AN INVESTIGATION OF THE C-Ni-V TERNARY PHASE DIAGRAM AND DEVELOPMENT OF ABRASION-RESISTANT ALLOYS

AYODEJI OLUWATOYIN APATA

A thesis submitted to the Faculty of Engineering and the Built Environment, University of the Witwatersrand, in fulfilment of the requirements for the degree of Doctor of Philosophy in Engineering (Metallurgy and Materials Engineering).

Johannesburg, March 2014

DECLARATION

I, Ayodeji Oluwatoyin Apata, declare that this thesis is my own work except where otherwise acknowledged. It is being submitted for the degree of Doctor of Philosophy in Engineering at the University of the Witwatersrand, Johannesburg. It has not been submitted previously at this, or any other University for any degree of examination.

_____ _____

Signature Date

ABSTRACT

This study investigated the C-Ni-V ternary phase diagram and identification of possible abrasive-resistance alloys. Twenty-four alloys were made from the elemental components and were arc-melted under an argon atmosphere, using Ti as an oxygen-getter. These alloys were analysed in both the as-cast condition, and after annealing for 1000°C and water quenching. Microstructural characterization was carried out in a SEM with EDX, and was done to confirm the phases. The results were used to plot a solidification projection and all binary phases extended into ternary, except for ~Ni_8V, ~NiV_3 and ~V_2C which were not found, due to the sample compositions chosen. The extensions of the binary phases were: ~Ni_3V: ~15 at.% C; ~Ni_2V: ~20 at.% C; σ′: ~18 at.% C; (Ni): ~27 at.% C; ~V_8C_7: ~2 at.% Ni; ~V_6C_5: ~2 at.% Ni and ~VC: ~2 at.% Ni. The liquidus surface was derived, and three ternary invariant reactions were identified. The isothermal section at 1000°C was also constructed.

Hardness of the alloys was studied in both conditions. Alloys with (Ni) (188-402HV_5) were found to be ductile with low hardness. Alloys containing (V), ~Ni_3V and ~Ni_2V were identified as hard phases (533-1052 HV_5). Alloys with σ′ phase were very hard (1065-1266 HV_5) extremely brittle with cracks. Fracture toughness of the C-Ni-V alloys 0.9-5.2 (MPa.m$^{-1/2}$) were comparable with ceramics 0.5-5.3(MPa.m$^{-1/2}$).

The wear behaviour of the alloys was characterized by sliding the carbide alloys against a Cr-steel ball in a pin-on-disc configuration. There were several co-existing wear mechanisms: abrasion, adhesion and the formation of a thin tribolayers. The wear coefficients for a 10N contact load after a sliding wear path of 300m varied between 0.1 x 10^{-6} and 7.6 x 10^{-6} (mm^3/Nm), which was not as good as WC-Co hard metals, but close.

DEDICATION

The thesis is dedicated to almighty God maker of heaven and earth and my parents: Benson Apata and Victoria Apata for giving me the right path.

ACKNOWLEDGEMENTS

I would like to thank the following people and organisations for their contribution to this work:

- The Almighty God, the creator and custodian of knowledge for leading me successfully in all I went through while trying to achieve this academic goal.

- My main supervisor, Prof. L.A. Cornish for her motherly guidance and for taking pains to read and correct the manuscript of this project. My unreserved appreciation goes to other supervisors: Prof. M.J. Witcomb, Prof. G.O. Rading and Prof. P.K. Jain.

- The financial assistance of Africa Materials Science and Engineering Network (AMSEN), a Carnegie-RISE Network and DST/NRT Centre of Excellence in Strong Materials (CoE-SM) are gratefully acknowledged.

- My employer, The Federal Polytechnics Idah, Kogi State, Nigeria for granting me the study leave.

- MINTEK and Edson Mahuma for manufacturing of samples.

- Dr N. Sacks and Engr. E. Ogunmuyiwa for the wear tests.

- To the following people: Mr and Mrs Ikotun, Mr and Mrs Adams, the Dominion Family and everybody that rendered one assistance or the other for me in the course of this programme. May God in His infinite mercy bless you all. Amen.

- My colleagues in the research group for their love, concern and understanding during the course of my study. Wish them all the best of luck in their entire endeavor in life.

- Finally, my sincere gratitude goes to my dear wife Mrs. Funke Apata who is always there for me in every step I took. Dear, every time I think about you, I bless the day I met you.

THE LORD IS MY STRENGTH

A.O. APATA 2014

TABLE OF CONTENTS

DECLARATION ii
ABSTRACT iii
DEDICATION iv
ACKNOWLEDGEMENTS v
TABLE OF CONTENTS vi
LIST OF FIGURES xi
LIST OF TABLES xxx
CHAPTER ONE 1
1.1 INTRODUCTION 1
1.2 BACKGROUND AND MOTIVATION 2
CHAPTER TWO 4
2.0 LITERATURE REVIEW 4
2.1 Cemented Carbides 4
2.2 Nickel-based alloys 7
2.3 Phase diagrams 9
2.3.1 V-C phase diagram 9
2.3.2 Solid phases 11
2.3.3 Binary Ni-V phase diagram 20
2.3.4 Solid phases 22
2.3.5 Phase reaction 22
2.3.6 Binary Ni-C phase diagram 24
2.3.7 Solid phases 25
2.3.8 Ni-V-C tenary system 27
2.4 Tribology 28
2.4.1 Friction 29
2.5 Sliding wear 32
CHAPTER THREE 33

3.0 EXPERIMENTAL PROCEDURE 33
3.1 Sample selection 33
3.2 Manufacturing and sectioning of the samples 35
3.3 Sample annealing 37
3.4 Metallographic preparation 37
3.5 Sample characterization 37
3.5.1 Scanning electron microscopy and energy dispersive X-ray analysis 37
3.5.2 X-ray diffraction (XRD) 38
3.6 Mechanical testing 40
3.6.1 Hardness tests 40
3.6.2 Toughness 40
3.6.3 Palmqvist fracture toughness (K_{IC}) 41
3.6.4 Sliding wear and friction tests 41
CHAPTER FOUR 44
4.0 RESULTS 44
4.1 Characterizations of as-cast alloys 44
4.1.1 Nominal $Ni_{10}:V_{50}:C_{40}$ (at.%), Sample 1 44
4.1.2 Nominal $Ni_{20}:V_{40}:C_{40}$ (at.%), Sample 2 50
4.1.3 Nominal $Ni_{24}:V_{50}:C_{26}$ (at.%),Sample 3 56
4.1.4 Nominal $Ni_{40}:V_{50}:C_{10}$ (at.%), Sample 4 62
4.1.5 Nominal $Ni_{53}:V_{37}:C_{10}$ (at.%), Sample 5 67
4.1.6 Nominal $Ni_{64}:V_{25}:C_{11}$ (at.%), Sample 6 72
4.1.7 Nominal $Ni_{70}:V_{10}:C_{20}$ (at.%), Sample 7 78
4.1.8 Nominal $Ni_{60}:V_{30}:C_{10}$ (at.%), Sample 8 84
4.1.9 Nominal $Ni_{30}:V_{65}:C_{5}$ (at.%), Sample 9 90
4.1.10 Nominal $Ni_{20}:V_{35}:C_{45}$ (at.%), Sample 10 96
4.1.11 Nominal $Ni_{10}:V_{80}:C_{10}$ (at.%), Sample 11 102
4.1.12 Nominal $Ni_{5}:V_{75}:C_{20}$ (at.%), Sample 12 109
4.1.13 Nominal $Ni_{14}:V_{64}:C_{22}$ (at.%), Sample 13 116
4.1.14 Nominal $Ni_{28}:V_{54}:C_{18}$ (at.%), Sample 14 122
4.1.15 Nominal $Ni_{32}:V_{56}:C_{12}$ (at.%), Sample 15 129

4.1.16 Nominal $Ni_{39}:V_{42.8}:C_{18.2}$ (at.%), Sample 17 135
4.1.17 Nominal $Ni_{66.4}:V_{16.1}:C_{17.5}$ (at.%), Sample 18 142
4.1.18 Nominal $Ni_{68}:V_{14}:C_{18}$ (at.%), Sample 19 148
4.1.19 Nominal $Ni_{59}:V_{27.2}:C_{13.8}$ (at.%), Sample 20 154
4.1.20 Nominal $Ni_{59}:V_{27.2}:C_{13.8}$ (at.%), Sample 21 159
4.1.21 Nominal $Ni_{49}:V_{33.3}:C_{17.7}$ (at.%), Sample 22 166
4.1.22 Nominal $Ni_{24}:V_{58.6}:C_{17.4}$ (at.%), Sample 23 171
4.1.23 Nominal $Ni_{22.1}:V_{49.1}:C_{28.8}$ (at.%), Sample 24 177
4.2 Phase analysis of alloys – annealed at 1000 °C for 1000 hours 184
4.2.1 Heat treated nominal $Ni_{64}:V_{25}:C_{11}$ (at.%), Sample 6H 184
4.2.2 Heat treated nominal $Ni_{70}:V_{10}:C_{20}$ (at.%), Sample 7H 189
4.2.3 Heat treated nominal $Ni_{60}:V_{30}:C_{10}$ (at.%), Sample 8H 194
4.2.4 Heat treated nominal $Ni_{20}:V_{35}:C_{45}$ (at.%), Sample 10H 200
4.2.5 Heat treated nominal $Ni_{10}:V_{80}:C_{10}$ (at.%), Sample 11H 206
4.2.6 Heat treated nominal $Ni_{5}:V_{75}:C_{20}$ (at.%), Sample 12H 213
4.2.7 Heat treated nominal $Ni_{14}:V_{64}:C_{22}$ (at.%), Sample 13H 219
4.2.8 Heat treated nominal $Ni_{28}:V_{54}:C_{18}$ (at.%), Sample 14H 224
4.2.9 Heat treated nominal $Ni_{32}:V_{56}:C_{12}$ (at.%), Sample 15H 230
4.2.10 Heat treated nominal $Ni_{39}:V_{42.8}:C_{18.2}$ (at.%), Sample 17H 237
4.2.11 Heat treated nominal $Ni_{66.4}:V_{16.1}:C_{17.5}$ (at.%), Sample 18H 243
4.2.12 Heat treated nominal $Ni_{68}:V_{14}:C_{18}$ (at.%), Sample 19H 250
4.2.13 Heat treated nominal $Ni_{59}:V_{27.2}:C_{13.8}$ (at.%), Sample 20H 255
4.2.14 Heat treated nominal $Ni_{39}:V_{42.8}:C_{18.2}$ (at.%), Sample 21H 260
4.2.15 Heat treated nominal $Ni_{49}:V_{33.3}:C_{17.7}$ (at.%), Sample 22H 267
4.2.16 Heat treated nominal $Ni_{22.1}:V_{49.1}:C_{28.8}$ (at.%), Sample 24H 272
4.3 Mechanical properties 279
4.3.1 Hardness test results 279
4.3.1.1 Hardness results of as-cast specimen 279
4.3.1.2 Toughness 279
4.3.1.3 Fracture toughness (KIC), for as-cast samples 285
4.3.1.4 Heat treated hardness test results 285

4.3.1.5 Fracture toughness (KIC) for heat treated samples 291
4.3.2 Sliding wear and friction test results 291
4.3.2.1 Friction results (as-cast samples) for Samples 19 to 24 291
4.3.2.2 Sliding wear volume of as-cast samples 295
4.3.2.3 Wear surface analysis of as-cast samples 296
4.3.2.4 Friction results of heat treated samples 300
4.3.2.5 Sliding wear volume of heat treated samples 304
4.3.2.6 Wear surface analysis for heat treated samples 304
CHAPTER FIVE 307
5.0 DISCUSSION 307
5.1 X-ray results 307
5.3 Liquidus projection surface 320
5.4 Isothermal section at 1000 °C 324
5.5 Mechanical properties 326
5.5.1 Hardness 326
5.5.2 Toughness 329
5.5.3 Fracture toughness (K_{IC}) 332
5.5.4 Friction response of the as-cast samples 333
5.5.5 Sliding wear volume of as-cast samples 335
5.5.6 Wear surface analysis of as-cast samples 336
5.5.7 Friction response of heat treated samples 337
5.5.8 Sliding wear volume of heat treated samples 338
5.5.9 Wear surface analysis of heat treated samples 341
5.5.10 Comparison with literature data 341
5.5.11. Comparison of phase diagrams with VC-coated Ni 349
5.5.12. Comparison of the investigated C-Ni-V alloyed with rapidly solidified thick deposit of Fe-C-V-Cr-Ni alloy by plasma spraying Hos *et al.* [2009]. 353
5.5.13. Comparison of hardnesses of the alloys with σ′ volume fractions 354
CHAPTER SIX 356
6.0 CONCLUSIONS AND RECOMMENDATIONS 356
6.1 CONCLUSIONS 356

6.2 RECOMMENDATIONS 360
REFERENCES 361
APPENDIX A 370
APPENDIX B 374

LIST OF FIGURES

Figure 2.1.Cross-section of the as-coated: (a) optical, (b) Scanning Auger microscopy and heat treated at (c) 850° C 45 min (d) 1000°C 45 min sample, showing the points where chemical analyses were performed [2009Rui]. **6**
Figure 2. 2. Binary V-C equilibrium phase diagram [1985Car]. **11**
Figure 2. 3. Calculated V-C phase diagram [1991Lee]. **15**
Figure 2.4. Calculated V-C phase diagram compared with experimental data [1969Rud]. **15**
Figure 2.5. Equilibrium phase diagram of the V–C system with consideration of the ordering of nonstoichiometric cubic and hexagonal vanadium carbides VC_y and V_2C_y [1999Lip]..... **17**
Figure 2.6. Calculated V–C phase diagram according to Huang [1991Hua]. **18**
Figure 2.7. Calculated V-C phase diagram according to Hu *et al*. [2006 Hu]..... **19**
Figure 2.8. Calculated phase diagram compared with the experimental data from various sources [2006Hu]. **19**
Figure 2.9. Calculated phase diagram in the ordering region compared with experimental data from various sources [2006Hu]. **20**
Figure 2.10. Ni-V binary phase diagram [1982Smi]. **21**
Figure 2.11. The Ni–V phase diagram, calculated using the modified CEF model for the sigma phase [2001Wat1]. **24**
Figure 2.12. Ni-C (graphite) phase diagram with selected data points for the Ni-rich eutectic composition and temperature [1989Sin]. **25**
Figure 2.13. Ni-C (graphite solid line) with metastable Ni-Ni_3C (dashed line) phase diagram [1989Sin]..... **26**
Figure 2.14.Complete isothermal section given at 1100°C (1373K) [1975Hol]. **27**
Figure 2.15. Complete isothermal section given at 1100°C (1373K) [1975Tel]. **28**
Figure 2.16. The coefficient of friction as a function of sliding distance. (a) A typical S-shaped curve illustrating the running in period. (b) Four hypothetical patterns that can be expected [2002Bhu]. **32**
Figure 3.1. Selected compositions of the ternary Ni -V- C samples..... **34**
Figure 3.2. Button Arc Furnace (BAF) showing constituent's element before melting. **36**
Figure 3.3 Button Arc Furnace (BAF) showing the sample button after melting. **36**
Figure 3.4. Measurement head of the tribometer. **42**
Figure 4.1. SEM-BSE image of nominal Ni_{10}:V_{50}:C_{40} (at.%), Sample, 1 in as-cast condition, showing graphite plates (very dark), dendrites ~V_6C_5 (medium grey) and matrix (light) ~Ni_3V. **45**
Figure 4.2. SEM-BSE image of nominal Ni_{10}:V_{50}:C_{40} (at.%), Sample 1, in as-cast condition, showing graphite plates (very dark), dendrites ~V_6C_5 (medium grey) and matrix (light) ~Ni_3V at higher magnification. **45**
Figure 4.3. EDX analyses of as-cast Ni_{10}:V_{50}:C_{40} (at.%), Sample 1. ..... **46**
Figure 4.4. Unlabelled XRD pattern of as-cast nominal Ni_{10}:V_{50}:C_{40} (at.%), Sample 1. ..... **47**

Figure 4.5. XRD pattern of as-cast nominal $Ni_{10}:V_{50}:C_{40}$ (at.%), Sample 1, showing identified ~V_6C_5 peaks. **47**
Figure 4.6. XRD pattern of as-cast nominal $Ni_{10}:V_{50}:C_{40}$ (at.%), Sample 1, showing identified ~Ni_3V peaks. **48**
Figure 4.7. XRD pattern of as-cast nominal $Ni_{10}:V_{50}:C_{40}$ (at.%), Sample 1, showing identified C peaks. **48**
Figure 4.8. XRD pattern of as-cast nominal $Ni_{10}:V_{50}:C_{40}$ (at.%), Sample 1, showing all identified phases. **49**
Figure 4.9. SEM-BSE image of nominal $Ni_{20}:V_{40}:C_{40}$ (at.%), Sample 2, in as-cast condition, showing graphite plates (very dark), ~V_8C_7 dendrites (medium grey) and (Ni) matrix (light). .. **51**
Figure 4.10. SEM-BSE image of nominal $Ni_{20}:V_{40}:C_{40}$ (at.%), Sample 2, in as-cast condition, showing graphite plates (very dark), ~V_8C_7 dendrites (medium grey) and (Ni) matrix (light) at higher magnification. **51**
Figure 4.11. EDX analyses of as-cast $Ni_{20}:V_{40}:C_{40}$ (at.%), Sample 2. ..... **52**
Figure 4.12. Unlabelled XRD pattern of as-cast nominal $Ni_{20}:V_{40}:C_{40}$ (at.%), Sample 2. ..... **53**
Figure 4.13. XRD pattern of as-cast nominal $Ni_{20}:V_{40}:C_{40}$ (at.%), Sample 2, showing identified ~V_8C_7 peaks. **53**
Figure 4.14. XRD pattern of as-cast nominal $Ni_{20}:V_{40}:C_{40}$ (at.%), Sample 2, showing identified (Ni) peaks. **54**
Figure 4.15. XRD pattern of as-cast nominal $Ni_{20}:V_{40}:C_{40}$ (at.%), Sample 2, showing identified C peaks. **54**
Figure 4.16. XRD pattern of as-cast nominal $Ni_{20}:V_{40}:C_{40}$ (at.%), Sample 2, showing all identified peaks. **55**
Figure 4.17. SEM-BSE image of nominal $Ni_{24}:V_{50}:C_{26}$ (at.%), Sample 3, in the as-cast condition, showing ~V_6C_5 dendrites (dark) and ~Ni_2V matrix (light). **57**
Figure 4.18. SEM-BSE image of nominal $Ni_{24}:V_{50}:C_{26}$ (at.%), Sample 3, in the as-cast condition, showing ~V_6C_5 dendrites (dark) with C flakes and ~Ni_2V matrix (light) at higher magnification. **57**
Figure 4.19. EDX analyses of as-cast $Ni_{24}:V_{50}:C_{26}$ (at.%), Sample 3. ..... **58**
Figure 4.20. Unlabelled XRD pattern of as-cast nominal $Ni_{24}:V_{50}:C_{26}$(at.%), Sample 3. ..... **59**
Figure 4.21. XRD pattern of as-cast nominal $Ni_{24}:V_{50}:C_{26}$ (at.%), Sample 3, showing identified $V_4C_{2.66}$ peaks. **59**
Figure 4.22. XRD pattern of as-cast nominal $Ni_{24}:V_{50}:C_{26}$ (at.%), Sample 3, showing identified V_6C_5 peaks. **60**
Figure 4.23. XRD pattern of as-cast nominal $Ni_{24}:V_{50}:C_{26}$ (at.%), Sample 3, showing identified Ni_2V peaks. **60**
Figure 4.24. XRD pattern of as-cast nominal $Ni_{24}:V_{50}:C_{26}$ (at.%), Sample 3, showing identified C peaks. **61**
Figure 4.25. XRD pattern of as-cast nominal $Ni_{24}:V_{50}:C_{26}$ (at.%), Sample 3, showing all identified peaks. **61**

Figure 4.26. SEM-BSE image of nominal $Ni_{40}:V_{50}:C_{10}$ (at.%), Sample 4, in the as-cast condition, showing ~VC dendrites (dark), ~Ni_2V matrix (light). **63**
Figure 4.27. SEM-BSE image of nominal $Ni_{40}:V_{50}:C_{10}$ (at.%), Sample 4, in the as-cast condition, showing ~VC needles (dark), ~Ni_2V matrix (light) and eutectic at higher magnification. **63**
Figure 4.28. EDX analyses of as-cast nominal $Ni_{40}:V_{50}:C_{10}$ (at.%), Sample 4. **64**
Figure 4.29. Unlabelled XRD pattern of as-cast nominal $Ni_{40}:V_{50}:C_{10}$ (at.%), Sample 4. **65**
Figure 4.30. XRD pattern of as-cast nominal $Ni_{40}:V_{50}:C_{10}$ (at.%), Sample 4, showing identified VC peaks. **65**
Figure 4.31. XRD pattern of as-cast nominal $Ni_{40}:V_{50}:C_{10}$ (at.%), Sample 4, showing identified Ni_2V peaks. **66**
Figure 4.32. XRD pattern of as-cast nominal $Ni_{40}:V_{50}:C_{10}$ (at.%), Sample 4, showing all the identified peaks. **66**
Figure 4.33. SEM-BSE image of nominal $Ni_{53}:V_{37}:C_{10}$ (at.%), Sample 5, in the as-cast condition, showing ~V_6C_5 dendrites (dark) and ~Ni_2V matrix (light). **68**
Figure 4.34. SEM-BSE image of nominal $Ni_{53}:V_{37}:C_{10}$ (at.%), Sample 5, in the as-cast condition, showing ~V_6C_5 dendrites (dark) ~Ni_2V matrix (light) and eutectic at higher magnification. **68**
Figure 4. 35. EDX analyses of as-cast nominal $Ni_{53}:V_{37}:C_{10}$ (at.%), Sample 5. **69**
Figure 4.36. Unlabelled XRD pattern of as-cast nominal $Ni_{53}:V_{37}:C_{10}$ (at.%), Sample 5. **70**
Figure 4.37. XRD pattern of as-cast nominal $Ni_{53}:V_{37}:C_{10}$ (at.%), Sample 5, showing identified V_6C_5 peaks. **70**
Figure 4.38. XRD pattern of as-cast nominal $Ni_{53}:V_{37}:C_{10}$ (at.%), Sample 5, showing identified Ni_2V peaks. **71**
Figure 4.39. XRD pattern of as-cast nominal $Ni_{53}:V_{37}:C_{10}$ (at.%), Sample 5, showing all identified peaks. **71**
Figure 4.40. SEM-BSE image of nominal $Ni_{64}:V_{25}:C_{11}$ (at.%), Sample 6, showing ~V_8C_7 dendrites (dark), ~Ni_3V matrix (light) and eutectic. **74**
Figure 4.41. SEM-BSE image of nominal $Ni_{64}:V_{25}:C_{11}$ (at.%), Sample 6, showing ~ V_8C_7 dendrites (dark), ~Ni_3V matrix (light) and eutectic with different colonies at higher magnification. **74**
Figure 4.42. EDX analyses of as-cast nominal $Ni_{64}:V_{25}:C_{11}$ (at.%), Sample 6. **75**
Figure 4.43. Unlabelled XRD pattern of as-cast nominal $Ni_{64}:V_{25}:C_{11}$ (at.%), Sample 6. **76**
Figure 4.44. XRD pattern of as-cast nominal $Ni_{64}:V_{25}:C_{11}$ (at.%) , Sample 6, showing identified Ni_3V peaks. **76**
Figure 4.45. XRD pattern of as-cast nominal $Ni_{64}:V_{25}:C_{11}$ (at.%), Sample 6, showing identified V_8C_7 peaks. **77**
Figure 4.46. XRD pattern of as-cast nominal $Ni_{64}:V_{25}:C_{11}$ (at.%), Sample 6, showing all the identified peaks. **77**
Figure 4.47. SEM-BSE image of nominal $Ni_{70}:V_{10}:C_{20}$ (at.%), Sample 7, in the as-cast condition, showing graphite plates (very dark), ~V_8C_7 dendrites (dark) and (Ni) matrix (light). **79**

Figure 4.48. SEM-BSE image of nominal $Ni_{70}:V_{10}:C_{20}$ (at.%), Sample 7, in the as-cast condition, showing graphite plates (very dark), ~V_8C_7 dendrites (dark), (Ni) matrix (light) and eutectic at higher magnification. **80**
Figure 4.49. EDX analyses of nominal $Ni_{70}:V_{10}:C_{20}$ (at.%), Sample 7, in the as-cast condition.. **81**
Figure 4.50. Unlabelled XRD pattern of as-cast nominal $Ni_{70}:V_{10}:C_{20}$ (at.%), Sample 7. ..... **82**
Figure 4.51. XRD pattern of as-cast nominal $Ni_{70}:V_{10}:C_{20}$ (at.%), Sample 7, showing (Ni) peaks. **82**
Figure 4.52. XRD pattern of as-cast nominal $Ni_{70}:V_{10}:C_{20}$ (at.%), Sample 7, showing C peaks.. **83**
Figure 4.53. XRD pattern of as-cast nominal $Ni_{70}:V_{10}:C_{20}$ (at.%), Sample 7, showing ~V_7C_8 peaks. **83**
Figure 4.54. XRD pattern of as-cast nominal $Ni_{70}:V_{10}:C_{20}$ (at.%), Sample 7, showing all identified phases..... **84**
Figure 4.55. SEM-BSE image of nominal $Ni_{60}:V_{30}:C_{10}$ (at.%), Sample 8, in the as-cast condition, showing ~V_8C_7 dendrites (dark), ~Ni_2V matrix (light) and eutectic. **86**
Figure 4.56. SEM-BSE image of nominal $Ni_{60}:V_{30}:C_{10}$ (at.%), Sample 8, in the as-cast condition, showing ~V_8C_7 dendrites (dark) with cracks, ~Ni_2V matrix (light) and eutectic at higher magnification. **86**
Figure 4.57. EDX analyses of as-cast nominal $Ni_{60}:V_{30}:C_{10}$ (at.%), Sample 8..... **87**
Figure 4.58. Unlabelled XRD pattern of as-cast nominal $Ni_{60}:V_{30}:C_{10}$ (at.%), Sample 8. ..... **88**
Figure 4.59. XRD pattern of as-cast nominal $Ni_{60}:V_{30}:C_{10}$ (at.%), Sample 8, showing identified ~V_8C_7 peaks. **88**
Figure 4.60. XRD pattern of as-cast nominal $Ni_{60}:V_{30}:C_{10}$ (at.%), Sample 8, showing identified ~Ni_2V peaks. **89**
Figure 4.61. XRD pattern of as-cast nominal $Ni_{60}:V_{30}:C_{10}$ (at.%), Sample 8, showing identified C peaks. **89**
Figure 4.62. XRD pattern of as-cast nominal $Ni_{60}:V_{30}:C_{10}$ (at.%), Sample 8, showing all identified phases..... **90**
Figure 4.63. SEM-BSE image of nominal $Ni_{30}:V_{65}:C_5$ (at.%), Sample 9, in the as-cast condition, showing ~VC dendrites (dark), σ′ matrix (light) and eutectic. **91**
Figure 4.64. SEM-BSE image of nominal $Ni_{30}:V_{65}:C_5$ (at.%), Sample 9 in the as-cast condition, showing primary ~VC dendrites (dark), σ′ matrix (light) and eutectic at higher magnification.. **92**
Figure 4.65. EDX analyses of as-cast nominal $Ni_{30}:V_{65}:C_5$ (at.%), Sample 9. ..... **93**
Figure 4.66. Unlabelled XRD pattern of as-cast nominal $Ni_{30}:V_{65}:C_5$ (at.%), Sample 9..... **94**
Figure 4.67. XRD pattern of nominal $Ni_{30}:V_{65}:C_5$ (at.%), Sample 9, in the as-cast condition, showing identified ~VC peaks. **94**
Figure 4.68. XRD pattern of nominal $Ni_{30}:V_{65}:C_5$ (at.%), Sample 9, in the as-cast condition, showing identified ~$V_4C_{2.66}$ peaks. **95**
Figure 4.69. XRD pattern of nominal $Ni_{30}:V_{65}:C_5$ (at.%), Sample 9, in the as-cast condition, showing all the identified peaks..... **95**

Figure 4.70. SEM-BSE image of nominal $Ni_{20}:V_{35}:C_{45}$ (at.%), Sample 10, in the as-cast condition, showing graphite flakes (very dark), ~V_8C_7 dendrites (dark), and (Ni) matrix (light). Pores can be seen at the top right corner..... **97**
Figure 4.71. SEM-BSE image of nominal $Ni_{20}:V_{35}:C_{45}$ (at.%), Sample 10, in the as-cast condition, showing graphite flakes (very dark), ~V_8C_7 dendrites (dark), and (Ni) matrix (light) at higher magnification. **98**
Figure 4.72. SEM-SE low magnification image of nominal $Ni_{20}:V_{35}:C_{45}$ (at.%), Sample 10, in the as-cast condition, showing pores. **98**
Figure 4.73. EDX analyses of as-cast nominal $Ni_{20}:V_{35}:C_{45}$ (at.%), Sample 10..... **99**
Figure 4.74. Unlabelled XRD pattern of as-cast nominal $Ni_{20}:V_{35}:C_{45}$ (at.%), Sample 10. ..... **100**
Figure 4.75. XRD pattern of nominal $Ni_{20}:V_{35}:C_{45}$ (at.%), Sample 10, in the as-cast condition, showing identified (Ni) peaks. **100**
Figure 4.76. XRD pattern of nominal $Ni_{20}:V_{35}:C_{45}$ (at.%), Sample 10, in the as-cast condition, showing identified ~V_8C_7 peaks. **101**
Figure 4.77. XRD pattern of nominal $Ni_{20}:V_{35}:C_{45}$ (at.%), Sample 10, in the as-cast condition, showing identified graphite peaks. **101**
Figure 4.78. XRD pattern of nominal $Ni_{20}:V_{35}:C_{45}$ (at.%), Sample 10, in the as-cast condition, showing all identified phases. **102**
Figure 4.79. SEM-BSE image of nominal $Ni_{10}:V_{80}:C_{10}$ (at.%), Sample 11, in the as-cast condition, showing ~VC dendrites (dark), (V) matrix (light) and eutectic. **103**
Figure 4.80. SEM-BSE image of nominal $Ni_{10}:V_{80}:C_{10}$ (at.%), Sample 11, in the as-cast condition, showing ~VC dendrites (dark), (V) matrix (light) and eutectic at higher magnification. **104**
Figure 4.81. EDX analyses of as-cast nominal $Ni_{10}:V_{80}:C_{10}$ (at.%), Sample 11..... **105**
Figure 4.82. Unlabelled XRD pattern of as-cast nominal $Ni_{10}:V_{80}:C_{10}$ (at.%), Sample 11. ..... **106**
Figure 4.83. XRD pattern of nominal $Ni_{10}:V_{80}:C_{10}$ (at.%), Sample 11, in the as-cast condition, showing identified $V_4C_{2.66}$ peaks. **106**
Figure 4.84. XRD pattern of nominal $Ni_{10}:V_{80}:C_{10}$ (at.%), Sample 11, in the as-cast condition, showing identified VC peaks. **107**
Figure 4.85. XRD pattern of nominal $Ni_{10}:V_{80}:C_{10}$ (at.%), Sample 11, in the as-cast condition, showing identified (V) peaks. **107**
Figure 4.86. XRD pattern of nominal $Ni_{10}:V_{80}:C_{10}$ (at.%), Sample 11, in the as-cast condition, showing identified NiV_3 peaks. **108**
Figure 4.87. XRD pattern of nominal $Ni_{10}:V_{80}:C_{10}$ (at.%), Sample 11, in the as-cast condition, showing all the identified peaks. **108**
Figure 4.88. SEM-BSE image of nominal $Ni_5:V_{75}:C_{20}$ (at.%), Sample 12, in the as-cast condition, showing ~VC dendrites (dark), a eutectic and matrix (medium). **110**
Figure 4.89. SEM-BSE image of as-cast nominal $Ni_5:V_{75}:C_{20}$ (at.%), Sample 12, showing ~VC dendrites with some pores at top of micrograph, and local light peritectic layer σ′and eutectic. **111**

Figure 4.90. SEM-BSE image of nominal $Ni_5:V_{75}:C_{20}$ (at.%), Sample 12 in the as-cast condition, showing ~VC dendrites with some cracks (dark) and peritectically formed σ′ (very light). **111**
Figure 4.91. EDX analyses of as-cast nominal $Ni_5:V_{75}:C_{20}$ (at.%), Sample 12. ..... **112**
Figure 4.92. Unlabelled XRD pattern of nominal $Ni_{20}:V_{35}:C_{45}$ (at.%), Sample 12, in the as-cast condition. **113**
Figure 4.93. XRD pattern of nominal $Ni_5:V_{75}:C_{20}$ (at.%), Sample 12, in the as-cast condition, showing identified ~V_2C peaks. **113**
Figure 4.94. XRD pattern of nominal $Ni_5:V_{75}:C_{20}$ (at.%), Sample 12, in the as-cast condition, showing identified (V) peaks. **114**
Figure 4.95. XRD pattern of nominal $Ni_5:V_{75}:C_{20}$ (at.%), Sample 12, in the as-cast condition, showing identified ~VC peaks. **114**
Figure 4.96. XRD pattern of nominal $Ni_5:V_{75}:C_{20}$ (at.%), Sample 12, in the as-cast condition, showing all the identified phases. **115**
Figure 4.97. SEM-BSE image of nominal $Ni_{14}:V_{64}:C_{22}$ (at.%), Sample 13, in the as-cast condition, showing ~VC needles (dark) and (Ni) matrix (light). **117**
Figure 4.98. SEM-BSE image of nominal $Ni_{14}:V_{64}:C_{22}$ (at.%), Sample 13, in the as-cast condition, showing ~VC dendrites (dark), (Ni) matrix (light) and fine eutectic at higher magnification. **117**
Figure 4.99. SEM-BSE image of nominal $Ni_{14}:V_{64}:C_{22}$ (at.%), Sample 13, in the as-cast condition, showing ~VC dendrites (dark), (Ni) matrix (light) and fine eutectic at higher magnification. **118**
Figure 4.100. Unlabelled XRD pattern of as-cast nominal $Ni_{14}:V_{64}:C_{22}$ (at.%), Sample 13. ..... **119**
Figure 4.101. XRD pattern of as-cast nominal $Ni_{14}:V_{64}:C_{22}$ (at.%), Sample 13, showing (Ni) peaks. **119**
Figure 4.102a. XRD pattern of as-cast nominal $Ni_{14}:V_{64}:C_{22}$ (at.%), Sample 13, showing identified V_6C_5 peaks. **120**
Figure 4.102b. XRD pattern of as-cast nominal $Ni_{14}:V_{64}:C_{22}$ (at.%), Sample 13, showing identified $V_4C_{2.66}$ peaks. **120**
Figure 4.104a. XRD pattern of as-cast nominal $Ni_{14}:V_{64}:C_{22}$ (at.%), Sample 13, showing identified VC peaks. **121**
Figure 4.104b. XRD pattern of as-cast nominal $Ni_{14}:V_{64}:C_{22}$ (at.%), Sample 13, showing all the identified peaks. **121**
Figure 4.106. SEM-BSE image of nominal $Ni_{28}:V_{54}:C_{18}$ (at.%), Sample 14, in the as-cast condition, showing ~VC dendrites (dark) with cracks, σ′ matrix (light) and eutectic (edge region). **123**
Figure 4.107. SEM-BSE image of nominal $Ni_{28}:V_{54}:C_{18}$ (at.%), Sample 14, in the as-cast condition, showing ~VC dendrites (dark), σ′matrix (light) at low magnification (middle region). **124**

Figure 4.108. SEM-BSE image of nominal $Ni_{28}:V_{54}:C_{18}$ (at.%), Sample 14, in the as-cast condition, showing ~VC dendrites (dark) with cracks, σ′ matrix (light) and eutectic at higher magnification (middle region). **124**
Figure 4.109. EDX analyses of as-cast nominal $Ni_{28}:V_{54}:C_{18}$ (at. %), Sample 14. ..... **125**
Figure 4.110. Unlabelled XRD pattern of as-cast nominal $Ni_{28}:V_{54}:C_{18}$ (at.%), Sample 14. ..... **126**
Figure 4.111. XRD pattern of as-cast nominal $Ni_{28}:V_{54}:C_{18}$ (at.%), Sample 14, showing identified VC peaks. **126**
Figure 4.112. XRD pattern of as-cast nominal $Ni_{28}:V_{54}:C_{18}$ (at.%), Sample 14, showing identified $V_4C_{2.66}$ peaks..... **127**
Figure 4.113. XRD pattern of as-cast nominal $Ni_{28}:V_{54}:C_{18}$ (at.%), Sample 14, showing identified C peaks. **127**
Figure 4.114. XRD pattern of as-cast nominal $Ni_{28}:V_{54}:C_{18}$ (at.%), Sample 14, showing all the identified peaks. **128**
Figure 4.115. SEM-BSE image of nominal $Ni_{32}:V_{56}:C_{12}$ (at.%), Sample 15, in the as-cast condition, showing ~V_8C_7 dendrites (dark) and σ′ matrix (light). **130**
Figure 4.116. SEM-BSE image of nominal $Ni_{32}:V_{56}:C_{12}$ (at.%), Sample 15, in the as-cast condition, showing ~V_8C_7 dendrites (dark), σ′ matrix (light) and eutectic at high magnification. **130**
Figure 4.117. SEM-SE image of nominal $Ni_{32}:V_{56}:C_{12}$ (at.%), Sample 15, in the as-cast condition, showing ~V_8C_7 dendrites (dark), σ′ matrix (light) and eutectic at high magnification. **131**
Figure 4.118. EDX analyses of as-cast nominal $Ni_{32}:V_{56}:C_{12}$ (at. %), Sample 15. ..... **132**
Figure 4.119. EDX analyses of as-cast nominal $Ni_{32}:V_{56}:C_{12}$ (at. %), Sample 15. ..... **133**
Figure 4.120. EDX analyses of as-cast nominal $Ni_{32}:V_{56}:C_{12}$ (at. %), Sample 15. ..... **133**
Figure 4.121. XRD pattern of as-cast nominal $Ni_{32}:V_{56}:C_{12}$ (at.%), Sample 15, showing identified $V_4C_{2.66}$ peaks..... **134**
Figure 4.122. XRD pattern of as-cast nominal $Ni_{32}:V_{56}:C_{12}$ (at.%), Sample 15, showing all the identified peaks. **134**
Figure 4.123. SEM-BSE image of nominal $Ni_{39}:V_{42.8}:C_{18.2}$ (at.%), Sample 17, in the as-cast condition, showing ~V_6C_5 dendrites (dark), ~Ni_2V matrix (light). **136**
Figure 4.124. SEM-BSE image of nominal $Ni_{39}:V_{42.8}:C_{18.2}$ (at.%), Sample 17, in the as-cast condition, showing ~V_6C_5 dendrites (dark), ~Ni_2V matrix (light) and eutectic at higher magnification. **137**
Figure 4.125. EDX analyses of as-cast nominal $Ni_{39}:V_{42.8}:C_{18.2}$ (at.%), Sample 17. ..... **138**
Figure 4.126. Unlabelled XRD pattern of as-cast nominal $Ni_{39}:V_{42.8}:C_{18.2}$ (at.%), Sample 17. **139**
Figure 4.127. XRD pattern of as-cast nominal $Ni_{39}:V_{42.8}:C_{18.2}$ (at.%), Sample 17, showing identified Ni_2V peaks..... **139**
Figure 4.128. XRD pattern of as-cast nominal $Ni_{39}:V_{42.8}:C_{18.2}$ (at.%), Sample 17, showing identified V_6C_5 peaks. **140**

Figure 4.129. XRD pattern of as-cast nominal $Ni_{39}:V_{42.8}:C_{18.2}$ (at.%), Sample 17, showing identified $V_4C_{2.66}$ peaks. **140**
Figure 4.130. XRD pattern of as-cast nominal $Ni_{39}:V_{42.8}:C_{18.2}$ (at.%), Sample 17, showing all the identified peaks. **141**
Figure 4.131. SEM-BSE image of nominal $Ni_{66.4}:V_{16.1}:C_{17.5}$ (at.%), Sample 18, in the as-cast condition, showing ~V_8C_7 dendrites (dark), (Ni) matrix (light). **142**
Figure 4.132. SEM-BSE image of nominal $Ni_{66.4}:V_{16.1}:C_{17.5}$ (at.%), Sample 18, in the as-cast condition, showing ~V_8C_7 dendrites (dark), (Ni) matrix (light) and eutectic at higher magnification. **143**
Figure 4.133. EDX analyses of as-cast nominal $Ni_{66.4}:V_{16.1}:C_{17.5}$ (at.%), Sample 18. **144**
Figure 4.134. Unlabelled XRD pattern of as-cast nominal $Ni_{66.4}:V_{16.1}:C_{17.5}$ (at.%), Sample 18. **145**
Figure 4.135. XRD pattern of as-cast nominal $Ni_{66.4}:V_{16.1}:C_{17.5}$ (at.%), Sample 18, showing identified V_8C_7 peaks. **145**
Figure 4.136. XRD pattern of as-cast nominal $Ni_{66.4}:V_{16.1}:C_{17.5}$ (at.%), Sample 18, showing identified Ni peaks. **146**
Figure 4.137. XRD pattern of as-cast nominal $Ni_{66.4}:V_{16.1}:C_{17.5}$ (at.%), Sample 18, showing identified $V_4C_{2.66}$ peaks. **146**
Figure 4.138. XRD pattern of as-cast nominal $Ni_{66.4}:V_{16.1}:C_{17.5}$ (at.%), Sample 18, showing identified C peaks. **147**
Figure 4.139. XRD pattern of as-cast nominal $Ni_{66.4}:V_{16.1}:C_{17.5}$ (at.%), Sample 18, showing all the identified peaks. **147**
Figure 4.140. SEM-BSE image of nominal $Ni_{68}:V_{14}:C_{18}$ (at.%), Sample 19, in the as-cast condition, showing ~V_8C_7 dendrites (dark), (Ni) matrix (light) and ~VC + (Ni) eutectic. **149**
Figure 4.141. SEM-BSE image of nominal $Ni_{68}:V_{14}:C_{18}$ (at.%), Sample 19, in the as-cast condition, showing ~V_8C_7 dendrites (dark), (Ni) matrix (light) and ~VC + (Ni) and C + (Ni) eutectics at higher magnification. **150**
Figure 4.142. EDX analyses of as-cast nominal $Ni_{68}:V_{14}:C_{18}$ (at.%), Sample 19. **151**
Figure 4.143. Unlabelled XRD pattern of as-cast nominal $Ni_{68}:V_{14}:C_{18}$ (at.%), Sample 19. **152**
Figure 4.144. XRD pattern of as-cast nominal $Ni_{68}:V_{14}:C_{18}$ (at.%), Sample 19, showing identified V_8C_7 peaks. **152**
Figure 4.145. XRD pattern of as-cast nominal $Ni_{68}:V_{14}:C_{18}$ (at.%), Sample 19, showing identified (Ni) peaks. **153**
Figure 4.146. XRD pattern of as-cast nominal $Ni_{68}:V_{14}:C_{18}$ (at.%), Sample 19, showing all the identified peaks. **153**
Figure 4.147. SEM-BSE image of nominal $Ni_{59}:V_{27.2}:C_{13.8}$ (at.%), Sample 20, in the as-cast condition, showing ~V_8C_7 dendrites (dark), and C + (Ni) eutectic. **155**
Figure 4.148. SEM-BSE image of nominal $Ni_{59}:V_{27.2}:C_{13.8}$ (at.%), Sample 20, in the as-cast condition, showing ~V_8C_7 dendrites (dark), (Ni) matrix (light), and ~VC + (Ni) and C + (Ni) eutectics at higher magnification. **155**
Figure 4.149. EDX analyses of as-cast nominal $Ni_{59}:V_{27.2}:C_{13.8}$ (at.%), Sample 20. **156**

Figure 4.150. Unlabelled XRD pattern of as-cast nominal $Ni_{59}:V_{27.2}:C_{13.8}$ (at.%), Sample 20. . **157**
Figure 4.151. XRD pattern of as-cast nominal $Ni_{59}:V_{27.2}:C_{13.8}$ (at.%), Sample 20, showing identified ~V_8C_7 peaks. **157**
Figure 4.152. XRD pattern of as-cast nominal $Ni_{59}:V_{27.2}:C_{13.8}$ (at.%), Sample 20, ... **158**
Figure 4.153. XRD pattern of as-cast nominal $Ni_{59}:V_{27.2}:C_{13.8}$ (at.%), Sample 20, ... **158**
Figure 4.154. XRD pattern of as-cast nominal $Ni_{59}:V_{27.2}:C_{13.8}$ (at.%), Sample 20, ... **159**
Figure 4.155. SEM-BSE image of nominal $Ni_{39}:V_{42.8}:C_{18.2}$ (at.%), Sample 21, in the as-cast condition, showing ~V_6C_5 needles (dark) and (Ni) matrix (light). **161**
Figure 4.156. SEM-BSE image of nominal $Ni_{39}:V_{42.8}:C_{18.2}$ (at.%), Sample 21, in the as-cast condition, showing ~V_6C_5 needles (dark) and (Ni) matrix (light), and ~VC + (Ni) and C + (Ni) eutectic at higher magnification. **161**
Figure 4.157. EDX analyses of as-cast nominal $Ni_{39}:V_{42.8}:C_{18.2}$ (at.%), Sample 21. ..... **162**
Figure 4.158. Unlabelled XRD pattern of as-cast nominal $Ni_{39}:V_{42.8}:C_{18.2}$ (at.%), Sample 21. . **163**
Figure 4.159. XRD pattern of as-cast nominal $Ni_{39}:V_{42.8}:C_{18.2}$ (at.%), Sample 21, showing identified ~Ni_2V peaks. **163**
Figure 4.160. XRD pattern of as-cast nominal $Ni_{39}:V_{42.8}:C_{18.2}$ (at.%), Sample 21, showing identified C peaks. **164**
Figure 4.161. XRD pattern of as-cast nominal $Ni_{39}:V_{42.8}:C_{18.2}$ (at.%), Sample 21, showing identified ~V_6C_5 peaks. **164**
Figure 4.162. XRD pattern of as-cast nominal $Ni_{39}:V_{42.8}:C_{18.2}$ (at.%), Sample 21, showing all the identified peaks. **165**
Figure 4.163. SEM-BSE image of nominal $Ni_{49}:V_{33.3}:C_{17.7}$ (at.%), Sample 22, in the as-cast condition, showing ~V_8C_7 dendrites (dark), and matrix (light). **167**
Figure 4.164. SEM-BSE image of nominal $Ni_{49}:V_{33.3}:C_{17.7}$ (at.%), Sample 22, in the as-cast condition, showing ~V_8C_7 dendrites (dark), and ~Ni_2V + ~VC and (Ni) + C eutectics at higher magnification. **167**
Figure 4.165. EDX analyses of as-cast nominal $Ni_{49}:V_{33.3}:C_{17.7}$ (at.%), Sample 22. ..... **168**
Figure 4.166. Unlabelled XRD pattern of as-cast nominal $Ni_{49}:V_{33.3}:C_{17.7}$ (at.%), Sample 22. . **169**
Figure 4.167. XRD pattern of as-cast nominal $Ni_{49}:V_{33.3}:C_{17.7}$ (at.%), Sample 22, showing identified ~Ni_2V peaks. **169**
Figure 4.168. XRD pattern of as-cast nominal $Ni_{49}:V_{33.3}:C_{17.7}$ (at.%), Sample 22, showing identified ~V_8C_7 peaks. **170**
Figure 4.169. XRD pattern of as-cast nominal $Ni_{49}:V_{33.3}:C_{17.7}$ (at.%), Sample 22, showing identified C peaks. **170**
Figure 4.170. XRD pattern of as-cast nominal $Ni_{49}:V_{33.3}:C_{17.7}$ (at.%), Sample 22, showing all the identified peaks. **171**
Figure 4.171. SEM-BSE image of nominal $Ni_{24}:V_{58.6}:C_{17.4}$ (at.%), Sample 23, in the as-cast condition, showing ~V_6C_5 dendrites (dark) and σ′ matrix (light). **172**

Figure 4.172. SEM-BSE image of nominal $Ni_{24}:V_{58.6}:C_{17.4}$ (at.%), Sample 23, in the as-cast condition, showing ~V_6C_5 dendrites (dark), σ′ matrix (light) and eutectic at high magnification. **173**
Figure 4.173. EDX analyses of as-cast nominal $Ni_{24}:V_{58.6}:C_{17.4}$ (at.%), Sample 23. ..... **174**
Figure 4.174. Unlabelled XRD pattern of as-cast nominal $Ni_{24}:V_{58.6}:C_{17.4}$ (at.%), Sample 23. . **175**
Figure 4.175. XRD pattern of as-cast nominal $Ni_{24}:V_{58.6}:C_{17.4}$ (at.%), Sample 23, showing identified ~V_6C_5 peaks **175**
Figure 4.176. XRD pattern of as-cast nominal $Ni_{24}:V_{58.6}:C_{17.4}$ (at.%), Sample 23, showing identified (V) peaks **176**
Figure 4.177. XRD pattern of as-cast nominal $Ni_{24}:V_{58.6}:C_{17.4}$ (at.%), Sample 23, showing all the identified peaks. **176**
Figure 4.178. SEM-BSE image of nominal $Ni_{22.1}:V_{49.1}:C_{28.8}$ (at.%), Sample 24, in the as-cast condition, showing ~V_8C_7 needles (dark) and ~Ni_2V matrix (light). **178**
Figure 4.179. SEM-BSE image of nominal $Ni_{22.1}:V_{49.1}:C_{28.8}$ (at.%), Sample 24, in the as-cast condition, showing ~V_8C_7 needles (dark) and ~Ni_2V matrix (light). **179**
Figure 4.180. SEM-BSE image of nominal $Ni_{22.1}:V_{49.1}:C_{28.8}$ (at.%), Sample 24, in the as-cast condition, showing ~V_8C_7 needles (dark) and ~Ni_2V matrix (light) at higher magnification. ... **179**
Figure 4.181. EDX analyses of as-cast nominal $Ni_{22.1}:V_{49.1}:C_{28.8}$ (at.%), Sample 24. ..... **180**
Figure 4.182. Unlabelled XRD pattern of as-cast nominal $Ni_{22.1}:V_{49.1}:C_{28.8}$ (at.%), Sample 24. **181**
Figure 4.183. XRD pattern of as-cast nominal $Ni_{22.1}:V_{49.1}:C_{28.8}$ (at.%), Sample 24, showing identified ~V_8C_7 peaks. **181**
Figure 4.184. XRD pattern of as-cast nominal $Ni_{22.1}:V_{49.1}:C_{28.8}$ (at.%), Sample 24, showing identified ~Ni_2V peaks. **182**
Figure 4.185. XRD pattern of as-cast nominal $Ni_{22.1}:V_{49.1}:C_{28.8}$ (at.%), Sample 24, showing identified ~$V_4C_{2.66}$ peaks. **182**
Figure 4.186. XRD pattern of as-cast nominal $Ni_{22.1}:V_{49.1}:C_{28.8}$ (at.%), Sample 24, showing all the identified peaks. **183**
Figure 4.187. BSE-SEM image of heat treated $Ni_{64}:V_{25}:C_{11}$ (at.%), Sample 6H, showing ~V_8C_7 dendrites (dark) and ~Ni_3V matrix (light) at low magnification. **185**
Figure 4.188. BSE-SEM image of heat treated $Ni_{64}:V_{25}:C_{11}$ (at.%), Sample 6H, showing ~V_8C_7 dendrites (dark), ~Ni_3V matrix (light) and eutectic with different colonies at higher magnification. **185**
Figure 4.189. EDX analyses of heat treated nominal $Ni_{64}:V_{25}:C_{11}$ (at.%), Sample 6H. **186**
Figure 4.190. Unlabelled XRD pattern of heat treated nominal $Ni_{64}:V_{25}:C_{11}$ (at.%), Sample 6H. **187**
Figure 4.191. XRD pattern of heat treated nominal $Ni_{64}:V_{25}:C_{11}$ (at.%), Sample 6H, showing identified ~V_8C_7 peaks. **187**
Figure 4.192. XRD pattern of heat treated nominal $Ni_{64}:V_{25}:C_{11}$ (at.%), Sample 6H, showing identified ~Ni_3V peaks. **188**

Figure 4.193. XRD pattern of heat treated nominal $Ni_{64}:V_{25}:C_{11}$ (at.%), Sample 6H, showing all the identified peaks. **188**
Figure 4.194. BSE-SEM images of heat treated $Ni_{70}:V_{10}:C_{20}$ (at.%), Sample 7H, showing graphite flakes (very dark), ~V_8C_7 dendrites (dark) and (Ni) matrix (light). **190**
Figure 4.195. BSE-SEM images of heat treated $Ni_{70}:V_{10}:C_{20}$ (at.%), Sample 7H, showing graphite flakes (very dark), ~V_8C_7 dendrites (dark) and (Ni) matrix (light). **190**
Figure 4.196. EDX analyses of heat treated nominal $Ni_{70}:V_{10}:C_{20}$ (at.%), Sample 7H. **191**
Figure 4.197. Unlabelled XRD pattern of heat treated nominal $Ni_{70}:V_{10}:C_{20}$ (at.%), Sample 7H. **192**
Figure 4.198. XRD pattern of heat treated nominal $Ni_{70}:V_{10}:C_{20}$ (at.%), Sample 7H, showing identified ~V_8C_7 peaks. **192**
Figure 4.199. XRD pattern of heat treated nominal $Ni_{70}:V_{10}:C_{20}$ (at.%), Sample 7H, showing identified C peaks. **193**
Figure 4.200. XRD pattern of heat treated nominal $Ni_{70}:V_{10}:C_{20}$ (at.%), Sample 7H, showing identified (Ni) peaks. **193**
Figure 4.201. XRD pattern of heat treated nominal $Ni_{70}:V_{10}:C_{20}$ (at.%), Sample 7H, showing all the identified peaks. **194**
Figure 4.202. BSE-SEM image of heat treated $Ni_{60}:V_{30}:C_{10}$ (at.%), Sample 8H, showing ~V_8C_7 dendrites (dark) and (Ni) matrix (light) at low magnification. **195**
Figure 4.203. BSE-SEM image of heat treated $Ni_{60}:V_{30}:C_{10}$ (at.%), Sample 8H, showing ~V_8C_7 dendrites (dark), (Ni) matrix (light) and eutectic at higher magnification. **196**
Figure 4.204. EDX analyses of heat treated nominal $Ni_{60}:V_{30}:C_{10}$ (at.%), Sample 8H. **197**
Figure 4.205. Unlabelled XRD pattern of heat treated nominal $Ni_{60}:V_{30}:C_{10}$ (at.%), Sample 8H. **198**
Figure 4.206. XRD pattern of heat treated nominal $Ni_{60}:V_{30}:C_{10}$ (at.%), Sample 8H, showing identified (Ni) peaks. **198**
Figure 4.207. XRD pattern of heat treated nominal $Ni_{60}:V_{30}:C_{10}$ (at.%), Sample 8H, showing identified ~V_8C_7 peaks. **199**
Figure 4.208. XRD pattern of heat treated nominal $Ni_{60}:V_{30}:C_{10}$ (at.%), Sample 8H, showing all the identified peaks. **199**
Figure 4.209. BSE-SEM image of heat treated $Ni_{20}:V_{35}:C_{45}$ (at.%), Sample 10H, showing ~V_8C_7 dendrites (dark), graphite flakes (very dark) and (Ni) matrix (light). **201**
Figure 4.210. BSE-SEM image of heat treated $Ni_{20}:V_{35}:C_{45}$ (at.%), Sample 10H, showing ~V_8C_7 dendrites (dark), graphite flakes (very dark) and (Ni) matrix (light). **201**
Figure 4.211. EDX analyses of heat treated nominal $Ni_{20}:V_{35}:C_{45}$ (at.%), Sample 10H. **202**
Figure 4.212. Unlabelled XRD pattern of heat treated nominal $Ni_{20}:V_{35}:C_{45}$ (at.%), Sample 10H. **203**
Figure 4.213. XRD pattern of heat treated nominal $Ni_{20}:V_{35}:C_{45}$ (at.%), Sample 10H, showing identified ~V_8C_7 peaks. **203**

Figure 4.214. XRD pattern of heat treated nominal $Ni_{20}:V_{35}:C_{45}$ (at.%), Sample 10H, showing identified (Ni) peaks. **204**
Figure 4.215. XRD pattern of heat treated nominal $Ni_{20}:V_{35}:C_{45}$ (at.%), Sample 10H, showing identified C peaks. **204**
Figure 4.216. XRD pattern of heat treated nominal $Ni_{20}:V_{35}:C_{45}$ (at.%), Sample 10H, showing identified ~$V_4C_{2.66}$ peaks. **205**
Figure 4.217. XRD pattern of heat treated nominal $Ni_{20}:V_{35}:C_{45}$ (at.%), Sample 10H, showing all the identified peaks. **205**
Figure 4.218. BSE-SEM image of heat treated $Ni_{10}:V_{80}:C_{10}$ (at.%), Sample 11H, showing ~VC dendrites (dark), (V) matrix (medium) and σ′ (light) at low magnification. **207**
Figure 4.219. BSE-SEM image of heat treated $Ni_{10}:V_{80}:C_{10}$ (at.%), Sample 11H, showing ~VC dendrites (dark), (V) matrix (medium) and σ′ (light) at higher magnification. **208**
Figure 4.220. EDX analyses of heat treated nominal $Ni_{10}:V_{80}:C_{10}$ (at.%), Sample 11H. **209**
Figure 4.221. Unlabelled XRD pattern of heat treated nominal $Ni_{10}:V_{80}:C_{10}$ (at.%), Sample 11H. **210**
Figure 4.222. XRD pattern of heat treated nominal $Ni_{10}:V_{80}:C_{10}$ (at.%), Sample 11H, showing identified ~VC peaks. **210**
Figure 4.223. XRD pattern of heat treated nominal $Ni_{10}:V_{80}:C_{10}$ (at.%), Sample 11H, showing identified (V) peaks. **211**
Figure 4.224. XRD pattern of heat treated nominal $Ni_{10}:V_{80}:C_{10}$ (at.%), Sample 11H, showing identified ~NiV_3 peaks. **211**
Figure 4.225. XRD pattern of heat treated nominal $Ni_{10}:V_{80}:C_{10}$ (at.%), Sample 11H, showing all the identified peaks. **212**
Figure 4.226. BSE-SEM image of heat treated $Ni_5:V_{75}:C_{20}$ (at.%), Sample 12H, showing ~VC dendrites (dark) and (V) matrix (medium). **213**
Figure 4.227. BSE-SEM image of heat treated $Ni_5:V_{75}:C_{20}$ (at.%), Sample 12H, showing ~VC dendrites (dark) and (V) matrix (medium). **214**
Figure 4.228. EDX analyses of heat treated nominal $Ni_5:V_{75}:C_{20}$ (at.%), Sample 12H. **215**
Figure 4.229. Raw XRD pattern of heat treated nominal $Ni_5:V_{75}:C_{20}$ (at.%), Sample 12H. **216**
Figure 4.230. XRD pattern of heat treated nominal $Ni_5:V_{75}:C_{20}$ (at.%), Sample 12H, showing identified ~VC peaks. **216**
Figure 4.231. XRD pattern of heat treated nominal $Ni_5:V_{75}:C_{20}$ (at.%), Sample 12H, showing identified (V) peaks. **217**
Figure 4.232. XRD pattern of heat treated nominal $Ni_5:V_{75}:C_{20}$ (at.%), Sample 12H, showing identified ~$V_4C_{2.66}$ peaks. **217**
Figure 4.233. XRD pattern of heat treated nominal $Ni_5:V_{75}:C_{20}$ (at.%), Sample 12H, showing all the identified peaks. **218**
Figure 4.234. BSE-SEM image of heat treated nominal $Ni_{14}:V_{64}:C_{22}$ (at.%), Sample 13H, showing ~VC dendrites (dark), ~Ni_2V (light) and σ′ (medium). **220**

Figure 4.235. BSE-SEM image of heat treated nominal $Ni_{14}:V_{64}:C_{22}$ (at.%), Sample 13H, showing ~VC dendrites (dark), ~Ni_2V (light) and σ′ (medium). **220**
Figure 4.236. EDX analyses of heat treated nominal $Ni_{14}:V_{64}:C_{22}$ (at.%), Sample 13H. **221**
Figure 4.237. Unlabelled XRD pattern of heat treated nominal $Ni_{14}:V_{64}:C_{22}$ (at.%), Sample 13H. **222**
Figure 4.238. XRD pattern of heat treated nominal $Ni_{14}:V_{64}:C_{22}$ (at.%), Sample 13H, showing identified ~Ni_2V peaks. **222**
Figure 4.239. XRD pattern of heat treated nominal $Ni_{14}:V_{64}:C_{22}$ (at.%), Sample 13H, showing identified ~VC peaks. **223**
Figure 4.240. XRD pattern of heat treated nominal $Ni_{14}:V_{64}:C_{22}$ (at.%), Sample 13H, showing all the identified peaks. **223**
Figure 4.241. BSE-SEM image of heat treated nominal $Ni_{28}:V_{54}:C_{18}$ (at.%), Sample 14H, showing ~VC dendrites (dark) and σ′ matrix (light) at low magnification. **225**
Figure 4.242. BSE-SEM image of heat treated nominal $Ni_{28}:V_{54}:C_{18}$ (at.%), Sample 14H, showing ~VC dendrites (dark) and σ′ matrix (light) at low magnification. **226**
Figure 4.243. EDX analyses of heat treated nominal $Ni_{28}:V_{54}:C_{18}$ (at.%), Sample 14H. **227**
Figure 4.244. Unlabelled XRD pattern of heat treated nominal $Ni_{28}:V_{54}:C_{18}$ (at.%), Sample 14H. **228**
Figure 4.245. XRD pattern of heat treated nominal $Ni_{28}:V_{54}:C_{18}$ (at.%), Sample 14H, showing identified ~VC peaks. **228**
Figure 4.246. XRD pattern of heat treated nominal $Ni_{28}:V_{54}:C_{18}$ (at.%), Sample 14H, showing identified ~$V_4C_{2.66}$ peaks. **229**
Figure 4.247. XRD pattern of heat treated nominal $Ni_{28}:V_{54}:C_{18}$ (at.%), Sample 14H, showing all the identified peaks. **229**
Figure 4.248. BSE-SEM image of heat treated nominal $Ni_{32}:V_{56}:C_{12}$ (at.%), Sample 15H, showing ~VC dendrites (dark) and σ′ matrix (light) at low magnification. **231**
Figure 4.249. BSE-SEM image of heat treated nominal $Ni_{32}:V_{56}:C_{12}$ (at.%), Sample 15H, showing ~VC dendrites (dark) with cracks and σ′ matrix (light) at higher magnification. **232**
Figure 4.250. EDX analyses of heat treated nominal $Ni_{32}:V_{56}:C_{12}$ (at.%), Sample 15H. **233**
Figure 4.251. Unlabelled XRD pattern of heat treated nominal $Ni_{32}:V_{56}:C_{12}$ (at.%), Sample 15H. **234**
Figure 4.252. XRD pattern of heat treated nominal $Ni_{32}:V_{56}:C_{12}$ (at.%), Sample 15H, showing identified ~VC peaks. **234**
Figure 4.253a. XRD pattern of heat treated nominal $Ni_{32}:V_{56}:C_{12}$ (at.%), Sample 15H, showing identified ~$V_4C_{2.66}$ peaks. **235**
Figure 4.253b. XRD pattern of heat treated nominal $Ni_{32}:V_{56}:C_{12}$ (at.%), Sample 15H, showing identified C peaks. **235**
Figure 4.255. XRD pattern of heat treated nominal $Ni_{32}:V_{56}:C_{12}$ (at.%), Sample 15H, showing all the identified peaks. **236**

Figure 4.256. BSE-SEM image of heat treated nominal $Ni_{39}:V_{42.8}:C_{18.2}$ (at.%), Sample 17H, showing ~V_6C_5 dendrites (dark) and ~Ni_2V matrix (light) at low magnification. **237**
Figure 4.257. BSE-SEM image of heat treated nominal $Ni_{39}:V_{42.8}:C_{18.2}$ (at.%), Sample 17H, showing ~V_6C_5 dendrites (dark) with needles (dark) and ~Ni_2V matrix (light) at higher magnification. **238**
Figure 4.258. EDX analyses of heat treated nominal $Ni_{39}:V_{42.8}:C_{18.2}$ (at.%), Sample 17H. **239**
Figure 4.259. Unlabelled XRD pattern of heat treated nominal $Ni_{39}:V_{42.8}:C_{18.2}$ (at.%), Sample 17H. **240**
Figure 4.260. XRD pattern of heat treated nominal $Ni_{39}:V_{42.8}:C_{18.2}$ (at.%), Sample 17H, showing identified ~V_6C_5 peaks. **240**
Figure 4.261. XRD pattern of heat treated nominal $Ni_{39}:V_{42.8}:C_{18.2}$ (at.%), Sample 17H, showing identified $V_4C_{2.66}$ peaks. **241**
Figure 4.262a. XRD pattern of heat treated nominal $Ni_{39}:V_{42.8}:C_{18.2}$ (at.%), Sample 17H, showing identified ~Ni_2Vpeaks. **241**
Figure 4.262b. XRD pattern of heat treated nominal $Ni_{39}:V_{42.8}:C_{18.2}$ (at.%), Sample 17H, showing identified C peaks. **242**
Figure 4.264. XRD pattern of heat treated nominal $Ni_{39}:V_{42.8}:C_{18.2}$ (at.%), Sample 17H, showing all the identified peaks. **242**
Figure 4.265. BSE-SEM image of heat treated nominal $Ni_{66.4}:V_{16.1}:C_{17.5}$ (at.%), Sample 18H, showing ~V_8C_7 dendrites (dark) and (Ni) matrix (light) at low magnification. **244**
Figure 4.266. BSE-SEM image of heat treated nominal $Ni_{66.4}:V_{16.1}:C_{17.5}$ (at.%), Sample 18H, showing ~V_8C_7 dendrites (dark), (Ni) matrix (light) and eutectic at higher magnification. **245**
Figure 4.267. EDX analyses of heat treated nominal $Ni_{66.4}:V_{16.1}:C_{17.5}$ (at.%), Sample 18H. **246**
Figure 4.268. Unlabelled XRD pattern of heat treated nominal $Ni_{66.4}:V_{16.1}:C_{17.5}$ (at.%), Sample 18H. **247**
Figure 4.269. XRD pattern of heat treated nominal $Ni_{66.4}:V_{16.1}:C_{17.5}$ (at.%), Sample 18H, showing identified (Ni) peaks. **247**
Figure 4.270. XRD pattern of heat treated nominal $Ni_{66.4}:V_{16.1}:C_{17.5}$ (at.%), Sample 18H, showing identified C peaks. **248**
Figure 4.271. XRD pattern of heat treated nominal $Ni_{66.4}:V_{16.1}:C_{17.5}$ (at.%), Sample 18H, showing identified ~V_8C_7 peaks. **248**
Figure 4.272. XRD pattern of heat treated nominal $Ni_{66.4}:V_{16.1}:C_{17.5}$ (at.%), Sample 18H, showing all the identified peaks. **249**
Figure 4.273. BSE-SEM images of heat treated $Ni_{68}:V_{14}:C_{18}$ (at.%), Sample 19H, showing ~V_8C_7 dendrites (dark) and (Ni) matrix (light). **250**
Figure 4.274. BSE-SEM images of heat treated $Ni_{68}:V_{14}:C_{18}$ (at.%), Sample 19H, showing ~V_8C_7 dendrites (dark), (Ni) matrix (light) and eutectic at higher magnification. **251**
Figure 4.275. EDX analyses of heat treated nominal $Ni_{68}:V_{14}:C_{18}$ (at.%), Sample 19H. **252**
Figure 4.276. Unlabelled XRD pattern of heat treated nominal $Ni_{68}:V_{14}:C_{18}$ (at.%), Sample 19H. **253**

Figure 4.277. XRD pattern of heat treated nominal $Ni_{68}:V_{14}:C_{18}$ (at.%), Sample 19H, showing identified (Ni) peaks. **253**
Figure 4.278. XRD pattern of heat treated nominal $Ni_{68}:V_{14}:C_{18}$ (at.%), Sample 19H, showing identified ~V_8C_7 peaks. **254**
Figure 4.279. XRD pattern of heat treated nominal $Ni_{68}:V_{14}:C_{18}$ (at.%), Sample 19H, showing all identified peaks. **254**
Figure 4.280. BSE-SEM images of heat treated $Ni_{59}:V_{27.2}:C_{13.8}$ (at.%), Sample 20H, showing ~V_8C_7 dendrites (dark) and (Ni) (light). **256**
Figure 4.281. BSE-SEM images of heat treated $Ni_{59}:V_{27.2}:C_{13.8}$ (at.%), Sample 20H, showing ~V_8C_7 dendrites (dark) and (Ni) + ~VC (light) and (Ni) + C (dark) eutectics. **256**
Figure 4.282. EDX analyses of heat treated $Ni_{59}:V_{27.2}:C_{13.8}$ (at.%), Sample 20H. **257**
Figure 4.283. Unlabelled XRD pattern of heat treated nominal $Ni_{59}:V_{27.2}:C_{13.8}$ (at.%), Sample 20H. **258**
Figure 4.284. XRD pattern of heat treated nominal $Ni_{59}:V_{27.2}:C_{13.8}$ (at.%), Sample 20H, showing identified (Ni) peaks. **258**
Figure 4.285. XRD pattern of heat treated nominal $Ni_{59}:V_{27.2}:C_{13.8}$ (at.%), Sample 20H, showing identified C peaks. **259**
Figure 4.286. XRD pattern of heat treated nominal $Ni_{59}:V_{27.2}:C_{13.8}$ (at.%), Sample 20H, showing identified ~V_8C_7 peaks. **259**
Figure 4.287. XRD pattern of heat treated nominal $Ni_{59}:V_{27.2}:C_{13.8}$ (at.%), Sample 20H, showing all identified peaks. **260**
Figure 4.288. BSE-SEM images of heat treated nominal $Ni_{39}:V_{42.8}:C_{18.2}$ (at.%), Sample 21H, showing ~V_6C_5 needles (dark), and ~Ni_2V matrix (light). **261**
Figure 4.289. BSE-SEM images of heat treated nominal $Ni_{39}:V_{42.8}:C_{18.2}$ (at.%), Sample 21H, showing ~V_6C_5 needles (dark), and ~Ni_2V matrix (light) at higher magnification. **262**
Figure 4.290. EDX analyses of heat treated nominal $Ni_{39}:V_{42.8}:C_{18.2}$ (at.%), Sample 21H. **263**
Figure 4.291. Unlabelled XRD pattern of heat treated nominal $Ni_{39}:V_{42.8}:C_{18.2}$ (at.%), Sample 21H. **264**
Figure 4.292. XRD pattern of heat treated nominal $Ni_{39}:V_{42.8}:C_{18.2}$ (at.%), Sample 21H, showing identified ~V_6C_5 peaks. **264**
Figure 4.293. XRD pattern of heat treated nominal $Ni_{39}:V_{42.8}:C_{18.2}$ (at.%), Sample 21H, showing identified C peaks. **265**
Figure 4.294. XRD pattern of heat treated nominal $Ni_{39}:V_{42.8}:C_{18.2}$ (at.%), Sample 21H, showing identified ~Ni_2V peaks. **265**
Figure 4.295. XRD pattern of heat treated nominal $Ni_{39}:V_{42.8}:C_{18.2}$ (at.%), Sample 21H, showing all the identified peaks. **266**
Figure 4.296. BSE-SEM image of heat treated $Ni_{49}:V_{33.3}:C_{17.7}$ (at.%), Sample 22H, showing ~V_8C_7 dendrites (dark), ~Ni_2V matrix (light) and coarsened ~VC + ~N_2V and C + ~Ni_2V eutectics. **267**

Figure 4.297. BSE-SEM image of heat treated $Ni_{49}:V_{33.3}:C_{17.7}$ (at.%), Sample 22H, showing ~V_8C_7 dendrites (dark), ~Ni_2V matrix (light) and coarsened ~VC + ~Ni_2V and C + ~Ni_2V eutectic at higher magnification. **268**
Figure 4.298. EDX analyses of annealed nominal $Ni_{49}:V_{33.3}:C_{17.7}$ (at.%), Sample 22H. **269**
Figure 4.299. Unlabelled XRD pattern of heat treated nominal $Ni_{49}:V_{33.3}:C_{17.7}$ (at.%), Sample 22H. **270**
Figure 4.300. XRD pattern of heat treated nominal $Ni_{49}:V_{33.3}:C_{17.7}$ (at.%), Sample 22H, showing identified ~V_8C_7 peaks. **270**
Figure 4.301. XRD pattern of heat treated nominal $Ni_{49}:V_{33.3}:C_{17.7}$ (at.%), Sample 22H, showing identified ~Ni_2V peaks. **271**
Figure 4.302. XRD pattern of heat treated nominal $Ni_{49}:V_{33.3}:C_{17.7}$ (at.%), Sample 22H, showing identified C peaks. **271**
Figure 4.303. XRD pattern of heat treated nominal $Ni_{49}:V_{33.3}:C_{17.7}$ (at.%), Sample 22H, showing all identified peaks. **272**
Figure 4.304. BSE-SEM image of heat treated $Ni_{22.1}:V_{49.1}:C_{28.8}$ (at.%), Sample 24H, showing ~V_8C_7 dendrites (dark) and ~Ni_2V (light). **273**
Figure 4.305. BSE-SEM image of heat treated nominal $Ni_{22.1}:V_{49.1}:C_{28.8}$ (at.%), Sample 24H, showing ~V_8C_7 coarsened needles (dark) and ~Ni_2V matrix (light). **274**
Figure 4.306. EDX analyses of annealed nominal $Ni_{22.1}:V_{49.1}:C_{28.8}$ (at.%), Sample 24H. **275**
Figure 4.307. Unlabelled XRD pattern of heat treated nominal $Ni_{22.1}:V_{49.1}:C_{28.8}$ (at.%), Sample 24H. **276**
Figure 4.308. XRD pattern of heat treated nominal $Ni_{22.1}:V_{49.1}:C_{28.8}$ (at.%), Sample 24H, showing identified ~V_8C_7 peaks. **276**
Figure 4.309. XRD pattern of heat treated nominal $Ni_{22.1}:V_{49.1}:C_{28.8}$ (at.%), Sample 24H, showing identified ~VC peaks. **277**
Figure 4.310. XRD pattern of heat treated nominal $Ni_{22.1}:V_{49.1}:C_{28.8}$ (at.%), Sample 24H, showing identified ~Ni_2V peaks. **277**
Figure 4.311. XRD pattern of heat treated nominal $Ni_{22.1}:V_{49.1}:C_{28.8}$ (at.%), Sample 24H, showing all the identified peaks. **278**
Figure 4.312. Optical micrographs of the macrohardness indentations in the as-cast Ni-V-C samples. **281**
Figure 4.312 (cont.). Optical micrographs of the macrohardness indentations in the as-cast Ni-V-C samples. **282**
Figure 4.312 (cont.). Optical micrographs of the macrohardness indentations in the as-cast Ni-V-C samples. **283**
Figure 4.312 (cont.). Optical micrographs of the macrohardness indentations in the as-cast Ni-V-C samples. **284**
Figure 4.316. Comparison of the hardnesses between the heat treated and as-cast samples. **286**
Figure 4.317. Optical micrographs of the macrohardness indentations in the heat treated Ni-V-C samples. **288**

Figure 4.317. (cont.). Optical micrographs of the macrohardness indentations in the heat treated Ni-V-C samples. **289**
Figure 4.317. (cont.). Optical micrographs of the macrohardness indentations in the heat treated Ni-V-C samples. **290**
Figure 4.320. Friction coefficient evolution with sliding distance for as-cast nominal $Ni_{68}:V_{14}:C_{18}$ (at.%), Sample 19. ..... **292**
Figure 4.321. Friction coefficient evolution with sliding distance for as-cast nominal $Ni_{59}:V_{27.2}:C_{13.8}$ (at.%), Sample 20. ..... **292**
Figure 4.322. Friction coefficient evolution with sliding distance for as-cast nominal $Ni_{39}:V_{42.8}:C_{18.2}$ (at.%), Sample 21. ..... **293**
Figure 4.323. Friction coefficient evolution with sliding distance for as-cast nominal $Ni_{49}:V_{33.3}:C_{17.7}$ (at.%), Sample 22. ..... **293**
Figure 4.324. Friction coefficient evolution with sliding distance for as-cast nominal $Ni_{24}:V_{58.6}:C_{17.4}$ (at.%), Sample 23. ..... **294**
Figure 4.325. Friction coefficient evolution with sliding distance for as-cast nominal $Ni_{22.1}:V_{49.1}:C_{28.8}$ (at.%) Sample 24. ..... **294**
Figure 4.326. SEM images in SE mode of the wear track of: (a) as-cast $Ni_{68}:V_{14}:C_{18}$ (at.%) Sample 19, (b) $Ni_{59}:V_{27.2}:C_{13.8}$ (at.%), Sample 20, (c) $Ni_{39}:V_{42.8}:C_{18.2}$,(at.%) Sample 21, (d) $Ni_{49}:V_{33.3}:C_{17.7}$,(at.%) Sample 22, (e) $Ni_{24}:V_{58.6}:C_{17.4}$ (at.%) Sample 23, and (f) $Ni_{22.1}:V_{49.1}:C_{28.8}$ (at.%), Sample 24, after sliding 300m at $3ms^{-1}$ under a contact load 10N. **297**
Figure 4.327. SEM images in SE mode of the wear scars on the ball used to produce the as-cast wear tracks shown in Figure 4.317: (a) as-cast $Ni_{68}:V_{14}:C_{18}$ (at.%) Samples 19, (b) $Ni_{59}:V_{27.2}:C_{13.8}$ (at.%), Sample 20, (c) $Ni_{39}:V_{42.8}:C_{18.2}$,(at.%) Sample 21, (d) $Ni_{49}:V_{33.3}:C_{17.7}$,(at.%) Sample 22, (e) $Ni_{24}:V_{58.6}:C_{17.4}$ (at.%) Sample 23, and (f) $Ni_{22.1}:V_{49.1}:C_{28.8}$ (at.%), Sample 24, after sliding 300m at $3ms^{-1}$ under a contact load 10N. **298**
Figure 4.328. Friction coefficient evolution with sliding distance for heat treated $Ni_{68}:V_{14}:C_{18}$ (at.%), Sample 19H. **300**
Figure 4.329. Friction coefficient evolution with sliding distance for heat treated $Ni_{59}:V_{27.2}:C_{13.8}$ (at.%), Sample 20H. **301**
Figure 4.330. Friction coefficient evolution with sliding distance for heat treated $Ni_{39}:V_{42.8}:C_{18.2}$ (at.%), Sample 21H. **301**
Figure 4.331. Friction coefficient evolution with sliding distance for heat treated $Ni_{49}:V_{33.3}:C_{17.7}$ (at.%), Sample 22H. **302**
Figure 4.332. Friction coefficient evolution with sliding distance for heat treated $Ni_{22.1}:V_{49.1}:C_{28.8}$ (at.%) Sample 24H. **302**
Figure 4.333. Comparison of the penetration depth of the Cr steel ball between heat treated and as-cast samples. **303**
Figure 4.334. SEM images in SE mode of the wear track of: (a) heat treated $Ni_{68}:V_{14}:C_{18}$ (at.%) Samples 19H, (b) $Ni_{59}:V_{27.2}:C_{13.8}$ (at.%) Sample 20H, (c) $Ni_{39}:V_{42.8}:C_{18.2}$,(at.%) Sample 21H, (d)

$Ni_{49}:V_{33.3}:C_{17.7}$,(at.%) Sample 22H, (f) and $Ni_{22.1}:V_{49.1}:C_{28.8}$ (at.%), Sample 24H, after sliding 300m at $3ms^{-1}$ under a contact load 10N. **305**
Figure 4.335. SEM images in SE mode of the wear scars on the ball used to produce the heat treated wear tracks shown in Figure 4.334: (a) heat treated $Ni_{68}:V_{14}:C_{18}$ (at.%) Samples 19H, (b) $Ni_{59}:V_{27.2}:C_{13.8}$ (at.%) Sample 20H, (c) $Ni_{39}:V_{42.8}:C_{18.2}$,(at.%) Sample 21H, (d) $Ni_{49}:V_{33.3}:C_{17.7}$,(at.%) Sample 22H, (f) and $Ni_{22.1}:V_{49.1}:C_{28.8}$ (at.%), Sample 24H, after sliding 300m at $3ms^{-1}$ under a contact load 10N. **306**
Figure 5.1. Plotted data for as-cast samples of the C-Ni-V system (at.%). **317**
Figure 5.2. Solidification projection for C-Ni-V for the as-cast results (at.%). **319**
Figure 5.3. Liquidus projection for C-Ni-V for the as-cast results (at.%). **323**
Figure 5.4. Plotted data for isothermal section of the C-Ni-V system (at.%) at 1000°C (Sample numbers in red). **324**
Figure 5.5. Isothermal section of the C-Ni-V system (at.%) at 1000°C. **325**
Figure 5.6. Hardness values of as-cast C-Ni-V alloys superposed on the solidification projection (at.%). **327**
Figure 5.7. Hardness values of C-Ni-V alloys annealed (1000°C, 1000h) and quenched, superposed on the isothermal section (at.%). **328**
Figure 5.8. Summary of the slip modes of as-cast C-Ni-V alloys, superposed on the solidification projection (at.%). **329**
Figure 5.9. Summary of the slip modes of as-cast C-Ni-V alloys, superposed on the solidification projection (at.%). **330**
Figure 5.10. Summary of the slip modes of heat treated C-Ni-V alloys, superposed on the isothermal section (at.%). **331**
Figure 5.11. Summary of the deformation responses of heat treated C-Ni-V alloys, superposed on the 1000°C isothermal projection (at.%). **332**
Figure 5.12. Summary of the penetration depth (μm) of the ball on to the as-cast samples and the wear coefficients superposed on the solidification projection (at.%). **336**
Figure 5.13. The dependence of wear track and wear coefficient on the hardness values in as-cast condition. **336**
Figure 5.14. Summary of the penetration depth (μm) of the ball on to the heat treated samples and the wear coefficients superimposed on the isothermal section (at.%). **339**
Figure 5.15. Dependence of wear track and wear coefficient on the hardness values in annealed condition. **340**
Figure 5.16. Comparison of the wear coefficients of the heat treated and as-cast samples. **340**
Figure 5.17. Solidification projection showing the superposed VC-coated Ni data (at.%) [2009Rui]. **350**
Figure 5.18. Isothermal section showing the superposed VC-coated Ni data (at.%). **352**
Figure 5.19. SEM images of cross-sections of Fe-C-V-Cr-Ni alloy: (a) as-cast without holding the melt: (b) as-cast after keeping the melt for 1.9ks: (c) as-sprayed deposit [2009Hos] ... ...Error! Bookmark not defined.

Figure 5.20. Relationship between σ′ volume fractions and hardness of the as-cast and heat treated samples. **350**
Figure 6.1. Solidification projection for C-Ni-V for the as-cast results (at.%). **356**
Figure 6.2. Projected liquidus surface for the C-Ni-V system (at.%). **357**
Figure 6.3. Isothermal section of the C-Ni-V system (at.%) at 1000°C. **358**

LIST OF TABLES

Table 2.1. Chemical of the phases measured by AES punctual analysis on as-coated samples [2009Rui] **5**
Table 2.2. Chemical of the phases in the heat treated samples at 1000°C, for 45 minutes measured by AES punctual analysis [2009Rui]. **5**
Table 2.3. Invariant reactions of V-C system [1962Sto, 1966Tre, 1968Rud, 1973Sha, 1983Emm, 1998Wie, 1999Lip, 2006Hu]. **12**
Table 2.4. V-C crystal structure data [1985Car]. **13**
Table 2.5. Comparison between calculated and experimentally reported invariant equilibrium data for the V-C system (at. % C) [1969Rud, 1985Car, 1991Lee]. **16**
Table 2.6. Ni-V crystal structure data [1982Smi]. **22**
Table 2.7. Invariant points in the Ni-V system [1982Smi]… **23**
Table 2.8. Ni-C crystal structure data [1989Sin]. **26**
Table 3.1. Selected compositions of the ternary C-Ni-V samples. **34**
Table 3.2. Test conditions for wear and friction tests. **42**
Table 4.1. EDX phase composition of as-cast nominal $Ni_{10}:V_{50}:C_{40}$ (at.%), Sample 1… **46**
Table 4.2. XRD peaks for as-cast nominal $Ni_{10}:V_{50}:C_{40}$ (at.%), Sample 1. ..... **49**
Table 4.2 (cont.). XRD peaks for as-cast nominal $Ni_{10}:V_{50}:C_{40}$ (at.%), Sample 1. ..... **50**
Table 4.4. EDX phase composition of as-cast nominal $Ni_{20}:V_{40}:C_{40}$ (at.%), Sample 2. ..... **52**
Table 4.5. XRD peaks for as-cast nominal $Ni_{20}:V_{40}:C_{40}$ (at.%), Sample 2. ..... **55**
Table 4.6. EDX phase compositions of as-cast nominal $Ni_{24}:V_{50}:C_{26}$ (at.%), Sample 3. ..... **58**
Table 4.7. XRD peaks for as-cast nominal $Ni_{24}:V_{50}:C_{26}$ (at.%), Sample 3. ..... **62**
Table 4.8. EDX phase composition of as-cast nominal $Ni_{40}:V_{50}:C_{10}$ (at.%), Sample 4. ..... **64**
Table 4.9. XRD peaks for as-cast nominal $Ni_{40}:V_{50}:C_{10}$ (at.%), Sample 4. ..... **67**
Table 4.10. EDX phase composition of as-cast nominal $Ni_{53}:V_{37}:C_{10}$ (at.%), Sample 5. ..... **69**
Table 4.11. XRD peaks for as-cast nominal $Ni_{53}:V_{37}:C_{10}$ (at.%), Sample 5. ..... **72**
Table 4.12. EDX phase composition of as-cast nominal $Ni_{64}:V_{25}:C_{11}$ (at.%), Sample 6. ..... **75**
Table 4.13. XRD peaks for as-cast nominal $Ni_{64}:V_{25}:C_{11}$ (at.%), Sample 6. ..... **78**
Table 4.14. EDX phase composition of as-cast nominal $Ni_{70}:V_{10}:C_{20}$ (at.%), Sample 7. ..... **80**
Table 4.15. XRD peaks for as-cast nominal $Ni_{70}:V_{10}:C_{20}$ (at.%), Sample 7. ..... **84**
Table 4.16. EDX phase composition of as-cast nominal $Ni_{60}:V_{30}:C_{10}$ (at.%), Sample 8. ..... **87**
Table 4.17. XRD peaks for as-cast nominal $Ni_{60}:V_{30}:C_{10}$ (at.%), Sample 8. ..... **90**
Table 4.18. EDX phase analyses of as-cast nominal $Ni_{30}:V_{65}:C_5$ (at.%), Sample 9. ..... **92**
Table 4.19. XRD peaks for as-cast nominal $Ni_{30}:V_{65}:C_5$ (at.%), Sample 9. ..... **96**
Table 4.20. EDX phase analyses of as-cast nominal $Ni_{20}:V_{35}:C_{45}$ (at.%), Sample 10. ..... **99**
Table 4.21. XRD peaks for as-cast nominal $Ni_{20}:V_{35}:C_{45}$ (at.%), Sample 10. ..... **102**
Table 4.22. EDX phase analyses of as-cast nominal $Ni_{10}:V_{80}:C_{10}$ (at.%), Sample 11. ..... **104**
Table 4.23. XRD peaks for as-cast nominal $Ni_{10}:V_{80}:C_{10}$ (at.%), Sample 11. ..... **109**
Table 4.24. EDX phase analyses of as-cast nominal $Ni_5:V_{75}:C_{20}$ (at.%), Sample 12. ..... **112**

Table 4.25. XRD peaks for as-cast nominal $Ni_5:V_{75}:C_{20}$ (at.%), Sample 12. ..... **115**
Table 4.26 (cont.). XRD peaks for as-cast nominal $Ni_5:V_{75}:C_{20}$ (at.%), Sample 12. ..... **116**
Table 4.27. EDX phase analyses of as-cast nominal $Ni_{14}:V_{64}:C_{22}$ (at.%), Sample 13. ..... **118**
Table 4.28. XRD peaks for as-cast nominal $Ni_{14}:V_{64}:C_{22}$ (at.%), Sample 13. ..... **122**
Table 4.29. EDX phase analyses of as-cast nominal $Ni_{28}:V_{54}:C_{18}$ (at.%), Sample 14. ..... **125**
Table 4.30. XRD peaks for as-cast nominal $Ni_{28}:V_{54}:C_{18}$ (at.%), Sample 14. ..... **128**
Table 4.30 (cont.). XRD peaks for as-cast nominal $Ni_{28}:V_{54}:C_{18}$ (at.%), Sample 14. ..... **129**
Table 4.31. Phase analyses of as-cast nominal $Ni_{32}:V_{56}:C_{12}$ (at.%), Sample 15. ..... **131**
Table 4.32. XRD peaks for as-cast nominal $Ni_{32}:V_{56}:C_{12}$ (at.), Sample 15. ..... **135**
Table 4.33. Phase analyses of as-cast nominal $Ni_{39}:V_{42.8}:C_{18.2}$ (at.%), Sample 17. ..... **137**
Table 4.34. XRD peaks for as-cast nominal $Ni_{39}:V_{42.8}:C_{18.2}$ (at.), Sample 17. ..... **141**
Table 4.35. Phase analyses of as-cast nominal $Ni_{66.4}:V_{16.1}:C_{17.5}$ (at.%), Sample 18. ..... **143**
Table 4.36. XRD peaks for as-cast nominal $Ni_{66.4}:V_{16.1}:C_{17.5}$ (at.%), Sample 18. ..... **148**
Table 4.37. EDX phase analyses of as-cast nominal $Ni_{68}:V_{14}:C_{18}$ (at.%), Sample 19. ..... **150**
Table 4.38. XRD peaks for as-cast nominal $Ni_{68}:V_{14}:C_{18}$ (at.%), Sample 19. ..... **154**
Table 4.39. EDX phase analyses of as-cast nominal $Ni_{59}:V_{27.2}:C_{13.8}$ (at.%), Sample 20. ..... **156**
Table 4.40. XRD peaks for as-cast nominal $Ni_{59}:V_{27.2}:C_{13.8}$ (at.%), Sample 20. ..... **159**
Table 4.41. EDX phase analyses of as-cast nominal $Ni_{39}:V_{42.8}:C_{18.2}$ (at.%), Sample 21. ..... **162**
Table 4.42. XRD peaks for as-cast nominal $Ni_{39}:V_{42.8}:C_{18.2}$ (at.%), Sample 21. ..... **165**
Table 4.43. EDX phase analyses of as-cast nominal $Ni_{49}:V_{33.3}:C_{17.7}$ (at.%), Sample 22. ..... **168**
Table 4.44. XRD peaks for as-cast nominal $Ni_{49}:V_{33.3}:C_{17.7}$ (at.%), Sample 22. ..... **171**
Table 4.45. EDX phase analyses of as-cast nominal $Ni_{24}:V_{58.6}:C_{17.4}$ (at.%), Sample 23. ..... **173**
Table 4.46. XRD peaks for as-cast nominal $Ni_{24}:V_{58.6}:C_{17.4}$ (at.%), Sample 23. ..... **177**
Table 4.47. EDX phase analyses of as-cast nominal $Ni_{22.1}:V_{49.1}:C_{28.8}$ (at.%), Sample 24. ..... **180**
Table 4.48. XRD peaks for as-cast nominal $Ni_{22.1}:V_{49.1}:C_{28.8}$ (at.%), Sample 24. ..... **183**
Table 4.49. EDX phase analyses of annealed nominal $Ni_{64}:V_{25}:C_{11}$ (at.%), Sample 6H. **186**
Table 4.50. XRD peaks for heat treated nominal $Ni_{64}:V_{25}:C_{11}$ (at.%), Sample 6H. **189**
Table 4.51. EDX phase analyses of annealed nominal $Ni_{70}:V_{10}:C_{20}$ (at.%), Sample 7H. **191**
Table 4.52. XRD peaks for heat treated nominal $Ni_{70}:V_{10}:C_{20}$ (at.%), Sample 7H. **194**
Table 4.53. EDX phase analyses of annealed nominal $Ni_{60}:V_{30}:C_{10}$ (at.%), Sample 8H. **196**
Table 4.54. XRD peaks for heat treated nominal $Ni_{60}:V_{30}:C_{10}$ (at.%), Sample 8H. **200**
Table 4.55. EDX phase analyses of annealed nominal $Ni_{20}:V_{35}:C_{45}$ (at.%), Sample 10H. **202**
Table 4.56. XRD peaks for heat treated nominal $Ni_{20}:V_{35}:C_{45}$ (at.%), Sample 10H. **206**
Table 4.57. EDX phase analyses of annealed nominal $Ni_{10}:V_{80}:C_{11}$ (at.%), Sample 11H. **208**
Table 4.58. XRD peaks for heat treated nominal $Ni_{10}:V_{80}:C_{10}$ (at.%), Sample 11H. **212**
Table 4.59. EDX phase analyses of annealed nominal $Ni_5:V_{75}:C_{20}$ (at.%), Sample 12H. **214**
Table 4.60. XRD peaks for heat treated nominal $Ni_5:V_{75}:C_{20}$ (at.%), Sample 12H. **218**
Table 4.60. (cont.). XRD peaks for heat treated nominal $Ni_5:V_{75}:C_{20}$ (at.%), Sample 12H. **219**
Table 4.62. EDX phase analyses of annealed nominal $Ni_{14}:V_{64}:C_{22}$ (at.%), Sample 13H. **221**
Table 4.63. XRD peaks for heat treated nominal $Ni_{14}:V_{64}:C_{22}$ (at.%), Sample 13H. **224**

Table 4.64. EDX phase analyses of annealed nominal $Ni_{28}:V_{54}:C_{18}$ (at.%), Sample 14H. **226**
Table 4.65. XRD peaks for heat treated nominal $Ni_{28}:V_{54}:C_{18}$ (at.%), Sample 14H. **230**
Table 4.66. EDX phase analyses of annealed nominal $Ni_{32}:V_{56}:C_{12}$ (at.%), Sample 15H. **232**
Table 4.67. XRD peaks for heat treated nominal $Ni_{32}:V_{56}:C_{12}$ (at.%), Sample 15H. **236**
Table 4.68. EDX phase analyses of annealed nominal $Ni_{39}:V_{42.8}:C_{18.2}$ (at.%), Sample 17H. **238**
Table 4.69. XRD peaks for heat treated nominal $Ni_{39}:V_{42.8}:C_{18.2}$ (at.%), Sample 17H. **243**
Table 4.70. EDX phase analyses of annealed nominal $Ni_{66.4}:V_{16.1}:C_{17.5}$ (at.%), Sample 18H. .. **245**
Table 4.71. XRD peaks for heat treated nominal $Ni_{66.4}:V_{16.1}:C_{17.5}$ (at.%), Sample 18H. **249**
Table 4.72. EDX phase analyses of annealed nominal $Ni_{68}:V_{14}:C_{18}$ (at.%), Sample 19H. **251**
Table 4.73. XRD peaks for heat treated nominal $Ni_{68}:V_{14}:C_{18}$ (at.%), Sample 19H. **255**
Table 4.74. EDX phase analyses of annealed nominal $Ni_{59}:V_{27.2}:C_{13.8}$ (at.%), Sample 20H. **257**
Table 4.75. XRD peaks for heat treated nominal $Ni_{59}:V_{27.2}:C_{13.8}$ (at.%), Sample 20H. **260**
Table 4.76. EDX phase analyses of annealed nominal $Ni_{39}:V_{42.8}:C_{18.2}$ (at.%), Sample 21H. **262**
Table 4.77. XRD peaks for heat treated nominal $Ni_{39}:V_{42.8}:C_{18.2}$ (at.%), Sample 21H. **266**
Table 4.78. EDX phase analyses of annealed nominal $Ni_{49}:V_{33.3}:C_{17.7}$ (at.%), Sample 22H. **268**
Table 4.79. XRD peaks for heat treated nominal $Ni_{39}:V_{42.8}:C_{18.2}$ (at.%), Sample 22H. **272**
Table 4.80. EDX phase analyses of annealed nominal $Ni_{22.1}:V_{49.1}:C_{28.8}$ (at.%), Sample 24H. . **274**
Table 4.81. XRD peaks for heat treated nominal $Ni_{22.1}:V_{49.1}:C_{28.8}$ (at.%), Sample 24H. **278**
Table 4.82. Macrohardness measurements of as-cast ternary Ni-C-V alloys using a 5kg load. **280**
Table 4.83. Palmqvist fracture toughness (MPa√m) values measured from the as-cast Ni-V-C alloys. **285**
Table 4.84. Macrohardness measurements of heat treated ternary Ni-C-V alloys using a 5kg load. **287**
Table 4.85. Palmqvist fracture toughness (MPa√m) values measured from the heat treated Ni-V-C alloys. **291**
Table 4.86. Sliding wear and friction test results for as-cast samples. **295**
Table 4.87. EDX area analyses of as-cast samples. **299**
Table 4.88. Sliding wear and friction test results for heat treated samples. **304**
Table 4.89. EDX area analyses of heat treated samples. **304**
Table 5.1a. XRD peaks assumed to be from σ′ in as-cast samples **315**
Table 5.1b. XRD peaks assumed to be from σ′ in heat treated samples **315**
Table 5.3. Extents of the binary phases into the C-Ni-V system. **319**
Table 5.4. Solidification reactions of the C-Ni-V system. **321**
Table 5.4 (cont.). Solidification reactions of the C-Ni-V system **322**
Table 5.6. Ternary invariant reactions of the C-Ni-V system. **323**
Table 5.7. Examples of room-temperature plane strain fracture toughness values [1993Dow, 1994Cal]. **333**
Table 5.8. Hypothetical friction patterns followed for each sliding system under each test condition [2002Bhu]. **333**

Table 5.9. Hypothetical friction patterns followed for each heat treated samples sliding system under each test condition [2002Bhu]. **337**
Table 5.10. Wear scar dimensions and volumetric wear rate for WC–10wt%Co and WC–12wt%Co slid for 10km at 0.3ms^{-1} against WC–6wt%Co as function of contact load [2010Bon]. **342**
Table 5.11. Wear rate for WC-Co Grade S6 slid for 3800m at 100ms^{-1} [1999Yan]. **342**
Table 5.12. Wear rate for VC-Ni Slide for 300m at 0.3ms^{-1} (Present work). **343**
Table 5.13. Wear scar dimensions and volumetric wear rate for as-cast samples slid for 300m at 0.3ms^{-1} **347**
Table 5.14. Wear scar dimensions and volumetric wear rate for heat treated samples slid for 300m at 0.3ms^{-1} **348**
Table 5.15. Composition of the phases measured by AES punctual analysis on as-coated samples [2009Rui]. **349**
Table 5.16. Composition of the phases in the heat treated samples at 1000ºC, for 45 minutes measured by AES punctual analysis [2009Rui]. **351**
Table 5.17. Nominal compositions (at.%), phases, hardness and approximate σ′ volume fractions (%) of the as-cast samples. **351**
Table 5.18. Nominal compositions (at.%), phases, hardness and approximate σ′ volume fractions (%) of the heat treated samples. **351**

CHAPTER ONE

1.1 INTRODUCTION

Applications requiring high wear resistance often make use of composite materials consisting of fine hard ceramic particles dispersed in a transition metal matrix (Ni, Co, Cr) which serves as tough binder. Ceramic materials include WC, TiC, VC, NbC, B_4C, TaC and Al_2O_3 [1991Tie]. The mechanical stability of these systems, which in turn determine tool performance, depends on the characteristics of the intergranular phases [1997Lir]. The majority of cutting tools are fabricated from cemented carbides which contain hard abrasion-resistant carbides dispersed in a relatively soft matrix to achieve both good abrasion resistance and fracture toughness. Over the years, considerable research effort has gone into understanding the role of microstructural features such as carbide grain size and distribution, binder content in controlling the mechanical behavior of the cermets [1988Ala, 2003Tah]. Due to the different crystalline phases and complex microstructure developed in the VC-Ni system [2009Rui], it was necessary to study the C-V-Ni ternary system, the microstructure and mechanical properties in order to define a suitable composition and processing route to obtain a material with acceptable hardness and wear resistance.

Vanadium carbide (VC) has a reportedly outstanding tribological behaviour, combining high abrasion resistance with a low friction coefficient [2009Rui]. The abrasion resistance of vanadium carbide is related to its high hardness, which is superior to other similar compounds of transition metals in groups VB and VIB, except TiC [2009Rui]. Additionally, VC has fast oxidation kinetics that leads to the formation of vanadium oxide and oxycarbide surface layers, which are characterized by low shear strength and friction coefficient comparable to those of solid lubricants [1975San, 1997Gri, 2000Lug]. Despite the attractive tribological properties, industrial applications of VC are still limited. It is included as a minor constituent in cemented carbides, to enhance wear performance, to inhibit grain growth and decrease density [1997Luy, 2001And, 2001Are, 2002Wit, 2003Lee, 2005Fan, 2007Has].

1.2 BACKGROUND AND MOTIVATION

The development of materials that will perform efficiently in service is acknowledged to be one of the driving forces propelling research in the metallurgical and materials engineering discipline. The knowledge of a material's use is governed by understanding of the interdependence between the materials processing, structure and properties [2001Fle]. The grasp of these interrelations has been referred to as the central paradigm of the profession. Practical harnessing of these interactions has precipitated studies on how to develop novel alloys and metallic materials; an area commonly referred to as microstructure development/alloy development [2000Fle]. In crystalline solids, novel structures can be developed by a thorough understanding of the principles of phase transformation. In non-ferrous alloys, phase transformations are extensively utilized to develop novel structures with improved properties. However, principles involved in developing microstructure in practice are influenced by factors such as the nature of the material, level of technological sophistication, technical know-how, economic and social factors in a particular environment.

In South Africa, as well in as other less well-developed countries, the non-ferrous industries have not advanced to the level of more developed nations. This limits the non-ferrous alloys products that can be processed by these countries. This inevitably engenders importation and further contributes to the perpetual paralysis of not only the non-ferrous sector and allied industries, but also to a great extent the metallurgical and materials engineering discipline by virtue of low research challenges, motivation and redundancy. Limited research has been conducted into nickel-based vanadium carbide. In particular, the phase diagram work and structure property relations have been poorly documented. This project, aimed at investigating the carbon-nickel-vanadium phase diagram, would potentially extend the use of nickel-based alloys into different applications, e.g. those where wear resistance is important. It could also extend the use of vanadium into other areas.

Kundig [1981Kun] reported that in the late 1970s, the price of tungsten carbide suddenly increased by more than 200% and many manufacturers of hard metals sponsored research into vanadium-based cemented carbide with the hope of finding a substitute for tungsten carbide-based cemented carbides. When the price returned to normal, most research was stopped. South Africa has the world's largest reserves of vanadium, but is at present an

importer of tungsten [1983Fis]. Also, the report shows that world production of vanadium pentoxide is 60,000 tonnes of which 40% is produced by South Africa (the balance being China at 25% and Russia at 20%) and is growing by 6% per year [www.chemlink.com, 2009]. It is therefore in South Africa's interests to find new uses for vanadium, and in particular to find ways to replace at least some tungsten with vanadium.

A study focusing on graded metal-carbide composites produced by solid state transformations in VC-coated Ni started in Venezuela [2009Rui], but the workers were having difficulties because there were problems manufacturing samples with the targeted microstructures. It was realized that the targeted microstructures were inconsistent with the C-Ni-V phase diagram. Therefore, in order to realize the targeted microstructures, an investigation of the carbon-nickel-vanadium ternary phase diagram has to be carried out, which is the focus of this research. Additionally, suitable samples with hard particles in a softer matrix will be optimized for abrasive resistance. The final application could be in a more aggressive environment than conventional WC-Co hardmetals, since Ni is more corrosion-resistant than Co [2008San].

CHAPTER TWO

2.0 LITERATURE REVIEW

2.1 Cemented Carbides

Cemented carbides are group of sintered materials, the outstanding properties of which are high hardness and wear resistance [2008Bon]. These materials are made up of very fine particles of refractory metal carbides, cemented together by a metal or alloy of the iron group. In these combinations the main component (carbide phase) provides hardness and wear resistance while the ductile binder contributes the toughness.

Over the past few decades, the development of surface treatment processes has been viewed as a means of meeting increasing demands on component performance [1993Dan]. Post processing of cheap machined materials by surface coating has proven to be an effective substitute to expensive tool materials in terms of both quality and cost. The more conventional coating processes such as plating, carburizing, and nitriding have been inadequate in meeting the increasing demands on performance [2001Mir].

Considerable success in terms of wear resistance and spalling resistance has been achieved with more recently-developed coating techniques. Amongst the most significant of these techniques, is the Chemical Vapour Deposition (CVD) process, used mainly for the application of carbide coatings [1993Dan]. This process produces coatings with excellent wear and seizure resistance, as well as good adhesion, thus reducing component failure by spalling. Another process, called the Toyota Diffusion (TD) process which was developed in the early 1980s has also generated carbide coatings with wear and seizure resistance equivalent to that of CVD, at the same time reducing spalling significantly [1980Ara].

Surface engineering options, consisting of in-situ formation of relatively thick layers of graded steel-VC composites, were more recently studied [2007Wan1]. A new cast sintering process was reported, where the solidification of steel substrate is combined with surface sintering of ferrovanadium and carbon, forming carbide reinforcements [2007Wan2]. Another recently-proposed process was laser-assisted VC incrustation in steel substrates,

which produced a well-adhered composite coating, crack and porosity free; this composite is promoted for enhancing service life of die-casting dies [2002Sha].

Ruiz *et al.* [2009Rui] used coatings to produce graded metal-carbide composites by solid state transformations in nickel substrate, followed by heat treatment. It was reported that the observed microstructural modifications suggested the potential tailoring of a graded material for wear control, conformed by an external thin carbide layer, followed by a thicker cermets zone (Figure 2.1a, b and Table 2.1). The cermets layer was expected to be wear resistant and tough, as it contained hard VC particles in a ductile Ni matrix, so might endure wear during the normal lifetime of parts. The thickness of this layer could be varied by the CVD parameters, while the size and density of the hard carbide reinforcements was controlled by the duration of the exposure above the formation temperature of Ni_3V phase (1045°C) (Figure 2.1c and d and Table 2.2). However, the targeted microstructures were not obtained, possibly due to the production route.

Table 2.1. Chemical of the phases measured by AES punctual analysis on as-coated samples [2009Rui].

	Reported composition (at.%)[2009Rui]			
Regions and phases	C	V	Ni	Sum
A: External layer	15	53	25	93
B: Discrete carbide in the matrix	26	57	13	96
C: Continuous carbide	25	50	21	96
D: Ni_2V	0	35	62	97
E: Ni_3V	6	21	69	96
F: Ni matrix	0	0	87.5	87.5

Table 2.2. Chemical of the phases in the heat treated samples at 1000°C, for 45 minutes measured by AES punctual analysis [2009Rui].

Regions and phases	Compositions measured Reported [2009Rui](at.%)			
	C	V	Ni	Sum
A: V_8C_7	55	28	16	99
B: M_2C	36	24	40	100
C: M_2C	24	28	47	99
D: Ni_3V	0	37	61	98
E: About the same with D	0	37	61	98
F: Ni matrix	0	0	89	89

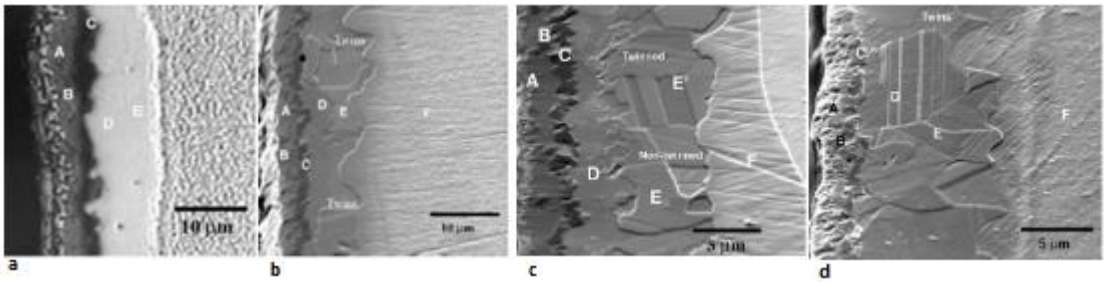


Figure 2.1.Cross-section of the as-coated: (a) optical, (b) Scanning Auger microscopy and heat treated at (c) 850º C 45 min, (d) 1000ºC 45 min sample, showing the points where chemical analyses were performed [2009Rui].

Viswanadham and Precht [1980Vis] provided a detailed crystallographic characterization of the C-Ni-V system. At high carbon to metal (C/M) ratios, the carbide was principally V_8C_7 or V_8C_7 + V_6C_5, while at low C/M ratios the carbides were V_6C_5 or V_6C_5 + V_4C_3. They stated the possibility of nickel being contained in a well-defined VC_x structure (where x takes the value: 0.75, 0.83 or 0.87), as well as the multicomponent character of the binder which contains a C-Ni-V solid solution and intermetallic compounds. They concluded that at low vanadium contents, the carbide can withstand the stresses generated by plastic flow in the binder if certain microstructural requirements, such as binder composition, carbide grain size and distribution, are met. At high vanadium contents in the binder, the binder hardness was high and stresses generated by plastic flow in the binder led to cleavage of the carbide grains under most achievable microstructural conditions. They also reported that binder strengthening is a viable means to achieve cermet systems that combine both high hardness and toughness, only when the cleavage energy of the carbide phase is sufficiently high to withstand the stresses generated by plastic flow in the binder. Otherwise, cleavage of the carbide phase will be the dominant fracture mode and overall mechanical performance of the cermet system will deteriorate.

Allen and Douglas [1999All] carburized Ni-2V, Ni-5V and Ni-12V (wt%) to produce internal-carbide zones in both alloys between 700-1000ºC. They observed that the carbide regions in Ni-12V appeared to contain at least two different precipitate structures. The zone adjacent to the alloy gas interface contained mostly spherical and small rod-like precipitates, while the inner zone contained much longer rods and grain-boundary attack. Further

observations shown that the carbide zones in Ni-5V were similar to those formed in Ni-12V except that the spherical precipitates formed in grain boundaries of Ni-5V specimens were not as dense as those formed in grain boundaries of Ni-12V. They also reported that carburization of Ni-2V formed mainly thin surface scales with carbides observed within the substrates of several specimens.

Niki and Masato [1970Nik] also studied the systems Ni-Ti-C, Ni-V-C, Ni-Cb-C, Ni-Mo-C, Ni-Ta-C and Ni-W-C by means of gas carburization and electron probe microanalysis in the nickel-rich portion. The results showed that the increase in hardness was negligible with the carburization.

Surface alloying with application of high temperature plasma jet of armco-iron and carbon steel was studied by Yakyshin *et al*. [1994Yak], Luan and Yan [2002Yan]. Microscopic examination, X-ray spectrum microanalysis and microhardness measurements show that the technique allowed surface alloying to a depth of 20-45μm with alloying element concentration up to 20mass%. It was also reported that microhardness of alloyed layer exceeds that of complex-alloyed cold worked steels.

2.2 Nickel-based alloys

The high wear resistance of cemented carbides explains their use in many fields, e.g. cutting tools, seals and bearings. The surfaces in sliding contact are not only subjected to mechanical wear, but also to chemically aggressive environments and corrosion can play an important role in the degradation of the material [2000Eng]. It is apparent that materials subjected to slurry environments must not only resist the erosion of solid particles and liquids, but also be resistant to damage caused by corrosion. These two factors may interact synergistically to produce wear rates that are greater than the sum of their separate effects. The ability of any material to resist the synergistic action of slurry erosion and corrosion is thus of the utmost importance. The characteristic high hardness and fracture toughness of WC-Co cermets have in the past made them materials of choice for use as cutting tools, mining bits, sandblasting nozzles, and for a variety of other wear resistant applications. In most cases, cobalt has been used as the tough metal binder phase, due to its excellent wetting, adhesion and adequate mechanical properties. However, cobalt, has low corrosion resistance and thus to improve the wear resistance in aggressive environments, other metallic alloy compositions have to be

formulated [1997Wen]. Indeed, substitution and/or replacement of Co by Ni was found to improve the resulting corrosion resistance as well as the wear performance of cemented carbides in corrosive environments [2008Bon].

Viatour [1978Via] reported that in most nickel-based cermets, metal carbide forms during solidification and was mainly at and around the grain boundaries. The mechanical properties of the cast nickel-based alloys were affected strongly by the morphology and distribution of the carbide. On solidification, the morphology and distribution of metal carbide varied with the alloy composition, which also affected the composition of metal carbide [1986Yos]. Since the properties such as the morphology and distribution of metal carbide depend on its composition, therefore it is important to control the morphology and distribution of metal carbide with superior mechanical properties.

Hoshiyama *et al.* [2009Hos] used Fe-C-V-Cr-Ni alloy powder in low-pressure plasma sprayed to produce rapidly solidified alloy deposits based on a stainless cast iron with finely dispersed vanadium carbide particles. The as-sprayed deposit was made up of γFe, αFe, V_8C_7, and Cr_7C_3. The fine precipitates of about 0.4 mm in the as-sprayed deposit were carbide. With increasing heat treatment temperature up to 1273 K, the carbide particles coarsen. The as-sprayed deposit had finer vanadium carbide than that of the Fe-C-V-Cr-Ni cast. With increasing heat treatment temperature above 1073 K, the coarsening of the vanadium and chromium carbide precipitates and elimination of saturation of matrix with vanadium, chromium, and carbon in the deposit result in the decrease in hardness of the Fe-C-V-Cr-Ni deposit.

Shurin *et al.* [1988Shu] reported on Ni-V-Nb-C quaternary system which they investigated along the Ni-$VC_{0.87}$-$NbC_{0.8}$ section in the as-cast and annealed conditions. They concluded that The Ni-$VC_{0.87}$-$NbC_{0.9}$ system has a ternary eutectic in the solidification of which the equilibrium phases are an Ni-base solid solution, (V, Nb)C carbide containing 10% $NbC_{0.9}$ and 90% $VC_{0.7}$, and (V, Nb)C carbide containing 20% $VC_{0.87}$ and 80% $NbC_{0.9}$. The point of the four-phase nonvariant equilibrium was in the region of the alloy containing 3% $NbC_{0.9}$ and 6% $VC_{0.87}$ and the temperature of the equilibrium was 1300±15°C.

Whitefield *et al.* [1997Whi] and Brieseck *et al*. [2012Bri] reported that to obtain good distribution of the metal carbide for nickel-based carbide alloys, the VC grain size must be ≤ 2 μm, otherwise a large VC grain size makes the alloy brittle. Since there are the advantages of inhibition of grain growth and to form hard, wear resistant vanadium rich carbides by using vanadium, a greater understanding of the system is needed, such as the phases and their reactions. Therefore it is necessary to study the binary phase diagrams first, in order to progress to the more complicated C-Ni-V ternary.

However, information about the structure of Ni-VC alloys and the effect of the composition on properties is limited. There is limited information relating to the phase equilibrium diagram for the system C-Ni-V. In order to systematically develop and investigate the C-Ni-V system, a combination of experimentation and interpretation will be undertaken. This research will develop and investigate nickel-vanadium carbide composite materials for better wear resistance, and the result will be compared with a conventional tungsten carbide WC.

2.3 Phase diagrams

Generally, phase diagrams are one of the most important sources of information concerning the behaviour of elements, compounds and solutions. They provide the knowledge of phase composition and phase stability as a function of temperature (T), pressure (P) and composition (C). Furthermore, they permit the study and control of important processes such as phase separation, solidification, sintering, purification, growth and doping of single crystals for technological and other applications. Although phase diagrams provide information about systems at equilibrium, they also assist in predicting phase relations, compositional changes and structures in systems not at equilibrium. Binary phase diagrams of systems comprising nickel, vanadium and carbon were reviewed. An understanding of the binary diagrams is necessary for identification of the boundary phases of the C-Ni-V ternary.

2.3.1 V-C phase diagram

Storms and McNeal [1962Sto] proposed a detailed phase diagram for the first time. They measured the melting point of vanadium metal at 1888°C and determined the temperatures and compositions of three invariant reactions:

Liquid ↔ (V) + V_2C

Liquid + $VC_x \leftrightarrow V_2C$ and

Liquid + graphite $\leftrightarrow VC_x$.

Rudy *et al.* [1968Rud] re-investigated the phases by means of X-ray diffraction, melting point, differential thermal analysis (DTA), chemical analysis and metallographic examination, indicating the melting behaviour of VC_x as congruent at 2625°C with 49.5 at.% C rather than peritectic. Their results were confirmed by Precht and Hollox [1968Pre], Tret'yachenko and Erementо [1966Tre], but with different reaction temperatures (2800°C with 45.5 at% C).

Although the existence of the V_4C_{3-x} phase is well accepted, the experimental data on its temperature range is scattered and sometimes even inconsistent. Storms and McNeal [1962Sto] reported the decomposition temperature of 1344°C. Later, other investigators, [1968Rud, 1973Sto], observed this phase above 1500°C. Khaenko and Fak [1978Kha] estimated the decomposition temperature between 1262°C and 1600°C. Carlson *et al*. [1985Car] gave 1350°C, and explained observation of this phase in samples annealed at temperature higher than 1350°C by its subsequent formation during the cooling period. Wiesenberger *et al*. [1998Wie] investigated the formation of V_4C_{3-x} by wedge-type diffusion couples. It was found that this phase contained 37.9 at.% C and had a very narrow (about 0.4 at.% C) homogeneity range. The decomposition temperature was assumed to be around 1875°C, and the lowest temperature of the existing range was reported as1267°C. Hu *et al*. [2006Hu] considered the thermodynamic re-assessment of the V-C system to be more reliable, because the calculated phase diagram and thermodynamic properties were in good agreement with experimental data from various sources.

The V-C phase diagram [1985Car] is given in Figure 2.2 and invariant reactions [2006Hu] are listed in Table 2.1. Carlson *et al.* [1985Car] investigated the vanadium-rich solvus of V–C system for the temperature range from 1100°C to 1650°C. The solubility decreased from a maximum of 4.3 at.% C at 1650°C to 0.5 at.% C at 1100°C. The liquidus curves were determined by Adelsberg and Cadoff [1966Ade] who equilibrated V or VC with C at different temperatures and chemically analyzed the liquid phase in equilibrium with the solid at each temperature. The V-rich boundary of V_2C was measured by Storms and McNeal

[1962Sto] and the C-rich boundary of V_2C was observed to be nearly independent of temperature. Most researchers placed this boundary near the ideal stoichiometry of 33.3 at.% C, others indicated the hyperstoichiometry of 35 at.% C [1998Wie, 1976Arb]. The V-rich boundary of VC_x was measured by Wiesenberger *et al*. [1998Wie] using EPMA (electron probe micro-analyser). The C-rich boundary of VC_x did not extend to 50 at.% C [1962Sto, 1968Rud,1998Wie], but decreased from 47 at.% C at 1000°C to 46 at.% C at 2625°C.

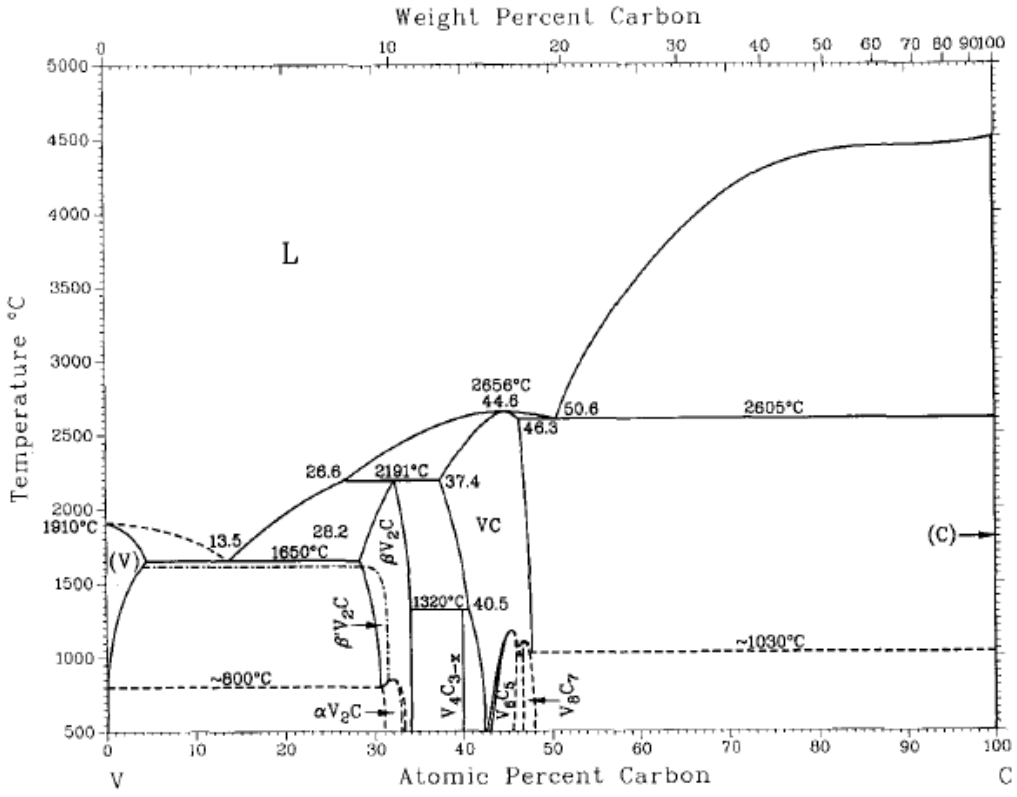


Figure 2.2. Binary V-C equilibrium phase diagram [1985Car].

2.3.2 Solid phases

At elevated temperatures, only two intermediate phases (V_2C and VC) exist; both exhibit wide ranges of homogeneity. Decreasing temperature results in a peritectoid reaction between V_2C and VC near 1320°C to form the V_4C_{3-x} phase; this in contrast to V2C and VC appears to be nearly invariant in stoichiometry. The crystal structure of V_4C_{3-x} was determined by Yvon and Parthe [1970Yvo] with single crystal X- ray methods. There is general agreement that the structures (Table 2.3) of all forms of V_2C are based on a cph sublattice of V atoms. Bowman [1965Bow] used both X-ray and neutron diffraction to

examine a C-rich powder specimen with a small amount of VC impurity and, after equilibration at 1400°C, found no ordering of the interstitial C atoms.

Table 2.3. Invariant reactions of V-C system [1962Sto, 1966Tre, 1968Rud, 1973Sha, 1983Emm, 1998Wie, 1999Lip, 2006Hu].

Reaction	T (°C)	Composition (at.% C)			Reference
$V_2C + VC_x \leftrightarrow V_4C_{3-x}$	1877	35 ± 1	39.5	37.9 ± 0.4	[1998Wie]
	1876	33.1	39.4	37.9	[2006Hu]
$V_4C_{3-x} \leftrightarrow V_2C + VC_x$	1267	37.9 ± 0.4	35 ± 1	41.9	[1998Wie]
	1262	37.9	33.3	42.1	[2006Hu]
$V_8C_7 \leftrightarrow VC_x$	1112 ± 8	0.467	---	---	[1983Emm]
	1124 ± 15	0.467	---	---	[1973Sha]
	1110	0.467	---	---	[2006Hu]
$VC_x \pm \leftrightarrow V_6C_5 + V_8C_7$	1060 ± 5	0.460	---	0.467	[1999Lip]
	1092	0.459	0.451	0.467	[2006Hu]
Liq ↔ V_2C + (V)	1630 ± 20	---	8.7	25	[1962Sto]
	1650 ± 7	15 ± 1	5.5 ± 1	27 ± 0.5	[1968Rud]
	1650 ± 10	14	4	30	[1966Tre]
	1649	13.3	3.78	29.3	[2006Hu]
Liq + $VC_x \leftrightarrow V_2C$	2165 ± 25	36	---	37.5	[1962Sto]
	2187 ± 10	35 ± 0.5	28 ± 3	37 ± 0.7	[1968Rud]
	2165	33.3	28 ± 1.5	37 ± 1.5	[1966Tre]
	2229	32.5	25.8	37.1	[2006Hu]
$VC_x \leftrightarrow$ Liq	2648 ± 12	43 ± 0.5	---	---	[1962Sto]
	2800 ± 20	47.5	---	---	[1966Tre]
	2658	43.3	---	---	[2006Hu]
Liq ↔ VC_x + C	2650 ± 35	---	46	---	[1962Sto]
	2625 ± 12	49.5 ± 0.5	46 ± 0.3	---	[1968Rud]
	2606	49.5	45.2	---	[2006Hu]

This disordered hexagonal structure is designated βV_2C in Figure 2.2. Yvon [1967Yvo] also examined powder specimens with neutron diffraction and found evidence for ordering of the C atoms in material that was equilibrated at 900°C for seven days, although the composition was not closely specified. This ordered structure was also hexagonal, with reflection intensities being compatible with an εFe_2N-type structure. The *a* parameter of the ordered structure was approximately $\sqrt{3}$ times the *a* parameter of the disordered structure, and the *c*

parameters of both the ordered and disordered structures were approximately equal. This hexagonal ordered structure is designated β'V_2C in Figure 2.2.

Table 2.4. V-C crystal structure data [1985Car].

Phase	**Homogeneity range, at.%C**	**Pearson Symbol**	**Space group**	***Strukturbericht* designation**	**Prototype**
(V)	0 to 4.3	c*I*2	*Im*3*m*	*A*2	W
αV_2C	31 to 33	*oP*12	*Pbcn*	…	ζFe_2N
βV_2C	27 to 34	*hP*3	*P*63/*mm*c	*L'3*	W_2C
β'V_2C	27.5 to 31.5	*hP*9	*P*31*m*	…	Ni_3N
V_4C_{3-x}	~40	*hR*20	*R*3*m*	*B*1	…
VC	37 to 48	c*F*8	*Fm*3*m*	…	NaCl
V_6C_5	43 to 46	*mB*44	*B*2	…	…
V_7C_8	47 to 48	c*P*60	*P*$4_1$32 P$4_3$32	…	…
(C)	100	*hP*4	*P*6_3/*mm*c	*A*9	C (graphite)

Failure to detect the ordered hexagonal structure during earlier investigations with X-ray techniques was attributed to the large difference in scattering power between vanadium and carbon such that vanadium normally dominates the diffraction intensities. There is evidence [1967Yvo, 1976Arb] that additional ordering occurs in V_2C below ~800°C to produce an orthorhombic structure. This is designated αV_2C in Figure 2.2. Neutron diffraction data [1967Yvo] showed all diffraction maxima from this phase to have intensities and indices compatible with the ζFe_2N-type structure; however, X-ray diffraction patterns from this polymorph of V_2C showed one or more extraneous maxima [1967Yvo, 1976Arb]. Such extraneous maxima led Rudy [1968Rud] and Arbuzov [1976Arb] to report *a* and *b* lattice parameters to be doubled or quadruple those of the ζFe_2N-type structure.

In common with other Group IV and V transition metal carbides, VC at high temperatures has a C-deficient NaCl-type (rock-salt) structure with the cubic lattice parameter increasing with C composition [1985Car]. They also reported that C atoms in the cubic rock-salt structure ordered at lower temperatures to produce two different superstructures V_6C_5 and V_8C_7. The V_6C_5 phase forms congruently near 1184°C and shows a range of homogeneity that broadens with decreasing temperature. A trigonal structure with space group symmetry

$P3_1$ or $P3_2$, depending on the sense of the screw axis rotation, was first proposed by Venables [1968Ven] on the basis of electron microscopy, diffraction, and nuclear magnetic resonance.

Billingham [1972Bill] proposed a monoclinic structure of V_6C_5 differing from the trigonal structure in that, the helical arrays of vacancies that form the screw axes undergo periodic displacements in position, but not in direction or sense of rotation, after every third vacancy. Only minor differences should appear in the diffraction patterns from the two different structures, but a pattern consistent with the monoclinic form was found by Billingham [1972Bill]. Hiraga [1973Hir] made a further investigation of the structure of this phase and, although agreed that the monoclinic structure was the true basic structure, suggested that vacancy distributions at non-stoichiometric compositions could better be described on the basis of an orthorhombic unit cell three times the size of the monoclinic unit cell.

Carlson and his co-workers [1985Car] proposed an assessed phase diagram using mainly the results given by other authors [1968Rud, 1962Sto, 1984Gha].They reported the phase relationships shown in Figure 2.2 for the region between 27 at.% C and 34 at.% C must be considered tentative. First, crystallographic data indicate that the V-rich portions of the high-temperature form of V_2C are identifiably different, with distinguishable space group symmetry from the C-rich high-temperature form [1976Arb, 1978Kha, 1965Bow]. On this basis, the C-rich portion in the high-temperature region of Figure 2.2 was designated βV_2C and the V-rich portion was designated $\beta' V_2C$. A question remained as to the order of the transition between the β and β' forms. Both the β and β' crystal structures are hexagonal and their V sublattices are identical. The empty C sublattices in the two structures are identical, but in βV_2C the C sublattice sites are statistically occupied, whereas in $\beta' V_2C$ some of the C sublattice sites are preferentially occupied and others are preferentially vacant. These crystallographic considerations, in combination with the lack of any experimental evidence for a two-phase separation between the β and β' forms, are the basis for suggesting that the $\beta' V_2C \leftrightarrow \beta V_2C$ transformation is higher order, as indicated by the dash-dot line in Figure 2.2.

Lee and Lee [1991Lee] calculated the system by CALPHAD technique, and the result is shown in Figure 2.3. V-C system: The calculated phase boundaries were compared with

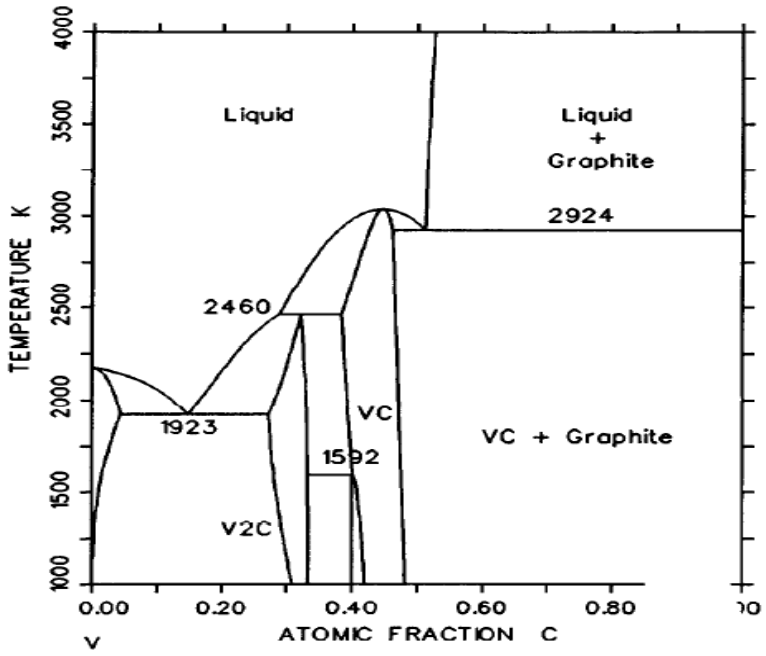


Figure 2.3. Calculated V-C phase diagram [1991Lee].

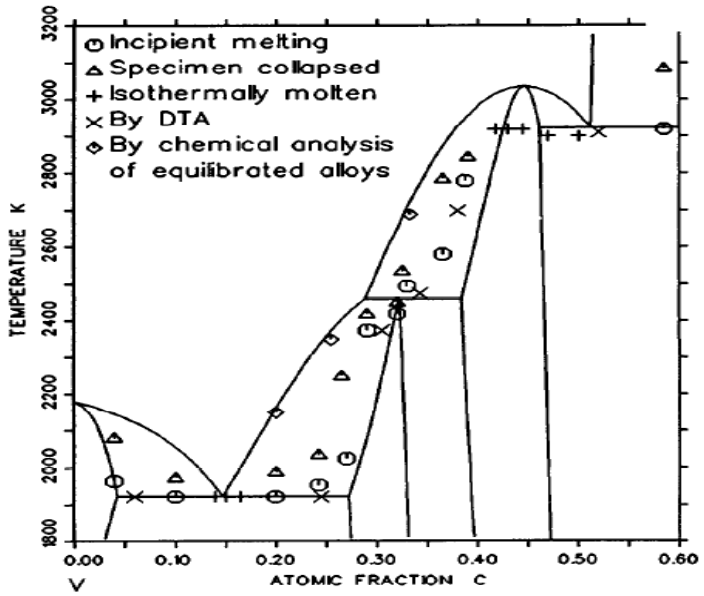


Figure 2.4. Calculated V-C phase diagram compared with experimental data [1969Rud].

experimental data by Rudy [1969Rud] in Figure 2.4, and the calculated invariant reactions and the congruent melting point of VC were compared with experimental data by Lee and Lee [1991Lee] (Table 2.5).

Table 2.5. Comparison between calculated and experimentally reported invariant equilibrium data for the V-C system (at.% C) [1969Rud, 1985Car, 1991Lee].

T(K) : V + V_2C = L				**Reference**
1923	4.30	14.71	27.23	[1991Lee]
1923	4.30	15	27	[1985Car]
1923±7	5.5±1	15±1	27±0.5	[1969Rud]
T (K) : L + VC = V_2C				**Reference**
2460	28.86	38.38	32.18	[1991Lee]
2460	29.5	37	34	[1985Car]
2460±10	28±3	37±0.7	35±0.5	[1969Rud]
T(K) : VC + Graphite = L				**Reference**
2924	46.14	100.00	51.19	[1991Lee]
2943	46	100.00	53.5	[1985Car]
2898±12	46±0.3	100.00	49.5±0.5	[1969Rud]
T(K) : VC = L				**Reference**
3035	44.60	44.60		[1991Lee]
3073	45.5	45.5		[1985Car]
2921±12	43 ±0.5	43±0.5		[1969Rud]

According to Lipatnikov *et al*. [1999Lip], a major difficulty in constructing a phase diagram of the V–C system resides in that the upper boundary of the homogeneity region of disordered cubic vanadium carbide. VC_y is the $VC_{0.88}$ carbide rather than an $MC_{1.0}$ carbide of stoichiometric composition, as is the case with carbides of other transition metals. The unusual position of the upper boundary of the homogeneity region for the VC_y carbide caused the formation in VC_y of an ordered M_8C_7-type phase that does not exist in other systems. Experimental data for the temperatures and heats of formation of the $V_6C_5 \leftrightarrow VC_y$ and $V_8C_7 \leftrightarrow VC_y$ phase transformations enabled the ordering of the VC_y carbide in the phase diagram of the V–C system to be defined as shown in Figure 2.5. Phase equilibria in the region of ordering of non-stoichiometric cubic VC_y carbide were calculated by the Order Parameter Functional (OPF) method.

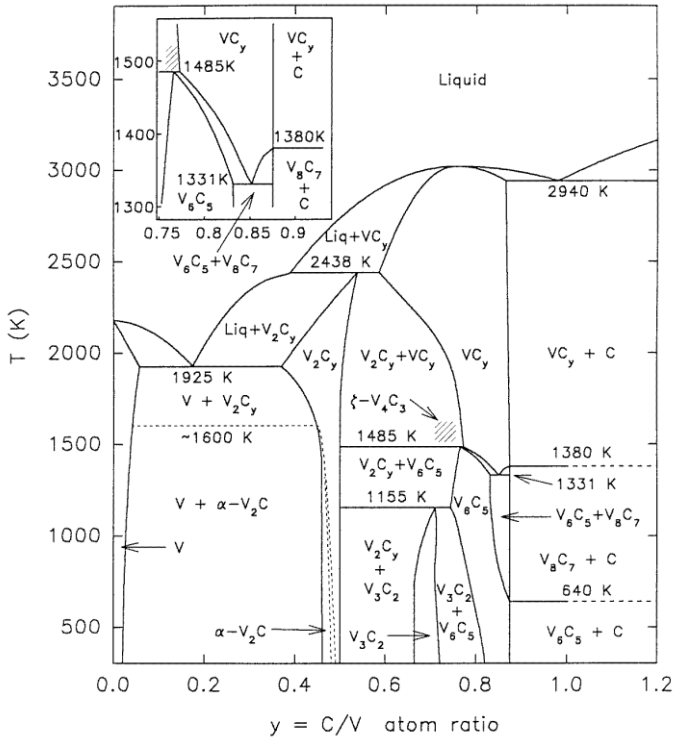


Figure 2.5. Equilibrium phase diagram of the V–C system with consideration of the ordering of nonstoichiometric cubic and hexagonal vanadium carbides VC_y and V_2C_y [1999Lip].

Lipatnikov *et al*. [1999Lip] concluded that V_8C_7, V_6C_5 and V_3C_2 are the ordered phases of cubic carbide VC_y and α-V_2C is an ordered phase of lower hexagonal carbide V_2C_y (β-V_2C). The inset in Figure 2.5 is the extended part of the ordering region near the upper boundary of the homogeneity region of VC_y.

Huang *et al*. [2005Hua], using the assessment of Lee and Lee [1991Lee] and their earlier work [1991Hua], optimized the system by the CALPHAD technique. The optimizations were in good agreement with the corresponding experimental data. However, their [1991Lee] thermodynamic calculations were based on different reference state values for the pure elements. In the work of Huang [1991Hua], the V and C reference state were taken from the SGTE database [1991Din], allowing extrapolation of the low order to high-order

systems with the same reference state. However, in the optimization of Lee and Lee [1991Lee], the lattice stability of bcc-V was set as a reference, which is inconsistent with thermodynamic calculations of Huang *et al*. [1991Hua]. The calculated V–C phase diagram using the thermodynamic description by Huang is presented in Figure 2.7, which shows three intermediate carbides: V_2C_x, V_3C_2 and VC_x. The V_2C_x and VC_x carbides exhibit a wide homogeneity range due to the carbon deficiency at high temperature, which is shown in Figure 2.6 by these phases "leaning toward" V at high temperature.

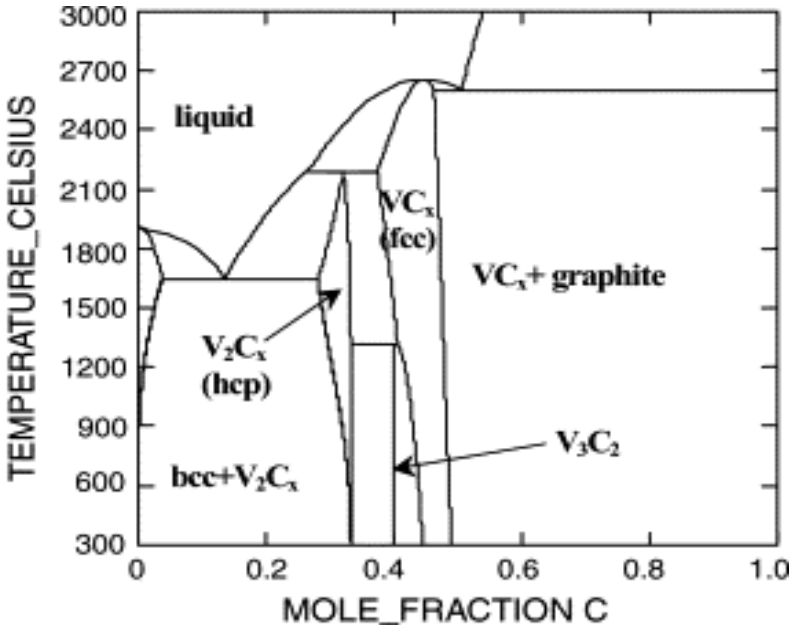


Figure 2.6. Calculated V–C phase diagram according to Huang [1991Hua].

Hu *et al*. [2006Hu] also used optimization method to derive Figure 2.7. Figure 2.8 shows the comparison between the calculated phase diagram and experimental data. The authors remarked that most of the experimental data were well described, except for the calculated liquidus, which has lower carbon content than experimental values.

Hu *et al*. [2006Hu] also inferred that below the eutectic temperature is a two-phase region V_6C_5 +V_8C_7, which is in good agreement with the experimental data as shown in Figure 2.9, an enlarged phase diagram of the order–disorder transformation region compared with the experimental data. The two-phase region narrows with decreasing temperature. Also, the carbon content of V_6C_5 increases to 0.455 which the ideal stoichiometry of V_6C_5, rather than 0.467 as calculated by Lipatnikov *et al*. [1999Lip]. Hu *et al*. [2006Hu] also claimed that

their results were more reasonable, considering the experimental data of V0.546C0.454, which is in the two-phase region in the range from 1000 to1200K (727 to 927ºC).

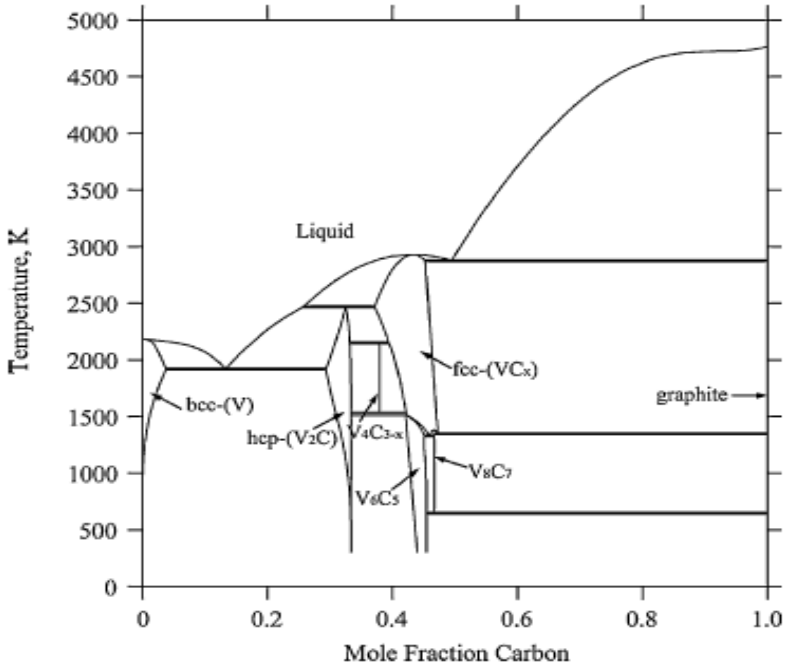


Figure 2.7. Calculated V-C phase diagram according to Hu *et al*. [2006 Hu].

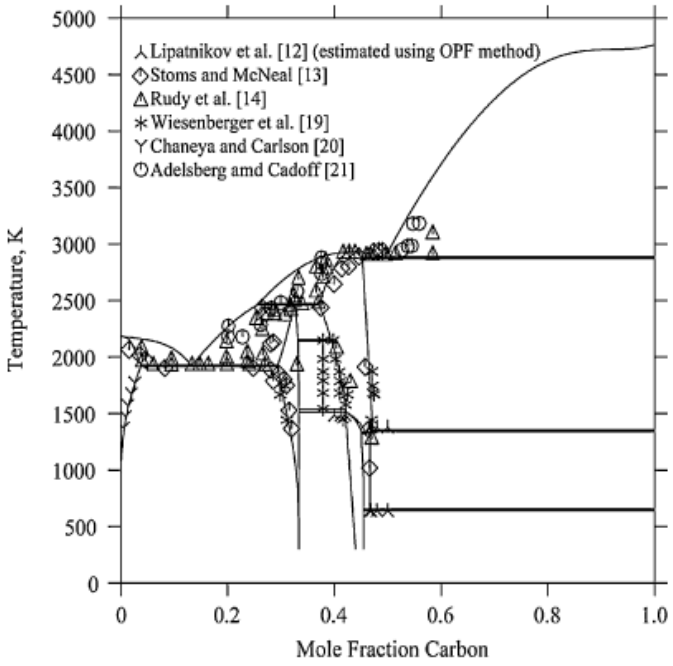


Figure 2.8. Calculated phase diagram compared with the experimental data from various sources [2006Hu].

It can be seen that the dashed line in Figure 2.9 [1999Lip] using order parameter functional (OPF) method causes the $V_{0.546}C_{0.454}$ to be in the single-phase region of V_6C_5 in this temperature range. The calculated temperature for $VC_x + V_2C \leftrightarrow V_6C_5$ is 1512 K (1239°C) which is higher than 1485K (1212°C) calculated by Lipatnikov *et al*. [1999Lip]. Considering the lack of experimental data and 1540K (1267°C) being reported as the lowest limit of V_4C_{3-x} by Wiesenberger *et al*. [1998Wie], the 1512K (1239°C) value obtained in this work is acceptable [2006Hu].

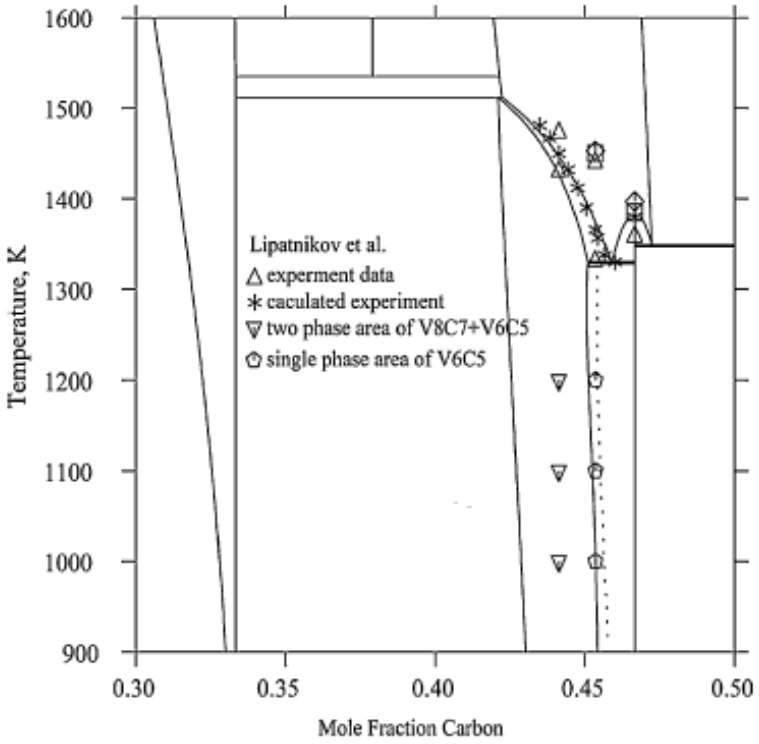


Figure 2.9. Calculated phase diagram in the ordering region compared with experimental data from various sources [2006Hu].

2.3.3 Binary Ni-V phase diagram

Several investigations to clarify the phase equilibria have been performed. Giebelhausen [1915Gie], Pearson *et al*. [1952Pea], Stevens *et al*. [1970Ste], Daire *et al*. [1969Dai], Moreen

et al. [1971Mor] and Tanner [1972Tan]. Results of these works were used by Smith *et al.* [1982Smi] to construct the assessed phase diagram in Figure 2.10.

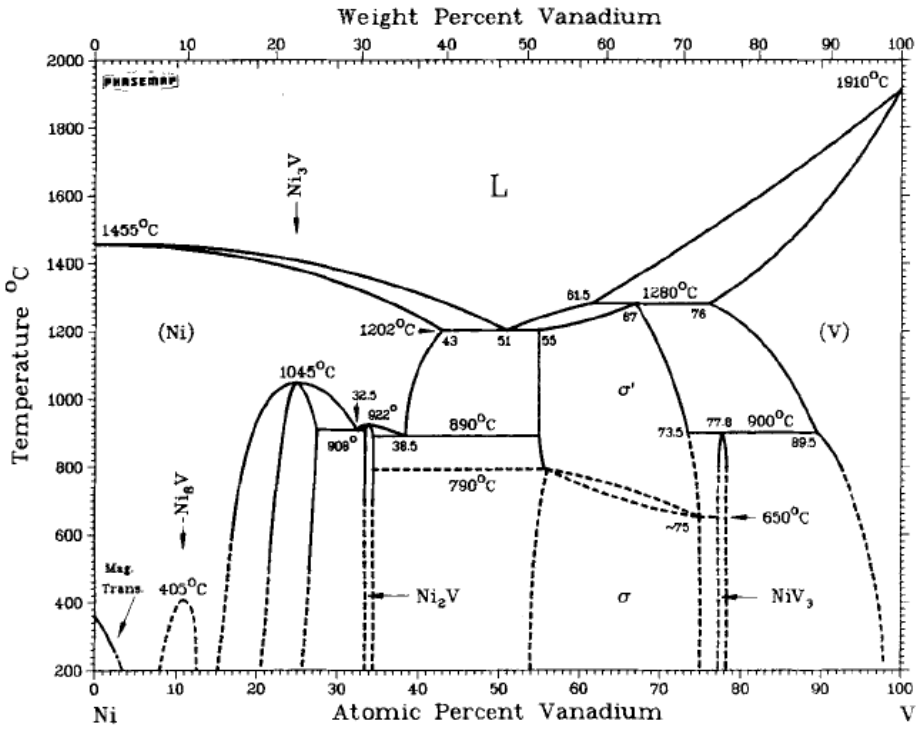


Figure 2.10. Ni-V binary phase diagram [1982Smi].

2.3.4 Solid phases

Table 2.6 shows the solid phases and their crystal data.

Table 2.6. Ni-V crystal structure data [1982Smi].

Phase	Composition, at.%V	Pearson symbol	Space group	*Strukturbericht* designation	Prototype
(Ni)	0 to 4.3	c*F*4	F*m*$\bar{3}$*m*	*A*1	Cu
Ni_8V	-11.1	*tI*18	...	…	$NbNi_8$
Ni_3V	-21 to 25.6	*tI*8	I4/*mmm* σ	$D0_{22}$	$TiAl_3$
Ni_2V	- 33.3	*oI*6	...	…	$MoPt_2$
σ	57.5 to ~75	*tP*30	*P*42/*mnm*	$D8_b$	σCrFe
NiV_3	75.7 to 78	*cP*8	*Pm*$\bar{3}$*n*	*A*15	Cr_3Si
(V)	76 to 100	c*I*2	*Im*$\bar{3}$*m*	*A*2	W

2.3.5 Phase Reactions

Smith *et al*. [1982Smi] have reviewed the crystallographic, phase diagram and thermodynamic literature on the Ni-V system up to the end of 1982 as part of the American Society for Metals-US National Bureau of Standards Binary Phase Diagram Assessment Programme. The system is characterized by extensive solid solubility, a broad single-phase σ phase field ranging from 55 to 75 mol.% V and four additional intermediate phases whose compositions correspond to the formulae Ni_8V, Ni_3V, Ni_2V and NiV_3. Solidification of liquid occurs through a peritectic reaction L + (V) ↔ σ at 1280°C and a eutectic reaction L ↔ (Ni) + σ at 1202°C. On the Ni side, the (Ni) phase undergoes three transformations to give Ni_8V, Ni_3V, and Ni_2V phases having congruent transformation temperatures of 405°C, 1045°C and 922°C respectively. Two eutectoid reactions (Ni) ↔Ni_3V + Ni_2V and (Ni) ↔ Ni_2V + σ occur at 908°C and 890°C, respectively. The NiV_3 phase occurs through a peritectoid reaction (V) + σ ↔ NiV_3 at 900°C. There is controversy regarding the low-temperature transformation (σ ↔ σ′) of the σ phase [1982Smi]. Thermodynamic optimizations of the Ni–V system have been carried out using experimental phase diagram and thermodynamic data available from the literature by Watson and Hayes [2001Wat2]. In

the optimization, model was used to describe the thermodynamic properties of the sigma phase. Table 2.7 shows the phase equilibrium [1982Smi].

Table 2.7. Invariant points in the Ni-V system [1982Smi].

Reaction	**T(°C)**	**Type of Reaction**	**Mole Fraction V**		
L + (V) ↔ σ	1280	Peritectic	0.67	0.615	0.76
L↔(Ni) + σ	1202	Eutectic	0.51	0.43	0.55
Ni_3V↔(Ni)	1045	Congruent	…	0.25	…
Ni_2V ↔(Ni)	922	Congruent	…	0.333	…
(Ni) ↔Ni_3V + Ni_2V	908	Eutectoid	0.325	0.275	0.33
σ + (V)↔ NiV_3	900	Peritectoid	0.778	0.738	0.895
(Ni) ↔ Ni_2V + σ	890	Eutectic	0.385	0.345	0.55
Ni_8V ↔(Ni)	405	Congruent	…	0.11	…

Thermodynamic optimisations of the Ni–V system were carried out by Watson *et al.* [2001Wat1], Watson and Hayes [2001Wat2] using experimental phase diagram and thermodynamic data available from the literature. In each optimisation, different model was used to describe the thermodynamic properties of the sigma phase. Temperature and composition dependent parameters of the Gibbs energy expressions were adjusted during the optimisations using a least-squares fitting computer program so that the differences between the experimental data and corresponding values generated from the optimised Gibbs energy expressions were minimized. The difference models adopted were: substitutional model which was found to be poor. Compound energy formation (CEF) was also employed, this was choosing because it reflects the crystallography of the phase more closely than the substitutional model. The fit of the calculated phase boundaries to the experimental data were good, however the σ-phase field was quite wide. The modified CEF model was finally adopted, in this way, a set of Gibbs energy expressions were produced which was smoother than the previous optimisations and consistent with the phase diagram and thermodynamic properties of the system as shown in Figure 2.11.

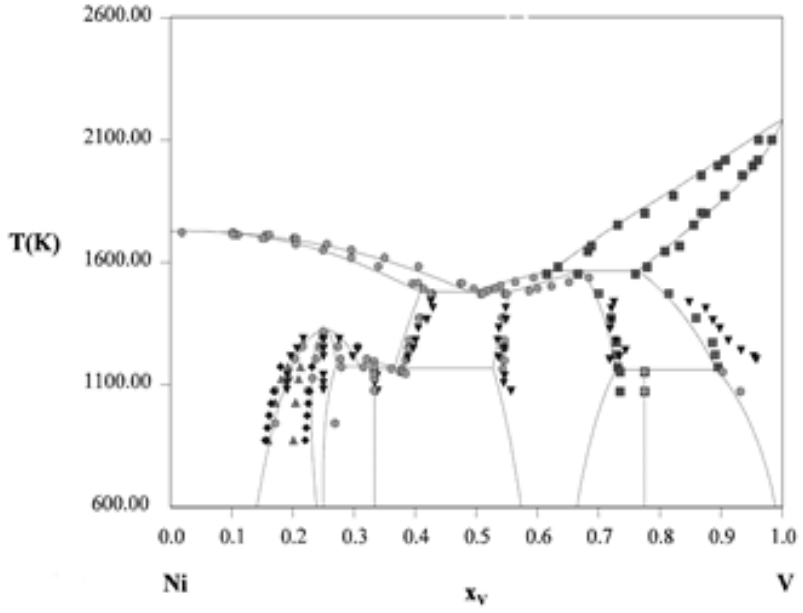


Figure 2.11. The Ni–V phase diagram, calculated using the modified CEF model for the sigma phase [2001Wat1].

2.3.6 Binary Ni-C phase diagram

The equilibrium phase diagram for the Ni-C (graphite) system is given in Figure 2.12. The system consists of a simple eutectic with limited terminal solubility of C in fcc (Ni) and very limited (unresolvable in Figure 2.12) terminal solid solubility of Ni in C (graphite). The eutectic composition and temperature were investigated by several authors [1967Rut, 1969Luc, 1978Kau, 1981Ers]. The DTA data of Lucas [1969Luc] have been used to fix the eutectic temperature at 1326.5ºC. Data for the Ni-rich solidus are non-existent. Therefore, the solidus in Figure 2.12 has been constructed simply by interpolating between the melting point of pure fcc Ni (1455ºC) and the maximum solid solubility of C (2.7 at.% C) in (Ni) reported by Singleton and Nash [1989Sin].

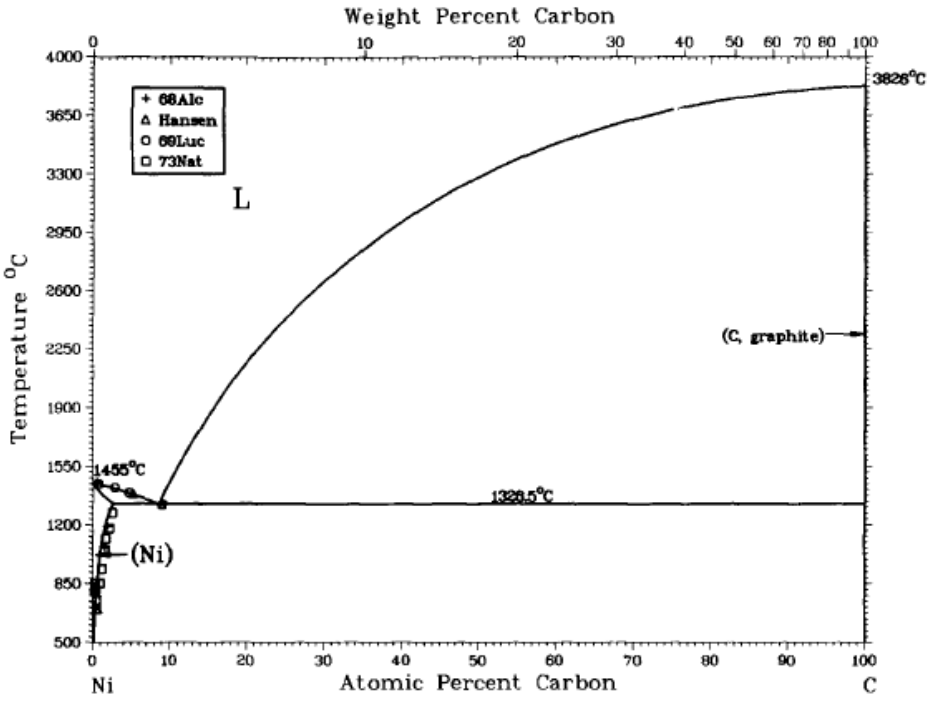


Figure 2.12. Ni-C (graphite) phase diagram with selected data points for the Ni-rich eutectic composition and temperature [1989Sin].

2.3.7 Solid phases

No stable carbides have been reported in the Ni-C (graphite) system, but a metastable carbide (Ni_3C) can be produced. Singleton and Nash reported that by splat quenching (~106°C/s) a molten Ni-C alloy produced a highly supersaturated fcc phase, along with Ni_3C [1989Sin]. Subsequent work by Ershova *et al*. [1981Ers] facilitated the construction of a metastable equilibrium diagram that incorporated Ni_3C together with an extended solid solution of C in fcc (Ni) (Figure 2.13). Major inconsistencies at concentrations greater than 25 at.% C between the metastable diagrams presented by Ershova *et al*. [981Ers] has led to the omission of this portion of the diagram in Figure 2.13. A summary of the structural data available for the Ni-C (graphite) system and the Ni-Ni_3C metastable system is given in Table 2.8 [1989Sin].

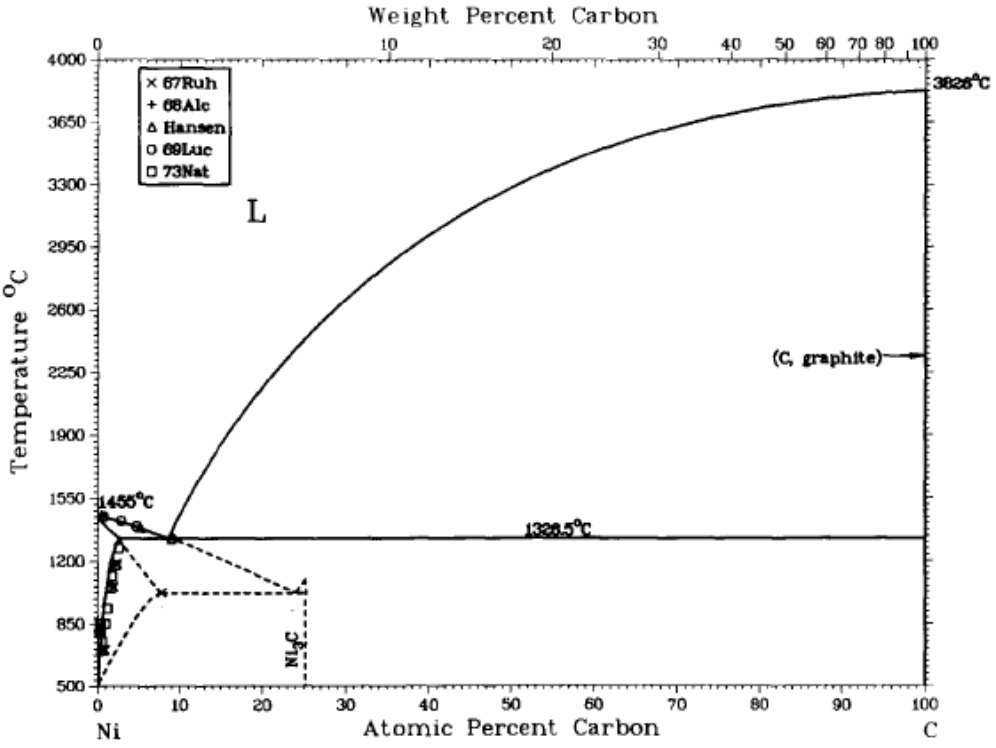


Figure 2.13. Ni-C (graphite solid line) with metastable Ni-Ni_3C (dashed line) phase diagram [1989Sin].

Table 2.8. Ni-C crystal structure data [1989Sin].

Phases	**Composition, at.%C**	**Pearson symbol**	**Space group**	**Strukturbericht Designation**	**Prototype**
(Ni)	0 to 2.7	*cF*4	$Fm\bar{3}m$	*A*1	Cu
C (graphite)	…	*hP*4	$P6_3/mmc$	*A*9	C (graphite)
Metastable phases					
Ni_3C		*oP*16	*Pnmα*	$D0_{11}$	Fe_3C
(Ni)	7.4	*cF*4	$Fm\bar{3}m$	*A*1	Cu

2.3.8 Ni-V-C ternary system

The Ni-V-C system at 1100ºC has been reported by Telegus [1971Tel] and Holleck [1975Hol]. Figure 2.14 shows the isothermal section by Holleck [1975Hol] and Figure 2.15 shows the isothermal section by Telegus [1971Tel]. Both diagrams exhibit many two-phase fields. The C regions in both diagrams are similar because of the very limited solubility in carbon. There is some uncertainty with regard to the isothermal section given by Holleck, [1975Hol] and one of the phases, CNi_2V_4, is questionable, as are its three-phase regions.

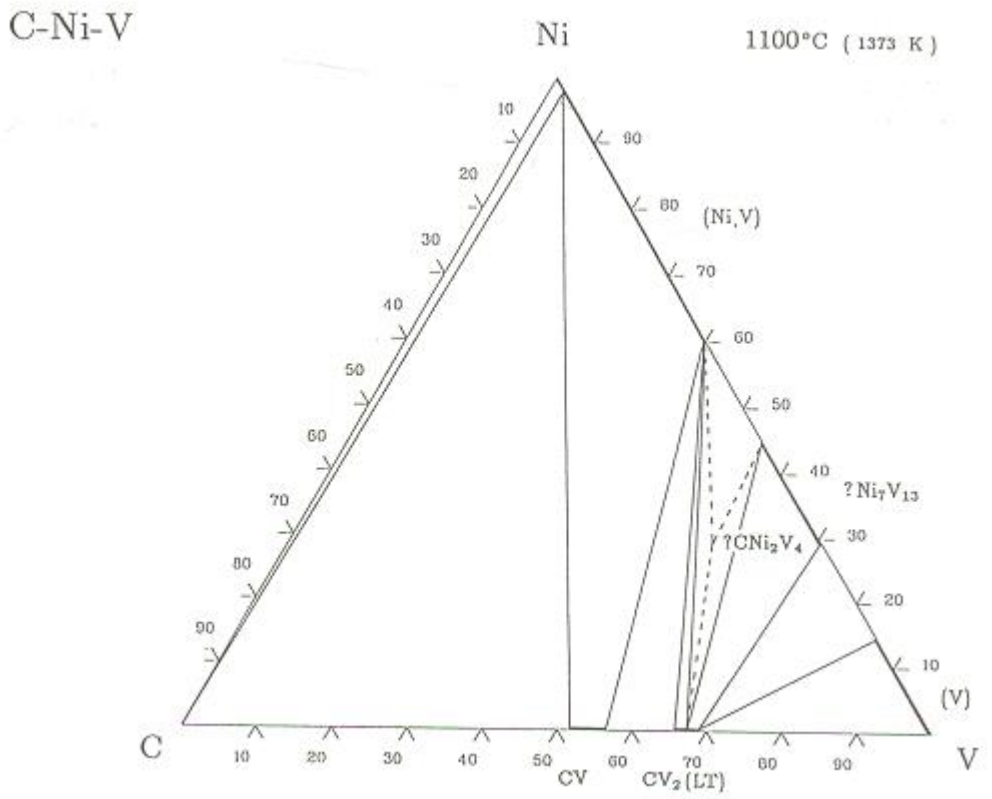


Figure 2.14. Complete isothermal section given at 1100ºC (1373K) [1975Hol].

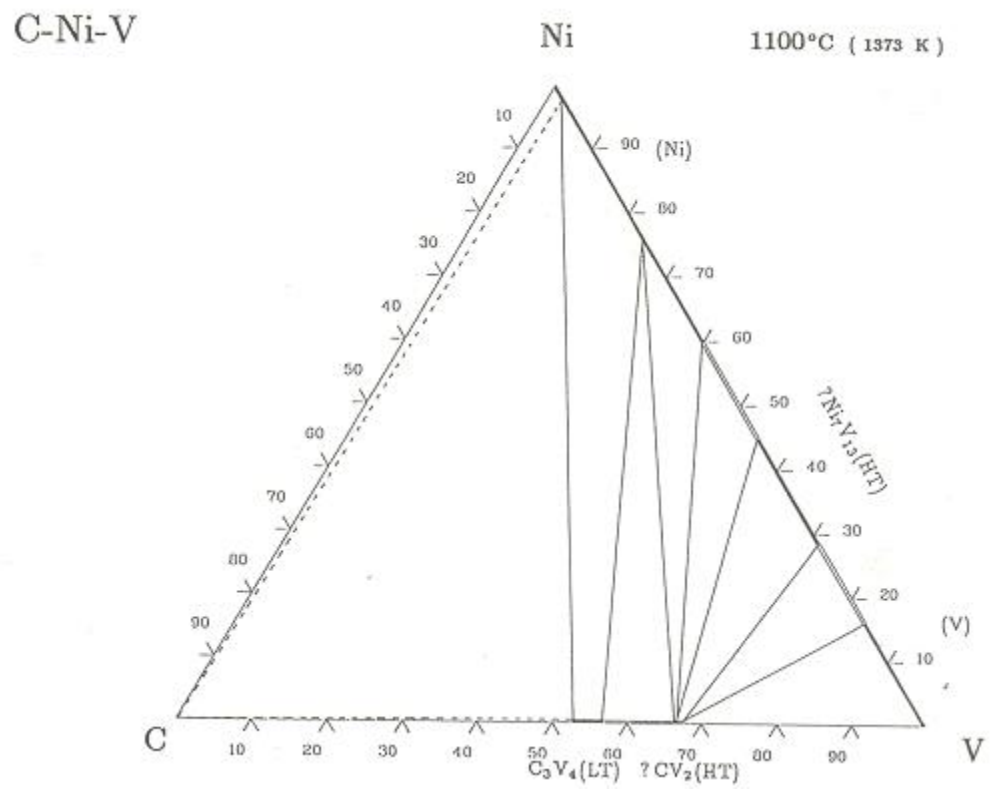


Figure 2.15. Complete isothermal section given at 1100ºC (1373K) [1975Tel].

2.4 Tribology

Tribology, defined as 'the science and technology of interacting surfaces [1992Hut], involves the study of friction, wear and lubrication. These three factors are fundamentally linked together and each contributes significantly to the success or failure of a given system of surfaces in relative motion to each other.

Many applications existing today do not allow for lubrication. In the absence of lubrication, as is the case with dry sliding wear, the friction and wear response of the system will be more significant in determining the failure modes and lifetimes of the system components. Thus the material properties and the parameters of the operating system which affect friction and wear become vital to improve the tribological response within the system.

This sections summarised the main components of the tribological system namely, friction and dry sliding wear.

2.4.1 Friction

Friction can be defined as the resistance experienced by one body when moving against another body [1992Hut]. Friction is usually described or compared by using μ, known as the coefficient of friction. This coefficient of friction is indicative of the relationship between the frictional force experienced, F, and the normal load on the object, W [1992Hut]:

$$\mu = F/W$$

For most common materials sliding in air, the value of μ usually lies between 0.1 and 1. The equation is an expression of the Laws of Friction.

There are two types of coefficients of friction that are required to accurately describe a system experiencing friction. The first is the static coefficient of friction, μ_s, which describes the system in which an object remains stationary although a force is being exerted against it. The second is the kinetic coefficient of friction, μ_k, which is used to describe the system when an object is moved from its point of rest due to a force being exerted against it and the object continues to move under the applied force. [2002Bhu] .

There are three Laws of Friction generally applied to metals [1992Hut, 2002Bhu]. The laws state that the frictional forces are:

i. Proportional to the normal load on the object,
ii. Independent of the area of contact and
iii. Independent of the sliding velocity.

The third law only applies once motion has started [2002Bhu] and thus only kinetic friction with its kinetic coefficient of friction μ_k is independent of sliding velocity and does not change for moderate speeds [1992Hut]. It is important to acknowledge that friction is not a material property but rather a system response [2002Bhu]. There are various factors that influence the friction properties of materials. For example, oxide films, composition, microstructure, environmental conditions and the applied loads all affect how the material will respond to the friction experienced [1992Hut]. With metals, temperature has a

significant effect on friction. When the temperature of a metal increases it changes the mechanical properties and the rate of oxidation and there is the possibility of phase transformations, all of which affect frictional behaviour [1992Hut].

Friction plays a contributory role to the rate of wear within a given system although no accurate relationship, producing realistic results, has been defined. Although sliding velocity does not usually affect friction, it does affect the frictional energy dissipation which in turn affects the temperature at the sliding interface [1992Hut]. Measuring the friction coefficient during a wear test allows changes in the sliding behaviour of the material to be monitored and often corresponds to changes in the wear pattern and hence the wear mechanisms which often renders valuable information of the material properties.

When considering sliding friction, it has been accepted that the total intrinsic frictional force consists of two components [2002Bhu]. That of the force required to shear the asperities known as the adhesive friction component and that of the force required to supply the energy of deformation known as the ploughing component. For brittle materials the fracture of adhesive contacts and brittle deformation need to be considered. Therefore fracture toughness plays a vital role.

The pattern of a friction response graph during dry sliding wear can often provide detailed information. These graphs are typically presented in an S-shaped curve as shown in Figure 2.16 [2002Bhu]. The shape of these friction curves may be influenced by the interface materials as well as the operating conditions. During sliding, changes occur between the surfaces and within the surface materials that affect the friction and wear properties. The initial sliding period during which the frictional forces stabilize is often referred to as the run-in period. During this time high asperities may be worn down, surface films may be removed or new films formed or structural changes within the material may occur. After this initial period new changes may occur at the interfaces of the two sliding bodies such as roughening and/or the presence of trapped wear particles which may lead to an increase in the friction level or causing it to increase to a new steady state plateau [2002Bhu]. The transitions that friction could possibly undergo during a wear test can generally be grouped into four patterns as illustrated in Figure 2.16 [2002Bhu].

The first pattern (I) shows that friction stays at an initial level for a period of time and then slowly increases to another steady state value. This pattern is often associated with identical metals sliding against each other. This response is a result of ploughing due to roughening of the surface and entrapped wear particles.

In smooth surfaces involving elastic deformation with a dominant adhesive component of friction, an increase in the friction level is associated with the smoothing of the surfaces resulting in a larger component of adhesive friction [2002Bhu].

The second pattern (II) shows that friction stays at an initial level for a period of time and then increases to a higher level after which it decreases slightly and then levels off. This decrease in friction is due to the smoothing of two hard surfaces experiencing plastic deformation which results in a decrease in the ploughing component. If the surfaces experience elastic contact where the adhesive component is dominant a decrease in the adhesive component of the friction is due to the decreased real contact area as a result of the ploughing which is due to the roughening and wear debris [2002Bhu].

Pattern three (III) shows that friction increases to a high value at which it remains for a period of time and then decreases to a lower value. Shortly afterward it increases again to a high level. This pattern can often be repetitive. The decrease in the friction level during plastic contact is thought to be due to the ejection of wear particles from the contact surfaces and then subsequently the formation of new wear particles contributes to the increase in the friction levels [2002Bhu].

Pattern four (IV) is similar to pattern (III) however the high and low levels are not repetitive but rather unpredictable. The sharp rise in the friction level and its erratic behaviour is usually associated with incompatible material pairing [2002Bhu].

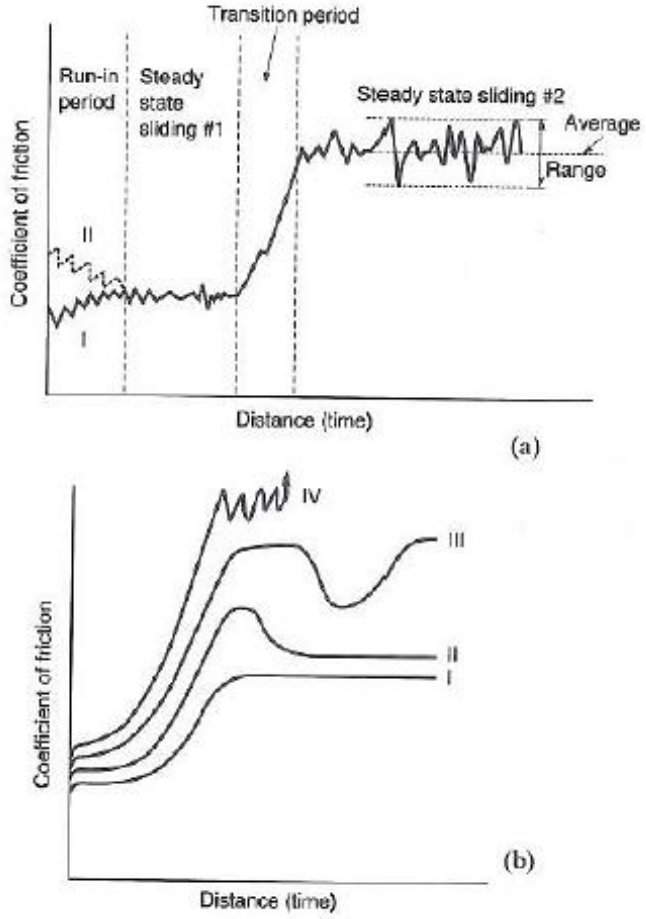


Figure 2.16. The coefficient of friction as a function of sliding distance. (a) A typical S-shaped curve illustrating the running in period. (b) Four hypothetical patterns that can be expected [2002Bhu].

2.5 Sliding wear

Sliding wear refers to the wear that occurs when one body is sliding over another body [1992Hut]. It results in deformation of a material's surface generally due to a breakdown of lubrication which is often referred to as scuffing when it occurs at high speeds. Galling is a result of severe sliding wear and causes harsh surface damage due to localized welding during un-lubricated conditions at low speeds [1992Hut].

Tests executed to investigate sliding wear can be performed using numerous test configurations, the geometries may differ but the basic principle remains the same; one body is held stationary whilst the other body is in motion. One of the most common configurations used is that of the pin-on-disc, which is also used in the current work.

CHAPTER THREE

3.0 EXPERIMENTAL PROCEDURE

3.1 Sample selection

Twenty-four samples were prepared in three stages, since only six samples could be prepared at a time in the arc-melter. Each new set of sample compositions was selected to resolve queries from the previous set. Two-phase samples were targeted because more information could be gleaned per sample. The last six (19-24) were also prepared in order to complete the liquidus surface projection and wear test. The nominal compositions in atomic percent were converted to weight percent according to the relation:

$$wt.\%\ Ni = \frac{at.\%Ni\ \times at.\ wt.of\ Ni}{(at.\%Ni\ \times at.\ wt.of\ Ni) + (at.\%V\ \times at.\ wt.of\ V) + (at.\%C\ \times at.wt\ of\ C)}$$

where the abbreviations at. and wt. stand for atomic and weight respectively.

The detail of the conversion is shown in Appendix A. The targeted compositions were converted to 3g as shown in Table 3.1 and plotted in Figure 3.1.

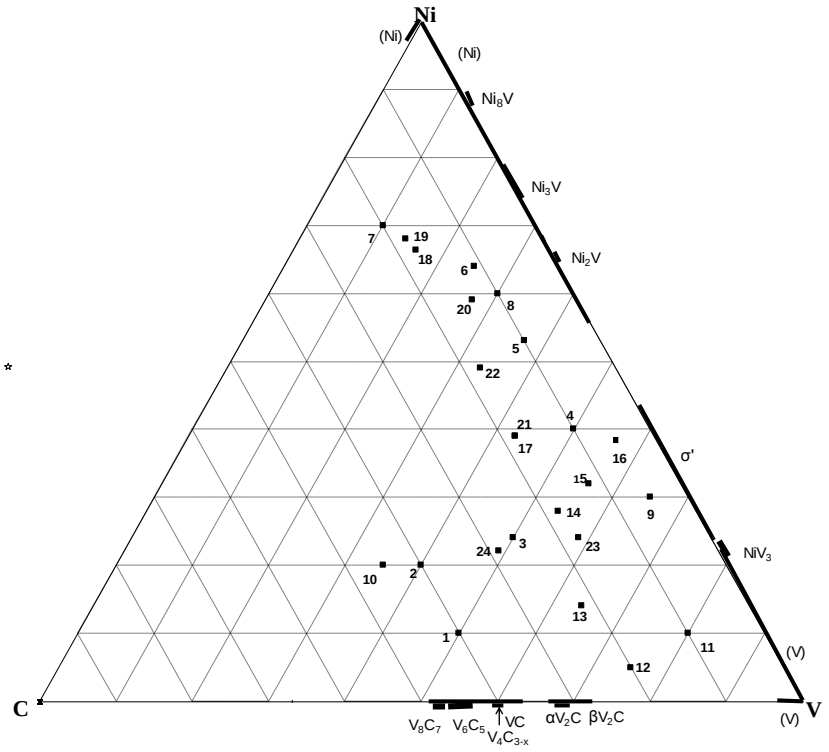


Figure 3.1. Selected compositions of the ternary Ni -V- C samples.

Table 3.1. Selected compositions of the ternary C-Ni-V samples.

Sample no	Atomic %			Weight %			Weighted Samples (3g)		
	Ni	V	C	Ni	V	C	Ni	V	C
1	10	50	40	16	17.6	13.4	0.48	2.12	0.40
2	20	40	40	31.8	55.2	13.0	0.95	1.66	0.39
3	24	50	26	24.0	50.0	26.0	0.98	1.80	0.22
4	40	50	10	46.8	50.8	2.4	1.40	1.53	0.07
5	53	37	10	60.8	36.8	2.4	1.82	1.11	0.07
6	64	25	11	72.8	24.7	2.5	2.18	0.74	0.08
7	70	10	20	85	10	5	2.55	0.30	0.15
8	60	30	10	68	30	2	2.04	0.90	0.06
9	30	65	5	34	65	1	1.03	1.93	0.04
10	20	35	45	34	51	15	1.04	1.51	0.45
11	10	80	10	12	85	3	0.36	2.55	0.09
12	5	75	20	6.7	87.7	5.5	0.18	2.67	0.15
13	14	64	22	18.9	75	6.1	0.57	2.25	0.18
14	28	54	18	35.6	59.8	4.6	1.07	1.79	0.14
15	32	56	12	38.5	58.5	3	1.15	1.77	0.08
16	38	57	5	42.9	55.9	1.2	1.28	1.68	0.04
17	39	42.8	18.2	48.8	46.5	4.7	1.46	1.40	0.14
18	66.4	16.1	17.5	79.1	16.6	4.3	1.88	0.50	0.12

19	68	14	18	81.1	14.5	4.4	2.43	0.44	0.13
20	59	27.2	13.8	69.1	27.6	3.3	2.07	0.83	0.10
21	39	42.8	18.2	48.8	46.5	4.7	1.46	1.40	0.14
22	49	33.3	17.7	60.1	35.5	4.4	1.80	1.07	0.13
23	24	58.6	17.4	30.6	64.9	4.5	0.92	1.94	0.14
24	22. 1	49.1	28.8	31.2	60.5	8.3	0.94	1.81	0.25

3.2 Manufacturing and sectioning of the samples

Alloy buttons of mass ~3g were prepared from chips and rods of the respective elements. The purity of the Ni, V and C was at least 99.65%. The combined elements were melted in button arc-furnace (BAF) at Mintek, according to their standard preparation method PMD-SOP-O37, in an argon (of at least 99.999% purity) atmosphere on a water-cooled copper hearth. Before each button melt took place, a button of titanium was melted, which act as an oxygen getter. Each button was turned over and re-melted at least three times to ensure thorough mixing of the elements. Six samples could be prepared per arc-melt as shown in Figures 3.1 and 3.2. The arc-melting electrode is equipped with a tungsten tip.

The cooling rate of the arc-melted samples is not known, but it was not fast enough to freeze in the high temperature binary phases, as solid-state decompositions were observed in the microstructures. The mass losses of the samples were monitored. All the recorded weight losses were less than 5%.

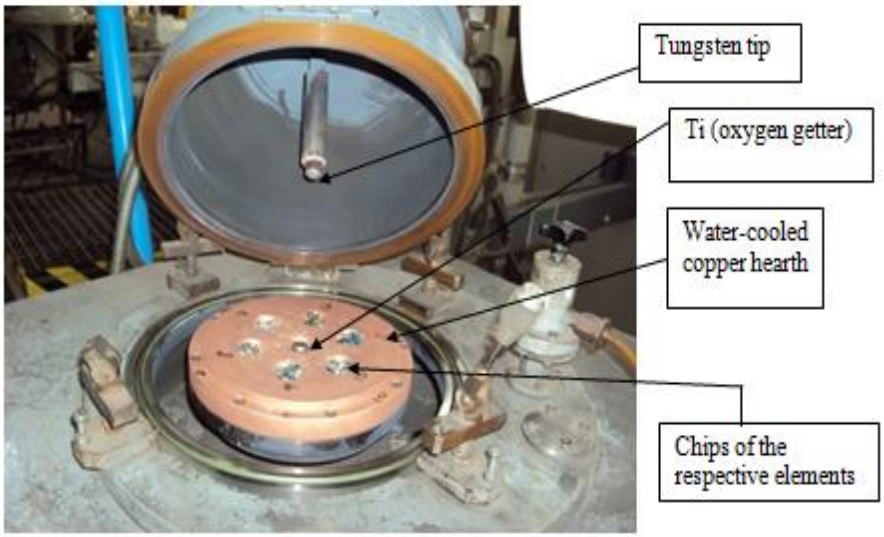


Figure 3.2. Button Arc Furnace (BAF) showing constituent's element before melting.

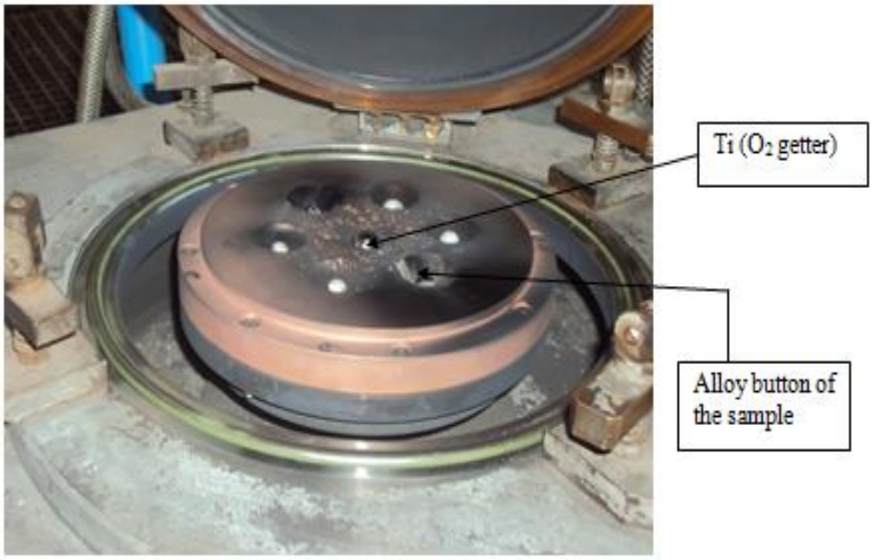


Figure 3.3. Button Arc Furnace (BAF) showing the sample button after melting.

Precautions taken during sample production:

- It was ensured that the chamber was cleaned of any residue on its surface.
- To remove as much as oxygen as possible, the chamber was flushed with argon twice before melting.

- The chamber was flushed thoroughly with argon gas until the material was cool; and argon was slowly bled whilst keeping the vacuum pump running.

- In every melting cycle, Ti was the melted first, followed by the samples.

The alloys were designated according to their nominal compositions in atomic percent. The as-cast alloy buttons were cut into two halves using a STRUERS automatic cutting machine with Accutom® cutting wheel.

3.3 Sample annealing

Before heat treatment, it proved necessary to seal off the specimens in vacuum ampoules for homogenization annealing by evacuating air and sealing while the vacuum pump was running. One half of each sample was heat treated at 1000°C for 1000 hours in a tube furnace, followed by quenching in water by removing the ampoules from the tube furnace as quickly as possible in order to retain the phases at 1000°C.

3.4 Metallographic preparation

Both halves of each sample (as-cast and annealed) were prepared for metallographic examination. Samples were mounted in conductive bakelite in a mounting press, which was heated at 180°C for approximately 3minutes and then water cooled for 1.5 minutes under 250bar. They were ground to 1200 grit on SiC paper and polished using diamond impregnated clothes of 6μm down to 1μm followed by an oxide polishing (OP-S) system, by which polishing is achieved through a combination of chemical treatment (the solution has a pH of 8) and gentle abrasive action. The samples were polished for 15 minutes using the least possible pressure. The reason for using OPS was to provide a better surface, by etching and polishing, i.e. mechanical and chemical effect.

3.5 Sample characterization

3.5.1 Scanning electron microscopy and energy dispersive X-ray analysis

The microstructure was examined initially with optical microscope to check for homogeniety prior to examination using a LEO 1525 field-emission scanning electron microscope (FE-SEM). The samples were examined at higher magnifications in backscattered electron mode (BSE) to distinguish between the phases, as the intensity of the backscattered electrons is a

function of the atomic number of the phase, i.e. different phases have a different amount of backscattered electrons associated with them and this shows as different contrast in the resulting micrograph. The higher the average atomic numbers of the phase, the more electrons are backscattered and the brighter the phase appears in the micrograph. The secondary electron (SE) mode was used to check if the samples contained any pores or cavities.

The phases and overall composition of the samples were analyzed using an energy dispersive X-ray spectroscopy (EDX) system with Oxford INCA software. The resolution of the EDS detector was 132eV. All samples were analysed at 10mm working distance and 12kV accelerating voltage. The quantification was carried out using pure elemental standards. where possible layer features were analysed (i.e. where the phases were larger than 3μm). The results quoted are the average of at least five composition determinations. For each phase the standard deviation was calculated.

3.5.2 X-ray diffraction (XRD)

To confirm and identify phases, conventional X-ray diffraction (XRD) was performed on a Phillips PW-1810 general- purpose system, by using λCuKα radiation, at an operating power of 40kV and 20mA. The starting measuring angle was 10° to 90° (2θ) with a step size of 0.02^o and a counting time of 5 seconds per data point. Phillips PW-1810 was used to identify the first and second batch as-cast samples. D2 Phaser was used for other batch and the heat treated samples. But λCoKα radiation, at the same operating power as Phillip was used. Also the starting measuring angle was 20° to 100° (2θ) with a step size of 0.02^o and a counting time of 5 seconds per data point.

XRD is a suitable technique for phase analyses incorporating lattice parameter and lattice type determinations on crystalline materials. XRD can also be used to determine and evaluate the effect of a solute on the lattice parameter of a phase.

XRD is based on the Bragg diffraction [1913Bra]. When a crystalline material is irradiated by a monochromatic source of X-rays, reflections will occur from the various lattice planes in the crystal. Each reflecting plane will diffract a portion of the X-ray beam as governed by the relationship:

$$n\lambda = 2d \sin\theta$$

Where

λ = wavelength of the incident radiation,

d = interplanar spacing,

θ = incident angle of radiation with the plane, and

n = a small integer.

The reflections are characteristic of the particular crystal structure and give the d- spacings for a phase, from which the lattice parameter can be calculated through the relationship (for a cubic phase)

$$d^2 = \frac{a^2}{h^2 + k^2 + l^2}$$

Where:

d = the interplanar spacing,

a = the lattice parameter, and

h, k and l = Miller indices of the plane from which the reflection originates.

Phases are identified in XRD by matching the phase under investigation to standard patterns, which are available in the International Crystallography Diffraction Database (ICDD) [2001ICD] and International Crystal Structure Database (ICSD) [2002ICS]. However, there are many phases not yet included in these databases, and the standard patterns are normally only for end- member phases, solid solutions are not included.

Some of the binary phases may show solubility for the third element in the system, which shifts the position of the reflections, e.g. (V) with some C is different from pure V. Some of the diffraction patterns also had overlaps on the major peaks. These complicated the XRD identification significantly.

3.6 Mechanical testing

3.6.1 Hardness tests

Vickers macrohardness measurements were conducted on the alloys on both as-cast and heat treated samples using a Vickers hardness tester. A 5 kg load was used, and at least five measurements taken on random areas on the surface of the samples to obtain an average hardness value of the alloys. Care was taken to ensure that each individual indentation was more than two diameters away from another indentation to avoid work hardening effects. In all measurements, the load was applied for ~15 seconds.

The diamond-pyramid hardness number (DPH), or Vickers hardness number (VHN) can be determined according to the following equations [1988Die]:

$$\text{DPH} = \frac{2\text{PSin}\left(\frac{\theta}{2}\right)}{(L^2)}$$

$$\text{DPH} = \frac{1.854\text{P}}{(L^2)}$$

Where:

P = Applied load (kg)

L = Average length of diagonals (mm)

θ = Angle between opposite faces of diamond (136°)

This is equivalent to measuring the average diagonal and obtaining values from the correct tables.

3.6.2 Toughness

Micrographs of the hardness indentations were taken using Leica DM6000 optical microscope to obtain a qualitative evaluation of the alloys' toughness. The alloys were categorized by slip modes, with planar slip having reasonable toughness or plastic deformation and wavy slip having high toughness. The alloys which had cracks were categorized under alloys with cracking.

3.6.3 Palmqvist fracture toughness (K_{IC})

The Palmqvist fracture toughness values were derived using Shetty's equation [1985She, 1990Spi].

$$K_{IC} = 0.0889\sqrt{\frac{HVP}{\sum a}}$$

Where:

K_{IC} = Fracture toughness (MPa$\sqrt{m}$)

HV= Hardness of the samples (N/m^2)

P = Applied load (N)

$\sum a$ = Crack length at each corner (m)

$\frac{p}{\sum a}$ = Applied load over sum of crack length (N/m).

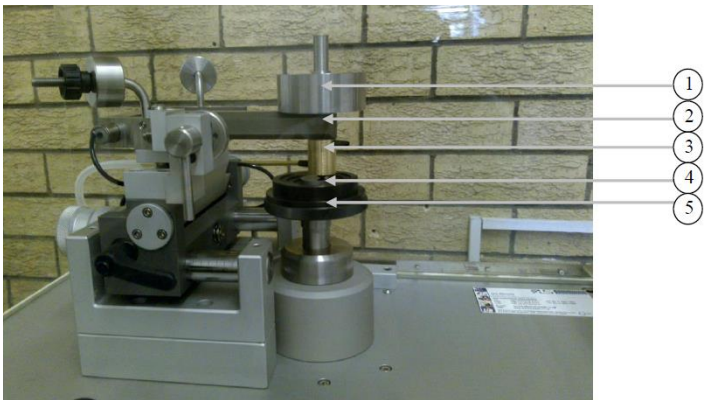
3.6.4 Sliding wear and friction tests

The sliding wear and friction tests were conducted using a CSM tribometer with a pin-on-disc configuration. In this work, the 100Cr-steel balls were the pins and the six selected samples (those with the best microstructures) were the disc. The tribometer had an elastic blade which served as an arm which held the ball with the aid of an adapter fix in one position. Figure 3.4 illustrates the measurement head of the tribometer. There was a disc-holder mandrel to which the sample was fixed. Test parameters that were varied included the applied load on the ball, the speed at which the sample rotated the wear track radius of the ball on the sample, and the total sliding distance.

Prior to each test, the ball and the sample were each fitted into their correct positions in the tribometer. Once this setup was completed, the TriboX InstrumX software was initiated to commence a test. The input parameters and data sampling parameters were first verified in the input sheet. The tests were run at constant operating conditions as listed in Table 3.2. The 100Cr-steel balls used had a hardness range of 600-800HV and a diameter of 6mm.

Table 3.2. Test conditions for wear and friction tests.

Wear track radius	5.00 mm
Linear speed	0.30 m/s
Applied Load	10.00N
Sliding distance	300.00 m
Acquisition rate	30 Hz
Temperature	25 ± 3°C



1- Test Load.
2- Elastic blade
3- Adapter
4- Substrate
5- Disc-holder mandrel

Figure 3.4. Measurement head of the tribometer.

During a test, the tribometer software measured the static and dynamic friction coefficients as well as the penetration depth for the duration of the test. These data were used to derive the friction response of the contact partners and to calculate the wear rates of the contact partners. Prior to testing the sample surfaces were metallographically prepared as described in Section 3.3.

After the friction and sliding wear test, the ball and the sample were then examined using a Motic stereo microscope where the wear scar is measured. In order to calculate the wear rate, the worn volume of the ball and the sample were obtained.

For the ball with spherical geometry:

$$\text{Height of the spherical cap } (h) = R - \sqrt{R^2 - \frac{d^2}{4}}$$

$$\text{Volume of the spherical cap } (v) = \frac{1}{3}\pi h^2 (3.R - h)$$

$$\text{Wear rate} = \frac{v}{D.\,Fn}$$

where:

R- Sphere radius

h- Height of the spherical cap

d- Worn cap diameter

v- Volume of the spherical cap

D- Measurement distance

Fn- Applied load (nomal)

For the sample:

Area of the wear tract which was calculated with a circle formula: $A = \pi r^2$ and then the maximum depth penetration (P) was taken from the tribology Excel file. The worn track section (S) = A x P and the wear rate was calculated from:

$$\text{Wear Rate}_{\text{Sample}} = \frac{S}{D.\,Fn}$$

CHAPTER FOUR

4.0 RESULTS

4.1 Characterizations of as-cast alloys

Sample 16 was not analyzed further because of titanium contamination found in the microstructure. Samples up to Sample 24 were for phase diagram derivation, whereas Samples 19-24 were chosen for wear test after analysing the previous samples.

4.1.1 Nominal $Ni_{10}:V_{50}:C_{40}$ (at.%), Sample 1

The microstructures of alloys were revealed using SEM. Figures 4.1 and 4.2 show the microstructure of the nominal $Ni_{10}:V_{50}:C_{40}$ (at.%) alloy. The microstructure showed fine medium grey ~V_6C_5 surrounded by light ~Ni_3V phases (Figure 4.2).

Table 4.1 gives the phase analyses, which are shown graphically in Figure 4.3. The overall composition lies within the tie-triangle of the phases, signifying that the alloy is likely to be in equilibrium, and no phases were missed. The phase results are sensible, despite the variation between the nominal composition and overall composition, $Ni_{4.6}:V_{40.7}:C_{54.7}$ (at.%). The EDX analyses of Sample 1 are shown in Appendix B1.

The structure is deduced to have formed by:	L → graphite
followed by	L + graphite → ~VC
and	L → ~VC + (Ni) sparse eutectic
then	~VC → ~V_6C_5 in solid state.
	~ (Ni) → ~Ni_3V in solid state.

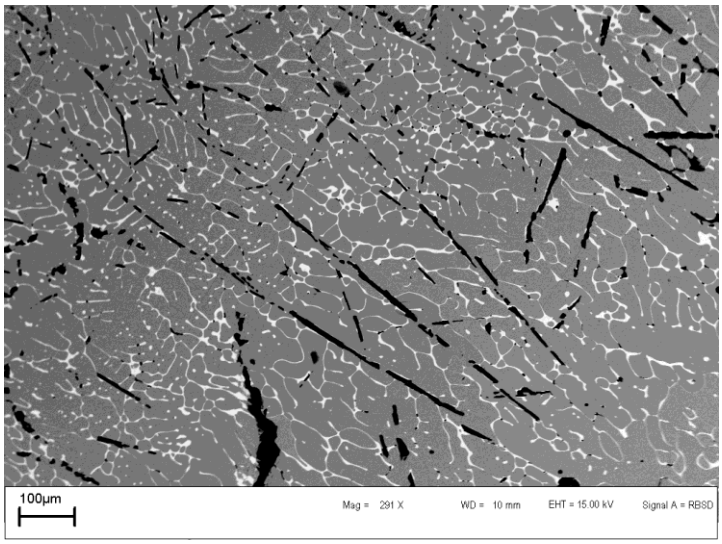


Figure 4.1. SEM-BSE image of nominal $Ni_{10}:V_{50}:C_{40}$ (at.%), Sample, 1 in as-cast condition, showing graphite plates (very dark), dendrites ~V_6C_5 (medium grey) and matrix (light) ~Ni_3V.

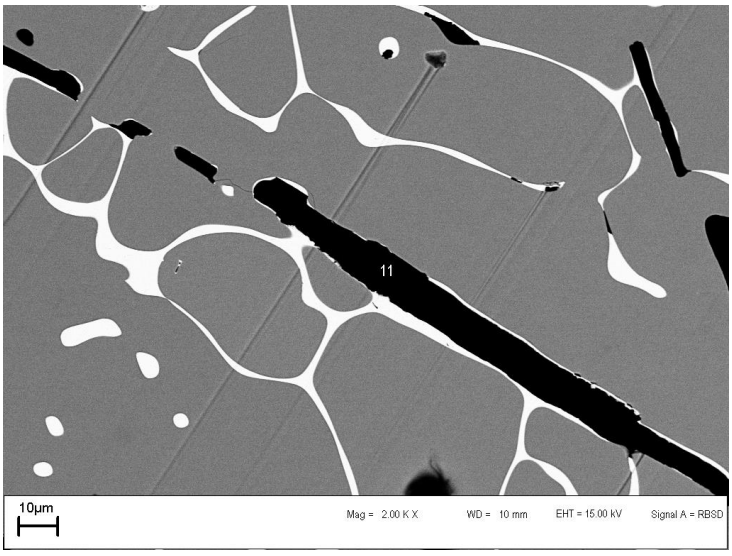


Figure 4.2. SEM-BSE image of nominal $Ni_{10}:V_{50}:C_{40}$ (at.%), Sample 1, in as-cast condition, showing graphite plates (very dark), dendrites ~V_6C_5 (medium grey) and matrix (light) ~Ni_3V at higher magnification.

Table 4.1. EDX phase composition of as-cast nominal $Ni_{10}:V_{50}:C_{40}$ (at.%), Sample 1.

Phase Description	C	V	Ni	Phase
Overall	54.7 ± 1.1	40.7 ± 1.4	4.6 ± 0.6	-
Dark	100 ± 0.0	0	0	graphite
Light	15.5 ± 0.1	17.3 ± 0.6	67.2 ± 0.5	~Ni_3V
Medium	43.5 ± 0.3	56.5 ± 0.3	00.0 ± 0.0	~V_6C_5

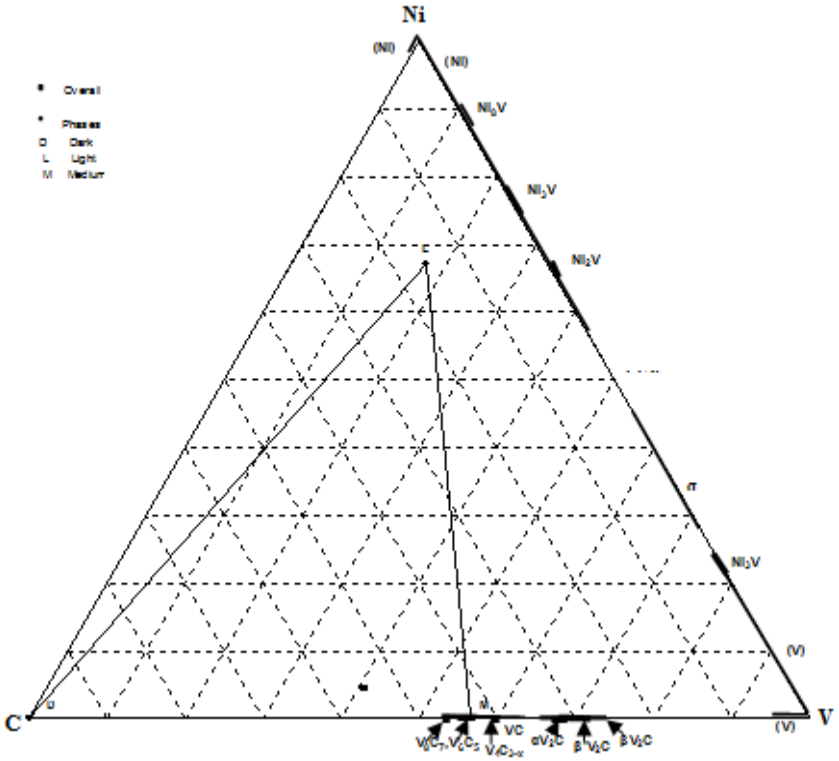


Figure 4.3. EDX analyses of as-cast $Ni_{10}:V_{50}:C_{40}$ (at.%), Sample 1.

The XRD pattern, Figures 4.4 to 4.8, shows the experimental pattern of the sample with the database lines for each of the phases. The pattern had overlapping peaks of the different phases at 2θ = 44º. The highest intensity peaks were ~V_6C_5, at about 2θ = 37.5º and 63.5º. The XRD pattern (Figure 4.8) confirmed the presence of ~V_6C_5, ~Ni_3V and graphite. All peaks could be matched and Table 4.3 contains the identified peaks.

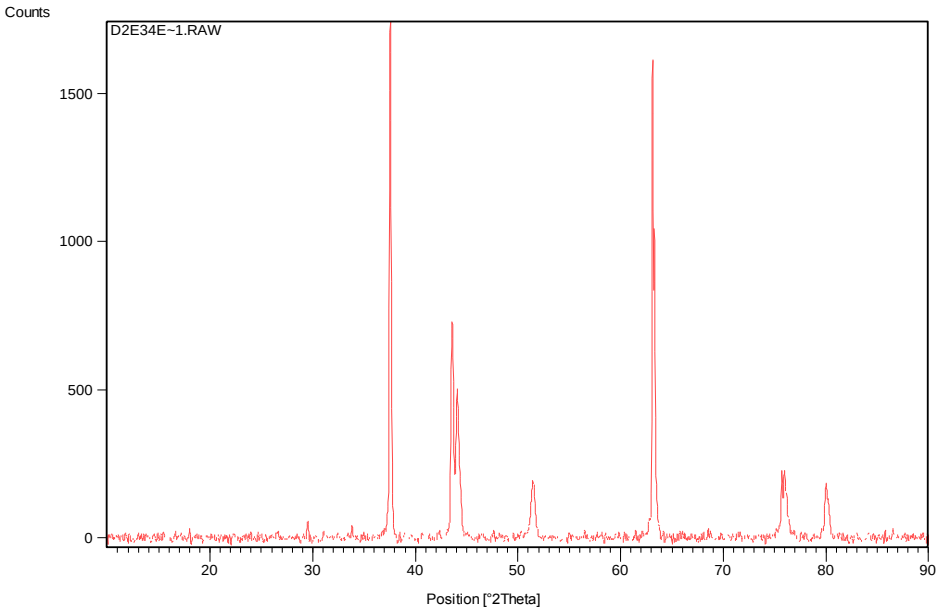


Figure 4.4. Unlabelled XRD pattern of as-cast nominal Ni_{10}:V_{50}:C_{40} (at.%), Sample 1.

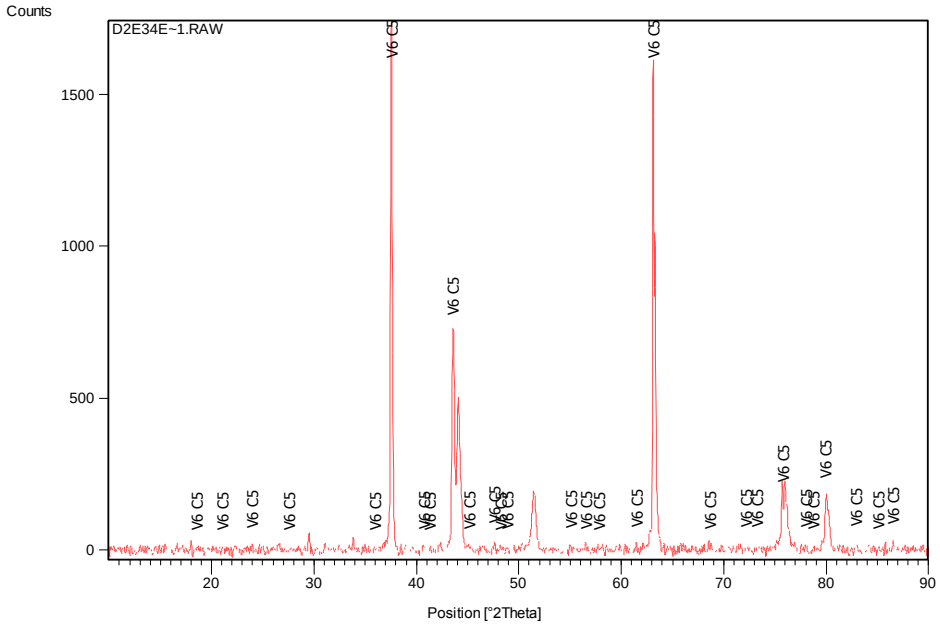


Figure 4.5. XRD pattern of as-cast nominal Ni_{10}:V_{50}:C_{40} (at.%), Sample 1, showing identified ~V_6C_5 peaks.

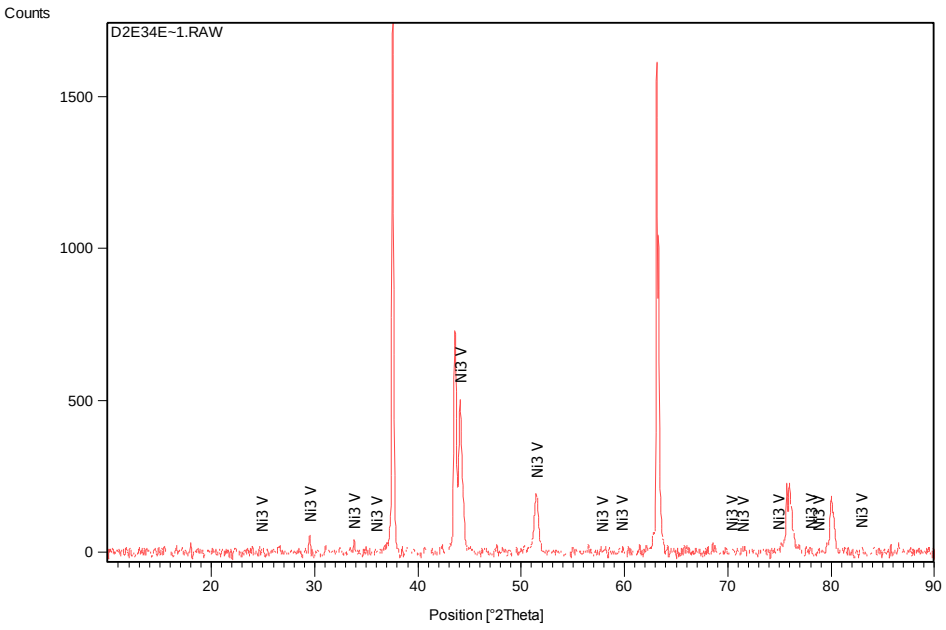


Figure 4.6. XRD pattern of as-cast nominal $Ni_{10}:V_{50}:C_{40}$ (at.%), Sample 1, showing identified ~Ni_3V peaks.

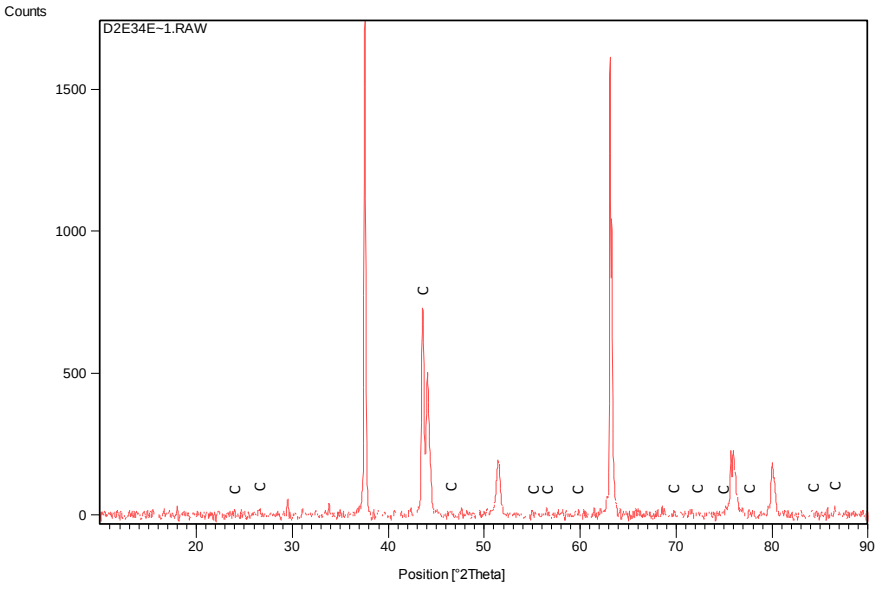


Figure 4.7. XRD pattern of as-cast nominal $Ni_{10}:V_{50}:C_{40}$ (at.%), Sample 1, showing identified C peaks.

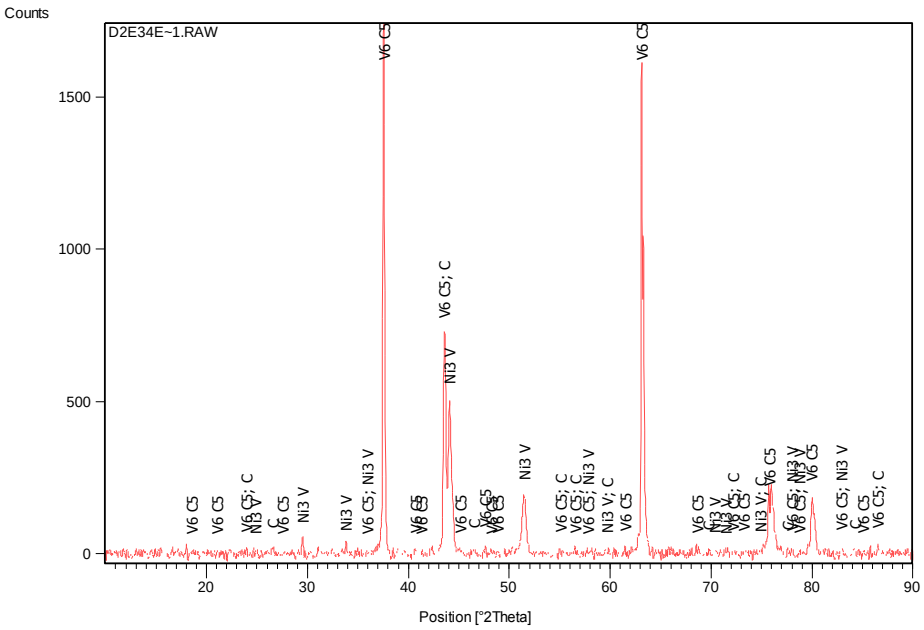


Figure 4.8. XRD pattern of as-cast nominal $Ni_{10}:V_{50}:C_{40}$ (at.%), Sample 1, showing all identified phases.

Table 4.2. XRD peaks for as-cast nominal $Ni_{10}:V_{50}:C_{40}$ (at.%), Sample 1.

Position 2θ (°)	Height (counts)	Relative Intensity (%)	Phases
18.5061	1.67	0.10	V_6C_5
21.0616	2.37	0.14	V_6C_5
23.9496	7.25	0.42	V_6C_5, C
24.8228	1.69	0.10	Ni_3V
26.5576	16.16	0.93	C
27.5983	1.55	0.09	V_6C_5
29.5353	36.12	2.07	Ni_3V
33.8016	9.69	0.56	Ni_3V
35.9337	1.78	0.10	V_6C_5, Ni_3V
37.5622	1745.81	100.00	V_6C_5
40.7410	6.06	0.35	V_6C_5
41.3172	3.54	0.20	V_6C_5
43.5549	708.95	40.61	V_6C_5 , C
44.0930	496.24	28.42	V_6C_5, Ni_3V
45.1601	5.99	0.34	V_6C_5
46.5576	17.59	1.01	V_6C_5, C
47.6275	23.93	1.37	V_6C_5
48.2597	0.99	0.06	$V_6 C_5$
48.8814	4.50	0.26	V_6C_5

Table 4.3 (cont.). XRD peaks for as-cast nominal $Ni_{10}:V_{50}:C_{40}$ (at.%), Sample 1.

51.4920	180.11	10.32	V_6C_5, Ni_3V
55.0832	6.70	0.38	V_6C_5, C,
56.5656	4.98	0.28	V_6C_5, C,
57.7857	2.06	0.12	V_6C_5, Ni_3V
59.6774	3.66	0.21	V_6C_5, C, Ni_3V
61.4799	10.03	0.57	V_6C_5
63.1068	1600.82	91.69	V_6C_5
68.6372	6.13	0.35	V_6C_5
69.7820	11.09	0.64	V_6C_5, C
70.4019	4.80	0.27	V_6C_5, Ni_3V
71.4893	2.32	0.13	V_6C_5, Ni_3V
72.2179	12.71	0.73	V_6C_5, C
73.2904	11.11	0.64	V_6C_5
74.8465	9.02	0.52	V_6C_5, C, Ni_3V
75.8276	159.57	9.14	V_6C_5
77.5765	9.75	0.56	V_6C_5, C
78.0547	12.42	0.71	Ni_3V
78.7570	5.89	0.34	V_6C_5, Ni_3V
79.9836	174.45	9.99	V_6C_5
82.9616	15.34	0.88	V_6C_5, Ni_3V
84.2321	13.66	0.78	V_6C_5
85.0959	6.32	0.36	V_6C_5
86.5686	17.96	1.03	V_6C_5, C, Ni_3V

4.1.2 Nominal $Ni_{20}:V_{40}:C_{40}$ (at.%), Sample 2

An SEM-BSE image of nominal $Ni_{20}:V_{40}:C_{40}$ (at.%) in the as-cast condition are shown in Figure 4.9. A possible sparse eutectic is shown in Figure 4.10. The alloy consisted of plates (very dark) identified as graphite which were randomly distributed, ~V_7C_8 dendrites (medium grey) and a (Ni) matrix with light contrast.

The phase compositions are given in Table 4.4, and are plotted in Figure 4.11, showing the overall composition to lie within the tie-triangle of the phases. The overall composition was very different from the nominal composition. This could explain why the carbon content of the matrix was high. The EDX analyses of Sample 2 are shown in Appendix B2.

The structure was formed by: $L \rightarrow$ graphite

Followed by	L + graphite → ~VC
And	L → ~VC + (Ni) sparse eutectic
Then	~VC → ~V_8C_7 in solid state.

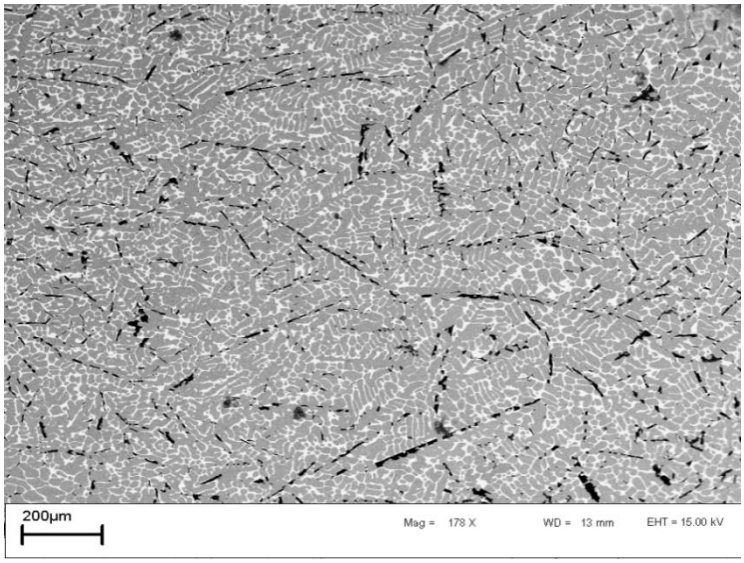


Figure 4.9. SEM-BSE image of nominal Ni_{20}:V_{40}:C_{40} (at.%), Sample 2, in as-cast condition, showing graphite plates (very dark), ~V_8C_7 dendrites (medium grey) and (Ni) matrix (light).

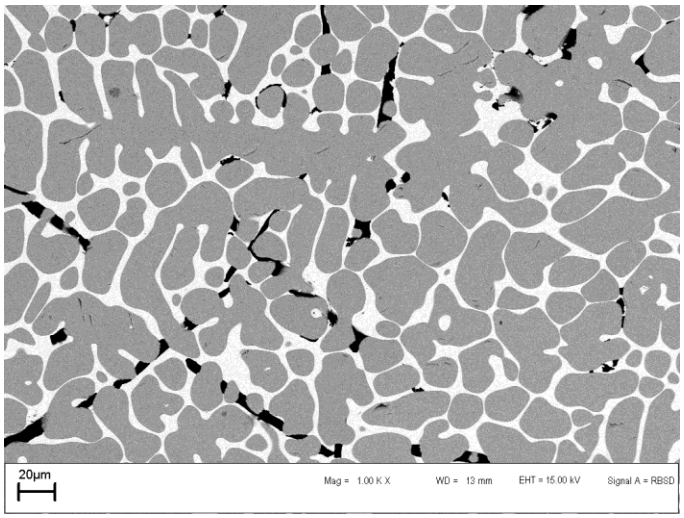


Figure 4.10. SEM-BSE image of nominal Ni_{20}:V_{40}:C_{40} (at.%), Sample 2, in as-cast condition, showing graphite plates (very dark), ~V_8C_7 dendrites (medium grey) and (Ni) matrix (light) at higher magnification.

Table 4.4. EDX phase composition of as-cast nominal $Ni_{20}:V_{40}:C_{40}$ (at.%), Sample 2.

Phase Description	C	V	Ni	Phase
Overall	60.5 ± 0.9	31.1 ± 0.5	8.4 ± 0.7	-
Dark	100 ± 0.0	0	0	graphite
Light	18.1 ± 0.1	4.7 ± 0.6	77.2 ± 0.3	(Ni)
Medium	48.7 ± 0.5	51.3 ± 0.5	00.0 ± 0.0	~V_8C_7

Figures 4.12 to 4.16 show the X-ray diffraction (XRD) pattern of the sample with the database lines for each of the phases. The XRD pattern (Figure 4.16) confirmed the presence of ~V_8C_7, (Ni) and graphite. All peaks could be matched, except 2θ = 29.4° and 33.6° which could not be identified. Table 4.5 shows the identified peaks together with their phases.

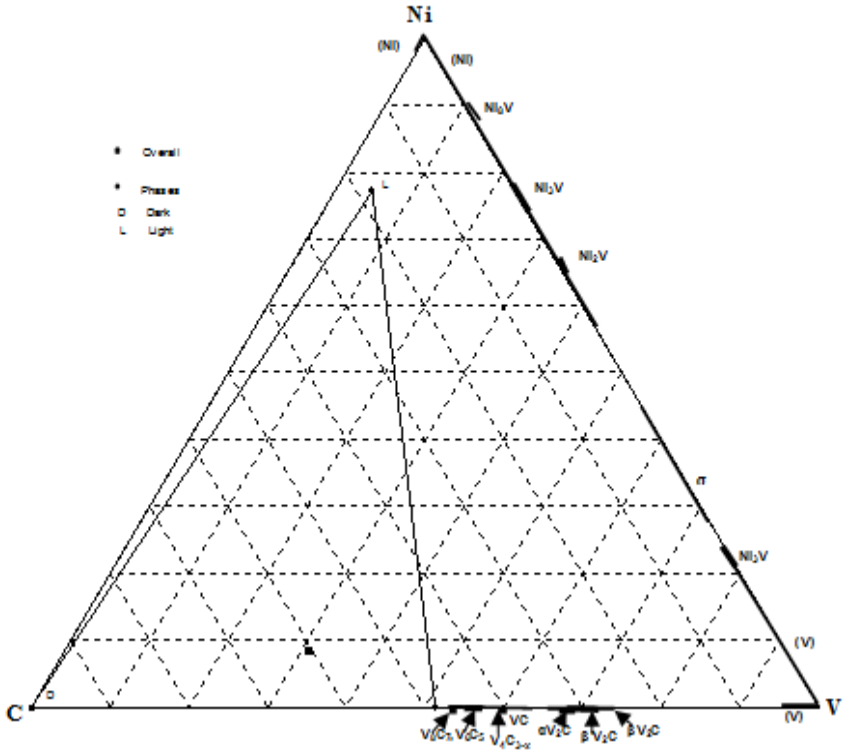


Figure 4.11. EDX analyses of as-cast $Ni_{20}:V_{40}:C_{40}$ (at.%), Sample 2.

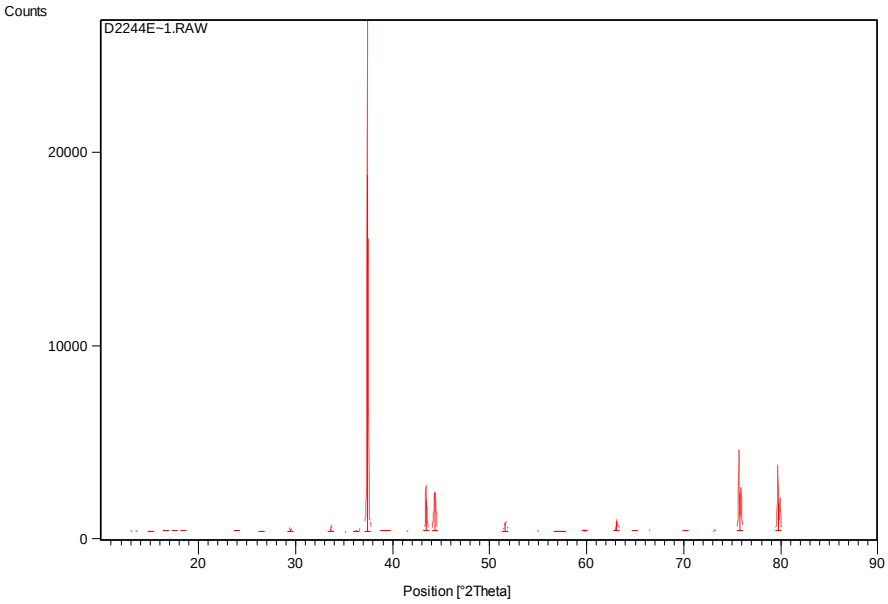


Figure 4.12. Unlabelled XRD pattern of as-cast nominal $Ni_{20}:V_{40}:C_{40}$ (at.%), Sample 2.

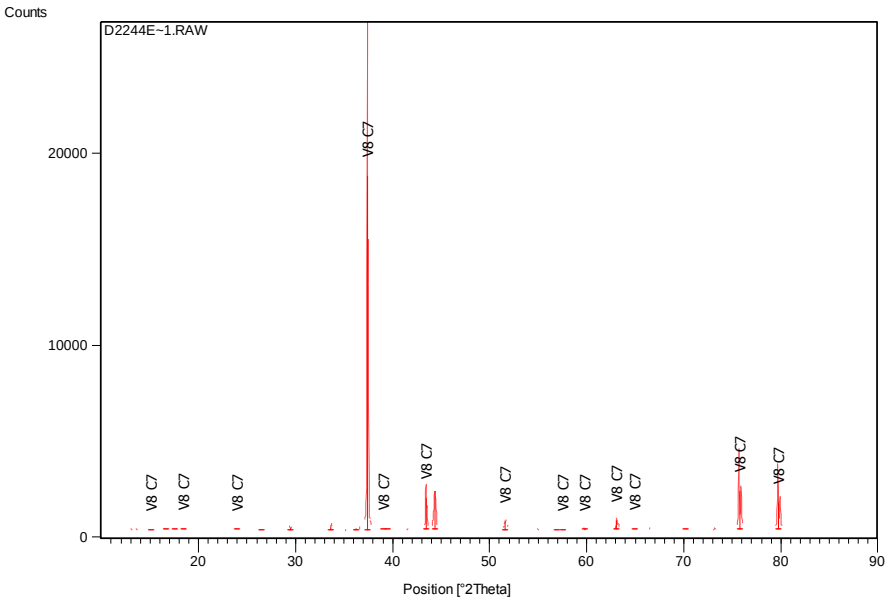


Figure 4.13. XRD pattern of as-cast nominal $Ni_{20}:V_{40}:C_{40}$ (at.%), Sample 2, showing identified ~V_8C_7 peaks.

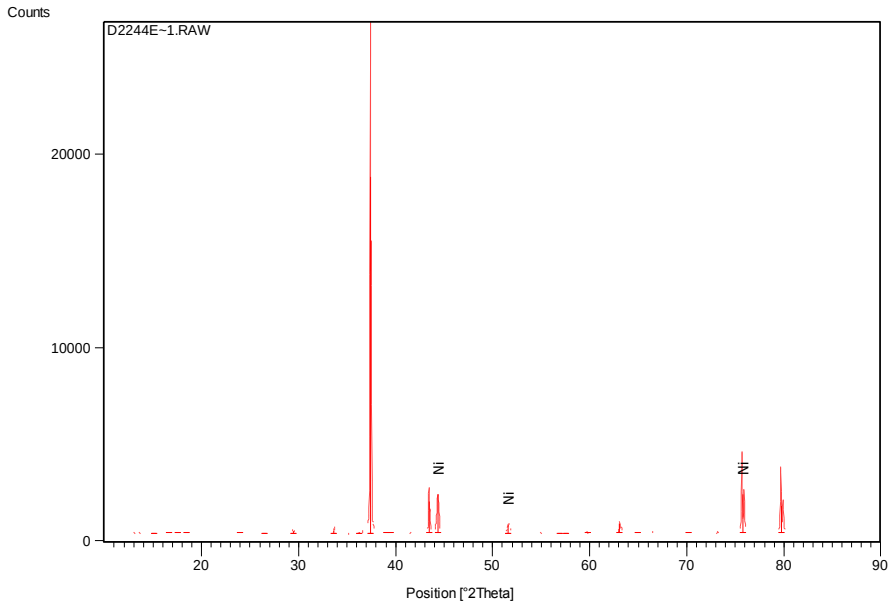


Figure 4.14. XRD pattern of as-cast nominal $Ni_{20}:V_{40}:C_{40}$ (at.%), Sample 2, showing identified (Ni) peaks.

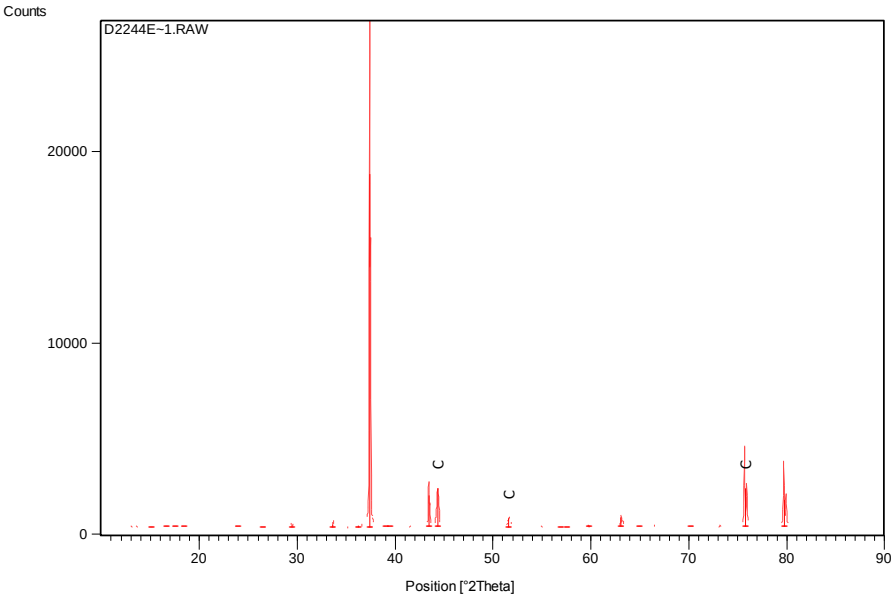


Figure 4.15. XRD pattern of as-cast nominal $Ni_{20}:V_{40}:C_{40}$ (at.%), Sample 2, showing identified C peaks.

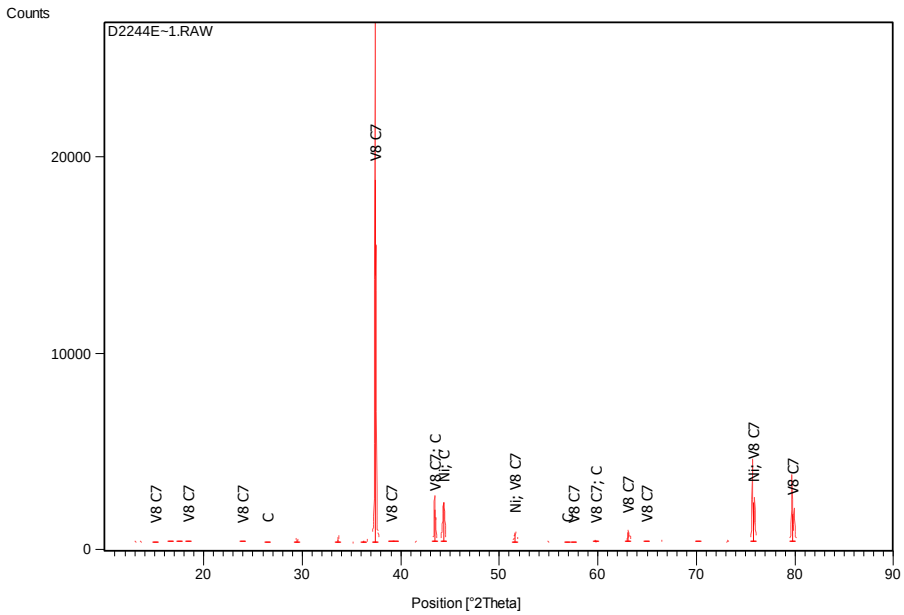


Figure 4.16. XRD pattern of as-cast nominal Ni_{20}:V_{40}:C_{40} (at.%), Sample 2, showing all identified peaks.

Table 4.5. XRD peaks for as-cast nominal Ni_{20}:V_{40}:C_{40} (at.%), Sample 2.

Position 2θ (º)	Height (counts)	Relative Intensity (%)	Phases
15.1138	26.48	0.14	V_8C_7
18.4481	66.61	0.36	V_8C_7
23.9242	15.01	0.08	V_8C_7
26.5263	43.92	0.24	V_8C_7
29.4601	147.48	0.80	Unidentified
33.6434	152.34	0.83	Unidentified
37.4286	18459.33	100.00	V_8C_7
39.0144	89.24	0.48	V_8C_7
43.4597	1647.10	8.92	V_8C_7
44.3587	2007.86	10.88	C, Ni
51.6202	471.35	2.55	C, Ni, V_8C_7
56.8726	26.12	0.14	V_8C_7
57.5729	26.22	0.14	V_8C_7
59.7763	27.76	0.15	V_8C_7
63.0673	453.01	2.45	V_8C_7
64.9526	17.71	0.10	V_8C_7
75.7561	2024.58	10.97	C, Ni, V_8C_7
79.7716	1380.53	7.48	V_8C_7

4.1.3 Nominal $Ni_{24}:V_{50}:C_{26}$ (at.%), Sample 3

An SEM-BSE image representative of nominal $Ni_{24}:V_{50}:C_{26}$ (at.%), Sample 3, in the as-cast condition is shown in Figure 4.17. The alloy had apparently two phases. These were dendrites whose contrasts were dark, identified as ~V_6C_5, the light regions (matrix) were identified as ~Ni_2V. There were needles growing on the primary phase, which were due to a retreating solvus with decreasing temperature. Figure 4.18 shows the microstructure of the alloy at higher magnification.

The phase compositions are shown in Table 4.6 and plotted in Figure 4.19, showing the overall compositions to be deviated from the tie-line connecting the two phases. The deviation was due to the graphite flakes which grew in a sparse Widmanstätten-like mode on the dendrites and into the matrix. This structure indicated growth in the solid state (i.e. with a favoured crystallographic relationship), rather than eutectic, and would push the overall analyses nearer to carbon. However, the standard deviation of the measurements was below 1at.%. The ~Ni_2V analyses might have been compromised by the C needles, so the true result probably had less carbon. Additionally, graphite was deposited from (Ni), probably before the latter become ~Ni_2V. The C was confirmed by XRD. The EDX analyses of Sample 3 are shown in Appendix B3.

The solidification sequence deduced from the microstructure was as follows:

$$L \rightarrow \sim VC$$

$$L + \sim VC \rightarrow (Ni)$$

And

$$\sim VC \rightarrow \sim V_6C_5$$

$$(Ni) \rightarrow \sim Ni_2V$$

The last two reactions occurred as solid state transformations, and carbon also precipitate in the solid state.

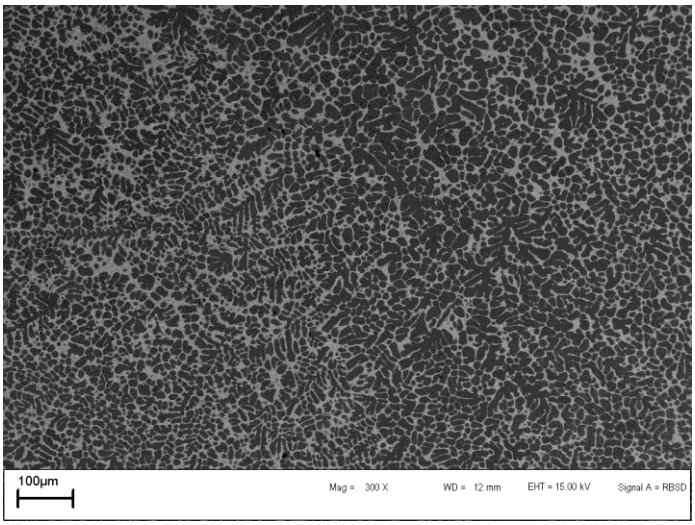


Figure 4.17. SEM-BSE image of nominal Ni_{24}:V_{50}:C_{26} (at.%), Sample 3, in the as-cast condition, showing ~V_6C_5 dendrites (dark) and ~Ni_2V matrix (light).

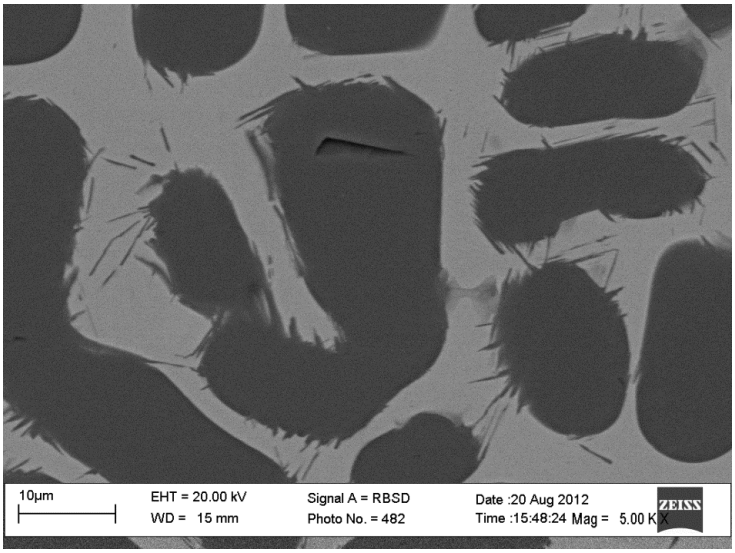


Figure 4.18. SEM-BSE image of nominal Ni_{24}:V_{50}:C_{26} (at.%), Sample 3, in the as-cast condition, showing ~V_6C_5 dendrites (dark) with C flakes and ~Ni_2V matrix (light) at higher magnification.

Table 4.6. EDX phase compositions of as-cast nominal $Ni_{24}:V_{50}:C_{26}$ (at.%), Sample 3.

Phase Description	C	V	Ni	Phase
Overall	38.2 ± 0.8	46.5 ± 0.4	15.3 ± 0.4	-
Dark	44.6 ± 0.8	55.0 ± 0.6	0.4 ± 0.3	~V_6C_5
Light	16.7 ± 0.2	31.2 ± 0.3	52.1 ± 0.4	~Ni_2V

The XRD pattern shown in Figures 4.20 to 4.25 was good, with a low signal to background ratio. The existence of $V_4C_{2.67}$, C, ~V_6C_5 and ~Ni_2V, was confirmed, as shown in Figures 4.21 to 4.24, with small shifts for the identified phases. A major peak was found at position $2\theta = 37.8^o$ which matched ~V_6C_5 and ~$V_4C_{2.67}$. Table 4.7 shows the identified peaks together with their phases. The presence of the two carbides shows that some transformation occurred at lower temperatures.

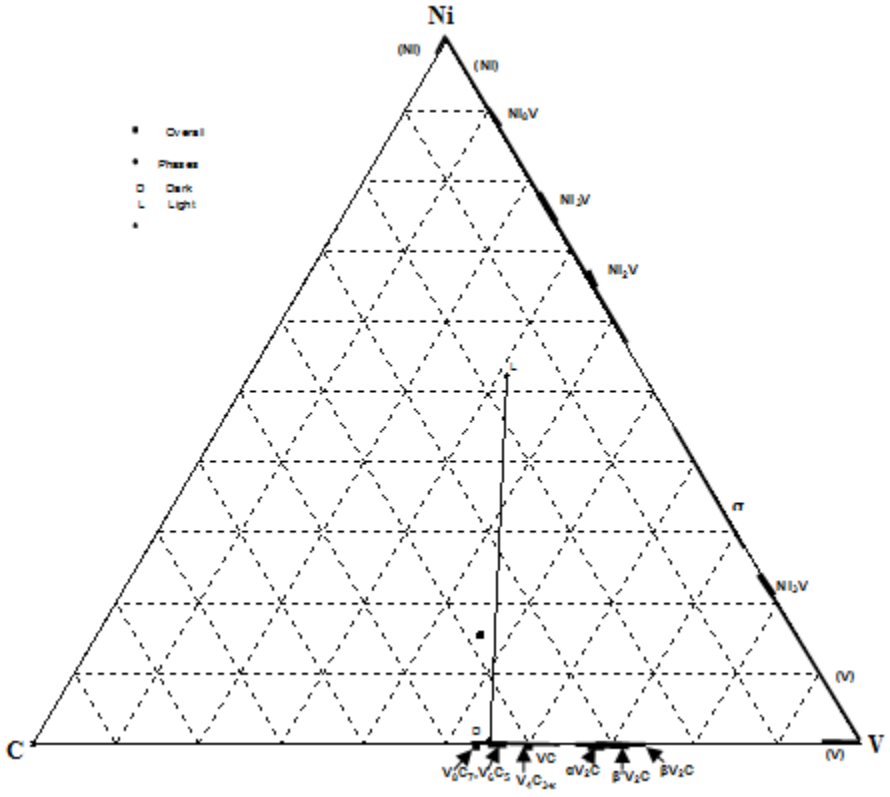


Figure 4.19. EDX analyses of as-cast $Ni_{24}:V_{50}:C_{26}$ (at.%), Sample 3.

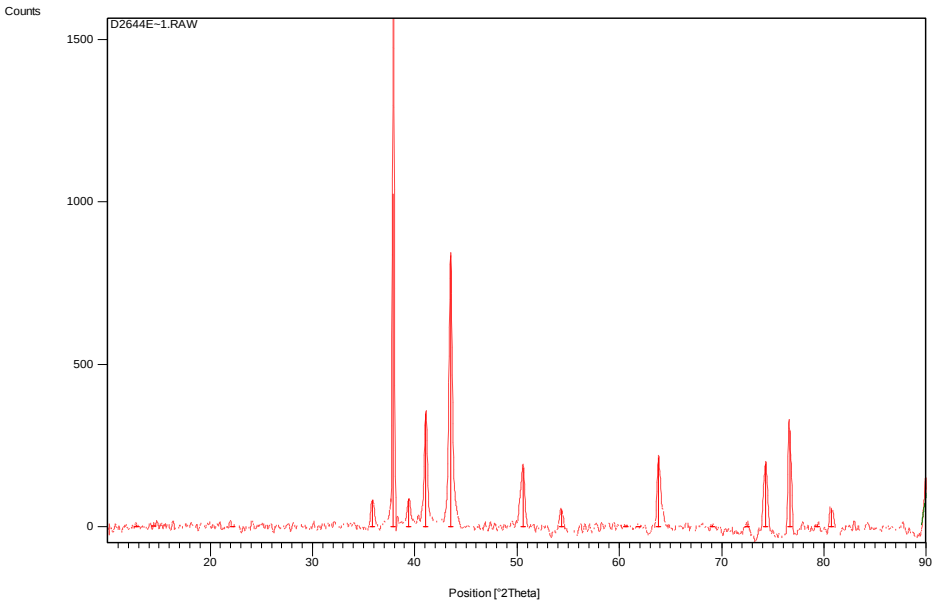


Figure 4.20. Unlabelled XRD pattern of as-cast nominal $Ni_{24}:V_{50}:C_{26}$(at.%), Sample 3.

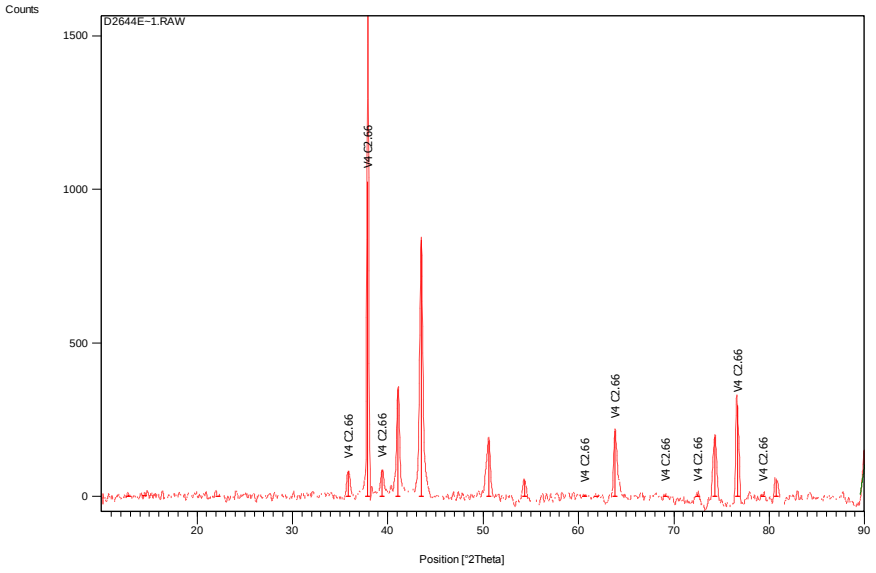


Figure 4.21. XRD pattern of as-cast nominal $Ni_{24}:V_{50}:C_{26}$ (at.%), Sample 3, showing identified $V_4C_{2.66}$ peaks.

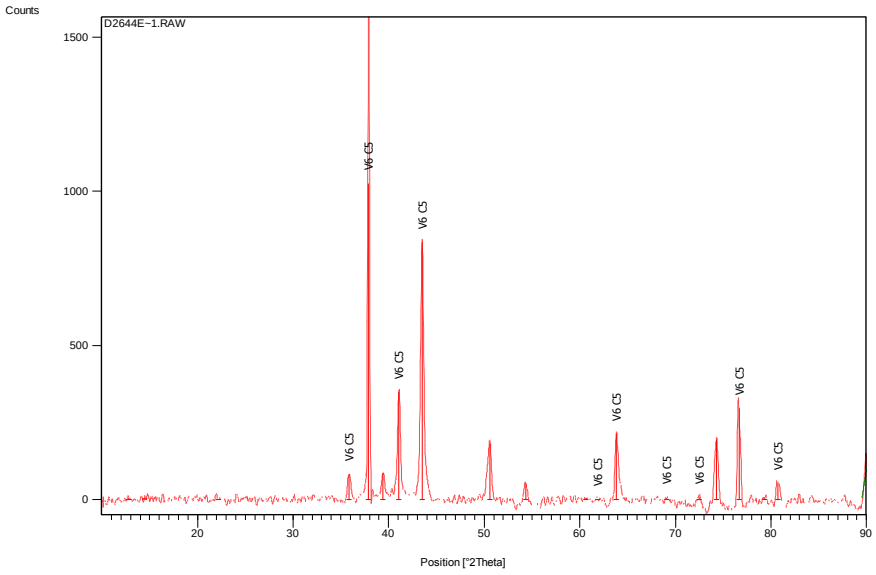


Figure 4.22. XRD pattern of as-cast nominal $Ni_{24}:V_{50}:C_{26}$ (at.%), Sample 3, showing identified V_6C_5 peaks.

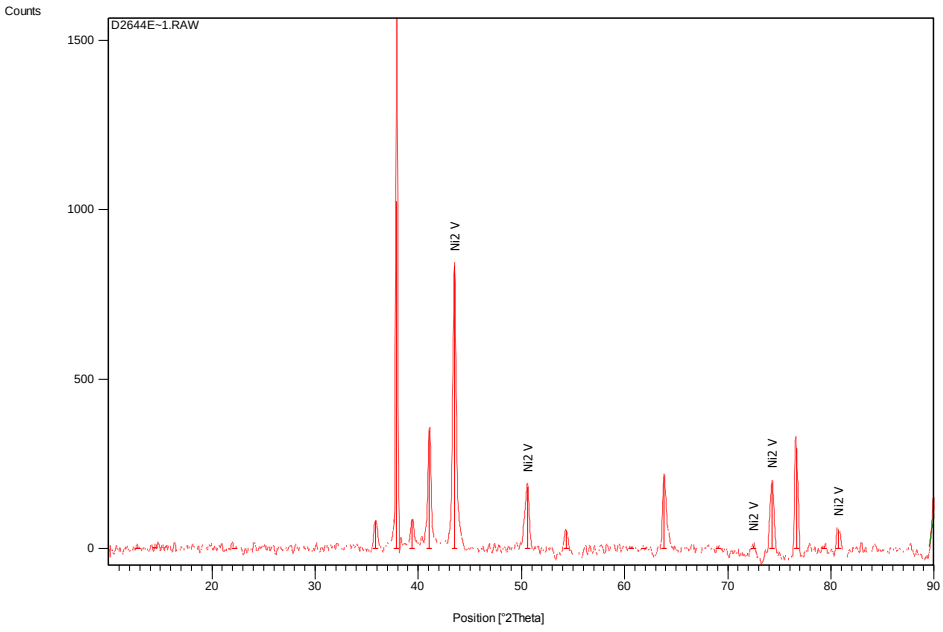


Figure 4.23. XRD pattern of as-cast nominal $Ni_{24}:V_{50}:C_{26}$ (at.%), Sample 3, showing identified Ni_2V peaks.

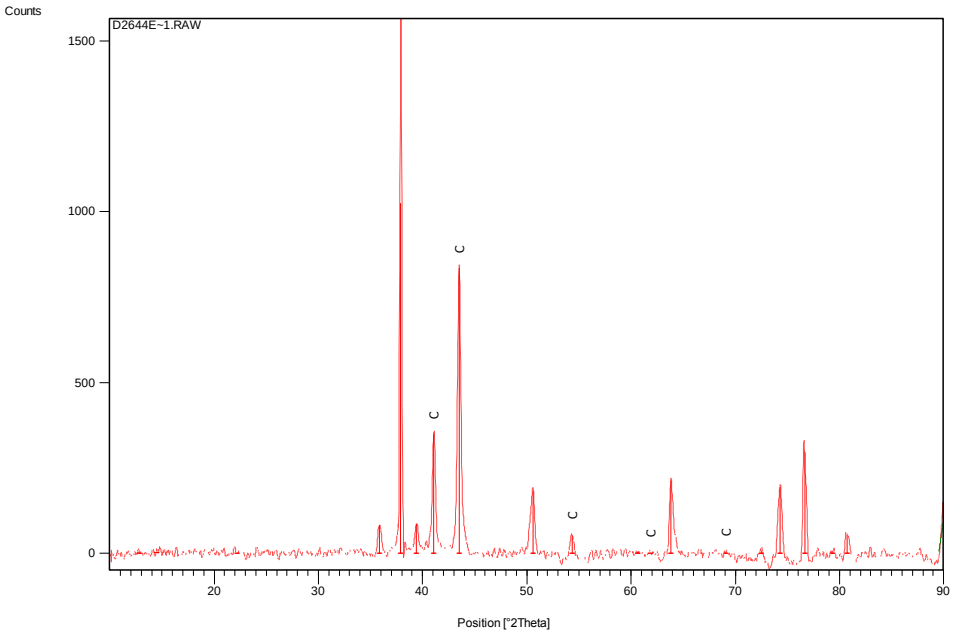


Figure 4.24. XRD pattern of as-cast nominal $Ni_{24}:V_{50}:C_{26}$ (at.%), Sample 3, showing identified C peaks.

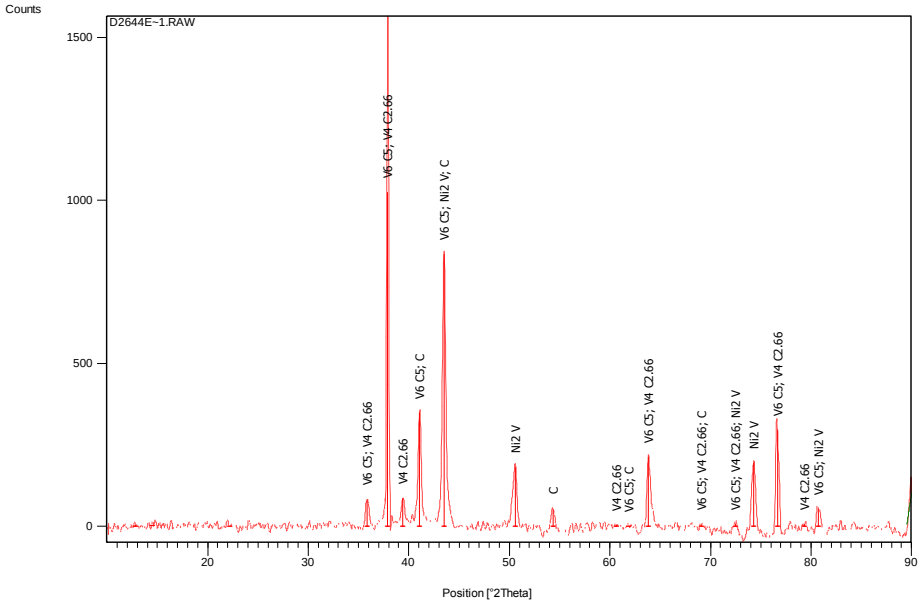


Figure 4.25. XRD pattern of as-cast nominal $Ni_{24}:V_{50}:C_{26}$ (at.%), Sample 3, showing all identified peaks.

Table 4.7. XRD peaks for as-cast nominal $Ni_{24}:V_{50}:C_{26}$ (at.%), Sample 3.

Position2θ (º)	Height (counts)	Relative Intensity (%)	Phases
35.8597	83.42	8.14	V_6C_5, $V_4C_{2.67}$
37.8880	1024.80	100.00	V_6C_5, $V_4C_{2.67}$
39.4195	84.69	8.26	$V_4C_{2.67}$
41.0930	348.91	34.05	V_6C_5, C
43.5001	835.24	81.50	C, Ni_2V,$V_4C_{2.67}$
50.6219	180.43	17.61	Ni_2V
54.3225	54.55	5.32	C
60.6618	3.90	0.38	$V_4C_{2.67}$
61.8720	1.00	0.10	V_6C_5, C
63.8209	212.66	20.75	V_6C_5, $V_4C_{2.67}$
69.1241	6.49	0.63	V_6C_5, C, $V_4C_{2.67}$
72.4669	8.56	0.84	V_6C_5, Ni_2V,$V_4C_{2.67}$
74.2808	194.24	18.95	Ni_2V
76.6478	297.27	29.01	V_6C_5, $V_4C_{2.67}$
79.3696	7.34	0.72	$V_4C_{2.67}$
80.7370	54.44	5.31	V_6C_5

4.1.4 Nominal $Ni_{40}:V_{50}:C_{10}$ (at.%), Sample 4

Figure 4.26 shows the microstructure of nominal $Ni_{40}:V_{50}:C_{10}$ (at.%), Sample 4, in the as-cast condition. The alloy showed a different morphology compared to other alloys, with dark ~VC needles surrounded by a light regions of two different contrasts ("light" and "medium") which had nearly the same composition and were identified as ~Ni_2V and regions of a fine mixture of ~VC + (Ni) eutectic as shown in Figure 4.27.

The phase compositions are shown in Table 4.8 and plotted in Figure 4.28, showing the overall compositions and the eutectic to be deviated from the tie-line joining the two phases. The deviation may be due to unidentified phases which may be present in the microstructure. However, the standard deviation of the measurements was below 1 at.%. The EDX analyses of Sample 4 are also shown in Appendix B4.

The solidification sequence deduced from the microstructure is as follows:

$$L \rightarrow \sim VC$$

followed by a eutectic reaction: $L \rightarrow \sim VC + (Ni)$

and $(Ni) \rightarrow \sim Ni_2V$ in solid state.

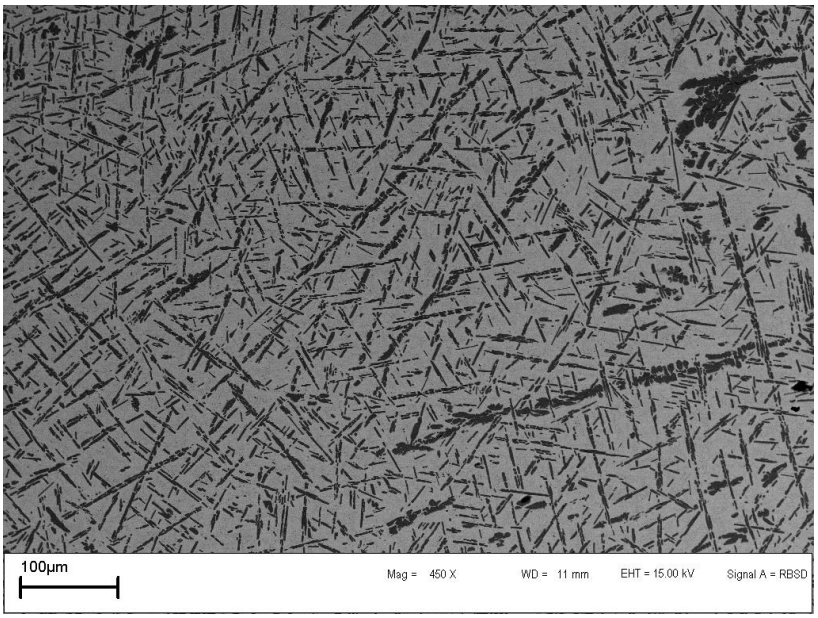


Figure 4.26. SEM-BSE image of nominal Ni_{40}:V_{50}:C_{10} (at.%), Sample 4, in the as-cast condition, showing ~VC dendrites (dark), ~Ni_2V matrix (light).

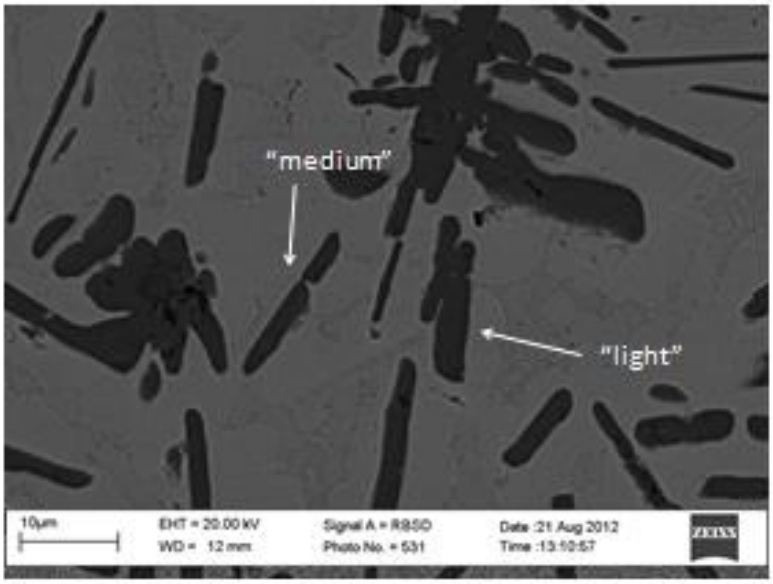


Figure 4.27. SEM-BSE image of nominal Ni_{40}:V_{50}:C_{10} (at.%), Sample 4, in the as-cast condition, showing ~VC needles (dark), ~Ni_2V matrix (light) and eutectic at higher magnification.

Table 4.8. EDX phase composition of as-cast nominal $Ni_{40}:V_{50}:C_{10}$ (at.%), Sample 4.

Phase Description	C	V	Ni	Phase
Overall	23.4 ± 1.2	44.6 ± 0.7	32.0 ± 0.9	-
Dark	36.7 ± 0.5	62.7 ± 0.5	0.6 ± 0.1	~VC
Light	16.1 ± 0.6	36.6 ± 0.4	47.8 ± 0.7	~Ni_2V
Medium	16.3 ± 0.9	35.9 ±1.2	47.8 ± 0.9	~Ni_2V
Eutectic	25.8 ± 0.9	44.4 ± 0.5	29.8 ± 1.4	~VC + (Ni)

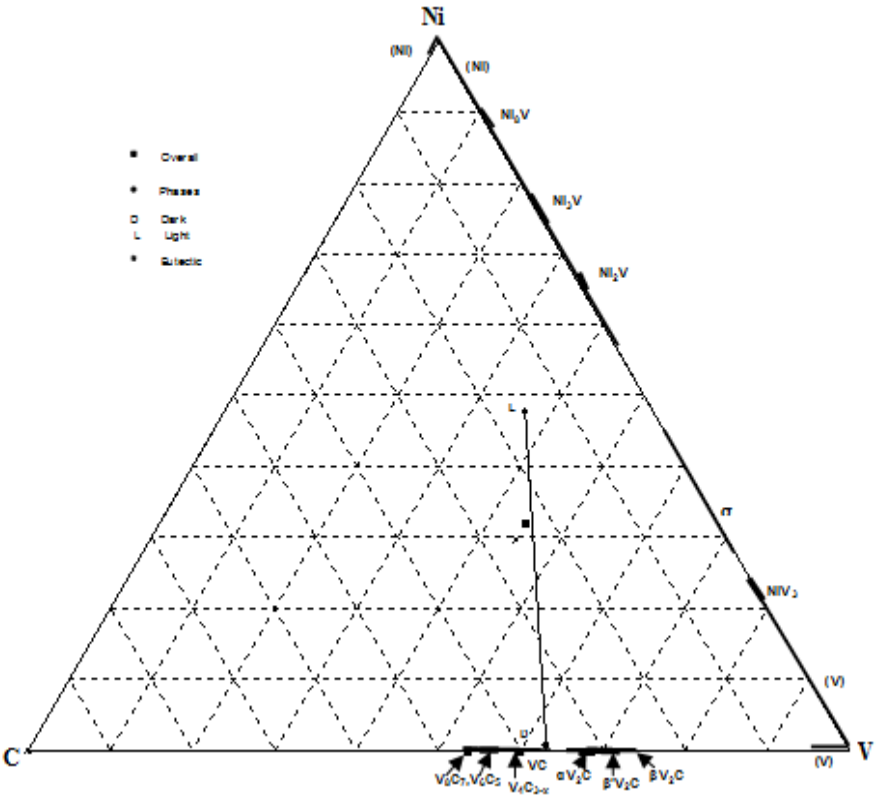


Figure 4.28. EDX analyses of as-cast nominal $Ni_{40}:V_{50}:C_{10}$ (at.%), Sample 4.

The XRD pattern shown in Figures 4.29 to 4.32 was good, with a high signal:background ratio. The existence of ~VC and ~Ni_2V was confirmed. The matches for the phases were good with the ICDD, but unidentified peaks at $2\theta = 41.70^o$, 43.97^o, 45.24^o, 46.39^o and 47.59^o were found By comparison with Sample 13, unidentified peaks was found to be $V_4C_{2.66}$. A

major peak was found at position 2θ = 43.10°, which matched ~Ni_2V. Carbon peaks could not be matched. Table 4.9 shows the identified peaks together with their phases.

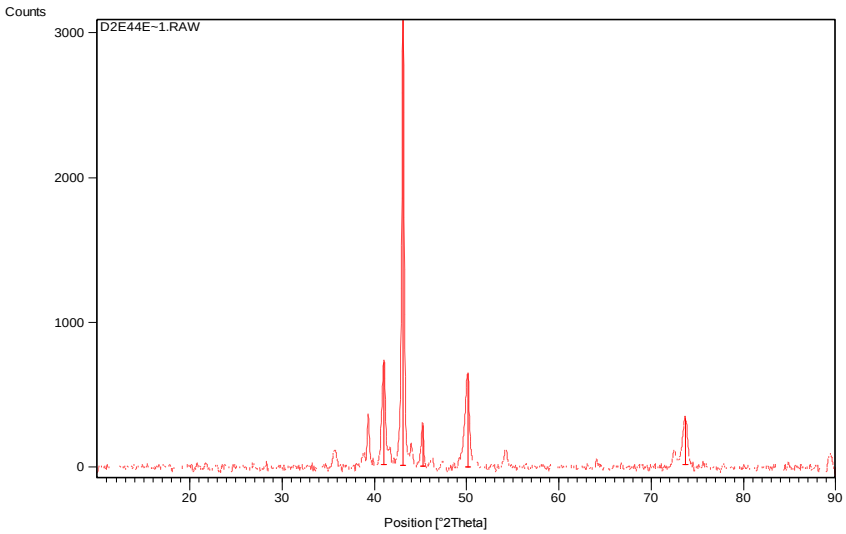


Figure 4.29. Unlabelled XRD pattern of as-cast nominal Ni_{40}:V_{50}:C_{10} (at.%), Sample 4.

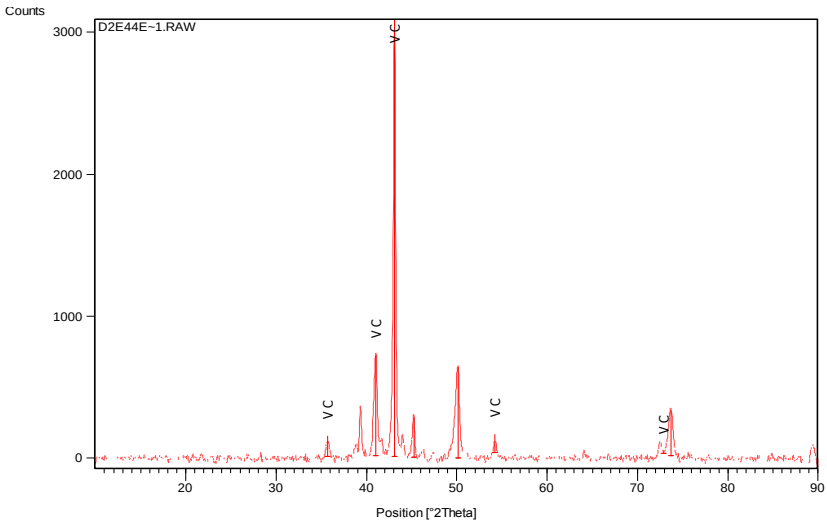


Figure 4.30. XRD pattern of as-cast nominal Ni_{40}:V_{50}:C_{10} (at.%), Sample 4, showing identified VC peaks.

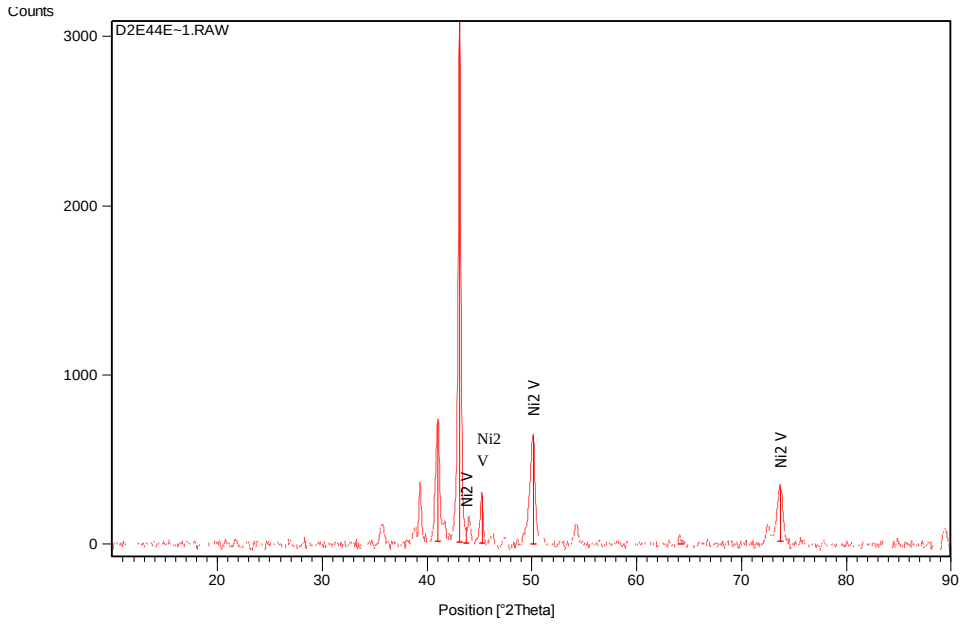


Figure 4.31. XRD pattern of as-cast nominal $Ni_{40}:V_{50}:C_{10}$ (at.%), Sample 4, showing identified Ni_2V peaks.

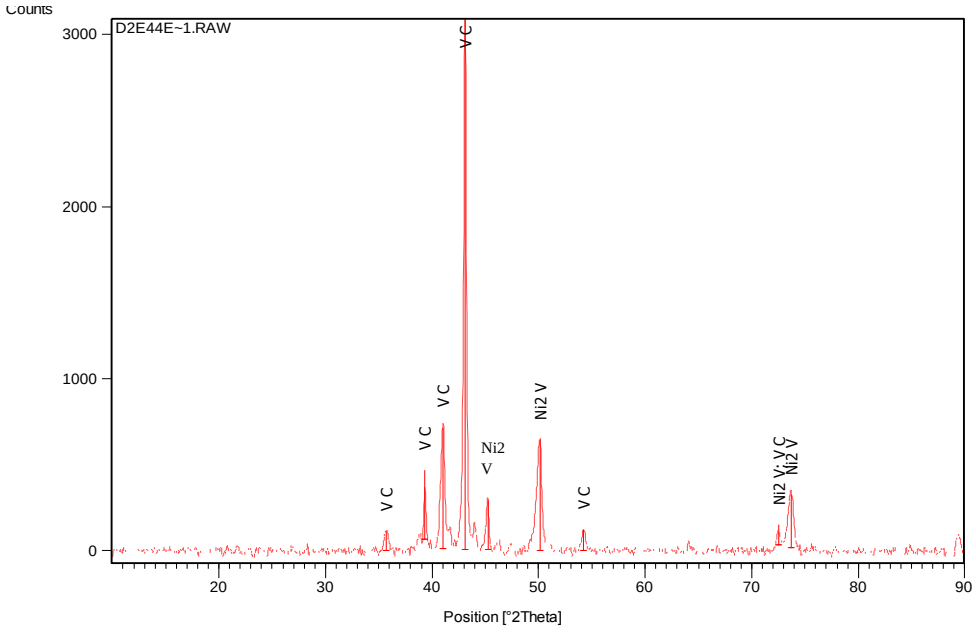


Figure 4.32. XRD pattern of as-cast nominal $Ni_{40}:V_{50}:C_{10}$ (at.%), Sample 4, showing all the identified peaks.

Table 4.9. XRD peaks for as-cast nominal $Ni_{40}:V_{50}:C_{10}$ (at.%), Sample 4.

Position 2θ (º)	Height (counts)	Relative Intensity. (%)	Phases
35.6951	115.00	3.73	VC
39.3353	405.53	13.15	VC
41.0596	701.00	22.73	VC
41.7049	133.87	4.34	$V_4C_{2.66}$
43.1012	3084.00	100.00	VC
43.9713	170.77	5.53	$V_4C_{2.66}$
45.2431	290.00	9.40	$V_4C_{2.66}$
46.3977	61.94	2.01	$V_4C_{2.66}$
47.5924	17.64	0.58	$V_4C_{2.66}$d
50.1244	649.00	21.04	Ni_2V
54.2204	125.00	4.05	VC
72.4937	122.58	3.97	VC, Ni_2V
73.7231	310.00	10.05	Ni_2V

4.1.5 Nominal $Ni_{53}:V_{37}:C_{10}$ (at.%), Sample 5

The nominal $Ni_{53}:V_{37}:C_{10}$ (at.%) alloy, Sample 5, possessed mainly dark dendrites identified as ~V_6C_5, as shown in Figure 4.33 at low magnification. Some pores were also identified in the microstructure. Figure 4.34 shows the microstructure of the alloy at higher magnification, showing the phases.

Table 4.10 gives the EDX analyses, and these are plotted in Figure 4.35. The overall composition was close to the tie-line joining the two phases, as was the eutectic composition. Also, the eutectic composition was seen to be close to the light phase, which is not surprising since it comprised mostly the light phase. Generally, there were small experimental errors for the phases. The EDX analyses of Sample 5 are shown in Appendix B5.

The solidification sequence deduced from the microstructure is as follows:

$$L \rightarrow \sim VC$$

$$L + \sim VC \rightarrow (Ni)$$

followed by a eutectic reactions: $L \rightarrow (Ni) + C(graphite)$

then ~VC → ~V_6C_5 in solid state

and (Ni) → ~Ni_2V in solid state.

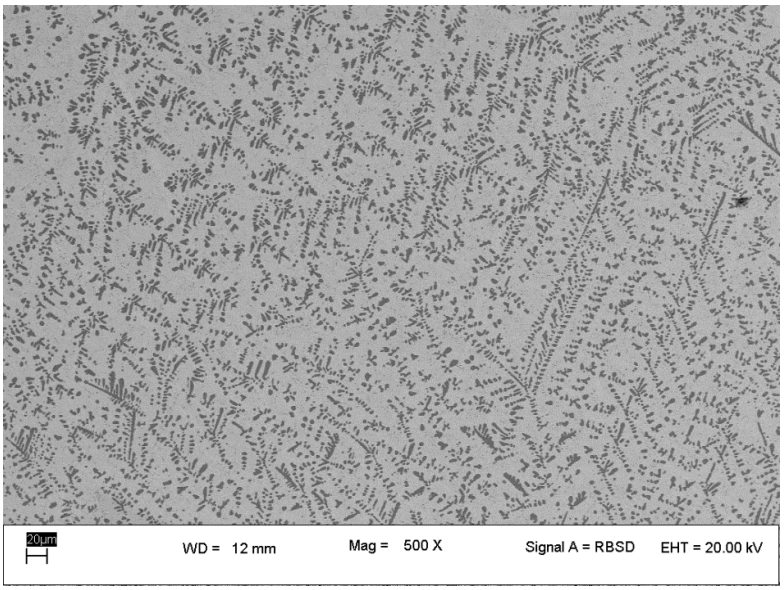


Figure 4.33. SEM-BSE image of nominal Ni_{53}:V_{37}:C_{10} (at.%), Sample 5, in the as-cast condition, showing ~V_6C_5 dendrites (dark) and ~Ni_2V matrix (light).

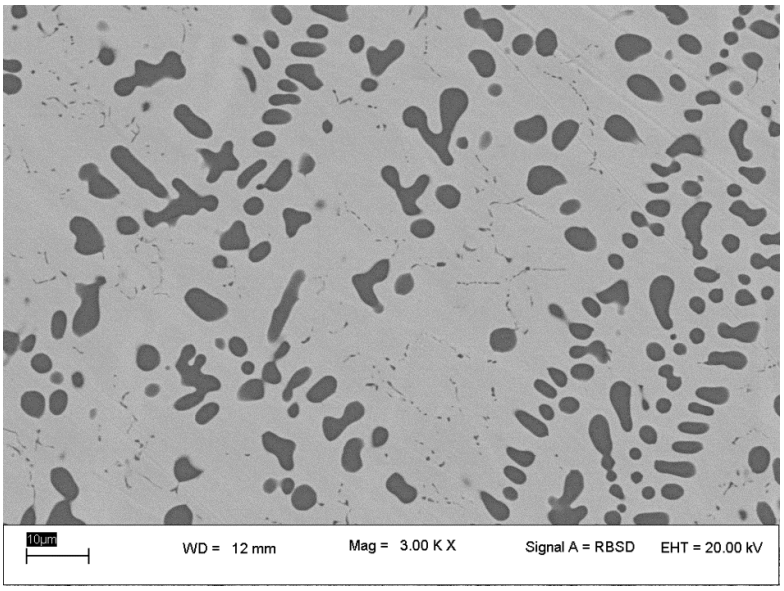


Figure 4.34. SEM-BSE image of nominal Ni_{53}:V_{37}:C_{10} (at.%), Sample 5, in the as-cast condition, showing ~V_6C_5 dendrites (dark) ~Ni_2V matrix (light) and eutectic at higher magnification.

Table 4.10. EDX phase composition of as-cast nominal $Ni_{53}:V_{37}:C_{10}$ (at.%), Sample 5.

Phase Description	C	V	Ni	Phase
Overall	22.4 ± 0.3	36.4 ± 0.3	41.2 ± 0.2	-
Dark	43.6 ± 0.2	55.5 ± 0.2	0.9 ± 0.02	~V_6C_5
Light	11.7 ± 0.6	27.0 ± 0.5	61.3 ± 0.8	~Ni_2V
Eutectic	13.8 ± 0.3	27.2 ± 0.1	59.0 ± 0.3	C + (Ni)

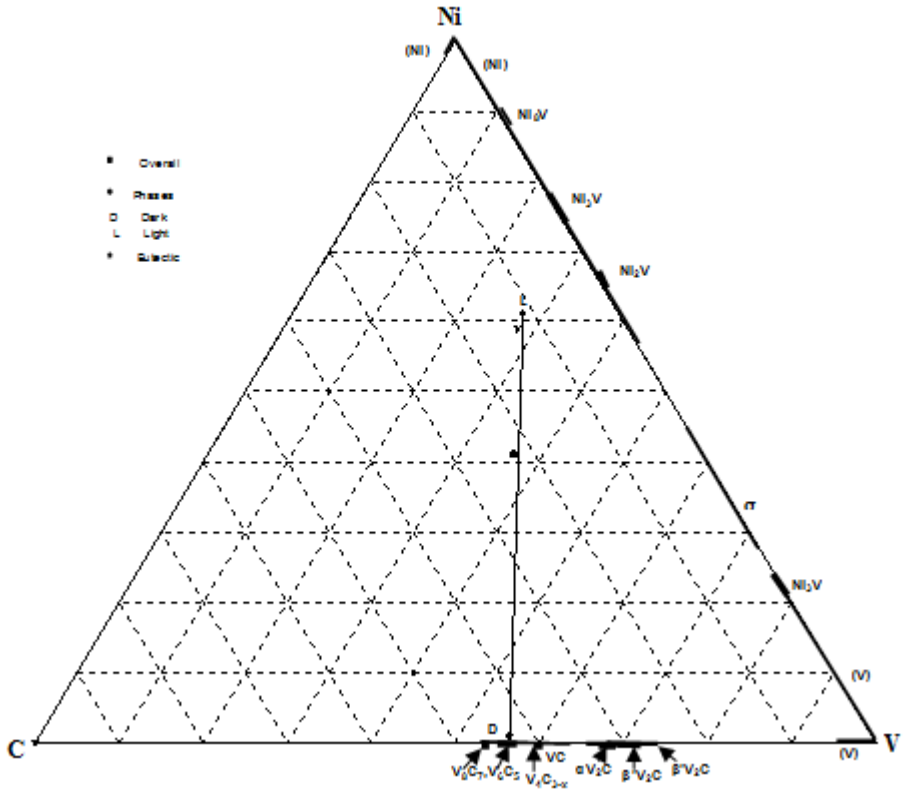


Figure 4.35 EDX analyses of as-cast nominal $Ni_{53}:V_{37}:C_{10}$ (at.%), Sample 5.

The XRD pattern, Figures 4.36 to 4.39, shows the experimental pattern of the Sample 5 with the fitted database lines. The pattern was poor with a high background:signal ratio, and very noisy, and some peaks might have not have been identified because they were lost in the background. The highest intensity peak was V_6C_5 at about $2\theta = 42.97^{o}$ (Figure 4.32). The

pattern confirmed the presence of ~V_6C_5 and ~Ni_2V (Figure 4.39) and there was no match for carbon but the peaks could have been lost in the background. Table 4.11 shows the identified peaks together with their phases.

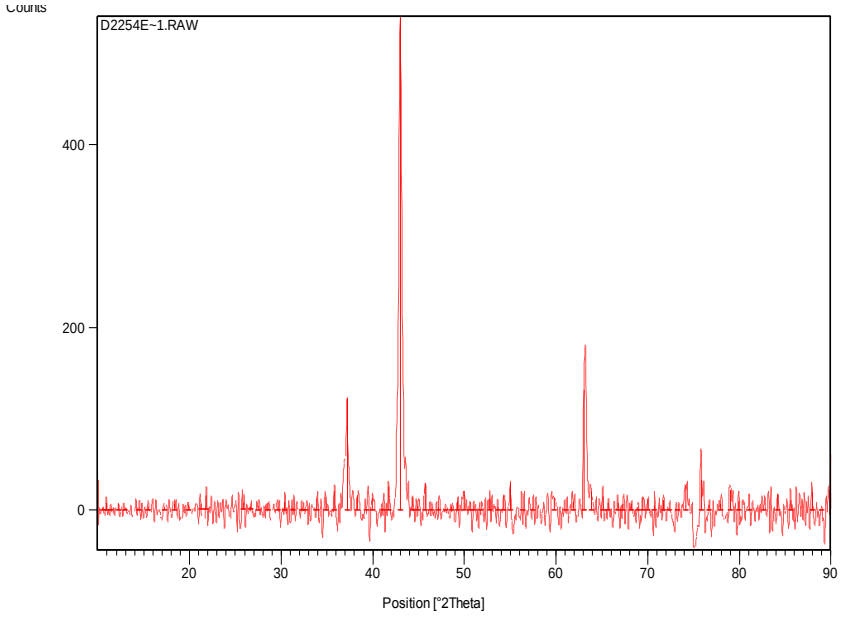


Figure 4.36 Unlabelled XRD pattern of as-cast nominal $Ni_{53}:V_{37}:C_{10}$ (at.%), Sample 5.

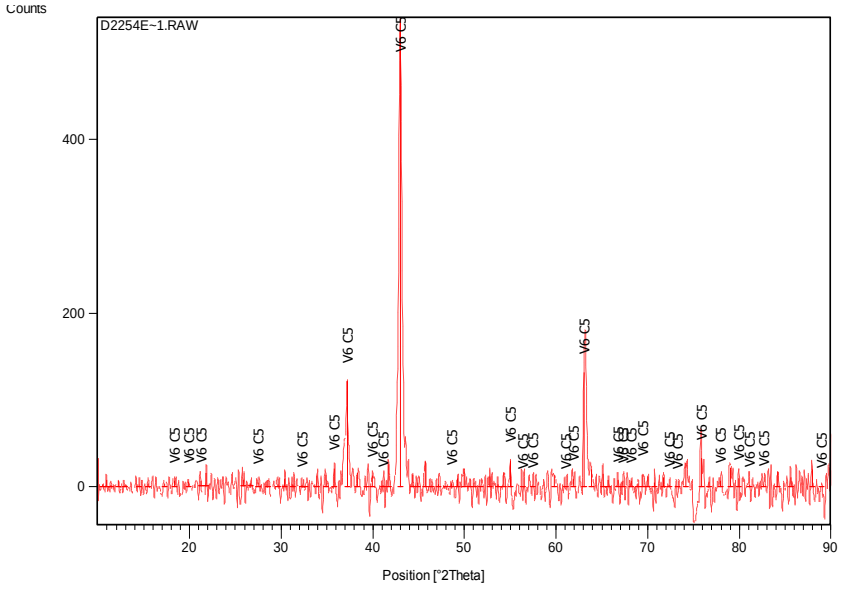


Figure 4.37 XRD pattern of as-cast nominal $Ni_{53}:V_{37}:C_{10}$ (at.%), Sample 5, showing identified V_6C_5 peaks.

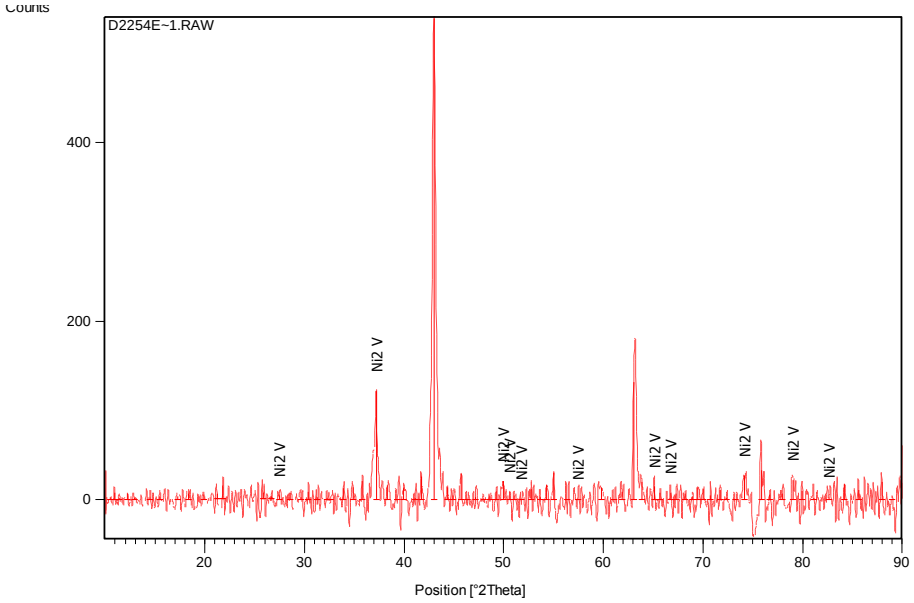


Figure 4.38 XRD pattern of as-cast nominal $Ni_{53}:V_{37}:C_{10}$ (at.%), Sample 5, showing identified Ni_2V peaks.

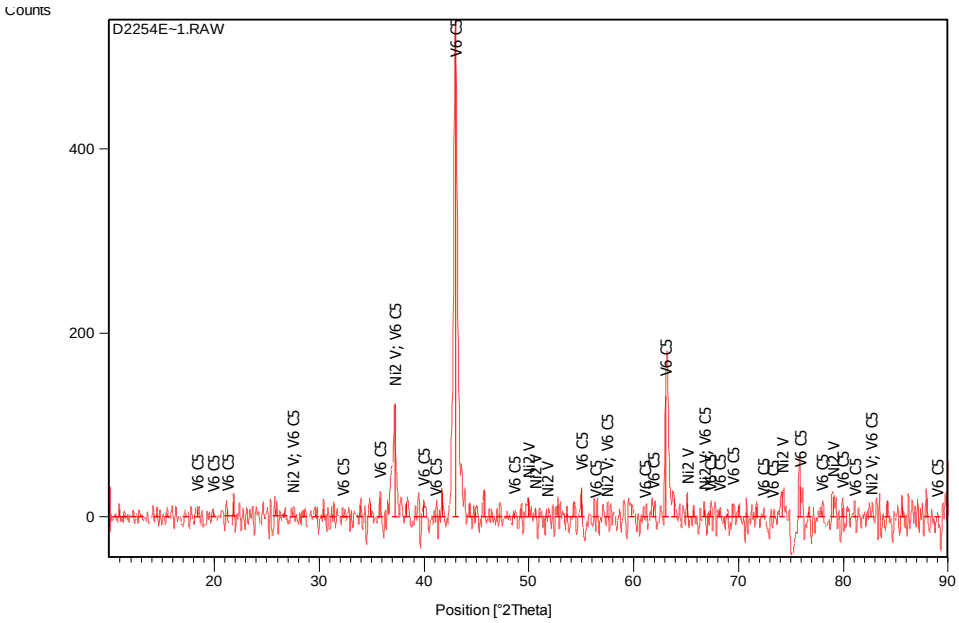


Figure 4.39 XRD pattern of as-cast nominal $Ni_{53}:V_{37}:C_{10}$ (at.%), Sample 5, showing all identified peaks.

Table 4.11. XRD peaks for as-cast nominal $Ni_{53}:V_{37}:C_{10}$ (at.%), Sample 5.

Position 2θ (°)	Height (counts)	Relative Intensity (%)	Phases
18.3247	7.46	1.38	V_6C_5
19.8817	6.53	1.21	V_6C_5
21.2166	6.26	1.16	V_6C_5
27.4596	4.98	0.92	V_6C_5, Ni_2V
32.2791	2.52	0.47	V_6C_5
35.8095	21.90	4.06	V_6C_5
37.1896	122.76	22.78	V_6C_5, Ni_2V
39.9140	13.62	2.53	V_6C_5
41.1186	2.73	0.51	V_6C_5
42.9712	538.95	100.00	V_6C_5
48.6392	4.16	0.77	V_6C_5
49.9417	21.12	3.92	Ni_2V
50.5631	9.20	1.71	Ni_2V
51.8006	1.10	0.20	Ni_2V
54.9943	30.54	5.67	V_6C_5
56.3828	0.26	0.05	V_6C_5
57.4463	1.44	0.27	V_6C_5, Ni_2V
61.0729	0.15	0.03	V_6C_5
61.8784	8.98	1.67	V_6C_5
63.0217	132.08	24.51	V_6C_5
65.1319	16.02	2.97	Ni_2V
66.7560	8.68	1.61	V_6C_5, Ni_2V
67.2808	7.45	1.38	V_6C_5
68.2032	7.12	1.32	V_6C_5
69.4714	14.60	2.71	V_6C_5
72.3256	2.50	0.46	V_6C_5
73.2368	0.01	0.00	V_6C_5
74.1871	27.35	5.08	Ni_2V
75.8990	33.41	6.20	V_6C_5
77.9562	7.30	1.35	V_6C_5
79.0583	22.48	4.17	Ni_2V
79.9118	10.44	1.94	V_6C_5
81.1465	2.82	0.52	V_6C_5
82.6329	3.86	0.72	V_6C_5, Ni_2V
88.9512	1.51	0.28	V_6C_5

4.1.6 Nominal $Ni_{64}:V_{25}:C_{11}$ (at.%), Sample 6

An SEM-BSE image representative of the centre and edge microstructures of nominal $Ni_{64}:V_{25}:C_{11}$ (at.%), Sample 6, in the as-cast condition is shown in Figure 4.40. The alloy had

apparently two phases. These were dendrites whose contrasts were dark, identified as ~V_8C_7 and the light regions (matrix) were identified as ~Ni_3V. The ~Ni_3V had different contrasts, depending on orientation. There were different eutectic colonies of dark and light phases surrounding dendrites. Figure 4.41 shows the microstructure of the alloy at higher magnification, with a noticeable edge effect around the dendrites.

The phase compositions are shown in Table 4.12 and plotted in Figure 4.42, showing the overall compositions to be deviated from the tie-line joining the two phases, but the eutectic was close to the light phase. The deviation may be due to unidentified phases which may be present in the microstructure. However, the standard deviation of the measurements was below 1 at.%. The EDX analyses of Sample 6 are also shown in Appendix B6.

The solidification sequence deduced from the microstructure is as follows:

$$L \rightarrow \sim VC$$

followed by $$L \rightarrow \sim VC + (Ni)$$

$$L \rightarrow (Ni) + C$$

then $$\sim VC \rightarrow \sim V_8C_7$$ in solid state.

and $$(Ni) \rightarrow \sim Ni_3V$$ in solid state.

There was also some solid state precipitation in the light phase, some of which was too fine to resolve properly.

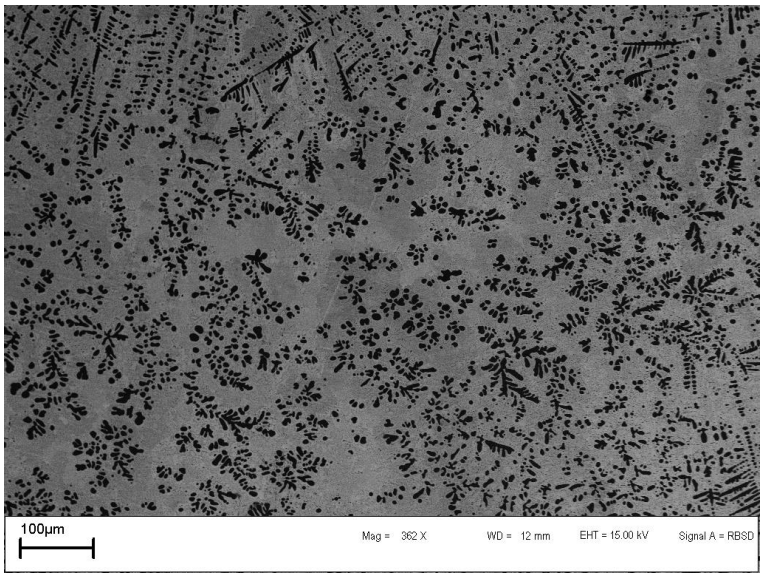


Figure 4.40. SEM-BSE image of nominal $Ni_{64}:V_{25}:C_{11}$ (at.%), Sample 6, showing ~V_8C_7 dendrites (dark), ~Ni_3V matrix (light) and eutectic.

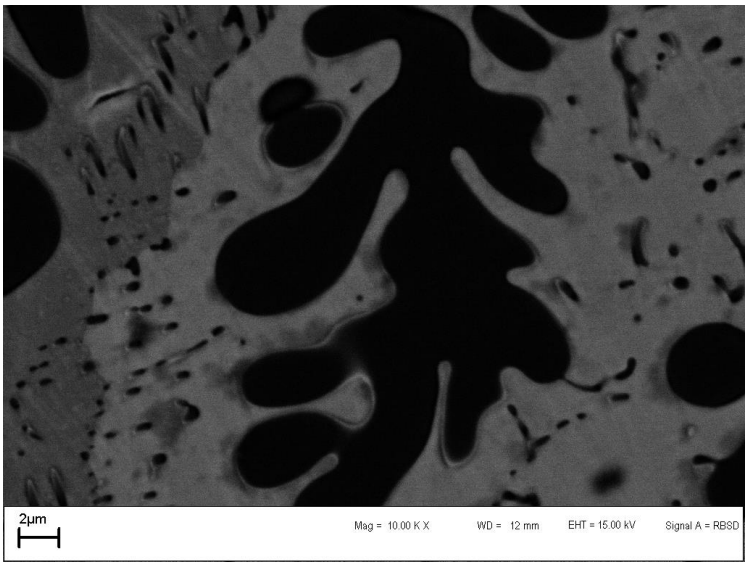


Figure 4.41. SEM-BSE image of nominal $Ni_{64}:V_{25}:C_{11}$ (at.%), Sample 6, showing ~V_8C_7 dendrites (dark), ~Ni_3V matrix (light) and eutectic with different colonies at higher magnification.

Table 4.12. EDX phase composition of as-cast nominal $Ni_{64}:V_{25}:C_{11}$ (at.%), Sample 6.

Phase Description	C	V	Ni	Phase
Overall	22.2 ± 0.3	26.0 ± 0.5	46.8 ± 0.3	-
Dark	46.6 ± 0.5	52.3 ± 0.8	1.1 ± 0.7	~V_8C_7
Light	14.3 ± 0.4	13.3 ± 0.3	72.4 ± 0.5	~Ni_3V
Eutectics	17.5 ± 0.5	16.1 ± 0.6	66.4 ± 0.2	~VC + (Ni) (Ni) + C

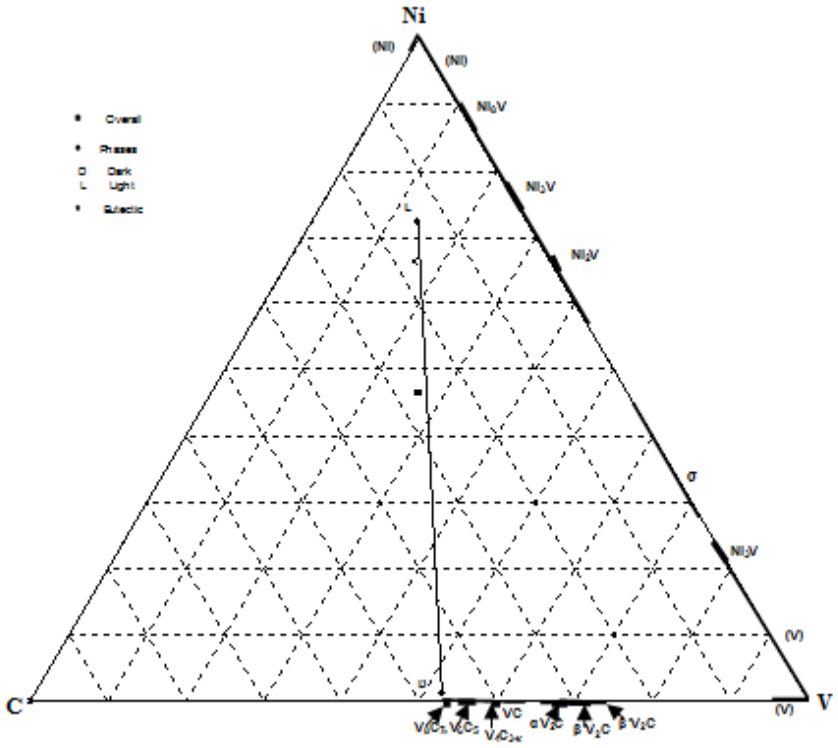


Figure 4.42. EDX analyses of as-cast nominal $Ni_{64}:V_{25}:C_{11}$ (at.%), Sample 6.

The XRD pattern shown in Figures 4.43 to 4.46 was good, with a high signal:background ratio. The existence of ~V_8C_7 and ~Ni_3V with the ICDD was confirmed by XRD, as shown in Figures 4.44 and 4.45 respectively. The matches for the ~Ni_3V phases were excellent. A major peak was found at position $2\theta = 44.18^{o}$, which matched ~Ni_3V. Carbon could not be

matched, but may have been in too small a proportion to be detected. Table 4.13 shows the identified peaks together with their phases.

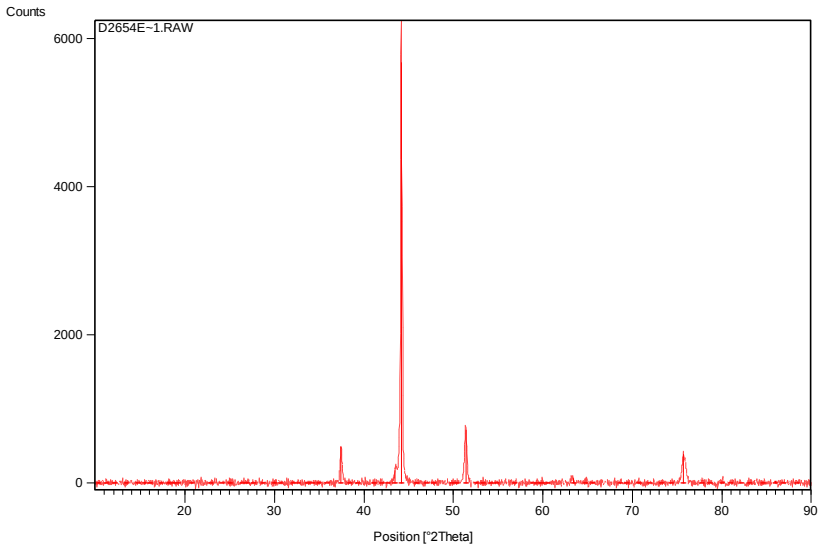


Figure 4.43. Unlabelled XRD pattern of as-cast nominal Ni_{64}:V_{25}:C_{11} (at.%), Sample 6.

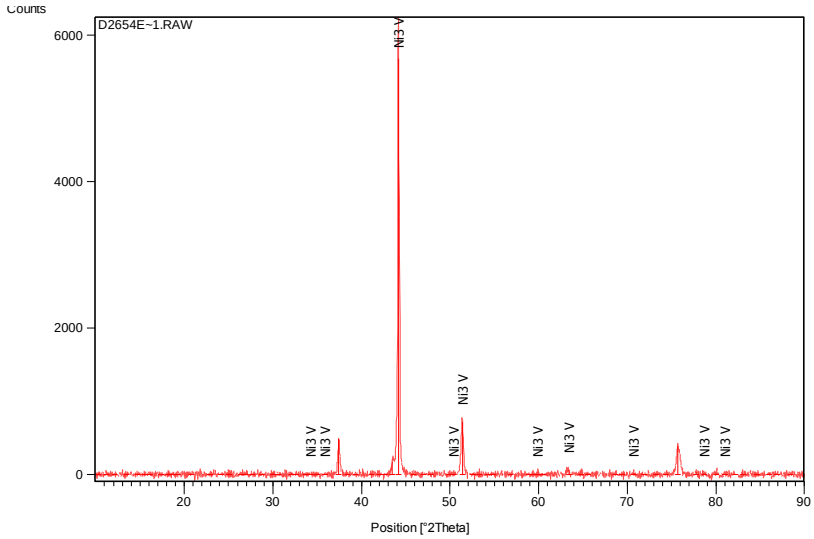


Figure 4.44. XRD pattern of as-cast nominal Ni_{64}:V_{25}:C_{11} (at.%), Sample 6, showing identified Ni_3V peaks.

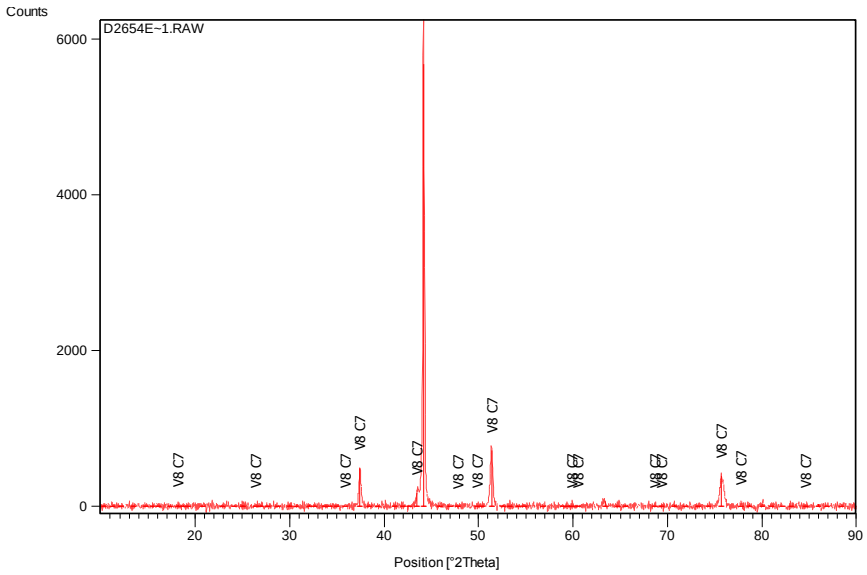


Figure 4.45. XRD pattern of as-cast nominal $Ni_{64}:V_{25}:C_{11}$ (at.%), Sample 6, showing identified V_8C_7 peaks.

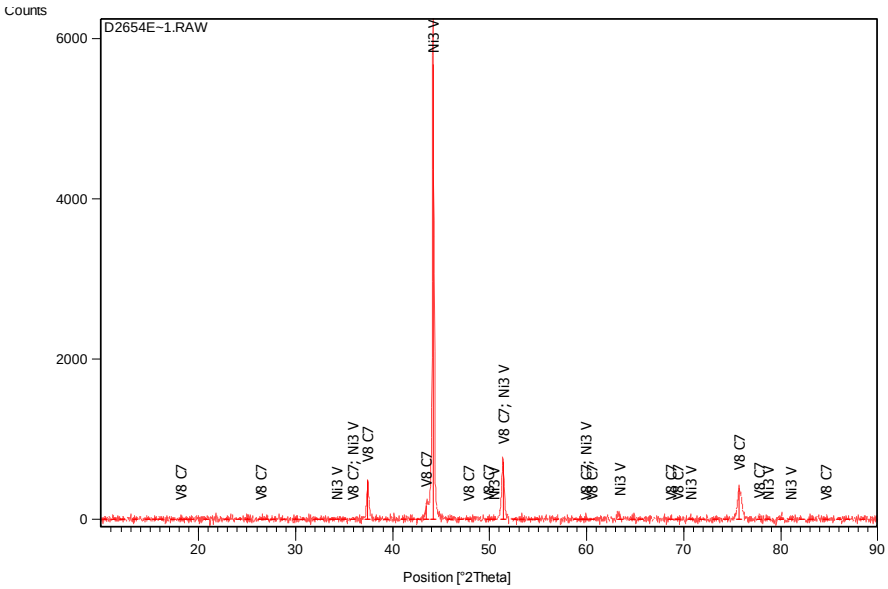


Figure 4.46. XRD pattern of as-cast nominal $Ni_{64}:V_{25}:C_{11}$ (at.%), Sample 6, showing all the identified peaks.

Table 4.13. XRD peaks for as-cast nominal $Ni_{64}:V_{25}:C_{11}$ (at.%), Sample 6.

Position 2θ (º)	Height (counts)	Relative Intensity (%)	Phases
18.2015	14.77	0.26	V_8C_7
26.4149	7.42	0.13	V_8C_7
34.2817	4.28	0.08	Ni_3V
35.8371	12.57	0.22	V_8C_7, Ni_3V
37.4551	484.12	8.52	V_8C_7
43.4670	173.71	3.06	V_8C_7
44.1893	5680.67	100.00	Ni_3V
47.7571	1.46	0.03	V_8C_7
49.8677	8.35	0.15	V_8C_7
50.4606	9.61	0.17	Ni_3V
51.3771	713.16	12.55	V_8C_7, Ni_3V
59.9349	6.28	0.11	V_8C_7, Ni_3V
60.5654	5.98	0.11	V_8C_7
63.3905	61.88	1.09	Ni_3V
68.6236	10.38	0.18	V_8C_7
69.3768	0.66	0.01	V_8C_7
70.7045	13.06	0.23	Ni_3V
75.6572	387.67	6.82	V_8C_7
77.7992	37.50	0.66	V_8C_7
78.6550	14.62	0.26	Ni_3V
81.0580	11.04	0.19	Ni_3V
84.6390	5.13	0.09	V_8C_7

4.1.7 Nominal $Ni_{70}:V_{10}:C_{20}$ (at.%), Sample 7

SEM-BSE images of nominal $Ni_{70}:V_{10}:C_{20}$ (at.%) in the as-cast condition are shown in Figures 4.47 and 4.48, taken at different areas of the sample. Figure 4.47 shows the microstructure at low magnification. The alloy consisted of graphite plates (very dark) which were randomly distributed, ~V_7C_8 dendrites that originally had round interfaces, then ended with a facetted morphology (dark) which formed on the dendrites, coarse blocky ~V_7C_8 in one of the eutectics, including the matrix with light contrast, which was identified as (Ni). At higher magnifications (Figure 4.48), the dendrites sometimes appeared facetted.

The phase compositions are shown in Table 4.14, and were plotted in Figure 4.49, showing the overall composition to lie within the tie-triangle of the phases. The overall composition was very different from the nominal composition in that the nickel and carbon composition

appeared to be swapped. Even if the system was over-reporting carbon, the phase results are sensible. At higher magnification (Figure 4.48), the eutectic was clearly seen, sometimes more globular (~VC + (Ni)) and sometimes with flakes ((Ni) + C). However, the standard deviation of the measurements was below 1 at.%. The EDX analyses of Sample 7 are shown in Appendix B7.

The structure was formed by: $L \rightarrow C$ (graphite)

followed by $L + C \rightarrow \sim VC$

and $L \rightarrow \sim VC + (Ni)$

$L \rightarrow C + (Ni)$

then $\sim VC \rightarrow \sim V_8C_7$ in solid state

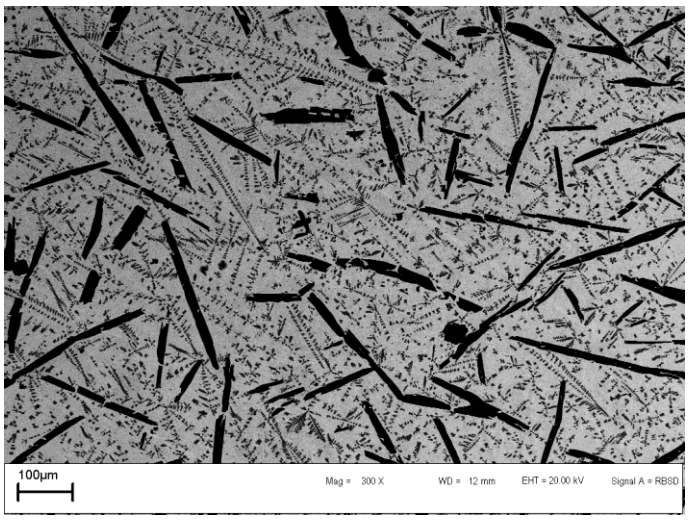


Figure 4.47. SEM-BSE image of nominal Ni_{70}:V_{10}:C_{20} (at.%), Sample 7, in the as-cast condition, showing graphite plates (very dark), ~V_8C_7 dendrites (dark) and (Ni) matrix (light).

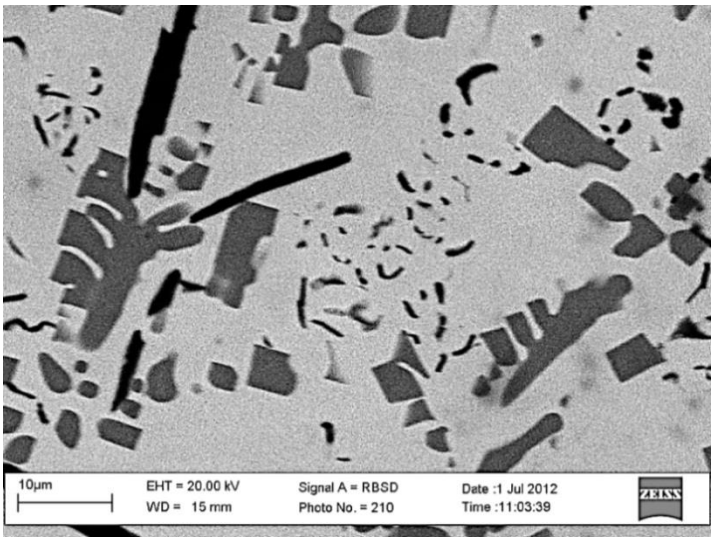


Figure 4.48. SEM-BSE image of nominal Ni_{70}:V_{10}:C_{20} (at.%), Sample 7, in the as-cast condition, showing graphite plates (very dark), ~V_8C_7 dendrites (dark), (Ni) matrix (light) and eutectic at higher magnification.

Table 4.14. EDX phase composition of as-cast nominal Ni_{70}:V_{10}:C_{20} (at.%), Sample 7.

Phase Description	C	V	Ni	Phase
Overall	73.6 ± 0.4	4.1 ± 0.2	22.3 ± 0.3	-
Needles	99.7 ± 0.1	0.02 ± 0.1	0.3 ± 0.1	Graphite
Dendrites	47.8 ± 0.4	49.1 ± 1.3	3.1 ± 1.7	~V_8C_7
Light	22.5 ± 1.3	2.0 ± 0.1	75.5 ± 1.2	(Ni)
Eutectics	70.4 ± 0.8	4.8 ± 0.1	25.0 ± 0.7	~VC + (Ni) C + (Ni)

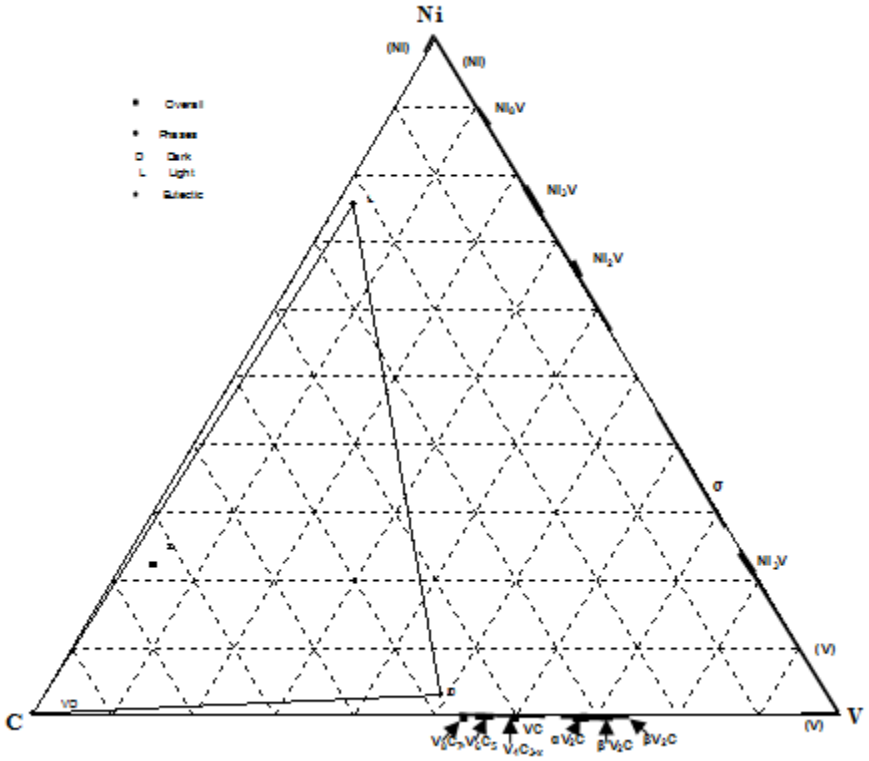


Figure 4.49. EDX analyses of nominal $Ni_{70}:V_{10}:C_{20}$ (at.%), Sample 7, in the as-cast condition.

Figures 4.50 to 4.54 show the experimental pattern of the sample with the database lines for each of the phases. The XRD pattern (Figure 4.54) confirmed the presence of ~V_8C_7, graphite and (Ni). The highest intensity peak at about 2θ = 46° shows that the peak is a probably a combination of C and (Ni). All peaks could be matched, except one at 2θ = 29°. Table 4.15 shows the identified peaks together with their phases.

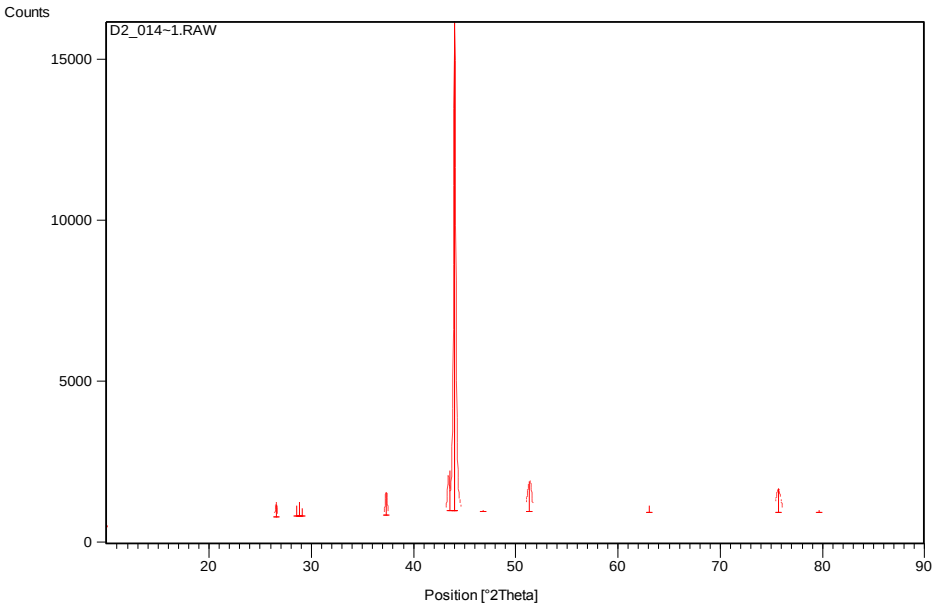


Figure 4.50. Unlabelled XRD pattern of as-cast nominal $Ni_{70}:V_{10}:C_{20}$ (at.%), Sample 7.

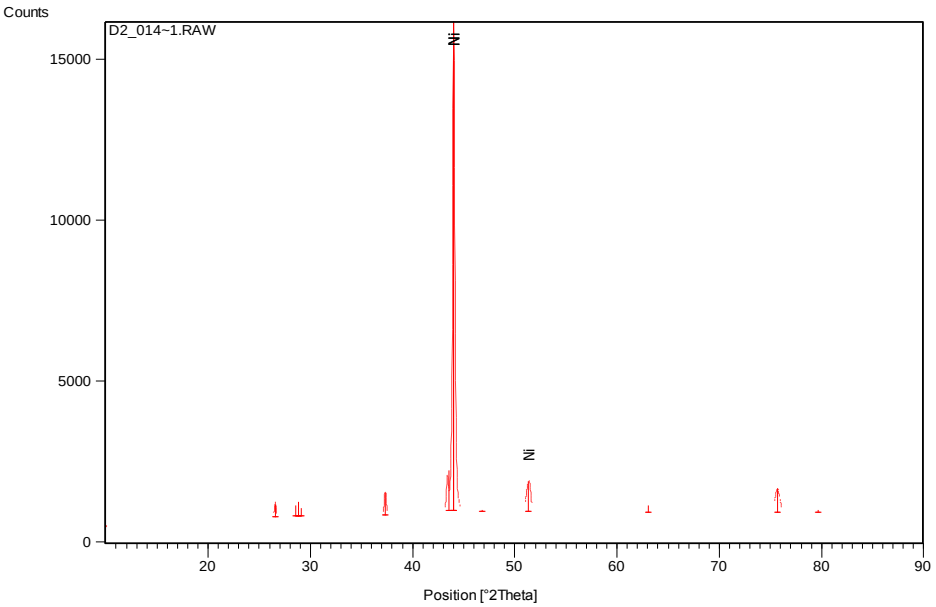


Figure 4.51. XRD pattern of as-cast nominal $Ni_{70}:V_{10}:C_{20}$ (at.%), Sample 7, showing (Ni) peaks.

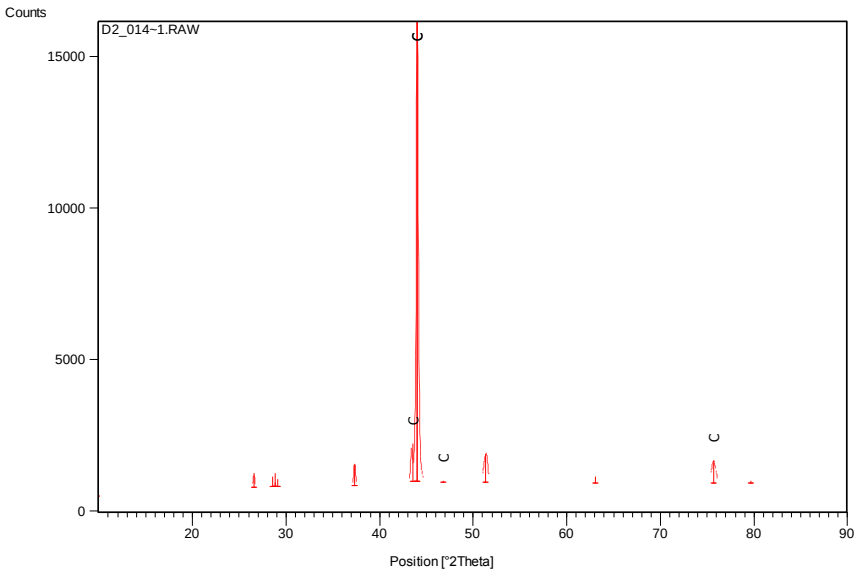


Figure 4.52. XRD pattern of as-cast nominal $Ni_{70}:V_{10}:C_{20}$ (at.%), Sample 7, showing C peaks.

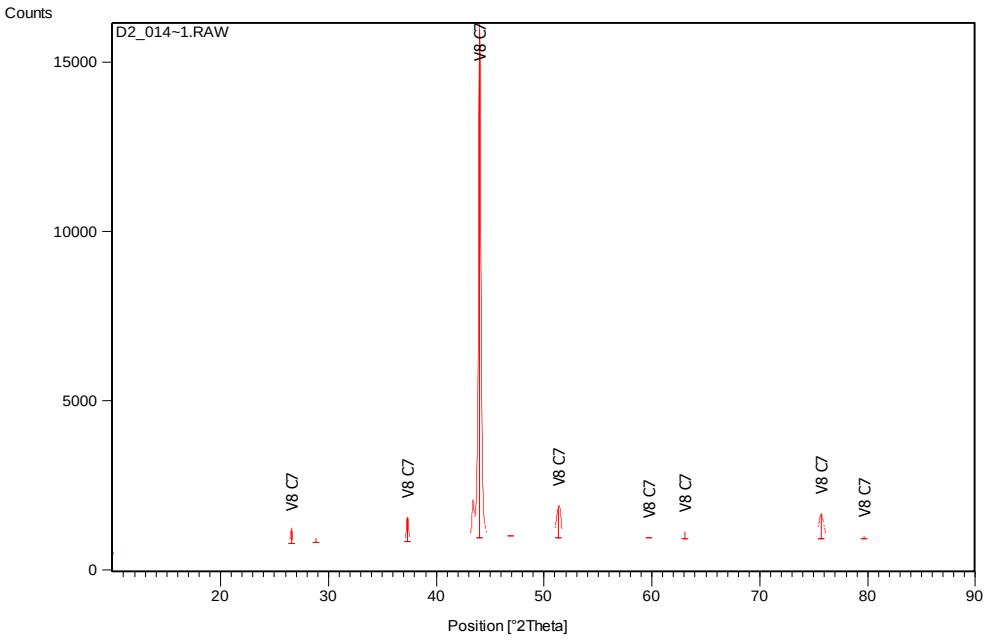


Figure 4.53. XRD pattern of as-cast nominal $Ni_{70}:V_{10}:C_{20}$ (at.%), Sample 7, showing ~V_7C_8 peaks.

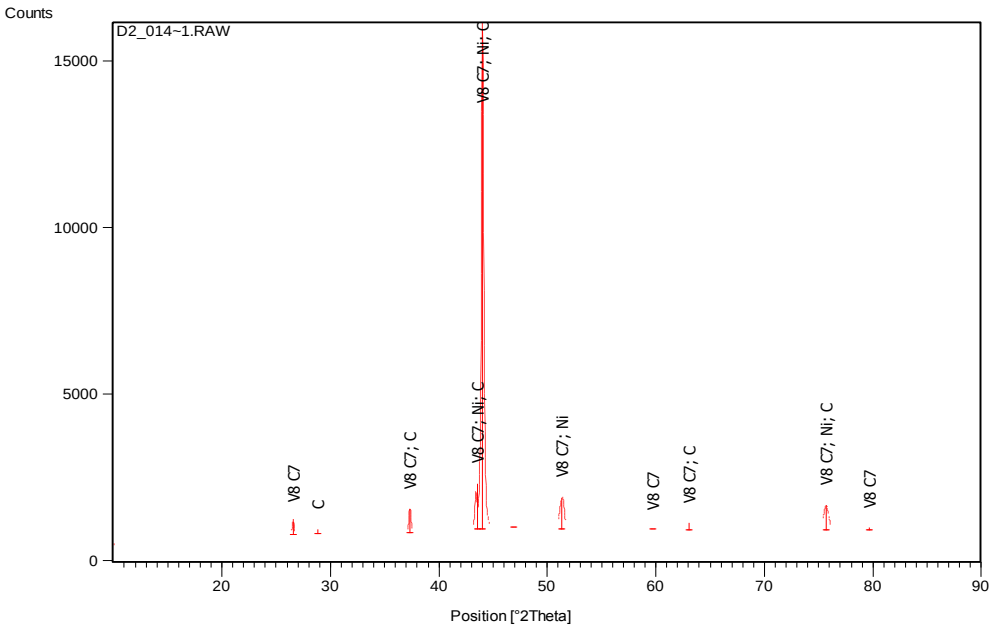


Figure 4.54. XRD pattern of as-cast nominal $Ni_{70}:V_{10}:C_{20}$ (at.%), Sample 7, showing all identified phases.

Table 4.15. XRD peaks for as-cast nominal $Ni_{70}:V_{10}:C_{20}$ (at.%), Sample 7.

Position 2θ (º)	Height (counts)	Relative Intensity. (%)	Phases
26.5575	383.46	1.90	V_8C_7
29.1419	270.40	1.34	Unidentified
37.3283	675.20	3.34	V_8C_7
43.5940	1259.40	6.23	C
44.0249	20210.91	100.00	Ni, C
44.0275	15189.76	75.16	V_8C_7, C
46.8149	65.05	0.32	C
51.3554	971.56	4.81	V_8C_7, Ni
63.0282	227.77	1.13	V_8C_7
75.6669	751.90	3.72	V_8C_7, C
79.6859	86.99	0.43	V_8C_7

4.1.8 Nominal $Ni_{60}:V_{30}:C_{10}$ (at.%), Sample 8

An SEM-BSE image representative of the centre and edge microstructures of nominal $Ni_{60}:V_{30}:C_{10}$ (at.%), Sample 8 in the as-cast condition is shown in Figure 4.55. The alloy had

apparently two contrasts. These were dark dendrites which were cracked, identified as ~V_8C_7, and the light regions (matrix) were identified as ~Ni_2V. There was a eutectic of dark and light phases surrounding the dendrites, and the (Ni) surrounding the dendrites was probably due to fast cooling [2009Xia]. Some pores were also identified in the microstructure. Figure 4.56 shows the microstructure of the alloy at higher magnification, showing that some of the dendrites had (Ni) around them. The eutectic had two different morphologies: globular and more flake-like.

The phase compositions are shown in Table 4.16 and plotted in Figure 4.57, showing the overall compositions to be deviated from the tie-line, but the eutectic overall was on the tie-line. The deviation may be due to some graphite which may be present in the microstructure, and would push the overall analyses nearer to carbon. The analyses over-reported C, which was very noticeable for ~V_8C_7, because the result had about ~4 at.% more C than reported in the binary [1985Car]. However, the standard deviation of the measurements was below 1 at.%. The EDX analyses of Sample 8 are shown in Appendix B8.

The deduced solidification sequence is:	$L \rightarrow$ ~VC
followed by a eutectic reaction	$L \rightarrow$ ~VC + (Ni) (globular)
	$L \rightarrow C$ + (Ni) (flake-like)
and	~VC $\rightarrow$ ~V_8C_7 in the solid state (~1050°C for binary [1985Car])
then	(Ni) $\rightarrow$ ~Ni_2V in the solid state (922°C for binary [1982Sim]).

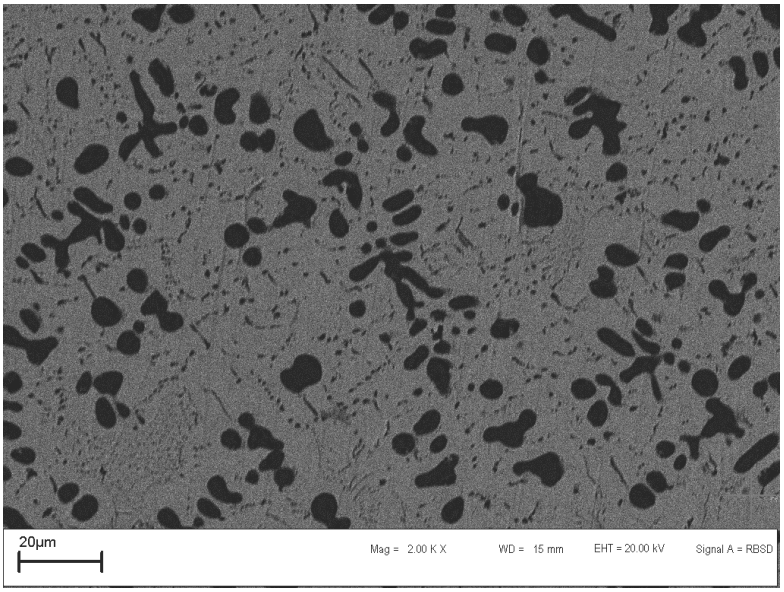


Figure 4.55. SEM-BSE image of nominal Ni_{60}:V_{30}:C_{10} (at.%), Sample 8, in the as-cast condition, showing ~V_8C_7 dendrites (dark), ~Ni_2V matrix (light) and eutectic.

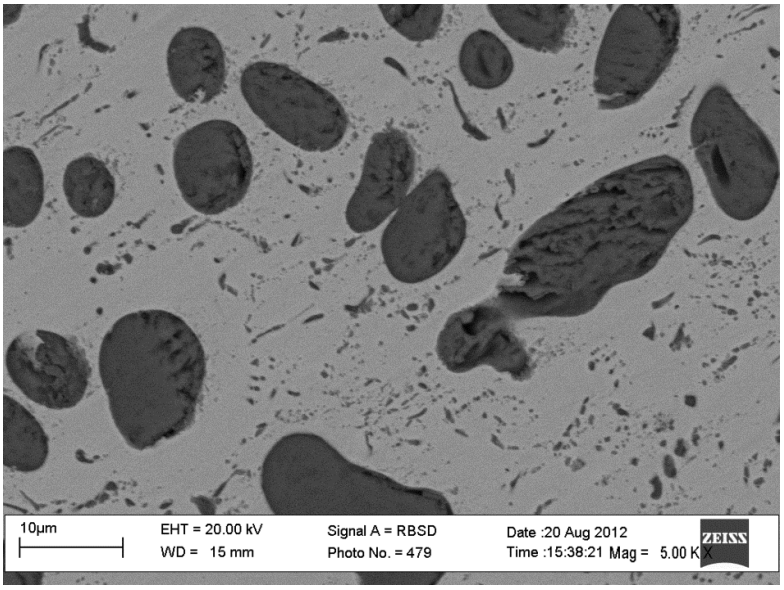


Figure 4.56. SEM-BSE image of nominal Ni_{60}:V_{30}:C_{10} (at.%), Sample 8, in the as-cast condition, showing ~V_8C_7 dendrites (dark) with cracks, ~Ni_2V matrix (light) and eutectic at higher magnification.

Table 4.16. EDX phase composition of as-cast nominal $Ni_{60}:V_{30}:C_{10}$ (at.%), Sample 8.

Phase Description	C	V	Ni	Phase
Overall	29.8 ± 0.8	26.5 ± 0.4	43.7 ± 0.5	-
Dark	48.6 ± 0.4	50.4 ± 0.4	1.0 ± 0.1	~V_8C_7
Light	18.7 ± 0.4	21.2 ± 0.4	60.1 ± 0.4	(Ni)
Eutectics	25.7 ± 0.5	28.5 ± 0.2	45.8 ± 0.6	~VC + (Ni) (Ni) + C

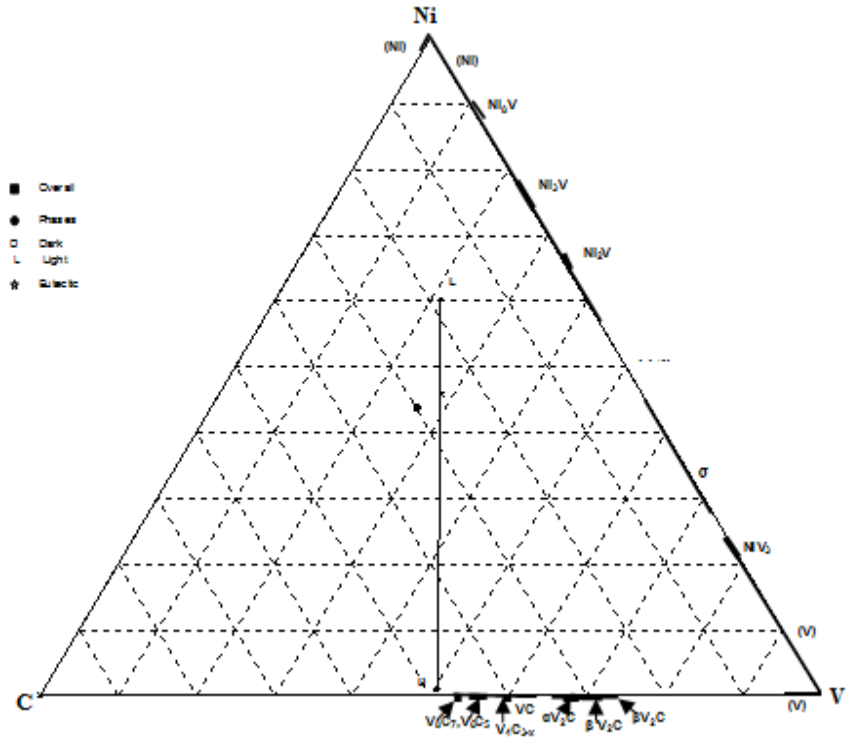


Figure 4.57. EDX analyses of as-cast nominal $Ni_{60}:V_{30}:C_{10}$ (at.%), Sample 8.

The XRD pattern, Figures 4.58 to 4.62, shows the experimental pattern of the sample with the database lines for each of the phases. The patterns had overlapping peaks of the different phases. The highest intensity peaks were ~V_8C_7, C and ~Ni_2V at about $2\theta = 43.95^{o}$. Figure

4.62 confirmed the presence of ~V_8C_7, C and ~Ni_2V. Table 4.17 shows the identified peaks together with their phases.

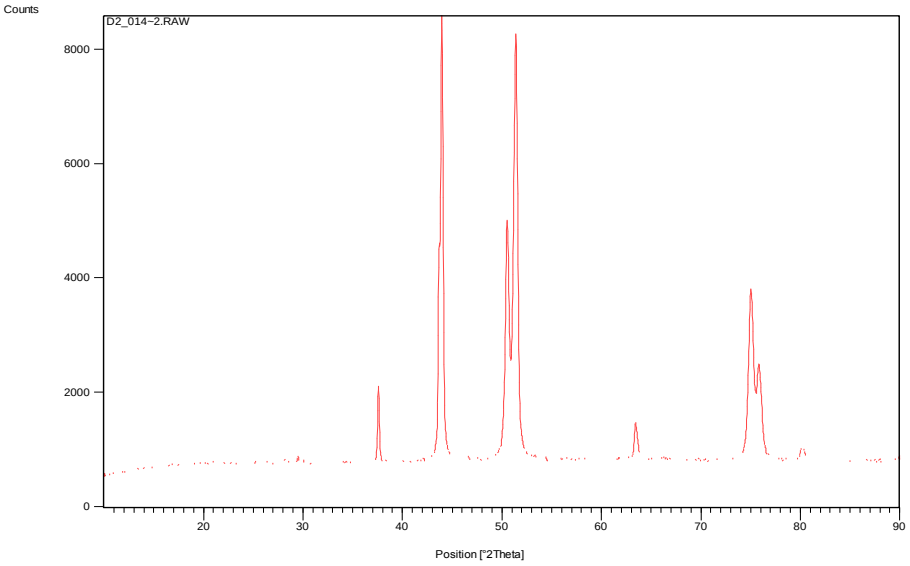


Figure 4.58. Unlabelled XRD pattern of as-cast nominal Ni_{60}:V_{30}:C_{10} (at.%), Sample 8.

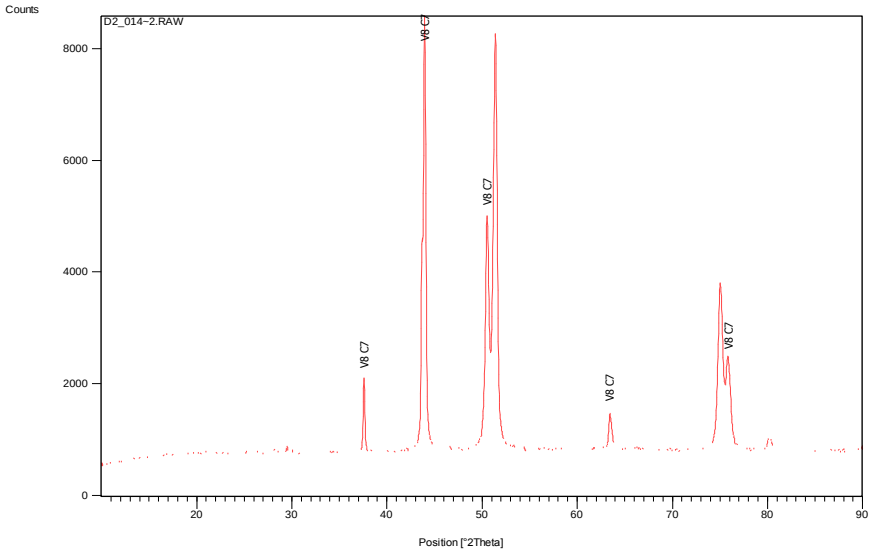


Figure 4.59. XRD pattern of as-cast nominal Ni_{60}:V_{30}:C_{10} (at.%), Sample 8, showing identified ~V_8C_7 peaks.

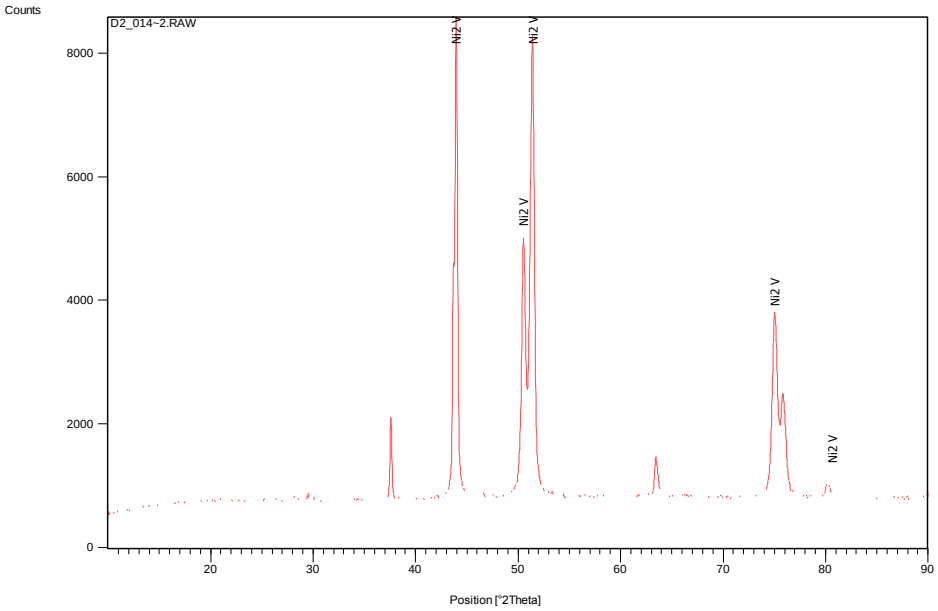


Figure 4.60. XRD pattern of as-cast nominal $Ni_{60}:V_{30}:C_{10}$ (at.%), Sample 8, showing identified ~Ni_2V peaks.

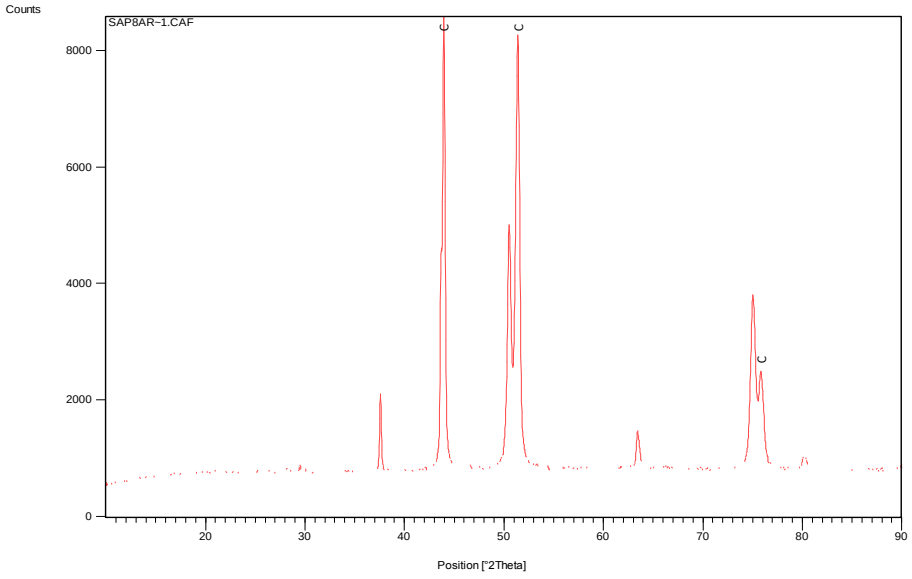


Figure 4.61. XRD pattern of as-cast nominal $Ni_{60}:V_{30}:C_{10}$ (at.%), Sample 8, showing identified C peaks.

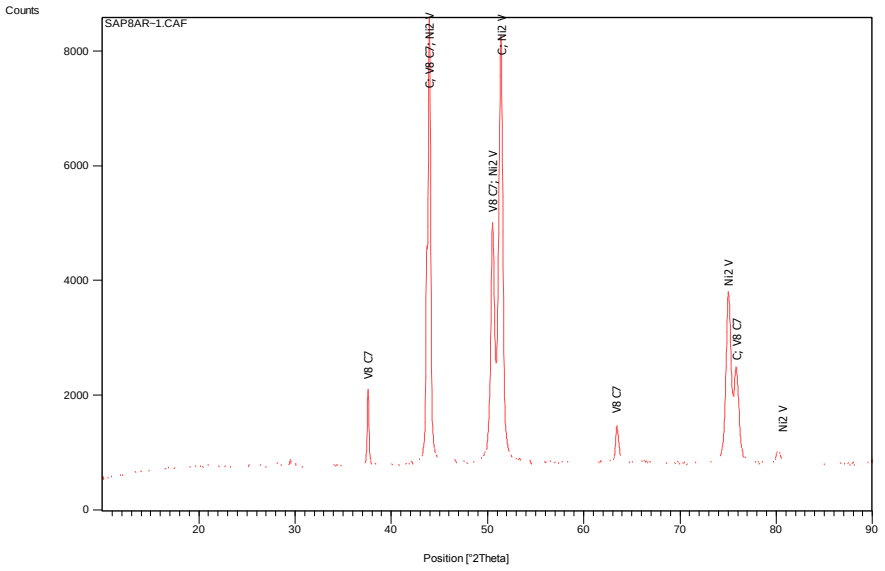


Figure 4.62. XRD pattern of as-cast nominal $Ni_{60}:V_{30}:C_{10}$ (at.%), Sample 8, showing all identified phases.

Table 4.17. XRD peaks for as-cast nominal $Ni_{60}:V_{30}:C_{10}$ (at.%), Sample 8.

Position 2θ (º)	Height (counts)	Relative Intensity (%)	Phases
37.5640	1286.00	16.45	V_8C_7
43.9542	7816.00	100.00	V_8C_7, Ni_2V, C
50.5214	4185.00	53.54	Ni_2V
51.4299	7443.00	95.23	Ni_2V, C
63.4114	672.00	8.60	V_8C_7
74.9856	2886.00	36.92	Ni_2V
75.9029	1598.00	20.45	V_8C_7, C
80.6364	328.40	4.20	Ni_2V

4.1.9 Nominal $Ni_{30}:V_{65}:C_5$ (at.%), Sample 9

The microstructure of nominal $Ni_{30}:V_{65}:C_5$ (at.%), Sample 9, showed dark dendrites and a eutectic with lighter regions (Figure 4.63). The microstructure of Sample 9 had more of the eutectic phase compared to other samples. At higher magnification (Figure 4.64), the eutectic shows two different morphologies; fine and coarse. Also, there were some pores identified in the microstructure.

Table 4.18 gives the EDX analyses, and these were plotted in Figure 4.65. The overall composition was off the tie-line between two phases, this may be due to an unidentified phase, which would be richer in Ni, possibly (Ni) or ~Ni_2V. The coarse and fine eutectic regions had the same compositions. This shows that the eutectic solidified with a slight range of compositions. Also, the eutectic was close to the overall composition, which is not surprising, since it comprised most of the sample. Generally, there were small experimental errors for the phases. The EDX analyses of Sample 12 are shown in Appendix B9.

The solidification sequence deduced from the microstructure is as follows:

$$L \rightarrow \sim VC$$

followed by the eutectic: $L \rightarrow \sim VC + \sigma'$.



Figure 4.63. SEM-BSE image of nominal Ni_{30}:V_{65}:C_5 (at.%), Sample 9, in the as-cast condition, showing ~VC dendrites (dark), σ′ matrix (light) and eutectic.

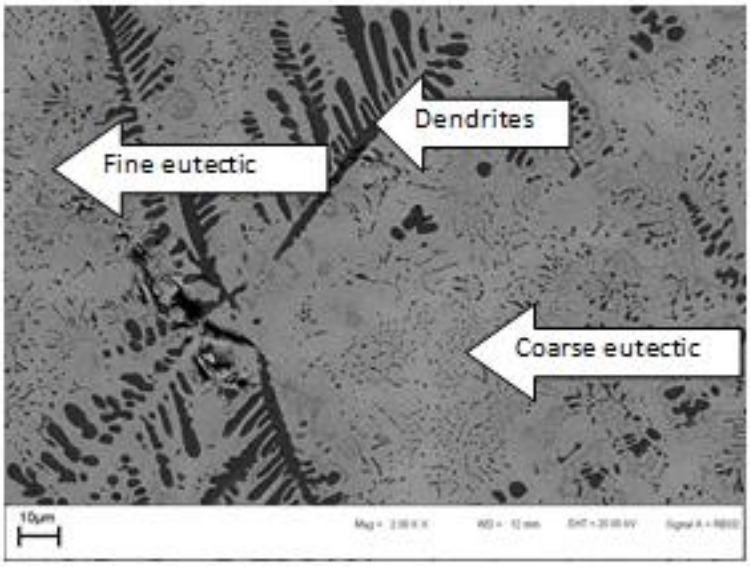


Figure 4.64. SEM-BSE image of nominal $Ni_{30}:V_{65}:C_5$ (at.%), Sample 9 in the as-cast condition, showing primary ~VC dendrites (dark), σ′ matrix (light) and eutectic at higher magnification.

Table 4.18. EDX phase analyses of as-cast nominal $Ni_{30}:V_{65}:C_5$ (at.%), Sample 9.

Phase Description	C	V	Ni	Phase
Overall	17.9 ± 0.4	57.4 ± 0.3	24.7 ± 0.2	-
Dark	35.1 ± 0.7	64.0 ± 0.6	0.9 ± 0.3	~VC
Light	10.4 ± 0.2	59.8 ± 0.7	29.8 ± 0.7	σ′
Fine eutectic	17.4 ± 0.2	58.6 ± 0.2	24.0 ± 0.4	~VC + σ′
Coarse eutectic	17.9 ± 0.1	58.5 ± 0.4	23.6 ± 0.4	~VC + σ′

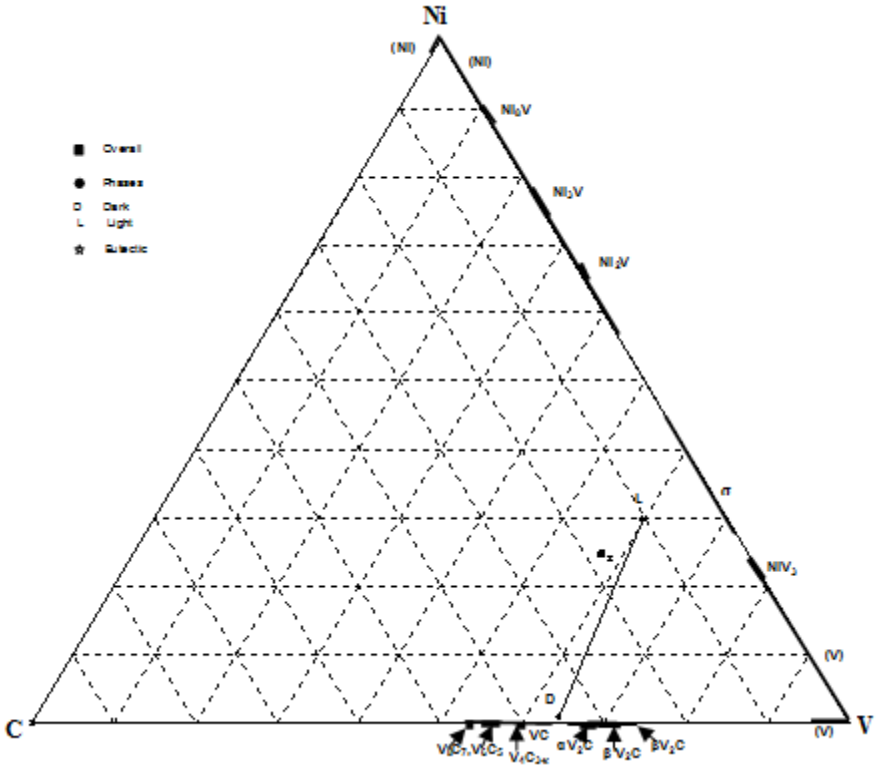


Figure 4.65. EDX analyses of as-cast nominal Ni_{30}:V_{65}:C_5 (at.%), Sample 9.

The XRD pattern shown in Figures 4.66 to 4.69 was fair, with a reasonable signal:background ratio, but having few sharp peaks. The presence of ~VC and perhaps ~$V_4C_{2.66}$ (which might not be present since it forms at lower temperatures in the solid state, and was not obvious in the microstructure) was indicated as shown in Figure 4.69. There were several unidentified peaks shown in Table 4.18 and none of Ni, Ni_2V or C could be matched. When the Ni-V system [1982Smi] was consulted, the identified peaks were assumed to be from σ′ (sigma) phase, which was not included in the International Crystallography Diffraction Database (ICDD) [2001ICD] and is likely to be complicated with many peaks. Table 4.19 shows the identified peaks together with their phases.

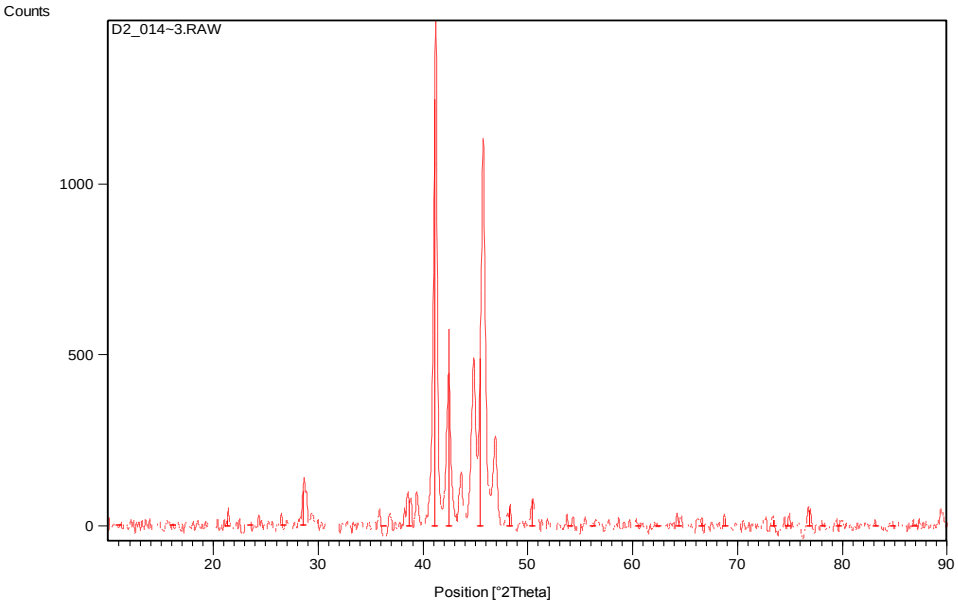


Figure 4.66. Unlabelled XRD pattern of as-cast nominal Ni_{30}:V_{65}:C_5 (at.%), Sample 9.

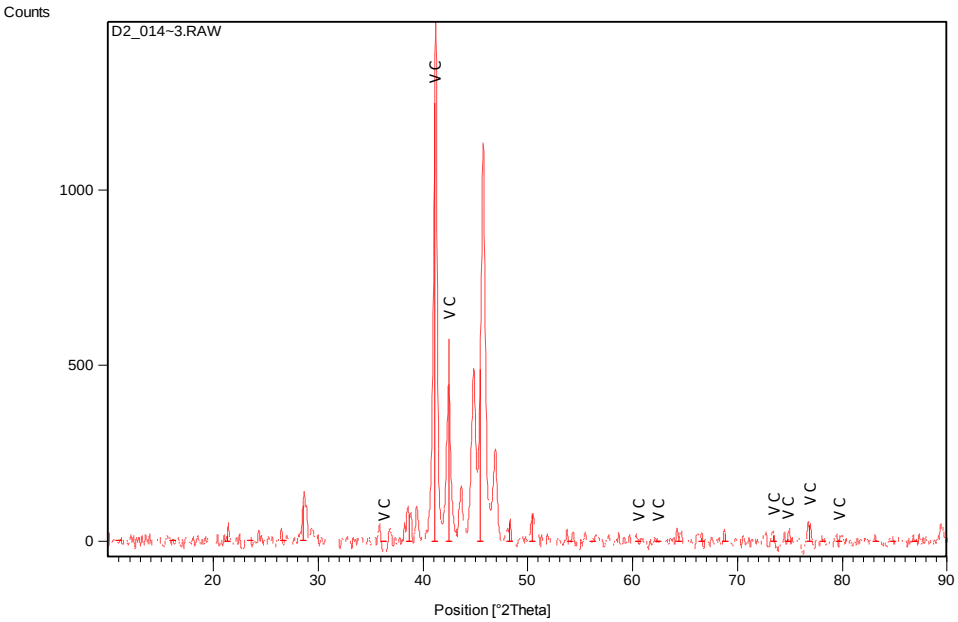


Figure 4.67. XRD pattern of nominal Ni_{30}:V_{65}:C_5 (at.%), Sample 9, in the as-cast condition, showing identified ~VC peaks.

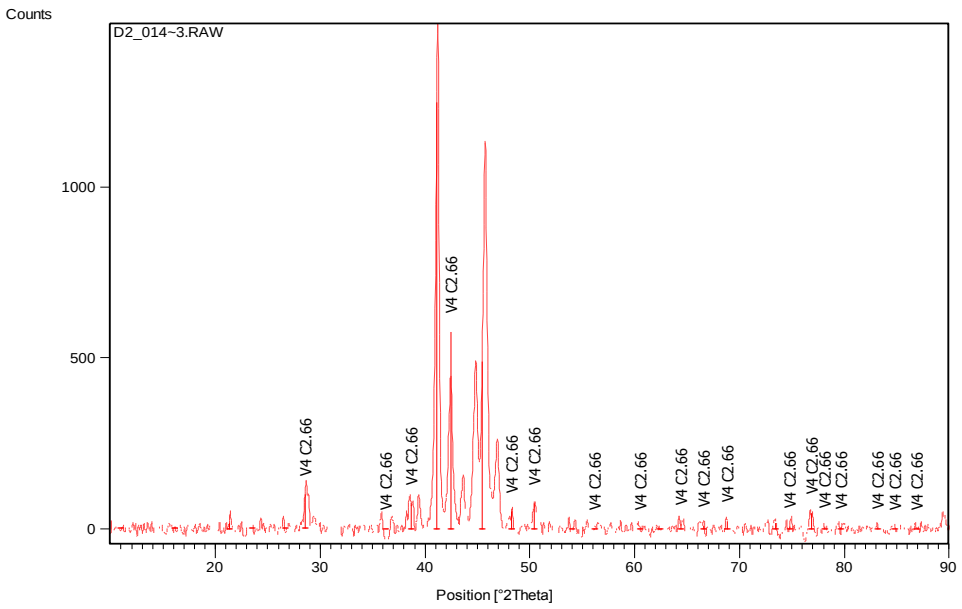


Figure 4.68. XRD pattern of nominal Ni_{30}:V_{65}:C_5 (at.%), Sample 9, in the as-cast condition, showing identified ~$V_4C_{2.66}$ peaks.

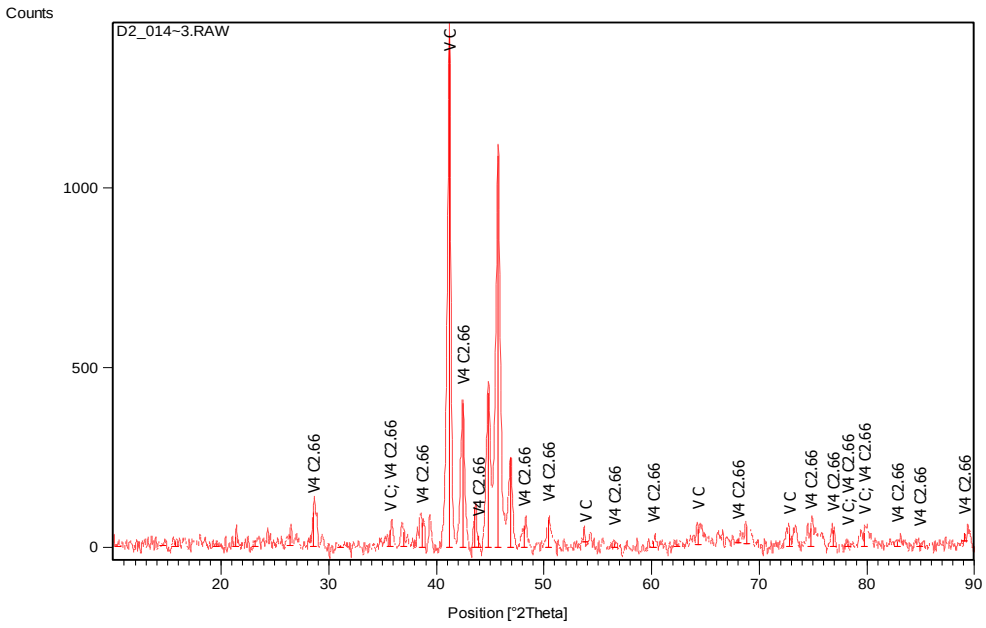


Figure 4.69. XRD pattern of nominal Ni_{30}:V_{65}:C_5 (at.%), Sample 9, in the as-cast condition, showing all the identified peaks.

Table 4.19. XRD peaks for as-cast nominal $Ni_{30}:V_{65}:C_5$ (at.%), Sample 9.

Position 2θ (º)	Height (counts)	Relative Intensity (%)	Phases
21.3408	39.68	0.29	Presumed σ′
26.3591	28.47	2.00	Presumed σ′
28.5901	97.11	6.83	$V_4C_{2.66}$,
31.0523	3.68	0.26	Presumed σ′
35.7123	47.09	3.31	VC, $V_4C_{2.66}$
36.9562	41.12	2.89	Presumed σ′
38.7038	68.78	4.83	$V_4C_{2.66}$
41.1889	1422.55	100.00	VC
42.4371	401.81	28.25	$V_4C_{2.66}$
43.5903	111.16	7.81	Presumed σ′
43.9060	32.80	2.31	$V_4C_{2.66}$
44.7872	428.62	30.13	Presumed σ′
45.7476	1087.56	76.45	Presumed σ′
46.9078	247.90	17.43	Presumed σ′
48.1900	59.77	4.20	$V_4C_{2.66}$
50.4478	76.34	5.37	$V_4C_{2.66}$
53.8640	1.00	0.07	VC
56.5864	10.14	0.71	$V_4C_{2.66}$
60.1362	17.29	1.22	$V_4C_{2.66}$
62.3549	6.91	0.49	Presumed σ′
64.3604	45.11	3.17	VC
68.0376	12.14	0.85	$V_4C_{2.66}$
68.8426	49.29	3.47	Presumed σ′
72.8013	36.16	2.54	VC
74.7845	53.11	3.73	$V_4C_{2.66}$
76.8566	47.72	3.35	$V_4C_{2.66}$
78.2408	9.01	0.63	VC, $V_4C_{2.66}$
79.7499	36.37	2.56	$V_4C_{2.66}$
82.8206	14.71	1.03	$V_4C_{2.66}$
84.8635	5.15	0.36	$V_4C_{2.66}$
89.0951	25.39	1.79	$V_4C_{2.66}$

4.1.10 Nominal $Ni_{20}:V_{35}:C_{45}$ (at.%), Sample 10

The image of nominal $Ni_{20}:V_{35}:C_{45}$ (at.%), Sample 10, in as-cast condition is shown in Figure 4.70. The alloy consisted of graphite flakes (very dark) which were randomly distributed, ~V_8C_7 dendrites (dark) and a (Ni) + VC sparse eutectic, where (Ni) had a light contrast. At higher magnification (Figure 4.71), the microstructure showed some of the graphite flakes

and the sparse eutectic. Figure 4.72 also shows the image of the pores taken in the secondary electron mode (SE).

The phase compositions are shown in Table 4.20 and were plotted in Figure 4.73, showing the overall composition to lie within the tie-triangle of the phases, signifying the alloy to be potentially at equilibrium. Despite the variation between the nominal composition and overall composition, $Ni_{2.4}$:$V_{25.9}$:$C_{71.7}$ (at.%), the phase results are sensible. The EDX analyses of Sample 10 are shown in Appendix B10.

The deduced solidification sequence is: L → graphite

followed by L + graphite → ~VC

and L → ~VC + (Ni)

then, in the solid state ~VC → ~V_8C_7

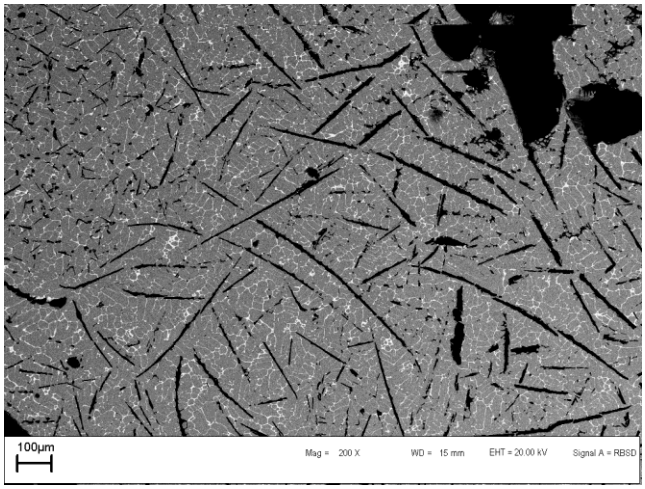


Figure 4.70. SEM-BSE image of nominal Ni_{20}:V_{35}:C_{45} (at.%), Sample 10, in the as-cast condition, showing graphite flakes (very dark), ~V_8C_7 dendrites (dark), and (Ni) matrix (light). Pores can be seen at the top right corner.

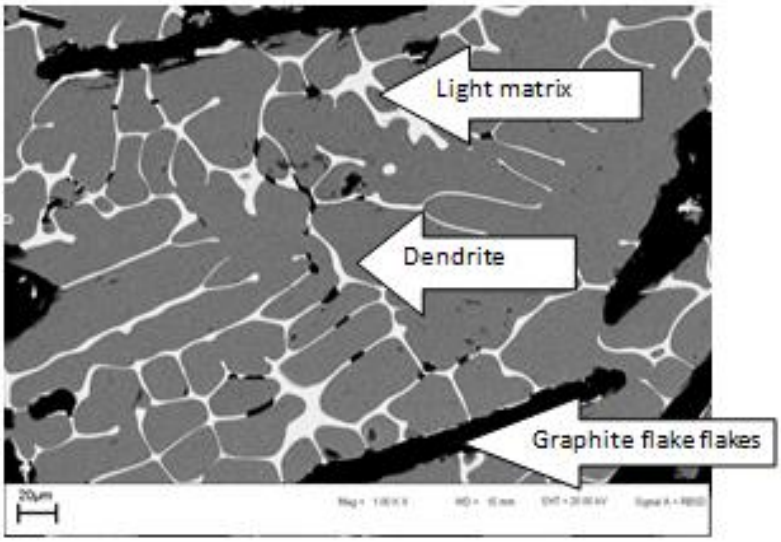


Figure 4.71. SEM-BSE image of nominal $Ni_{20}:V_{35}:C_{45}$ (at.%), Sample 10, in the as-cast condition, showing graphite flakes (very dark), ~V_8C_7 dendrites (dark), and (Ni) matrix (light) at higher magnification.

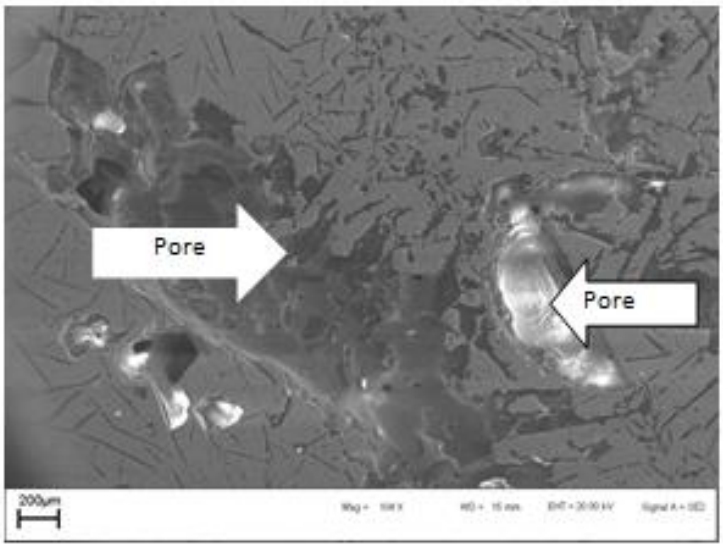


Figure 4.72. SEM-SE low magnification image of nominal $Ni_{20}:V_{35}:C_{45}$ (at.%), Sample 10, in the as-cast condition, showing pores.

Table 4.20. EDX phase analyses of as-cast nominal $Ni_{20}:V_{35}:C_{45}$ (at.%), Sample 10.

Phase Description	C	V	Ni	Phase
Overall	71.7 ± 0.2	25.9 ± 0.5	2.4 ± 0.3	-
Dark	49.3 ± 0.4	50.6 ± 0.4	0.1 ± 0.01	~V_8C_7
Light	18.6 ± 0.5	3.6 ± 0.1	77.8 ± 0.6	(Ni)
Very Dark	99.9 ± 0.0	0.1 ± 0.0	0.0 ± 0.0	Graphite

The existence of ~V_8C_7, (Ni) and graphite was confirmed by the XRD, as shown in Figures 4.74 to 4.78. The matches of the phases with the ICDD were good with minor peak shifts, showing the other element were present in the phases. The pattern had high background and few peaks, which could be as a result of the pores. The highest intensity peak was ~V_8C_7 at $2\theta = 51.39^{o}$. Table 4.21 shows the identified peaks together with their phases.

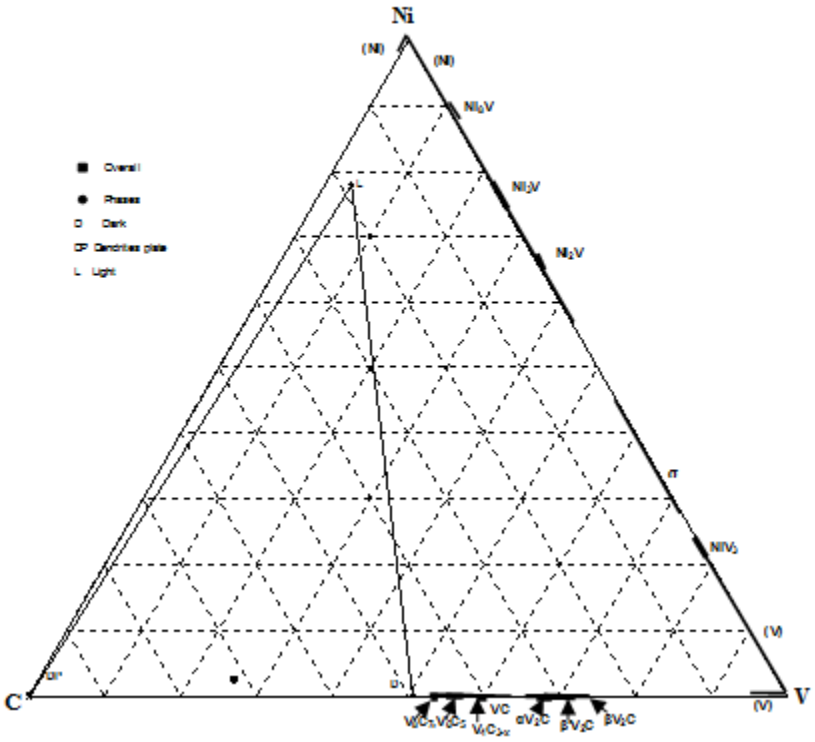


Figure 4.73. EDX analyses of as-cast nominal $Ni_{20}:V_{35}:C_{45}$ (at.%), Sample 10.

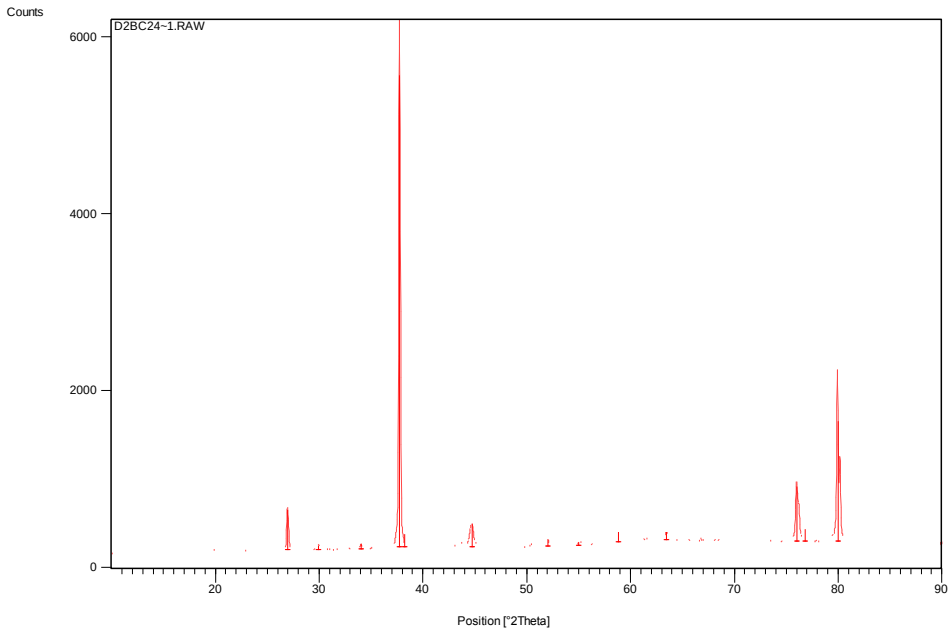


Figure 4.74. Unlabelled XRD pattern of as-cast nominal $Ni_{20}:V_{35}:C_{45}$ (at.%), Sample 10.

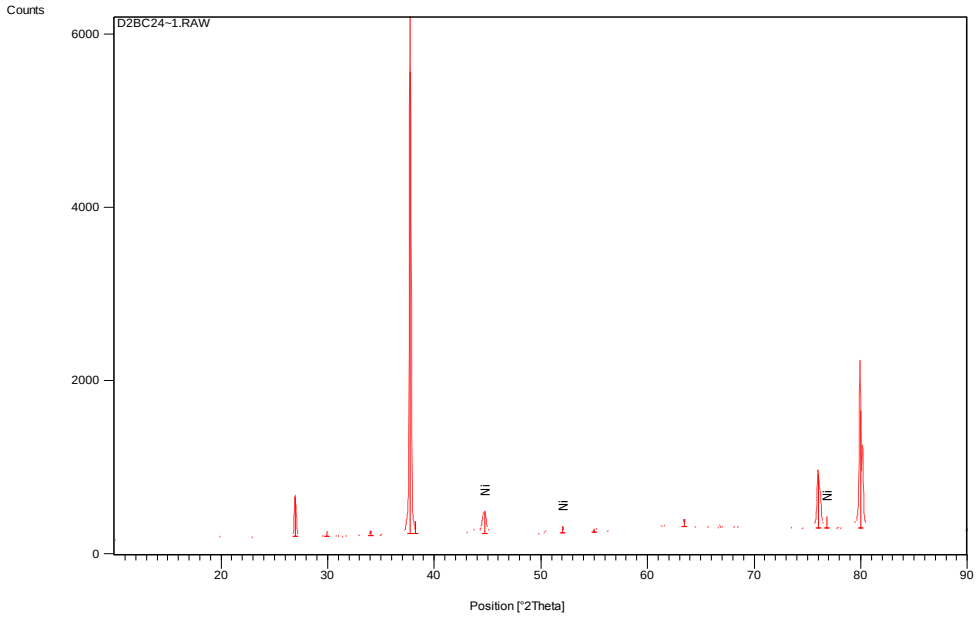


Figure 4.75. XRD pattern of nominal $Ni_{20}:V_{35}:C_{45}$ (at.%), Sample 10, in the as-cast condition, showing identified (Ni) peaks.

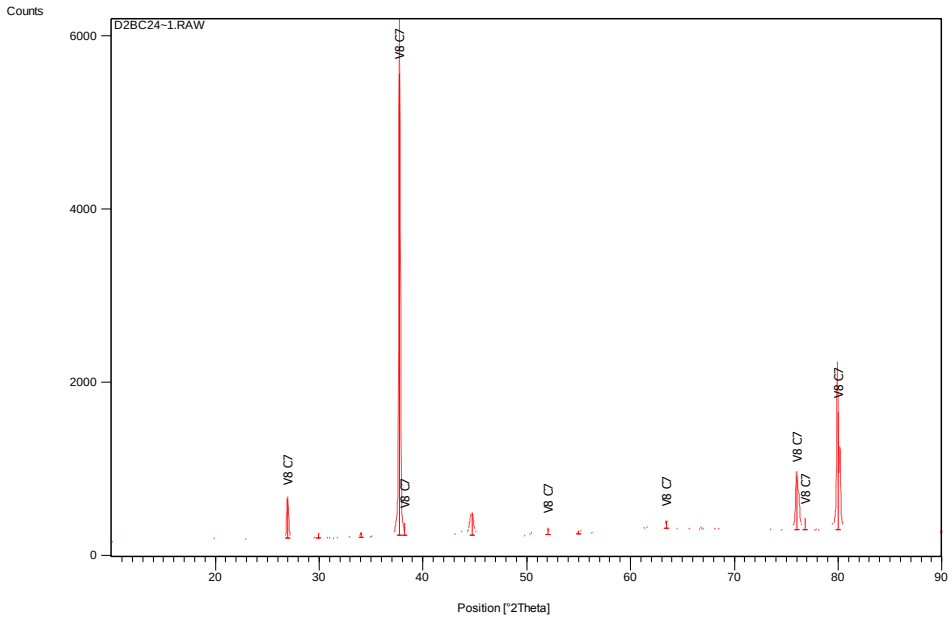


Figure 4.76. XRD pattern of nominal $Ni_{20}:V_{35}:C_{45}$ (at.%), Sample 10, in the as-cast condition, showing identified ~V_8C_7 peaks.

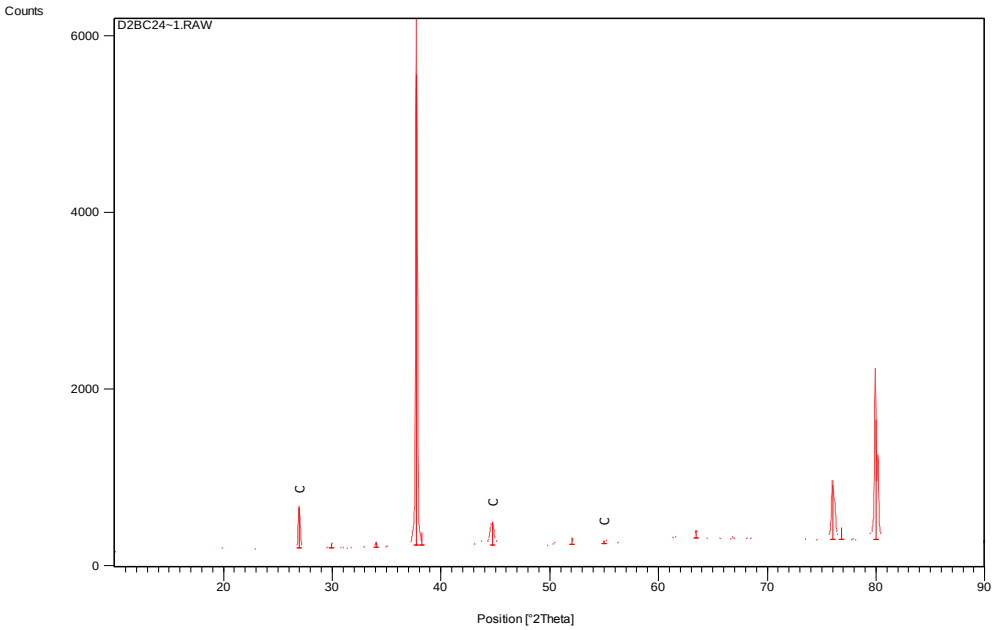


Figure 4.77. XRD pattern of nominal $Ni_{20}:V_{35}:C_{45}$ (at.%), Sample 10, in the as-cast condition, showing identified graphite peaks.

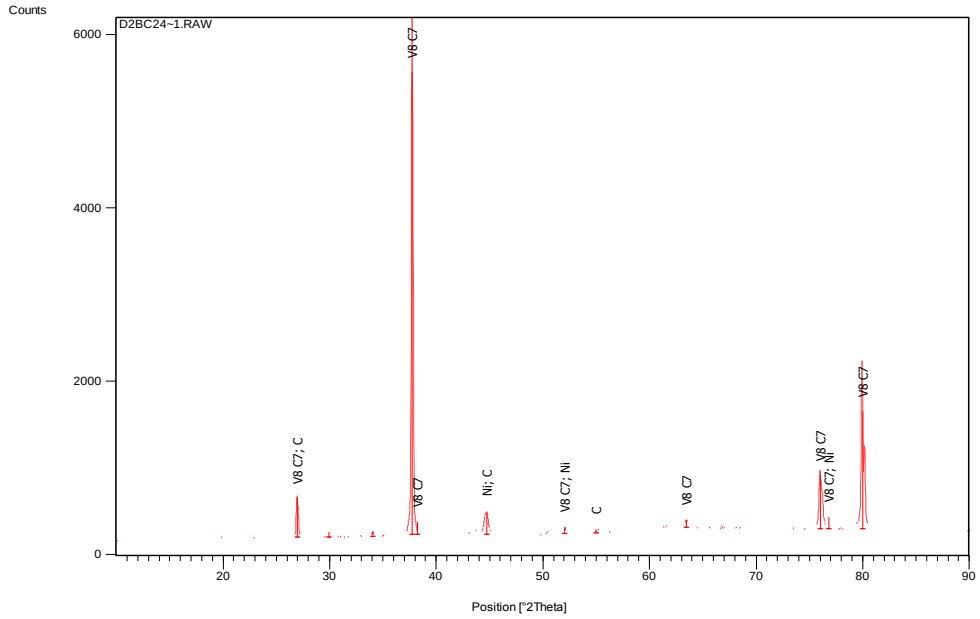


Figure 4.78. XRD pattern of nominal $Ni_{20}:V_{35}:C_{45}$ (at.%), Sample 10, in the as-cast condition, showing all identified phases.

Table 4.21. XRD peaks for as-cast nominal $Ni_{20}:V_{35}:C_{45}$ (at.%), Sample 10.

Position 2θ (º)	Height (counts)	Relative Intensity (%)	Phases
26.9678	450.36	8.44	C
37.7510	5336.28	100.00	V_8C_7
38.2380	139.40	2.61	V_8C_7
44.7114	259.77	4.87	Ni, C
52.0229	82.29	1.54	V_8C_7, Ni
55.0384	38.67	0.72	C
63.4911	85.18	1.60	V_8C_7
76.0575	617.50	11.57	V_8C_7
76.8220	138.90	2.60	V_8C_7, Ni
80.0034	1365.68	25.59	V_8C_7

4.1.11 Nominal $Ni_{10}:V_{80}:C_{10}$ (at.%), Sample 11

SEM-BSE images representative of the centre and edge microstructures of nominal $Ni_{10}:V_{80}:C_{10}$ (at.%), Sample 11, in the as-cast condition are shown in Figures 4.79 and 4.80.

The alloy had apparently two phases. These were partially facetted dendrites whose contrasts were dark, identified as ~VC, and the light regions (matrix) were identified as (V). In some places, there was a light phase, which was too small to analyse, but could have been ~V_2C. There was also a eutectic. Figure 4.80 shows the microstructure of the alloy at higher magnification.

The phase compositions are shown in Table 4.22 and plotted in Figure 4.81 showing the overall compositions to be deviated slightly from the tie-line connecting the two phases, although the eutectic was closer to the overall composition. The deviation may be due to some unidentified phases which may be present in the microstructure. However, the standard deviation of the measurements was below 1 at.%. The EDX analyses of Sample 11 are shown in Appendix B11.

The solidification sequence deduced from the microstructure is as follows:

$$L \rightarrow \sim VC$$

followed by a eutectic reaction $L \rightarrow \sim VC + (V)$

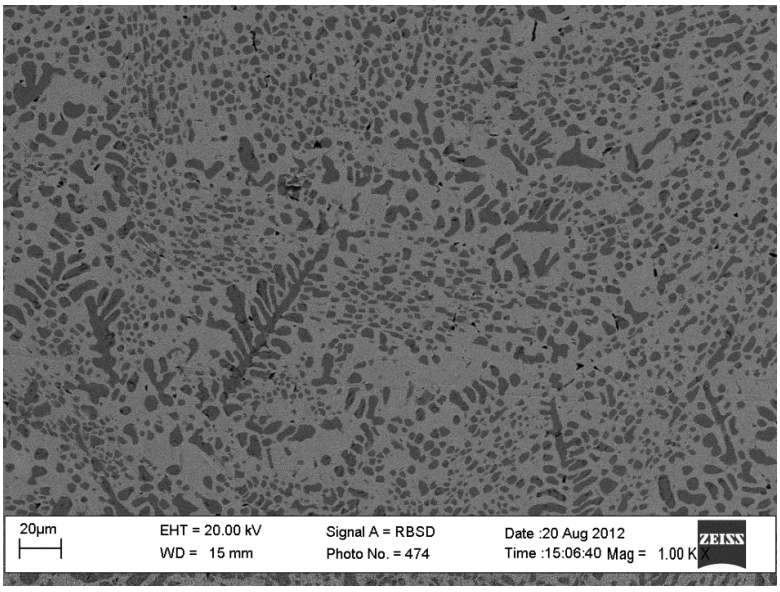


Figure 4.79. SEM-BSE image of nominal Ni_{10}:V_{80}:C_{10} (at.%), Sample 11, in the as-cast condition, showing ~VC dendrites (dark), (V) matrix (light) and eutectic.

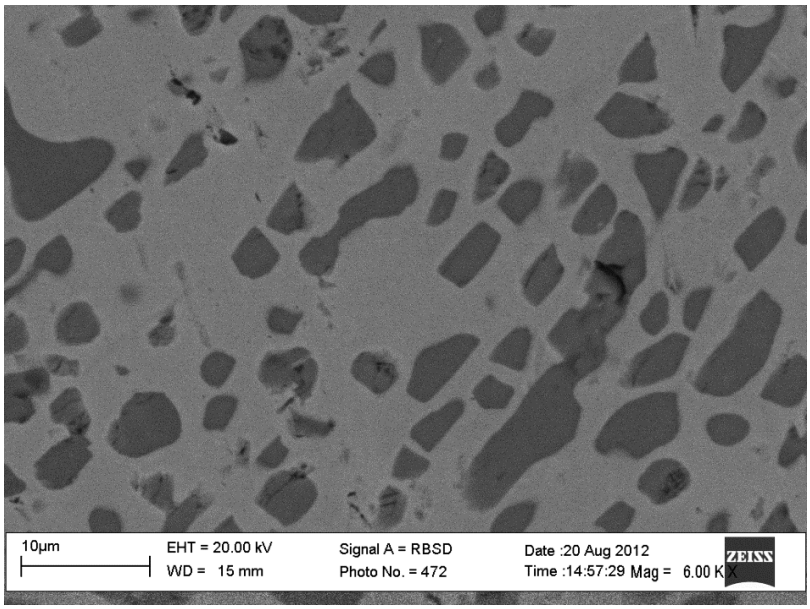


Figure 4.80. SEM-BSE image of nominal $Ni_{10}:V_{80}:C_{10}$ (at.%), Sample 11, in the as-cast condition, showing ~VC dendrites (dark), (V) matrix (light) and eutectic at higher magnification.

Table 4.22. EDX phase analyses of as-cast nominal $Ni_{10}:V_{80}:C_{10}$ (at.%), Sample 11.

Phase Description	C	V	Ni	Phase
Overall	25.1 ± 0.2	67.3 ± 0.5	7.6 ± 0.3	-
Dark	36.3 ± 0.4	62.5 ± 0.4	1.2 ± 0.01	~VC
Light	9.4 ± 0.5	71.8 ± 0.1	18.8 ± 0.6	(V)
Eutectic	24.3 ± 0.3	68.2 ± 0.8	7.8 ± 0.5	~VC + (V)

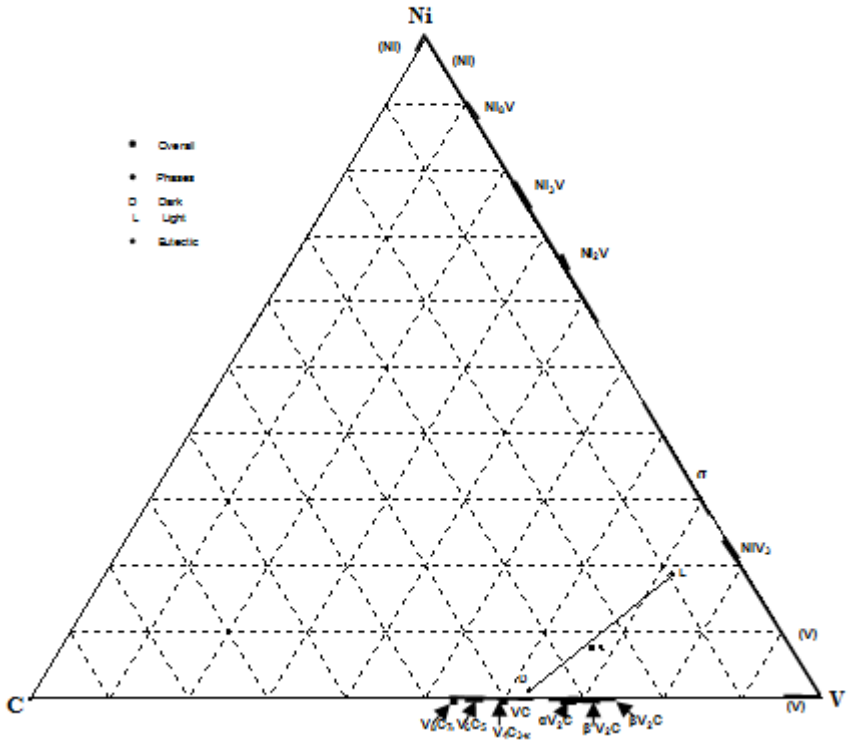


Figure 4.81. EDX analyses of as-cast nominal Ni_{10}:V_{80}:C_{10} (at.%), Sample 11.

The XRD pattern shown in Figures 4.82 to 4.87 was good, with a high signal:background ratio. The existence of VC, V, NiV_3 (possibly formed within (V)) and $V_4C_{2.66}$ (once again possibly not present, as it forms in the solid state at lower temperature [1985Car]) was identified. The matches for the phases with the ICDD were good, but with unidentified peaks at 2θ = 21.19°, 33.38° and 46.59°. A major peak was found at position 2θ = 42.66°, which matched V and $V_4C_{2.66}$. Table 4.23 shows the identified peaks together with their phases.

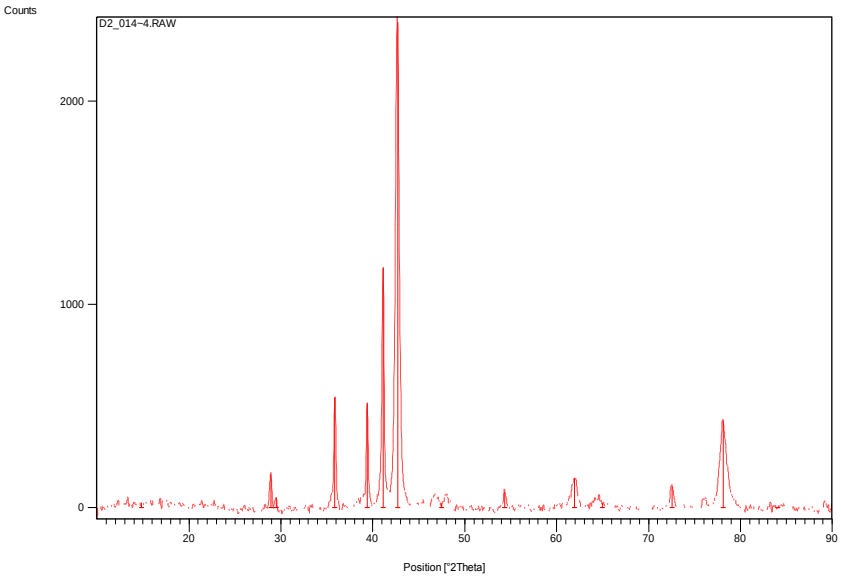


Figure 4.82. Unlabelled XRD pattern of as-cast nominal $Ni_{10}:V_{80}:C_{10}$ (at.%), Sample 11.

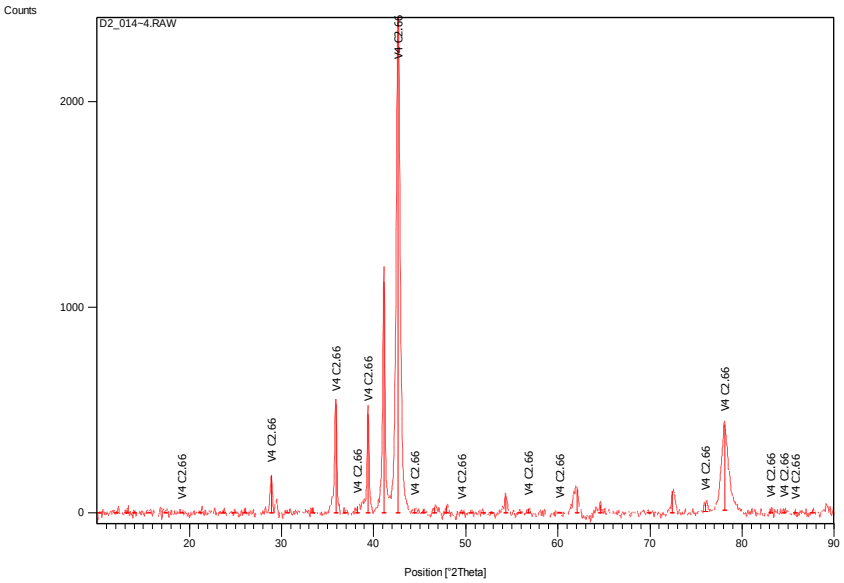


Figure 4.83. XRD pattern of nominal $Ni_{10}:V_{80}:C_{10}$ (at.%), Sample 11, in the as-cast condition, showing identified $V_4C_{2.66}$ peaks.

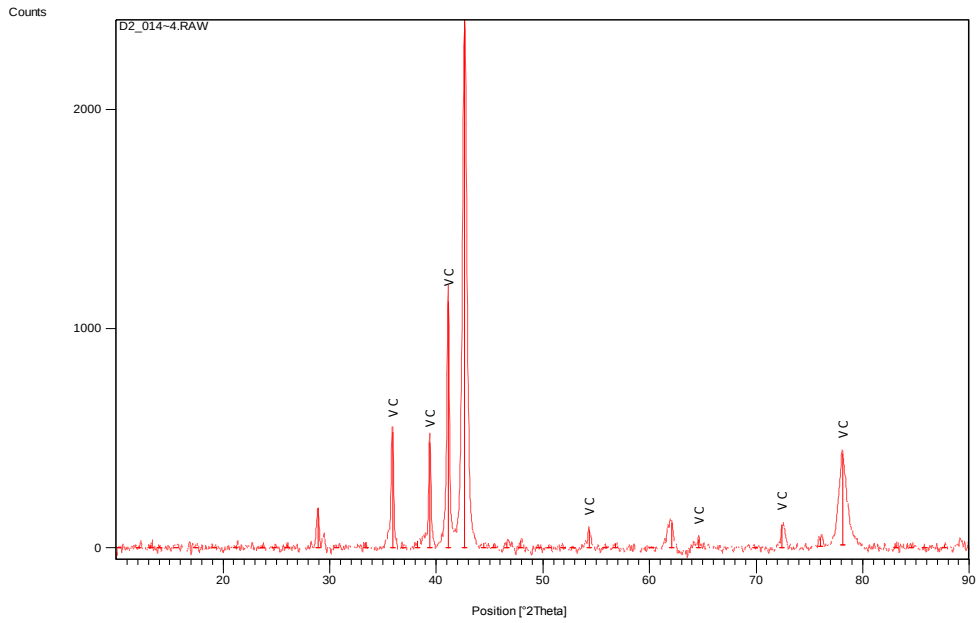


Figure 4.84. XRD pattern of nominal Ni_{10}:V_{80}:C_{10} (at.%), Sample 11, in the as-cast condition, showing identified VC peaks.

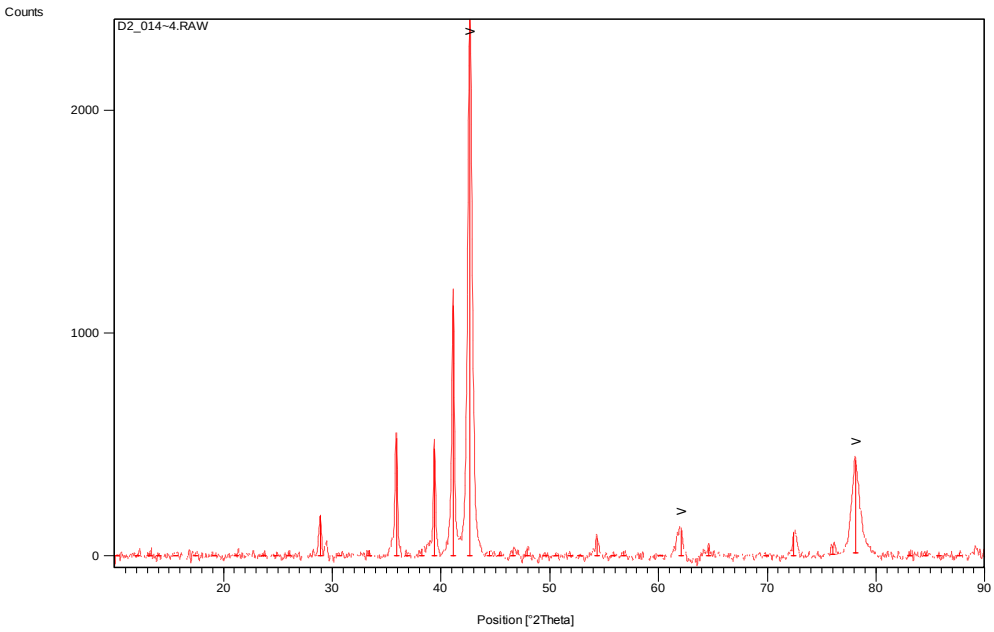


Figure 4.85. XRD pattern of nominal Ni_{10}:V_{80}:C_{10} (at.%), Sample 11, in the as-cast condition, showing identified (V) peaks.

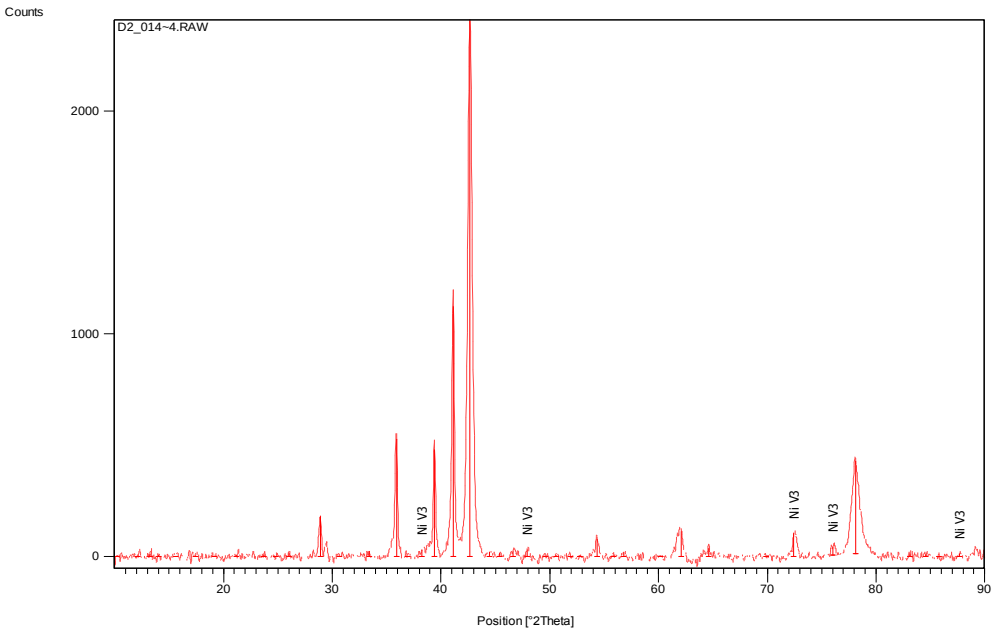


Figure 4.86. XRD pattern of nominal $Ni_{10}:V_{80}:C_{10}$ (at.%), Sample 11, in the as-cast condition, showing identified NiV_3 peaks.

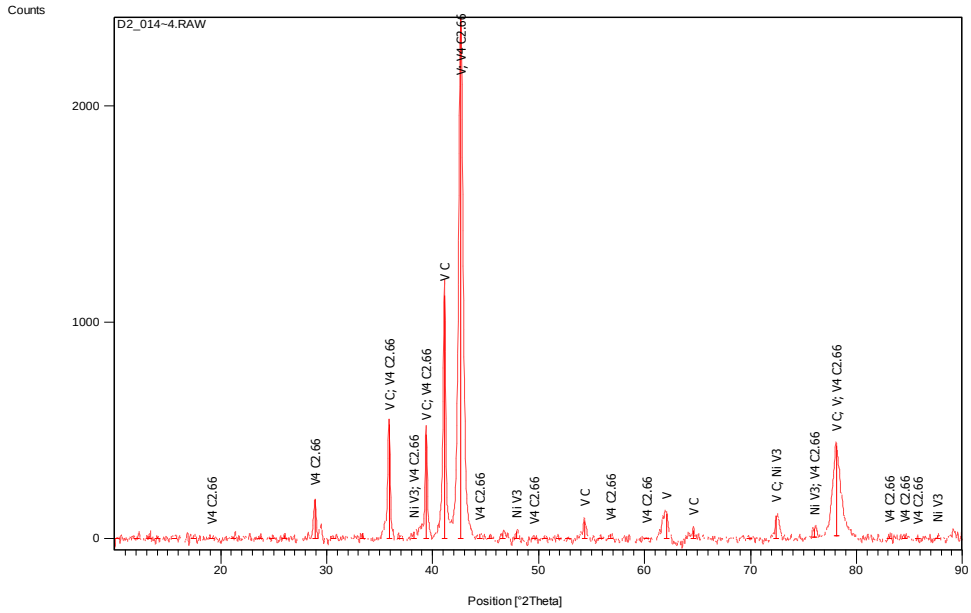


Figure 4.87. XRD pattern of nominal $Ni_{10}:V_{80}:C_{10}$ (at.%), Sample 11, in the as-cast condition, showing all the identified peaks.

Table 4.23. XRD peaks for as-cast nominal $Ni_{10}:V_{80}:C_{10}$ (at.%), Sample 11.

Position 2θ (º)	Height (counts)	Relative Intensity (%)	Phases
19.1877	2.16	0.09	$V_4C_{2.66}$
21.1950	7.61	0.32	Unidentified
28.9234	180.40	7.49	$V_4C_{2.66}$
33.3810	24.85	1.03	Unidentified
35.8970	529.74	21.99	$V_4C_{2.66}$, VC
38.2539	31.69	1.32	$V_4C_{2.66}$, NiV_3
39.4116	480.79	19.96	$V_4C_{2.66}$, VC
41.1104	1125.54	46.72	VC
42.6604	2408.85	100.00	$V_4C_{2.66}$, V
44.4353	23.14	0.96	$V_4C_{2.66}$
46.5981	24.47	1.02	Unidentified
47.9052	31.56	1.31	NiV_3
49.5760	4.07	0.17	$V_4C_{2.66}$
54.3886	78.52	3.26	VC
56.7915	17.91	0.74	$V_4C_{2.66}$
60.2228	7.22	0.30	$V_4C_{2.66}$
62.1217	113.27	4.70	V
64.6451	39.52	1.64	VC
72.4458	105.74	4.39	VC, NiV_3
76.0425	38.15	1.58	$V_4C_{2.66}$, NiV_3
78.1000	417.25	17.32	$V_4C_{2.66}$, VC,V
83.1344	10.47	0.43	$V_4C_{2.66}$
84.5857	8.22	0.34	$V_4C_{2.66}$
85.7818	4.65	0.19	$V_4C_{2.66}$
87.6952	13.13	0.55	NiV_3

4.1.12 Nominal $Ni_5:V_{75}:C_{20}$ (at.%), Sample 12

The nominal $Ni_5:V_{75}:C_{20}$ (at.%) alloy, Sample 12 possessed mainly ~VC dendrites (dark) and a light contrast matrix as shown in Figure 4.88 at low magnification. At high magnification, the dendrites had ragged edges showing a peritectic reaction (Figure 4.89) and locally, a light peritectically-formed phase around the dendrites which was too small to analyse accurately. Since Ni has the highest atomic number of the three components, this phase had more Ni, and so was likely to be σ′. There were some cracks in the alloy, mostly in the dendrites. Figure 4.90 shows the eutectic regions.

The phase compositions are shown in Table 4.24 and are plotted in Figure 4.91, showing the overall composition to be slightly off the tie-line joining the two phases, showing a phase (the light, peritectically formed phase) had not been analysed. The eutectic composition was closer to the overall composition. Also, the peritectically-formed phase was too small to be analysed accurately. The analyses had standard deviations below 1 at.%. The EDX analyses of Sample 12 are shown in Appendix B12.

The solidification sequence deduced from the microstructure is as follows:

$$L \rightarrow \sim VC$$

followed by a local peritectic reaction: $L + \sim VC \rightarrow \sigma'$

followed by eutectic reaction $L \rightarrow \sim VC + (V)$

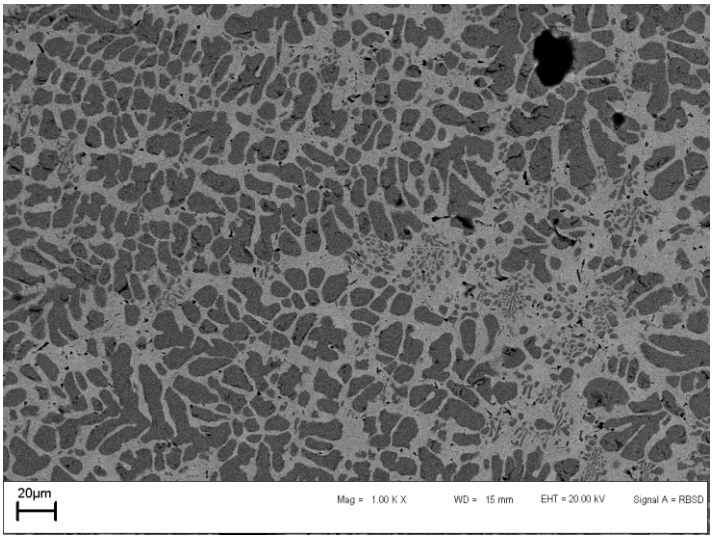


Figure 4.88. SEM-BSE image of nominal Ni_5:V_{75}:C_{20} (at.%), Sample 12, in the as-cast condition, showing ~VC dendrites (dark), a eutectic and matrix (medium).

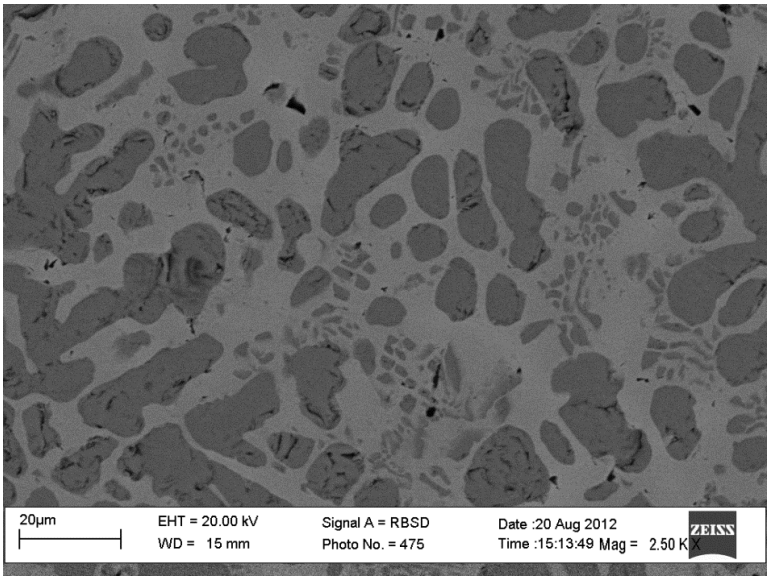


Figure 4.89. SEM-BSE image of as-cast nominal Ni_5:V_{75}:C_{20} (at.%), Sample 12, showing ~VC dendrites with some pores at top of micrograph, and local light peritectic layer σ′and eutectic.

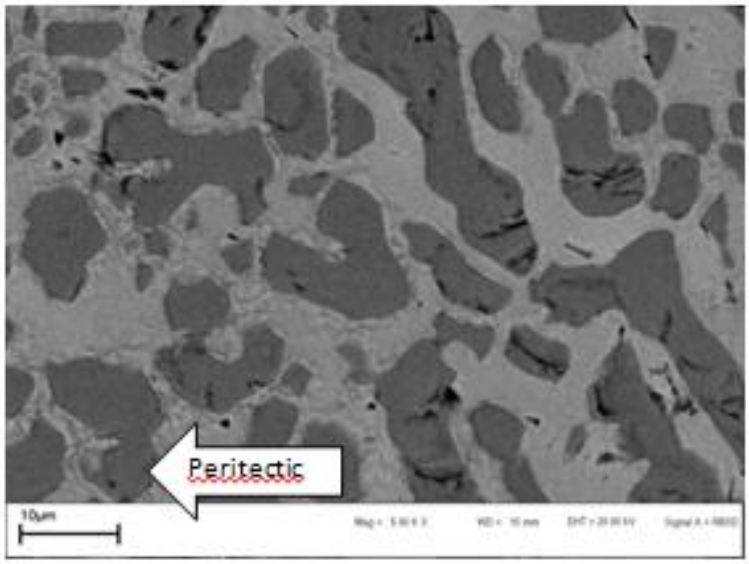


Figure 4.90. SEM-BSE image of nominal Ni_5:V_{75}:C_{20} (at.%), Sample 12 in the as-cast condition, showing ~VC dendrites with some cracks (dark) and peritectically formed σ′ (very light).

Table 4.24. EDX phase analyses of as-cast nominal $Ni_5:V_{75}:C_{20}$ (at.%), Sample 12.

Phase Description	C	V	Ni	Phase
Overall	28.2 ± 0.4	68.0 ± 0.4	3.8 ± 0.1	-
Dark	36.2 ± 0.5	63.7 ± 0.5	0.1 ± 0.1	~VC
Light	10.8 ± 0.5	79.4 ± 0.4	9.8 ± 0.3	(V)
Very light peritectic	Too small for analysis			σ′
Eutectic	29.2 ± 0.7	67.1 ± 0.5	3.7 ± 0.2	~VC + (V)

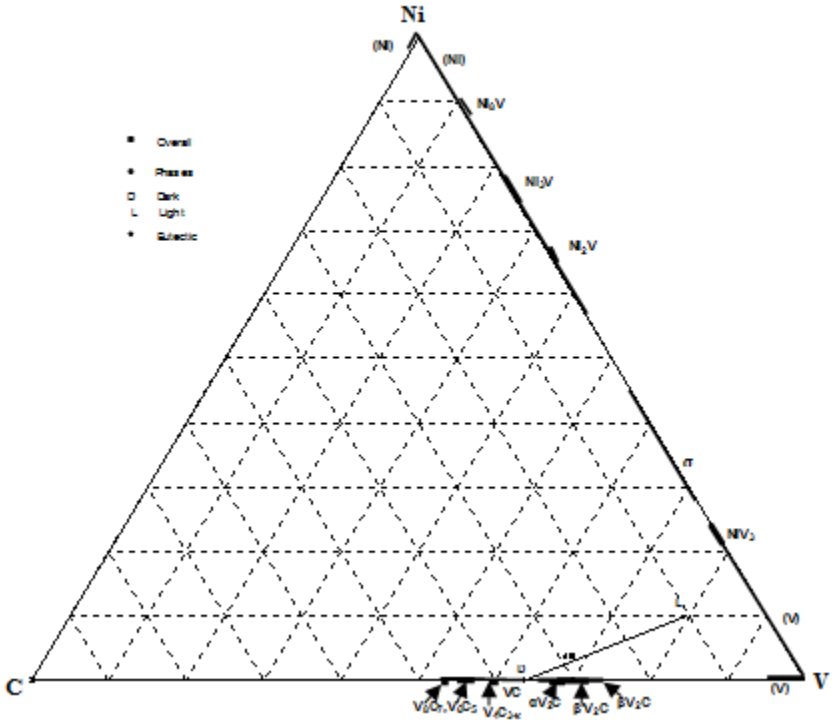


Figure 4.91. EDX analyses of as-cast nominal $Ni_5:V_{75}:C_{20}$ (at.%), Sample 12.

Figures 4.92 to 4.96 show the X-ray diffraction (XRD) pattern of the sample with the database lines for each of the phases. The XRD pattern identified the ~V_2C (Figure 4.93) although ~V_2C was not seen in the microstructure (and was not thought to be peritectic layer), (V) (Figure 4.94) and ~VC (Figure 4.95). All peaks could be matched, except those at

2θ = 28.31°, 38.22°, 47.44° and 61.70°. However, if the peritectic phase was σ′ it would have only generated small peaks, since it was present in a small proportion, and would not have contributed much to the XRD pattern. Tables 4.25 and 4.26 show the identified peaks together with their phases.

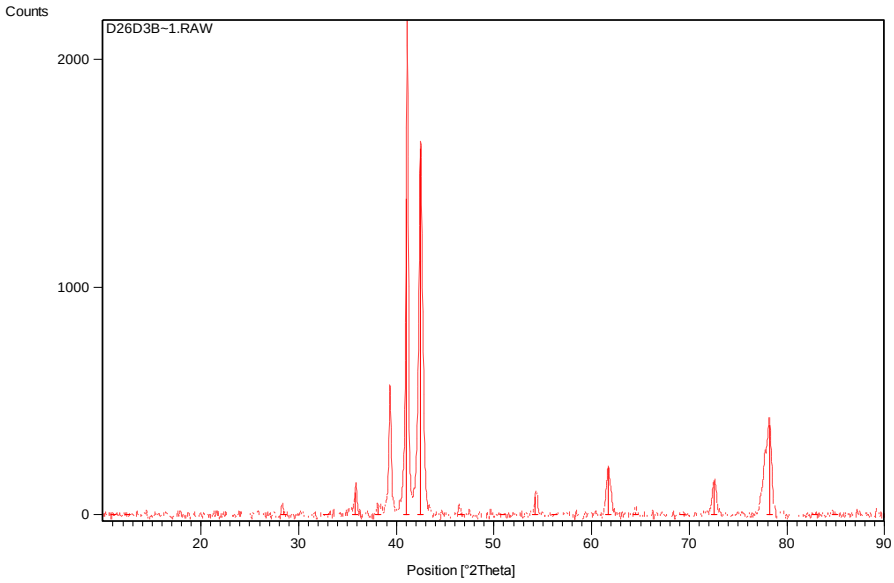


Figure 4.92. Unlabelled XRD pattern of nominal $Ni_{20}:V_{35}:C_{45}$ (at.%), Sample 12, in the as-cast condition.

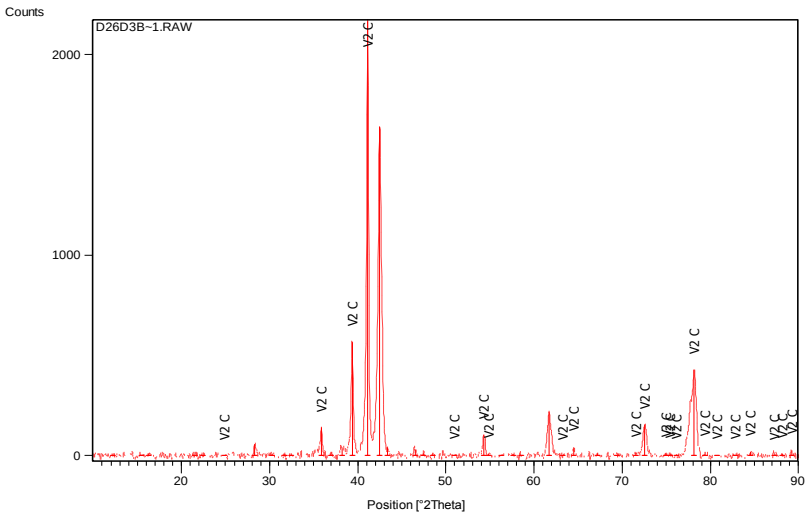


Figure 4.93. XRD pattern of nominal $Ni_5:V_{75}:C_{20}$ (at.%), Sample 12, in the as-cast condition, showing identified ~V_2C peaks.

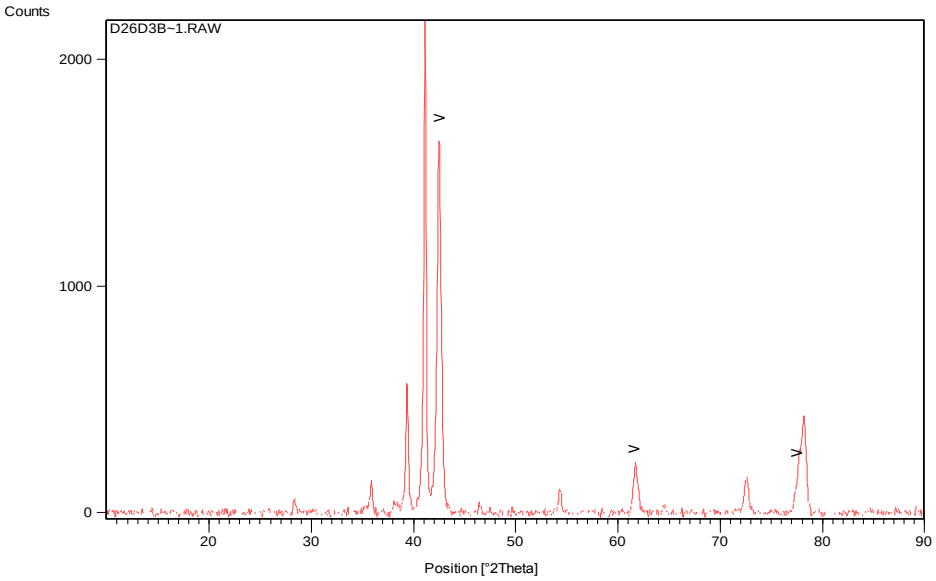


Figure 4.94. XRD pattern of nominal Ni_5:V_{75}:C_{20} (at.%), Sample 12, in the as-cast condition, showing identified (V) peaks.

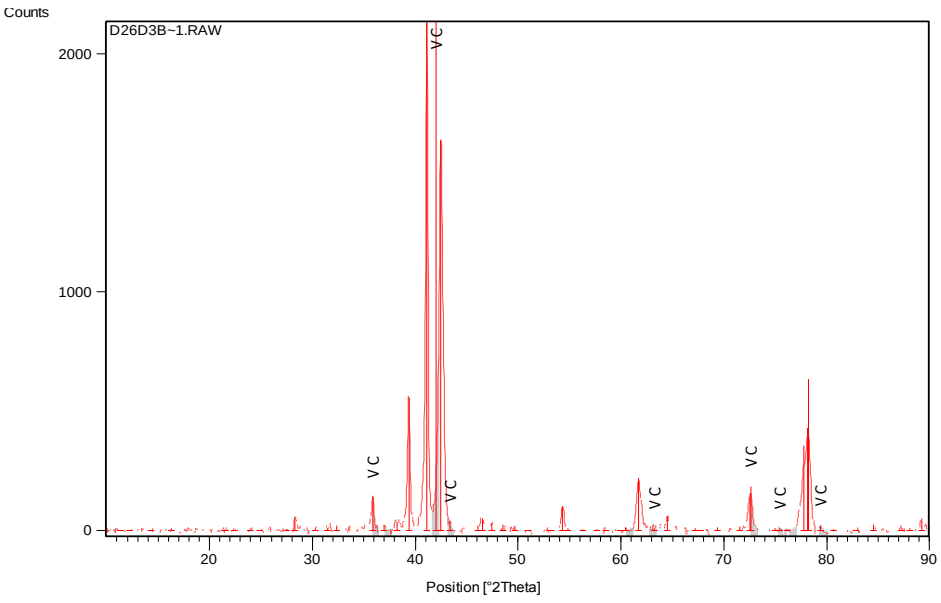


Figure 4.95. XRD pattern of nominal Ni_5:V_{75}:C_{20} (at.%), Sample 12, in the as-cast condition, showing identified ~VC peaks.

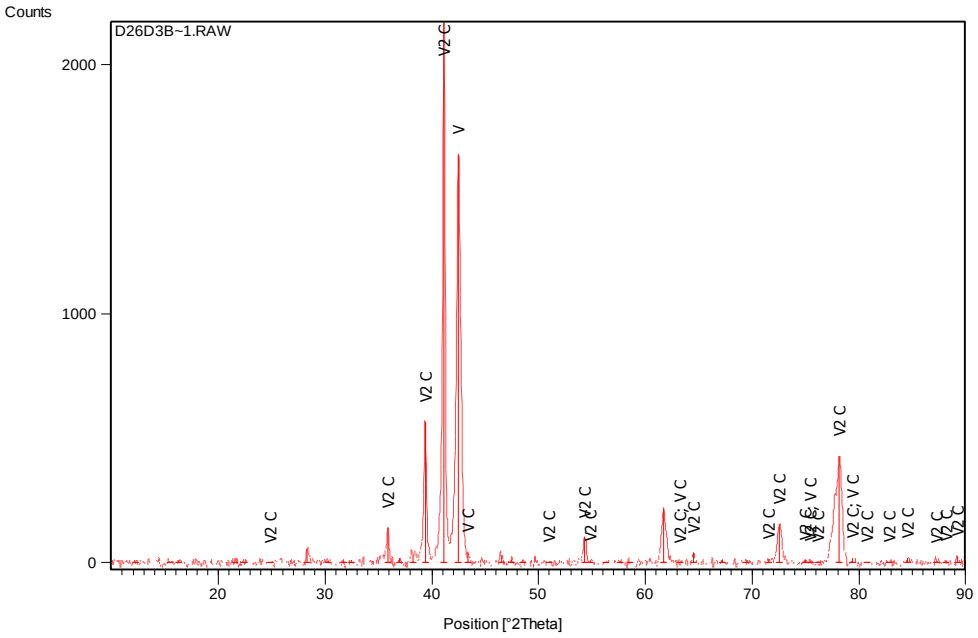


Figure 4.96. XRD pattern of nominal Ni_5:V_{75}:C_{20} (at.%), Sample 12, in the as-cast condition, showing all the identified phases.

Table 4.25. XRD peaks for as-cast nominal Ni_5:V_{75}:C_{20} (at.%), Sample 12.

Position 2θ (º)	Height (counts)	Relative Intensity (%)	Phases
24.9020	2.27	0.10	V_2C
28.3112	58.56	2.70	Presumed σ′
35.8753	140.69	6.50	V_2C
38.2219	35.36	1.63	Presumed σ′
39.3657	566.56	26.17	V_2C
41.1206	2165.09	100.00	V_2C
42.4979	1637.63	75.64	V
43.3751	40.73	1.88	VC
47.4413	11.05	0.51	Presumed σ′
50.9372	4.23	0.20	V_2C
54.3241	103.24	4.77	V_2C
54.8802	7.90	0.37	V_2C
61.7065	218.16	10.08	Presumed σ′
63.2205	0.68	0.03	V_2C, VC
64.5025	43.53	2.01	V_2C
71.5320	17.85	0.82	V_2C

Table 4.26 (cont.). XRD peaks for as-cast nominal Ni_5:V_{75}:C_{20} (at.%), Sample 12.

72.5510	156.30	7.22	V_2C
74.9340	13.57	0.63	V_2C
75.4452	9.20	0.42	V_2C, VC
76.1139	5.67	0.26	V_2C
78.1720	431.62	19.94	V_2C
79.4161	21.04	0.97	V_2C, VC
80.7956	4.33	0.20	V_2C
82.8318	3.82	0.18	V_2C
84.5818	21.51	0.99	V_2C
87.2757	1.71	0.08	V_2C
88.1120	9.66	0.45	V_2C
89.2140	26.95	1.24	V_2C

4.1.13 Nominal Ni_{14}:V_{64}:C_{22} (at.%), Sample 13

The nominal Ni_{14}:V_{64}:C_{22} (at.%), Sample 13, in the as-cast condition is shown in Figure 4.97. The alloy showed a different morphology compared to other alloys, with needles of ~VC (dark) surrounded by light regions (matrix) which were identified as (Ni) and regions of a fine mixture of ~VC + (Ni) eutectic as shown in Figure 4.98. Some of the light regions were slightly darker.

The phase compositions are shown in Table 4.27 and plotted in Figure 4.99. The overall compositions and the eutectic were seen to deviate slightly from the tie-line joining the two phases. However, the standard deviation of the measurements was below 1 at.%. The darker light matrix regions ("medium") are thought to be due to precipitation of ~V_6C_5, by extrapolation, which would have occurred in the solid state. The EDX analyses of Sample 13 are shown in Appendix B13.

The solidification sequence deduced from the microstructure is as follows:

$$L \rightarrow \sim VC$$

$$L + \sim VC \rightarrow (Ni)$$

followed by a eutectic reaction: $L \rightarrow \sim VC + (Ni)$ fine eutectic.

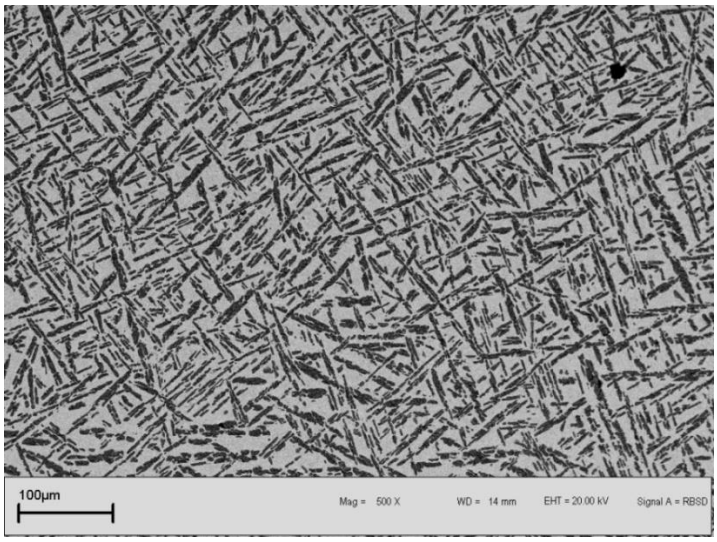


Figure 4.97. SEM-BSE image of nominal $Ni_{14}:V_{64}:C_{22}$ (at.%), Sample 13, in the as-cast condition, showing ~VC needles (dark) and (Ni) matrix (light).

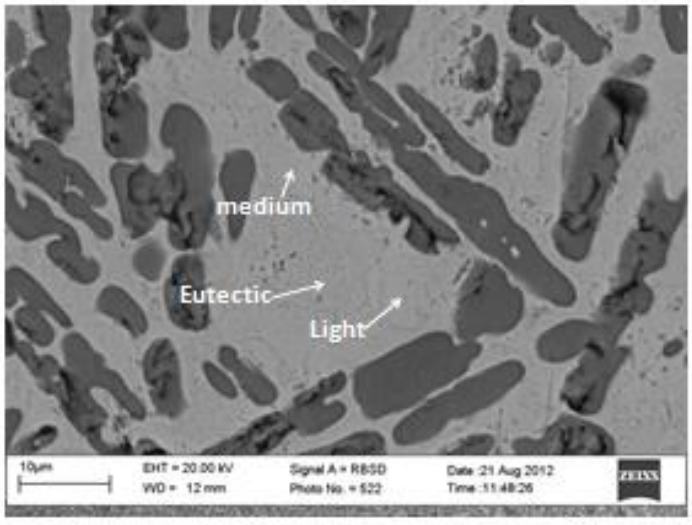


Figure 4.98. SEM-BSE image of nominal $Ni_{14}:V_{64}:C_{22}$ (at.%), Sample 13, in the as-cast condition, showing ~VC dendrites (dark), (Ni) matrix (light) and fine eutectic at higher magnification.

Table 4.26. EDX phase analyses of as-cast nominal $Ni_{14}:V_{64}:C_{22}$ (at.%), Sample 13.

Phase Description	C	V	Ni	Phase
Overall	30.1 ± 0.5	47.8 ± 0.3	22.1 ± 0.4	-
Dark	37.7 ± 0.3	61.9 ± 0.6	0.4 ± 0.06	~VC
Medium	35.1 ± 0.4	52.8 ± 0.6	12.1± 0.8	
Light	17.9 ± 0.7	41.0 ± 1.3	41.1 ± 0.8	(Ni)
Eutectic	28.5 ± 1.1	49.8 ± 0.4	21.7 ± 0.9	~VC + (Ni)

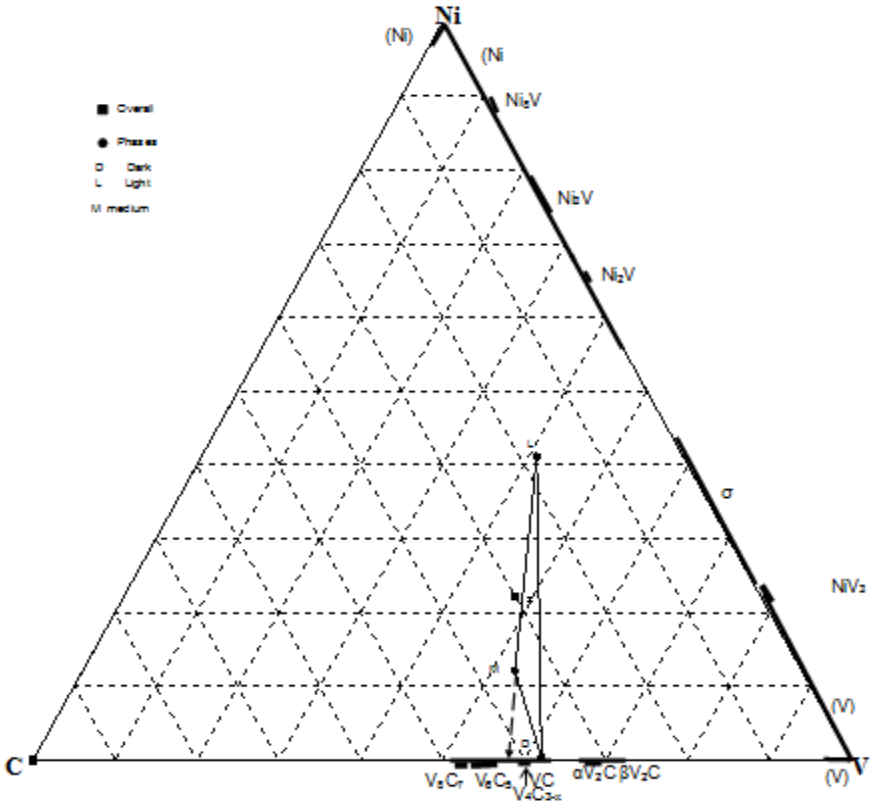


Figure 4.99. SEM-BSE image of nominal $Ni_{14}:V_{64}:C_{22}$ (at.%), Sample 13, in the as-cast condition, showing ~VC dendrites (dark), (Ni) matrix (light) and fine eutectic at higher magnification.

Figures 4.100 to 4.104 show the experimental pattern of the sample with the database lines for each of the phases. The patterns had overlapping peaks of the different phases. The highest intensity peaks were ~V_6C_5, ~VC and (Ni) at about 2θ = 48.17°. Figure 4.104 confirmed the presence of ~V_6C_5, ~VC, (Ni), and ~$V_4C_{2.66}$, although unidentified peaks could be seen. Table 4.28 shows the identified peaks together with their phases.

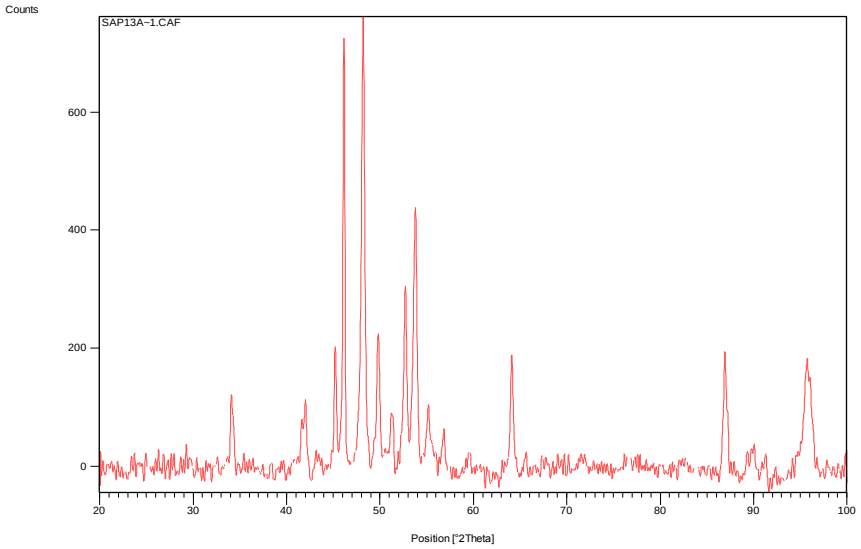


Figure 4.100. Unlabelled XRD pattern of as-cast nominal $Ni_{14}:V_{64}:C_{22}$ (at.%), Sample 13.

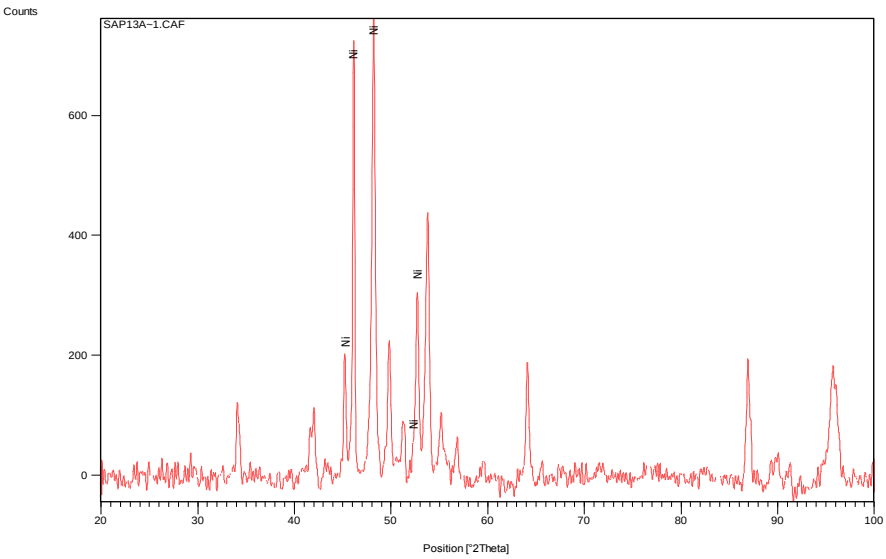


Figure 4.101. XRD pattern of as-cast nominal $Ni_{14}:V_{64}:C_{22}$ (at.%), Sample 13, showing (Ni) peaks.

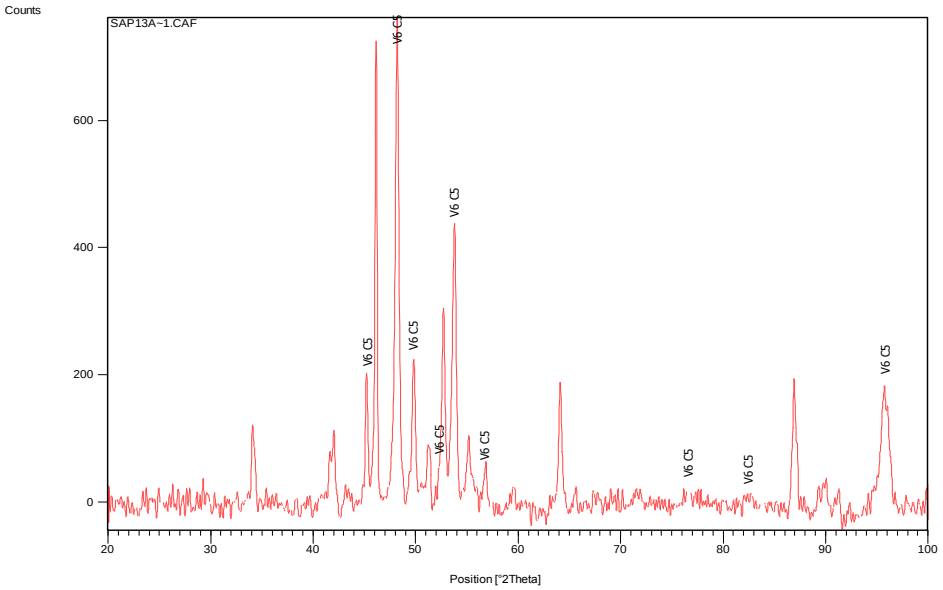


Figure 4.102a. XRD pattern of as-cast nominal $Ni_{14}:V_{64}:C_{22}$ (at.%), Sample 13, showing identified V_6C_5 peaks.

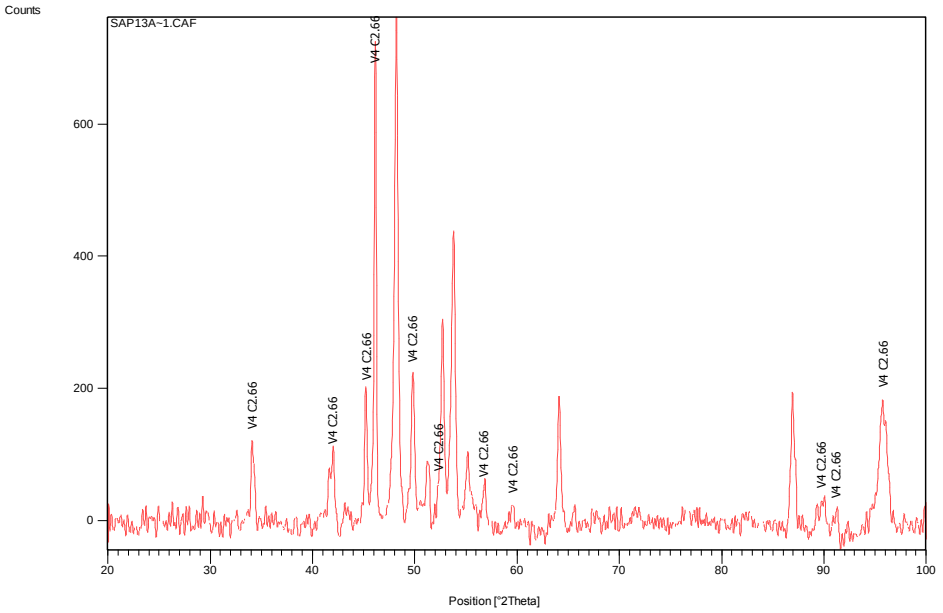


Figure 4.103b. XRD pattern of as-cast nominal $Ni_{14}:V_{64}:C_{22}$ (at.%), Sample 13, showing identified $V_4C_{2.66}$ peaks.

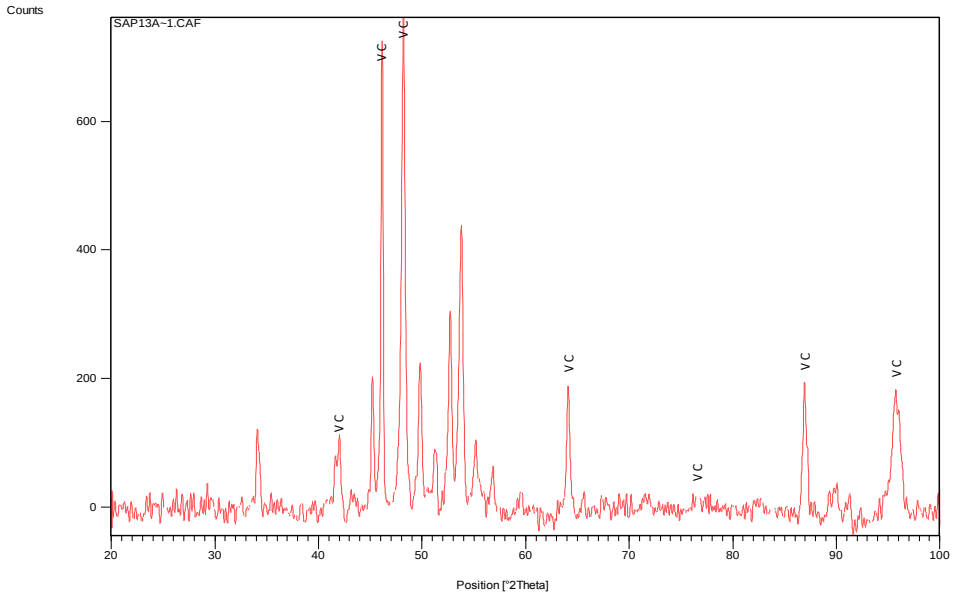


Figure 4.104a. XRD pattern of as-cast nominal $Ni_{14}:V_{64}:C_{22}$ (at.%), Sample 13, showing identified VC peaks.

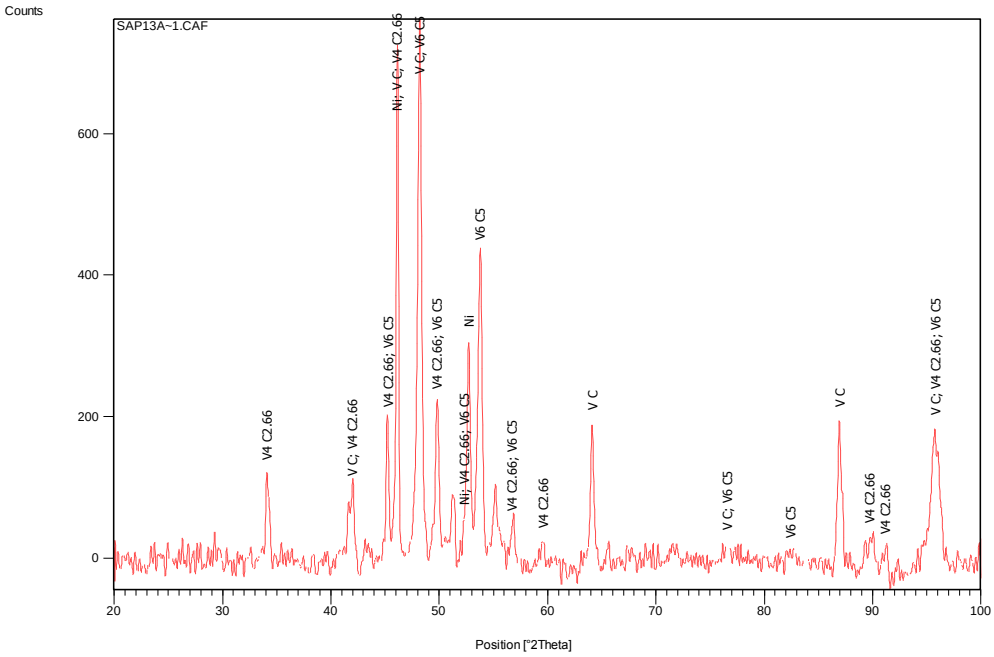


Figure 4.105b. XRD pattern of as-cast nominal $Ni_{14}:V_{64}:C_{22}$ (at.%), Sample 13, showing all the identified peaks.

Table 4.27. XRD peaks for as-cast nominal $Ni_{14}:V_{64}:C_{22}$ (at.%), Sample 13.

Position 2θ (º)	Height (counts)	Relative Intensity (%)	Phases
34.1072	118.00	15.65	$V_4C_{2.66}$
41.9470	96.00	12.73	$V_4C_{2.66}$,VC
43.3627	18.04	0.39	Unidentified
45.2460	187.00	24.80	$V_4C_{2.66}$,V_6C_5, Ni
46.1015	666.00	88.33	$V_4C_{2.66}$,VC, Ni
48.1775	754.00	100.00	VC,V_6C_5, Ni
49.7778	201.70	26.75	$V_4C_{2.66}$,V_6C_5
51.3395	75.03	9.82	Unidentified
52.2762	32.00	4.24	$V_4C_{2.66}$,V_6C_5, Ni
52.7136	282.22	37.43	Ni
53.7356	411.00	54.51	V_6C_5
55.2268	90.00	11.94	Unidentified
56.5560	11.00	1.46	$V_4C_{2.66}$
56.7120	33.00	4.38	V_6C_5
59.5771	20.00	2.65	$V_4C_{2.66}$
64.1272	187.00	24.80	VC
71.6228	15.00	1.99	Unidentified
76.5443	16.00	2.12	VC,V_6C_5
82.4489	7.00	0.93	V_6C_5
86.9575	191.00	25.33	VC
89.7449	28.00	3.71	$V_4C_{2.66}$
91.1759	12.00	1.59	$V_4C_{2.66}$
95.7511	179.00	23.74	$V_4C_{2.66}$,V_6C_5,VC

4.1.14 Nominal $Ni_{28}:V_{54}:C_{18}$ (at.%), Sample 14

Figure 4.106 shows the microstructure of the as-cast Sample 14. The microstructure shows two different regions: at the edge of the sample (Figure 4.106), which were characterised by dendrites, occasionally showing no arms, matrix and a eutectic comprising both phases. The centre of the sample (Figure 4.107) consisted of dark dendrites and light matrix at low magnification. A eutectic and some cracks in the dendrites, which may be due to brittleness or different coefficients of expansion between the phases, can be seen at higher magnification (Figure 4.108).

Table 4.29 gives the EDX analyses, and these were plotted in Figure 4.109. The overall composition was off the tie-line between two phases, showing that the ~VC in the eutectic had a layer C content than the primary ~VC (tending towards V_6C_5). The dendrites solidified with a range of morphologies, although the larger features were more needle-like than dendritic. The dendrites at the edge and middle regions had the same composition. Also, the eutectic was close to the overall composition. Generally, there were small experimental errors for the phases. The EDX analyses of Sample 14 are shown in Appendix B14.

The solidification sequence deduced from the microstructure is as follows:

$$L \rightarrow \sim VC$$

followed by the eutectic $L \rightarrow \sim VC + \sigma'$

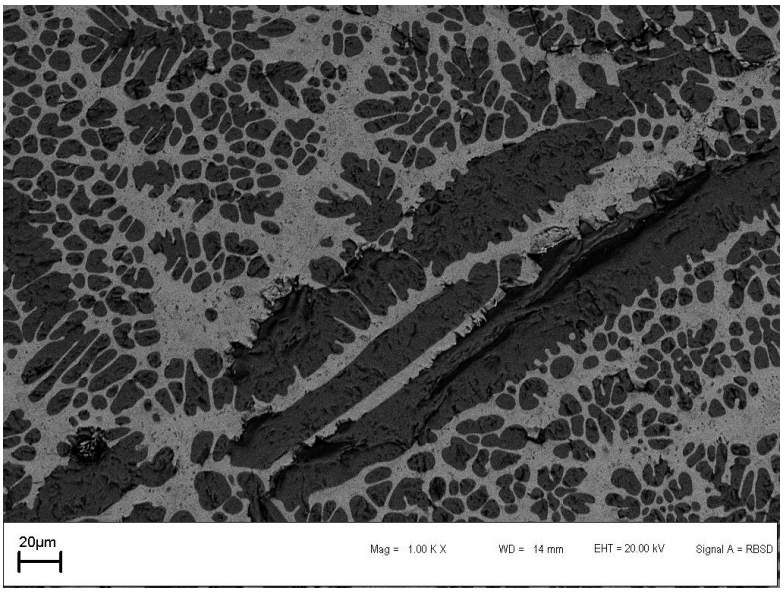


Figure 4.106. SEM-BSE image of nominal $Ni_{28}:V_{54}:C_{18}$ (at.%), Sample 14, in the as-cast condition, showing ~VC dendrites (dark) with cracks, σ′ matrix (light) and eutectic (edge region).

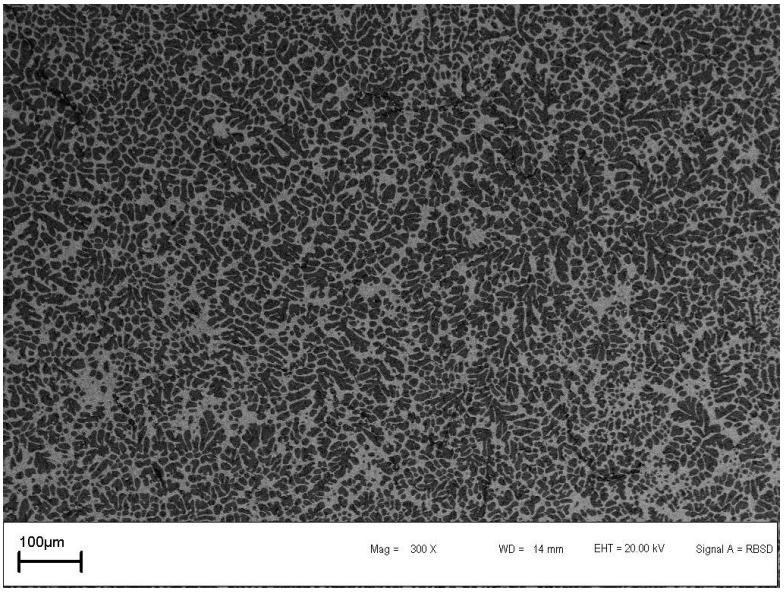


Figure 4.107. SEM-BSE image of nominal Ni_{28}:V_{54}:C_{18} (at.%), Sample 14, in the as-cast condition, showing ~VC dendrites (dark), σ′matrix (light) at low magnification (middle region).

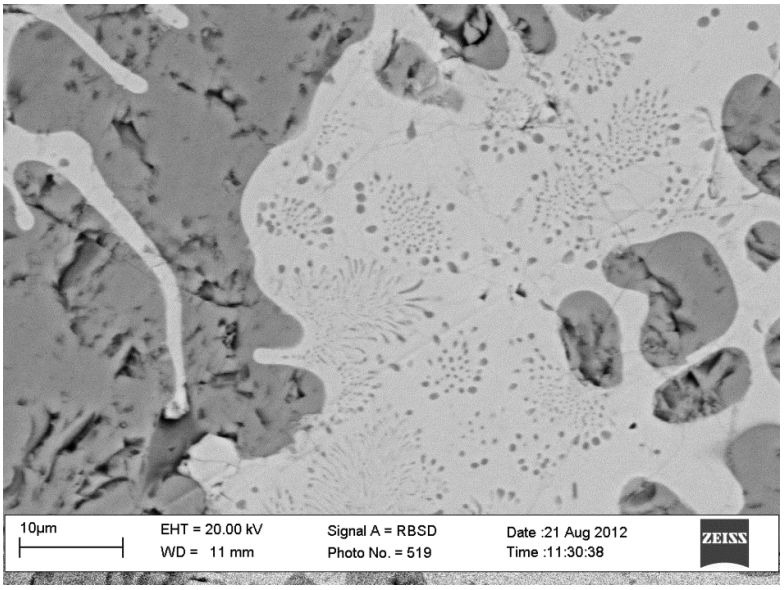


Figure 4.108. SEM-BSE image of nominal Ni_{28}:V_{54}:C_{18} (at.%), Sample 14, in the as-cast condition, showing ~VC dendrites (dark) with cracks, σ′ matrix (light) and eutectic at higher magnification (middle region).

Table 4.28. EDX phase analyses of as-cast nominal $Ni_{28}:V_{54}:C_{18}$ (at.%), Sample 14.

Phase Description	C	V	Ni	Phase
Overall	35.4 ± 0.4	55.3 ± 0.2	9.3 ± 0.3	-
Dark dendrites with arms	37.4 ± 0.4	62.3 ± 0.5	0.3 ± 0.1	~VC
Dark dendrites without arms	37.6 ± 0.5	62.1 ± 0.5	0.2 ± 0.01	~VC
Light	12.7 ± 0.6	56.7 ± 0.3	30.6 ± 0.5	σ′
Eutectic	35.2 ± 0.5	54.8 ± 0.4	10.0 ± 0.3	~VC + σ′

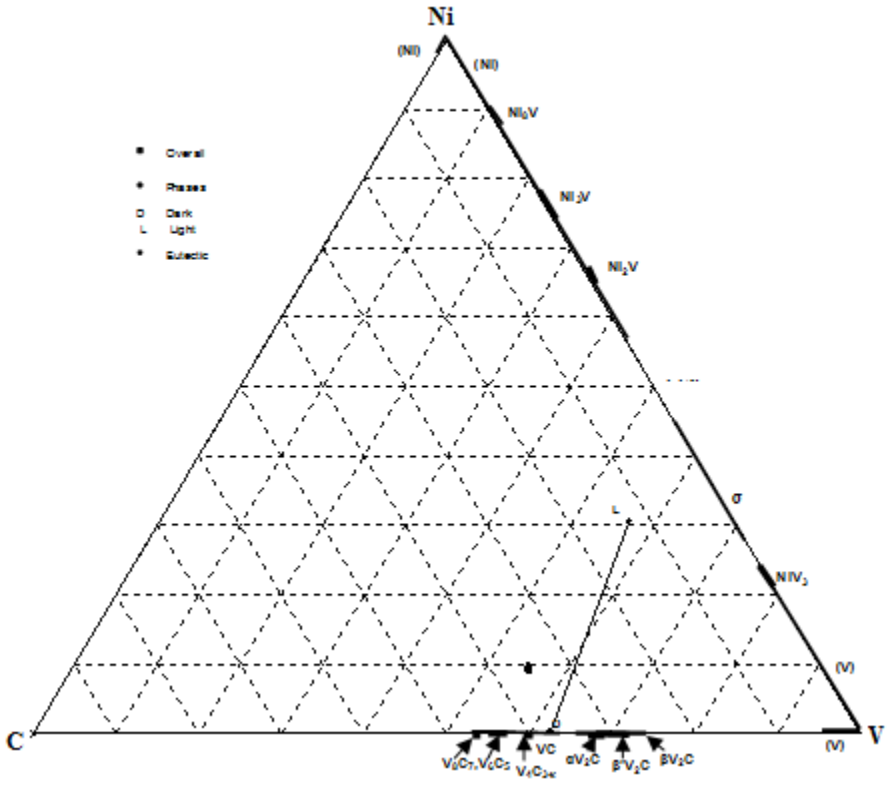


Figure 4.109. EDX analyses of as-cast nominal $Ni_{28}:V_{54}:C_{18}$ (at. %), Sample 14.

The XRD pattern shown in Figures 4.110 to 4.115 was fair, with a reasonable signal:background ratio, although the background was noisy. The presence of ~VC, C and ~$V_4C_{2.66}$ (which might not be present since it forms at lower temperatures in the solid state, and was not obvious in the microstructure) was indicated in Figure 4.113. There were several

unidentified peaks shown in Table 4.30, but when the Ni-V system [1982Smi] was consulted, they were assumed to be from the σ′ phase, which was not available in the International Crystallography Diffraction Database (ICDD) [2001ICD]. The presence of ~V_8C_7 and ~V_6C_5 could not be confirmed. Table 4.30 shows the identified peaks, together with their phases.

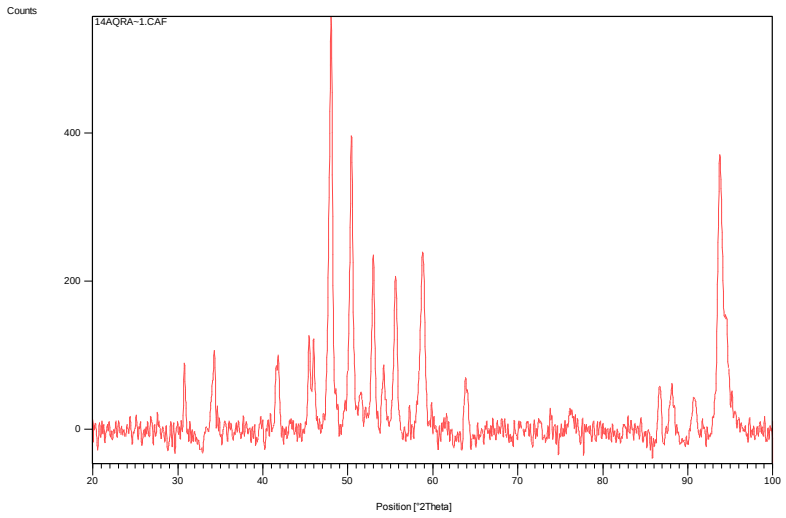


Figure 4.110. Unlabelled XRD pattern of as-cast nominal $Ni_{28}:V_{54}:C_{18}$ (at.%), Sample 14.

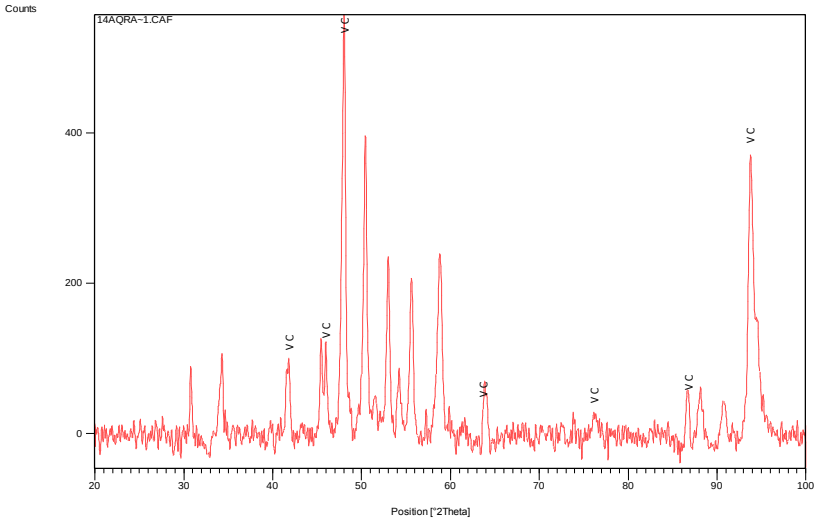


Figure 4.111. XRD pattern of as-cast nominal $Ni_{28}:V_{54}:C_{18}$ (at.%), Sample 14, showing identified VC peaks.

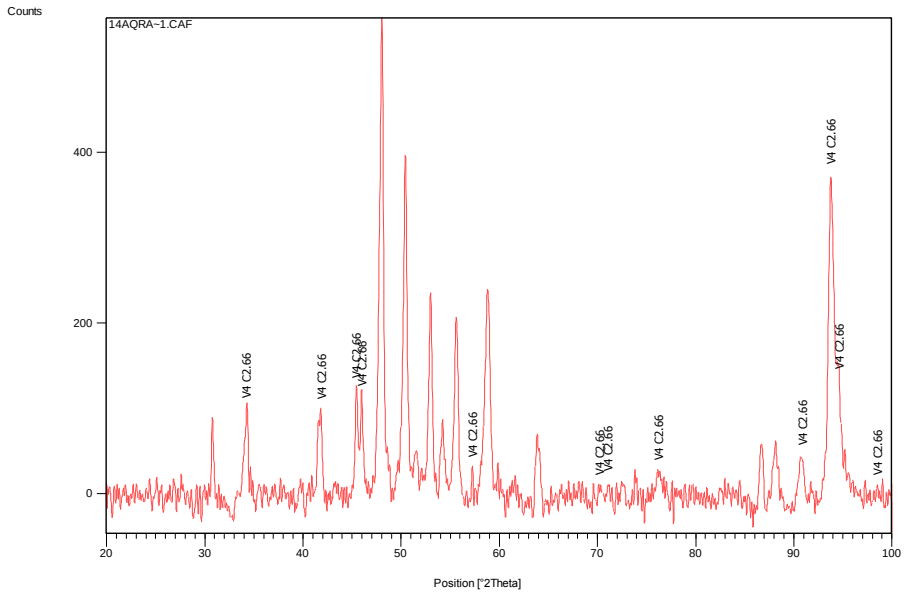


Figure 4.112. XRD pattern of as-cast nominal $Ni_{28}:V_{54}:C_{18}$ (at.%), Sample 14, showing identified $V_4C_{2.66}$ peaks.

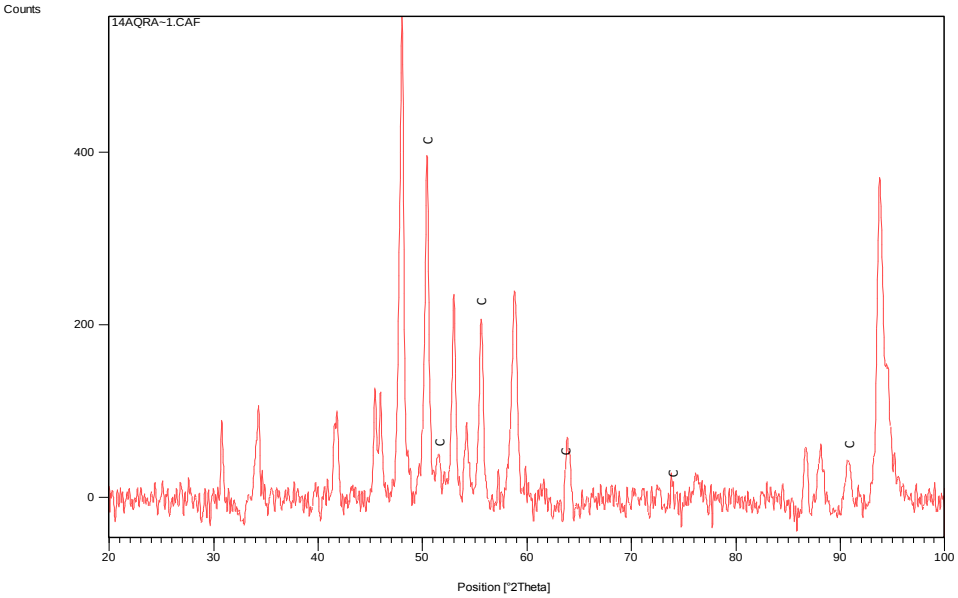


Figure 4.113. XRD pattern of as-cast nominal $Ni_{28}:V_{54}:C_{18}$ (at.%), Sample 14, showing identified C peaks.

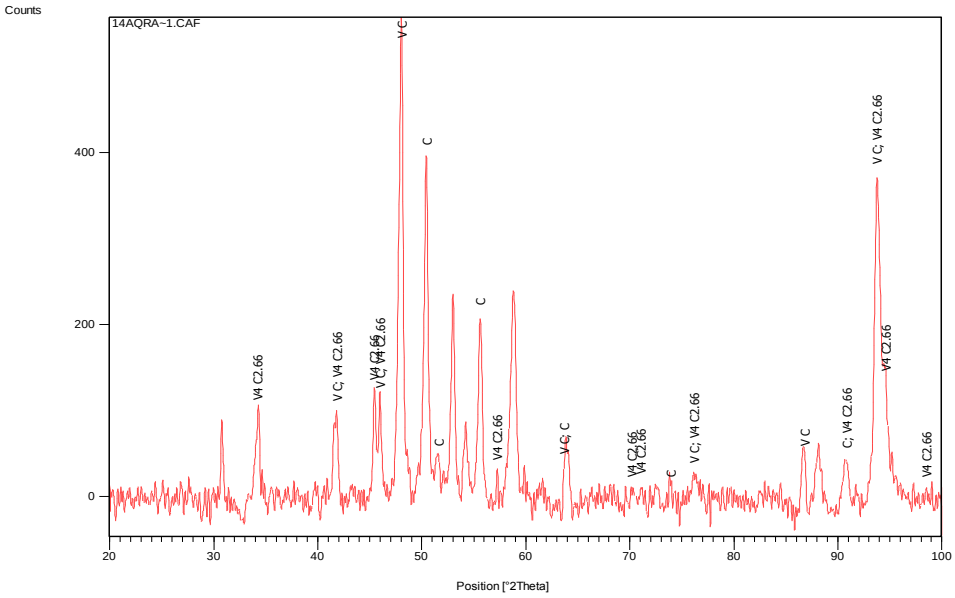


Figure 4.114. XRD pattern of as-cast nominal $Ni_{28}:V_{54}:C_{18}$ (at.%), Sample 14, showing all the identified peaks.

Table 4.29. XRD peaks for as-cast nominal $Ni_{28}:V_{54}:C_{18}$ (at.%), Sample 14.

Position 2θ (º)	Height (counts)	Relative Intensity (%)	Phases
30.7530	85.14	15.52	Presumed σ′
34.2311	96.04	17.50	$V_4C_{2.66}$
39.7792	10.32	1.88	Presumed σ′
41.8480	94.25	17.18	$V_4C_{2.66}$, VC
43.2431	12.46	2.27	Unidentified
45.4336	119.42	21.77	$V_4C_{2.66}$
46.0239	110.15	20.08	$V_4C_{2.66}$, VC
48.0653	548.64	100.00	VC
50.4473	393.27	71.68	C
51.6567	43.14	7.86	C
53.0068	233.50	42.56	Presumed σ′
54.1256	70.03	12.76	Presumed σ′
55.5990	208.05	37.92	C
57.2377	28.61	5.21	$V_4C_{2.66}$
58.8014	241.64	44.04	Presumed σ′
61.4658	10.28	1.87	Presumed σ′
63.6682	34.32	6.26	VC, C
70.2403	8.12	1.48	$V_4C_{2.66}$
71.0770	12.17	2.22	$V_4C_{2.66}$

Table 4.30 (cont.). XRD peaks for as-cast nominal $Ni_{28}:V_{54}:C_{18}$ (at.%), Sample 14.

72.5990	11.44	2.08	Presumed σ′
73.9776	8.67	1.58	C
76.2365	25.87	4.72	$V_4C_{2.66}$, VC
82.6589	4.83	0.88	Presumed σ′
86.8549	41.88	7.63	VC
88.2293	46.52	8.48	Presumed σ′
90.8577	41.38	7.54	$V_4C_{2.66}$, C
93.7453	369.09	67.27	$V_4C_{2.66}$, VC
94.6206	127.17	23.18	$V_4C_{2.66}$
98.5281	8.22	1.50	$V_4C_{2.66}$

4.1.15 Nominal $Ni_{32}:V_{56}:C_{12}$ (at.%), Sample 15

The microstructure of nominal $Ni_{32}:V_{56}:C_{12}$ (at.%), Sample 15, shows dark dendrites (some of which were cracked) identified as ~V_8C_7 and a eutectic with lighter regions identified as σ′ (Figure 4.115). The microstructure of Sample 15 had more of this eutectic compared to other samples. At higher magnification (Figure 4.116), more of the eutectic was visible, which was mainly lamellar and globular. With secondary electron imaging, the surface morphology showed some pores, possibly where material was removed on preparation (Figure 4.117).

Table 4.31 gives the EDX analyses, and these were plotted in Figure 4.118. The overall and eutectic compositions were off the tie-line between two phases, showing that the dark eutectic vanadium carbide component had a different composition from the dark dendrites. Also, the eutectic was close to the overall composition. Generally, there were small experimental errors for the phases. The EDX analyses of Sample 15 are shown in Appendix B15.

The deduced solidification sequence is: $L \rightarrow \sim VC$

followed by a eutectic reaction $L \rightarrow \sim VC + \sigma'$

then $\sim VC \rightarrow \sim V_8C_7$ in solid state transformation.

It was observed that the solidification sequence of Sample 15 is comparable to Sample 14. This may be due to the initial selected composition of the two samples before casting was close to the σ′-rich region.



Figure 4.115. SEM-BSE image of nominal Ni_{32}:V_{56}:C_{12} (at.%), Sample 15, in the as-cast condition, showing ~V_8C_7 dendrites (dark) and σ′ matrix (light).

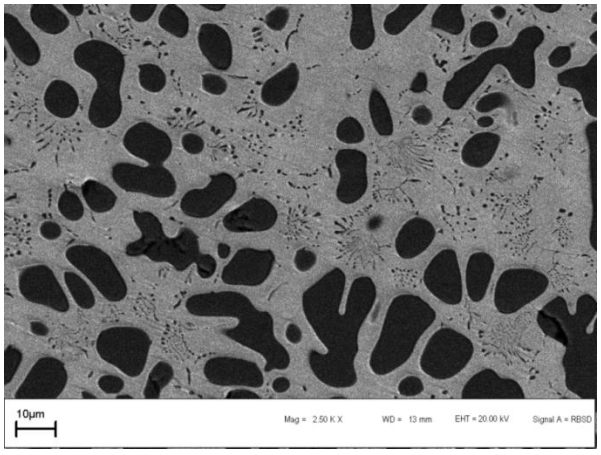


Figure 4.116. SEM-BSE image of nominal Ni_{32}:V_{56}:C_{12} (at.%), Sample 15, in the as-cast condition, showing ~V_8C_7 dendrites (dark), σ′ matrix (light) and eutectic at high magnification.

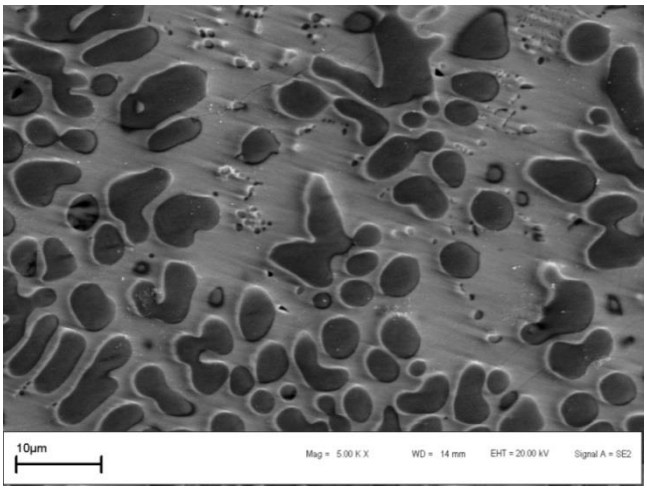


Figure 4.117. SEM-SE image of nominal $Ni_{32}:V_{56}:C_{12}$ (at.%), Sample 15, in the as-cast condition, showing ~V_8C_7 dendrites (dark), σ′ matrix (light) and eutectic at high magnification.

Table 4.30. Phase analyses of as-cast nominal $Ni_{32}:V_{56}:C_{12}$ (at.%), Sample 15.

Phase Description	**C**	**V**	**Ni**	**Phase**
Overall	29.9 ± 0.7	54.4 ± 0.7	15.7 ± 0.2	-
Dark	46.5 ± 0.5	52.5 ± 0.8	1.0 ± 0.5	~V_8C_7
Light	16.9 ± 0.9	49.6 ± 0.5	33.6 ± 0.8	σ′
Eutectic	28.7 ± 0.3	55.4 ± 0.3	15.9 ± 0.1	~VC + σ′

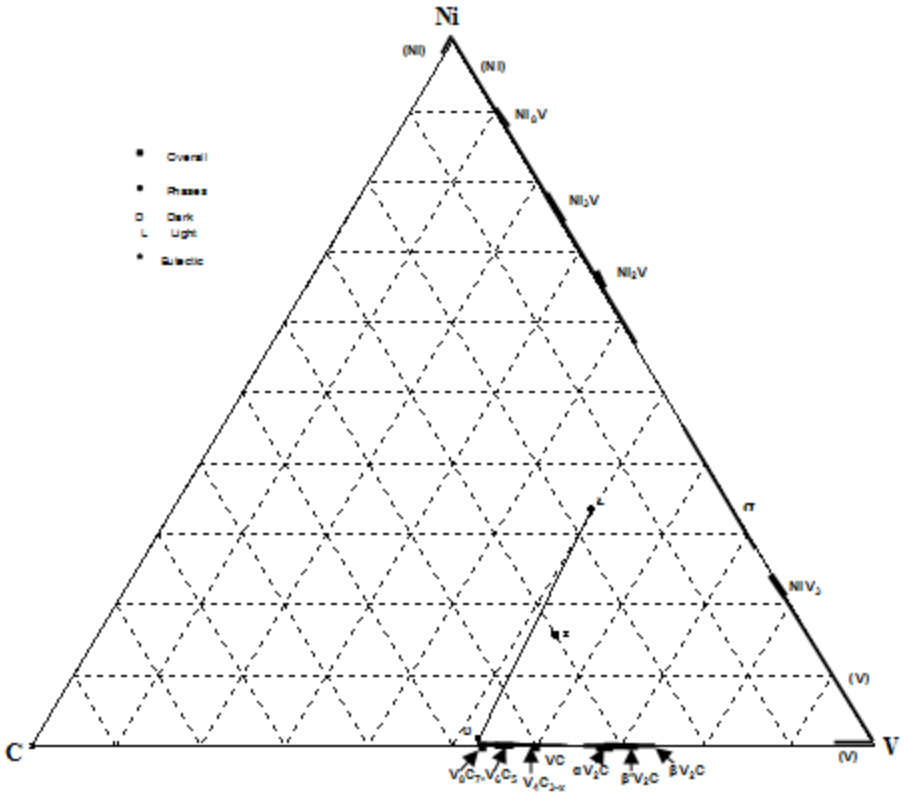


Figure 4.118. EDX analyses of as-cast nominal $Ni_{32}:V_{56}:C_{12}$ (at. %), Sample 15.

The XRD pattern shown in Figures 4.119 to 4.122 was reasonable, with a fair signal:background ratio. The hump at 2θ = 60 to 70° (Figure 4.119) before the background treatment may be due to presence of an amorphous phase. The hump was removed using the software, prior to the peaks being labelled. The existence of ~V_8C_7, and ~$V_4C_{2.66}$ (once again, possibly not present as it forms in the solid state at lower temperature) was identified. (V), ~V_2C and NiV_3 peaks could not be matched. The matches for the phases with the ICDD [2001ICD] were good, and the unidentified peaks which were assumed to be σ′, which had a similar composition to that analysed, according to the Ni-V binary [1982Smi]. A major peak was found at position 2θ = 45.06°, which matched both ~V_8C_7 and ~$V_4C_{2.66}$. Table 4.32 shows the identified peaks, together with their phases.

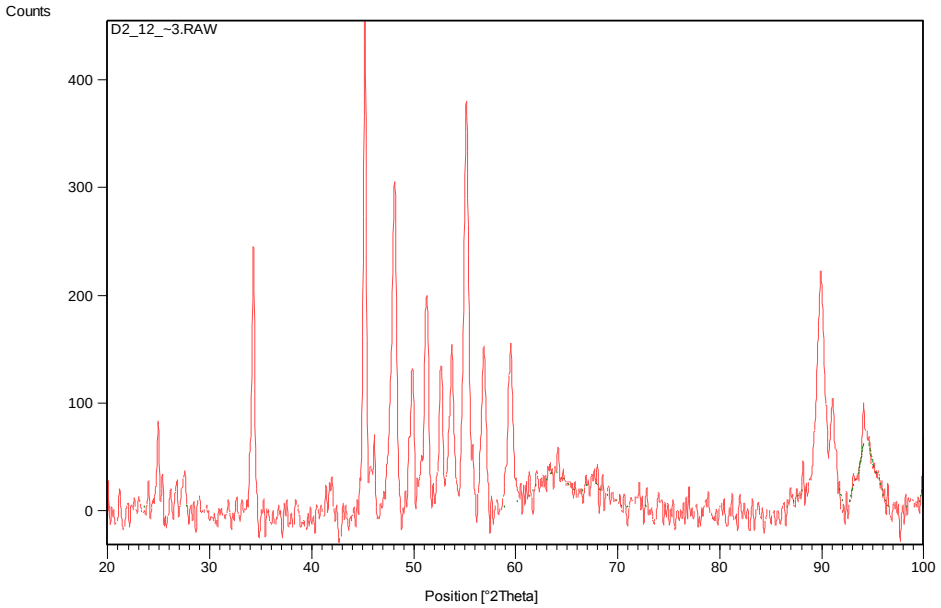


Figure 4.119. EDX analyses of as-cast nominal $Ni_{32}:V_{56}:C_{12}$ (at. %), Sample 15.

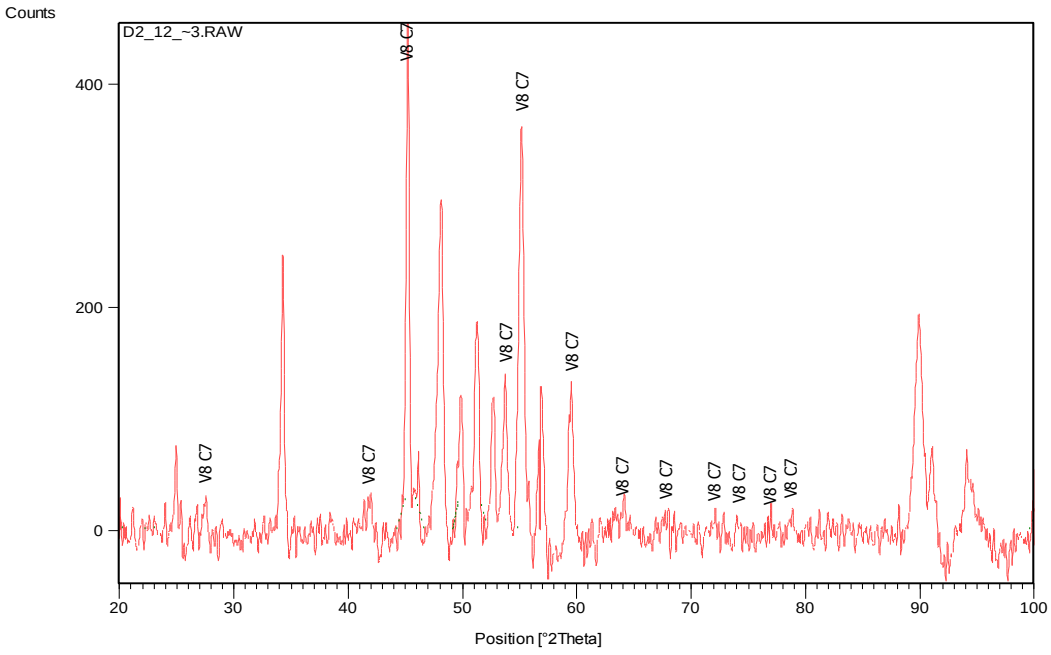


Figure 4.120. EDX analyses of as-cast nominal $Ni_{32}:V_{56}:C_{12}$ (at. %), Sample 15.

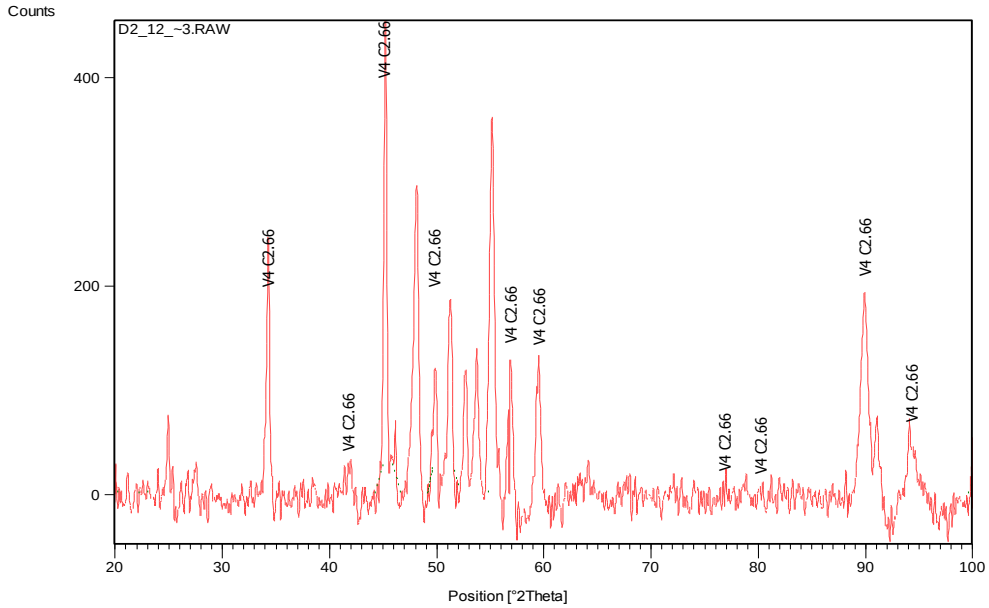


Figure 4.121. XRD pattern of as-cast nominal $Ni_{32}:V_{56}:C_{12}$ (at.%), Sample 15, showing identified $V_4C_{2.66}$ peaks.

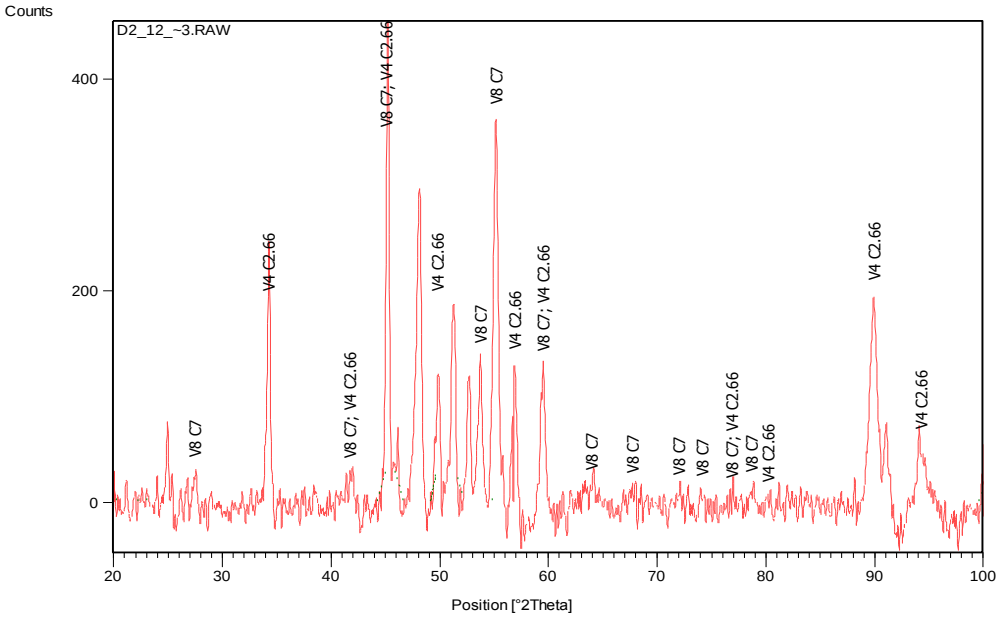


Figure 4.122. XRD pattern of as-cast nominal $Ni_{32}:V_{56}:C_{12}$ (at.%), Sample 15, showing all the identified peaks.

Table 4.31. XRD peaks for as-cast nominal $Ni_{32}:V_{56}:C_{12}$ (at.), Sample 15.

Position 2θ (º)	Height (counts)	Relative Intensity (%)	Phases
24.8257	25.66	5.87	Presumed σ′
27.4188	25.47	5.83	V_8C_7
28.8177	1.83	0.42	Presumed σ′
34.2090	181.10	41.46	$V_4C_{2.66}$
41.7584	24.57	5.62	$V_4C_{2.66}$, V_8C_7
45.0640	436.79	100.00	$V_4C_{2.66}$, V_8C_7
48.0922	295.86	67.73	Presumed σ′
49.7960	153.73	35.19	$V_4C_{2.66}$
52.6652	135.54	22.87	Presumed σ′
53.7116	129.10	29.56	V_8C_7
55.1488	355.84	81.47	V_8C_7
56.8751	127.57	29.21	$V_4C_{2.66}$
59.4717	125.11	28.64	$V_4C_{2.66}$, V_8C_7
63.9706	13.08	2.99	V_8C_7
67.7545	10.51	2.41	V_8C_7
71.9836	8.68	1.99	V_8C_7
74.1493	6.78	1.55	V_8C_7
76.8334	4.90	1.12	$V_4C_{2.66}$, V_8C_7
78.6877	11.01	2.52	V_8C_7
80.2032	1.57	0.36	$V_4C_{2.66}$
87.1246	12.06	2.04	Presumed σ′
89.9094	191.29	43.79	$V_4C_{2.66}$
91.0468	112.96	19.06	Presumed σ′
94.2629	51.32	11.75	$V_4C_{2.66}$
98.5964	5.70	0.96	Presumed σ′

4.1.16 Nominal $Ni_{39}:V_{42.8}:C_{18.2}$ (at.%), Sample 17

The nominal $Ni_{39}:V_{42.8}:C_{18.2}$ (at.%) alloy, Sample 17, possessed mainly dark dendrites identified as ~V_6C_5, surrounded by a eutectic of dark ~V_6C_5 and light ~Ni_2V phases and the light regions (matrix) as shown in Figure 4.123. Figure 4.124 shows the microstructure of the alloy at higher magnification. The as-cast alloy Sample 17 was similar to as-cast alloy Sample 5 in terms of morphology and solidification sequence.

The phase compositions are shown in Table 4.33 and plotted in Figure 4.125, showing the eutectic composition to be deviated from the tie-line between the dark primary phase and the light phase. This would be expected since there were some graphite flakes in the eutectic (Figure 4.123), even if a ~VC + (Ni) formed first. The deviation may be due to unidentified phases which may be present in the microstructure, especially considering the standard deviation of the measurements was below 1 at.%, meaning that the analyses were good. The EDX analyses of Sample 17 are shown in Appendix B16.

The deduced solidification sequence is: $L \rightarrow \sim VC$

followed by a eutectic reaction $L \rightarrow C + (Ni)$

followed by solid state reactions $\sim VC \rightarrow \sim V_6C_5$

$(Ni) \rightarrow \sim Ni_2V$

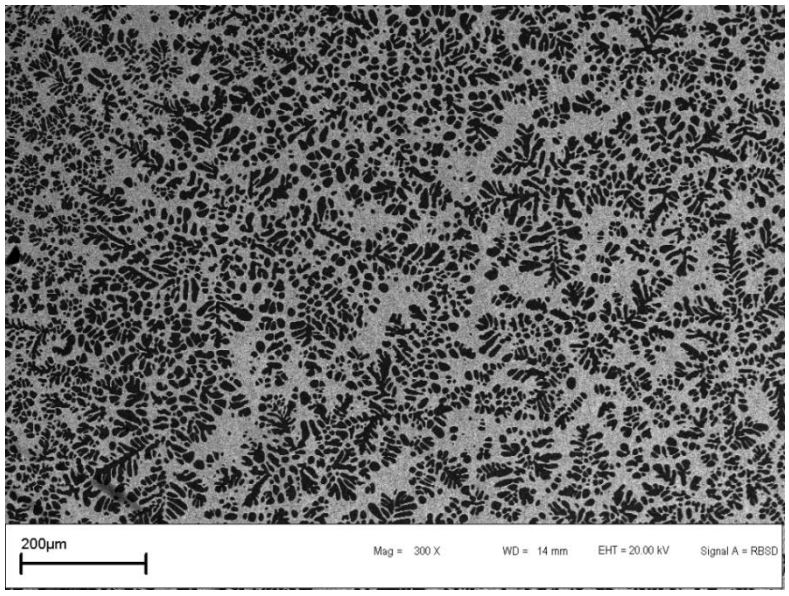


Figure 4.123. SEM-BSE image of nominal Ni_{39}:$V_{42.8}$:$C_{18.2}$ (at.%), Sample 17, in the as-cast condition, showing ~V_6C_5 dendrites (dark), ~Ni_2V matrix (light).

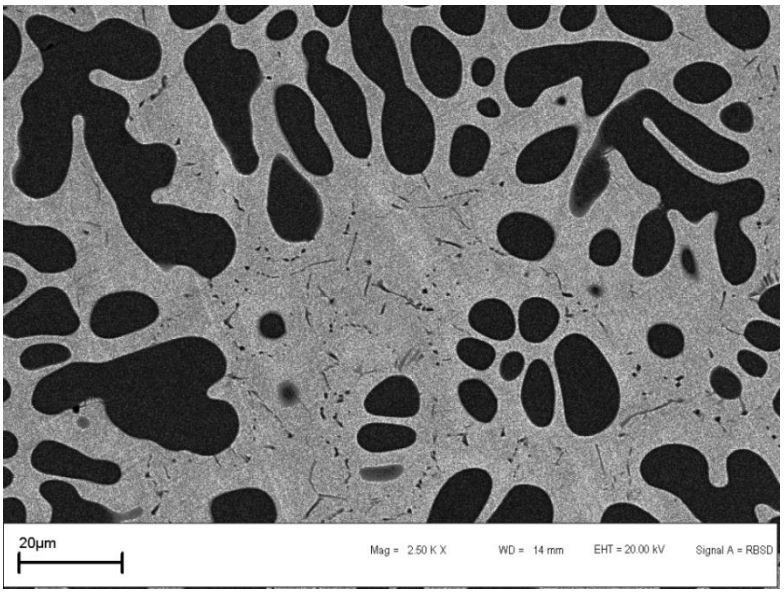


Figure 4.124. SEM-BSE image of nominal Ni_{39}:$V_{42.8}$:$C_{18.2}$ (at.%), Sample 17, in the as-cast condition, showing ~V_6C_5 dendrites (dark), ~Ni_2V matrix (light) and eutectic at higher magnification.

Table 4.32. Phase analyses of as-cast nominal Ni_{39}:$V_{42.8}$:$C_{18.2}$ (at.%), Sample 17.

Phase Description	**C**	**V**	**Ni**	**Phase**
Overall	34.1 ± 0.2	39.4 ± 0.4	26.5 ± 0.2	-
Dark	41.6 ± 0.2	57.8 ± 0.2	0.6 ± 0.1	~V_6C_5
Light	12.7 ± 0.6	28.6 ± 0.3	58.7 ± 0.5	~Ni_2V
Eutectics	32.6 ± 1.3	37.8 ± 0.9	29.6 ± 0.4	~VC + (Ni) (Ni) + C

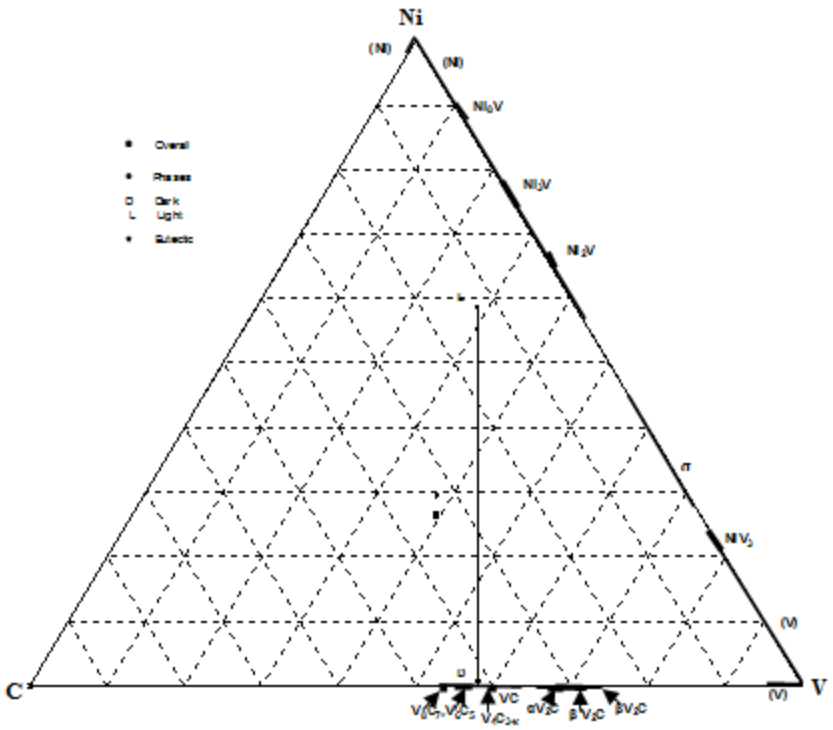


Figure 4.125. EDX analyses of as-cast nominal Ni_{39}:$V_{42.8}$:$C_{18.2}$ (at.%), Sample 17.

The XRD pattern, Figures 4.126 to 4.130, shows the experimental pattern of the Sample 17 with the database lines for each of the phases. The pattern was reasonable with a good signal:background ratio. The highest intensity peaks were V_6C_5 and Ni_2V, at about $2\theta = 51.10^o$. The pattern (Figure 4.130) confirmed the presence of ~V_6C_5, $V_4C_{2.66}$ and ~Ni_2V with unidentified peaks at $2\theta = 31.13^o$ and 64.11^o. By comparison with other spectra, C peaks were found at $2\theta = 51.10^o$, 55.69^o and 92.97^o. The difference in background between $2\theta = 60^o$ and 70° in Figure 4.128 compared to other pattern was due to background treatment. Table 4.34 shows the identified peaks, together with their phases.

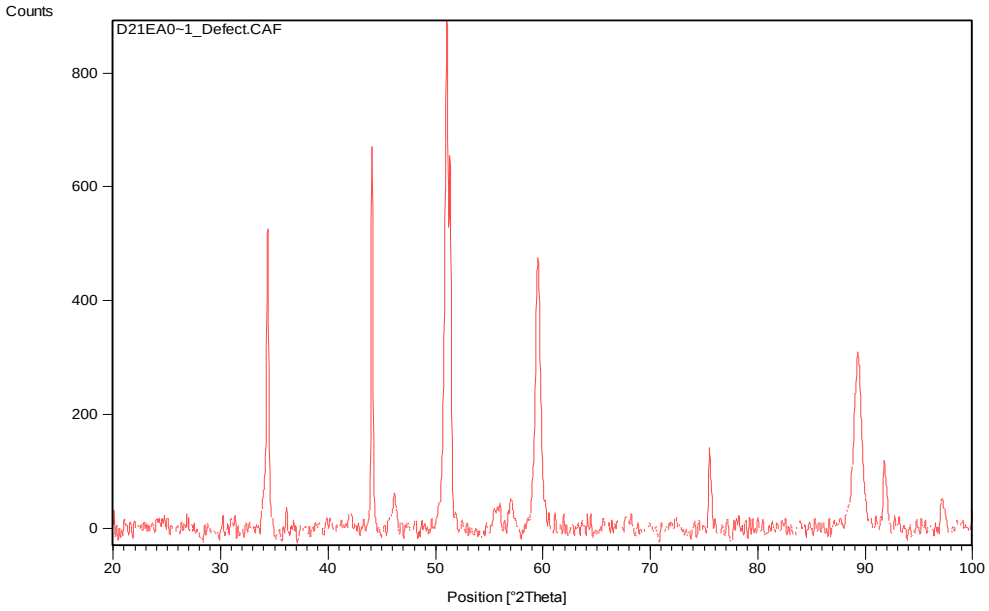


Figure 4.126. Unlabelled XRD pattern of as-cast nominal Ni_{39}:$V_{42.8}$:$C_{18.2}$ (at.%), Sample 17.

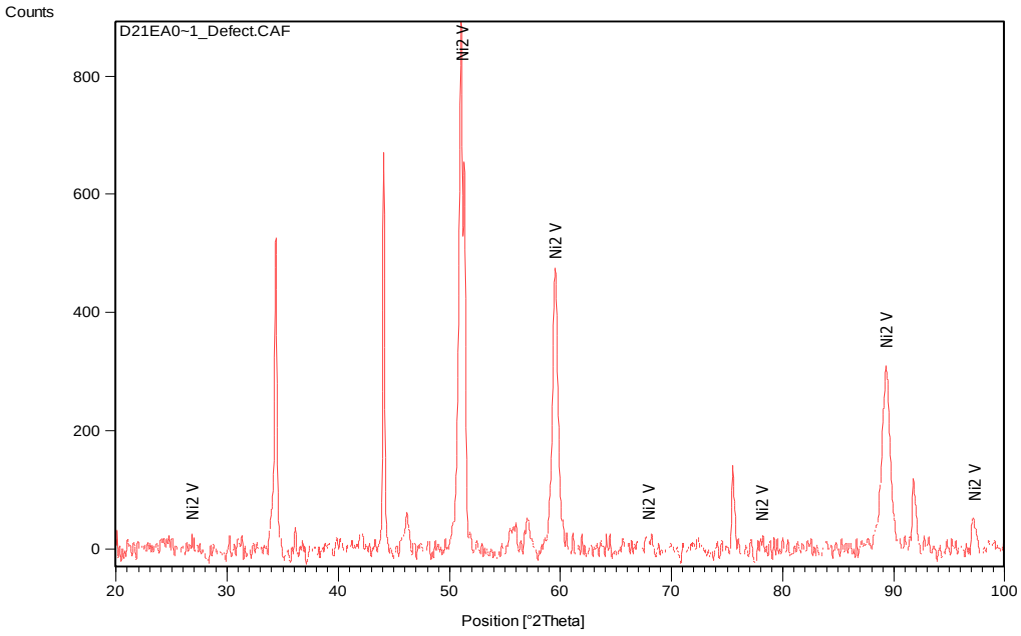


Figure 4.127. XRD pattern of as-cast nominal Ni_{39}:$V_{42.8}$:$C_{18.2}$ (at.%), Sample 17, showing identified Ni_2V peaks.

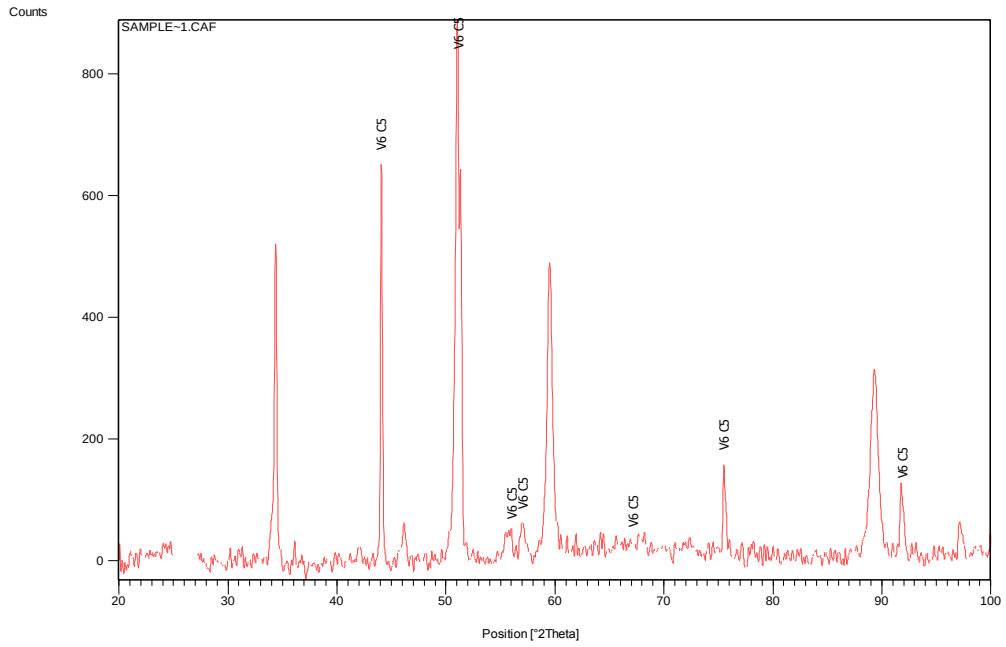


Figure 4.128. XRD pattern of as-cast nominal $Ni_{39}:V_{42.8}:C_{18.2}$ (at.%), Sample 17, showing identified V_6C_5 peaks.

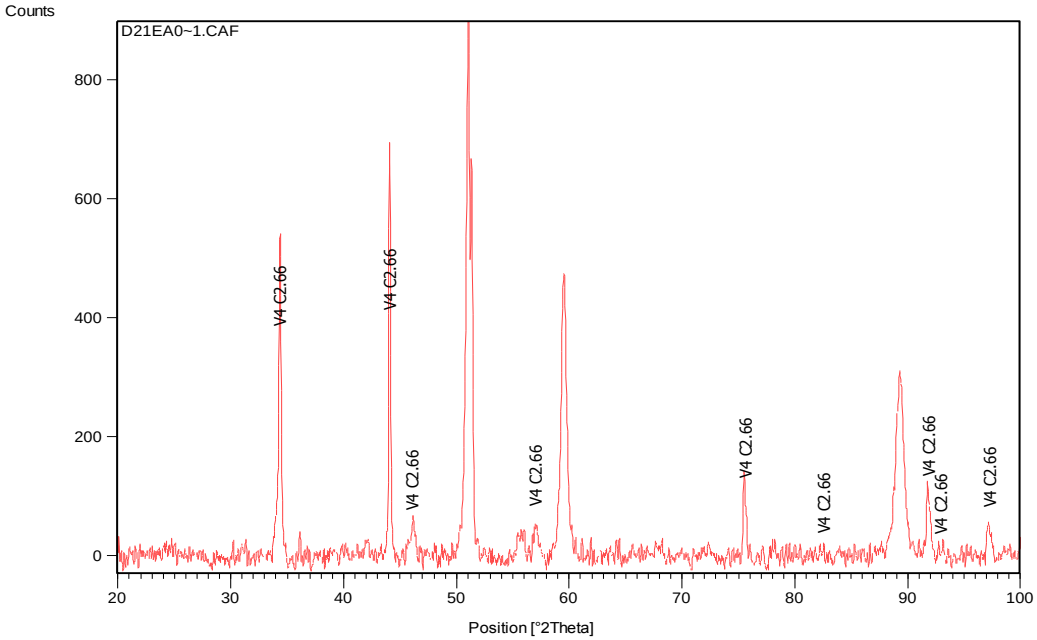


Figure 4.129. XRD pattern of as-cast nominal $Ni_{39}:V_{42.8}:C_{18.2}$ (at.%), Sample 17, showing identified $V_4C_{2.66}$ peaks.

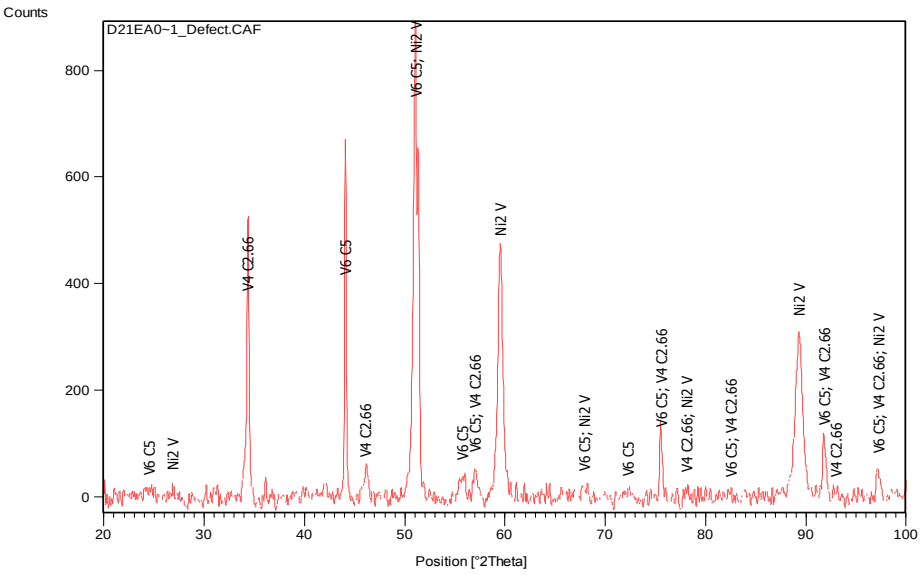


Figure 4.130. XRD pattern of as-cast nominal Ni_{39}:$V_{42.8}$:$C_{18.2}$ (at.%), Sample 17, showing all the identified peaks.

Table 4.33. XRD peaks for as-cast nominal Ni_{39}:$V_{42.8}$:$C_{18.2}$ (at.), Sample 17.

Position 2θ (º)	Height (counts)	Relative Intensity (%)	Phases
24.4639	6.95	0.88	V_6C_5
26.8653	16.40	2.07	Ni_2V
31.1310	5.53	0.70	Unidentified
34.3102	353.91	44.72	$V_4C_{2.66}$
44.0843	383.11	48.41	V_6C_5
46.0438	41.27	5.21	$V_4C_{2.66}$
51.1033	791.46	100.00	V_6C_5, Ni_2V,C
55.6966	36.58	4.62	V_6C_5, C
57.0053	50.27	6.35	$V_4C_{2.66}$, Ni_2V
59.5235	456.88	57.73	Ni_2V
64.1195	4.29	0.54	Unidentified
67.9288	13.68	1.73	V_6C_5, Ni_2V
72.2191	5.42	0.68	V_6C_5
75.6263	98.02	12.38	V_6C_5, $V_4C_{2.66}$
78.1186	12.85	1.62	$V_4C_{2.66}$, Ni_2V
83.9785	5.02	0.63	V_6C_5, $V_4C_{2.66}$
89.3104	298.49	37.71	Ni_2V
91.8492	98.26	12.41	V_6C_5, $V_4C_{2.66}$
92.9730	2.67	0.34	$V_4C_{2.66}$, C
97.2087	47.88	6.05	V_6C_5, Ni_2V, $V_4C_{2.66}$

4.1.17 Nominal $Ni_{66.4}$:$V_{16.1}$:$C_{17.5}$ (at.%), Sample 18

An SEM-BSE image of the representative microstructure of nominal $Ni_{66.4}$:$V_{16.1}$:$C_{17.5}$ (at.%), Sample 18, in the as-cast condition is shown in Figure 4.131 at low magnification. The alloy had two contrasts. These were dendrites whose contrast was dark, identified as ~V_8C_7 with cracks, the light regions (matrix) were identified as (Ni), and a eutectic of dark and light phases. Figure 4.132 shows the microstructure of the alloy at higher magnification.

The phase compositions are shown in Table 4.35 and plotted in Figure 4.133, showing the overall and the eutectic compositions to be deviated from the tie-line joining the two phases. The deviation was due to graphite, which was present in the second eutectic (as flakes), and would move the overall analyses nearer to carbon. The standard deviation of the measurements was below 1 at.%, which shows that the analysis was good. The EDX analyses of Sample 18 are shown in Appendix B17.

The deduced solidification sequence is: $L \rightarrow \sim VC$

followed by a eutectic reaction: $L \rightarrow C + (Ni)$

followed by solid state reaction: $\sim VC \rightarrow \sim V_8C_7$

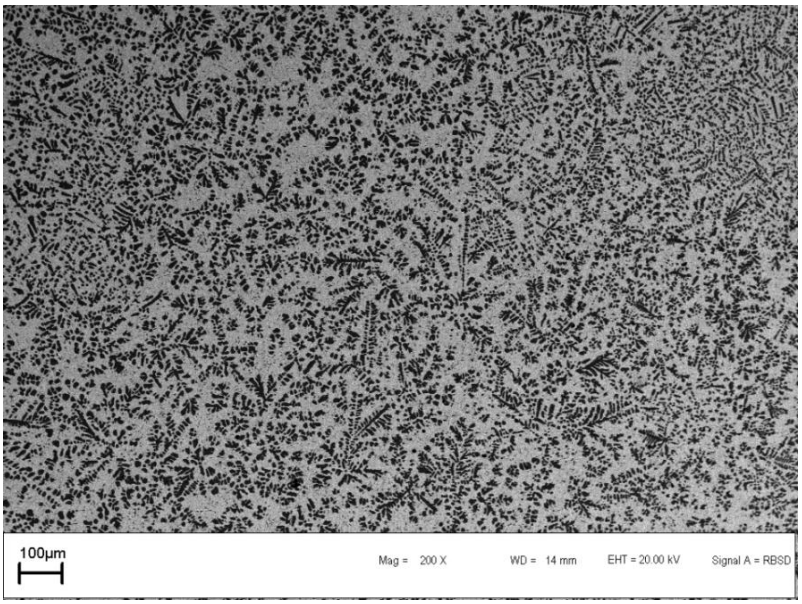


Figure 4.131. SEM-BSE image of nominal $Ni_{66.4}$:$V_{16.1}$:$C_{17.5}$ (at.%), Sample 18, in the as-cast condition, showing ~V_8C_7 dendrites (dark), (Ni) matrix (light).

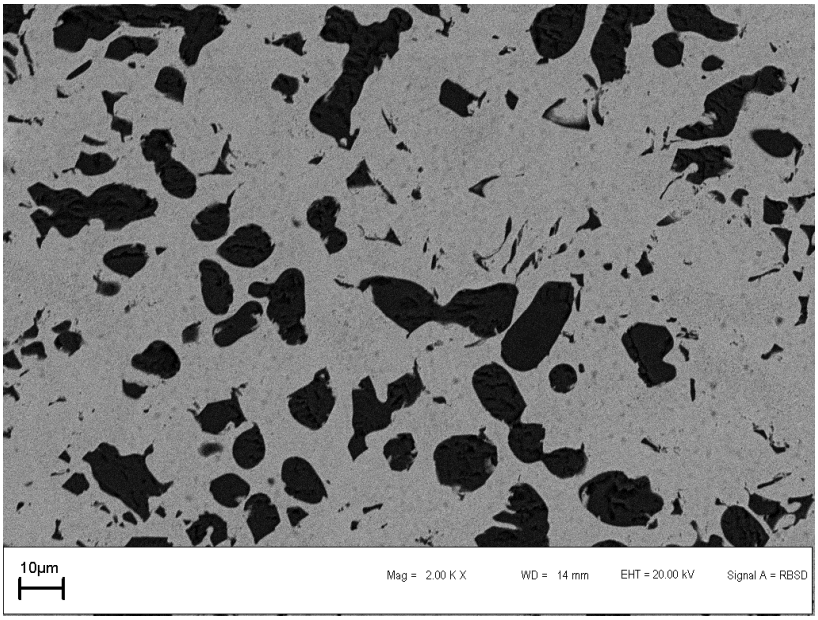


Figure 4.132. SEM-BSE image of nominal $Ni_{66.4}$:$V_{16.1}$:$C_{17.5}$ (at.%), Sample 18, in the as-cast condition, showing ~V_8C_7 dendrites (dark), (Ni) matrix (light) and eutectic at higher magnification.

Table 4.34. Phase analyses of as-cast nominal $Ni_{66.4}$:$V_{16.1}$:$C_{17.5}$ (at.%), Sample 18.

Phase Description	C	V	Ni	Phase
Overall	37.3 ± 0.6	20.2 ± 0.9	42.5 ± 0.3	-
Dark	46.0 ± 0.6	53.1 ± 0.6	1.0 ± 0.6	~V_8C_7
Light	20.0 ± 0.5	3.5 ± 0.3	76.5 ± 0.5	(Ni)
Eutectics	34.6 ± 0.4	17.4 ± 0.5	48.0 ± 0.5	~VC + (Ni) (Ni) + C

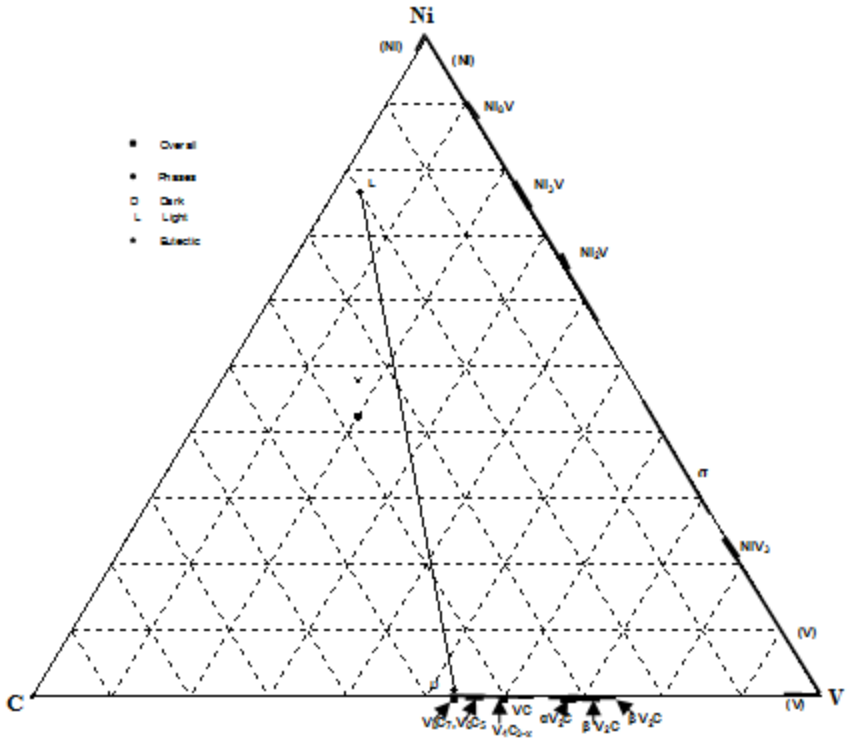


Figure 4.133. EDX analyses of as-cast nominal $Ni_{66.4}$:$V_{16.1}$:$C_{17.5}$ (at.%), Sample 18.

The XRD pattern shown in Figures 4.134 to 4.139 was reasonable, with a good signal:background ratio. The XRD pattern (Figure 4.139) confirmed the presence of ~V_8C_7, C, ~$V_4C_{2.66}$ and (Ni). The highest intensity peak at about $2\theta = 60.17^o$ shows that the peak is a combination of ~V_8C_7, ~$V_4C_{2.66}$, C and (Ni). All peaks could be matched, except the one at $2\theta = 56^o$, this could be an impurity. Table 4.36 shows the identified peaks, together with their phases.

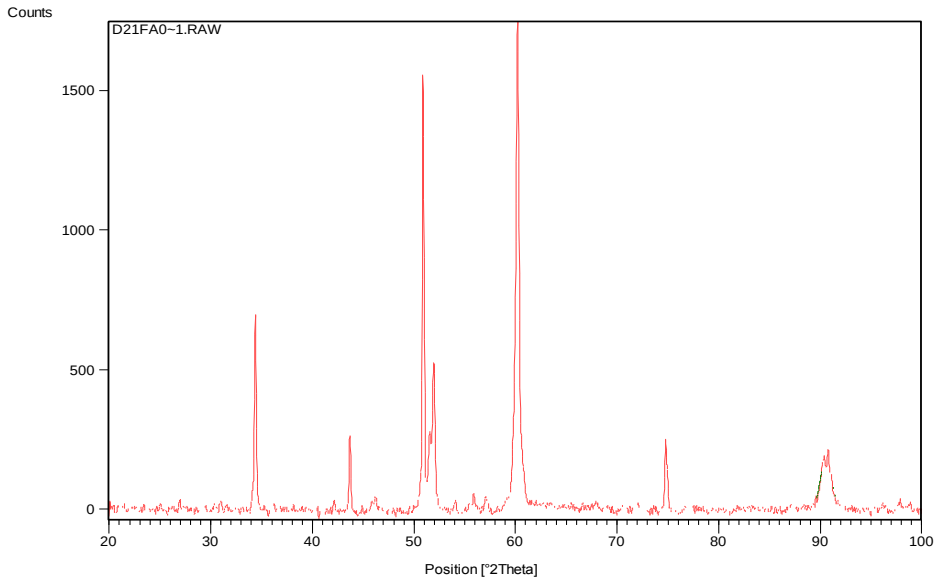


Figure 4.134. Unlabelled XRD pattern of as-cast nominal $Ni_{66.4}$:$V_{16.1}$:$C_{17.5}$ (at.%), Sample 18.

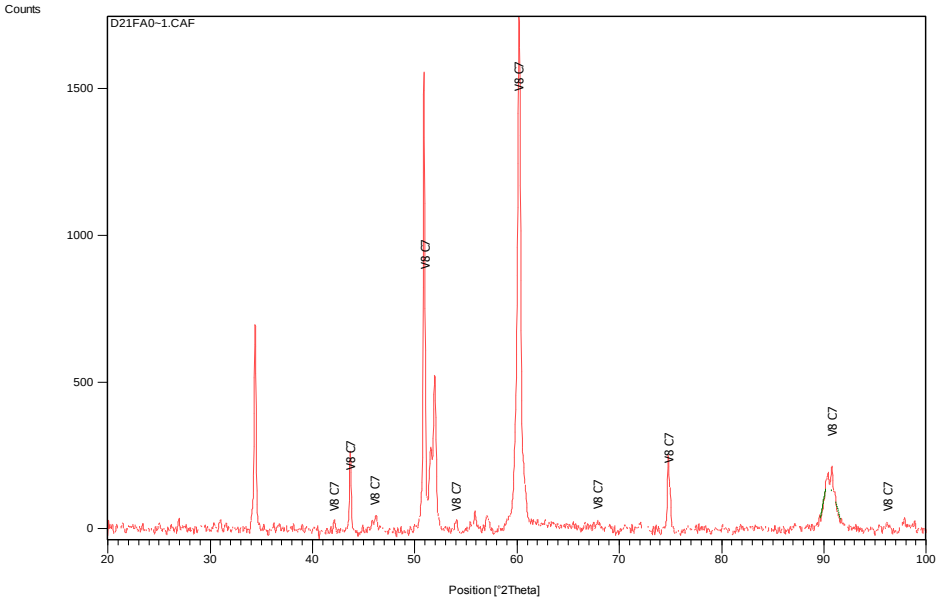


Figure 4.135. XRD pattern of as-cast nominal $Ni_{66.4}$:$V_{16.1}$:$C_{17.5}$ (at.%), Sample 18, showing identified V_8C_7 peaks.

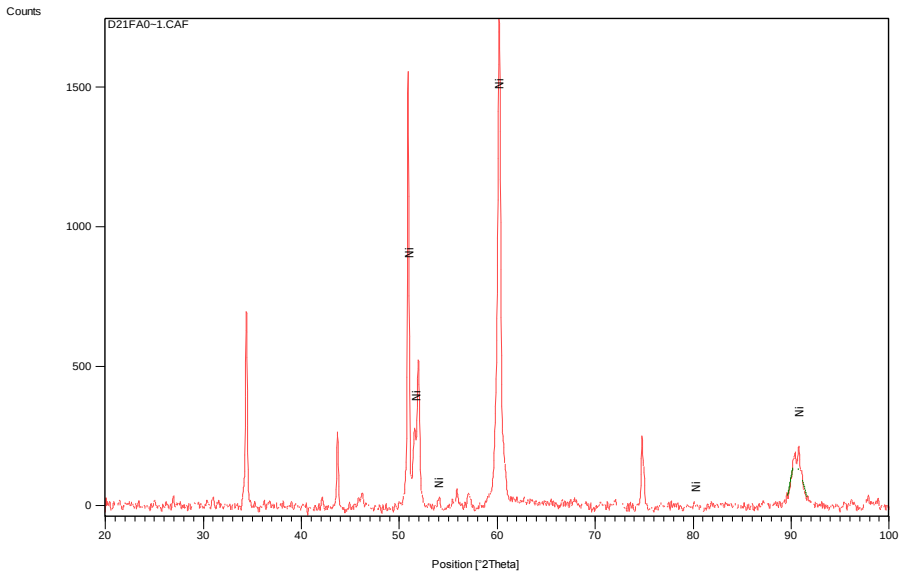


Figure 4.136. XRD pattern of as-cast nominal $Ni_{66.4}$:$V_{16.1}$:$C_{17.5}$ (at.%), Sample 18, showing identified Ni peaks.

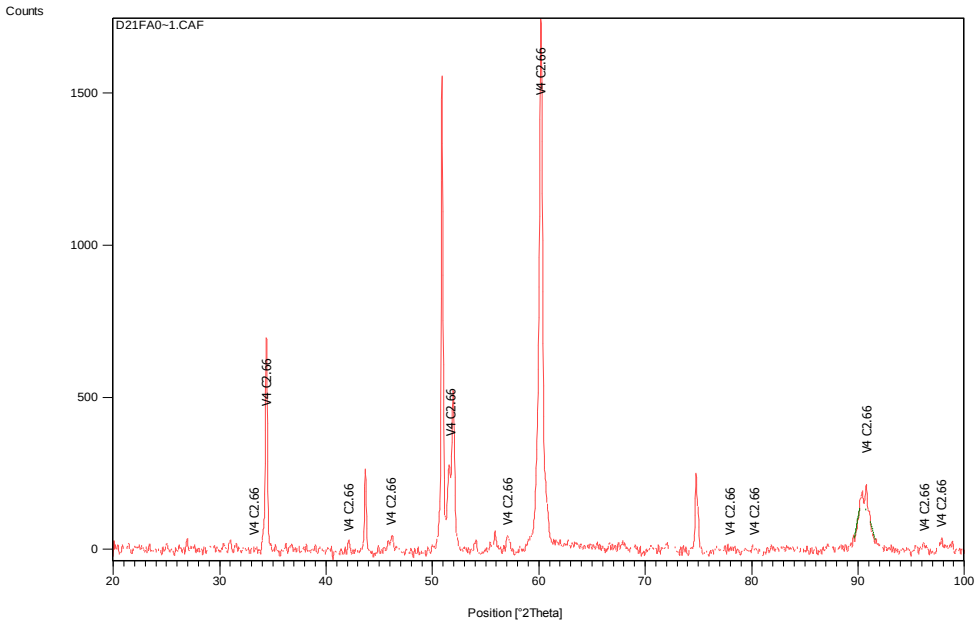


Figure 4.137. XRD pattern of as-cast nominal $Ni_{66.4}$:$V_{16.1}$:$C_{17.5}$ (at.%), Sample 18, showing identified $V_4C_{2.66}$ peaks.

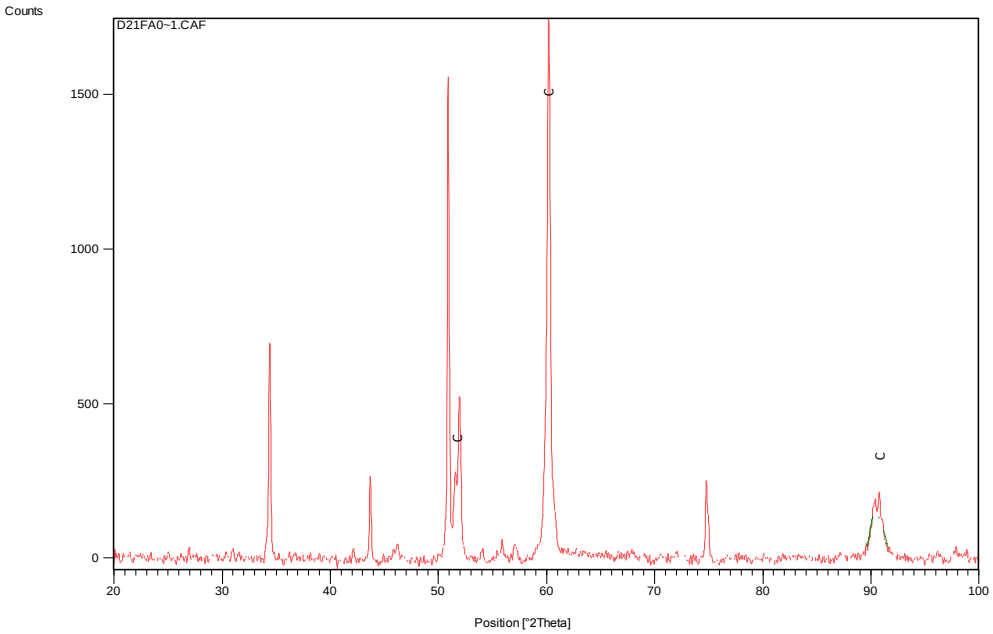


Figure 4.138. XRD pattern of as-cast nominal $Ni_{66.4}:V_{16.1}:C_{17.5}$ (at.%), Sample 18, showing identified C peaks.

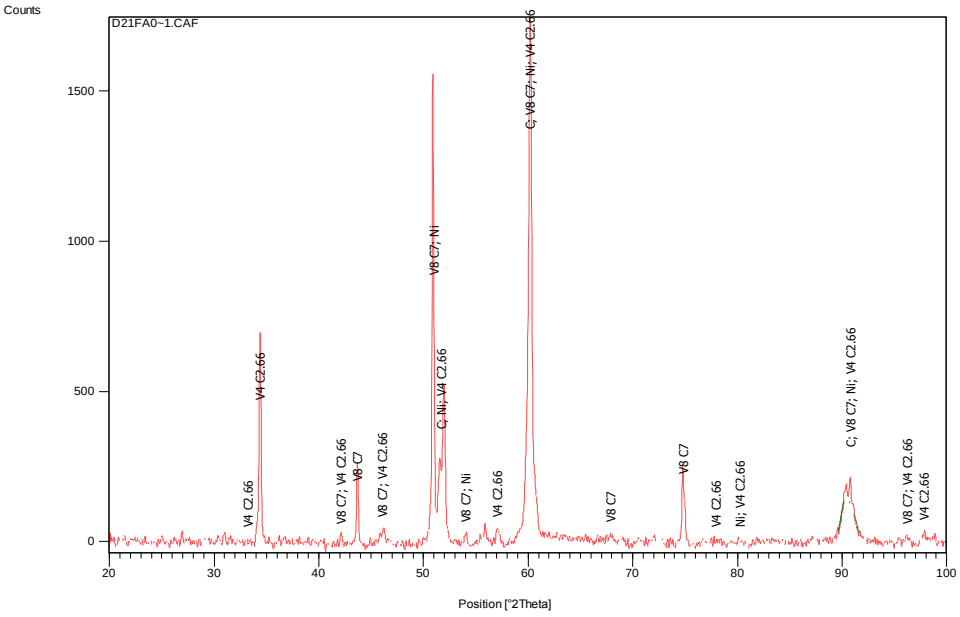


Figure 4.139. XRD pattern of as-cast nominal $Ni_{66.4}:V_{16.1}:C_{17.5}$ (at.%), Sample 18, showing all the identified peaks.

Table 4.35. XRD peaks for as-cast nominal $Ni_{66.4}:V_{16.1}:C_{17.5}$ (at.%), Sample 18.

Position 2θ (º)	Height (counts)	Relative Intensity (%)	Phases
33.2112	0.63	0.04	$V_4C_{2.66}$
34.3730	424.86	29.70	$V_4C_{2.66}$
42.1205	12.08	0.84	$V_4C_{2.66}$, V_8C_7
43.6635	153.00	10.70	V_8C_7
46.1042	33.41	2.34	V_8C_7
50.9723	835.42	58.41	V_8C_7, Ni
51.7011	324.30	22.67	$V_4C_{2.66}$, Ni, C
54.0059	15.57	1.09	V_8C_7, Ni
55.8796	51.95	3.63	Unidentified
57.0806	33.10	2.31	$V_4C_{2.66}$
60.1790	1430.36	100.00	$V_4C_{2.66}$, V_8C_7, Ni, C
67.9217	17.70	1.24	V_8C_7
74.8264	177.51	12.41	V_8C_7
77.9454	1.94	0.14	$V_4C_{2.66}$
80.2371	1.84	0.13	$V_4C_{2.66}$, Ni
90.7791	144.74	10.12	$V_4C_{2.66}$, V_8C_7, Ni, C
96.2004	12.54	0.88	$V_4C_{2.66}$, V_8C_7
97.7758	26.19	1.83	$V_4C_{2.66}$

4.1.18 Nominal $Ni_{68}:V_{14}:C_{18}$ (at.%), Sample 19

The nominal $Ni_{68}:V_{14}:C_{18}$ (at.%) alloy, Sample 19, possessed dark dendrites identified as ~V_8C_7, surrounded by a eutectic of ~VC + (Ni), and the light regions were identified as (Ni), as shown in Figure 4.140 at low magnification. Figure 4.141 shows the microstructure of the alloy at higher magnification, showing the eutectic in better detail which had both globular (~VC) and (flake-like) (C) attributes.

Table 4.37 gives the EDX analyses, and these are plotted in Figure 4.142. The overall and eutectic compositions were slightly off the tie-line between two phases, although still within the expected error. Also, the eutectic was close to the overall composition, which is not surprising, since it comprised most of the sample. The carbon in ~VC was over-reported as shown in the plot. Generally, there were small experimental errors for the phases. The EDX analyses of Sample 19 are shown in Appendix B18.

The deduced solidification sequence is: $L \rightarrow \sim VC$

followed by a eutectic reaction: $L \rightarrow \sim VC + (Ni)$

$L \rightarrow C + (Ni)$

followed by the solid state reaction: $\sim VC \rightarrow \sim V_8C_7$ (~1140ºC in the binary [1985Car]).

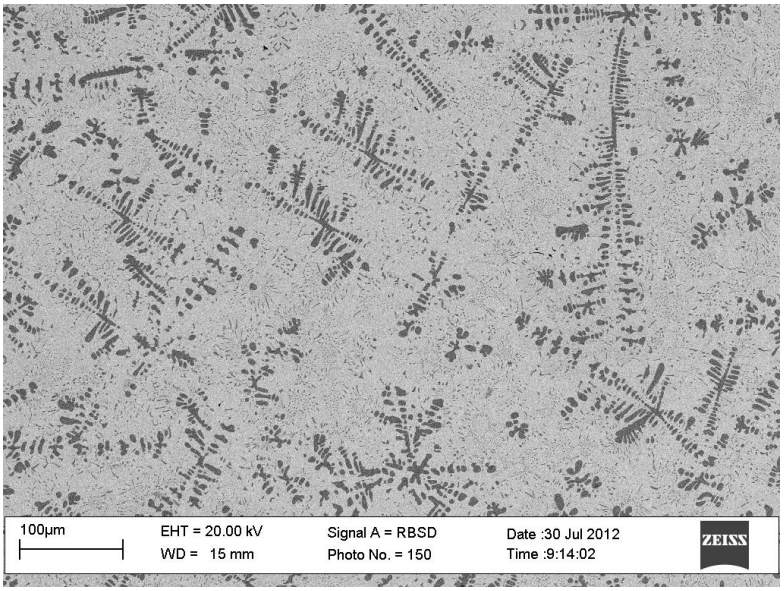


Figure 4.140. SEM-BSE image of nominal Ni_{68}:V_{14}:C_{18} (at.%), Sample 19, in the as-cast condition, showing ~V_8C_7 dendrites (dark), (Ni) matrix (light) and ~VC + (Ni) eutectic.

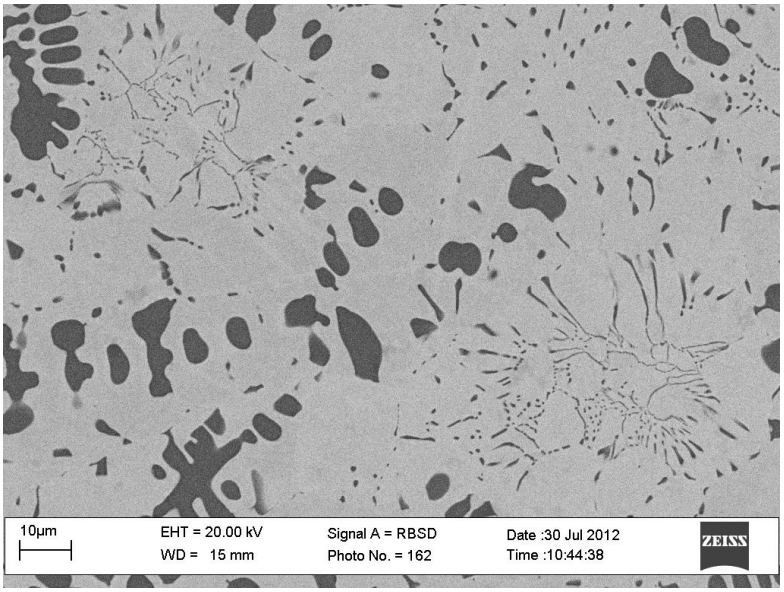


Figure 4.141. SEM-BSE image of nominal Ni_{68}:V_{14}:C_{18} (at.%), Sample 19, in the as-cast condition, showing ~V_8C_7 dendrites (dark), (Ni) matrix (light) and ~VC + (Ni) and C + (Ni) eutectics at higher magnification.

Table 4.36. EDX phase analyses of as-cast nominal Ni_{68}:V_{14}:C_{18} (at.%), Sample 19.

Phase Description	C	V	Ni	Phase
Overall	30.6 ± 0.7	14.7 ± 0.5	54.7 ± 0.9	-
Dark	49.2 ± 0.7	49.1 ± 0.2	1.7 ± 0.5	~V_8C_7
Light	27.6 ± 0.9	5.9 ± 0.2	66.5 ± 0.1	(Ni)
Eutectics	29.4 ± 0.4	13.7 ± 0.4	56.9 ± 0.6	~VC + (Ni) C + (Ni)

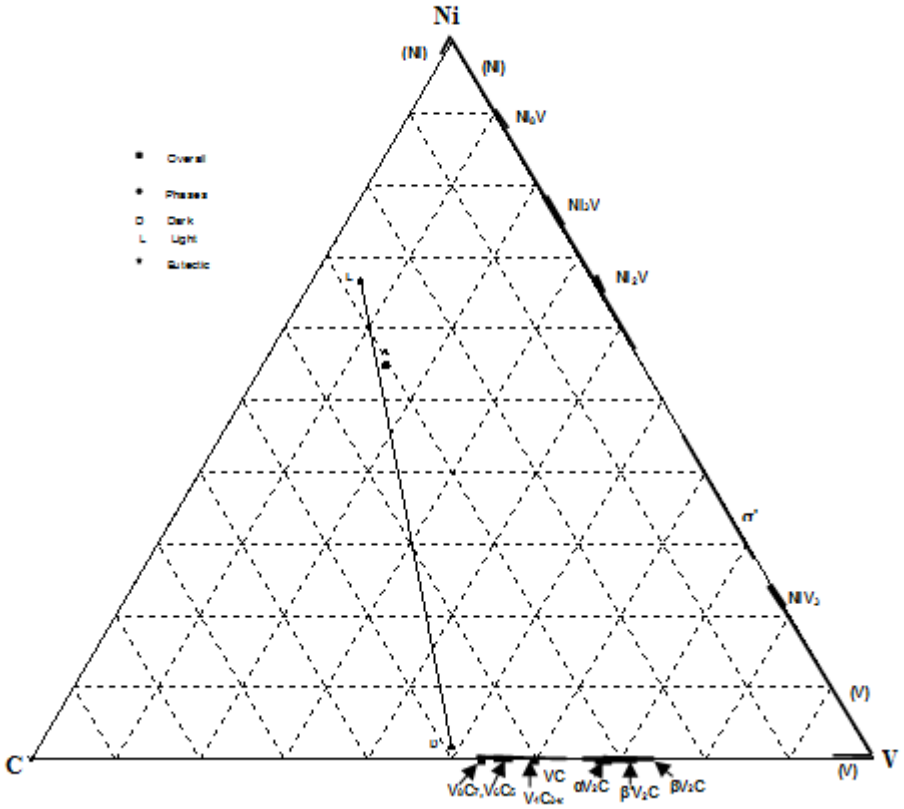


Figure 4.142. EDX analyses of as-cast nominal $Ni_{68}:V_{14}:C_{18}$ (at.%), Sample 19.

The XRD pattern shown in Figures 4.143 to 4.146 was reasonable, with a good signal to background ratio. The XRD pattern (Figure 4.146) confirmed the presence of ~V_8C_7 and (Ni), while C peaks at 2θ = 50.9º and ~54.3º could be matched with Figure 4.151. The highest intensity peak at about 2θ = 51.83º was for (Ni). All peaks could be matched. Table 4.38 shows the identified peaks, together with their phases.

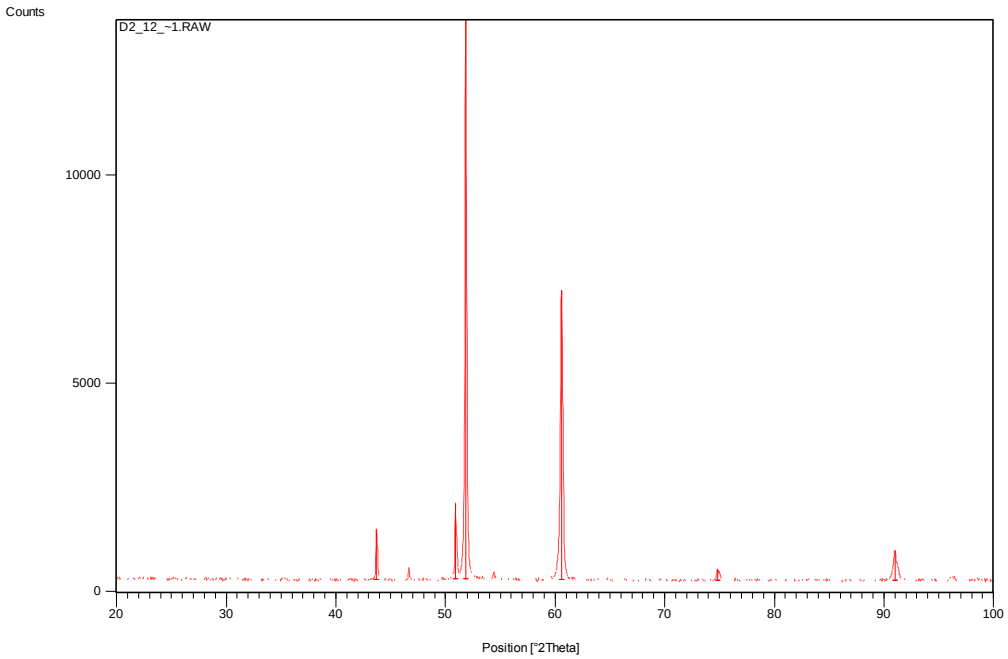


Figure 4.143. Unlabelled XRD pattern of as-cast nominal $Ni_{68}:V_{14}:C_{18}$ (at.%), Sample 19.

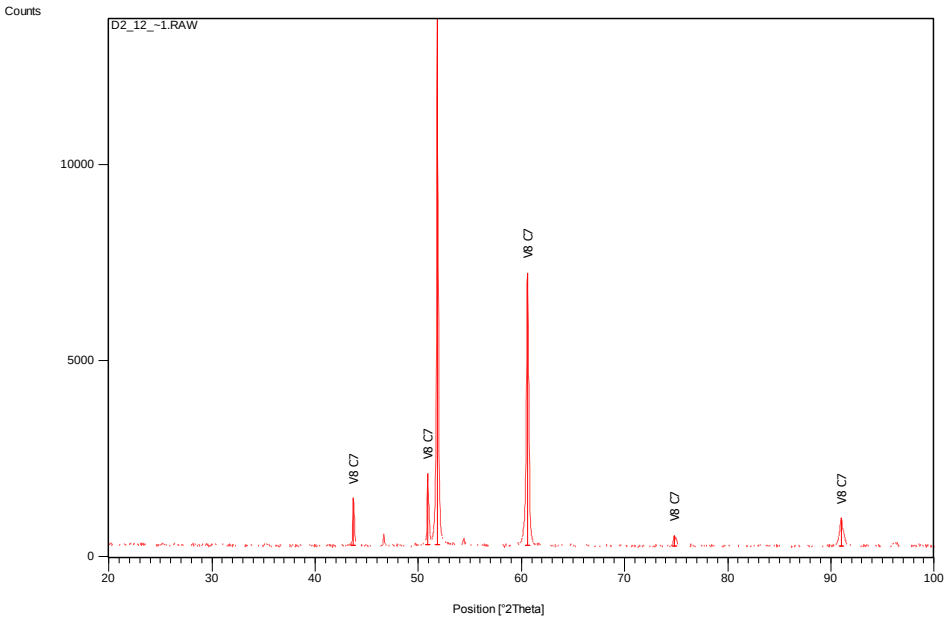


Figure 4.144. XRD pattern of as-cast nominal $Ni_{68}:V_{14}:C_{18}$ (at.%), Sample 19, showing identified V_8C_7 peaks.

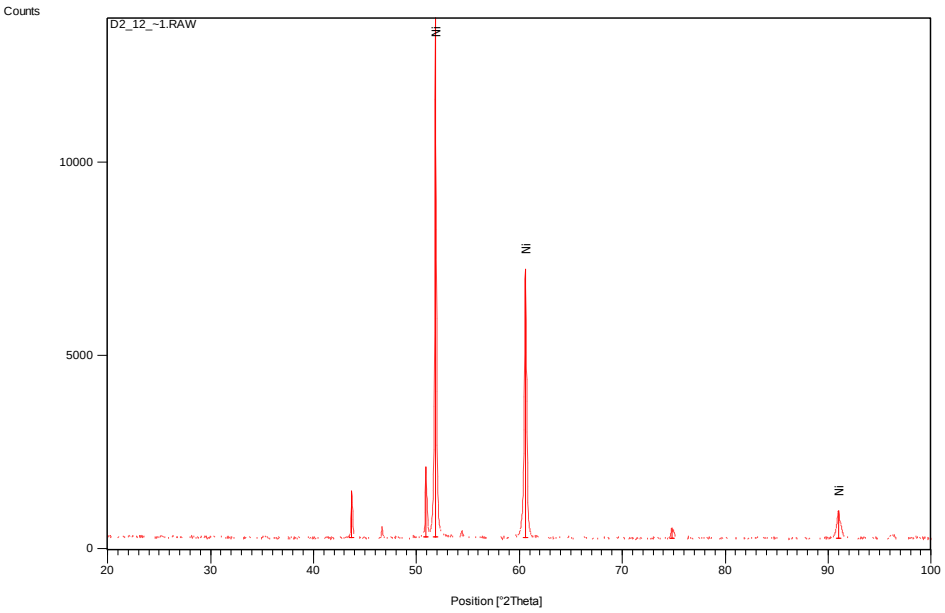


Figure 4.145. XRD pattern of as-cast nominal $Ni_{68}:V_{14}:C_{18}$ (at.%), Sample 19, showing identified (Ni) peaks.

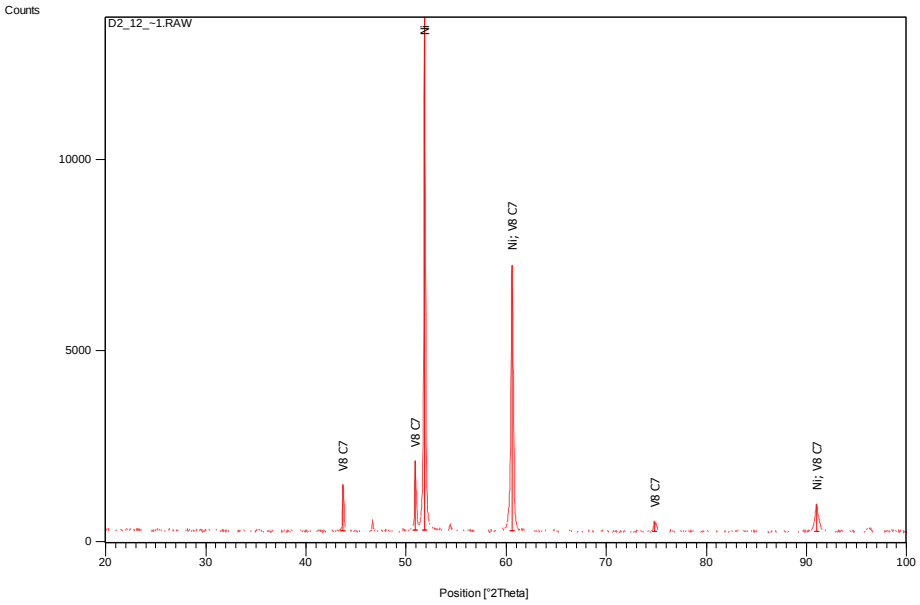


Figure 4.146. XRD pattern of as-cast nominal $Ni_{68}:V_{14}:C_{18}$ (at.%), Sample 19, showing all the identified peaks.

Table 4.37. XRD peaks for as-cast nominal $Ni_{68}:V_{14}:C_{18}$ (at.%), Sample 19.

Position 2θ (º)	Height (counts)	Relative Intensity (%)	Phases
43.7129	1219.72	9.05	V_8C_7, Ni
50.9136	1822.35	13.52	V_8C_7, Ni
51.8321	13482.89	100.00	Ni
60.5811	6945.14	51.51	V_8C_7, Ni
74.8429	260.50	1.93	V_8C_7, Ni
90.9931	711.27	5.28	V_8C_7, Ni

4.1.19 Nominal $Ni_{59}:V_{27.2}:C_{13.8}$ (at.%), Sample 20

An SEM-BSE image representative of the whole microstructure of nominal $Ni_{59}:V_{27.2}:C_{13.8}$ (at.%), Sample 20, in the as-cast condition is shown in Figure 4.147. The alloy had two contrasts. These were dendrites whose contrasts were dark, identified as ~V_8C_7, and the light regions were identified as (Ni). There was a eutectic of dark and light phases. Figure 4.148 shows the microstructure of the alloy at higher magnification, and the eutectic had both globular (~VC) and flake-like (C) characteristics.

The phase compositions are shown in Table 4.39 and plotted in Figure 4.149, showing the overall and eutectic compositions to be deviated slightly from the tie-line connecting the two phases, and on the more C-rich side, and the eutectic was close to the overall composition. The deviation may be due to some graphite, which may be present in the eutectic (Figure 4.148). The standard deviation of the measurements was below 1at.%, meaning that the analyses were good. The EDX analyses of Sample 20 are shown in Appendix B19.

The solidification sequence deduced from the microstructure is as follows:

$$L \rightarrow \sim VC$$

followed by a eutectic reaction:

$$L \rightarrow \sim VC + (Ni)$$

$$L \rightarrow C + (Ni)$$

followed by solid state reaction (~1140°C in the binary [1985Car]):

$$\sim VC \rightarrow \sim V_8C_7.$$

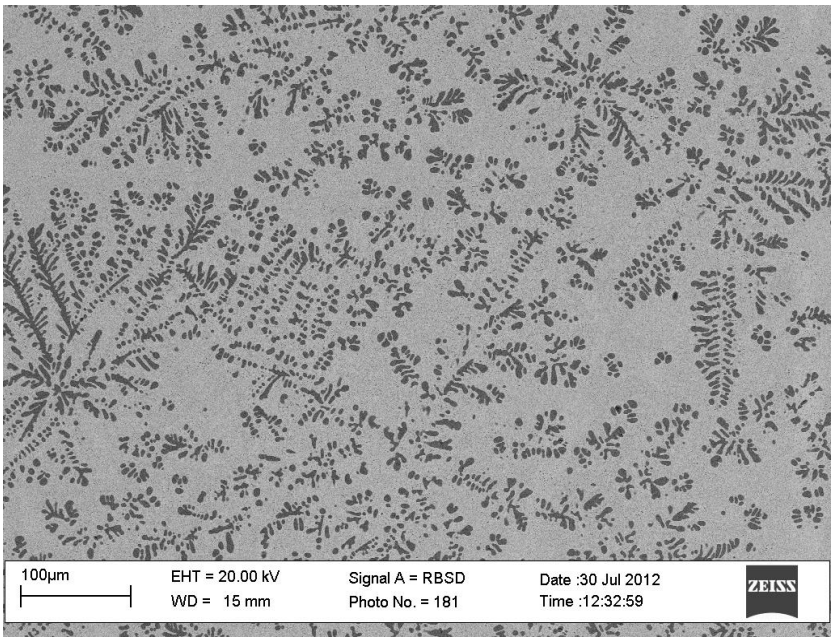


Figure 4.147. SEM-BSE image of nominal $Ni_{59}:V_{27.2}:C_{13.8}$ (at.%), Sample 20, in the as-cast condition, showing ~V_8C_7 dendrites (dark), and C + (Ni) eutectic.

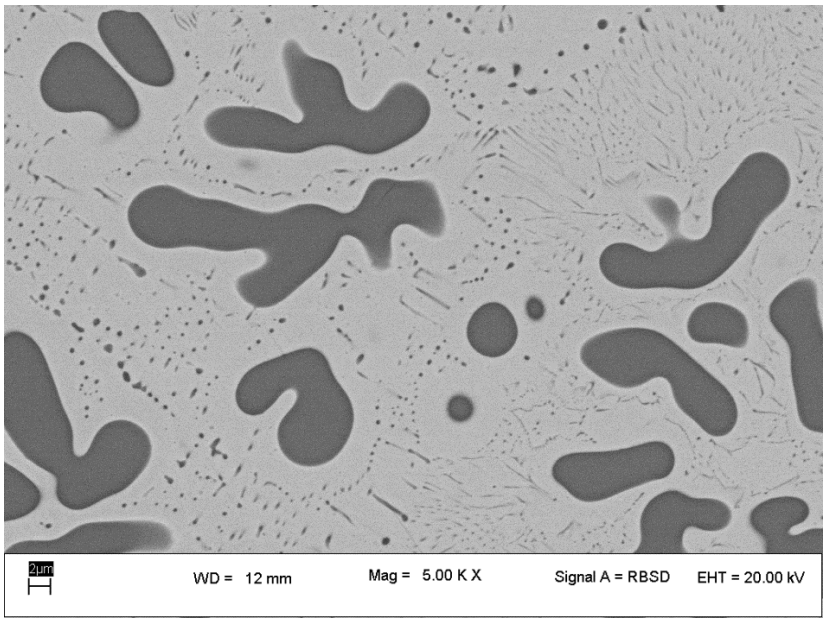


Figure 4.148. SEM-BSE image of nominal $Ni_{59}:V_{27.2}:C_{13.8}$ (at.%), Sample 20, in the as-cast condition, showing ~V_8C_7 dendrites (dark), (Ni) matrix (light), and ~VC + (Ni) and C + (Ni) eutectics at higher magnification.

Table 4.38. EDX phase analyses of as-cast nominal $Ni_{59}:V_{27.2}:C_{13.8}$ (at.%), Sample 20.

Phase Description	C	V	Ni	Phase
Overall	32.8 ± 0.7	23.3 ± 0.4	43.9 ± 0.6	-
Dark	48.8 ± 0.3	50.5 ± 0.2	0.7 ± 0.4	~V_8C_7
Light	21.3 ± 0.5	10.5 ± 0.4	68.2 ± 0.7	(Ni)
Eutectics	34.1 ± 0.2	23.9 ± 0.3	42.0 ± 0.7	~VC + (Ni) C + (Ni)

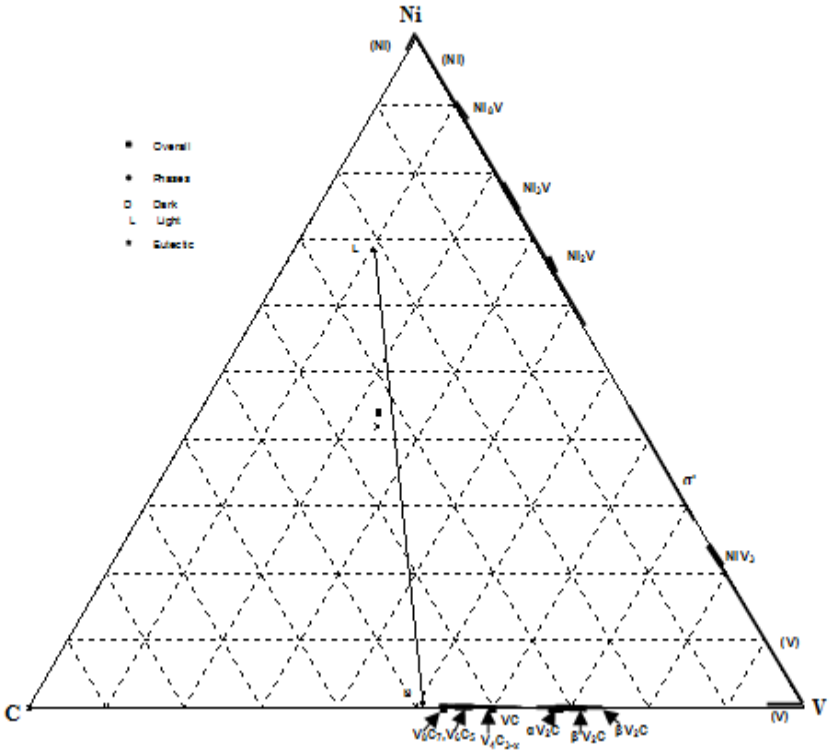


Figure 4.149. EDX analyses of as-cast nominal $Ni_{59}:V_{27.2}:C_{13.8}$ (at.%), Sample 20.

The XRD pattern (Figure 4.148) confirmed the presence of ~V_8C_7, graphite and (Ni). Figures 4.150 to 4.154 show the experimental peaks with the matched lines for each of the phases. The highest intensity peak at about $2\theta = 51.74^o$, was for (Ni) as was the case of Sample 19

(Figure 4.146). All peaks could be matched, except one at 2θ = 46.59°. Table 4.40 shows the identified peaks, together with their phases.

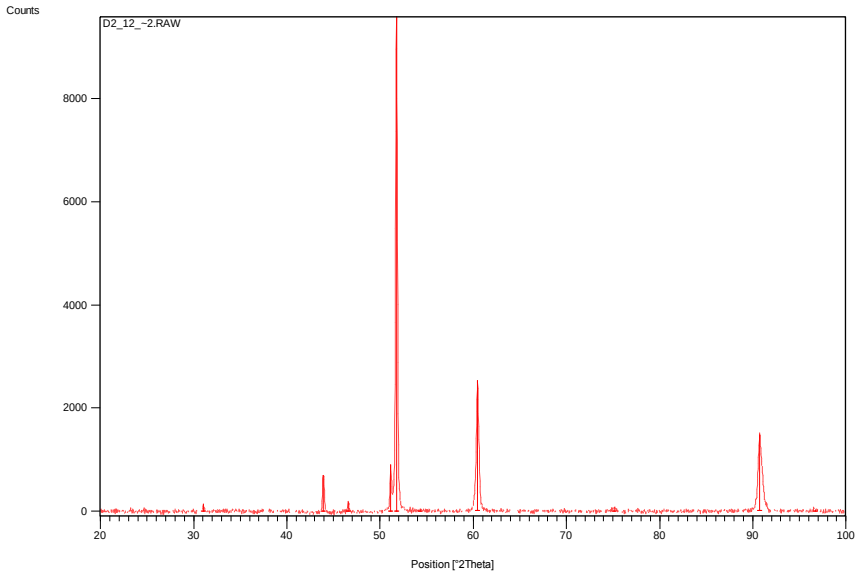


Figure 4.150. Unlabelled XRD pattern of as-cast nominal $Ni_{59}:V_{27.2}:C_{13.8}$ (at.%), Sample 20.

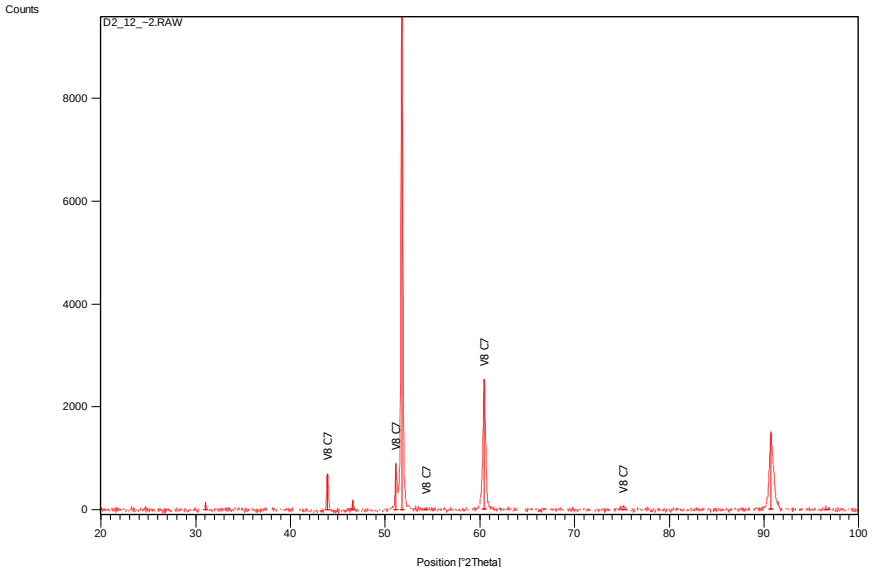


Figure 4.151. XRD pattern of as-cast nominal $Ni_{59}:V_{27.2}:C_{13.8}$ (at.%), Sample 20, showing identified ~V_8C_7 peaks.

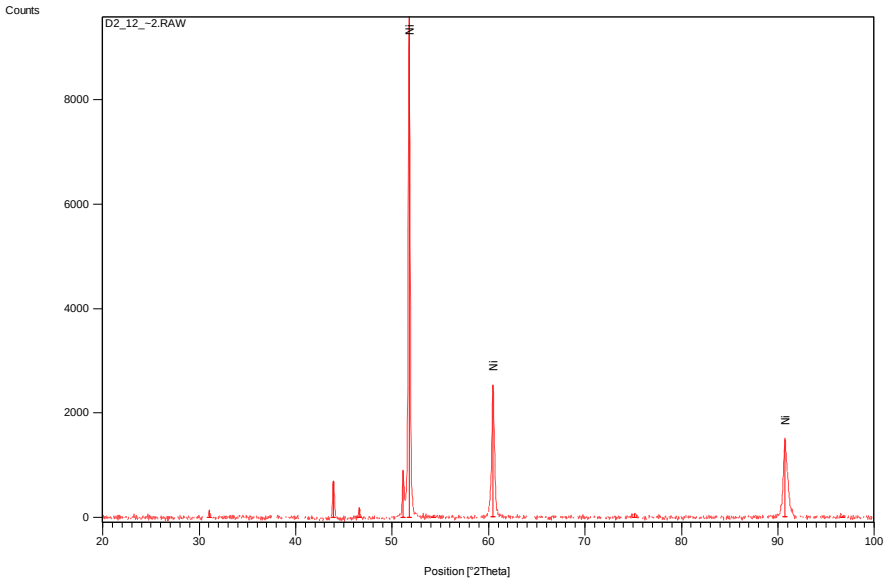


Figure 4.152. XRD pattern of as-cast nominal Ni_{59}:$V_{27.2}$:$C_{13.8}$ (at.%), Sample 20, showing identified (Ni) peaks.

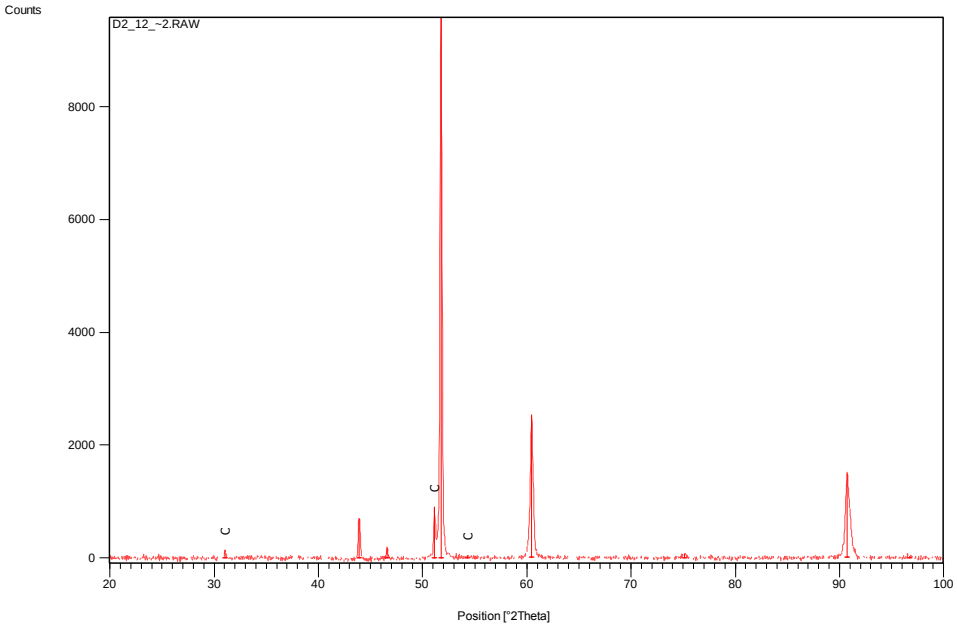


Figure 4.153. XRD pattern of as-cast nominal Ni_{59}:$V_{27.2}$:$C_{13.8}$ (at.%), Sample 20, showing identified C peaks.

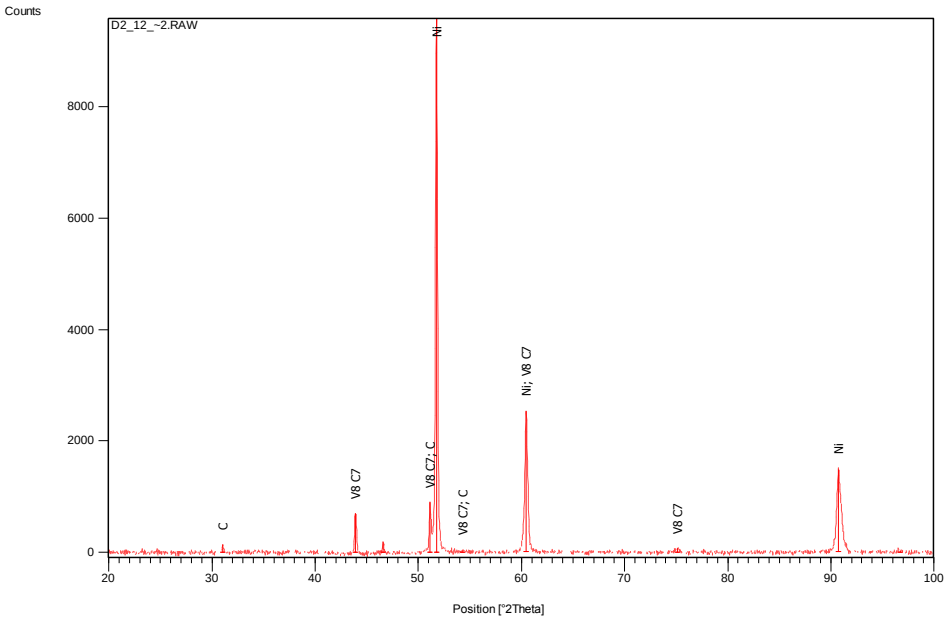


Figure 4.154. XRD pattern of as-cast nominal Ni_{59}:$V_{27.2}$:$C_{13.8}$ (at.%), Sample 20, showing all the identified peaks.

Table 4.39. XRD peaks for as-cast nominal Ni_{59}:$V_{27.2}$:$C_{13.8}$ (at.%), Sample 20.

Position 2θ (º)	Height (counts)	Relative Intensity (%)	Phases
31.0501	138.85	1.45	C
43.9151	698.83	7.29	V_8C_7
51.1289	900.22	9.39	V_8C_7, C
51.7489	9589.45	100.00	Ni
54.3452	45.92	0.48	V_8C_7, C
60.4684	2532.79	26.41	V_8C_7, Ni
75.1395	73.61	0.77	V_8C_7
90.7459	1482.48	15.46	Ni

4.1.20 Nominal Ni_{59}:$V_{27.2}$:$C_{13.8}$ (at.%), Sample 21

Figure 4.155 shows the microstructure of nominal Ni_{39}:$V_{42.8}$:$C_{18.2}$ (at.%), Sample 21 in the as-cast condition. The alloy showed a different morphology compared to most of the other alloys, except for Samples 4 and 13, with dark ~V_6C_5 needles surrounded by light regions

which were identified as ~Ni_2V, and regions of a fine mixture of ~VC + (Ni) eutectic as shown in Figure 4.156, although the discrete phases was sometimes flake-like. Some cracks were seen in the needles.

Table 4.41 gives the EDX analyses, and these are plotted in Figure 4.157. The overall composition was close to the tie-line joining the two phases, as was the eutectic composition. Generally, there were small experimental errors for the phases. The EDX analyses of Sample 21 are shown in Appendix B20.

The solidification sequence deduced from the microstructure is as follows:

$L \rightarrow$ ~VC

$L +$ ~VC $\rightarrow$ (Ni)

followed by eutectic reactions: $L \rightarrow$ ~VC + (Ni)

$L \rightarrow C +$ (Ni)

then solid state reaction: ~VC $\rightarrow$ ~V_6C_5 (~1184°C in the binary [1985Car])

(Ni) $\rightarrow$ ~Ni_2V (~922°C in the binary [1982Smi]).

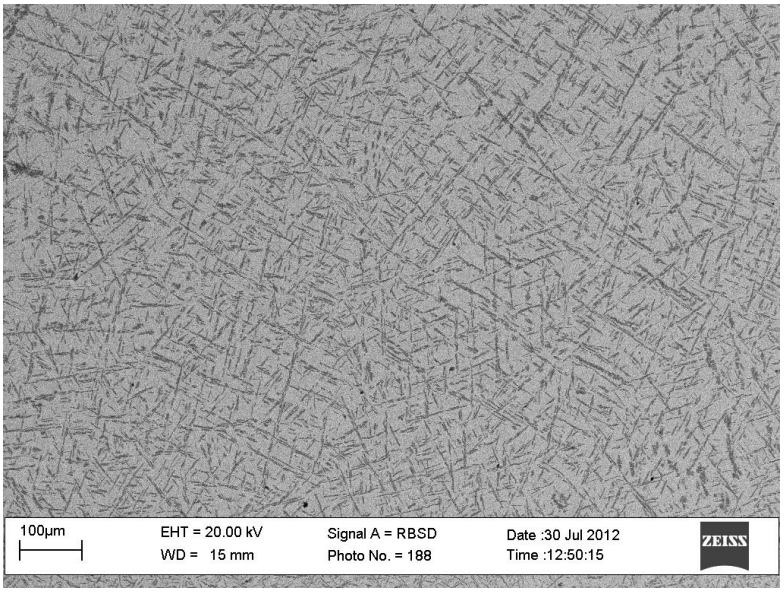


Figure 4.155. SEM-BSE image of nominal Ni_{39}:$V_{42.8}$:$C_{18.2}$ (at.%), Sample 21, in the as-cast condition, showing ~V_6C_5 needles (dark) and (Ni) matrix (light).

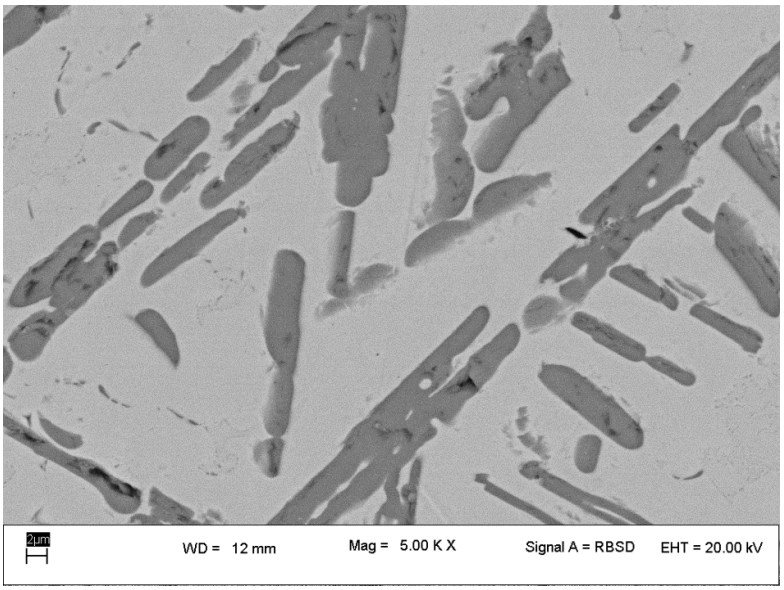


Figure 4.156. SEM-BSE image of nominal Ni_{39}:$V_{42.8}$:$C_{18.2}$ (at.%), Sample 21, in the as-cast condition, showing ~V_6C_5 needles (dark) and (Ni) matrix (light), and ~VC + (Ni) and C + (Ni) eutectic at higher magnification.

Table 4.40. EDX phase analyses of as-cast nominal $Ni_{39}:V_{42.8}:C_{18.2}$ (at.%), Sample 21.

Phase Description	C	V	Ni	Phase
Overall	24.7 ± 0.8	40.6 ± 0.7	34.7 ± 0.2	-
Dark	39.7 ± 0.7	59.2 ± 0.7	1.1 ± 0.4	~V_6C_5
Light	18.0 ± 0.9	33.2 ± 0.8	48.8 ± 0.6	~Ni_2V
Eutectics	27.0 ± 0.7	42.1 ± 0.7	30.9 ± 0.6	~VC + (Ni) C + (Ni)

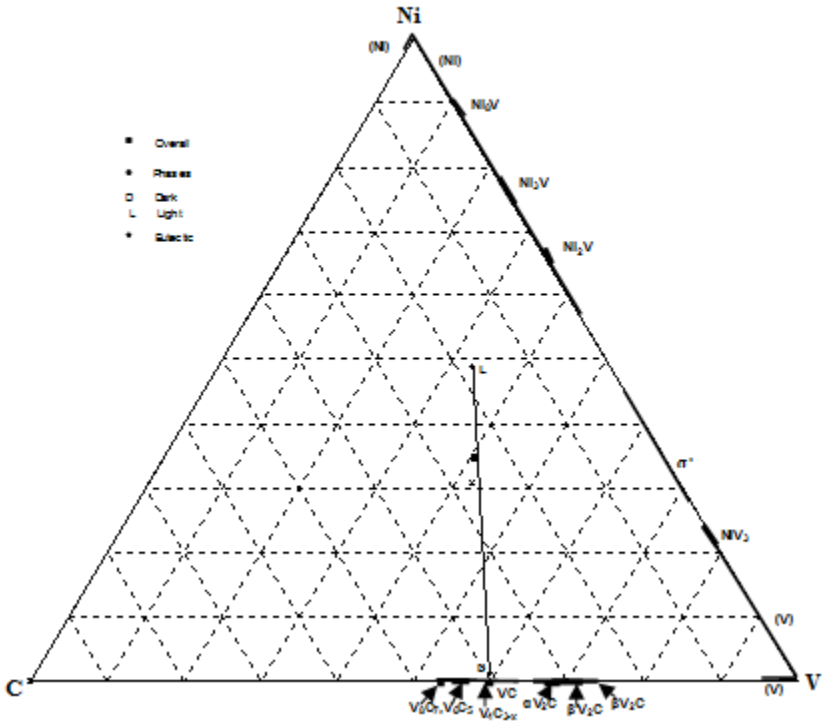


Figure 4.157. EDX analyses of as-cast nominal $Ni_{39}:V_{42.8}:C_{18.2}$ (at.%), Sample 21.

Figures 4.158 to 4.162 show the X-ray diffraction pattern of the sample with the matches for each of the phases. This confirmed the presence of ~Ni_2V (Figure 4.159), C (Figure 4.158) which can be seen as graphite flakes in the eutectic and ~V_6C_5 (Figure 4.161). The highest intensity peak was found at position $2\theta = 50.98^{o}$, which matched ~Ni_2V and C. All peaks

could be matched, except that at $2\theta = 42.16^{o}$. Table 4.42 shows the identified peaks together with their phases.

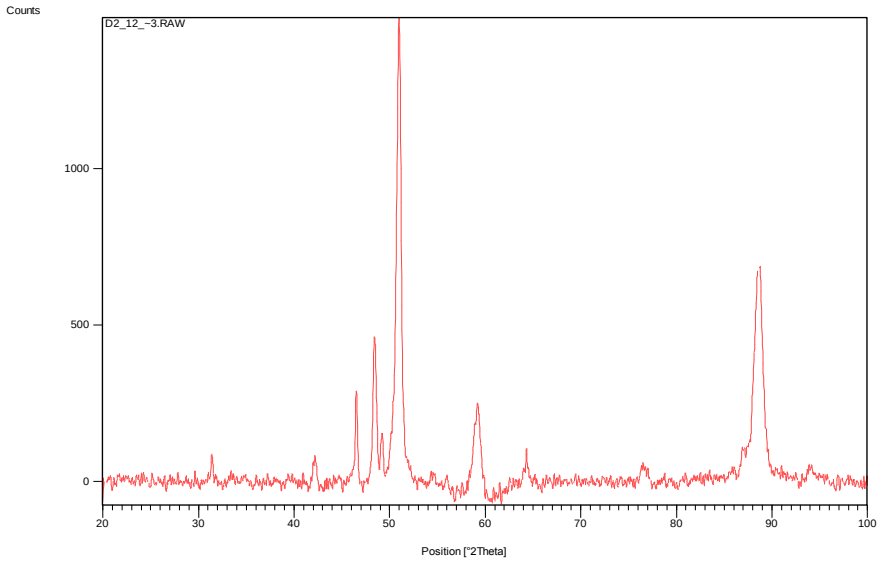


Figure 4.158. Unlabelled XRD pattern of as-cast nominal $Ni_{39}:V_{42.8}:C_{18.2}$ (at.%), Sample 21.

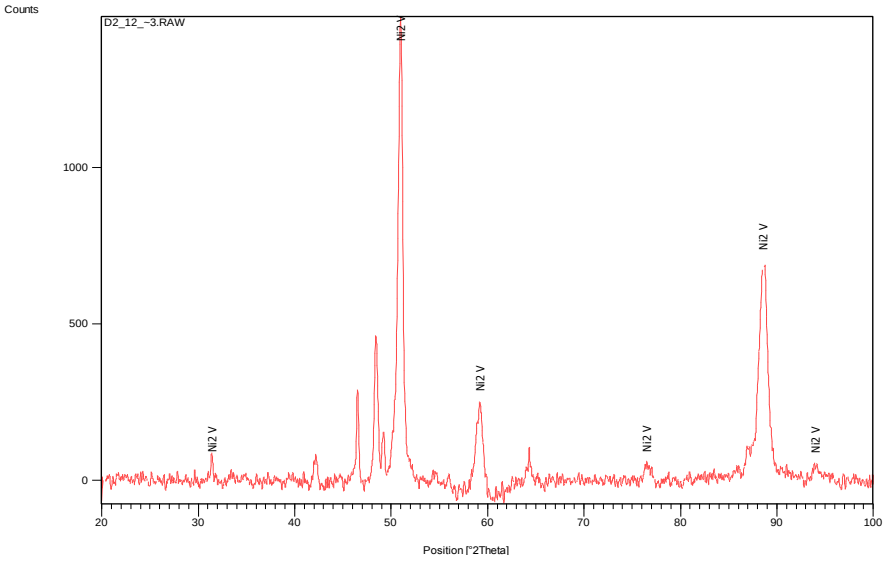


Figure 4.159. XRD pattern of as-cast nominal $Ni_{39}:V_{42.8}:C_{18.2}$ (at.%), Sample 21, showing identified ~Ni_2V peaks.

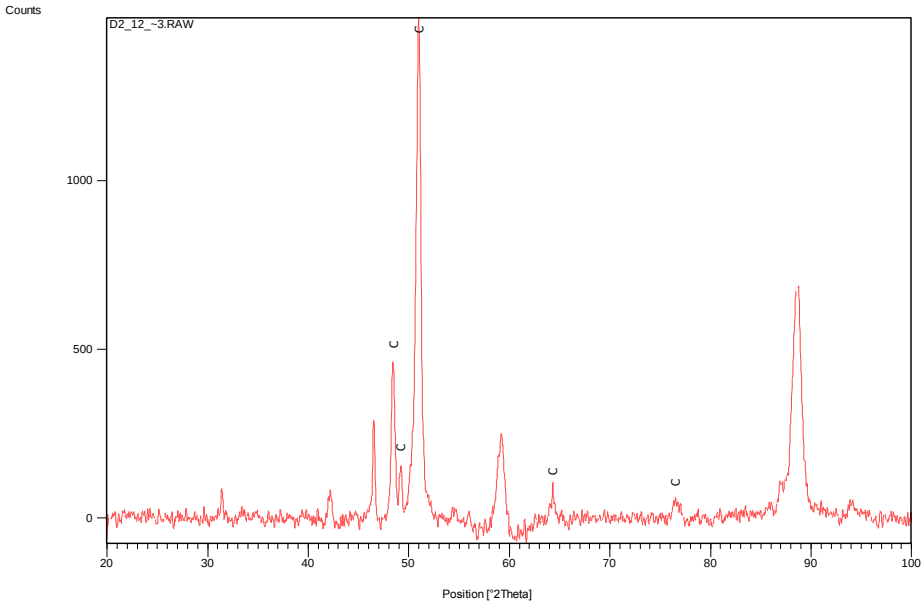


Figure 4.160. XRD pattern of as-cast nominal Ni_{39}:$V_{42.8}$:$C_{18.2}$ (at.%), Sample 21, showing identified C peaks.

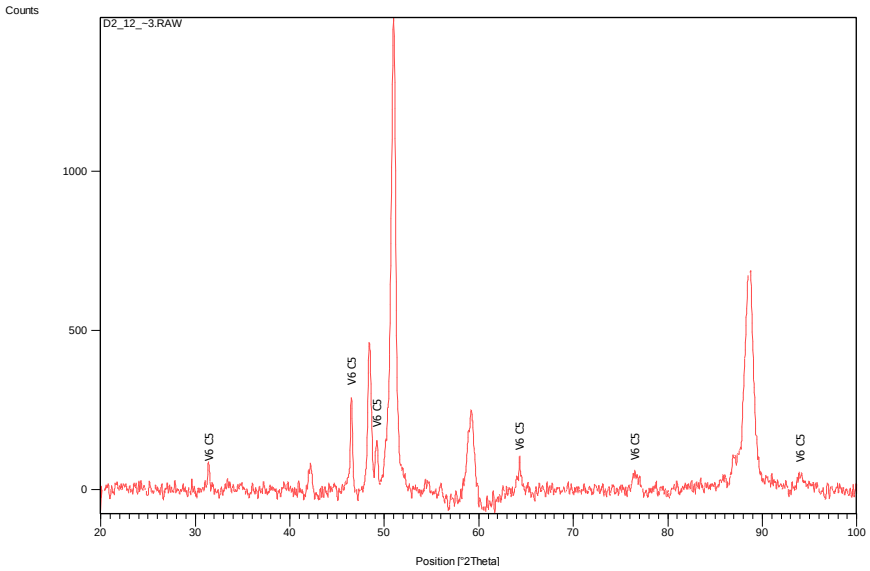


Figure 4.161. XRD pattern of as-cast nominal Ni_{39}:$V_{42.8}$:$C_{18.2}$ (at.%), Sample 21, showing identified ~V_6C_5 peaks.

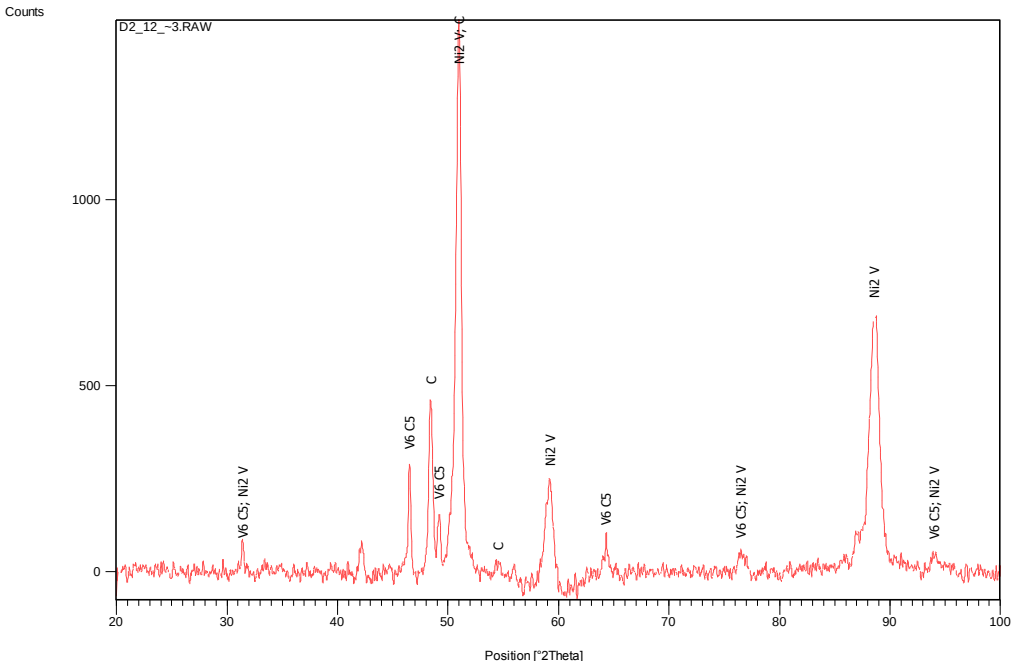


Figure 4.162. XRD pattern of as-cast nominal Ni_{39}:$V_{42.8}$:$C_{18.2}$ (at.%), Sample 21, showing all the identified peaks.

Table 4.41. XRD peaks for as-cast nominal Ni_{39}:$V_{42.8}$:$C_{18.2}$ (at.%), Sample 21.

Position 2θ (º)	Height (counts)	Relative Intensity (%)	Phases
31.3820	47.33	3.19	V_6C_5, Ni_2V
42.1626	67.36	4.54	Unidentified
46.5168	287.30	19.37	V_6C_5
48.4231	460.52	31.05	C
49.1995	154.38	10.41	V_6C_5, C
50.9865	1483.15	100.00	Ni_2V, C
54.5239	12.76	0.86	C
59.1887	243.57	16.42	Ni_2V
64.3137	82.13	5.54	V_6C_5,C
76.4900	49.05	3.31	V_6C_5, Ni_2V, C
88.5947	631.31	42.57	Ni_2V
93.9903	39.09	2.64	V_6C_5, Ni_2V

4.1.21 Nominal $Ni_{49}:V_{33.3}:C_{17.7}$ (at.%), Sample 22

An SEM-BSE image of the microstructure representative of nominal $Ni_{49}:V_{33.3}:C_{17.1}$ (at.%), Sample 22, in the as-cast condition is shown in Figure 4.163 at low magnification. The alloy had two discernable contrasts. These were dark dendrites identified as ~V_8C_7, and two eutectics: ~Ni_2V (globular) + ~VC (originally with (Ni)), and C (flakes) + (Ni) (then ~Ni_2V). Figure 4.164 shows the microstructure of the alloy at higher magnification.

The phase compositions are shown in Table 4.43 and plotted in Figure 4.165, showing the overall composition to be slightly deviated from the tie-line joining the two phases, and on the V-rich side. However, the standard deviation of the measurements was below 1at.%, which shows that the analyses were good. The EDX analyses of Sample 22 are shown in Appendix B21.

The deduced solidification sequence is: $L \rightarrow$ ~VC

followed by eutectic reactions: $L \rightarrow$ ~VC + (Ni)

$L \rightarrow C + (Ni)$

followed by solid state reactions: ~VC $\rightarrow$ ~V_8C_7 (~1140°C in the binary [1985Car])

(Ni) $\rightarrow$ ~Ni_2V (~922°C in the binary [1982Smi]).

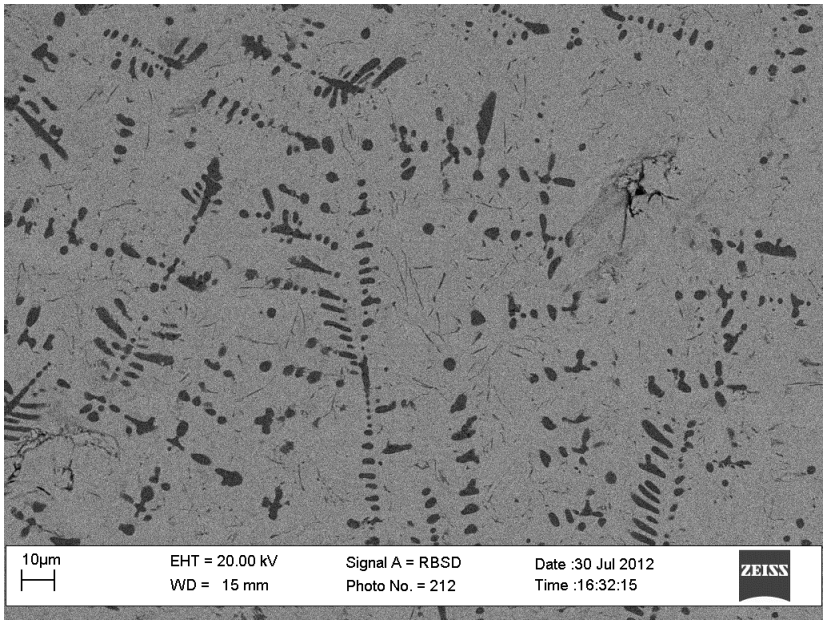


Figure 4.163. SEM-BSE image of nominal $Ni_{49}:V_{33.3}:C_{17.7}$ (at.%), Sample 22, in the as-cast condition, showing ~V_8C_7 dendrites (dark), and matrix (light).

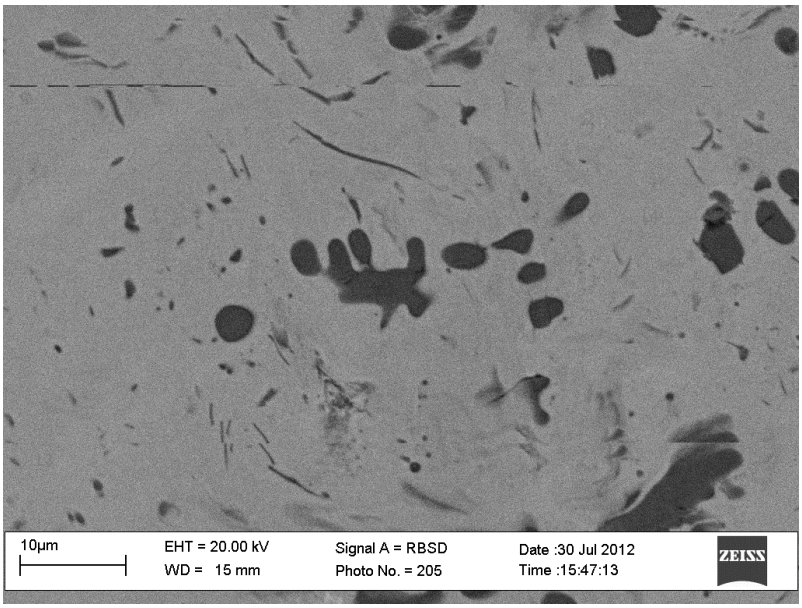


Figure 4.164. SEM-BSE image of nominal $Ni_{49}:V_{33.3}:C_{17.7}$ (at.%), Sample 22, in the as-cast condition, showing ~V_8C_7 dendrites (dark), and ~Ni_2V + ~VC and (Ni) + C eutectics at higher magnification.

Table 4.42. EDX phase analyses of as-cast nominal $Ni_{49}:V_{33.3}:C_{17.7}$ (at.%), Sample 22.

Phase Description	C	V	Ni	Phase
Overall	24.1 ± 0.5	35.0 ± 0.6	40.9 ± 0.3	-
Dark	48.4 ± 0.5	48.8 ± 0.4	2.8 ± 0.5	~V_8C_7
Light	19.6 ± 0.4	29.9 ± 0.2	50.5 ± 0.5	~Ni_2V
Eutectics	22.1 ± 0.6	32.1 ± 0.4	45.8 ± 0.5	~VC + (Ni) C + (Ni)

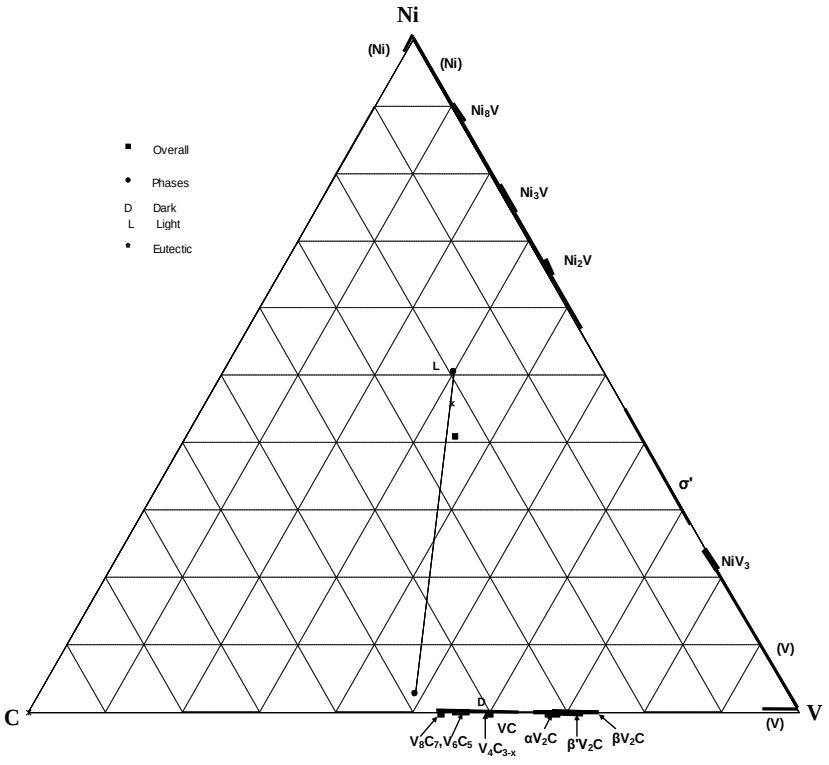


Figure 4.165. EDX analyses of as-cast nominal $Ni_{49}:V_{33.3}:C_{17.7}$ (at.%), Sample 22.

The XRD pattern, Figures 4.166 to 4.170, shows the matches for each of the phases. The pattern had overlapping peaks which had the highest intensity of the different phases at $2\theta = 50.76^{o}$. The XRD pattern (Figure 4.170) confirmed the presence of ~V_8C_7, ~Ni_2V and graphite. All peaks could be matched and Table 4.44 contains the identified peaks.

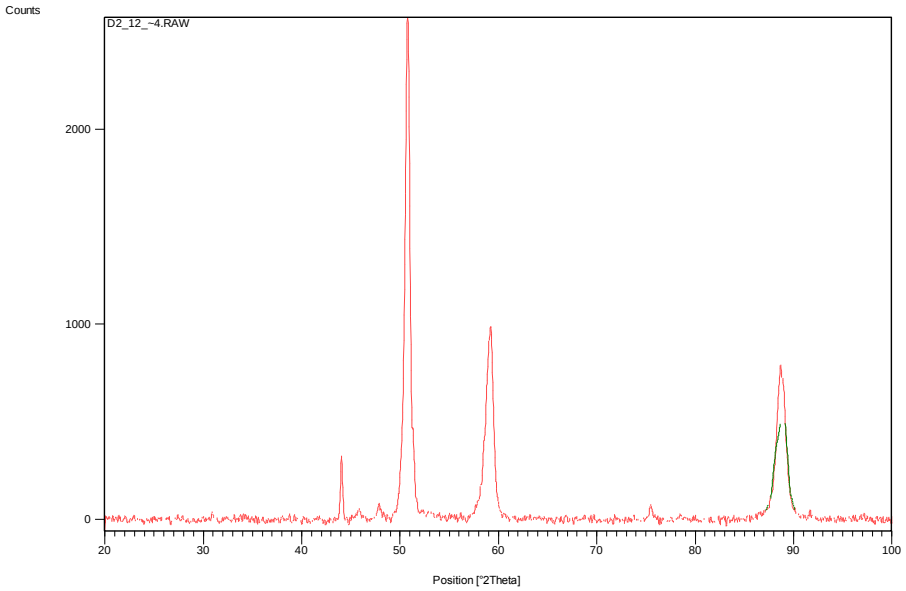


Figure 4.166. Unlabelled XRD pattern of as-cast nominal $Ni_{49}:V_{33.3}:C_{17.7}$ (at.%), Sample 22.

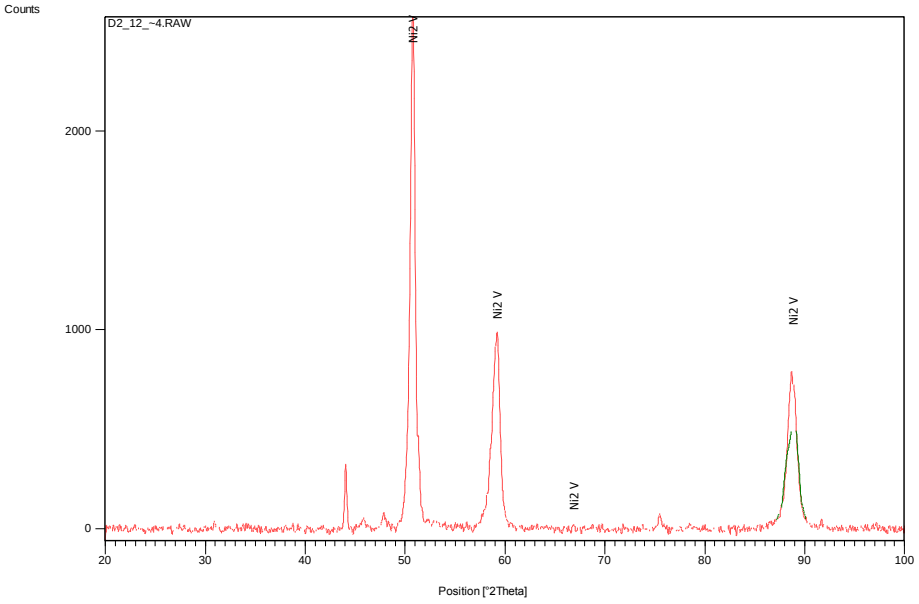


Figure 4.167. XRD pattern of as-cast nominal $Ni_{49}:V_{33.3}:C_{17.7}$ (at.%), Sample 22, showing identified ~Ni_2V peaks.

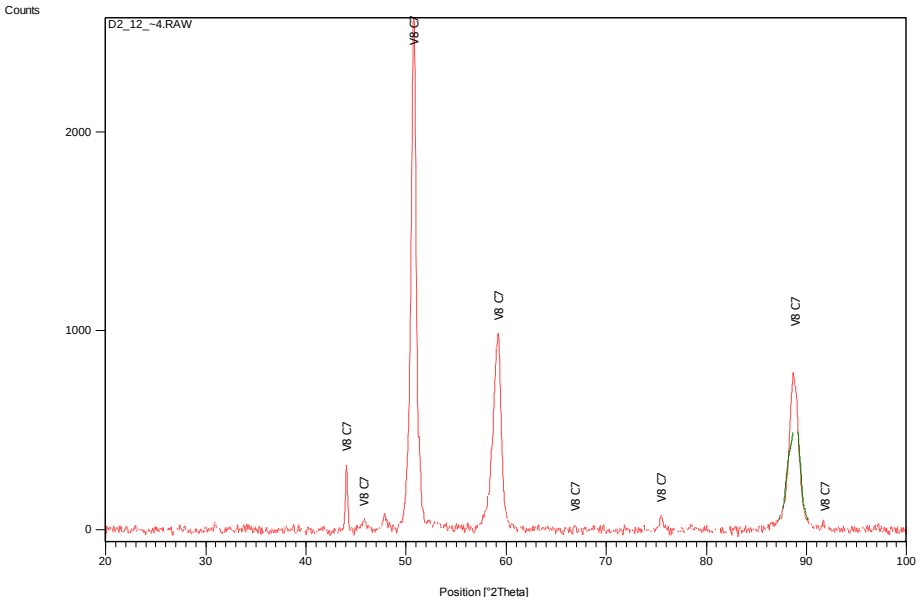


Figure 4.168. XRD pattern of as-cast nominal $Ni_{49}:V_{33.3}:C_{17.7}$ (at.%), Sample 22, showing identified ~V_8C_7 peaks.

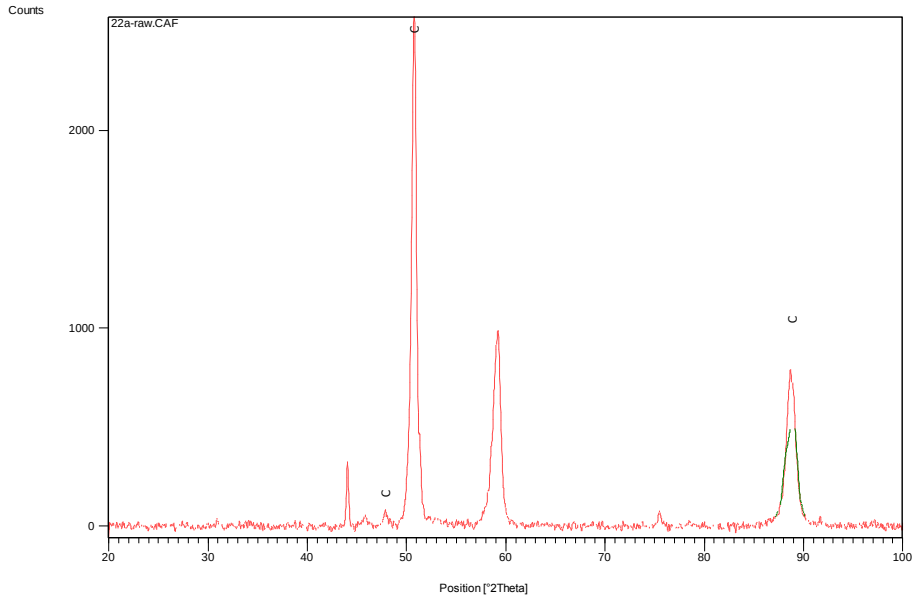


Figure 4.169. XRD pattern of as-cast nominal $Ni_{49}:V_{33.3}:C_{17.7}$ (at.%), Sample 22, showing identified C peaks.

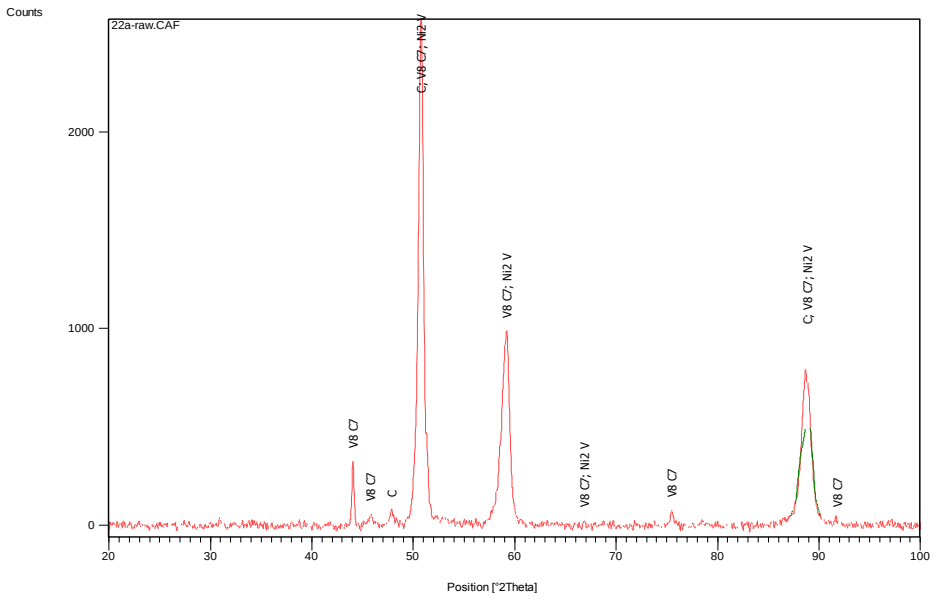


Figure 4.170. XRD pattern of as-cast nominal $Ni_{49}:V_{33.3}:C_{17.7}$ (at.%), Sample 22, showing all the identified peaks.

Table 4.43. XRD peaks for as-cast nominal $Ni_{49}:V_{33.3}:C_{17.7}$ (at.%), Sample 22.

Position 2θ (º)	Height (counts)	Relative Intensity (%)	Phases
44.0458	322.88	12.66	V_8C_7
45.7918	51.70	2.03	V_8C_7
47.8618	68.02	2.67	C
50.7692	2551.07	100.00	V_8C_7, Ni_2V, C
59.1922	953.88	37.39	V_8C_7, Ni_2V
66.8817	21.93	0.86	V_8C_7, Ni_2V
75.4699	71.55	2.80	V_8C_7
88.8480	464.20	18.20	V_8C_7, Ni_2V, C
91.8414	22.02	0.86	V_8C_7

4.1.22 Nominal $Ni_{24}:V_{58.6}:C_{17.4}$ (at.%), Sample 23

The nominal $Ni_{24}:V_{58.8}:C_{17.4}$ (at.%), Sample 23, in the as-cast condition is shown in Figure 4.171. The microstructure shows dark dendrites, identified as ~V_8C_7, with the lighter regions identified as σ′ and a eutectic of ~VC + σ′ (Figure 4.172). Also, there were some cracks, mainly in the dendrites.

The phase compositions are shown in Table 4.45 and plotted in Figure 4.173, with the overall composition to be deviated slightly from the tie-line connecting the two phases on the V-rich side and the eutectic was close to the overall composition. The standard deviation of the measurements was below 1at.%. Appendix B19 shows the EDX analyses of Sample 23.

The deduced solidification sequence is: $L \rightarrow \sim VC$

followed by a eutectic reaction: $L \rightarrow \sim VC + \sigma'$.

then $\sim VC \rightarrow \sim V_6C_5$ (solid state transformation [1985Car]).

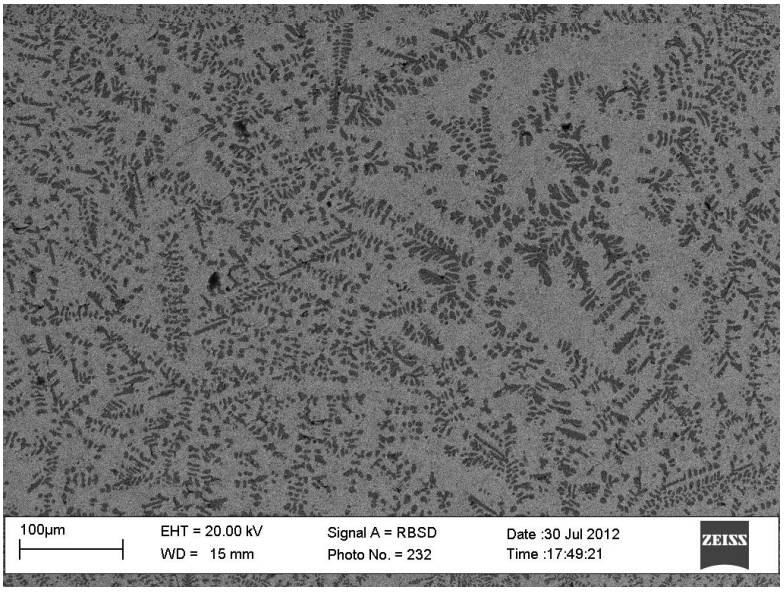


Figure 4.171. SEM-BSE image of nominal $Ni_{24}:V_{58.6}:C_{17.4}$ (at.%), Sample 23, in the as-cast condition, showing $\sim V_6C_5$ dendrites (dark) and σ′ matrix (light).

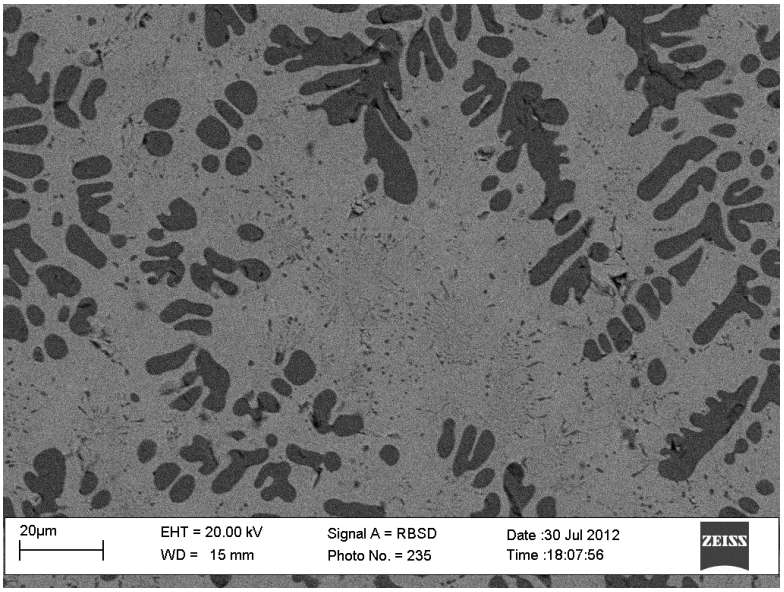


Figure 4.172. SEM-BSE image of nominal Ni_{24}:$V_{58.6}$:$C_{17.4}$ (at.%), Sample 23, in the as-cast condition, showing ~V_6C_5 dendrites (dark), σ′ matrix (light) and eutectic at high magnification.

Table 4.44. EDX phase analyses of as-cast nominal Ni_{24}:$V_{58.6}$:$C_{17.4}$ (at.%), Sample 23.

Phase Description	C	V	Ni	Phase
Overall	24.3 ± 0.9	51.8 ± 0.1	23.8 ± 0.4	-
Dark	42.9 ± 0.5	56.9 ± 0.6	0.2 ± 0.2	~V_6C_5
Light	16.8 ± 0.4	46.8 ± 0.8	36.4 ± 0.6	σ′
Eutectic	25.3 ± 0.5	50.9 ± 0.6	23.8 ± 0.5	~VC + σ′

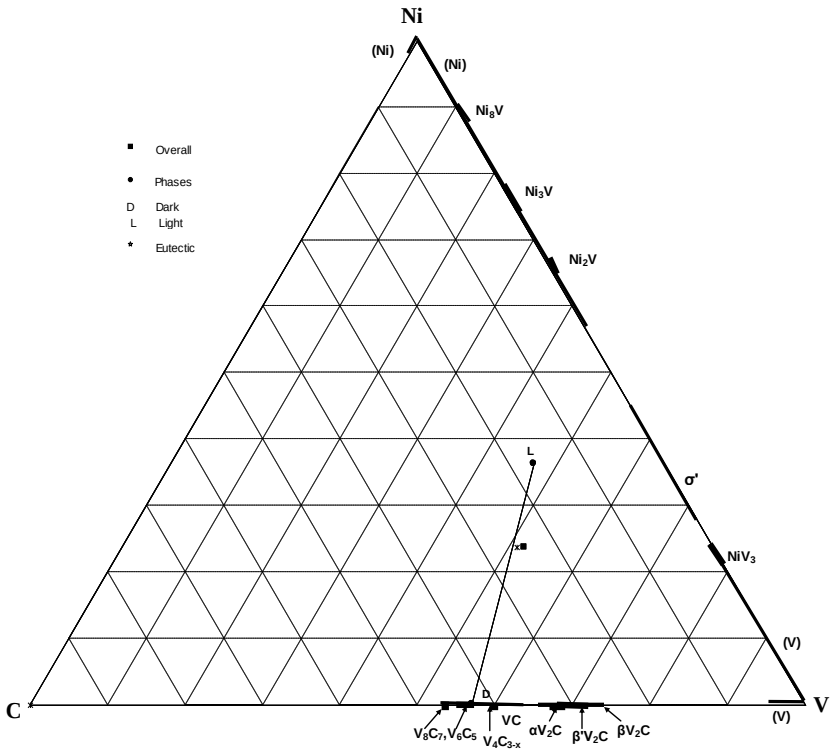


Figure 4.173. EDX analyses of as-cast nominal Ni_{24}:$V_{58.6}$:$C_{17.4}$ (at.%), Sample 23.

The XRD pattern shown in Figures 4.174 to 4.177 was fair, with a reasonable signal:background ratio, but being fairly noisy. The presence of ~V_6C_5 was shown in Figure 4.175, and perhaps (V) was indicated in Figure 4.176. There were several unidentified peaks shown in Table 4.46, which were assumed to be σ′ and were not included in the International Crystallography Diffraction Database (ICDD) [2001ICD]. Table 4.46 shows the identified peaks together with their phases.

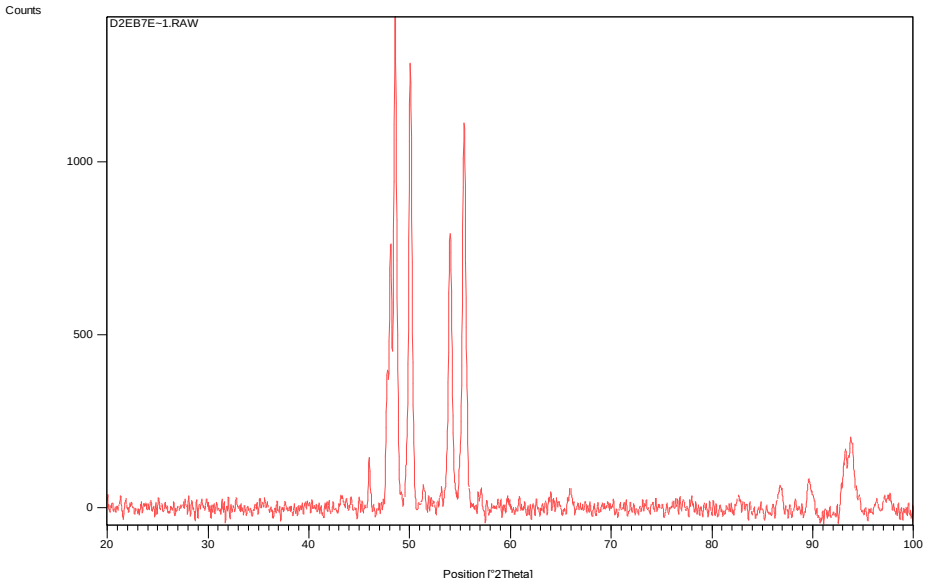


Figure 4.174. Unlabelled XRD pattern of as-cast nominal Ni_{24}:$V_{58.6}$:$C_{17.4}$ (at.%), Sample 23.

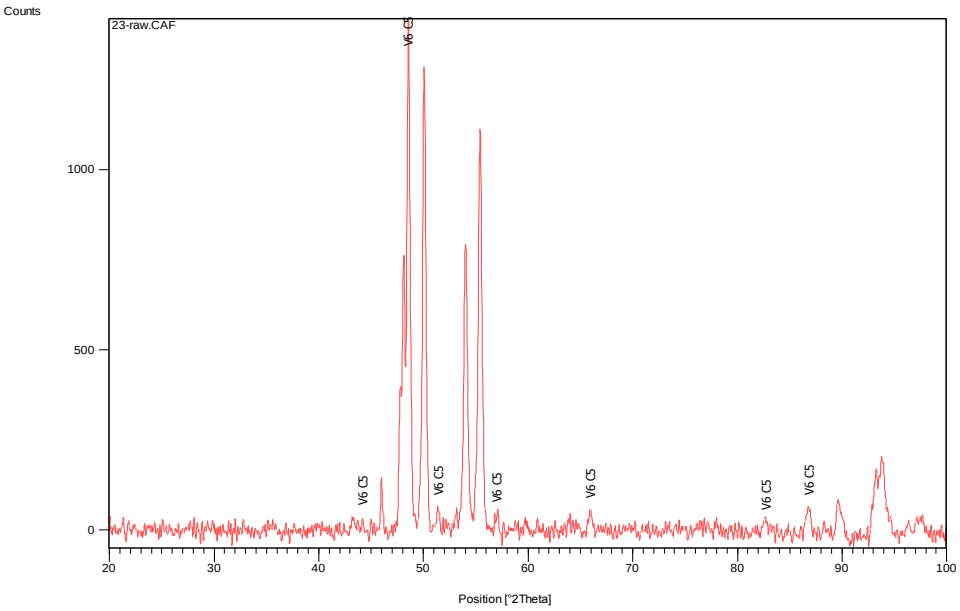


Figure 4.175. XRD pattern of as-cast nominal Ni_{24}:$V_{58.6}$:$C_{17.4}$ (at.%), Sample 23, showing identified ~V_6C_5 peaks.

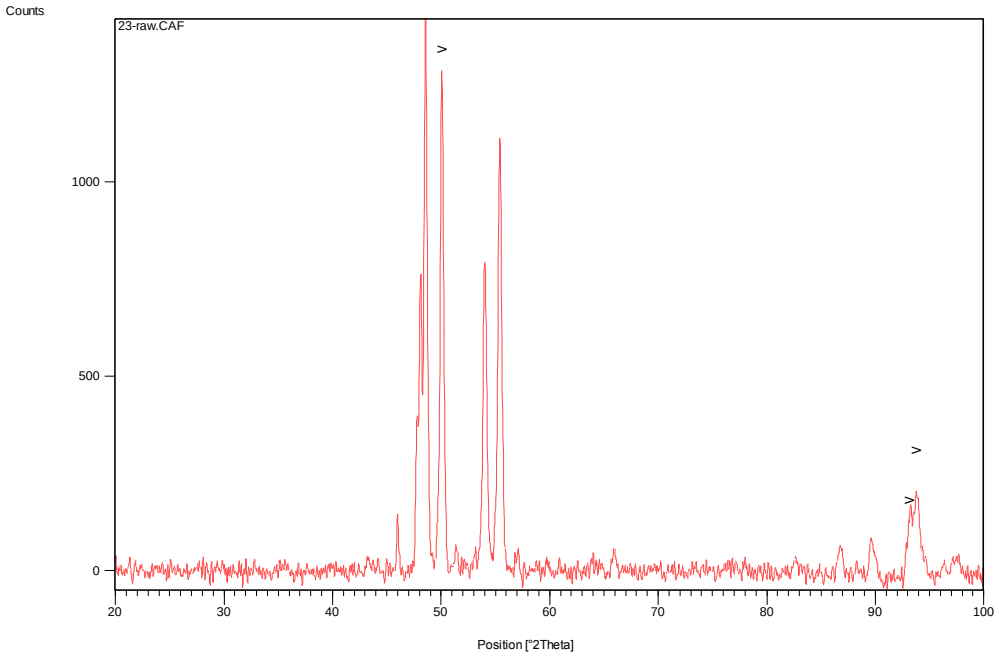


Figure 4.176. XRD pattern of as-cast nominal $Ni_{24}:V_{58.6}:C_{17.4}$ (at.%), Sample 23, showing identified (V) peaks.

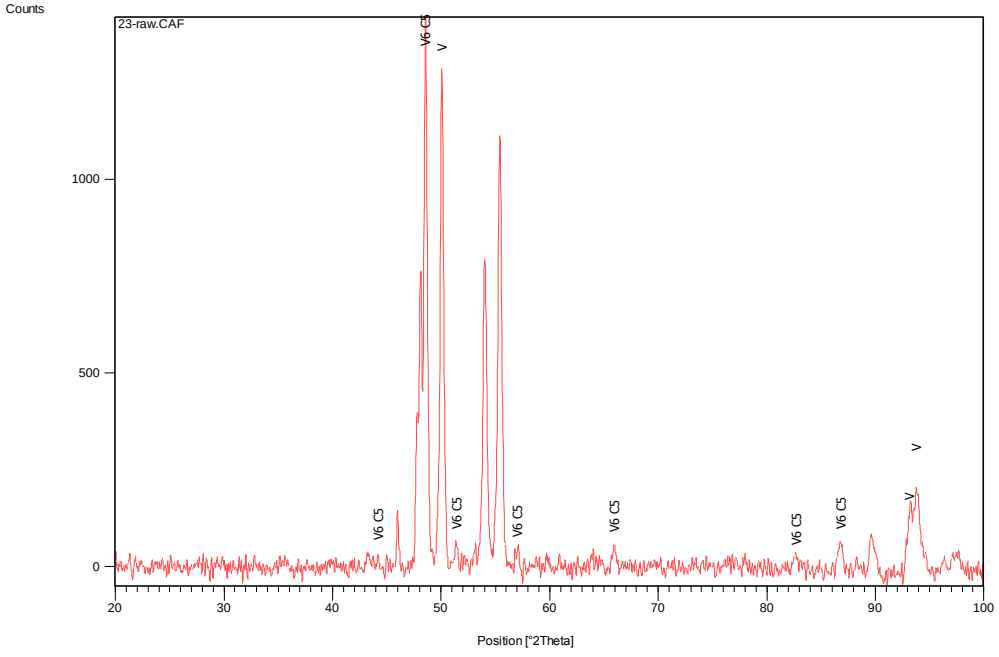


Figure 4.177. XRD pattern of as-cast nominal $Ni_{24}:V_{58.6}:C_{17.4}$ (at.%), Sample 23, showing all the identified peaks.

Table 4.45. XRD peaks for as-cast nominal Ni_{24}:$V_{58.6}$:$C_{17.4}$ (at.%), Sample 23.

Position 2θ (º)	Height (counts)	Relative Intensity (%)	Phases
44.1856	30.92	2.17	V_6C_5
45.9831	148.19	10.40	Presumed σ′
47.7145	316.22	22.18	Presumed σ′
48.5602	1425.38	100.00	V_6C_5
50.0670	1290.18	90.51	V
51.8715	33.86	2.38	V_6C_5
54.0214	794.74	55.76	Presumed σ′
55.4117	1111.83	78.00	Presumed σ′
57.0016	38.26	2.68	V_6C_5
63.9404	25.01	1.75	Presumed σ′
65.9091	48.22	3.38	V_6C_5
82.7408	17.36	1.22	V_6C_5
86.8170	59.11	4.15	V_6C_5
89.6258	82.94	5.82	Presumed σ′
93.1070	121.48	8.52	V
93.7818	244.20	17.13	V
97.4169	24.63	1.73	Presumed σ′

4.1.23 Nominal $Ni_{22.1}$:$V_{49.1}$:$C_{28.8}$ (at.%), Sample 24

Figure 4.178 shows the microstructure of nominal $Ni_{22.1}$:$V_{49.1}$:$C_{28.8}$ (at.%), Sample 24, in the as-cast condition and although similar in composition to Sample 3, it solidified differently. The alloy had a different morphology compared to other alloys, with dark ~V_8C_7 needles, sometimes in clumps (Figure 4.179), similar to those in Samples 4, 13 and 21, surrounded by light regions which were identified as ~Ni_2V. There was no eutectic (Figure 4.180). Some cracks and pores were seen in the needles. It is also possible that there is an orientation relationship between the needles and the matrix, which would be due to a solid state reaction.

The phase compositions are shown in Table 4.47 and plotted in Figure 4.181, showing the overall composition to be deviated from the tie-line joining the two phases, on the V-rich side. The deviation may be due to an unidentified phase which may be present in the microstructure, although the finer needles did appear darker. The analyses were reasonable, within the acceptable errors. The EDX analyses of Sample 24 are shown in Appendix B23.

The deduced solidification sequence is: $L \rightarrow \sim VC$

$L + \sim VC \rightarrow (Ni)$

followed by transformations in the solid state: $\sim VC \rightarrow \sim V_8C_7$ (~1140ºC in the binary [1985Car])

then $(Ni) \rightarrow \sim Ni_2V$ (~922ºC in the binary 1982Smi]).

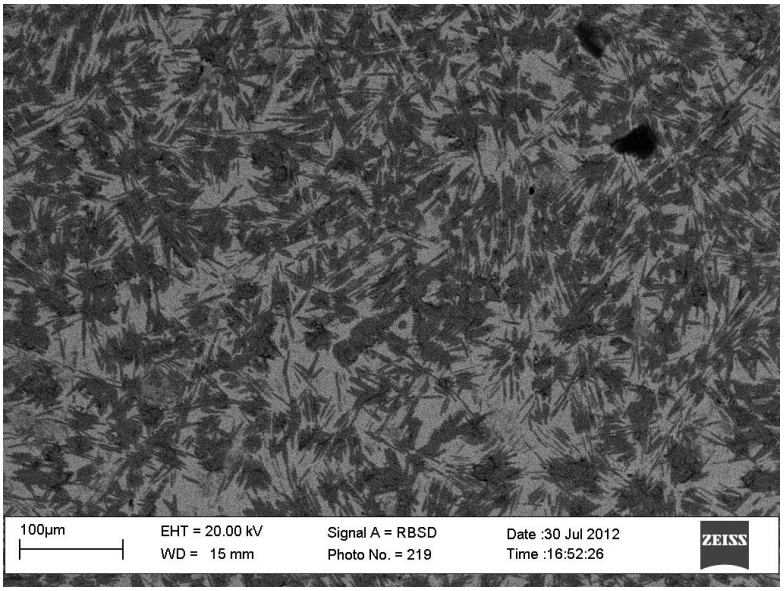


Figure 4.178. SEM-BSE image of nominal $Ni_{22.1}$:$V_{49.1}$:$C_{28.8}$ (at.%), Sample 24, in the as-cast condition, showing ~V_8C_7 needles (dark) and ~Ni_2V matrix (light).

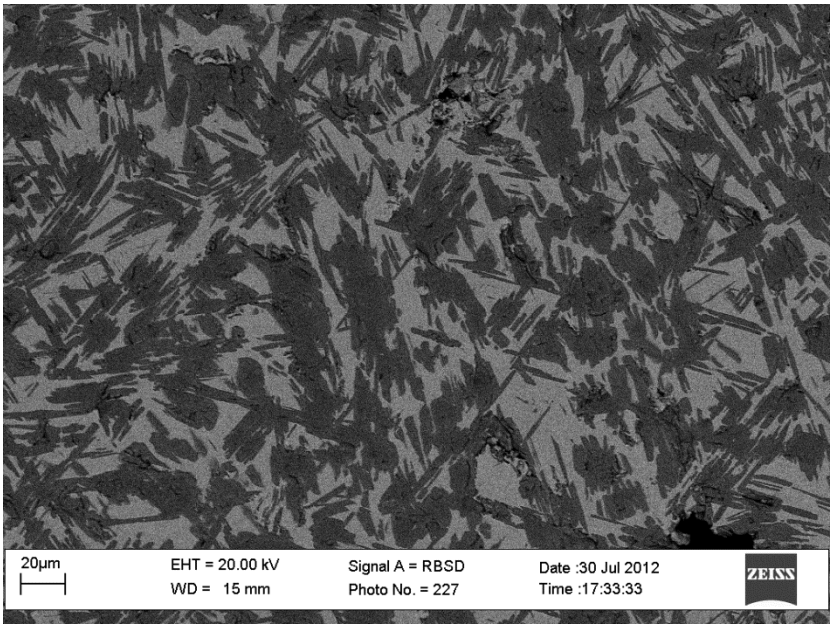


Figure 4.179. SEM-BSE image of nominal $Ni_{22.1}$:$V_{49.1}$:$C_{28.8}$ (at.%), Sample 24, in the as-cast condition, showing ~V_8C_7 needles (dark) and ~Ni_2V matrix (light).

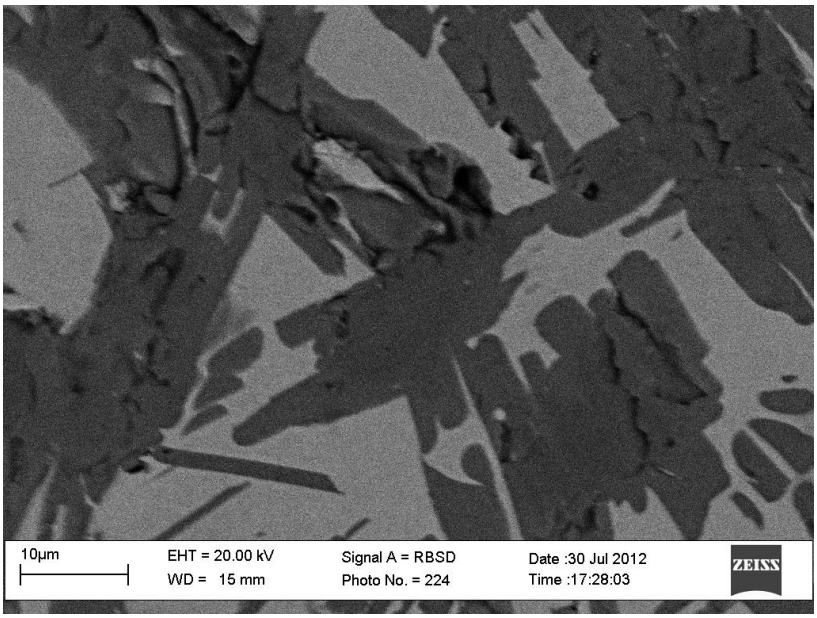


Figure 4.180. SEM-BSE image of nominal $Ni_{22.1}$:$V_{49.1}$:$C_{28.8}$ (at.%), Sample 24, in the as-cast condition, showing ~V_8C_7 needles (dark) and ~Ni_2V matrix (light) at higher magnification.

Table 4.46. EDX phase analyses of as-cast nominal $Ni_{22.1}:V_{49.1}:C_{28.8}$ (at.%), Sample 24.

Phase Description	C	V	Ni	Phase
Overall	36.3 ± 0.9	47.8 ± 0.9	15.9 ± 0.2	-
Dark	46.3 ± 0.8	53.3 ± 0.7	0.4 ± 0.1	~V_8C_7
Light	22.3 ± 0.7	31.9 ± 0.5	45.8 ± 0.7	~Ni_2V

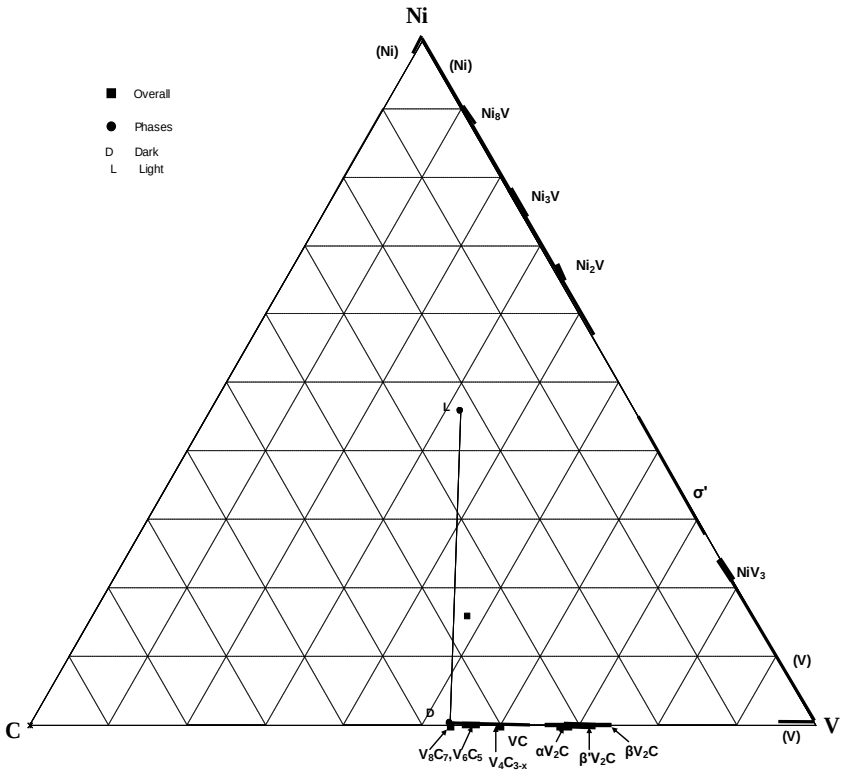


Figure 4.181. EDX analyses of as-cast nominal $Ni_{22.1}:V_{49.1}:C_{28.8}$ (at.%), Sample 24.

The XRD pattern shown in Figures 4.182 to 4.186 was fair, with a reasonable signal:background ratio. The peaks matched ~$V_4C_{2.66}$, which might not be present, since it forms at lower temperatures in the solid state, and were not obvious in the microstructure as shown in Figure 4.186 unless the finer needles were this phase (this is possible, because they did appear darker). The highest intensity peaks were V_8C_7 and Ni_2V, at $2\theta = 47.93^o$ and 50.86^o respectively. The pattern (Figure 4.186) confirmed the presence of V_8C_7, $V_4C_{2.66}$ and

Ni_2V with unidentified peaks at $2\theta = 41.72^o$ and 91.96^o. The unidentified peaks could not be matched with NiV_3 and V. Table 4.48 shows the identified peaks, together with their phases.

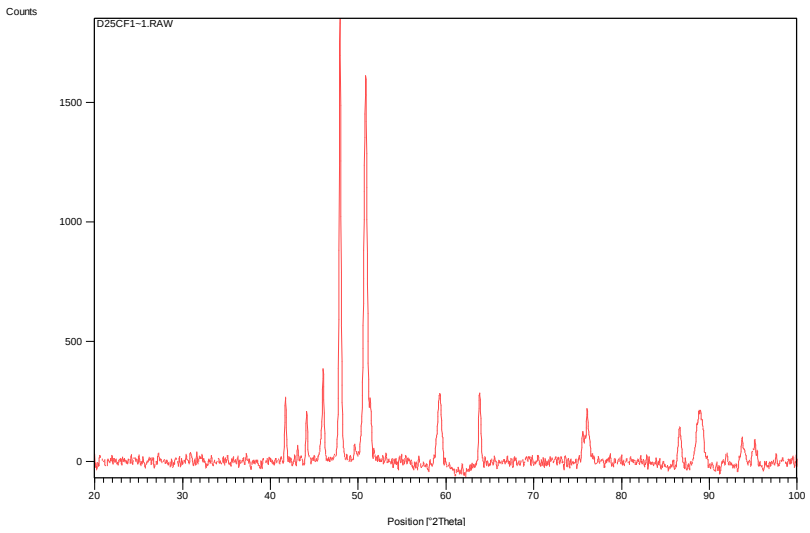


Figure 4.182. Unlabelled XRD pattern of as-cast nominal $Ni_{22.1}$:$V_{49.1}$:$C_{28.8}$ (at.%), Sample 24.

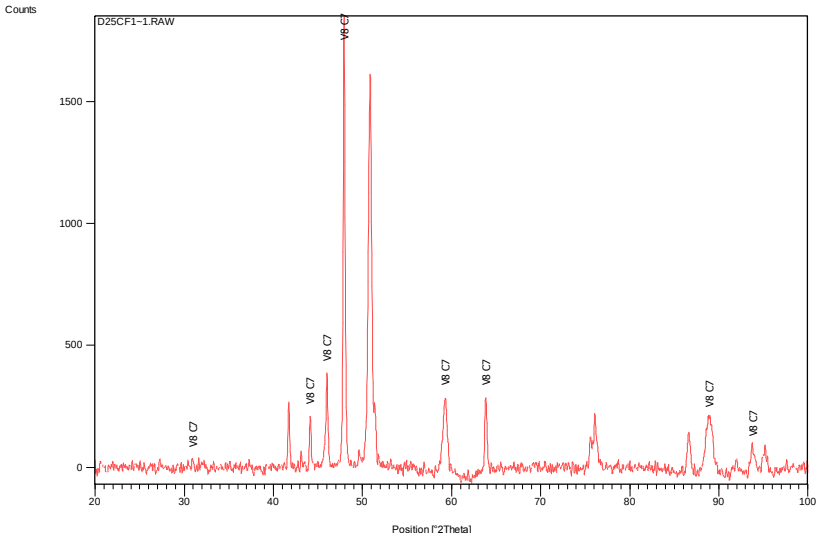


Figure 4.183. XRD pattern of as-cast nominal $Ni_{22.1}$:$V_{49.1}$:$C_{28.8}$ (at.%), Sample 24, showing identified ~V_8C_7 peaks.

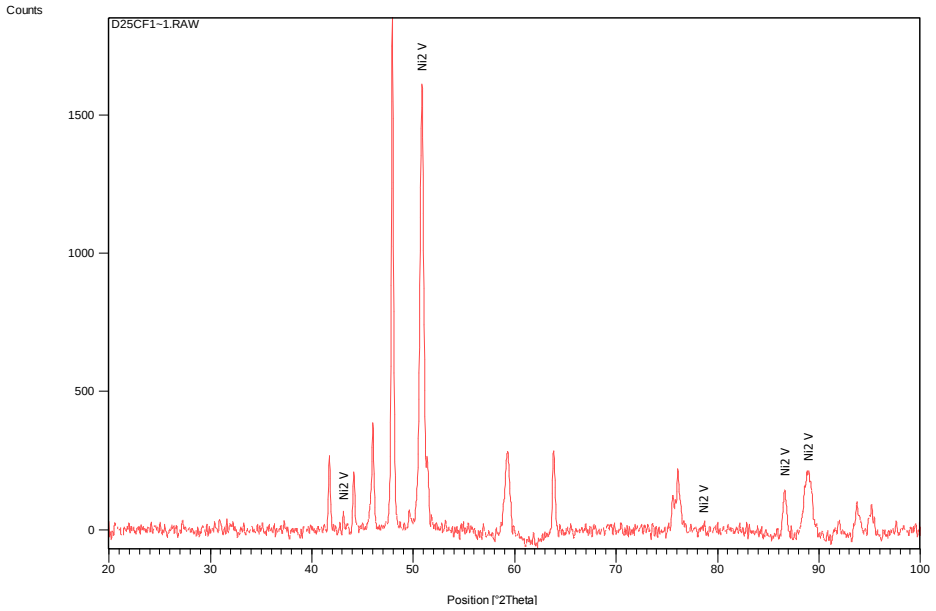


Figure 4.184. XRD pattern of as-cast nominal $Ni_{22.1}:V_{49.1}:C_{28.8}$ (at.%), Sample 24, showing identified ~Ni_2V peaks.

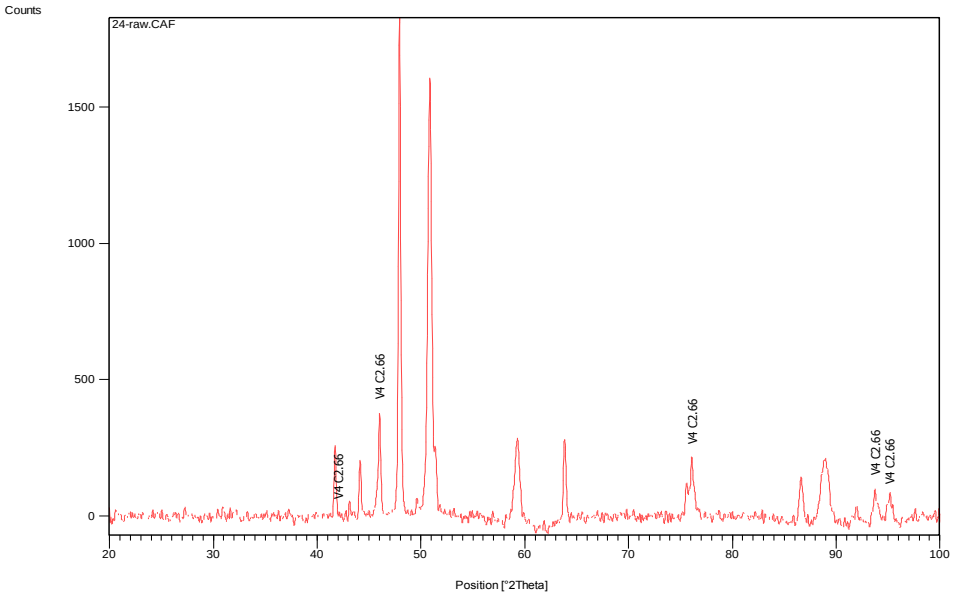


Figure 4.185. XRD pattern of as-cast nominal $Ni_{22.1}:V_{49.1}:C_{28.8}$ (at.%), Sample 24, showing identified ~$V_4C_{2.66}$ peaks.

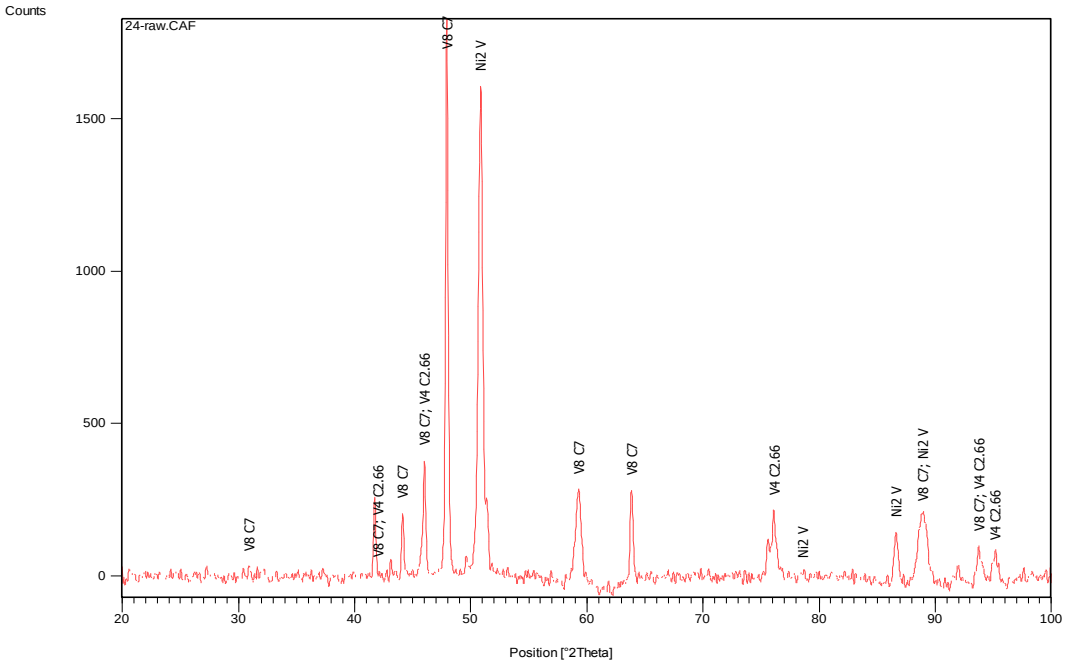


Figure 4.186. XRD pattern of as-cast nominal $Ni_{22.1}:V_{49.1}:C_{28.8}$ (at.%), Sample 24, showing all the identified peaks.

Table 4.47. XRD peaks for as-cast nominal $Ni_{22.1}:V_{49.1}:C_{28.8}$ (at.%), Sample 24.

Position 2θ (º)	Height (counts)	Relative Intensity (%)	Phases
30.9336	31.05	1.70	V_8C_7
41.7289	258.41	14.12	Unidentified
42.0201	12.00	0.66	$V_4C_{2.66}$
44.1411	202.79	11.08	V_8C_7, Ni_2V
46.0167	373.49	20.41	V_8C_7, $V_4C_{2.66}$
47.9336	1829.99	100.00	V_8C_7
50.8604	1595.33	87.18	Ni_2V
59.2873	284.02	15.52	V_8C_7
63.8371	280.03	15.30	V_8C_7
76.0959	212.98	11.64	$V_4C_{2.66}$
78.5751	9.76	0.53	Ni_2V
86.6221	142.04	7.76	Ni_2V
88.9283	197.52	10.79	V_8C_7, Ni_2V
91.9652	37.76	2.06	Unidentified
93.7384	98.72	5.39	V_8C_7, $V_4C_{2.66}$
95.1231	66.19	3.62	$V_4C_{2.66}$

4.2 Phase analysis of alloys – annealed at 1000 °C for 1000 hours

In this section, the heat treated samples results are presented. Five of the heat treated samples (Samples 1-5) had melted and fused with the crucibles, because the samples were not sealed in silica glass tubes. The heat treated Sample 9H was contaminated by titanium after heat treatment, and was not reported. There was no heat treated Sample 16H because the as-cast Sample 16 was contaminated by titanium. Heat treated Sample 23H was not analyzed further because of the contamination of Si found in the microstructure (which derived from the silica ampoule).

4.2.1 Heat treated nominal $Ni_{64}:V_{25}:C_{11}$ (at.%), Sample 6H

The SEM-BSE images of heat treated nominal $Ni_{64}:V_{25}:C_{11}$ (at.%), Sample 6H, at low and higher magnifications are shown in Figures 4.187 and 4.188. The microstructure of this alloy in the annealed condition was very similar to the as-cast condition (Figures 4.188, and 4.40). The alloy had two phases, ~V_8C_7 dendrites and the ~Ni_3V (matrix). The different eutectic colonies of globular and rod-like morphologies were retained and had coarsened (Figure 4.188).

Table 4.49 gives the phase analyses which are shown in Figure 4.189. Comparing Table 4.47 with Table 4.11, it can be seen that there were slight changes in composition after annealing: ~V_8C_7 had gained C and lost V, and ~Ni_3V had gained C and V and lost some Ni, which indicates a slightly sloping solvus. The EDX analyses of heat treated Sample 6 is shown in Appendix B24.

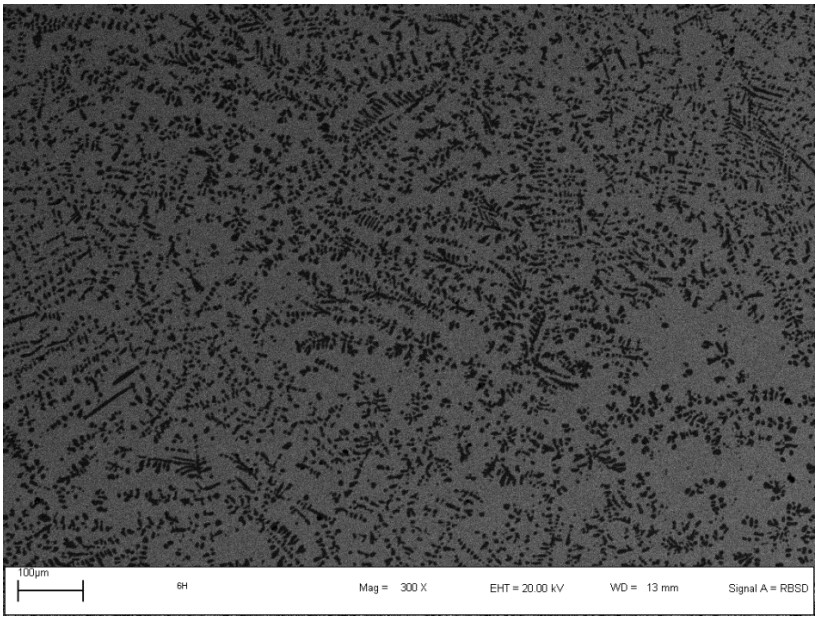


Figure 4.187. BSE-SEM image of heat treated $Ni_{64}:V_{25}:C_{11}$ (at.%), Sample 6H, showing ~V_8C_7 dendrites (dark) and ~Ni_3V matrix (light) at low magnification.

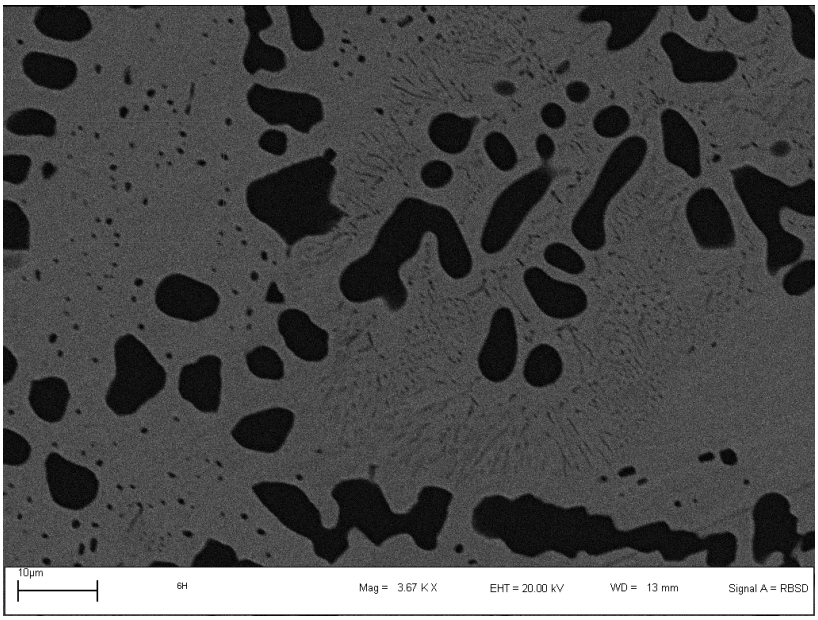


Figure 4.188. BSE-SEM image of heat treated $Ni_{64}:V_{25}:C_{11}$ (at.%), Sample 6H, showing ~V_8C_7 dendrites (dark), ~Ni_3V matrix (light) and eutectic with different colonies at higher magnification.

Table 4.48. EDX phase analyses of annealed nominal $Ni_{64}:V_{25}:C_{11}$ (at.%), Sample 6H.

Phase Description	C	V	Ni	Phase
Overall	26.9 ± 0.6	24.9 ± 0.3	48.2 ± 0.4	-
Dark	48.6 ± 0.4	50.2 ± 0.2	1.2 ±0.3	~V_8C_7
Light	15.5 ± 0.2	14.3 ± 0.4	70.2 ± 0.4	~Ni_3V
Eutectic	17.4 ± 0.5	15.3 ± 0.6	67.3 ± 0.5	~VC + (Ni)

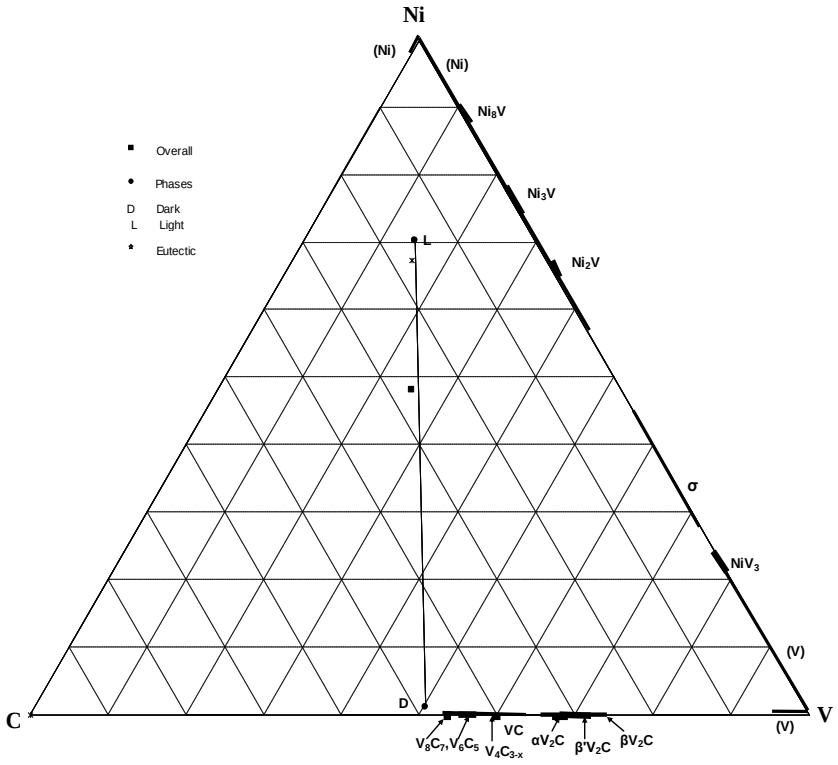


Figure 4.189. EDX analyses of heat treated nominal $Ni_{64}:V_{25}:C_{11}$ (at.%), Sample 6H.

Figures 4.190 to 4.193 show the XRD pattern for heat treated Sample 6H. The existence of ~V_8C_7 and ~Ni_3V were confirmed by XRD, as shown in Figures 4.191 and 4.192 respectively. The matches for the phases were excellent with the ICDD, but with unidentified peaks at about $2\theta = 55.38^o$ and 56.49^o. The ~Ni_3V peaks still retained the highest count at

position 2θ = 51.74° compared to as-cast sample (Figure 4.44). The ~V_8C_7 peaks were stronger in the annealed sample than for the as-cast specimen. Carbon could not be matched. Table 4.50 shows the identified peaks together with their phases.

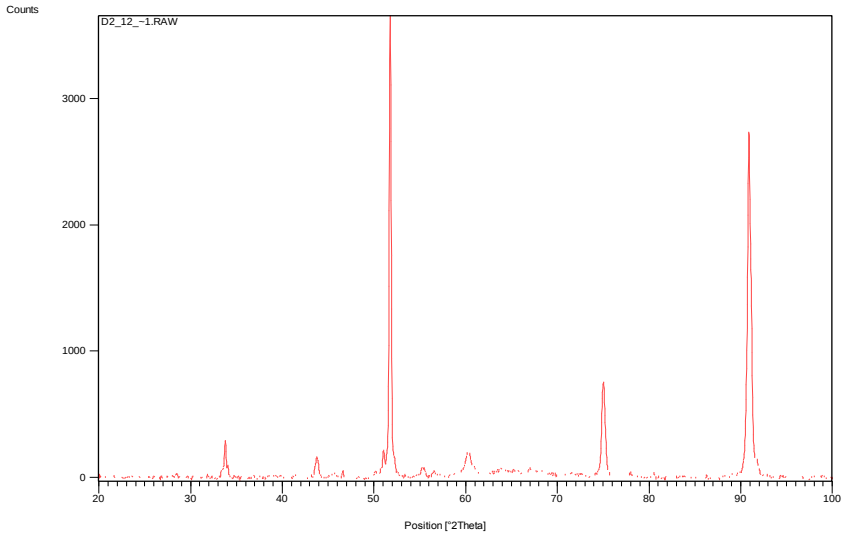


Figure 4.190. Unlabelled XRD pattern of heat treated nominal Ni_{64}:V_{25}:C_{11} (at.%), Sample 6H.

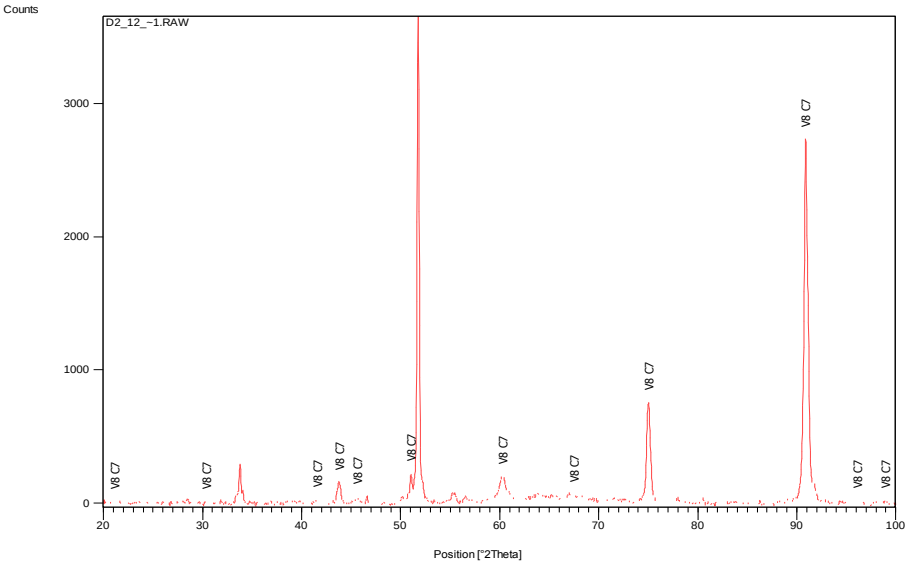


Figure 4.191. XRD pattern of heat treated nominal Ni_{64}:V_{25}:C_{11} (at.%), Sample 6H, showing identified ~V_8C_7 peaks.

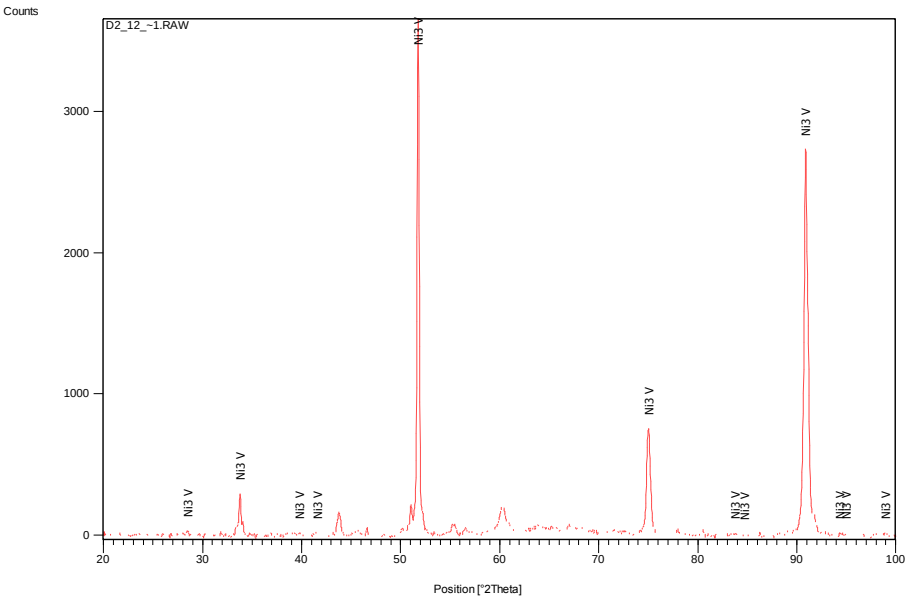


Figure 4.192. XRD pattern of heat treated nominal $Ni_{64}:V_{25}:C_{11}$ (at.%), Sample 6H, showing identified ~Ni_3V peaks.

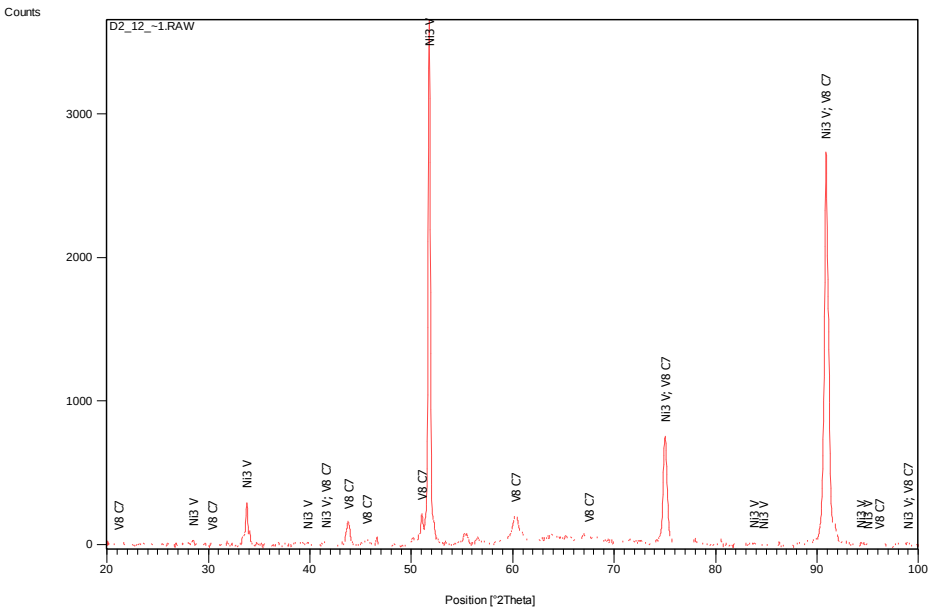


Figure 4.193. XRD pattern of heat treated nominal $Ni_{64}:V_{25}:C_{11}$ (at.%), Sample 6H, showing all the identified peaks.

Table 4.49. XRD peaks for heat treated nominal $Ni_{64}:V_{25}:C_{11}$ (at.%), Sample 6H.

Position 2θ (º)	Height (counts)	Relative Intensity (%)	Phases
21.1376	1.60	0.04	V_8C_7
28.5114	26.46	0.73	Ni_3V
30.4019	4.55	0.13	V_8C_7
33.7813	292.35	8.07	Ni_3V
39.7705	15.08	0.42	Ni_3V
41.5844	17.29	0.48	V_8C_7, Ni_3V
43.8208	149.25	4.12	V_8C_7
45.6133	40.52	1.12	V_8C_7
51.0395	211.26	5.83	V_8C_7
55.3794	74.07	2.05	Unidentified
56.4901	45.88	1.27	Unidentified
60.2928	194.92	5.38	V_8C_7
67.5204	57.20	1.58	V_8C_7
75.0441	750.31	20.72	V_8C_7, Ni_3V
83.8087	19.65	0.54	Ni_3V
84.7113	8.47	0.23	Ni_3V
90.8977	2727.10	75.30	Ni_3V
94.3186	18.48	0.51	Ni_3V
96.1233	11.05	0.31	Ni_3V

4.2.2 Heat treated nominal $Ni_{70}:V_{10}:C_{20}$ (at.%), Sample 7H

SEM-BSE images of $Ni_{70}:V_{10}:C_{20}$ (at.%), Sample 7H, in the heat treated condition are given in Figures 4.194 and 4.195. At low magnification, the alloy consisted of plates, which were randomly distributed, dendrites and the matrix. The heat treated sample showed a very similar microstructure to the as-cast sample (Figure 4.47). The phase compositions are shown in Table 4.51, and are plotted in Figure 4.196, showing the overall compositions to lie within the tie-triangle of the phases. The phase compositions of the heat treated Sample 7H varied slightly when compared to as-cast condition (Table 4.51, Table 4.14). The phases were identified as: graphite flakes, ~V_8C_7 dendrites and (Ni) matrix. The standard deviation of the measurements was below 1 at.%. The EDX analyses of Sample 7H are shown in Appendix B25. The ~V_8C_7 had lost some carbon, and the (Ni) matrix had gained carbon and lost Ni. It is possible that the matrix composition was affected by fine carbon precipitation.

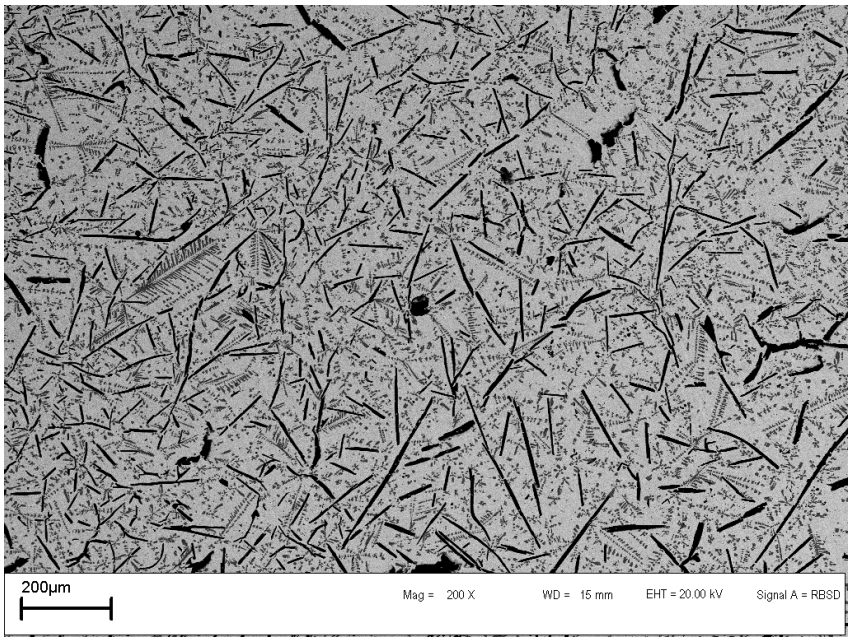


Figure 4.194. BSE-SEM images of heat treated Ni_{70}:V_{10}:C_{20} (at.%), Sample 7H, showing graphite flakes (very dark), ~V_8C_7 dendrites (dark) and (Ni) matrix (light).



Figure 4.195. BSE-SEM images of heat treated Ni_{70}:V_{10}:C_{20} (at.%), Sample 7H, showing graphite flakes (very dark), ~V_8C_7 dendrites (dark) and (Ni) matrix (light).

Table 4.50. EDX phase analyses of annealed nominal $Ni_{70}:V_{10}:C_{20}$ (at.%), Sample 7H.

Phase Description	C	V	Ni	Phase
Overall	50.2 ±1.1	7.9 ± 0.2	41.9 ± 0.8	-
Very dark	99.2 ±0.02	0.1±0.06	0.7±0.09	graphite
Dark	45.2 ± 0.7	50.9 ± 0.4	3.9 ± 0.5	~V_7C_8
Light	29.8 ± 0.4	1.7 ± 0.06	68.5 ± 0.5	(Ni)

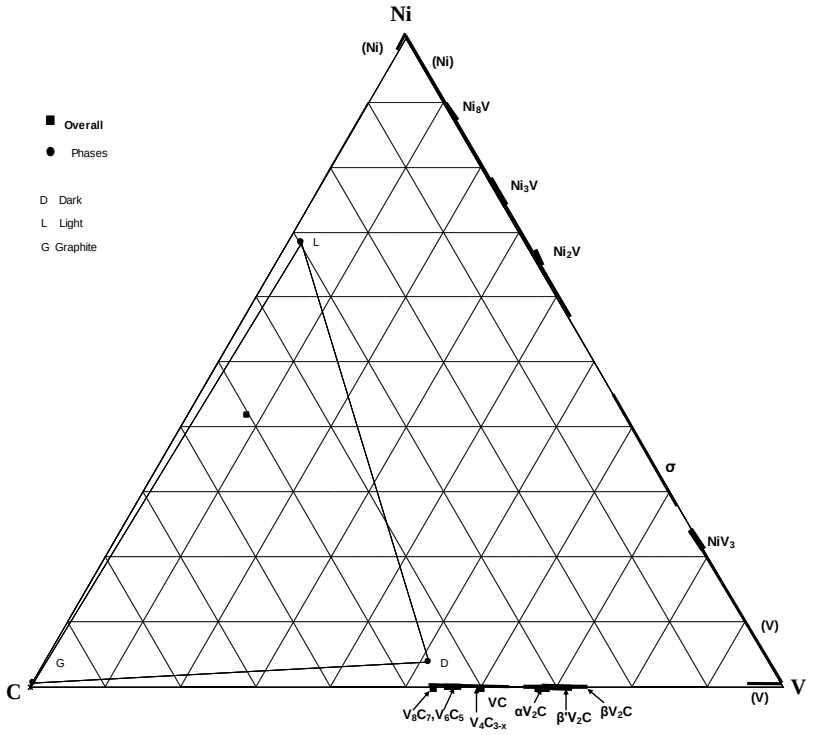


Figure 4.196. EDX analyses of heat treated nominal $Ni_{70}:V_{10}:C_{20}$ (at.%), Sample 7H.

Figures 4.197 to 4.201 show the experimental pattern of the sample, with the data for each of the phases. The XRD pattern (Figure 4.201) confirmed the presence of ~V_8C_7, graphite and (Ni). A major peak was found at $2\theta = 51.94^o$, which matched Ni. All peaks were matched except that at position $2\theta = 34.21^o$. Table 4.52 shows the identified peaks together with their phases. The nickel peaks were very high compared with the as-cast sample.

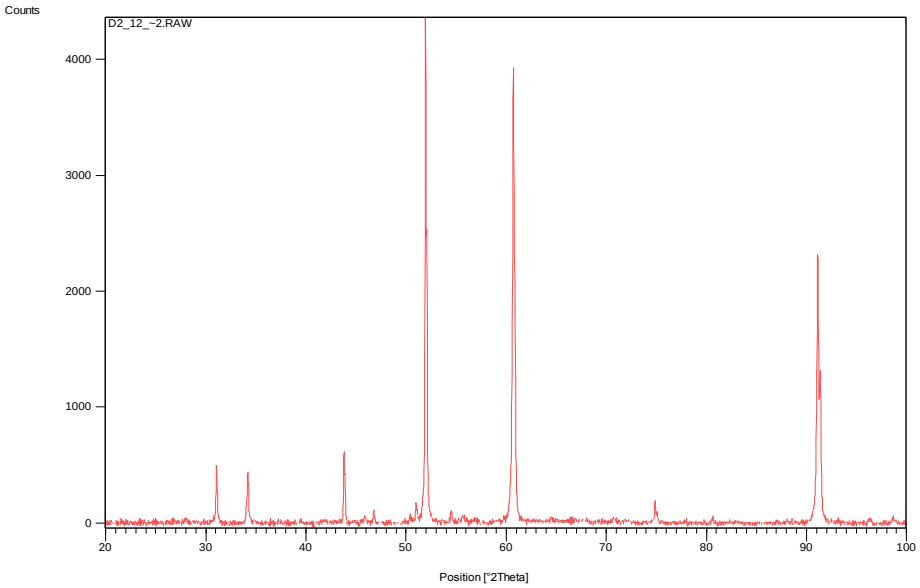


Figure 4.197. Unlabelled XRD pattern of heat treated nominal $Ni_{70}:V_{10}:C_{20}$ (at.%), Sample 7H.

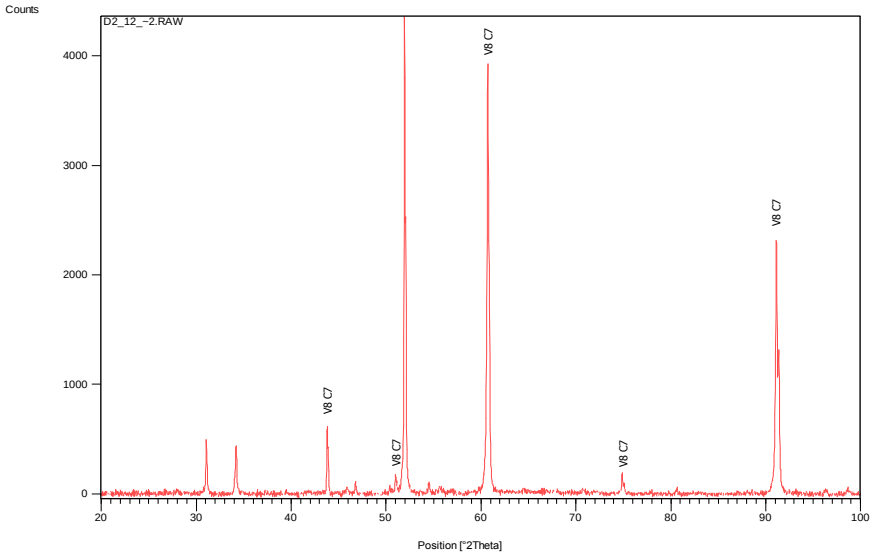


Figure 4.198. XRD pattern of heat treated nominal $Ni_{70}:V_{10}:C_{20}$ (at.%), Sample 7H, showing identified ~V_8C_7 peaks.

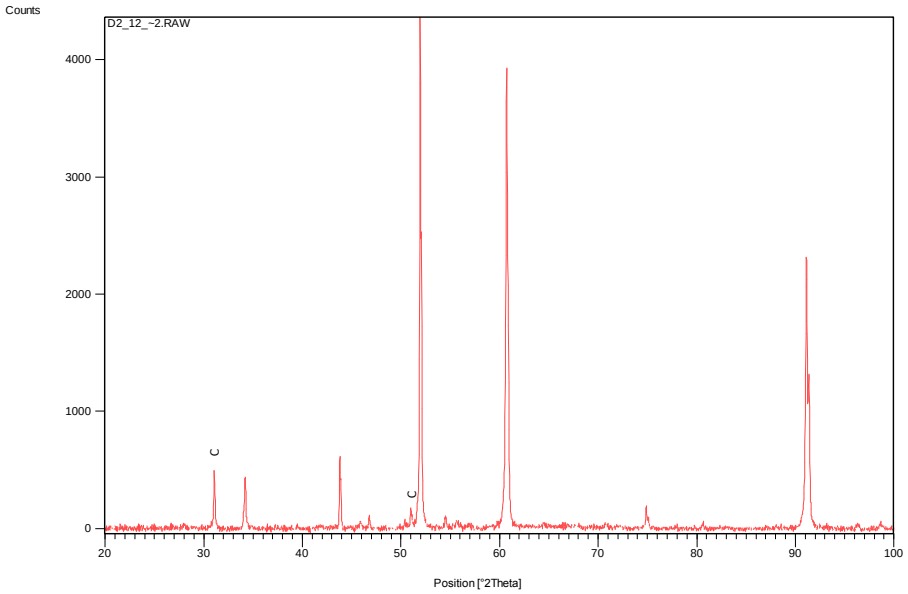


Figure 4.199. XRD pattern of heat treated nominal Ni_{70}:V_{10}:C_{20} (at.%), Sample 7H, showing identified C peaks.

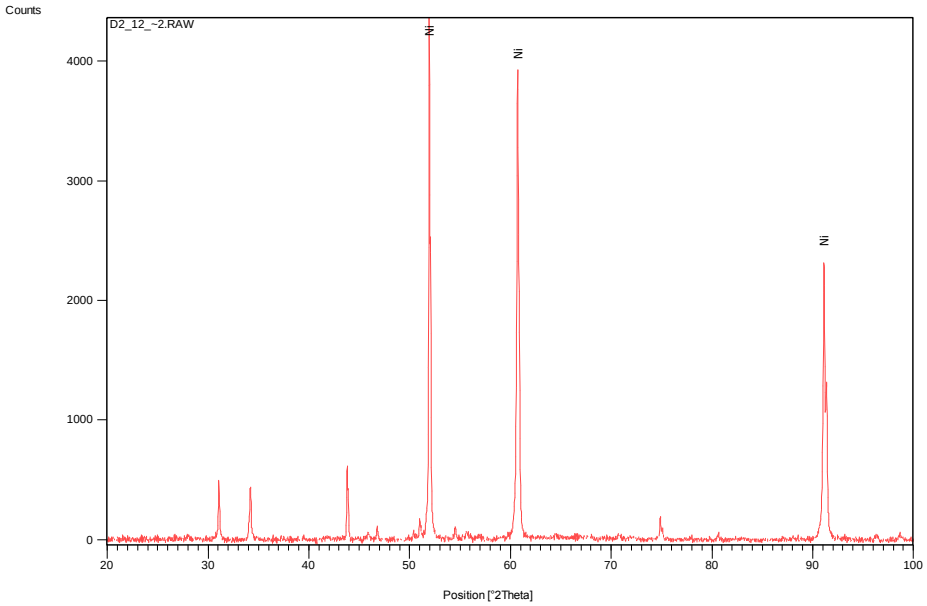


Figure 4.200. XRD pattern of heat treated nominal Ni_{70}:V_{10}:C_{20} (at.%), Sample 7H, showing identified (Ni) peaks.

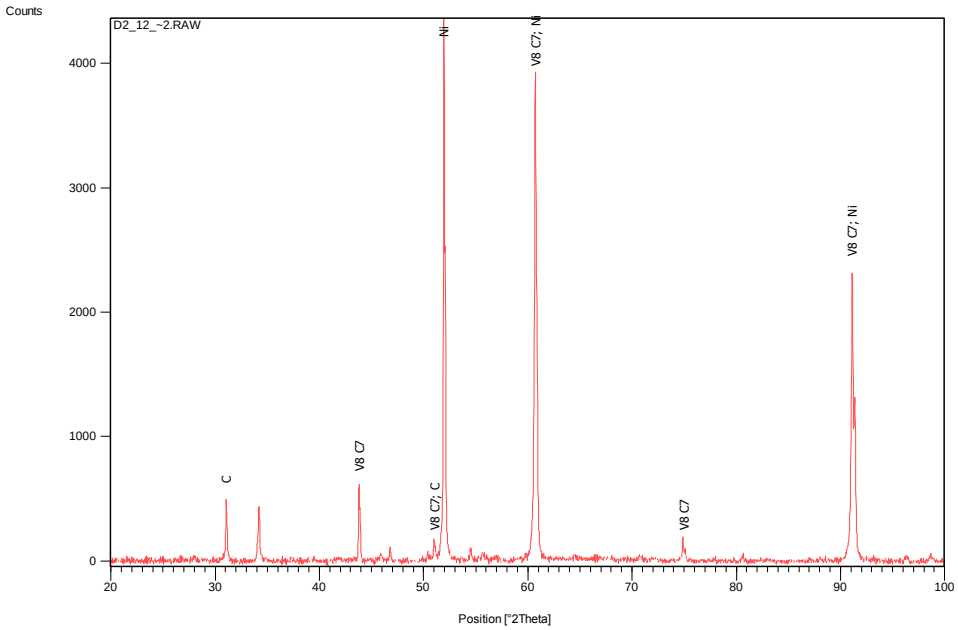


Figure 4.201. XRD pattern of heat treated nominal $Ni_{70}:V_{10}:C_{20}$ (at.%), Sample 7H, showing all the identified peaks.

Table 4.51. XRD peaks for heat treated nominal $Ni_{70}:V_{10}:C_{20}$ (at.%), Sample 7H.

Position 2θ (º)	Height (counts)	Relative Intensity (%)	Phases
31.0681	497.52	11.53	V_8C_7, C
34.2140	386.89	8.97	Unidentified
43.7973	606.56	14.06	V_8C_7
51.0351	135.57	3.14	V_8C_7, C
51.9460	4315.47	100.00	Ni
60.7083	3892.02	90.19	V_8C_7, Ni
74.9469	130.65	3.03	V_8C_7
91.1199	2332.25	54.04	V_8C_7, Ni
91.3823	1276.27	29.57	Unidentified

4.2.3 Heat treated nominal $Ni_{60}:V_{30}:C_{10}$ (at.%), Sample 8H

Figures 4.202 and 4.203 show the SEM-BSE images of $Ni_{60}:V_{30}:C_{10}$ (at.%), Sample 8, in the heat treated condition. The alloy had two different contrasts in the microstructure (Figure 4.203): dark dendrites, which was identified as ~V_8C_7, and the light matrix regions were identified as (Ni). There was a eutectic of dark and light phases, which were identified as

~V_8C_7 + (Ni). The heat treated sample showed a very similar microstructure to the as-cast sample (Figures 4.201, and 4.55), with coarsening of the dendrites and the eutectic, which would be expected. This led to the morphology of the ~V_8C_7 (dendrites) to be more facetted after the heat treatment. Two coarsened eutectic morphologies were observed (as in the as-cast sample), ~VC + (Ni) and (Ni) + C.

Table 4.53 gives the phase analyses for the alloy which are shown in Figure 4.204. Comparing Table 4.53 with Table 4.16, it could be seen that there was a significant change in composition during annealing, the ~Ni_2V phase which was seen in as-cast sample transformed back to (Ni) (with transformation temperature 906ºC [1982Smi]) (Figure 3.29). ~V_8C_7 had lost C and gained V on heat treatment and (Ni) had lost C and V, while gaining Ni. These changes show that the (Ni) solvus retreated at lower temperature. The EDX analyses of heat treated Sample 8 are shown in Appendix B26.

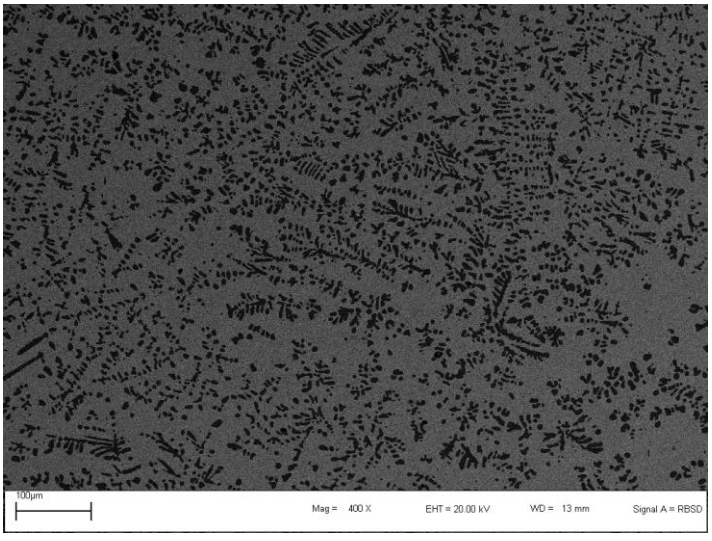


Figure 4.202. BSE-SEM image of heat treated Ni_{60}:V_{30}:C_{10} (at.%), Sample 8H, showing ~V_8C_7 dendrites (dark) and (Ni) matrix (light) at low magnification.

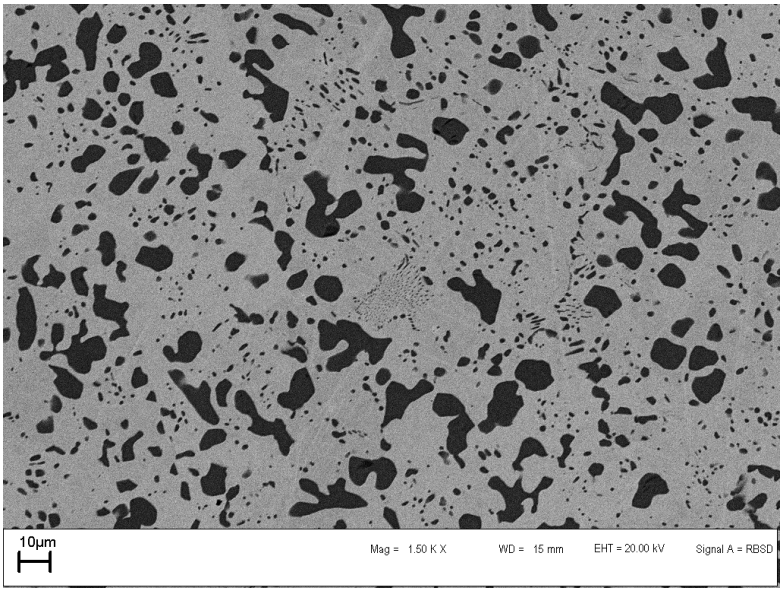


Figure 4.203. BSE-SEM image of heat treated $Ni_{60}:V_{30}:C_{10}$ (at.%), Sample 8H, showing ~V_8C_7 dendrites (dark), (Ni) matrix (light) and eutectic at higher magnification.

Table 4.52. EDX phase analyses of annealed nominal $Ni_{60}:V_{30}:C_{10}$ (at.%), Sample 8H.

Phase Description	C	V	Ni	Phase
Overall	22.2± 0.3	30.4±0.3	47.4± 0.3	-
Dark	45.9 ± 0.2	52.9 ± 0.3	1.2 ± 0.2	~V_8C_7
Light	15.9 ±0.2	20.9 ± 0.2	63.2 ± 0.4	(Ni)
Eutectic (fine)	21.9 ± 0.5	27.7 ± 0.6	50.4 ± 0.3	~V_8C_7 + (Ni)
Eutectic (coarsed)	21.8 ± 1.9	28.2 ± 1.1	50.0 ± 2.5	C + (Ni)

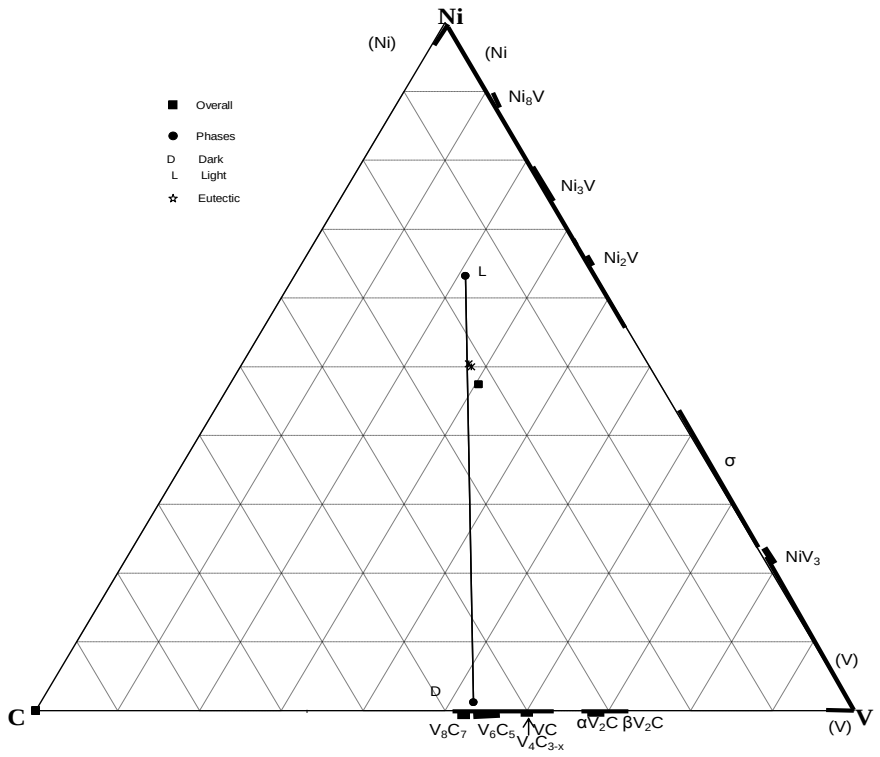


Figure 4.204. EDX analyses of heat treated nominal Ni_{60}:V_{30}:C_{10} (at.%), Sample 8H.

The XRD pattern (Figure 4.207) confirmed the presence of ~V_8C_7 and (Ni). Figures 4.205 to 4.208 show the experimental pattern of the sample with the database lines for each of the phases and Table 4.54 shows the identified peaks. The highest intensity peak at about 2θ = 51.66º was from (Ni). At 2θ = 60.68º and 91.11º there is an overlapping of ~V_8C_7 and (Ni) peaks. On annealing, the double peak at 2θ = 75.08º was much reduced, and also the peak at 2θ = 37.56º of the as-cast pattern had been lost. All peaks could be matched, except those at 2θ = 30.94º and 46.52º.

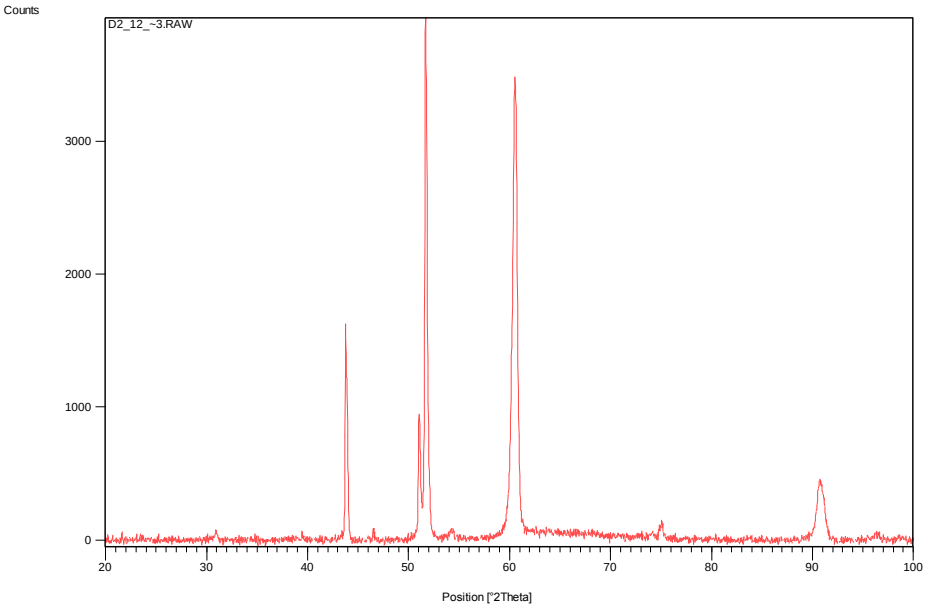


Figure 4.205. Unlabelled XRD pattern of heat treated nominal $Ni_{60}:V_{30}:C_{10}$ (at.%), Sample 8H.

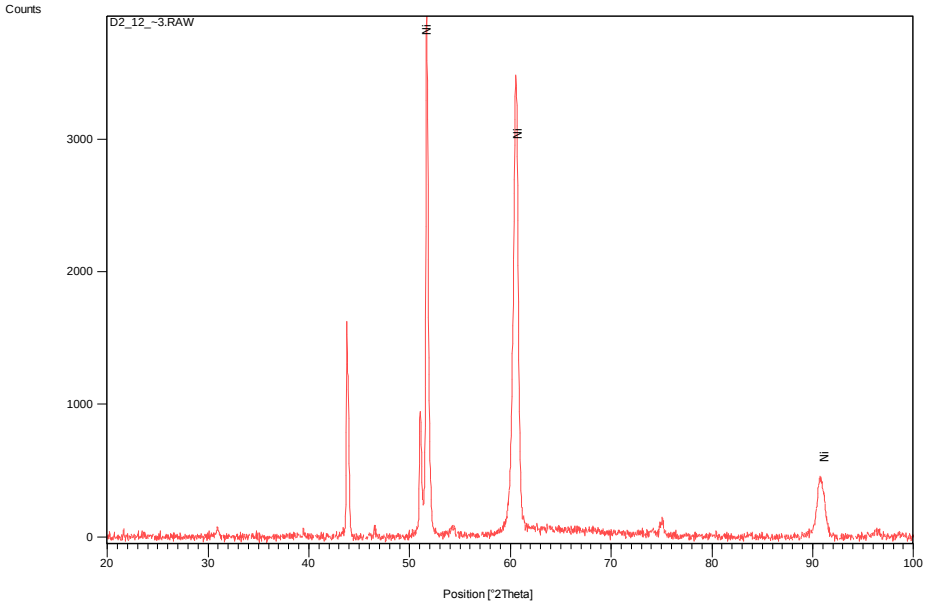


Figure 4.206. XRD pattern of heat treated nominal $Ni_{60}:V_{30}:C_{10}$ (at.%), Sample 8H, showing identified (Ni) peaks.

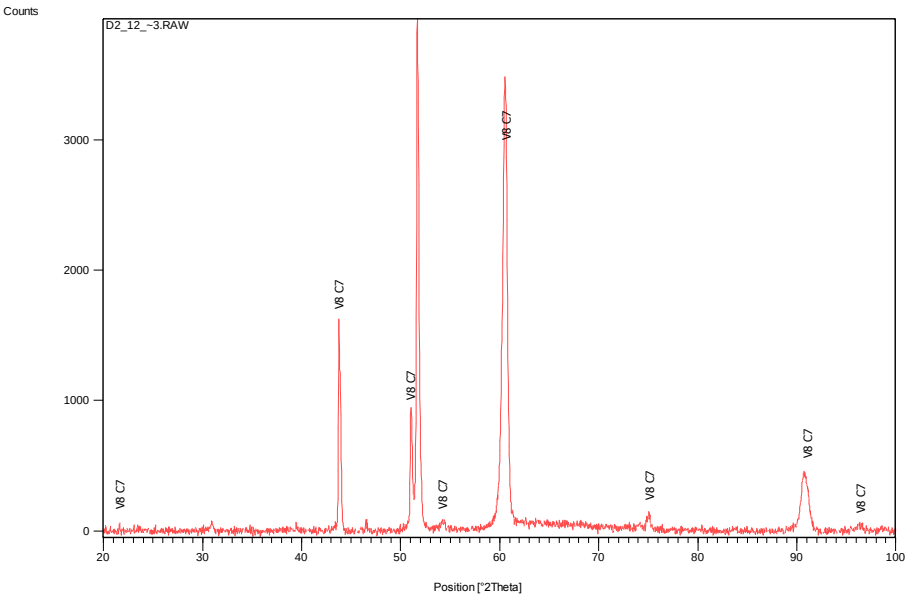


Figure 4.207. XRD pattern of heat treated nominal $Ni_{60}:V_{30}:C_{10}$ (at.%), Sample 8H, showing identified ~V_8C_7 peaks.

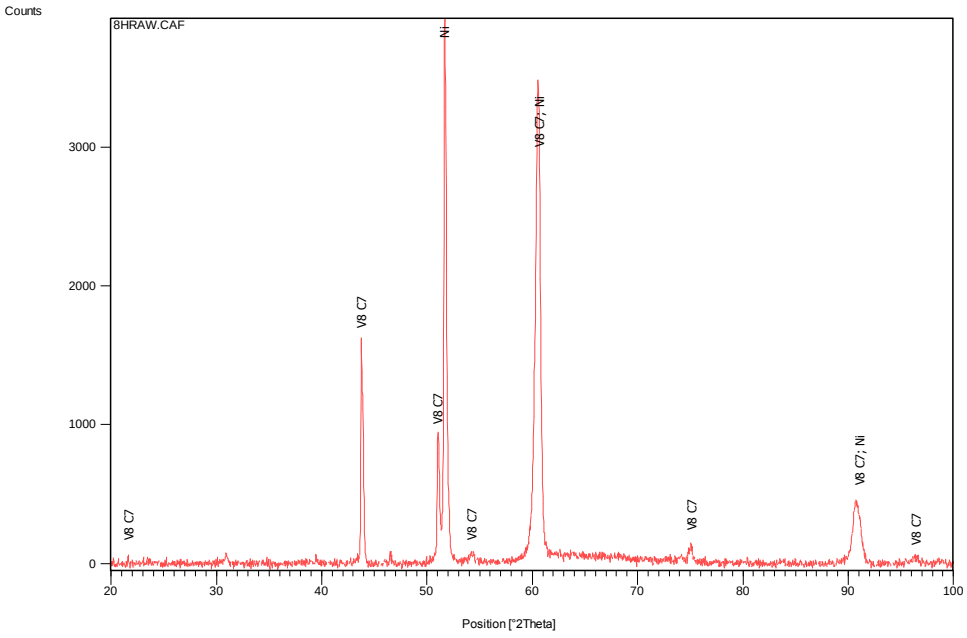


Figure 4.208. XRD pattern of heat treated nominal $Ni_{60}:V_{30}:C_{10}$ (at.%), Sample 8H, showing all the identified peaks.

Table 4.53. XRD peaks for heat treated nominal $Ni_{60}:V_{30}:C_{10}$ (at.%), Sample 8H.

Position 2θ (º)	Height (counts)	Relative Intensity (%)	Phases
21.6162	59.40	1.57	V_8C_7
30.9429	69.17	1.83	Unidentified
43.7590	1594.66	42.09	V_8C_7
46.5239	51.76	1.37	Unidentified
51.0191	896.70	23.67	V_8C_7
51.6657	3788.27	100.00	Ni
54.2527	66.03	1.74	V_8C_7
60.6868	2890.72	76.31	V_8C_7, Ni
75.0858	132.60	3.50	V_8C_7
91.1100	451.40	11.92	V_8C_7, Ni
96.4539	26.90	0.71	V_8C_7

4.2.4 Heat treated nominal $Ni_{20}:V_{35}:C_{45}$ (at.%), Sample 10H

The nominal $Ni_{20}:V_{35}:C_{45}$ (at.%), Sample 10H, in the annealed condition are shown in Figures 4.209 and 4.210. As was the case for Sample 10 in the as-cast condition (Figure 4.70), the annealed alloy showed dark dendrites with light regions between the dendrites, and graphite flakes. There were cracks around the graphite in ~V_8C_7, which had not been found in the as-cast alloy. The plot of the compositions (Table 4.55) identified the light phase as (Ni), the dark phase as ~V_8C_7, while the very dark phase was identified as graphite (Figure 4.211). The EDX analyses are shown in Appendix B27. On annealing, the ~V_8C_7 lost C and gained V, whereas (Ni) had gained V and lost a little Ni.

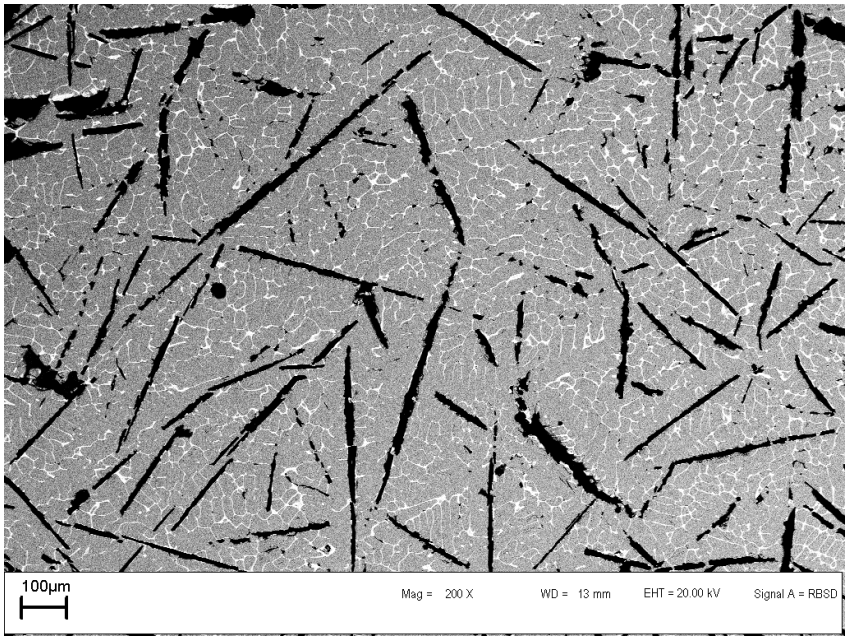


Figure 4.209. BSE-SEM image of heat treated $Ni_{20}:V_{35}:C_{45}$ (at.%), Sample 10H, showing ~V_8C_7 dendrites (dark), graphite flakes (very dark) and (Ni) matrix (light).

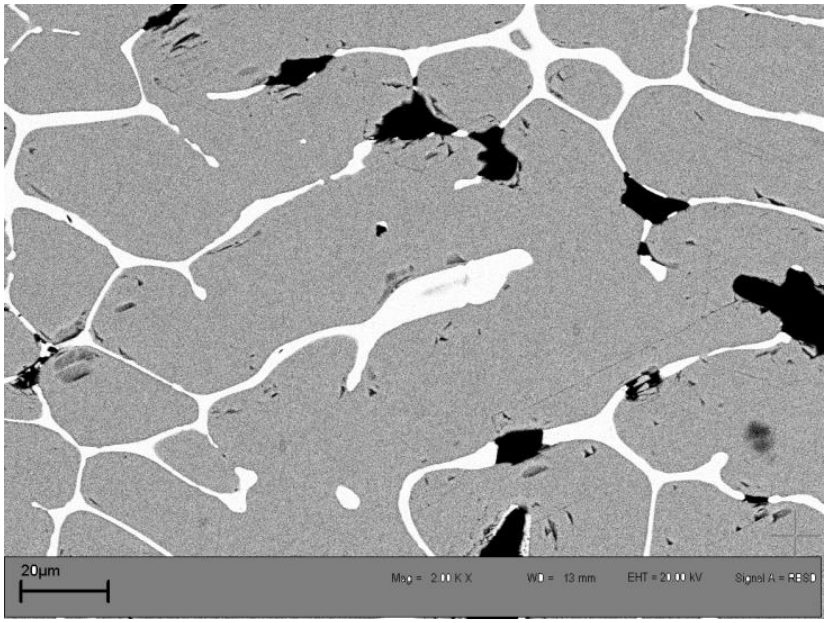


Figure 4.210. BSE-SEM image of heat treated $Ni_{20}:V_{35}:C_{45}$ (at.%), Sample 10H, showing ~V_8C_7 dendrites (dark), graphite flakes (very dark) and (Ni) matrix (light).

Table 4.54. EDX phase analyses of annealed nominal $Ni_{20}:V_{35}:C_{45}$ (at.%), Sample 10H.

Phase Description	C	V	Ni	Phase
Overall	72.1± 0.1	25.3± 1.0	2.6 ± 0.3	-
Dark	47.7 ± 0.5	52.0 ± 0.6	0.3 ± 0.1	~V_8C_7
Light	18.5 ± 1.3	5.0 ± 0.9	76.5 ± 0.4	(Ni)
Very dark	99.5 ± 0.4	0.5 ± 0.4	0	graphite

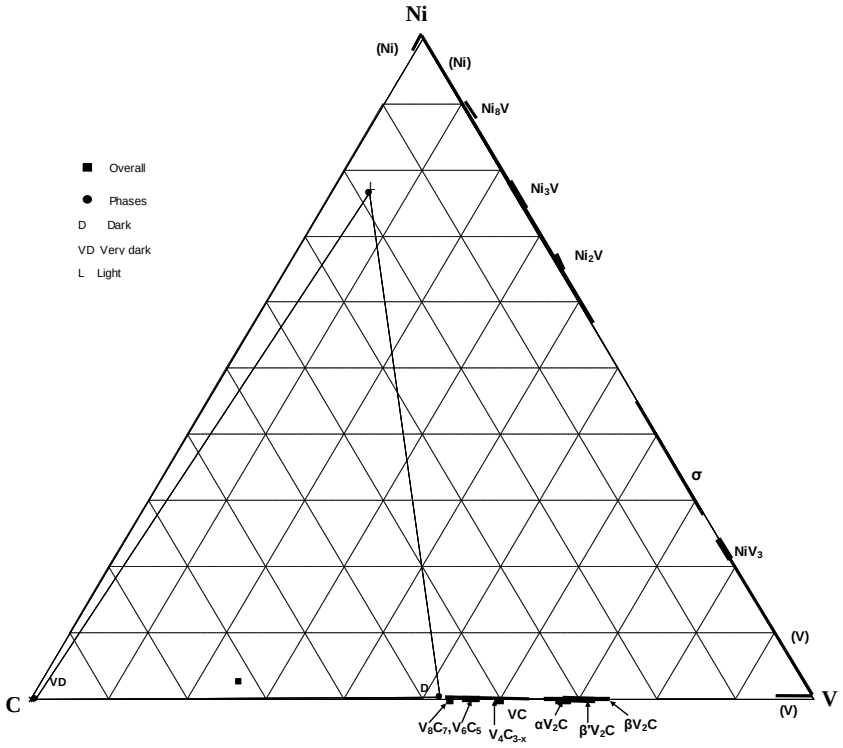


Figure 4.211. EDX analyses of heat treated nominal $Ni_{20}:V_{35}:C_{45}$ (at.%), Sample 10H.

The existence of ~V_8C_7, (Ni), graphite and ~$V_4C_{2.66}$ was confirmed by the XRD, although the pattern was extremely poor with low counts and high background as shown in Figures 4.212 to 4.217. In addition to the phases identified by EDX, ~$V_4C_{2.66}$ was also observed which was not identified in as-cast (Figure 4.76) condition. The highest intensity peak at

about 2θ = 52.11° (Figure 4.217) was a combination of ~V_8C_7, ~$V_4C_{2.66}$, C and (Ni). Table 4.56 shows both identified and unidentified peaks together with their phases.

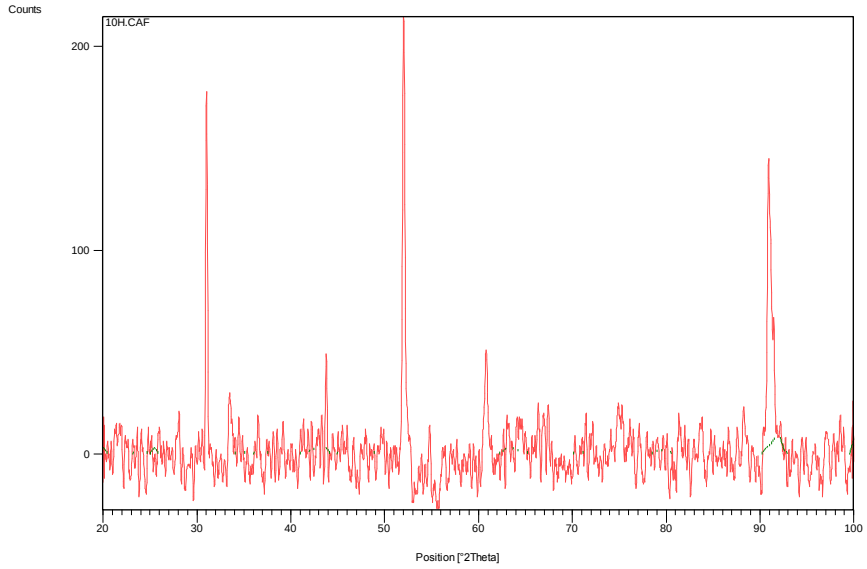


Figure 4.212. Unlabelled XRD pattern of heat treated nominal Ni_{20}:V_{35}:C_{45} (at.%), Sample 10H.

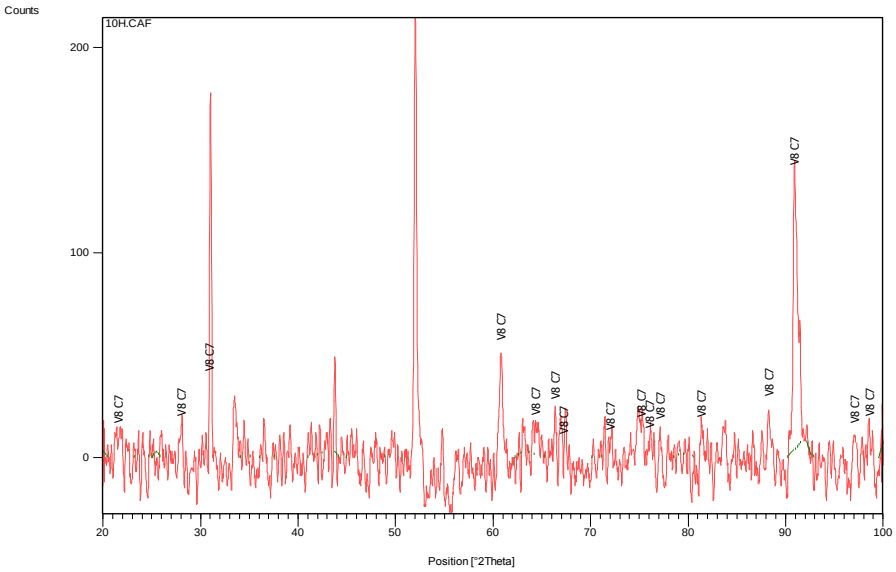


Figure 4.213. XRD pattern of heat treated nominal Ni_{20}:V_{35}:C_{45} (at.%), Sample 10H, showing identified ~V_8C_7 peaks.

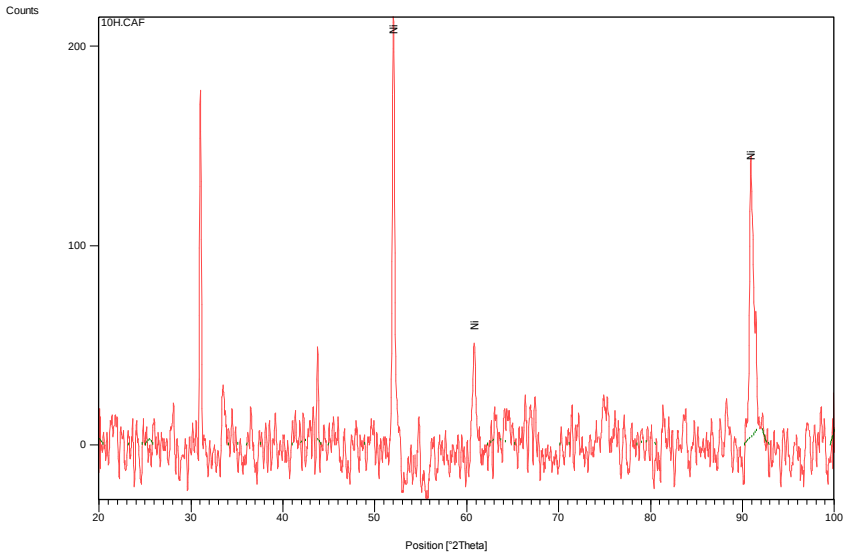


Figure 4.214. XRD pattern of heat treated nominal Ni_{20}:V_{35}:C_{45} (at.%), Sample 10H, showing identified (Ni) peaks.

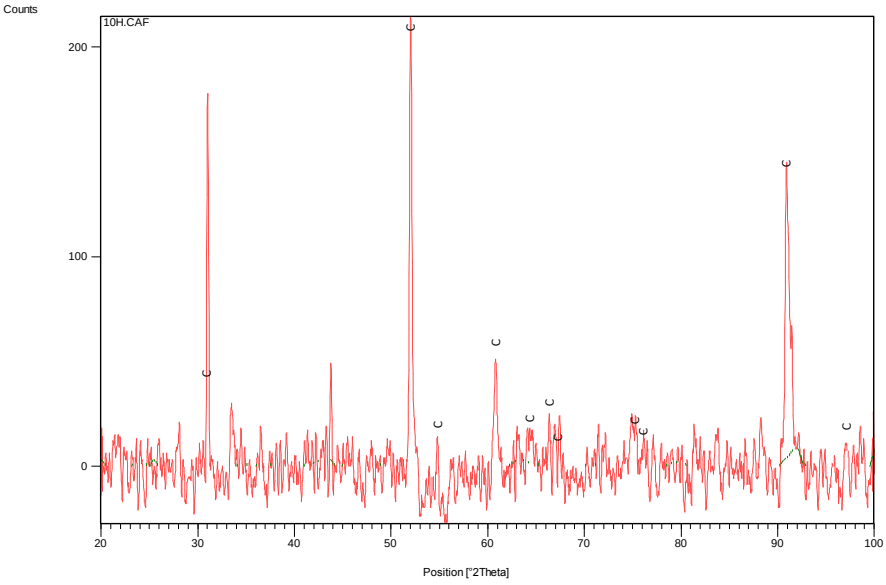


Figure 4.215. XRD pattern of heat treated nominal Ni_{20}:V_{35}:C_{45} (at.%), Sample 10H, showing identified C peaks.

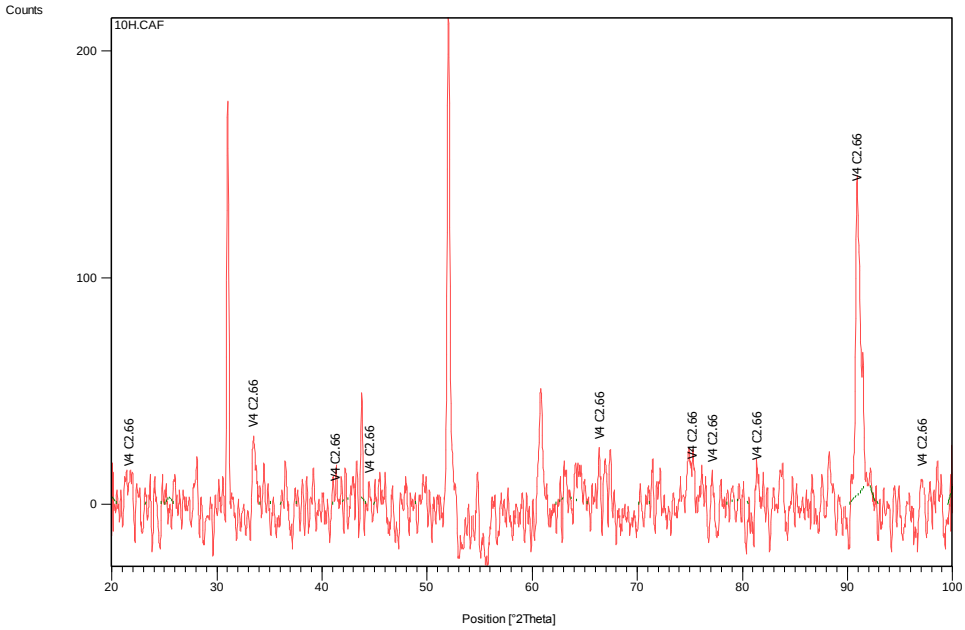


Figure 4.216. XRD pattern of heat treated nominal $Ni_{20}:V_{35}:C_{45}$ (at.%), Sample 10H, showing identified ~$V_4C_{2.66}$ peaks.

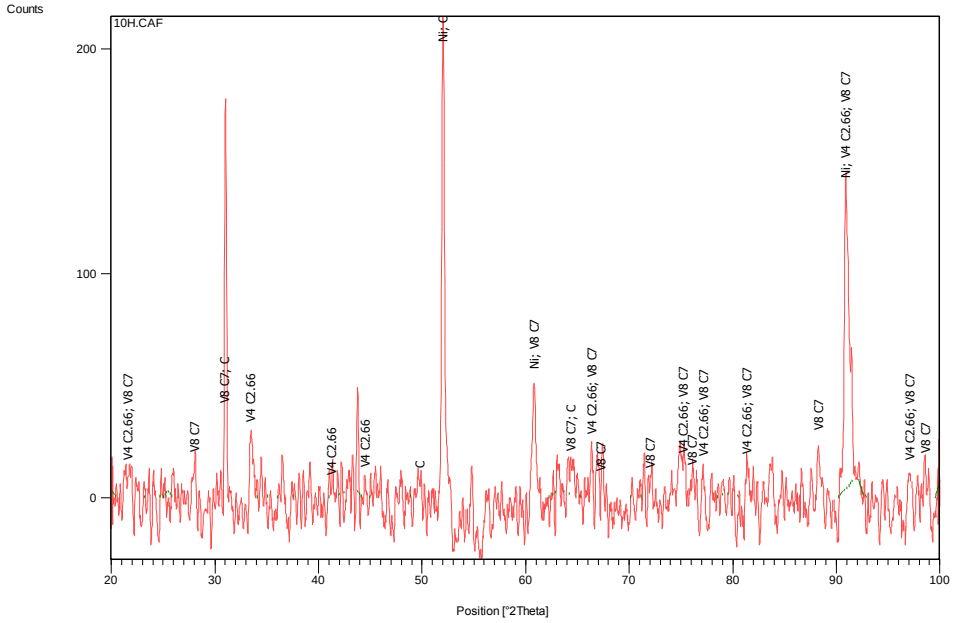


Figure 4.217. XRD pattern of heat treated nominal $Ni_{20}:V_{35}:C_{45}$ (at.%), Sample 10H, showing all the identified peaks.

Table 4.55. XRD peaks for heat treated nominal $Ni_{20}:V_{35}:C_{45}$ (at.%), Sample 10H.

Position 2θ (º)	Height (counts)	Relative Intensity (%)	Phases
21.5532	10.16	4.79	$V_4C_{2.66}$, V_8C_7
27.9744	14.04	6.62	V_8C_7
30.9324	35.59	16.79	V_8C_7, C
33.4336	27.56	13.00	$V_4C_{2.66}$
39.1333	11.09	5.23	Unidentified
41.2337	2.69	1.27	$V_4C_{2.66}$
44.5128	7.19	3.39	$V_4C_{2.66}$
49.7512	6.38	3.01	Unidentified
52.0208	211.99	100.00	C, Ni
54.7966	11.22	5.29	C
60.8246	50.62	23.88	V_8C_7, C, Ni
64.3868	13.29	6.27	V_8C_7, C
66.3551	22.28	10.51	$V_4C_{2.66}$, V_8C_7, C
67.2565	5.25	2.48	V_8C_7, C
72.0394	6.67	3.15	V_8C_7
75.1583	13.50	6.37	$V_4C_{2.66}$, V_8C_7, C
76.0571	8.16	3.85	V_8C_7, C
77.1332	12.21	5.76	$V_4C_{2.66}$, V_8C_7
81.3192	13.17	6.21	$V_4C_{2.66}$, V_8C_7
83.6995	14.54	6.86	Unidentified
88.2589	23.75	11.20	V_8C_7
90.8742	132.26	62.39	$V_4C_{2.66}$, V_8C_7, C, Ni
97.0985	10.31	4.86	$V_4C_{2.66}$, V_8C_7, C
98.5872	13.60	6.41	V_8C_7

4.2.5 Heat treated nominal $Ni_{10}:V_{80}:C_{10}$ (at.%), Sample 11H

SME-BSE images representative of the microstructure of nominal $Ni_{10}:V_{80}:C_{10}$ (at.%), Sample 11H, in heat treated condition are shown in Figures 4.218 and 4.219. The heat treated microstructure was very different from its as-cast structure, having a third phase (Figure 4.80). The alloy consisted of dark dendrites with more cracks than before, which may be due to brittleness or differences in the coefficient of thermal expansions of the phases, seen at higher magnification, with medium and light contrast phases. The eutectic appeared to have disappeared.

The phase compositions are shown in Table 4.57 and are plotted in Figure 4.220, showing the overall composition to lie within the tie-triangle of the phases. The position of the phases on the ternary plot (Figure 4.220) would suggest that the dark phase was VC, the light phase (V), and the medium phase was ~NiV_3. The position of the new phase, σ′, between the dark and the medium phases suggest that there was a separation of the as-cast (V) to (V) + σ′. The EDX analyses of heat treated Sample 11H are shown in Appendix B28.

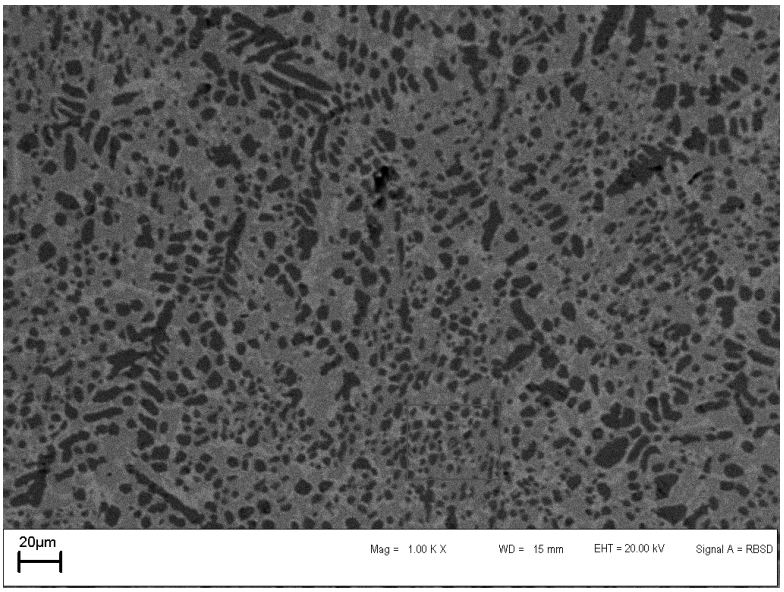


Figure 4.218. BSE-SEM image of heat treated Ni_{10}:V_{80}:C_{10} (at.%), Sample 11H, showing ~VC dendrites (dark), (V) matrix (medium) and σ′ (light) at low magnification.

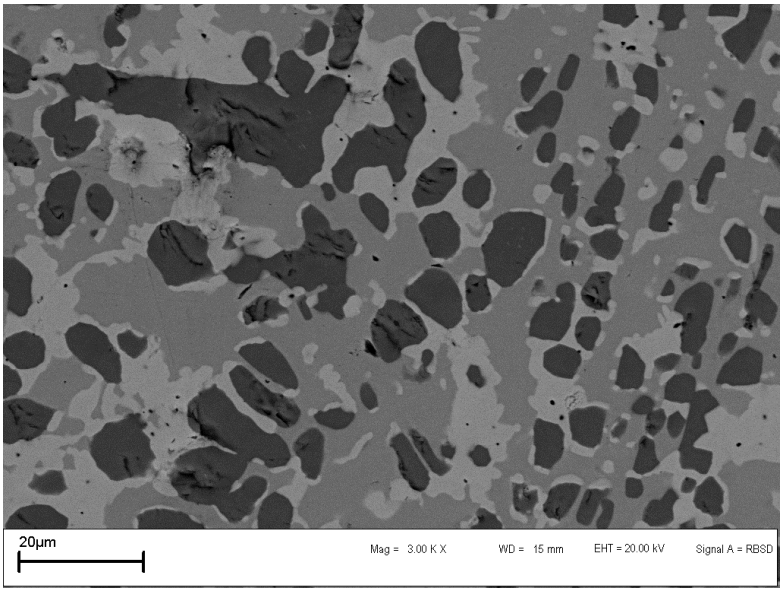


Figure 4.219. BSE-SEM image of heat treated $Ni_{10}:V_{80}:C_{10}$ (at.%), Sample 11H, showing ~VC dendrites (dark), (V) matrix (medium) and σ′ (light) at higher magnification.

Table 4.56. EDX phase analyses of annealed nominal $Ni_{10}:V_{80}:C_{11}$ (at.%), Sample 11H.

Phase Description	C	V	Ni	Phase
Overall	22.8 ± 0.4	69.0 ± 0.5	8.2 ± 0.2	-
Dark	36.9 ± 0.3	61.9 ± 0.3	1.2 ± 0.2	~VC
Light	10.4 ±0.4	67.4 ± 0.6	22.2 ± 0.6	σ′
Medium	9.9 ± 0.4	77.4 ± 0.7	12.7 ±0.4	(V)

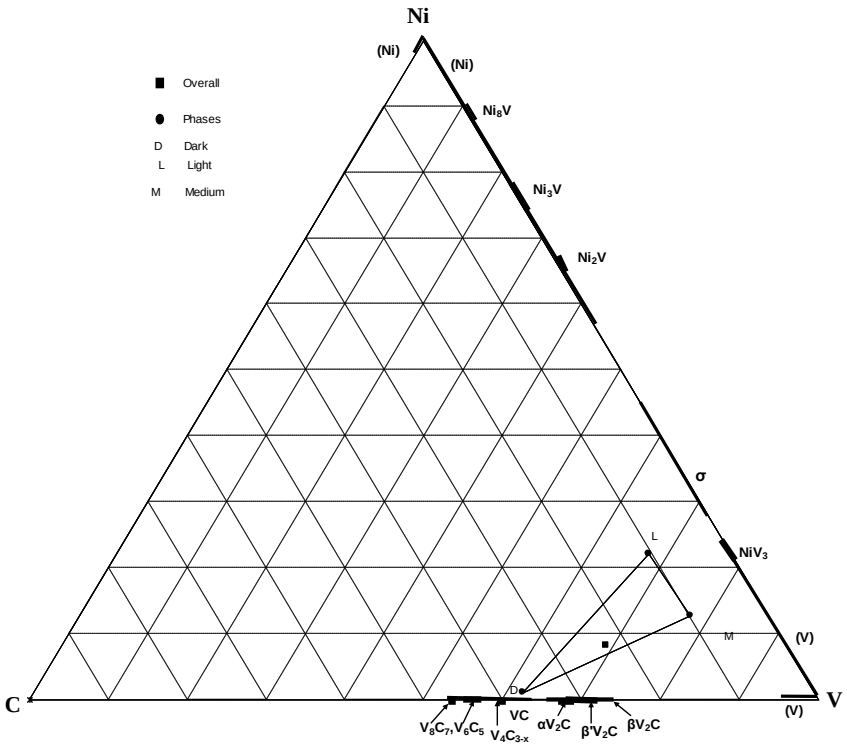


Figure 4.220. EDX analyses of heat treated nominal Ni_{10}:V_{80}:C_{10} (at.%), Sample 11H.

The XRD pattern shown in Figures 4.221 to 4.225 was fair, with a reasonable signal:background ratio, but not without noise and several sharp peaks. The presence of ~VC, ~NiV_3 and (V) were indicated as shown in Figure 4.225, with some unidentified peaks. However, the match with ~Ni_3V was poor, and the unidentified peaks were similar in angle and number to those of σ′, so the light phase was identified as σ′. A major peak was found at about $2\theta = 49.74^{o}$, which matched (V). Table 4.58 shows the identified peaks together with their phases.

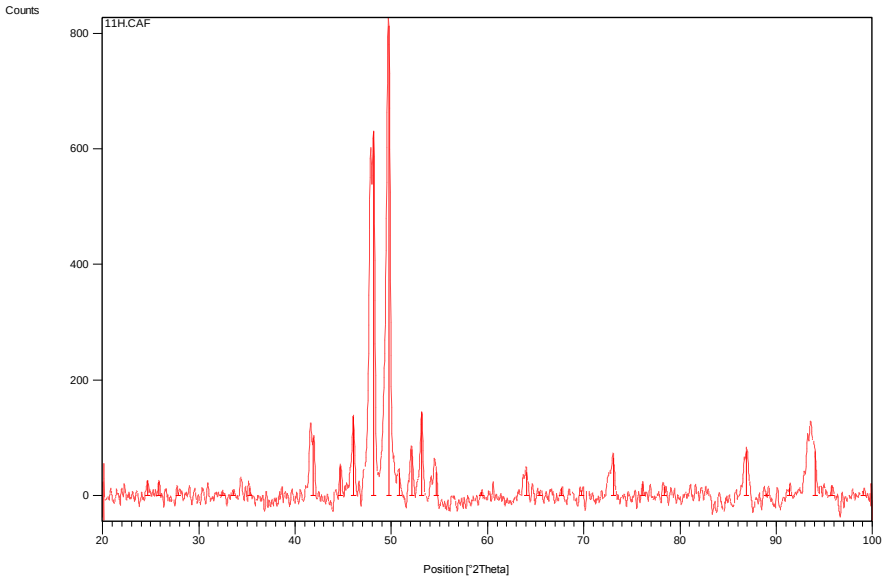


Figure 4.221. Unlabelled XRD pattern of heat treated nominal Ni_{10}:V_{80}:C_{10} (at.%), Sample 11H.

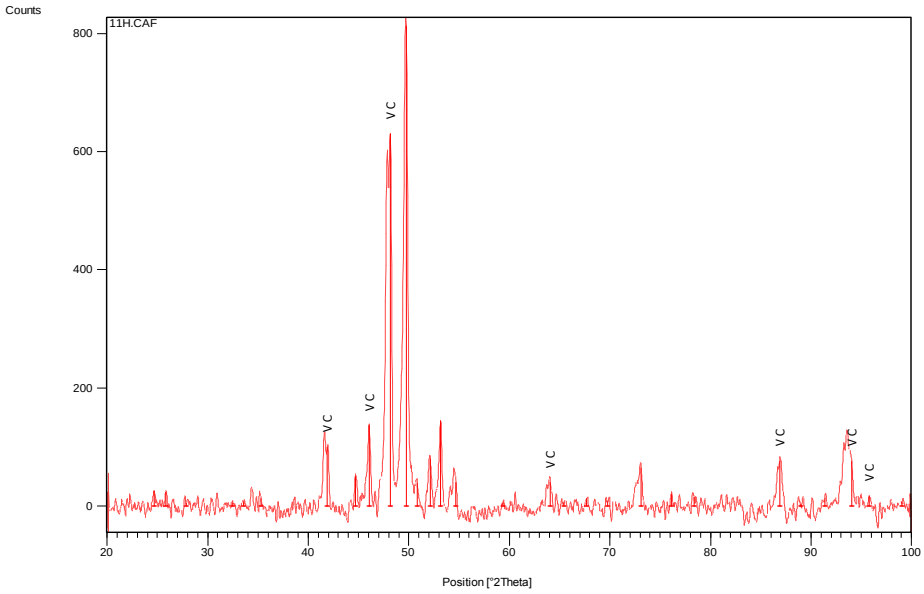


Figure 4.222. XRD pattern of heat treated nominal Ni_{10}:V_{80}:C_{10} (at.%), Sample 11H, showing identified ~VC peaks.

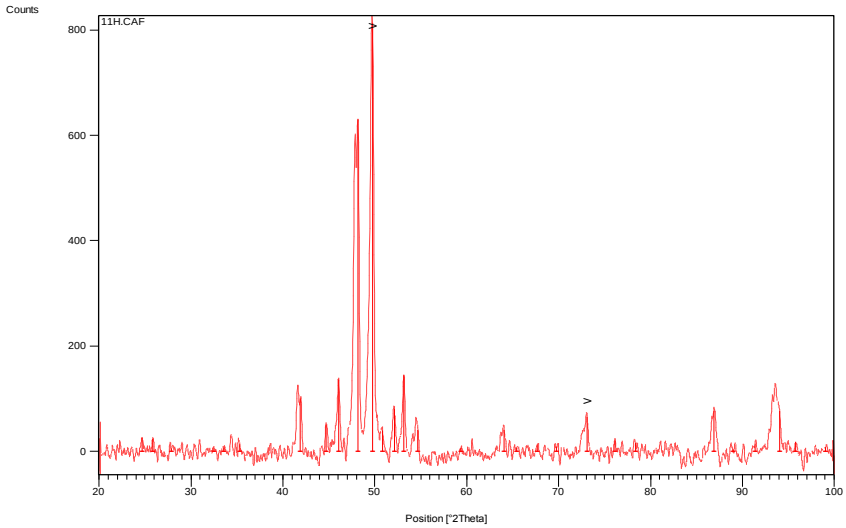


Figure 4.223. XRD pattern of heat treated nominal Ni_{10}:V_{80}:C_{10} (at.%), Sample 11H, showing identified (V) peaks.

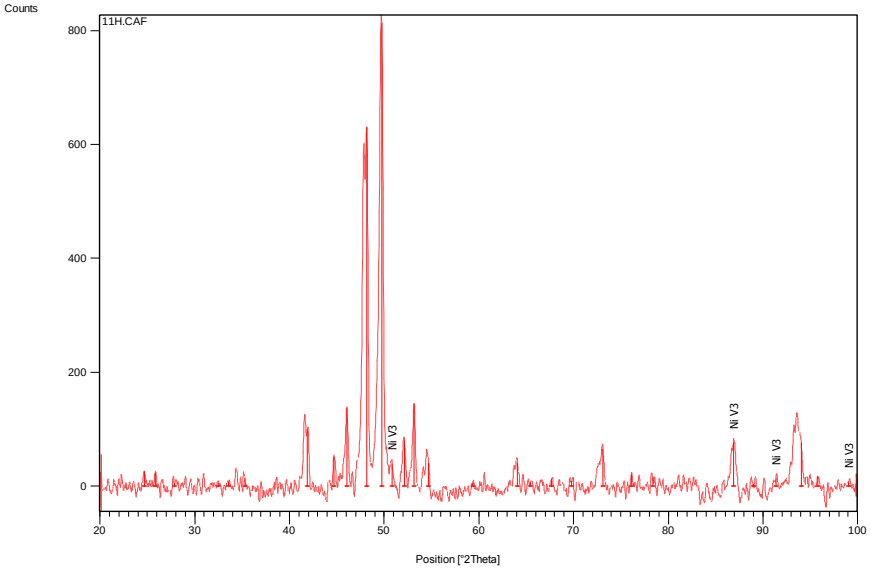


Figure 4.224. XRD pattern of heat treated nominal Ni_{10}:V_{80}:C_{10} (at.%), Sample 11H, showing identified ~NiV_3 peaks.

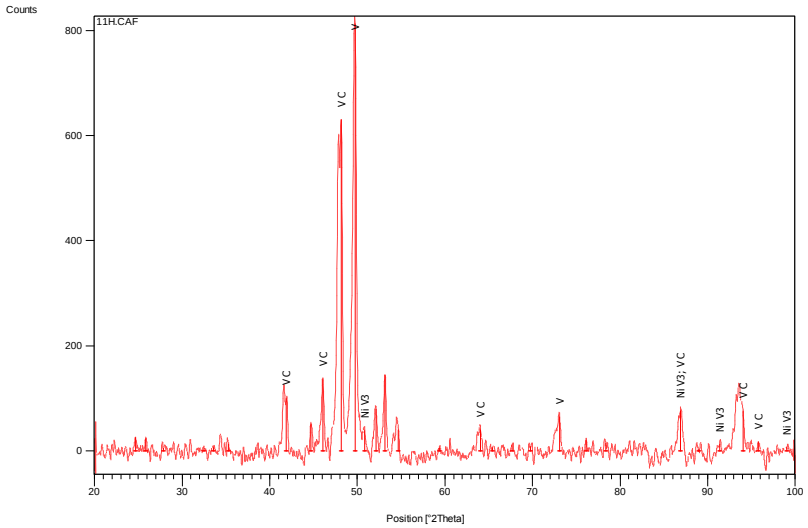


Figure 4.225. XRD pattern of heat treated nominal $Ni_{10}:V_{80}:C_{10}$ (at.%), Sample 11H, showing all the identified peaks.

Table 4.57. XRD peaks for heat treated nominal $Ni_{10}:V_{80}:C_{10}$ (at.%), Sample 11H.

Position 2θ (º)	Height (counts)	Relative Intensity (%)	Phases
33.5594	6.56	0.81	Presumed σ′
35.2787	13.57	1.67	Presumed σ′
41.9150	100.34	12.33	VC
44.6700	50.34	6.19	Presumed σ′
46.0688	136.45	16.77	VC
48.1493	630.43	77.48	VC
49.7419	813.68	100.00	V
50.8308	39.13	4.81	NiV_3
52.1066	79.98	9.83	Presumed σ′
53.1759	144.18	17.72	Presumed σ′
54.6955	40.83	5.02	Presumed σ′
64.0714	40.30	4.95	VC
69.7797	8.36	1.03	Presumed σ′
73.0883	64.96	7.98	V
76.1225	20.44	2.51	Presumed σ′
78.3463	15.28	1.88	Presumed σ′
86.8943	76.56	9.41	VC, NiV_3
91.3506	13.05	1.60	NiV_3
94.0179	76.72	9.43	VC
95.7810	17.20	2.11	VC
99.0720	7.73	0.95	NiV_3

4.2.6 Heat treated nominal $Ni_5:V_{75}:C_{20}$ (at.%), Sample 12H

The microstructure of nominal $Ni_5:V_{75}:C_{20}$ (at.%), Sample 12H in the annealed condition is shown in Figures 4.226 and 4.227. The bulk of the alloy sample (Figure 4.227) was fairly different from that of the as-cast condition (Figures 4.89 to 4.90). The heat treated alloy showed three different contrasts: dark, medium and a region near the dendrites (top left), which had a very light contrast, which might have been the locally occurring peritectically-formed phase. The eutectic of the as-cast condition had disappeared during annealing. There was also some porosity, as in the as-cast sample.

Table 4.59 gives the phase analyses for the alloy, also shown in Figure 4.228. The EDX analyses showed that there was hardly any composition difference between the medium and the light phases of the heat treated Sample 12H, but perhaps the latter were too small to analyse accurately or too thin (so that more X-rays came from the underlying (V)). Although the differences between the analyses of the light and medium phases were very small, they did support its identity to be σ′, because Ni was higher and V lower than the medium contrast phase. Also, the position of the phases on the ternary plot (Figure 4.228) suggested that the dark phase was VC and the light phase was (V). Appendix B29 shows the EDX analyses.

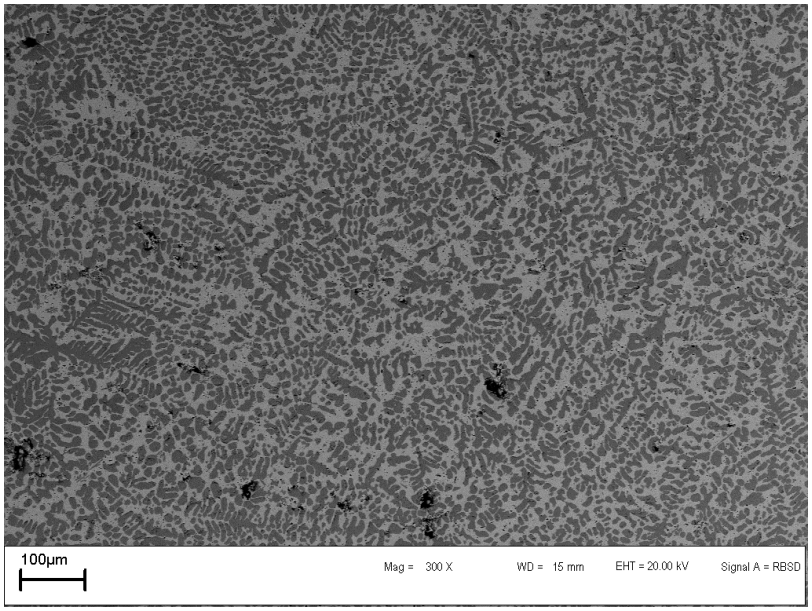


Figure 4.226. BSE-SEM image of heat treated $Ni_5:V_{75}:C_{20}$ (at.%), Sample 12H, showing ~VC dendrites (dark) and (V) matrix (medium).

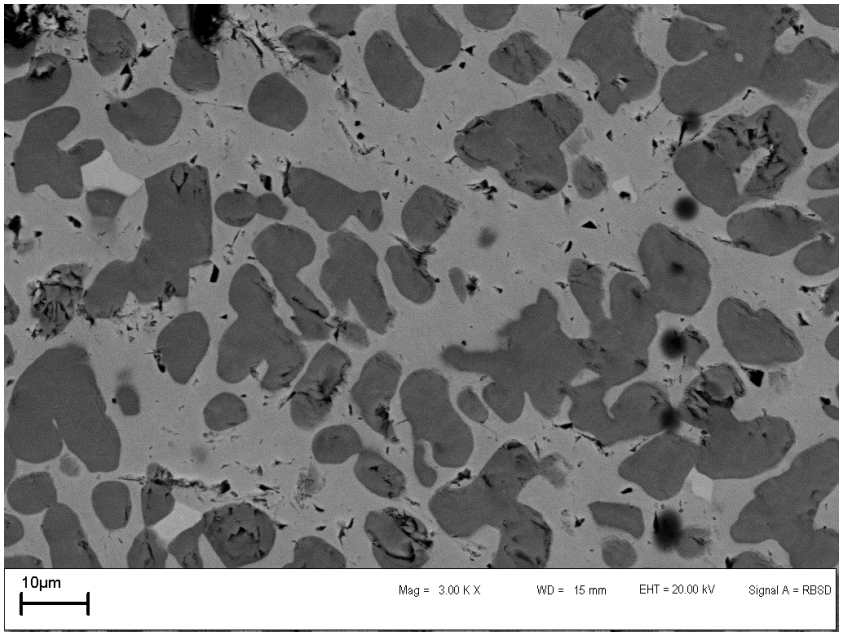


Figure 4.227. BSE-SEM image of heat treated Ni_5:V_{75}:C_{20} (at.%), Sample 12H, showing ~VC dendrites (dark) and (V) matrix (medium).

Table 4.58. EDX phase analyses of annealed nominal Ni_5:V_{75}:C_{20} (at.%), Sample 12H.

Phase Description	C	V	Ni	Phase
Overall	29.9 ± 0.4	66.8 ± 0.4	3.8 ± 0.1	-
Dark	38.0 ± 0.3	62.0 ± 0.3	0	~VC
Light	9.1 ± 0.5	80.1 ± 0.4	10.8 ± 0.3	Probably σ′
Medium	8.8 ± 0.5	81.2 ± 0.4	9.9 ± 0.1	(V)

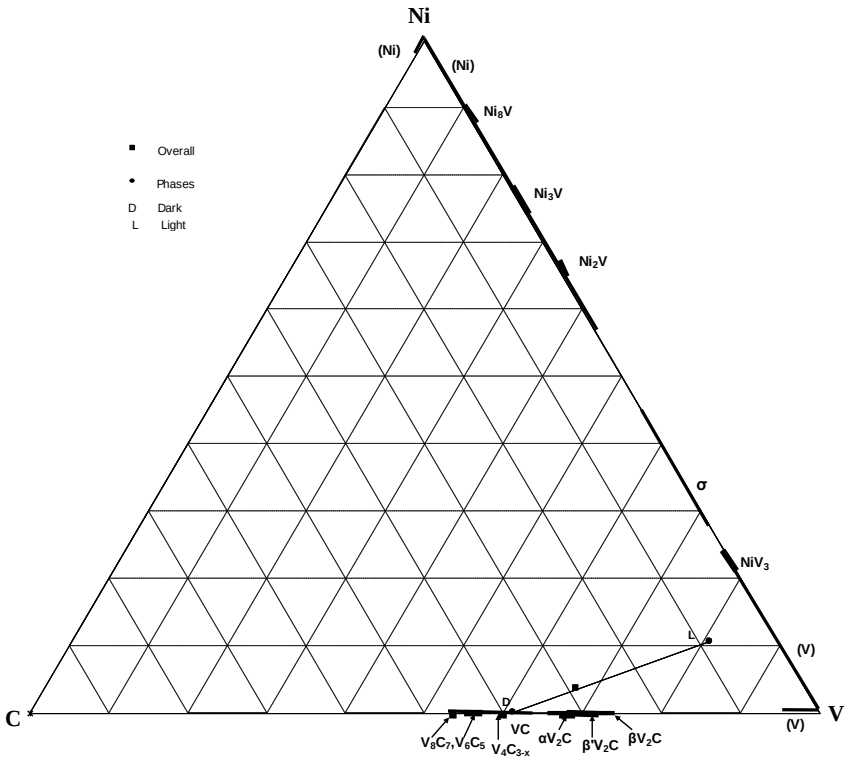


Figure 4.228. EDX analyses of heat treated nominal Ni_5:V_{75}:C_{20} (at.%), Sample 12H.

X-ray diffraction analysis was performed to confirm the phases in heat treated Sample 12H. Figures 4.229 to 4.233 show the experimental pattern of the sample with the database lines for each of the phases. The highest intensity peak was common for ~VC, ~$V_4C_{2.66}$ and (V) at about $2\theta = 93.83^{o}$ (Figure 4.233). Unidentified peaks were also seen. The identified peaks together with their phases are shown Table 4.60. The pattern was different from the as-cast, with some peaks the same, but with different intensities.

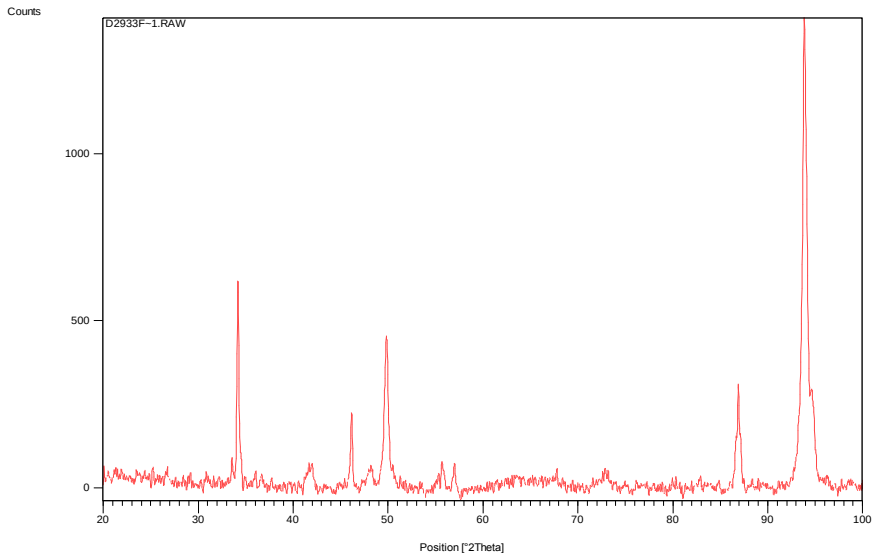


Figure 4.229. Raw XRD pattern of heat treated nominal Ni_5:V_{75}:C_{20} (at.%), Sample 12H.

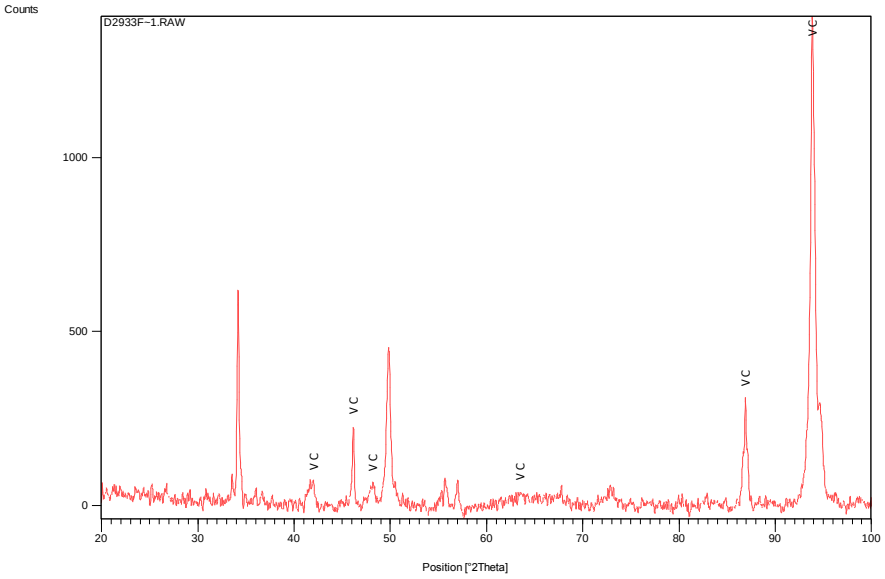


Figure 4.230. XRD pattern of heat treated nominal Ni_5:V_{75}:C_{20} (at.%), Sample 12H, showing identified ~VC peaks.

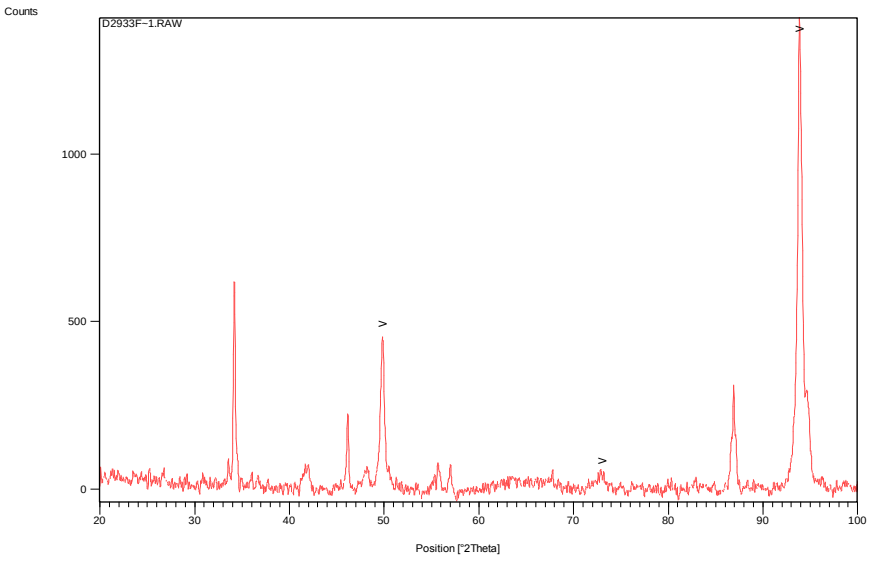


Figure 4.231. XRD pattern of heat treated nominal Ni_5:V_{75}:C_{20} (at.%), Sample 12H, showing identified (V) peaks.

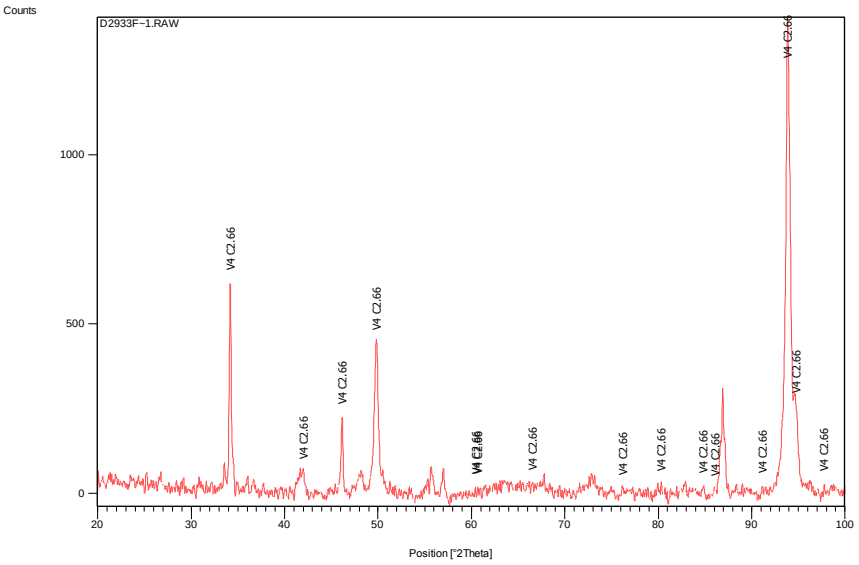


Figure 4.232. XRD pattern of heat treated nominal Ni_5:V_{75}:C_{20} (at.%), Sample 12H, showing identified ~$V_4C_{2.66}$ peaks.

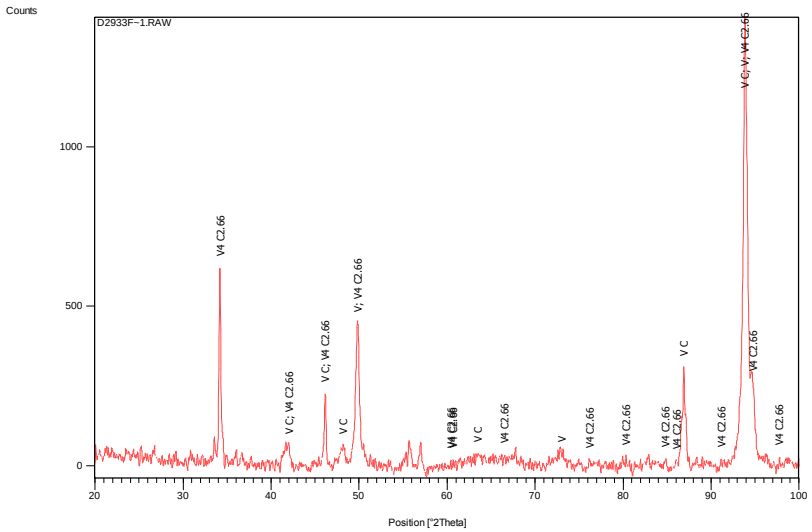


Figure 4.233. XRD pattern of heat treated nominal Ni_5:V_{75}:C_{20} (at.%), Sample 12H, showing all the identified peaks.

Table 4.59. XRD peaks for heat treated nominal Ni_5:V_{75}:C_{20} (at.%), Sample 12H.

Position 2θ (º)	Height (counts)	Relative Intensity (%)	Phases
20.9275	30.94	2.22	Possibly σ′
26.6896	48.41	3.47	Possibly σ′
29.2194	40.56	2.91	Possibly σ′
34.1863	618.24	44.36	$V_4C_{2.66}$
36.6567	32.67	2.34	Possibly σ′
38.9967	12.96	0.93	Possibly σ′
42.0397	60.65	4.35	$V_4C_{2.66}$, VC
46.1691	222.27	15.95	$V_4C_{2.66}$, VC
48.1879	59.16	4.24	VC
49.8613	442.75	31.77	$V_4C_{2.66}$,V
55.6675	73.34	5.26	Possibly σ′
56.9477	54.07	3.88	Possibly σ′
60.4323	17.92	1.29	$V_4C_{2.66}$
60.6785	16.85	1.21	$V_4C_{2.66}$
60.9413	15.66	1.12	$V_4C_{2.66}$
63.5074	33.57	2.41	VC
66.5142	31.03	2.23	$V_4C_{2.66}$
73.0084	35.28	2.53	V
76.1751	16.06	1.15	$V_4C_{2.66}$
84.8284	19.84	1.42	$V_4C_{2.66}$

Table 4.60 (cont.). XRD peaks for heat treated nominal $Ni_5:V_{75}:C_{20}$ (at.%), Sample 12H.

86.0751	12.56	0.90	$V_4C_{2.66}$
86.9086	300.76	21.58	VC
91.1844	18.98	1.36	$V_4C_{2.66}$
93.8361	1393.77	100.00	$V_4C_{2.66}$, VC, V
94.7759	256.48	18.40	$V_4C_{2.66}$
97.7715	26.49	1.90	$V_4C_{2.66}$

4.2.7 Heat treated nominal $Ni_{14}:V_{64}:C_{22}$ (at.%), Sample 13H

The microstructure of nominal $Ni_{14}:V_{64}:C_{22}$ (at.%), Sample 13H, in the annealed condition (Figures 4.234 and 4.235) was very different from its as-cast structure (Figures 4.97 and 4.98). The heat treated microstructure showed three contrasts, dark which was identified as ~VC, medium contrast, identified as σ′ with reference to the position of ternary plot (Figure 4.236), and a light phase which was identified as ~Ni_2V. The eutectic mixture in as-cast condition had disappeared during annealing, and also the ~VC needles had coarsened to become more globular.

Table 4.62 gives the phase analyses for the alloy, shown in Figure 4.236. The overall was not the same as the as-cast alloy ($Ni_{23.9}:V_{50.3}:C_{25.8}$ compared to $Ni_{22.1}:V_{47.8}:C_{30.1}$ (at.%) (as-cast)), which shows a loss of carbon. The ~VC had not changed composition significantly, and (Ni) had lost both C and V and gained Ni to become ~Ni_2V. The σ′ phase was identified. Thus, the nickel-rich phase has more nickel, and a new phase σ′ formed. The EDX analyses of heat treated Samples 13 are also shown in Appendix B30.

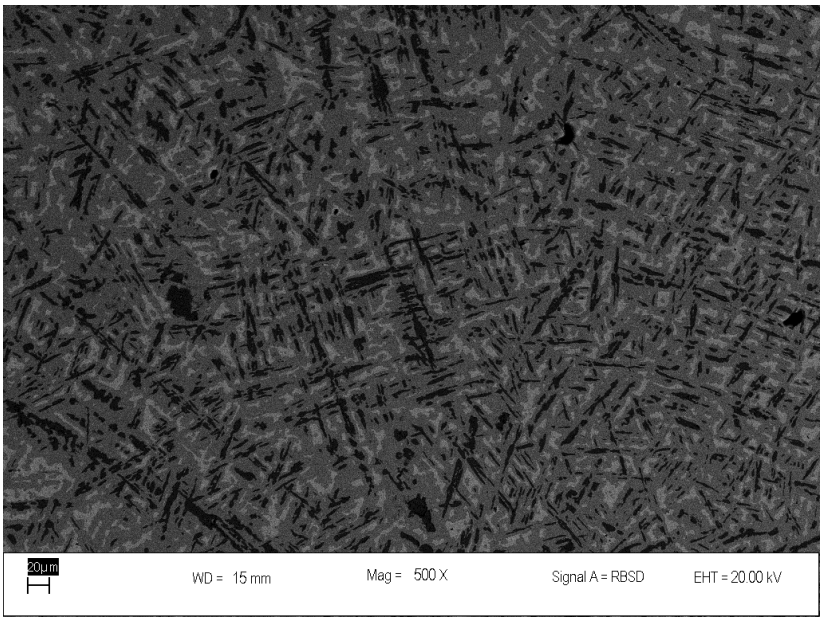


Figure 4.234. BSE-SEM image of heat treated nominal $Ni_{14}:V_{64}:C_{22}$ (at.%), Sample 13H, showing ~VC dendrites (dark), ~Ni_2V (light) and σ′ (medium).

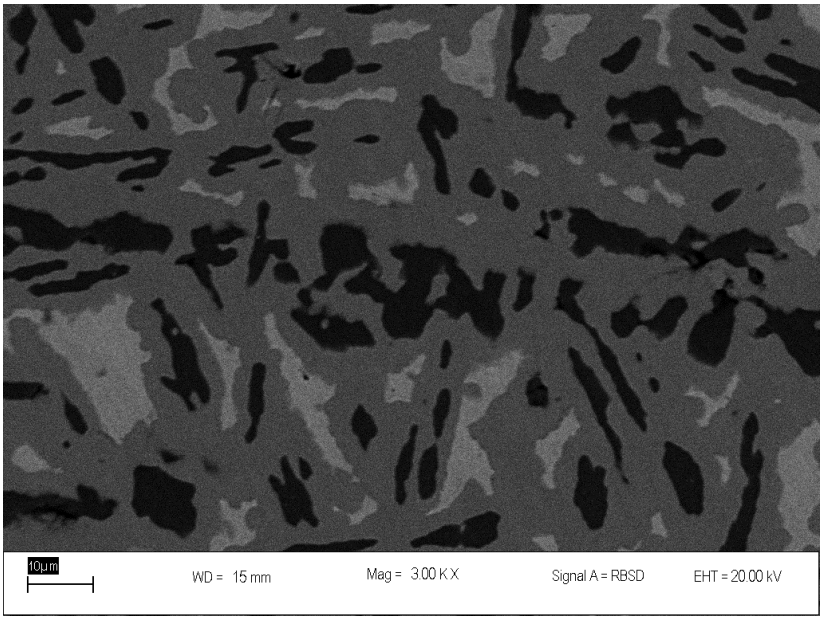


Figure 4.235. BSE-SEM image of heat treated nominal $Ni_{14}:V_{64}:C_{22}$ (at.%), Sample 13H, showing ~VC dendrites (dark), ~Ni_2V (light) and σ′ (medium).

Table 4.61. EDX phase analyses of annealed nominal $Ni_{14}:V_{64}:C_{22}$ (at.%), Sample 13H.

Phase Description	C	V	Ni	Phase
Overall	25.8 ± 0.7	50.3 ± 0.4	23.9 ± 0.4	-
Dark	37.4 ± 0.6	62.2 ± 0.7	0.4 ± 0.1	~VC
Light	14.7 ± 0.4	32.3 ± 0.4	53.0 ± 0.5	~Ni_2V
Medium	22.6 ± 0.5	51.9 ± 0.6	25.5 ± 0.4	σ′

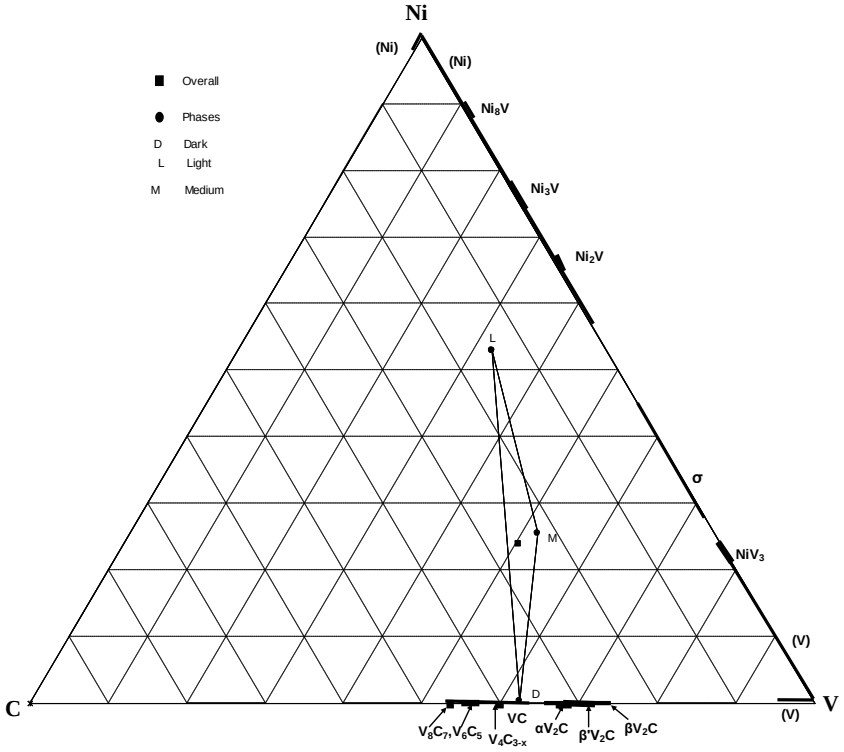


Figure 4.236. EDX analyses of heat treated nominal $Ni_{14}:V_{64}:C_{22}$ (at.%), Sample 13H.

Figures 4.237 to 4.240 show the XRD pattern for heat treated Sample 13. XRD analyses detected two phases (Figure 4.240), ~VC and ~Ni_2V, together with unidentified peaks, assumed to be σ. The pattern was very different from the as-cast pattern because the σ′ phase

had been formed on annealing. Table 4.63 shows the identified peaks together with their phases.

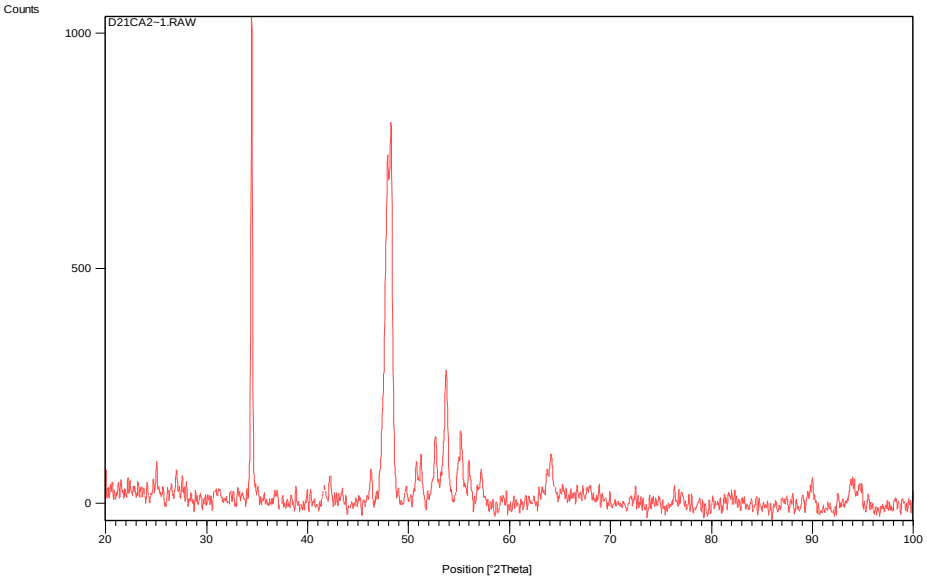


Figure 4.237. Unlabelled XRD pattern of heat treated nominal $Ni_{14}:V_{64}:C_{22}$ (at.%), Sample 13H.

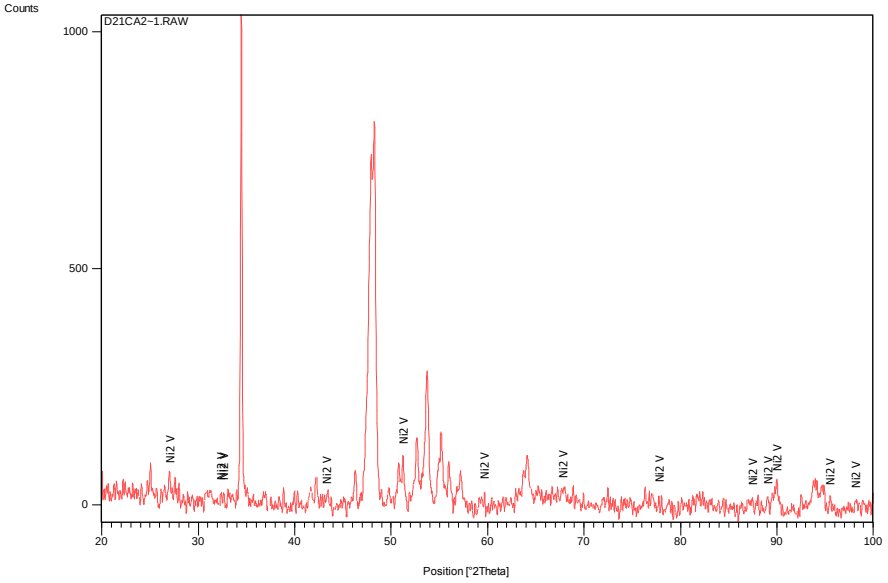


Figure 4.238. XRD pattern of heat treated nominal $Ni_{14}:V_{64}:C_{22}$ (at.%), Sample 13H, showing identified ~Ni_2V peaks.

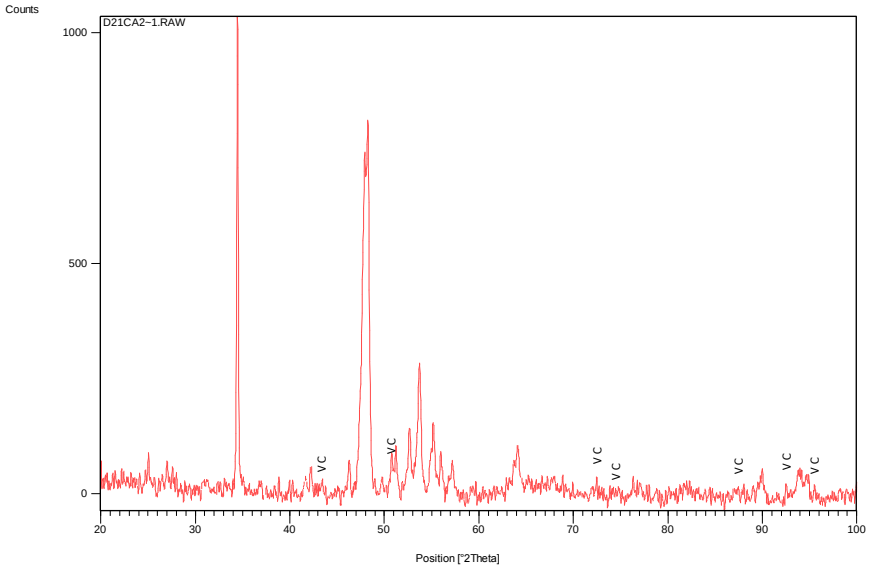


Figure 4.239. XRD pattern of heat treated nominal $Ni_{14}:V_{64}:C_{22}$ (at.%), Sample 13H, showing identified ~VC peaks.

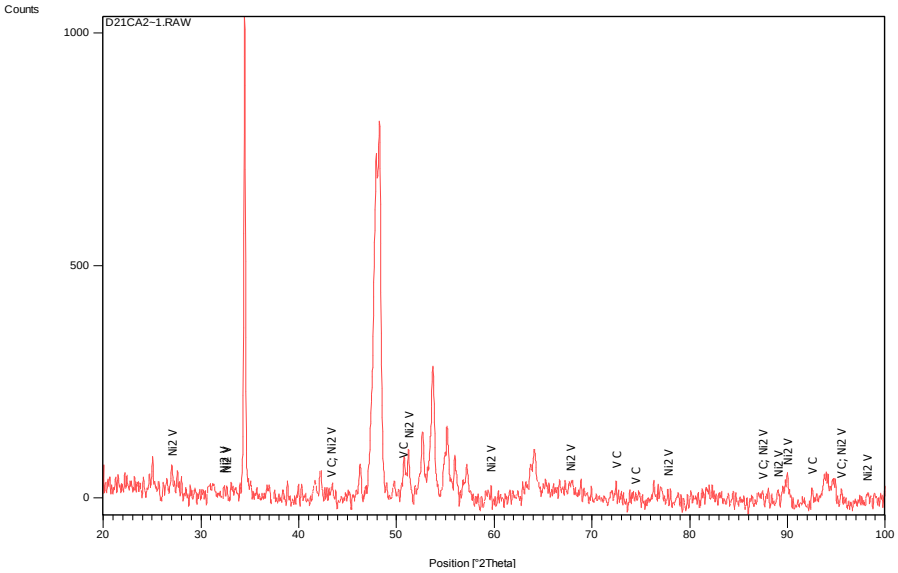


Figure 4.240. XRD pattern of heat treated nominal $Ni_{14}:V_{64}:C_{22}$ (at.%), Sample 13H, showing all the identified peaks.

Table 4.62. XRD peaks for heat treated nominal $Ni_{14}:V_{64}:C_{22}$ (at.%), Sample 13H.

Position 2θ (º)	Height (counts)	Relative Intensity (%)	Phases
25.6893	37.45	3.61	Presumed σ′
27.0435	61.89	5.96	Ni_2V
32.3205	25.41	2.45	Ni_2V
32.6568	25.96	2.50	Ni_2V
34.4576	1038.39	100.00	Presumed σ′
40.2886	27.32	2.63	Presumed σ′
42.2133	57.47	5.53	Presumed σ′
43.3235	17.40	1.68	Ni_2V, VC
47.9009	726.92	70.00	Presumed σ′
48.3344	721.68	69.50	Presumed σ′
50.7028	55.99	5.39	VC
51.2453	100.82	9.71	Ni_2V
51.8923	25.13	2.42	Presumed σ′
52.6133	135.25	13.02	Presumed σ′
53.7151	283.23	27.28	Presumed σ′
55.2120	148.70	14.32	Presumed σ′
57.2105	68.56	6.60	Presumed σ′
59.6798	26.58	2.56	Ni_2V
64.1309	99.38	9.57	Presumed σ′
67.8482	29.86	2.88	Ni_2V
72.4912	34.45	3.32	VC
74.4702	0.94	0.09	VC
77.7687	19.18	1.85	Ni_2V
87.4611	13.42	1.29	Ni_2V, VC
89.0481	16.70	1.61	Ni_2V
89.9864	44.04	4.24	Ni_2V
92.5272	22.21	2.14	VC
95.5172	14.87	1.43	Ni_2V, VC
98.1804	6.65	0.64	VC

4.2.8 Heat treated nominal $Ni_{28}:V_{54}:C_{18}$ (at.%), Sample 14H

As was the case for nominal $Ni_{28}:V_{54}:C_{18}$ (at.%), Sample 14 in the as-cast condition (Figures 4.106 and 4.107), the annealed alloy also showed two different regions. The edge of the sample consisted of dendrites (dark) which were identified as ~VC, occasionally showing no arms, with a ~VC + σ′ (light) eutectic. The middle region also consisted of dark dendrites and light matrix (Figures 4.241 and 4.242). The dendrites had not changed discernibly, but the eutectic had coarsened.

The phase analyses are given in Table 4.64 and plotted in Figure 4.243. It can be seen that the overall analysis lies outside that of the phase analyses. This suggested that a more C-rich phase had been missed. There were small differences between the EDX analyses of as-cast and the heat treated sample (Tables 4.29 and 4.64) for ~VC, and after heat treatment, σ′ had gaining C and V, but lost Ni. The eutectic had changed slightly; losing C and gained V. Appendix B31 shows the EDX analyses of heat treated Sample 14.

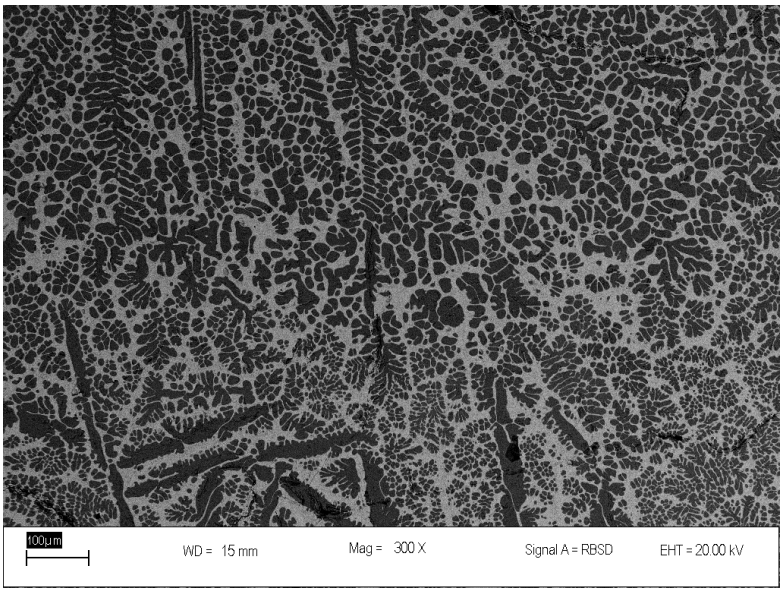


Figure 4.241. BSE-SEM image of heat treated nominal Ni_{28}:V_{54}:C_{18} (at.%), Sample 14H, showing ~VC dendrites (dark) and σ′ matrix (light) at low magnification.

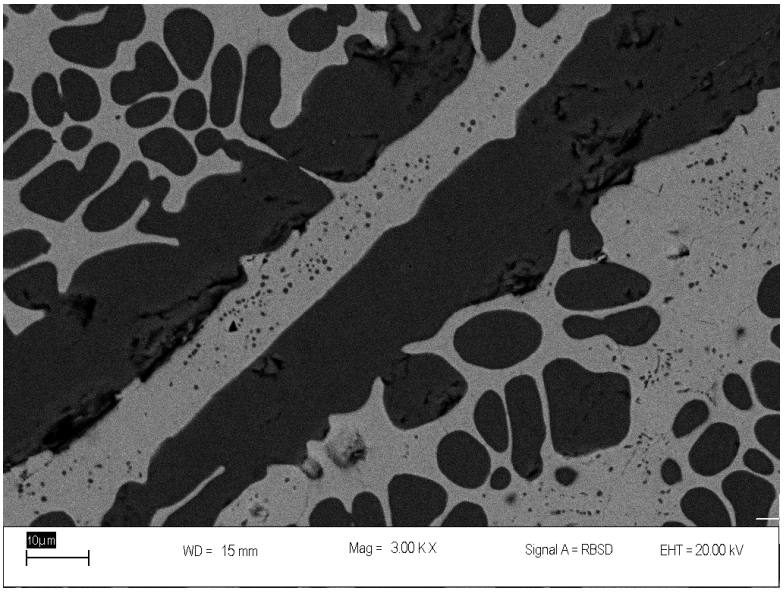


Figure 4.242. BSE-SEM image of heat treated nominal $Ni_{28}:V_{54}:C_{18}$ (at.%), Sample 14H, showing ~VC dendrites (dark) and σ′ matrix (light) at low magnification.

Table 4.63. EDX phase analyses of annealed nominal $Ni_{28}:V_{54}:C_{18}$ (at.%), Sample 14H.

Phase Description	C	V	Ni	Phase
Overall	32.4 ± 0.6	57.3 ± 0.4	10.1 ± 0.4	-
Dark	37.8 ± 0.6	61.8 ± 0.4	0.4 ± 0.2	~VC
Light	15.1 ± 0.3	52.1 ± 0.3	32.8 ± 0.1	σ′
Eutectic	31.7 ± 0.6	57.4 ± 0.3	10.9 ± 0.8	~VC + σ′

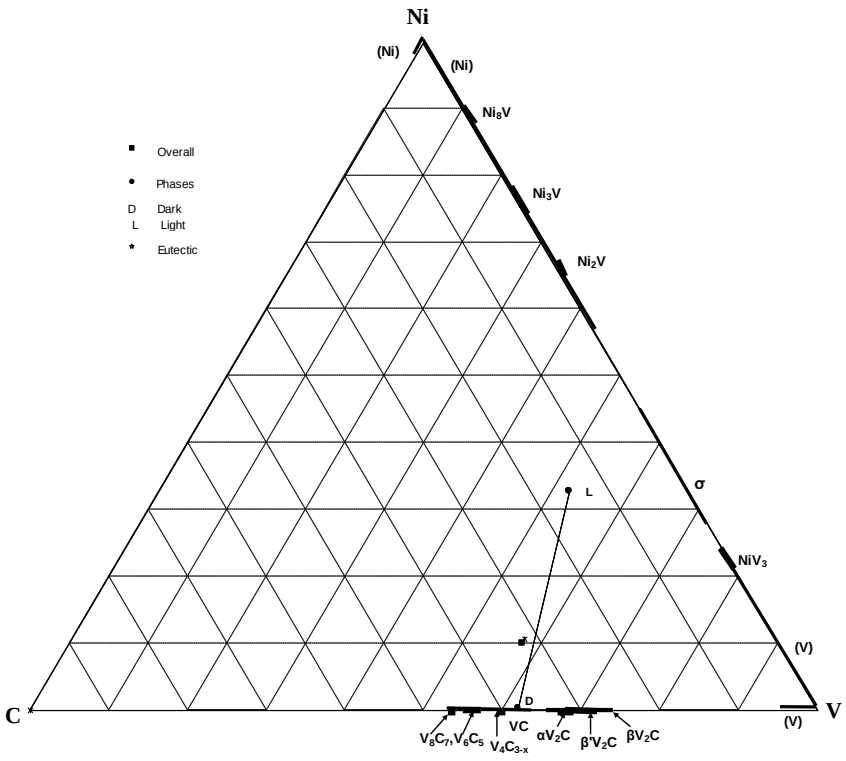


Figure 4.243. EDX analyses of heat treated nominal Ni_{28}:V_{54}:C_{18} (at.%), Sample 14H.

As in the as-cast condition (Figure 4.110), the presence of ~VC and ~$V_4C_{2.66}$ was identified by the XRD pattern as shown in Figures 4.244 to 4.247. Also there were several unidentified peaks shown in Figure 4.247; these were deduced to be σ′, which had the highest intensity peaks at about $2\theta = 50.26^{o}$. After heat treatment, the pattern was very different from the as-cast pattern. As a check the Ni, V_8C_7 and V_6C_5 peaks could not be matched. Table 4.65 shows the identified peaks together with their phases.

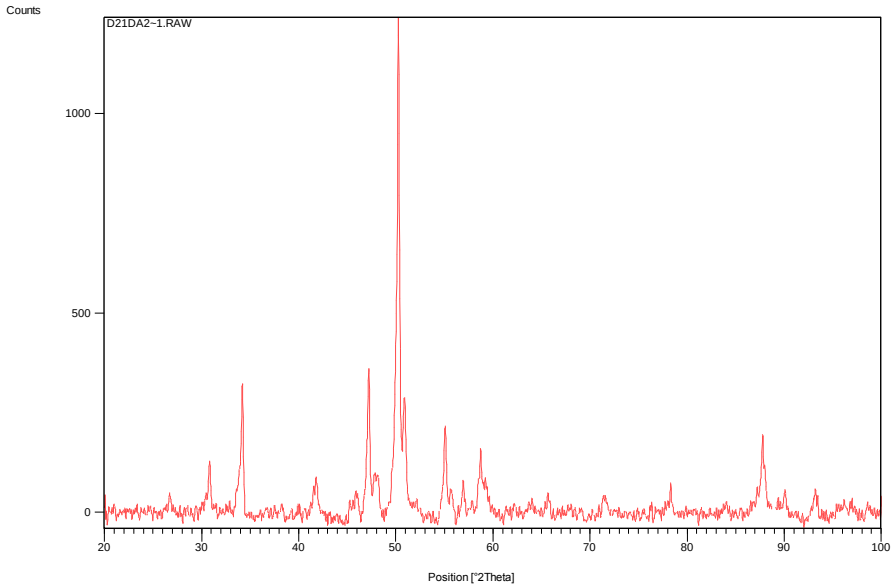


Figure 4.244. Unlabelled XRD pattern of heat treated nominal Ni_{28}:V_{54}:C_{18} (at.%), Sample 14H.

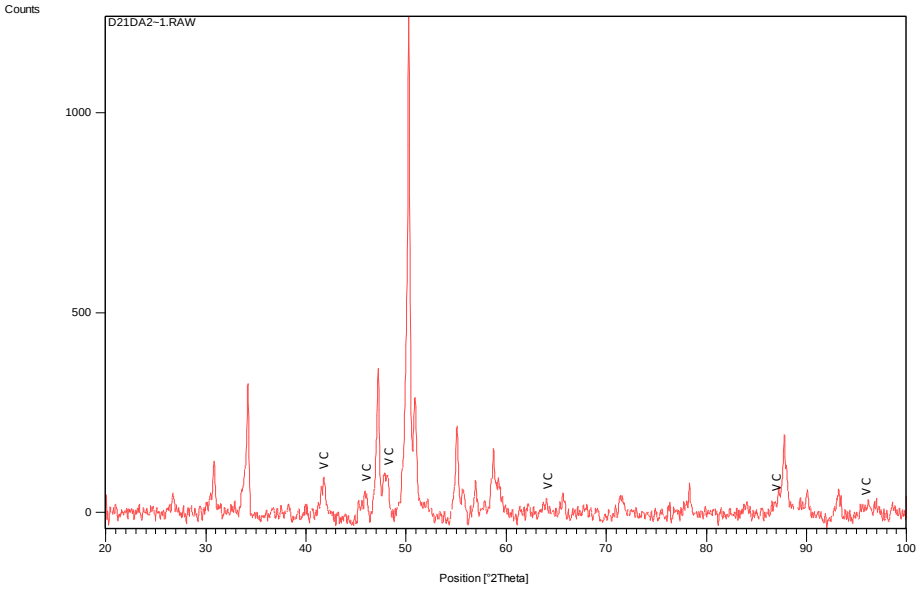


Figure 4.245. XRD pattern of heat treated nominal Ni_{28}:V_{54}:C_{18} (at.%), Sample 14H, showing identified ~VC peaks.

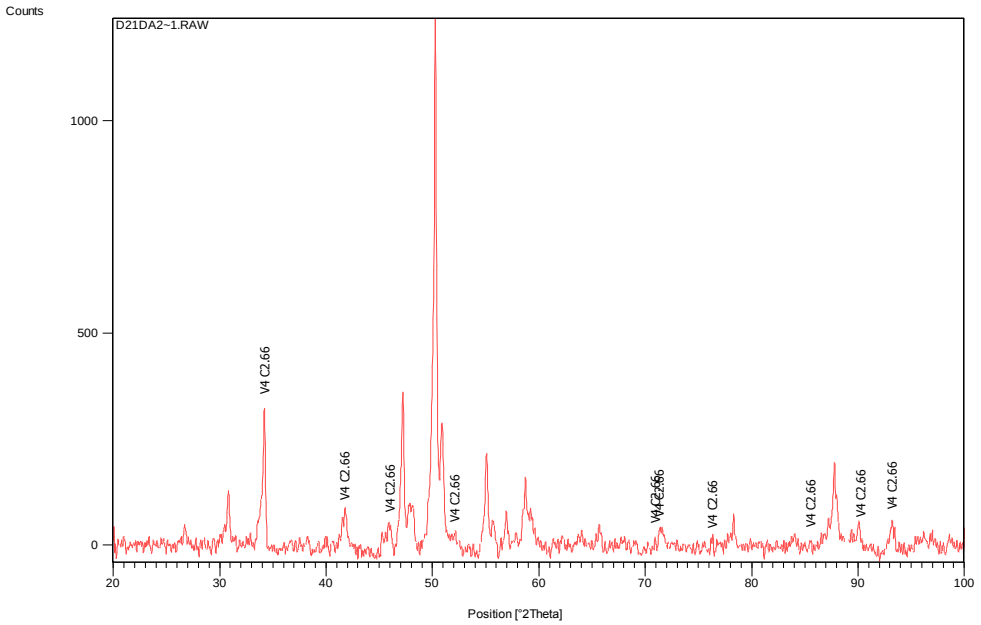


Figure 4.246. XRD pattern of heat treated nominal $Ni_{28}:V_{54}:C_{18}$ (at.%), Sample 14H, showing identified ~$V_4C_{2.66}$ peaks.

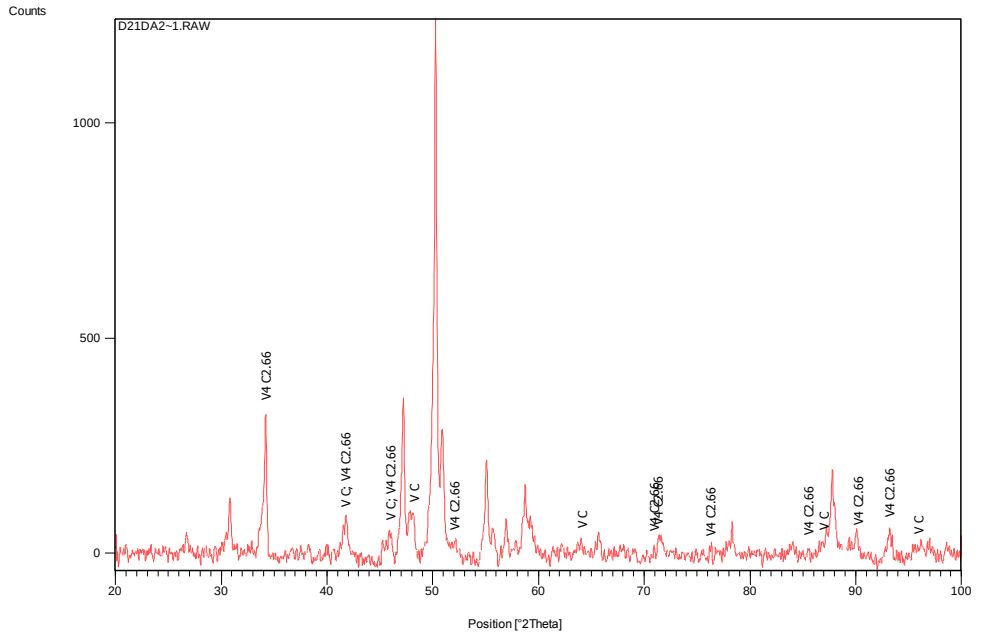


Figure 4.247. XRD pattern of heat treated nominal $Ni_{28}:V_{54}:C_{18}$ (at.%), Sample 14H, showing all the identified peaks.

Table 4.64. XRD peaks for heat treated nominal $Ni_{28}:V_{54}:C_{18}$ (at.%), Sample 14H.

Position 2θ (º)	Height (counts)	Relative Intensity (%)	Phases
26.6783	45.27	3.65	Presumed σ′
31.8853	11.51	0.93	Presumed σ′
34.1967	322.49	25.97	$V_4C_{2.66}$
41.7488	74.16	5.97	$V_4C_{2.66}$, VC
46.0034	44.58	3.59	$V_4C_{2.66}$, VC
47.2194	359.91	28.99	Presumed σ′
48.2098	83.82	6.75	VC
50.2607	1241.61	100.00	Presumed σ′
50.9530	272.24	21.93	Presumed σ′
52.0479	21.09	1.70	$V_4C_{2.66}$
55.6778	58.86	4.74	Presumed σ′
56.9227	73.43	5.91	Presumed σ′
58.7427	156.28	12.59	Presumed σ′
64.1111	21.65	1.74	VC
67.8875	7.80	0.63	Presumed σ′
70.9302	18.92	1.52	$V_4C_{2.66}$
71.3219	32.21	2.59	$V_4C_{2.66}$
76.2863	7.71	0.62	$V_4C_{2.66}$
78.3045	71.30	5.74	Presumed σ′
85.5411	8.83	0.71	$V_4C_{2.66}$
87.0021	18.94	1.53	VC
87.8292	167.39	13.48	Presumed σ′
90.1955	32.89	2.65	$V_4C_{2.66}$
93.1885	50.80	4.09	$V_4C_{2.66}$
95.8998	8.94	0.72	VC

4.2.9 Heat treated nominal $Ni_{32}:V_{56}:C_{12}$ (at.%), Sample 15H

The microstructure of nominal $Ni_{32}:V_{56}:C_{12}$ (at.%), Sample 15H, in the heat treated condition (Figures 4.248 and 4.249), showed only two contrasts as was the case of as-cast condition (Figure 4.115). However, the light phase appeared to have same structure with perhaps small traces remaining of the coarsened eutectic. The phases were identified as ~VC dendrites (dark) which was retained at high temperature after quenching, unlike in as-cast condition, where the ~VC phase had transformed to ~V_8C_7 in the solid state. The light phase was identified as σ′.

Table 4.66 gives the EDX analyses, and these are plotted in Figure 4.250. The overall compositions were off the tie-line (by about ± 4 at.%) between the two phases, possibly as a result phases not being at equilibrium. It can be seen that the EDX analyses for the annealed sample were significantly different from the as-cast sample (Tables 4.31 and. 4.66). The carbide had lost nearly 10 at.% C and gained nearly 10 at.% V after the heat treatment. The EDX analyses of heat treated Sample 14 are shown in Appendix B32.

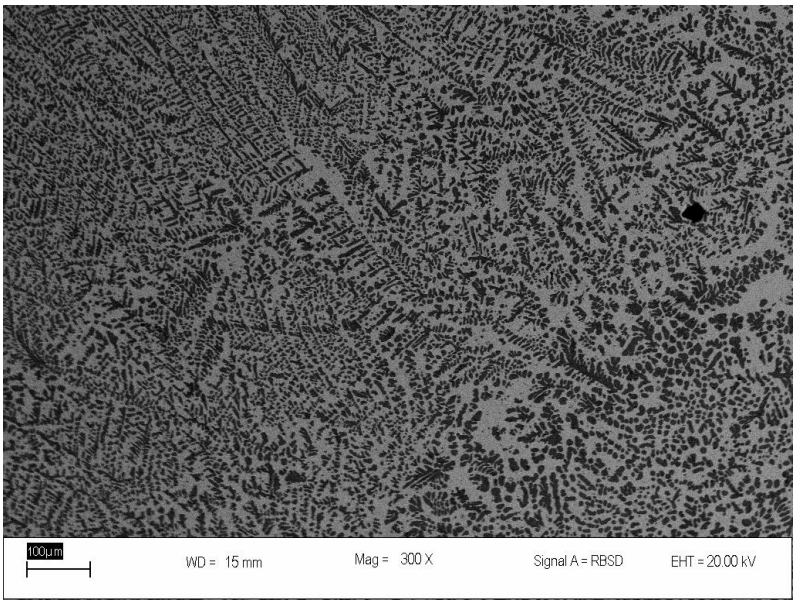


Figure 4.248. BSE-SEM image of heat treated nominal $Ni_{32}:V_{56}:C_{12}$ (at.%), Sample 15H, showing ~VC dendrites (dark) and σ′ matrix (light) at low magnification.

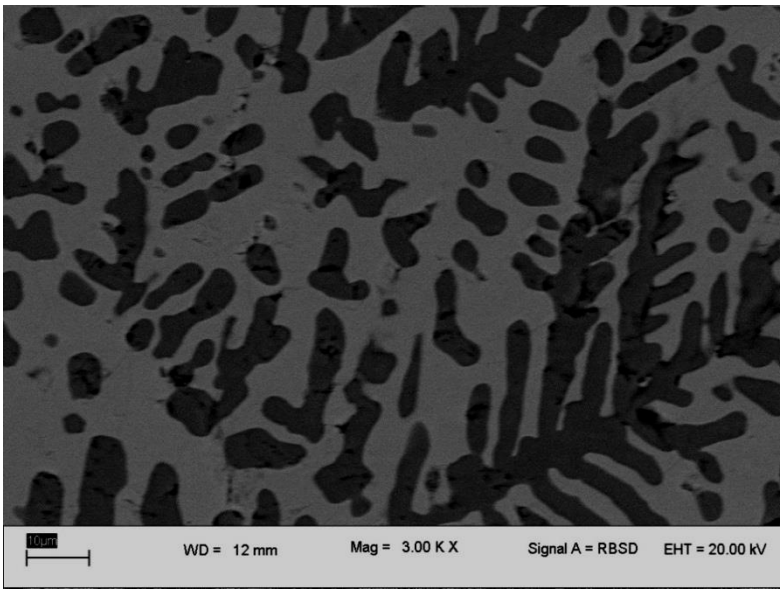


Figure 4.249. BSE-SEM image of heat treated nominal Ni_{32}:V_{56}:C_{12} (at.%), Sample 15H, showing ~VC dendrites (dark) with cracks and σ′ matrix (light) at higher magnification.

Table 4.65. EDX phase analyses of annealed nominal Ni_{32}:V_{56}:C_{12} (at.%), Sample 15H.

Phase Description	C	V	Ni	Phase
Overall	27.1 ± 0.2	55.9 ± 0.1	17.0 ± 0.1	-
Dark	36.6 ± 0.5	62.6 ± 1.1	0.8 ± 0.7	~VC
Light	11.6 ± 0.4	55.7 ± 0.3	32.7 ± 0.1	σ′

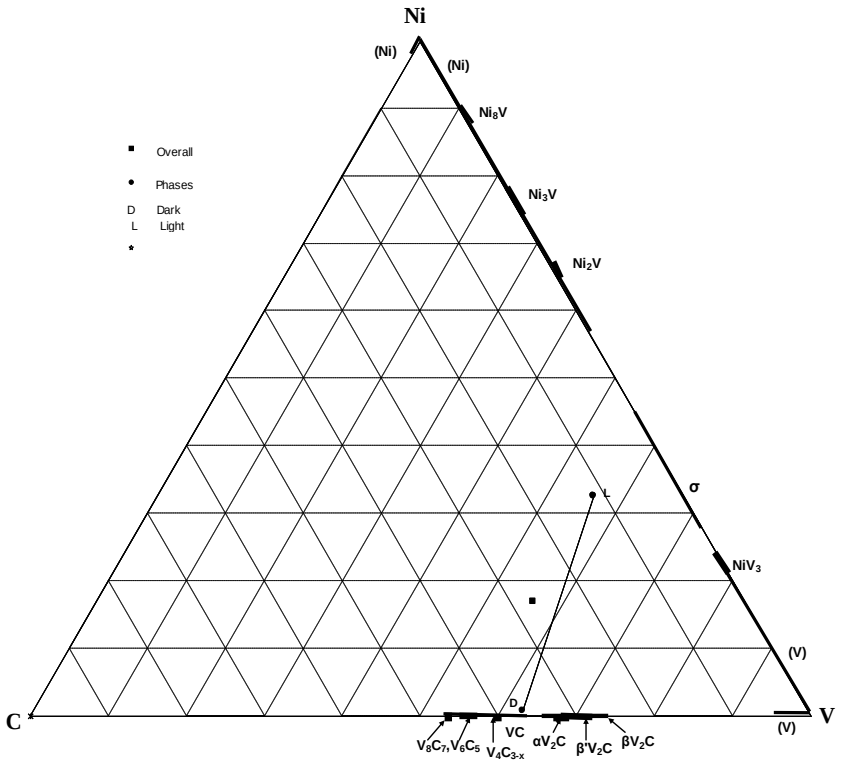


Figure 4.250. EDX analyses of heat treated nominal Ni_{32}:V_{56}:C_{12} (at.%), Sample 15H.

Figures 4.251 to 4.255 showed the XRD pattern of heat treated Sample 15. As was the case of the as-cast condition (Figure 4.119), a hump was also observed at $2\theta = 60$ to 70° (Figure 4.251), which may be due to the presence of an amorphous phase (possibly carbon). The pattern was very different from the as-cast specimen. The low number of peaks may be due to the cracks in the sample. The existence of ~VC, C and ~$V_4C_{2.66}$ was found. As in the as-cast sample (Figure 4.122), it was decided that the unidentified peaks were from σ′. Table 4.67 shows the identified peaks, together with their phases.

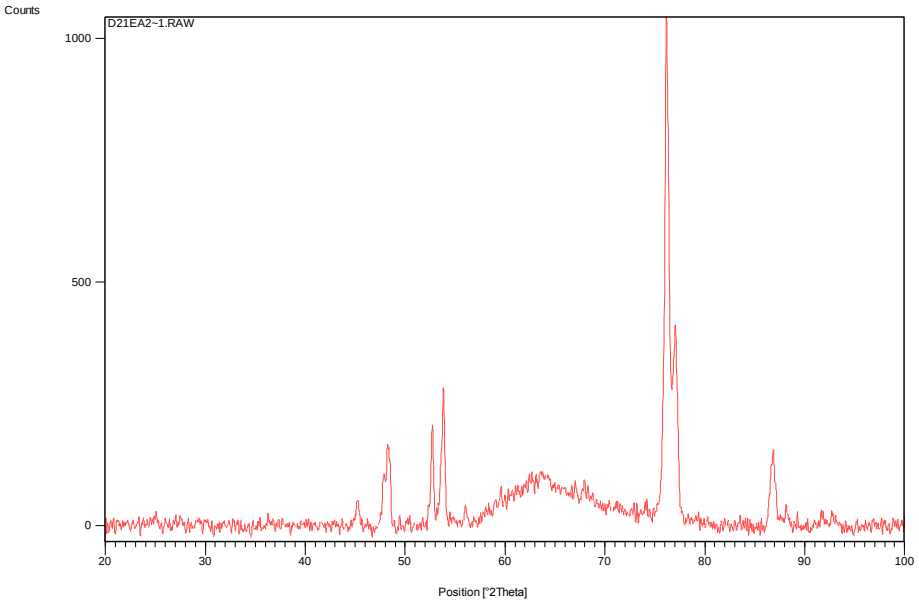


Figure 4.251. Unlabelled XRD pattern of heat treated nominal Ni_{32}:V_{56}:C_{12} (at.%), Sample 15H.

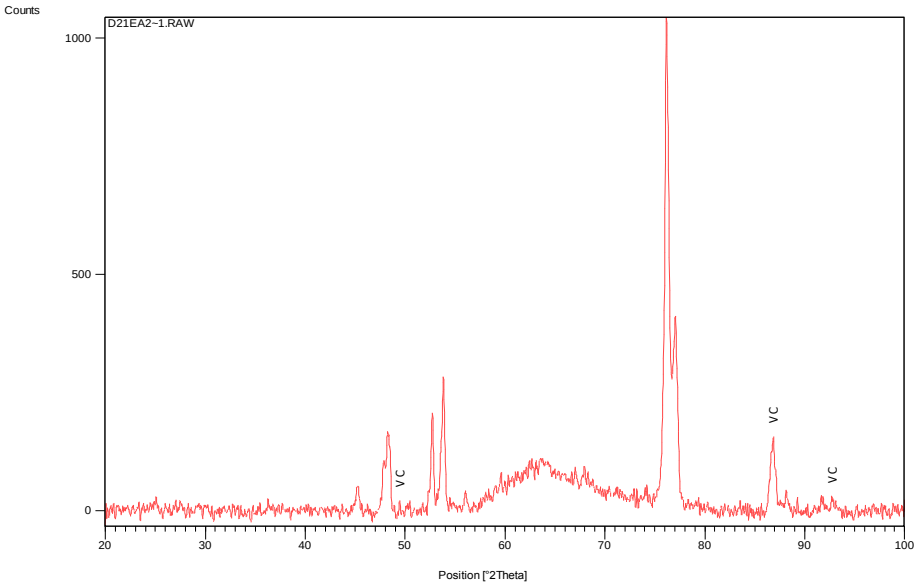


Figure 4.252. XRD pattern of heat treated nominal Ni_{32}:V_{56}:C_{12} (at.%), Sample 15H, showing identified ~VC peaks.

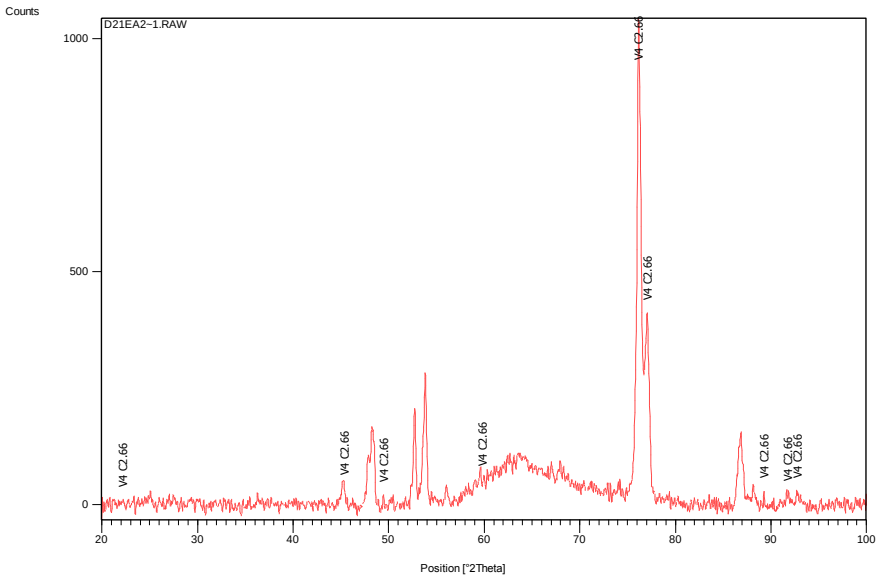


Figure 4.253a. XRD pattern of heat treated nominal $Ni_{32}:V_{56}:C_{12}$ (at.%), Sample 15H, showing identified ~$V_4C_{2.66}$ peaks.

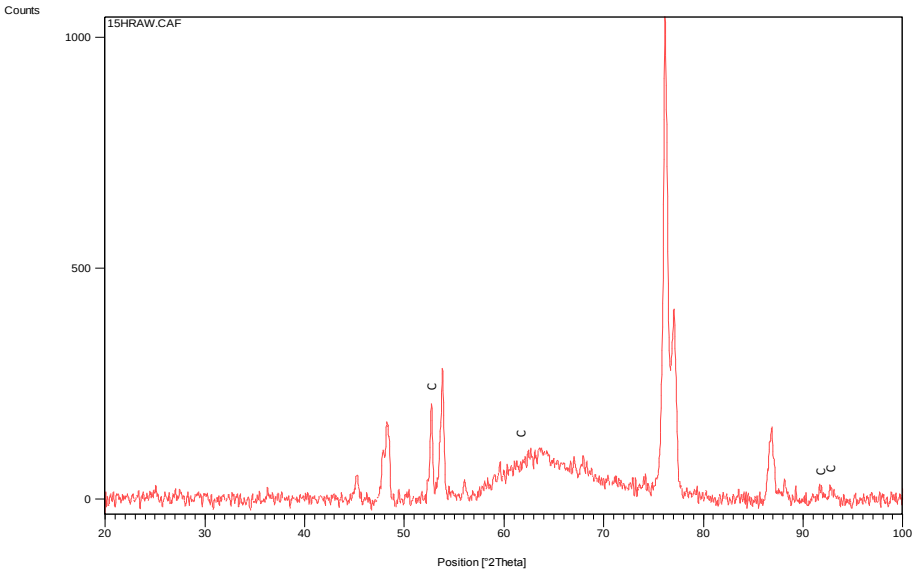


Figure 4.254b. XRD pattern of heat treated nominal $Ni_{32}:V_{56}:C_{12}$ (at.%), Sample 15H, showing identified C peaks.

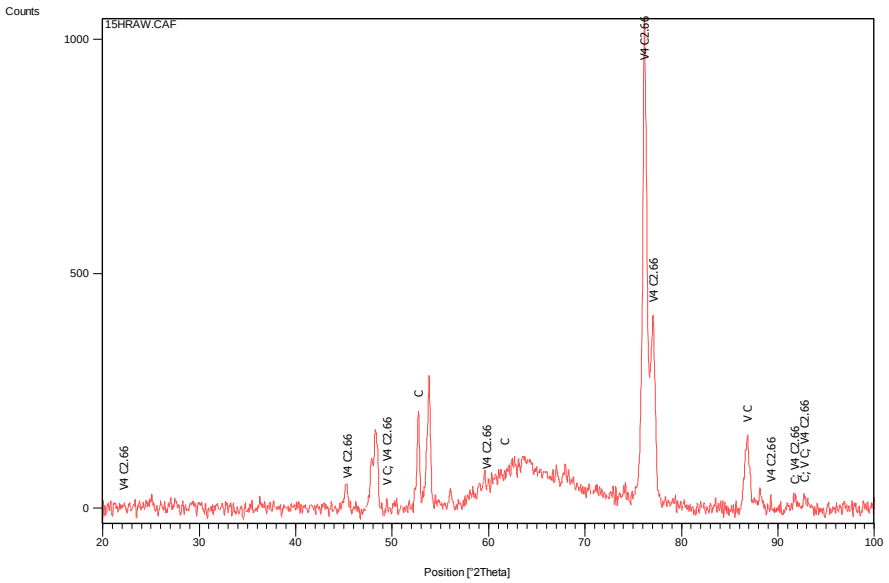


Figure 4.255. XRD pattern of heat treated nominal $Ni_{32}:V_{56}:C_{12}$ (at.%), Sample 15H, showing all the identified peaks.

Table 4.66. XRD peaks for heat treated nominal $Ni_{32}:V_{56}:C_{12}$ (at.%), Sample 15H.

Position 2θ (º)	Height (counts)	Relative Intensity (%)	Phases
22.1627	8.36	0.81	$V_4C_{2.66}$
45.3719	33.26	3.21	$V_4C_{2.66}$
48.5043	119.84	11.58	Presumed σ′
49.4517	19.45	1.88	$V_4C_{2.66}$, VC
52.7300	204.70	19.79	C
53.8534	272.41	26.33	Presumed σ′
56.0604	35.11	3.39	Presumed σ′
59.7865	52.89	5.11	$V_4C_{2.66}$
61.6785	103.00	9.96	C
76.1332	1034.51	100.00	$V_4C_{2.66}$
77.0689	409.96	39.63	$V_4C_{2.66}$
86.8575	153.01	14.79	VC
89.2806	26.84	2.59	$V_4C_{2.66}$
91.7444	21.14	2.04	$V_4C_{2.66}$, C
92.7158	25.82	2.50	$V_4C_{2.66}$, VC, C

4.2.10 Heat treated nominal $Ni_{39}:V_{42.8}:C_{18.2}$ (at.%), Sample 17H

The microstructure of nominal $Ni_{39}:V_{42.8}:C_{18.2}$ (at.%), Sample 17H, in heat treated condition is shown in Figures 4.256 and 4.257. The structure possessed mainly dark dendrites of two different morphologies with similar compositions, identified as ~V_6C_5, and a light region which was identified as ~Ni_2V. At higher magnification, the microstructure (Figure 4.257) was very different from its as-cast structure (Figure 4.124), and had needles on the dendrites. Also, the eutectic mixture in as-cast condition was retained after annealing, but had coarsened.

The phase compositions are shown in Table 4.68 and plotted in Figure 4.258. The overall analyses did not lie on the tie-line joining the two analysed phases, but there was graphite in the coarsened eutectic. There was no significant difference between the annealed and as-cast ~V_6C_5 compositions (Tables 4.68 and 4.33), although the ~Ni_2V phase had gained C and lost V, as well as gaining a little Ni. Appendix B33 shows the EDX analyses of heat treated Sample 17H.

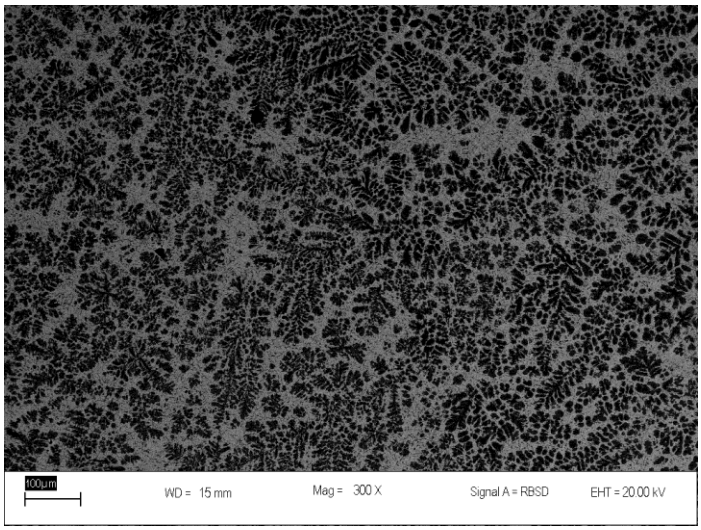


Figure 4.256. BSE-SEM image of heat treated nominal $Ni_{39}:V_{42.8}:C_{18.2}$ (at.%), Sample 17H, showing ~V_6C_5 dendrites (dark) and ~Ni_2V matrix (light) at low magnification.

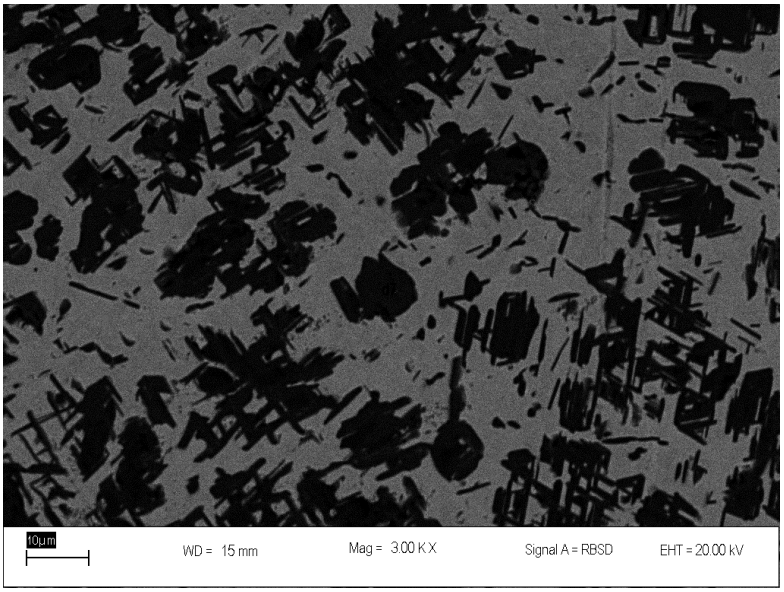


Figure 4.257. BSE-SEM image of heat treated nominal Ni_{39}:$V_{42.8}$:$C_{18.2}$ (at.%), Sample 17H, showing ~V_6C_5 dendrites (dark) with needles (dark) and ~Ni_2V matrix (light) at higher magnification.

Table 4.67. EDX phase analyses of annealed nominal Ni_{39}:$V_{42.8}$:$C_{18.2}$ (at.%), Sample 17H.

Phase Description	C	V	Ni	Phase
Overall	35.4 ± 0.7	37.5 ± 0.4	26.7 ± 0.4	-
Dark (globular)	42.9 ± 0.5	56.5 ± 0.3	0.6 ± 0.3	~V_6C_5
Needles	41.1 ± 1.4	57.5 ± 1.6	1.4 ± 0.3	~V_6C_5
Light	15.2 ± 0.7	23.2 ± 0.5	61.6 ± 0.6	~Ni_2V
Eutectic	37.7 ± 0.8	37.3 ± 0.6	25.0 ± 1.0	C + ~Ni_2V

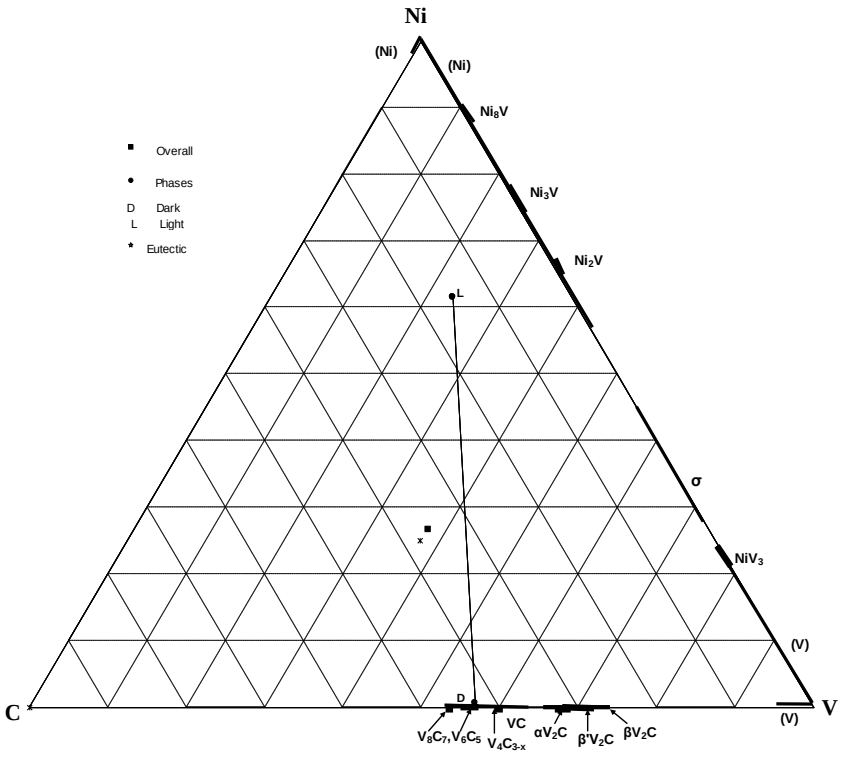


Figure 4.258. EDX analyses of heat treated nominal Ni_{39}:$V_{42.8}$:$C_{18.2}$ (at.%), Sample 17H.

The experimental XRD pattern of the heat treated alloy and the identified peaks for each phase are shown in Figures 4.259 to 4.264 and Table 4.69. The pattern was reasonable with a good signal:background ratio. The highest intensity peak were C and V_6C_5 at $2\theta = 51.4^o$. The pattern (Figure 4.264) confirmed the presence of C, V_6C_5, Ni_2V and $V_4C_{2.66}$ with unidentified peaks at $2\theta = 63.7$ and 76.1^o. The pattern was very different from that of the as-cast sample.

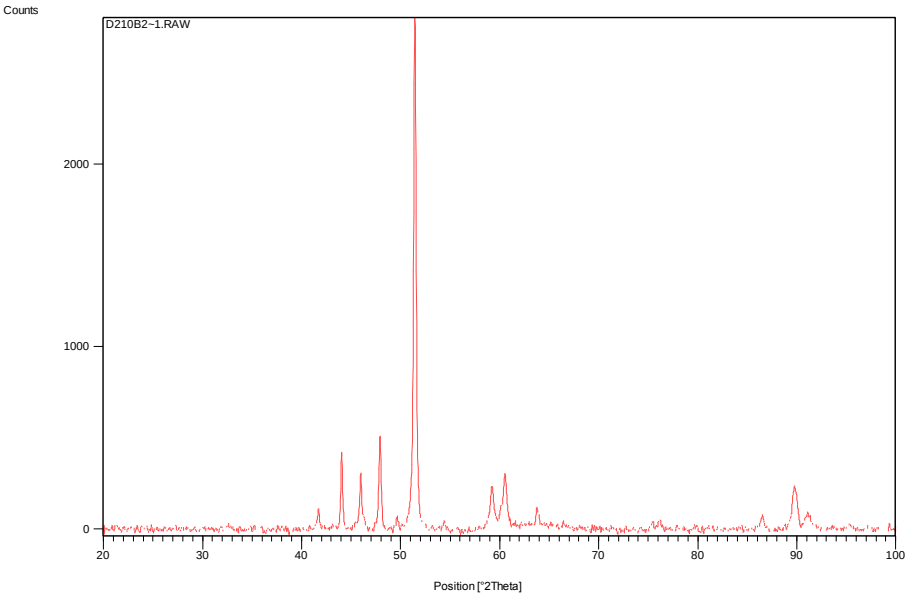


Figure 4.259. Unlabelled XRD pattern of heat treated nominal Ni_{39}:$V_{42.8}$:$C_{18.2}$ (at.%), Sample 17H.

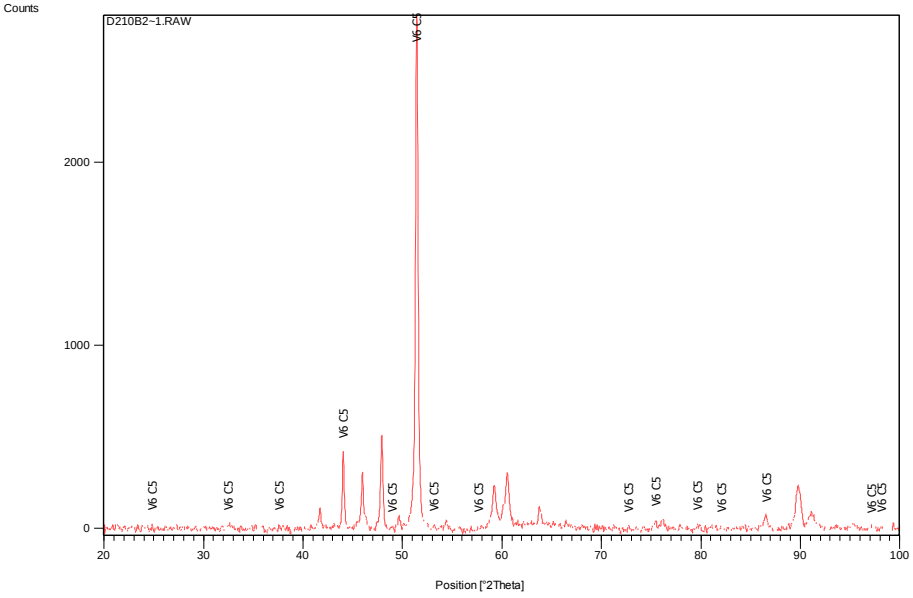


Figure 4.260. XRD pattern of heat treated nominal Ni_{39}:$V_{42.8}$:$C_{18.2}$ (at.%), Sample 17H, showing identified ~V_6C_5 peaks.

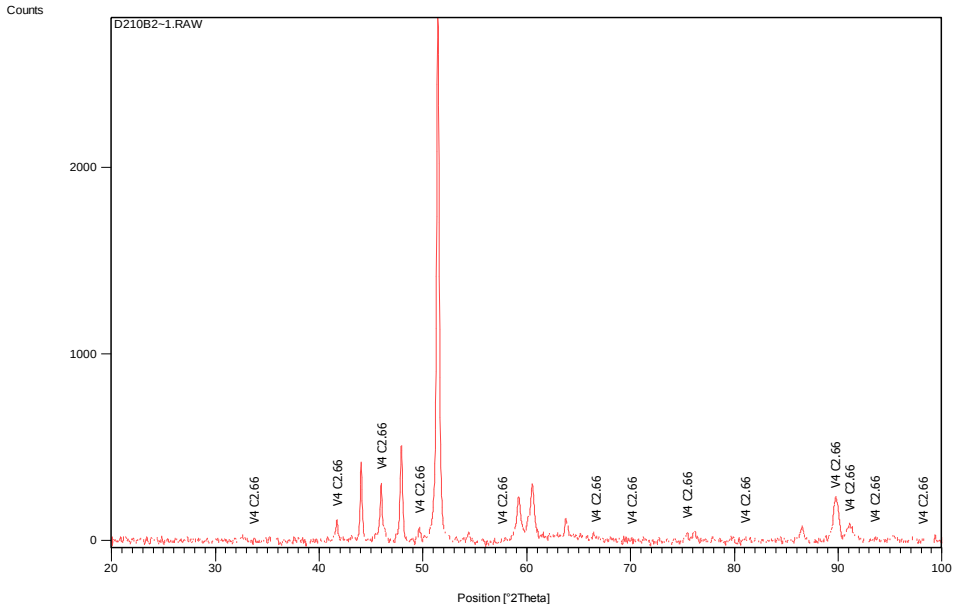


Figure 4.261. XRD pattern of heat treated nominal Ni_{39}:$V_{42.8}$:$C_{18.2}$ (at.%), Sample 17H, showing identified $V_4C_{2.66}$ peaks.

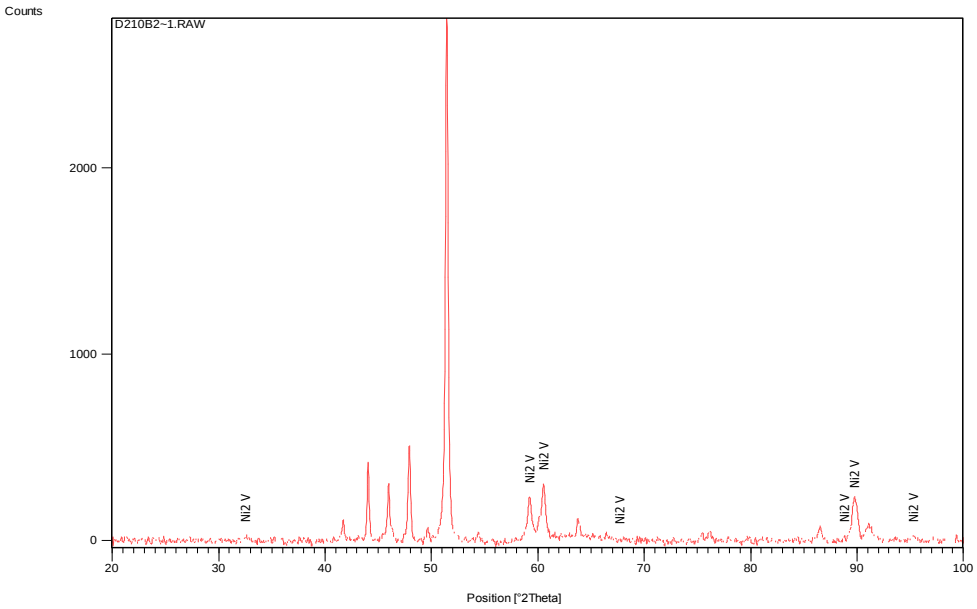


Figure 4.262a. XRD pattern of heat treated nominal Ni_{39}:$V_{42.8}$:$C_{18.2}$ (at.%), Sample 17H, showing identified ~Ni_2Vpeaks.

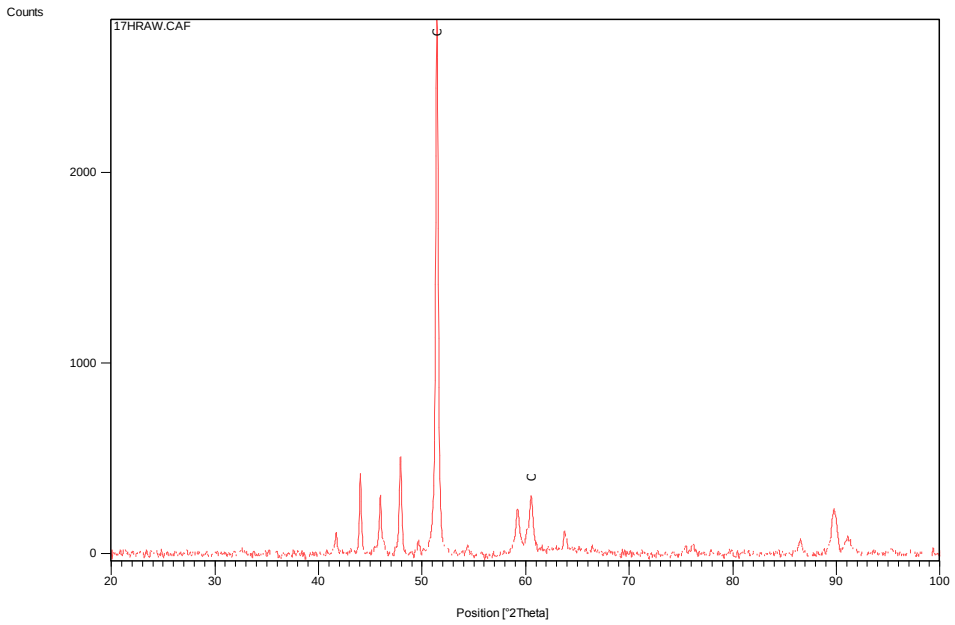


Figure 4.263b. XRD pattern of heat treated nominal $Ni_{39}:V_{42.8}:C_{18.2}$ (at.%), Sample 17H, showing identified C peaks.

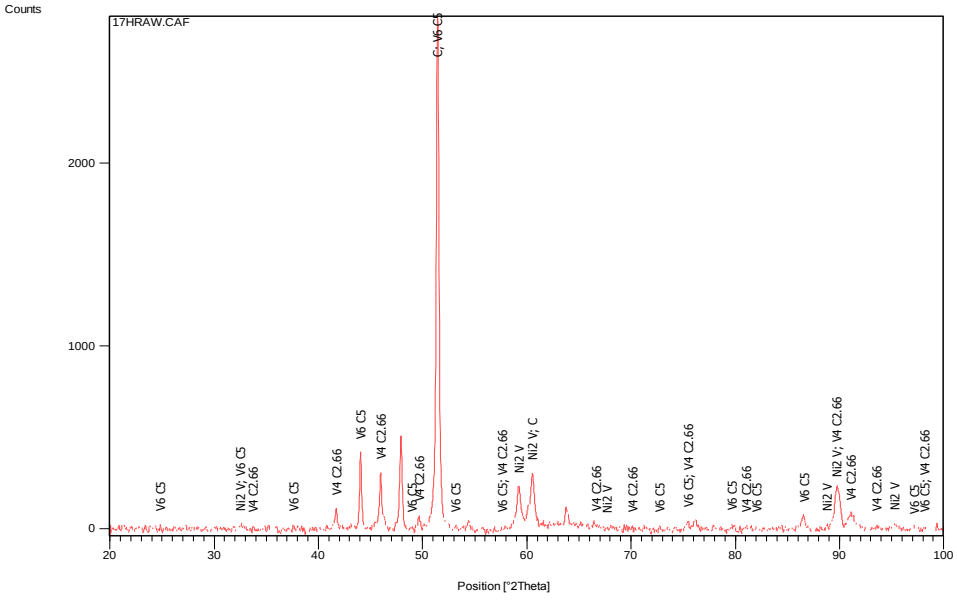


Figure 4.264. XRD pattern of heat treated nominal $Ni_{39}:V_{42.8}:C_{18.2}$ (at.%), Sample 17H, showing all the identified peaks.

Table 4.68. XRD peaks for heat treated nominal Ni_{39}:$V_{42.8}$:$C_{18.2}$ (at.%), Sample 17H.

Position 2θ (º)	Height (counts)	Relative Intensity (%)	Phases
24.8368	20.96	0.75	V_6C_5
32.5019	21.34	0.76	V_6C_5, Ni_2V
33.7521	14.09	0.50	V_6C_5
37.5845	23.93	0.85	$V_4C_{2.66}$
41.7137	111.74	3.99	$V_4C_{2.66}$
44.0341	414.47	14.79	V_6C_5
45.9711	304.72	10.87	$V_4C_{2.66}$
48.9552	13.78	0.49	V_6C_5
49.6507	72.31	2.58	$V_4C_{2.66}$
51.4316	2802.87	100.00	V_6C_5, C
53.1879	17.14	0.61	V_6C_5
57.6349	14.86	0.53	V_6C_5, $V_4C_{2.66}$
59.2249	232.63	8.30	Ni_2V
60.5436	303.29	10.82	Ni_2V, C
63.7457	118.42	4.23	Unidentified
66.6318	20.62	0.74	$V_4C_{2.66}$
67.6605	10.45	0.37	Ni_2V
70.1046	15.99	0.57	$V_4C_{2.66}$
72.7162	15.82	0.56	V_6C_5
75.4781	43.59	1.56	V_6C_5, $V_4C_{2.66}$
76.1553	45.79	1.63	Unidentified
79.6727	25.79	0.92	V_6C_5
81.0579	19.37	0.69	$V_4C_{2.66}$
82.0507	14.48	0.52	V_6C_5
86.5876	68.65	2.45	V_6C_5
88.7821	21.93	0.78	Ni_2V
89.6871	207.55	7.40	Ni_2V, $V_4C_{2.66}$
91.0907	79.66	2.84	$V_4C_{2.66}$
93.5663	21.34	0.76	$V_4C_{2.66}$
95.2783	25.13	0.90	Ni_2V
97.1393	9.38	0.33	V_6C_5
98.1736	13.91	0.50	V_6C_5, $V_4C_{2.66}$

4.2.11 Heat treated nominal $Ni_{66.4}$:$V_{16.1}$:$C_{17.5}$ (at.%), Sample 18H

An SEM-BSE image representative of the microstructure of nominal Ni_{66}:$V_{16.1}$:$C_{17.5}$ (at.%), Sample 18H, in the annealed condition is shown in Figure 4.265. The alloy had two contrasts. These were dark dendrites identified as ~V_8C_7, and the light matrix regions were identified as (Ni). At higher magnification, there was a eutectic of the dark and light phases

(Figure 4.266). In comparison with the as-cast condition (Figure 4.132), there was no significant difference in the microstructure, except that the dendrites were more facetted in heat treated condition. Also the alloy still retained its eutectic mixture after heat treatment, although it had rounded and coarsened.

Table 4.70 gives the phase analyses for the alloy, shown graphically in Figure 4.267. Comparing Tables 4.70 and Table 4.35, it can be seen that there was no significant change in composition during annealing. Also, the deviation of both overall and eutectic compositions from the tie-line joining the two phases was due to graphite, also present in the eutectic, which would push the overall analysis nearer to carbon. The EDX analyses of heat treated Sample 18H are shown in Appendix B34.

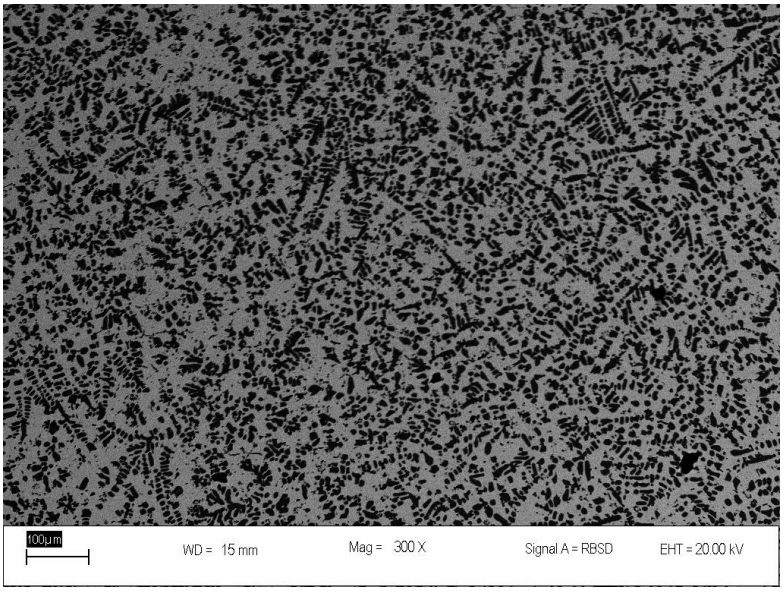


Figure 4.265. BSE-SEM image of heat treated nominal $Ni_{66.4}$:$V_{16.1}$:$C_{17.5}$ (at.%), Sample 18H, showing ~V_8C_7 dendrites (dark) and (Ni) matrix (light) at low magnification.

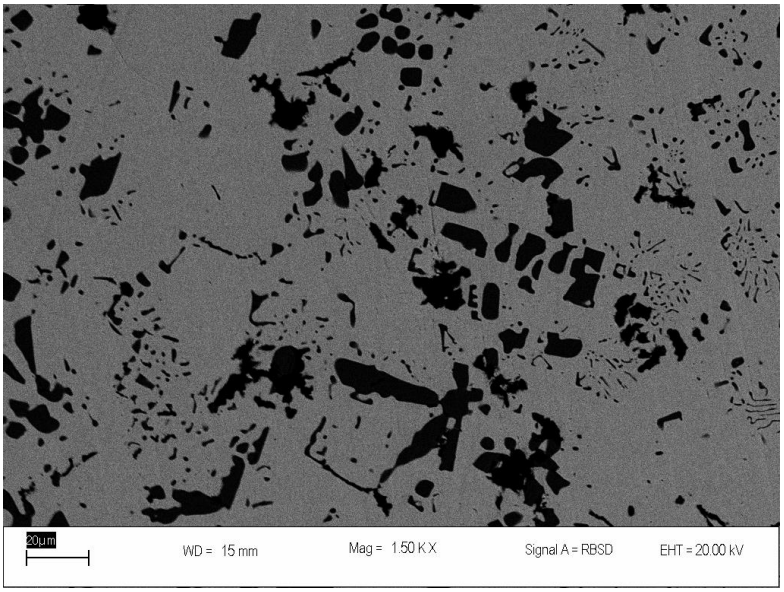


Figure 4.266. BSE-SEM image of heat treated nominal $Ni_{66.4}$:$V_{16.1}$:$C_{17.5}$ (at.%), Sample 18H, showing ~V_8C_7 dendrites (dark), (Ni) matrix (light) and eutectic at higher magnification.

Table 4.69. EDX phase analyses of annealed nominal $Ni_{66.4}$:$V_{16.1}$:$C_{17.5}$ (at.%), Sample 18H.

Phase Description	C	V	Ni	Phase
Overall	37.2 ± 0.5	18.2 ± 0.6	44.6 ± 0.4	-
Dark	47.4 ± 0.6	51.6 ± 0.6	1.0 ± 0.04	~V_8C_7
Light	18.5 ± 0.6	3.8 ± 0.6	77.7 ± 0.6	(Ni)
Eutectic	32.5 ± 0.5	22.6 ± 0.7	44.9 ± 1.0	C + (Ni)

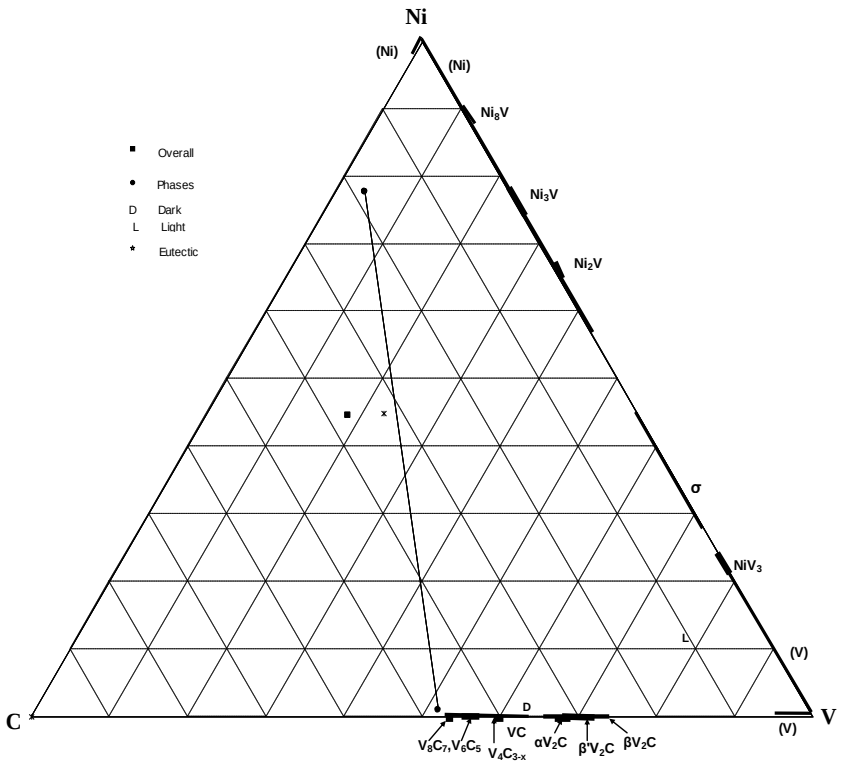


Figure 4.267. EDX analyses of heat treated nominal $Ni_{66.4}$:$V_{16.1}$:$C_{17.5}$ (at.%), Sample 18H.

As was the case of as-cast condition (Figure 4.134 to 4.139), the annealed XRD pattern also showed a good signal:background ratio, and the patterns were similar. The XRD pattern (Figure 4.272) confirmed the presence of ~V_8C_7, (Ni) and C. The highest intensity peak (at about $2\theta = 60.79^o$) was a combination of the (Ni) and ~V_8C_7 phases. All the identified peaks together with their phases are shown in Table 4.71.

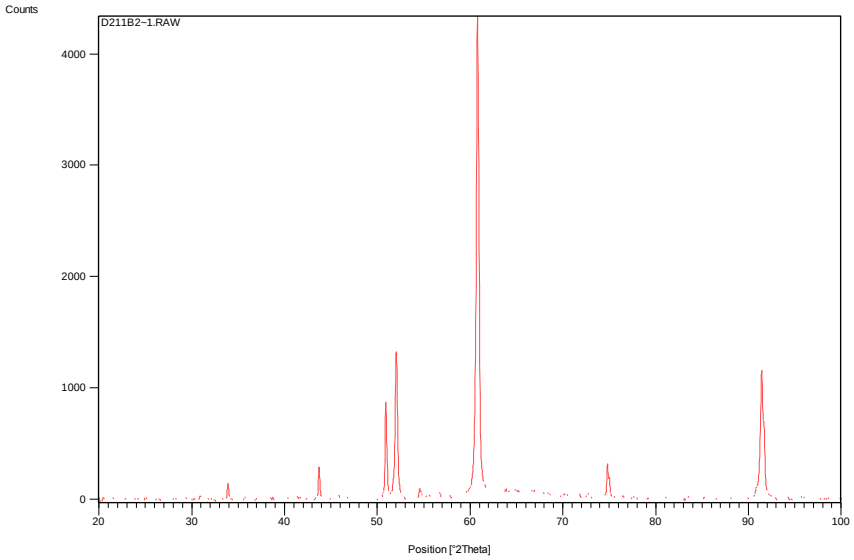


Figure 4.268. Unlabelled XRD pattern of heat treated nominal $Ni_{66.4}$:$V_{16.1}$:$C_{17.5}$ (at.%), Sample 18H.

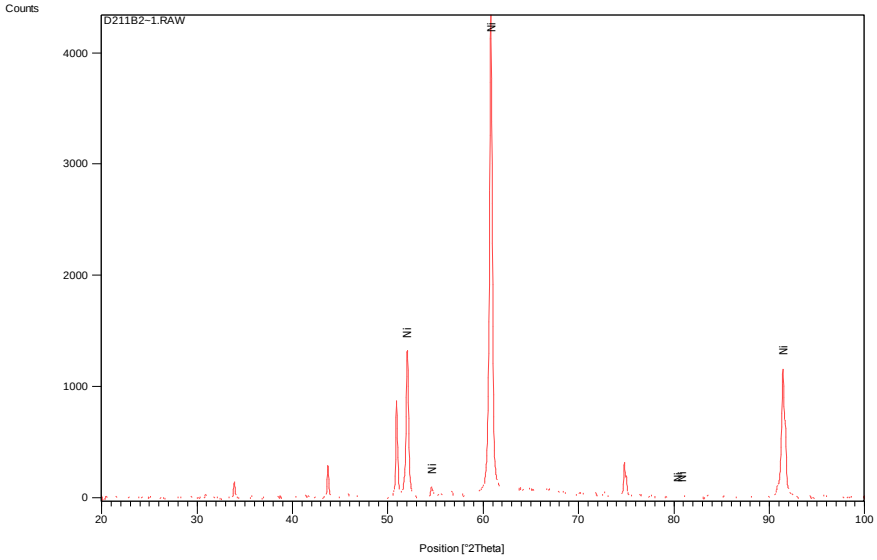


Figure 4.269. XRD pattern of heat treated nominal $Ni_{66.4}$:$V_{16.1}$:$C_{17.5}$ (at.%), Sample 18H, showing identified (Ni) peaks.

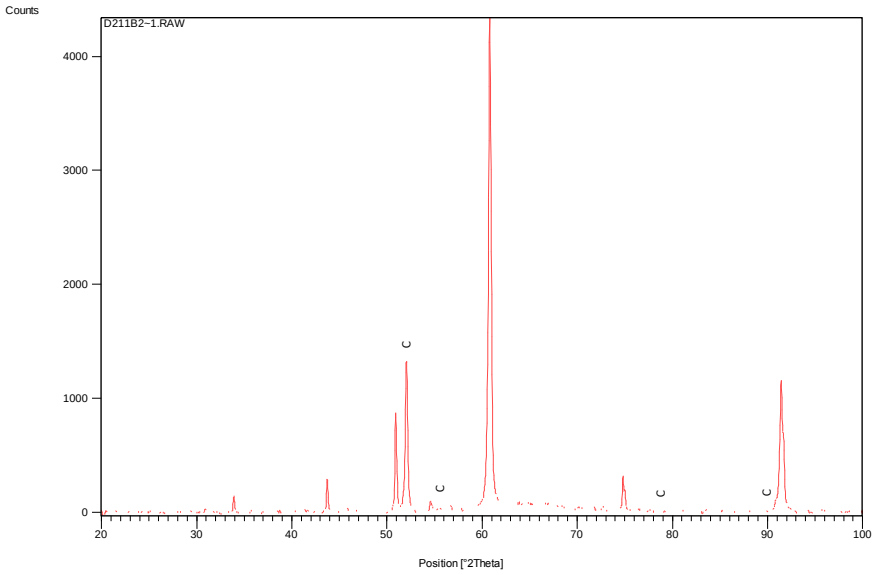


Figure 4.270. XRD pattern of heat treated nominal $Ni_{66.4}$:$V_{16.1}$:$C_{17.5}$ (at.%), Sample 18H, showing identified C peaks.

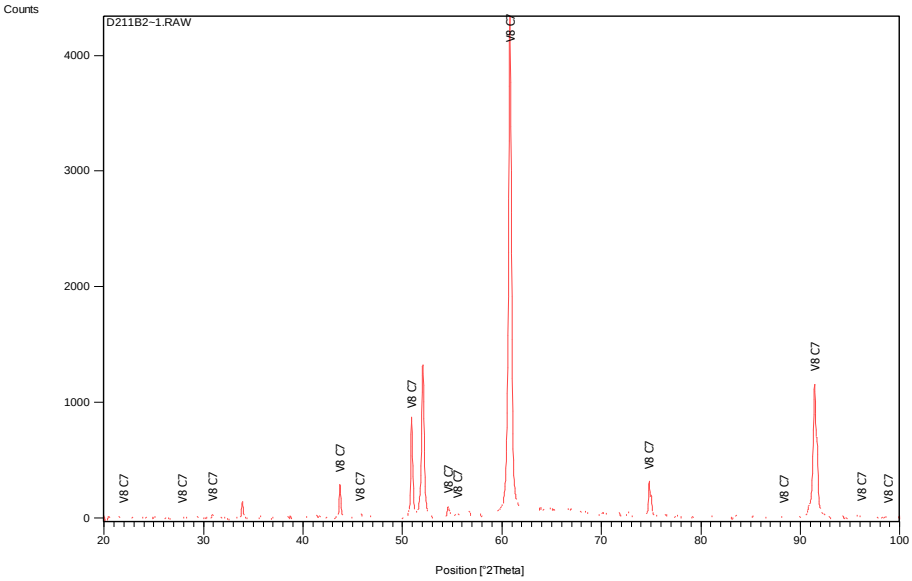


Figure 4.271. XRD pattern of heat treated nominal $Ni_{66.4}$:$V_{16.1}$:$C_{17.5}$ (at.%), Sample 18H, showing identified ~V_8C_7 peaks.

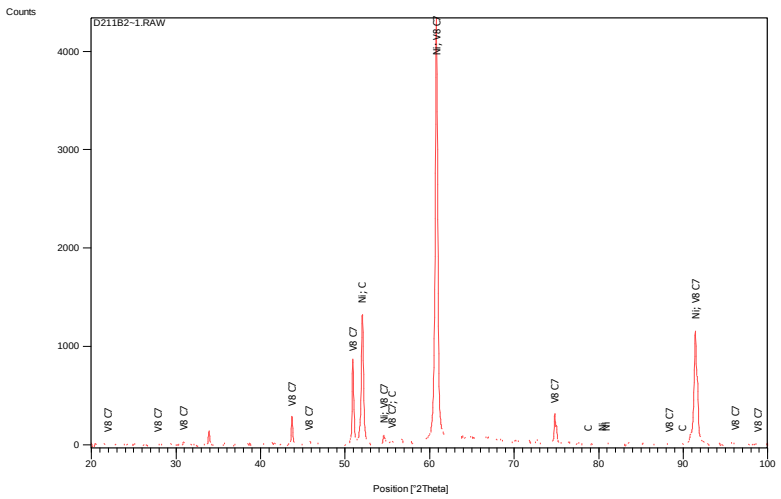


Figure 4.272. XRD pattern of heat treated nominal $Ni_{66.4}$:$V_{16.1}$:$C_{17.5}$ (at.%), Sample 18H, showing all the identified peaks.

Table 4.70. XRD peaks for heat treated nominal $Ni_{66.4}$:$V_{16.1}$:$C_{17.5}$ (at.%), Sample 18H.

Position 2θ (º)	Height (counts)	Relative Intensity (%)	Phases
21.9499	11.35	0.26	V_8C_7
27.8911	14.28	0.33	V_8C_7
30.8795	28.62	0.66	V_8C_7
43.6966	276.82	6.36	V_8C_7
45.7144	29.13	0.67	V_8C_7
50.8881	833.52	19.14	V_8C_7
52.0333	1312.30	30.13	Ni, C
54.5689	92.82	2.13	Ni, V_8C_7
55.5596	50.30	1.15	C, V_8C_7
60.7974	4355.74	100.00	Ni, V_8C_7
74.7909	301.87	6.93	V_8C_7
78.7451	15.65	0.36	C
80.3766	15.53	0.36	Ni
80.8222	17.48	0.40	Ni
88.3229	9.31	0.21	V_8C_7
89.8640	18.16	0.42	C
91.4170	1154.35	26.50	Ni, V_8C_7
96.1472	30.75	0.71	V_8C_7
98.8232	16.14	0.37	V_8C_7

4.2.12 Heat treated nominal $Ni_{68}:V_{14}:C_{18}$ (at.%), Sample 19H

The SEM-BSE images of heat treated nominal $Ni_{68}:V_{14}:C_{18}$ (at.%), Sample 19H are shown in Figures 4.273 and 4.274. The microstructure of alloy $Ni_{68}:V_{14}:C_{18}$ (at.%), Sample 19H, in the annealed condition was similar to the as-cast condition (Figures 4.274 and 4.141) with coarsening of the dendrites and the eutectic. The alloy had two main phases, the ~V_8C_7 dendrites and the (Ni) matrix, with possibly a small amount of C in the eutectic.

Table 4.72 gives the phase analyses which are shown in Figure 4.275. Comparing Table 4.72 with Table 4.37, it can be seen that there were changes in composition after annealing; ~V_8C_7 had lost C and gained V, and (Ni) had lost C and V and gained Ni. The EDX analyses can be found in Appendix B35.

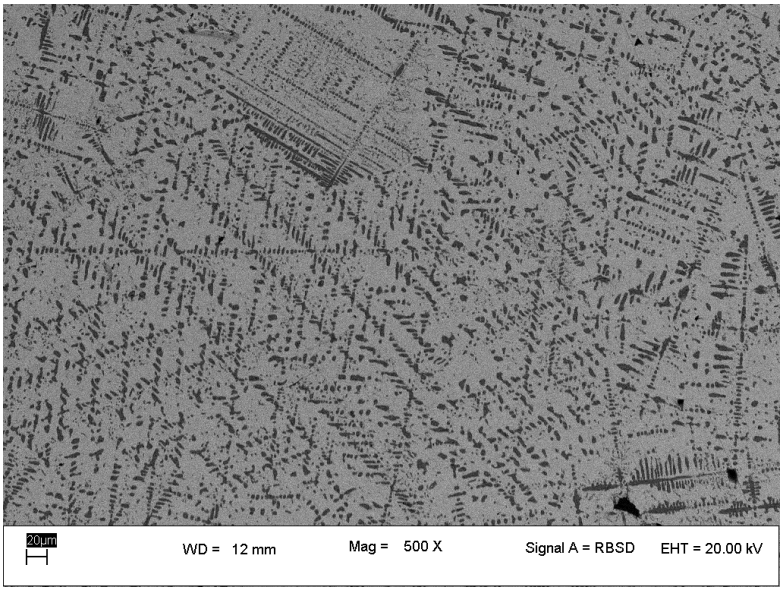


Figure 4.273. BSE-SEM images of heat treated $Ni_{68}:V_{14}:C_{18}$ (at.%), Sample 19H, showing ~V_8C_7 dendrites (dark) and (Ni) matrix (light).

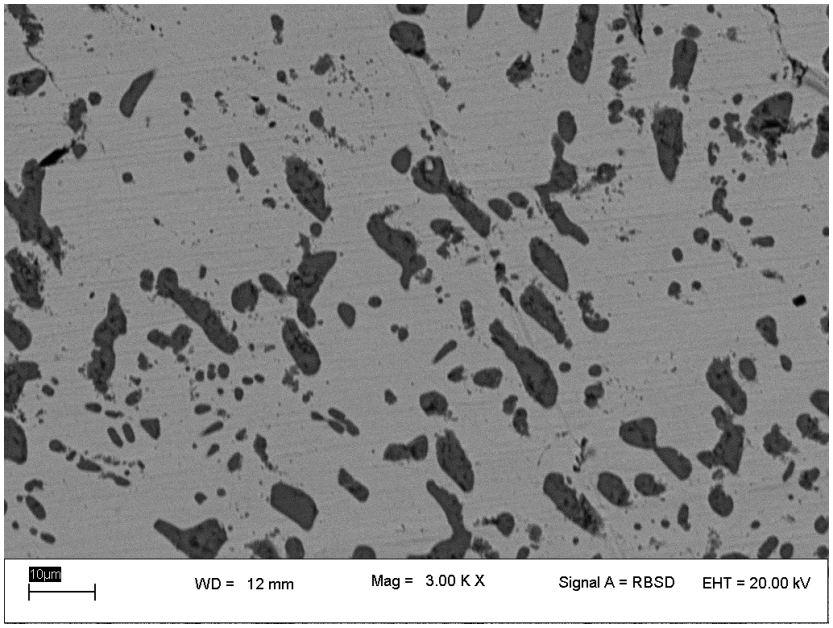


Figure 4.274. BSE-SEM images of heat treated $Ni_{68}:V_{14}:C_{18}$ (at.%), Sample 19H, showing ~V_8C_7 dendrites (dark), (Ni) matrix (light) and eutectic at higher magnification.

Table 4.71. EDX phase analyses of annealed nominal $Ni_{68}:V_{14}:C_{18}$ (at.%), Sample 19H.

Phase Description	C	V	Ni	Phase
Overall	33 ± 0.6	26.2 ± 0.4	40.8 ± 0.7	-
Dark	47.9 ± 1.0	50.6 ± 0.9	1.5 ± 0.3	~V_8C_7
Light	17.8 ± 0.2	4.4 ± 0.3	77.8 ± 0.2	(Ni)
Eutectic	30.5 ± 0.7	21.2 ± 1.0	48.3 ± 0.4	~V_8C_7 + (Ni)

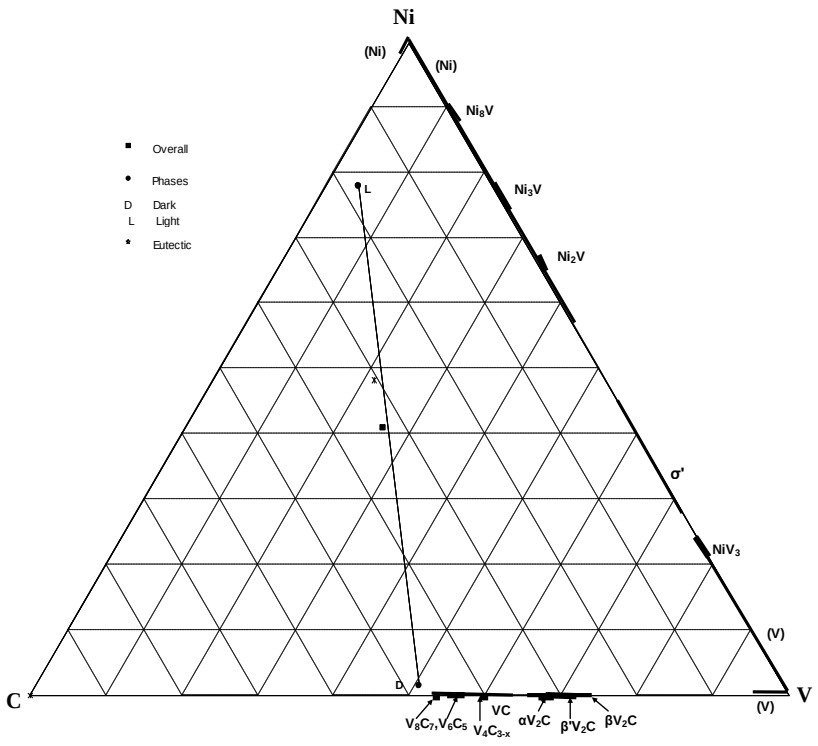


Figure 4.275. EDX analyses of heat treated nominal Ni_{68}:V_{14}:C_{18} (at.%), Sample 19H.

The XRD pattern shown in Figures 4.276 to 4.279 was good, with a high signal:background ratio. The existence of (Ni) and ~V_8C_7 was confirmed by XRD, as shown in Figures 4.277 and 4.278. Carbon peaks were not strongly confirmed, but could have been present at 2θ = ~51° and ~54°. The matches with the ICDD for the phases were excellent, but with unidentified peaks at about 2θ = 46.76° and 80.76°. The (Ni) peak retained the highest intensity at position 2θ = 51.96° as in the as-cast sample (Figure 4.145). Table 4.73 shows the identified peaks together with their phases.

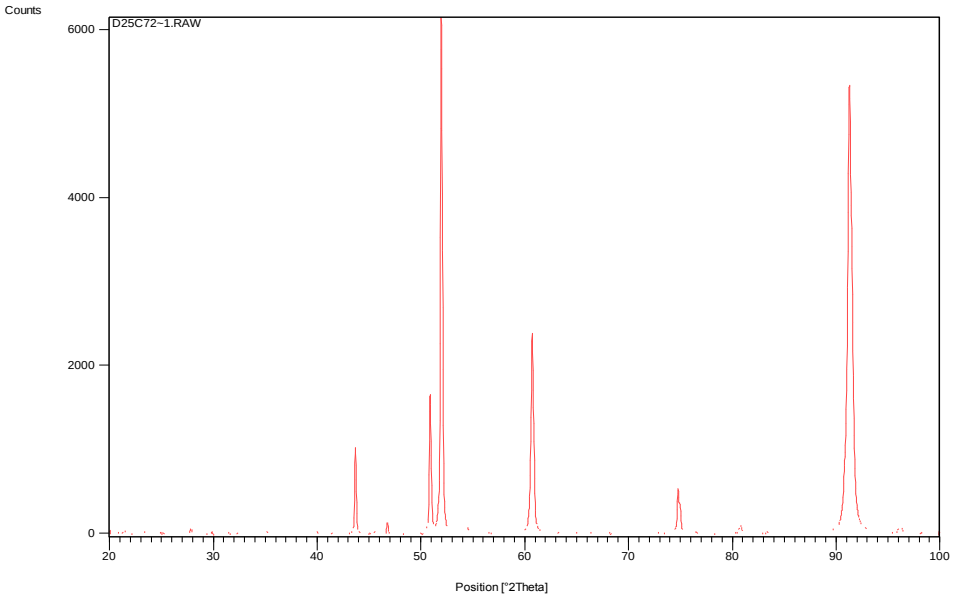


Figure 4.276. Unlabelled XRD pattern of heat treated nominal $Ni_{68}:V_{14}:C_{18}$ (at.%), Sample 19H.

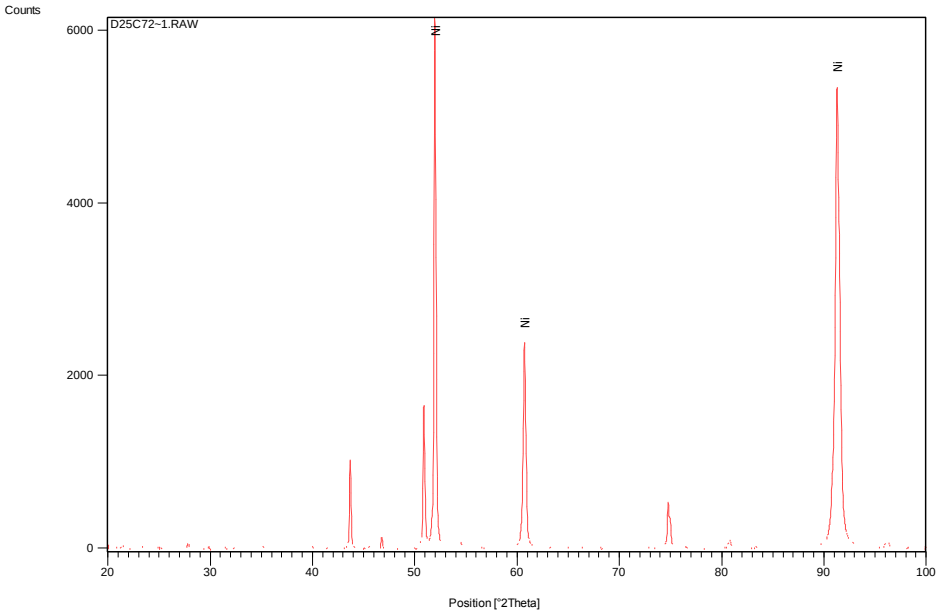


Figure 4.277. XRD pattern of heat treated nominal $Ni_{68}:V_{14}:C_{18}$ (at.%), Sample 19H, showing identified (Ni) peaks.

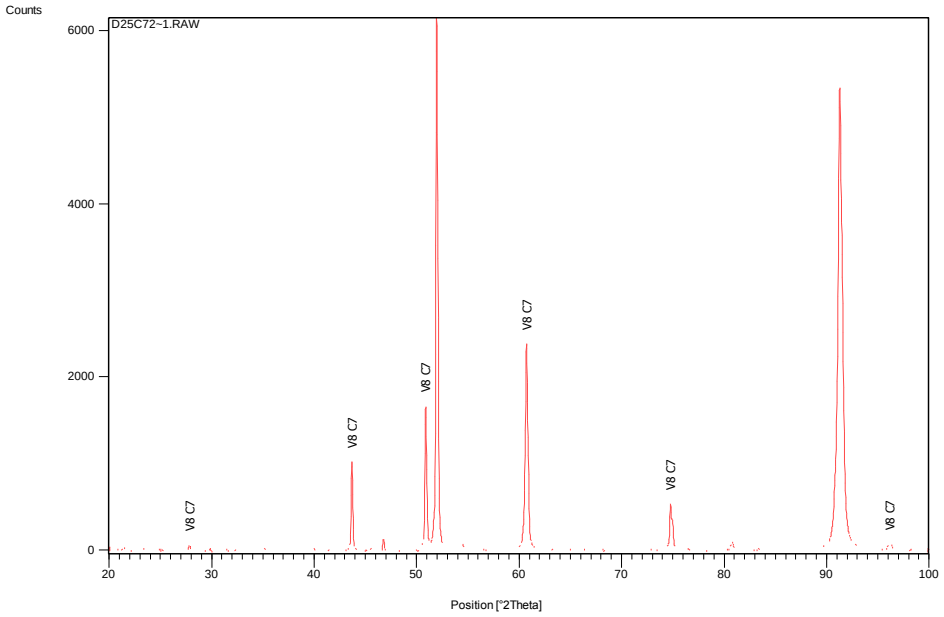


Figure 4.278. XRD pattern of heat treated nominal $Ni_{68}:V_{14}:C_{18}$ (at.%), Sample 19H, showing identified ~V_8C_7 peaks.

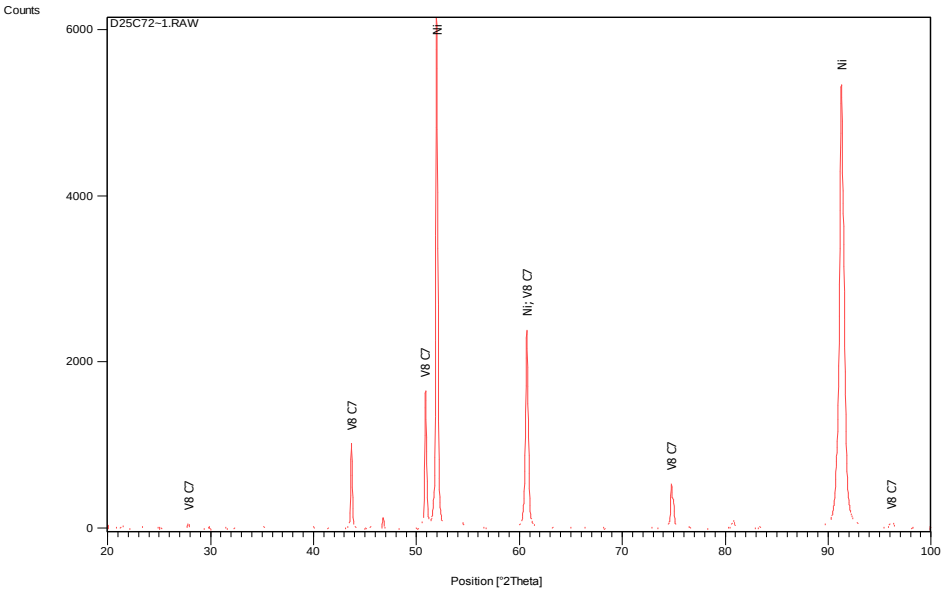


Figure 4.279. XRD pattern of heat treated nominal $Ni_{68}:V_{14}:C_{18}$ (at.%), Sample 19H, showing all identified peaks.

Table 4.72. XRD peaks for heat treated nominal $Ni_{68}:V_{14}:C_{18}$ (at.%), Sample 19H.

Position 2θ (º)	Height (counts)	Relative Intensity (%)	Phases
27.8330	57.98	0.94	V_8C_7
43.6821	1020.93	16.55	V_8C_7
46.7628	127.58	2.07	Unidentified
50.8773	1652.99	26.80	V_8C_7
51.9618	6168.04	100.00	Ni
60.7199	2373.85	38.49	V_8C_7, Ni
74.7706	529.83	8.59	V_8C_7
80.7687	93.83	1.52	Unidentified
91.2815	5293.15	85.82	Ni
96.1545	59.91	0.97	V_8C_7

4.2.13 Heat treated nominal $Ni_{59}:V_{27.2}:C_{13.8}$ (at.%), Sample 20H

Figures 4.280 and 4.281 show the SEM-BSE image of nominal $Ni_{59}:V_{27.2}:C_{13.8}$, Sample 20H, in the heat treated condition. The alloy had two different contrasts in the microstructure (Figure 4.280). There were dark dendrites, which were identified as ~V_8C_7, and the light matrix regions were identified as (Ni). The heat treated sample showed a very similar microstructure to the as-cast sample (Figures 4.280, and 4.147), with coarsening of the dendrites and the (Ni) + ~VC (globular) and C + (Ni) (flakes) eutectics, which would be expected.

Table 4.74 gives the phase analyses for the alloy, which are plotted in Figure 4.282. Comparing Tables 4.74 and 4.39, it could be seen that there was slight change in composition after annealing: ~V_8C_7 had lost C and gained some V, and (Ni) had gained C and lost V and Ni, which indicates slightly sloping solvi. The light phase was probably affected by the fine dark phase in the matrix. The EDX analyses are shown in Appendix B36.

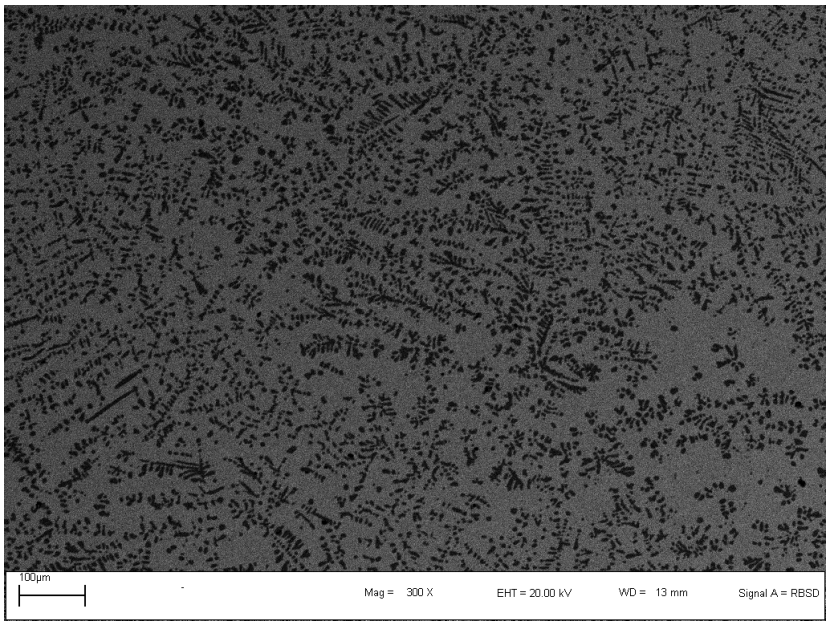


Figure 4.280. BSE-SEM images of heat treated Ni_{59}:$V_{27.2}$:$C_{13.8}$ (at.%), Sample 20H, showing ~V_8C_7 dendrites (dark) and (Ni) (light).

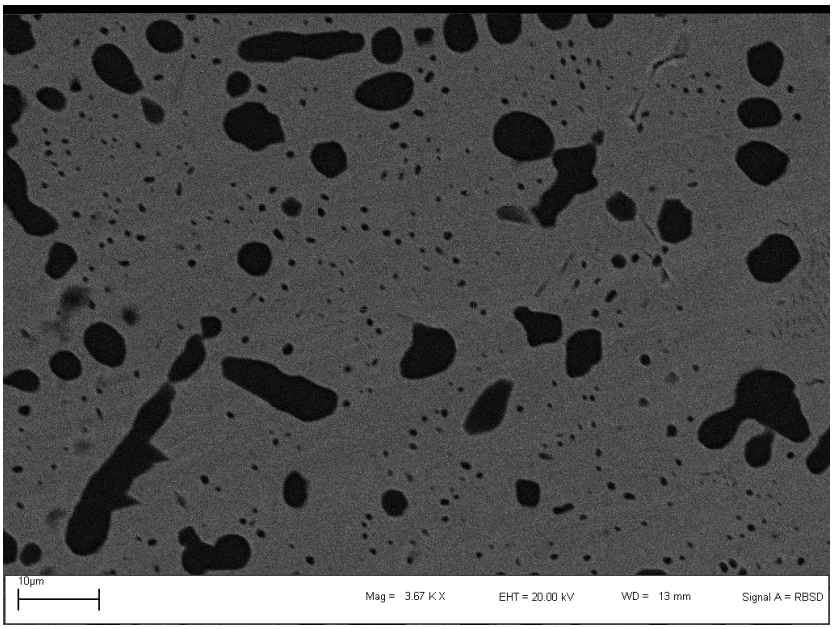


Figure 4.281. BSE-SEM images of heat treated Ni_{59}:$V_{27.2}$:$C_{13.8}$ (at.%), Sample 20H, showing ~V_8C_7 dendrites (dark) and (Ni) + ~VC (light) and (Ni) + C (dark) eutectics.

Table 4.73. EDX phase analyses of annealed nominal $Ni_{59}:V_{27.2}:C_{13.8}$ (at.%), Sample 20H.

Phase Description	C	V	Ni	Phase
Overall	32.6 ± 0.9	22.8 ± 0.4	44.6 ± 0.8	-
Dark	47 ± 0.5	52.7 ± 0.9	0.3 ± 0.02	~V_8C_7
Light	24.1 ± 0.2	13.9 ± 0.5	62 ± 0.3	(Ni)
Eutectics	27.2 ± 0.7	17.4 ± 0.8	55.4 ± 0.5	~VC + (Ni) C + (Ni)

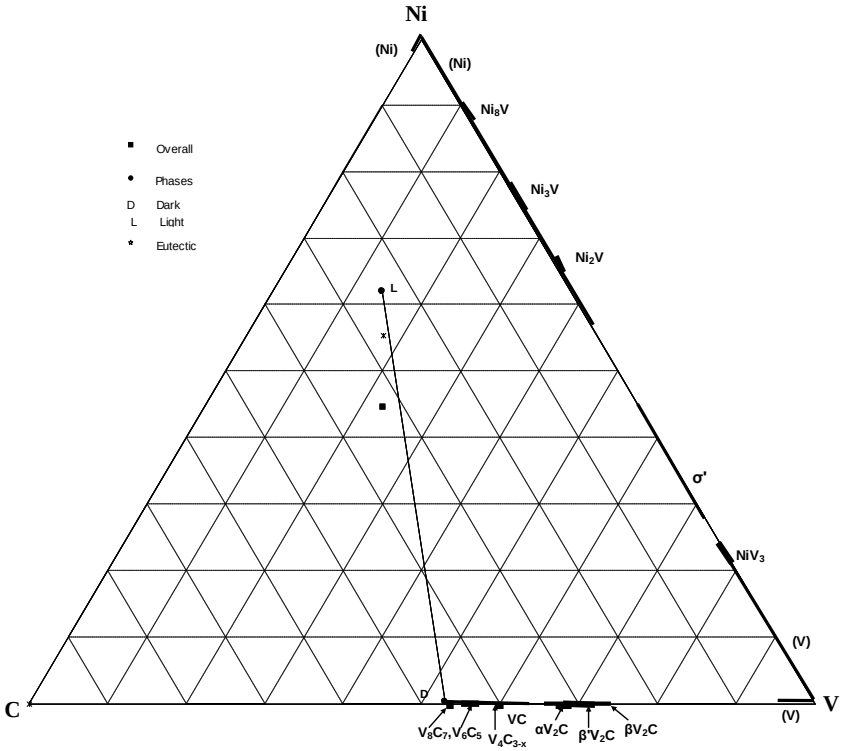


Figure 4.282. EDX analyses of heat treated $Ni_{59}:V_{27.2}:C_{13.8}$ (at.%), Sample 20H.

The XRD pattern (Figure 4.287) confirmed the presence of ~V_8C_7, C and (Ni). Figures 4.283 to 4.287 show the experimental pattern of the sample with the database lines for each of the phases and Table 4.75 shows the identified peaks. The highest intensity peak at $2\theta = 51.68^o$ was Ni, and is comparable to as-cast condition. The peak at $2\theta = 60.76^o$ was reduced on

annealing, and also the peak at 2θ = 51.12° of the as-cast pattern had been lost. There were extra peaks at 2θ = ~59° and ~70°. All peaks could not be matched, as shown in the table, but these were minor peaks.

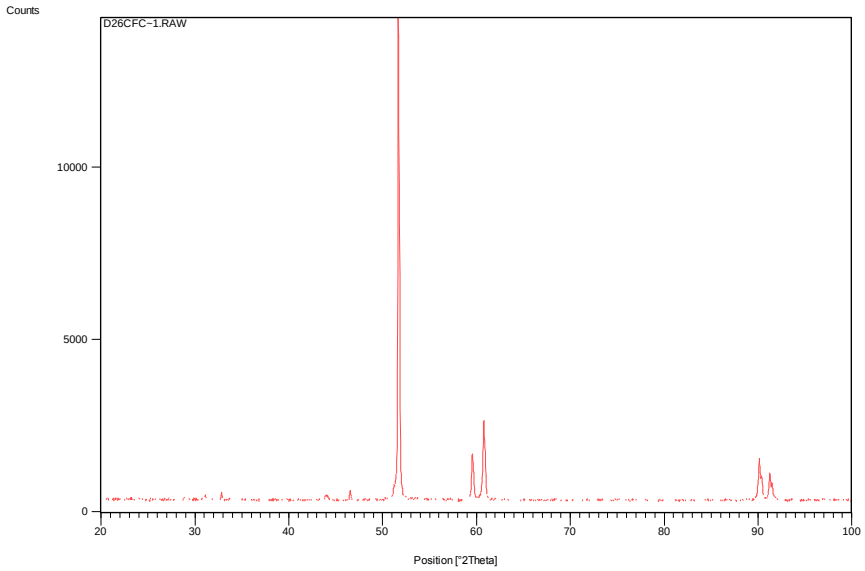


Figure 4.283. Unlabelled XRD pattern of heat treated nominal $Ni_{59}:V_{27.2}:C_{13.8}$ (at.%), Sample 20H.

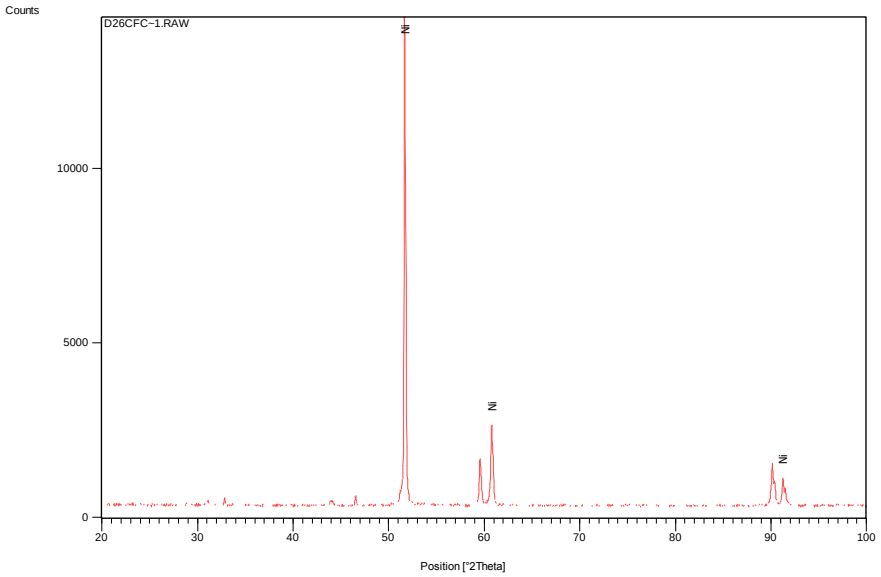


Figure 4.284. XRD pattern of heat treated nominal $Ni_{59}:V_{27.2}:C_{13.8}$ (at.%), Sample 20H, showing identified (Ni) peaks.

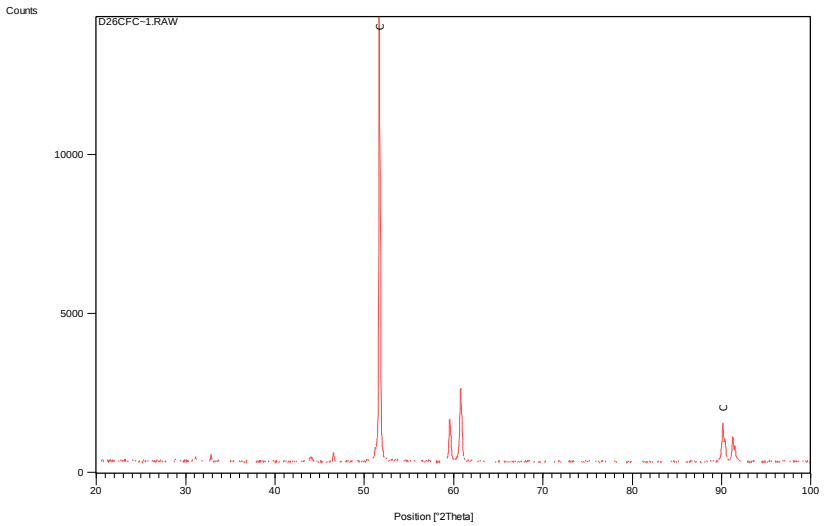


Figure 4.285. XRD pattern of heat treated nominal $Ni_{59}:V_{27.2}:C_{13.8}$ (at.%), Sample 20H, showing identified C peaks.

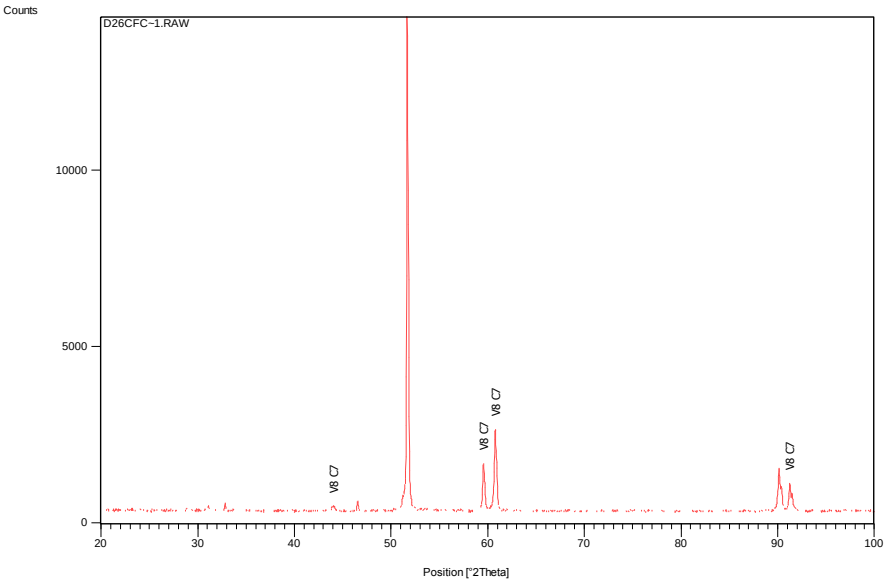


Figure 4.286. XRD pattern of heat treated nominal $Ni_{59}:V_{27.2}:C_{13.8}$ (at.%), Sample 20H, showing identified ~V_8C_7 peaks.

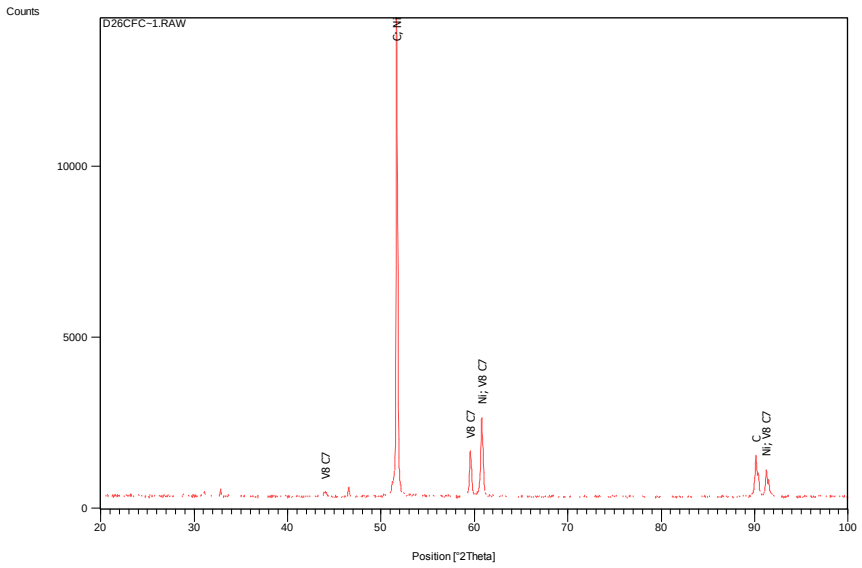


Figure 4.287. XRD pattern of heat treated nominal Ni_{59}:$V_{27.2}$:$C_{13.8}$ (at.%), Sample 20H, showing all identified peaks.

Table 4.74. XRD peaks for heat treated nominal Ni_{59}:$V_{27.2}$:$C_{13.8}$ (at.%), Sample 20H.

Position 2θ (º)	Height (counts)	Relative Intensity (%)	Phases
28.9124	56.68	0.82	Unidentified
31.1015	96.13	1.39	Unidentified
32.8517	132.57	1.92	Unidentified
44.0237	133.66	0.96	V_8C_7
46.5502	205.43	2.98	Unidentified
51.6822	13979.97	100.00	Ni, C
59.5658	1328.12	9.50	V_8C_7
60.7867	2295.95	16.42	V_8C_7, Ni
90.1427	1208.38	8.64	C
91.2620	782.15	5.59	V_8C_7, Ni

4.2.14 Heat treated nominal Ni_{39}:$V_{42.8}$:$C_{18.2}$ (at.%), Sample 21H

Figure 4.288 shows the microstructure of nominal Ni_{39}:$V_{42.8}$:$C_{18.2}$ (at.%), Sample 21H, in the heat treated condition. The microstructure of the alloy was very similar to the as-cast condition (Figures 4.288 and 4.155). The alloy had two phases, ~V_6C_5 needles with some

cracks (seen at higher magnification) (Figure 4.289) and the ~Ni_2V (matrix). The eutectic was coarsened.

Table 4.76 gives the phase analyses for the alloy, plotted in Figure 4.290. Comparing Tables 4.76 and 4.41, it can be seen that there were slight changes in composition after annealing: ~V_6C_5 had gained C and lost V, and ~Ni_2V had lost C and V and gained some Ni. The deviation of overall composition from the tie-line joining the two analysed phases is due to graphite in the eutectic, which pushes the overall analysis nearer to carbon. The EDX analyses of heat treated Sample 21H are shown in Appendix B37.

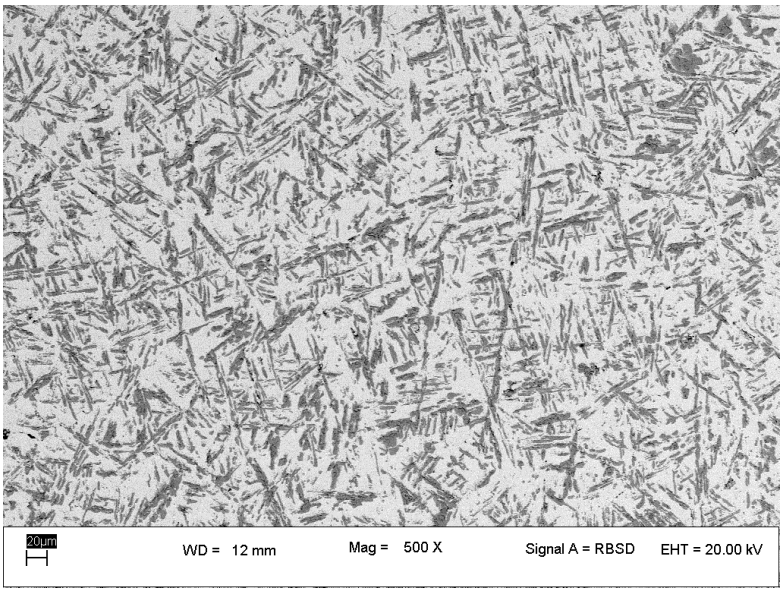


Figure 4.288. BSE-SEM images of heat treated nominal Ni_{39}:$V_{42.8}$:$C_{18.2}$ (at.%), Sample 21H, showing ~V_6C_5 needles (dark), and ~Ni_2V matrix (light).

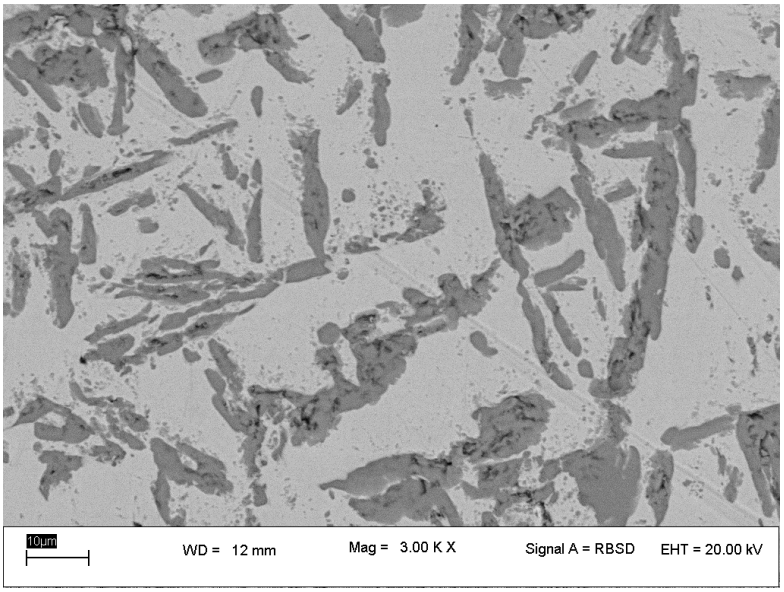


Figure 4.289. BSE-SEM images of heat treated nominal Ni_{39}:$V_{42.8}$:$C_{18.2}$ (at.%), Sample 21H, showing ~V_6C_5 needles (dark), and ~Ni_2V matrix (light) at higher magnification.

Table 4.75. EDX phase analyses of annealed nominal Ni_{39}:$V_{42.8}$:$C_{18.2}$ (at.%), Sample 21H.

Phase Description	C	V	Ni	Phase
Overall	25.4 ± 1.3	35.8 ± 1.2	38.8 ± 0.7	-
Dark	42.3 ± 0.5	56.8 ± 0.5	0.9 ± 0.02	~V_6C_5
Light	15.2 ± 1.3	31.8 ± 1.1	53.0 ± 0.4	~Ni_2V
Eutectics	30.2 ± 0.3	39.3 ± 0.8	30.5 ± 0.8	~V_6C_5 + ~Ni_2V C + ~Ni_2V

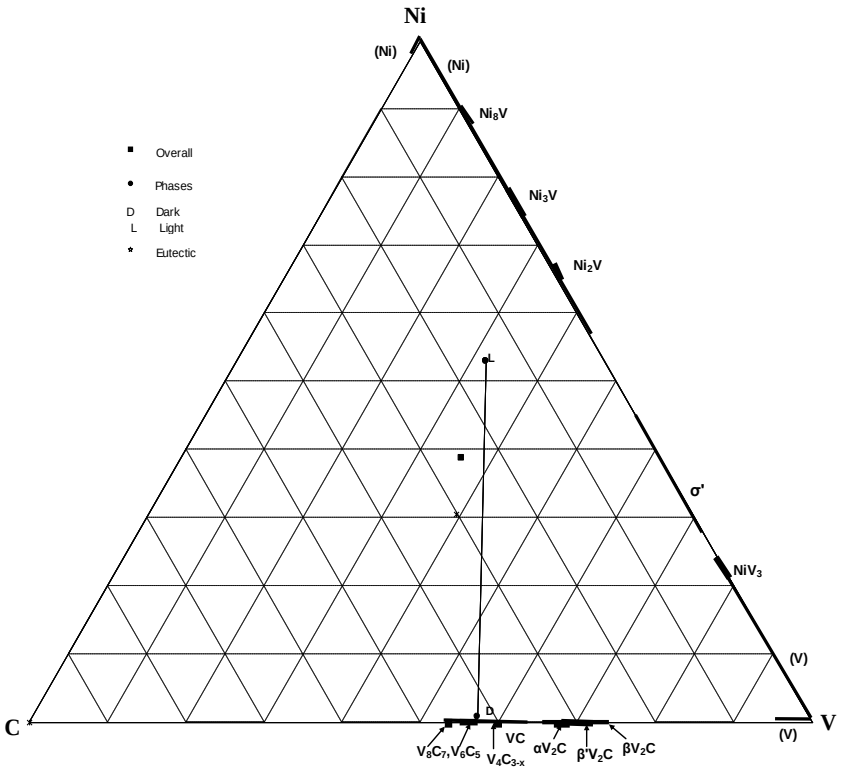


Figure 4.290. EDX analyses of heat treated nominal Ni_{39}:$V_{42.8}$:$C_{18.2}$ (at.%), Sample 21H.

Figures 4.291 to 4.295 show the XRD pattern for heat treated Sample 21H, which was similar to as-cast. The existence of ~V_6C_5, C and ~Ni_2V were confirmed, as shown in Figures 4.295. The matches for the phases with the ICDD were excellent, but there were unidentified peaks at 2θ = 46.43º, 48.54º and 55.42º. ~V_6C_5 had the highest intensity at position 2θ = 48.54º after annealing (Figure 4.295). Table 4.77 shows the identified peaks together with their phases.

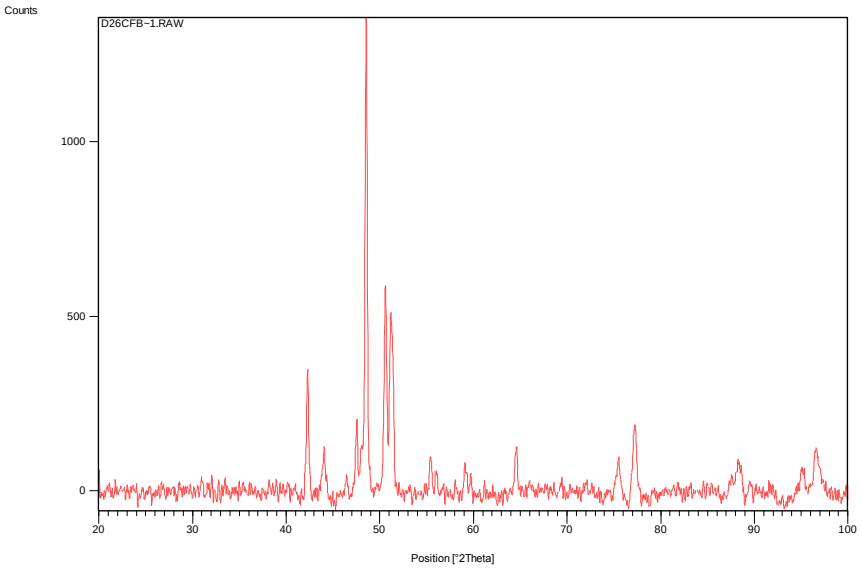


Figure 4.291. Unlabelled XRD pattern of heat treated nominal Ni_{39}:$V_{42.8}$:$C_{18.2}$ (at.%), Sample 21H.

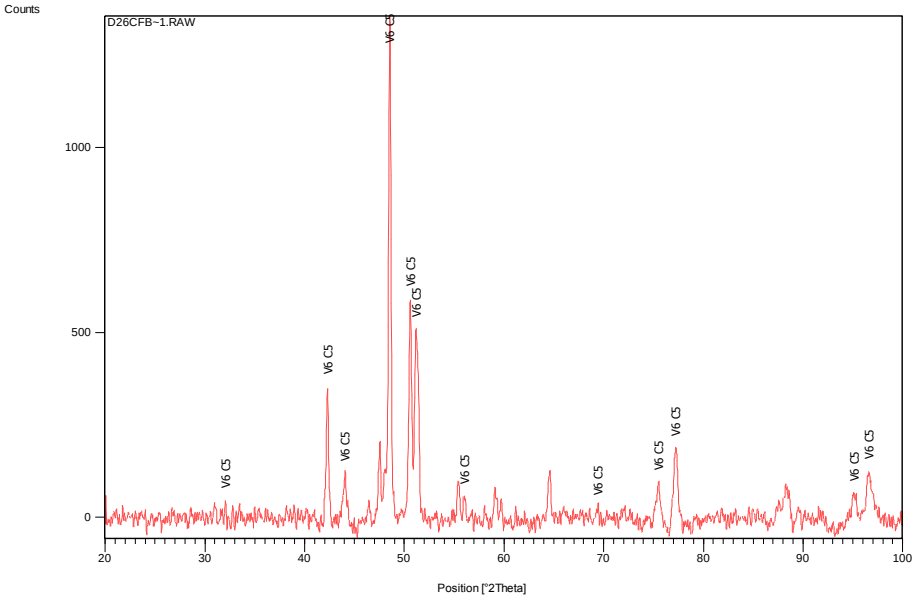


Figure 4.292. XRD pattern of heat treated nominal Ni_{39}:$V_{42.8}$:$C_{18.2}$ (at.%), Sample 21H, showing identified ~V_6C_5 peaks.

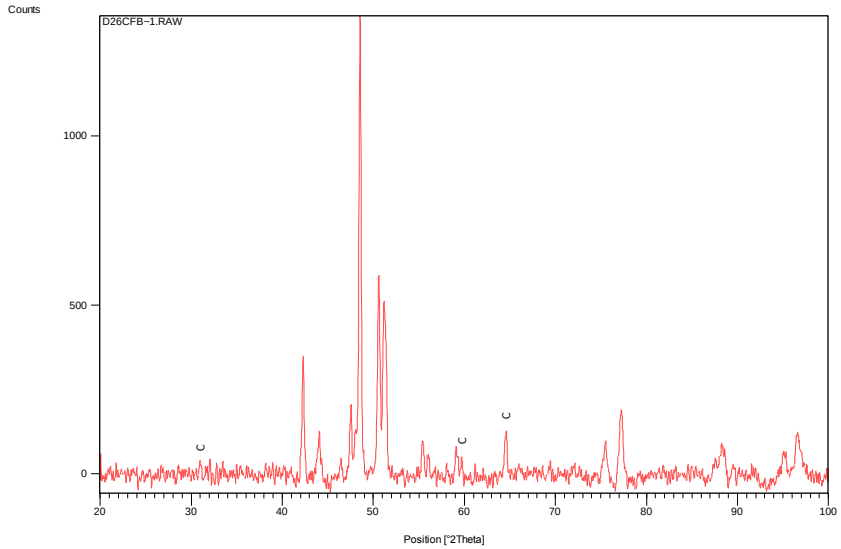


Figure 4.293. XRD pattern of heat treated nominal $Ni_{39}:V_{42.8}:C_{18.2}$ (at.%), Sample 21H, showing identified C peaks.

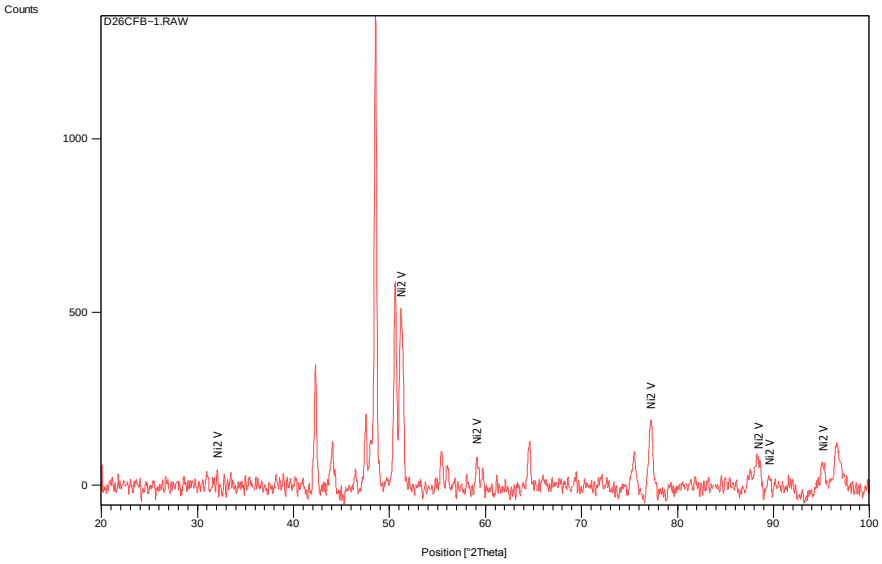


Figure 4.294. XRD pattern of heat treated nominal $Ni_{39}:V_{42.8}:C_{18.2}$ (at.%), Sample 21H, showing identified ~Ni_2V peaks.

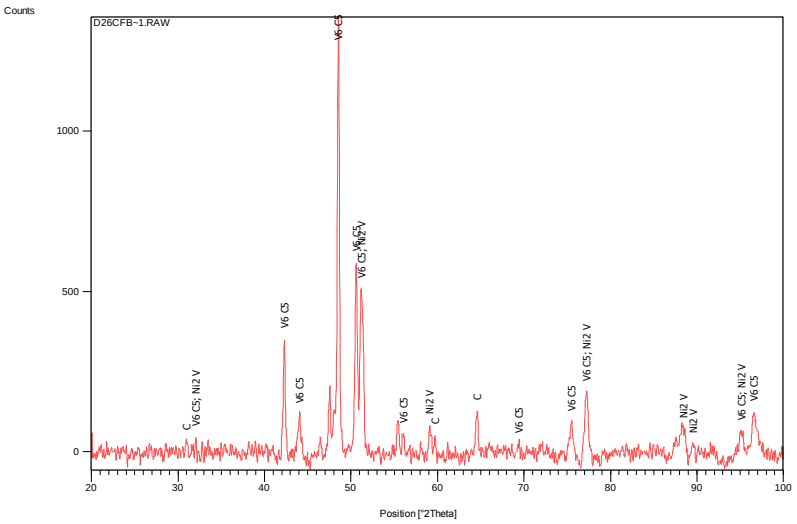


Figure 4.295. XRD pattern of heat treated nominal Ni_{39}:$V_{42.8}$:$C_{18.2}$ (at.%), Sample 21H, showing all the identified peaks.

Table 4.76. XRD peaks for heat treated nominal Ni_{39}:$V_{42.8}$:$C_{18.2}$ (at.%), Sample 21H.

Position 2θ (º)	Height (counts)	Relative Intensity (%)	Phases
31.0044	27.78	2.05	C
32.0772	42.40	3.12	V_6C_5, Ni_2V
42.2934	349.98	25.77	V_6C_5
44.0358	114.64	8.44	V_6C_5
46.4385	39.28	2.89	Unidentified
47.5272	196.11	14.44	Unidentified
48.5449	1358.00	100.00	V_6C_5
50.6001	587.93	43.29	V_6C_5
51.1973	505.99	37.26	V_6C_5, Ni_2V
55.4236	96.47	7.10	Unidentified
56.0205	53.63	3.95	V_6C_5
59.1039	80.82	5.95	Ni_2V
59.7079	48.19	3.55	C
64.5857	122.72	9.04	C
66.0416	16.53	1.22	Unidentified
69.3933	21.55	1.59	V_6C_5
75.4742	90.23	6.64	V_6C_5
77.2230	183.22	13.49	V_6C_5, Ni_2V
88.3949	68.08	5.01	Ni_2V
89.5583	20.13	1.48	Ni_2V
95.1385	61.42	4.52	V_6C_5, Ni_2V
96.5863	119.38	8.79	V_6C_5

4.2.15 Heat treated nominal $Ni_{49}:V_{33.3}:C_{17.7}$ (at.%), Sample 22H

Figures 4.296 and 4.297 show SEM-BSE images of $Ni_{49}:V_{33.3}:C_{17.7}$ (at.%), Sample 22H, in the heat treated condition. The alloy had two different contrasts in the microstructure. There were dark dendrites, which were identified as ~V_8C_7. The light matrix regions were identified as ~Ni_2V. There were eutectics of ~VC + (Ni) and C + ~Ni_2V. The heat treated sample showed very similar microstructures to the as-cast sample (Figures 4.296, and 4.163), with coarsening of the dendrites and the eutectics, which would be expected.

Table 4.78 gives the phase analyses for the alloy, which are shown in Figure 4.298. Comparing Table 4.78 with Table 4.43, it can be seen that there was a slight change in composition after annealing, the ~Ni_2V phase had gained C and Ni and lost V. There was no significant difference between the annealed and as-cast ~V_8C_7 compositions. The deviation of both overall and eutectic compositions from the tie-line joining the two analysed phases was again due to graphite, in the eutectic. The EDX analyses of heat treated Sample 22H are shown in Appendix B38.

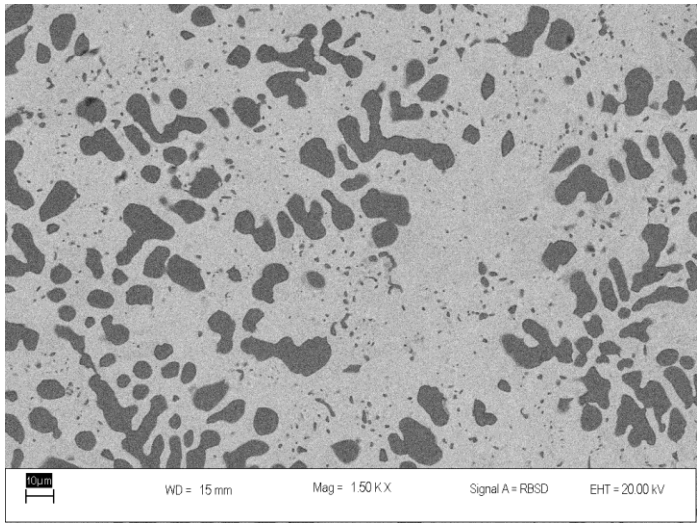


Figure 4.296. BSE-SEM image of heat treated $Ni_{49}:V_{33.3}:C_{17.7}$ (at.%), Sample 22H, showing ~V_8C_7 dendrites (dark), ~Ni_2V matrix (light) and coarsened ~VC + ~N_2V and C + ~Ni_2V eutectics.

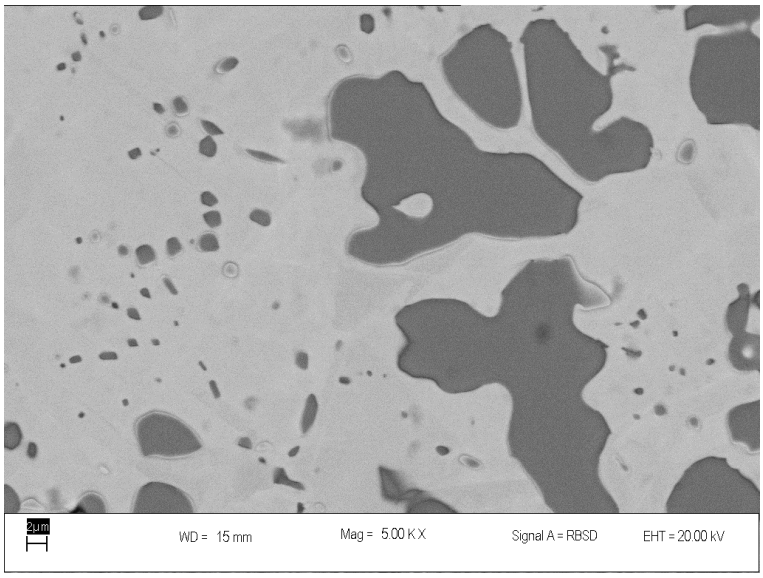


Figure 4.297. BSE-SEM image of heat treated $Ni_{49}:V_{33.3}:C_{17.7}$ (at.%), Sample 22H, showing ~V_8C_7 dendrites (dark), ~Ni_2V matrix (light) and coarsened ~VC + ~Ni_2V and C + ~Ni_2V eutectic at higher magnification.

Table 4.77. EDX phase analyses of annealed nominal $Ni_{49}:V_{33.3}:C_{17.7}$ (at.%), Sample 22H.

Phase Description	C	V	Ni	Phase
Overall	34.0 ± 0.6	30.0 ± 0.4	36.0 ± 0.8	-
Dark	47.7 ± 0.6	51.5 ± 0.6	0.8 ± 0.1	~V_8C_7
Light	21.1 ± 0.8	21.1 ± 0.3	57.8 ± 0.6	~Ni_2V
Eutectics	33.3 ± 1.1	30.8 ± 0.4	35.9 ± 0.7	~VC + ~Ni_2V ~VC + ~Ni_2V

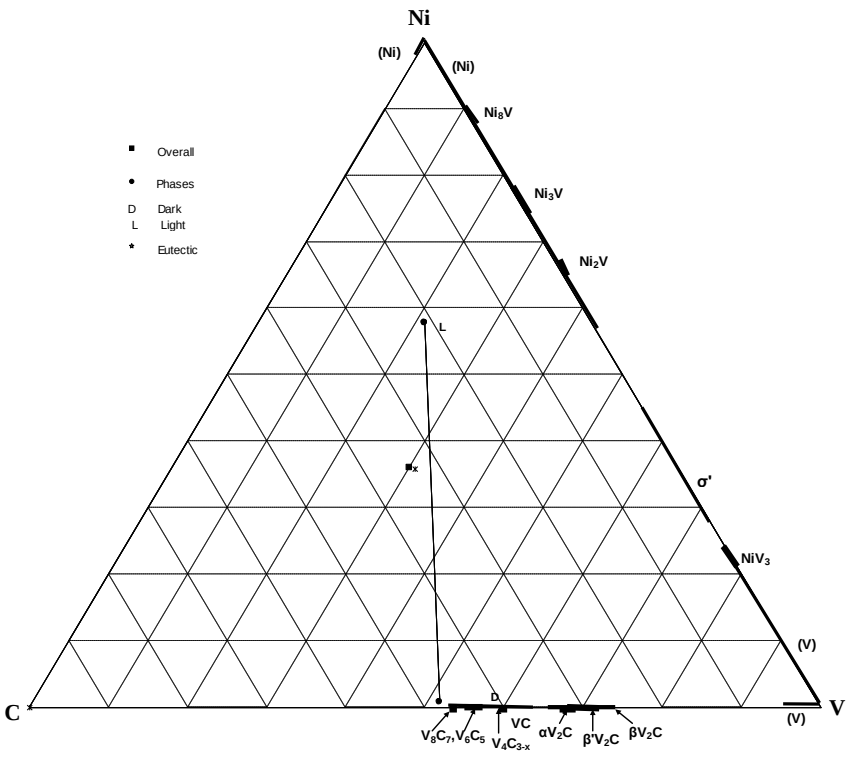


Figure 4.298. EDX analyses of annealed nominal $Ni_{49}:V_{33.3}:C_{17.7}$ (at.%), Sample 22H.

The XRD pattern (Figure 4.303) confirmed the presence of ~V_8C_7, C and Ni_2V. Figures 4.299 to 4.303 shows the experimental pattern of the sample with the database lines for each of the phases and Table 4.79 shows the identified peaks. The highest intensity peak at about $2\theta = 51.42^o$ shows that the peak is an overlapping of the three phases, which was comparable to as-cast sample. The heat treated peaks were much narrower than the as-cast peaks, showing that the phase compositions were closes, even though there was no difference in the EDX errors. On annealing, there was an extra peak at $2\theta = 59.24^o$. All peaks could be matched.

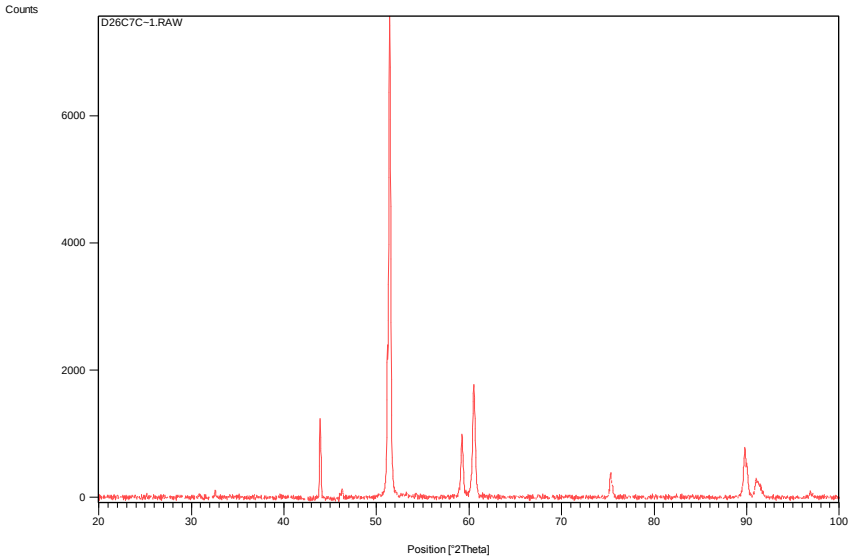


Figure 4.299. Unlabelled XRD pattern of heat treated nominal $Ni_{49}:V_{33.3}:C_{17.7}$ (at.%), Sample 22H.

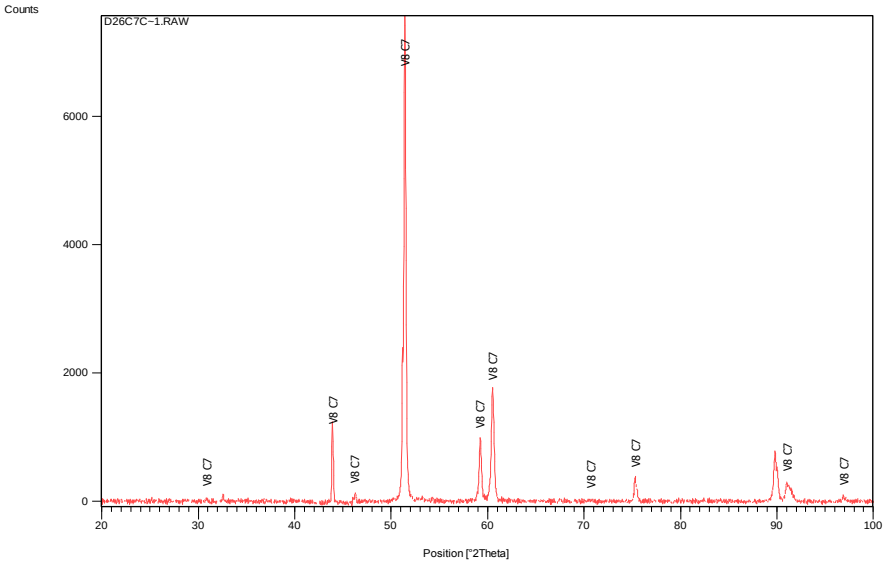


Figure 4.300. XRD pattern of heat treated nominal $Ni_{49}:V_{33.3}:C_{17.7}$ (at.%), Sample 22H, showing identified ~V_8C_7 peaks.

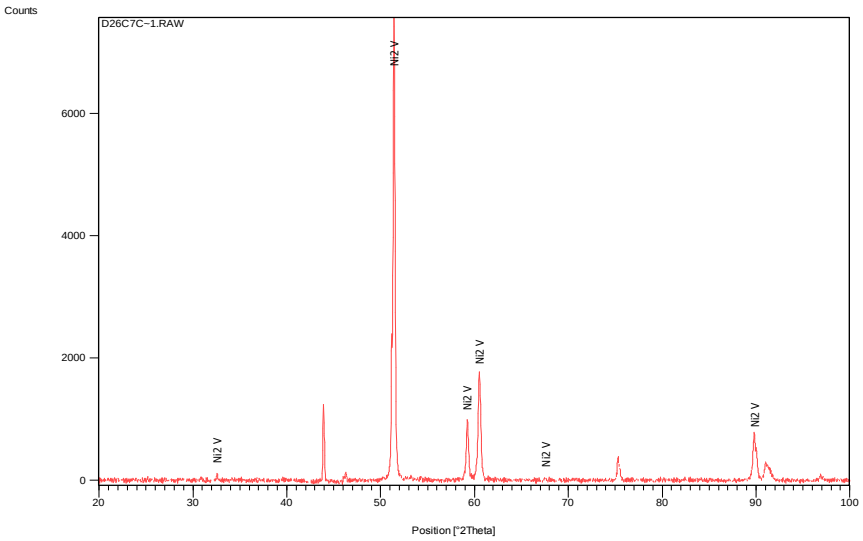


Figure 4.301. XRD pattern of heat treated nominal $Ni_{49}:V_{33.3}:C_{17.7}$ (at.%), Sample 22H, showing identified ~Ni_2V peaks.

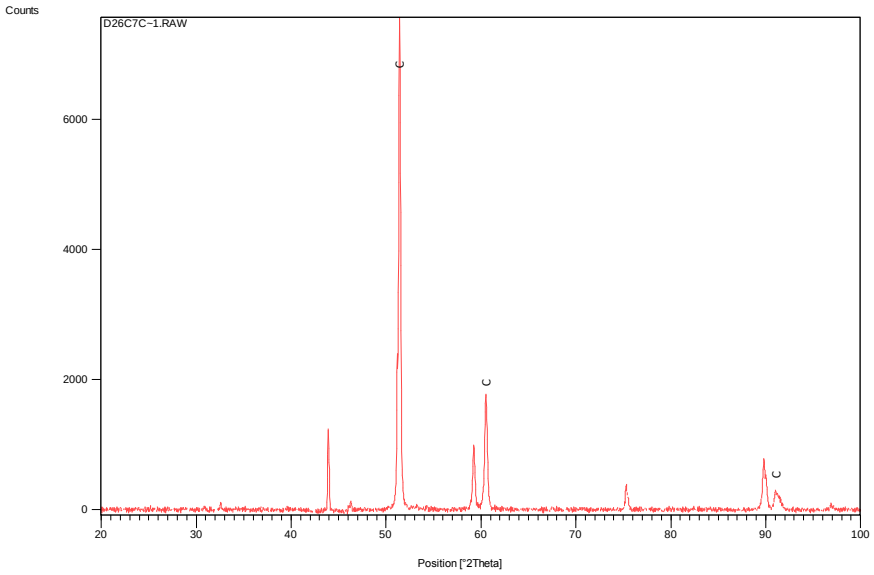


Figure 4.302. XRD pattern of heat treated nominal $Ni_{49}:V_{33.3}:C_{17.7}$ (at.%), Sample 22H, showing identified C peaks.

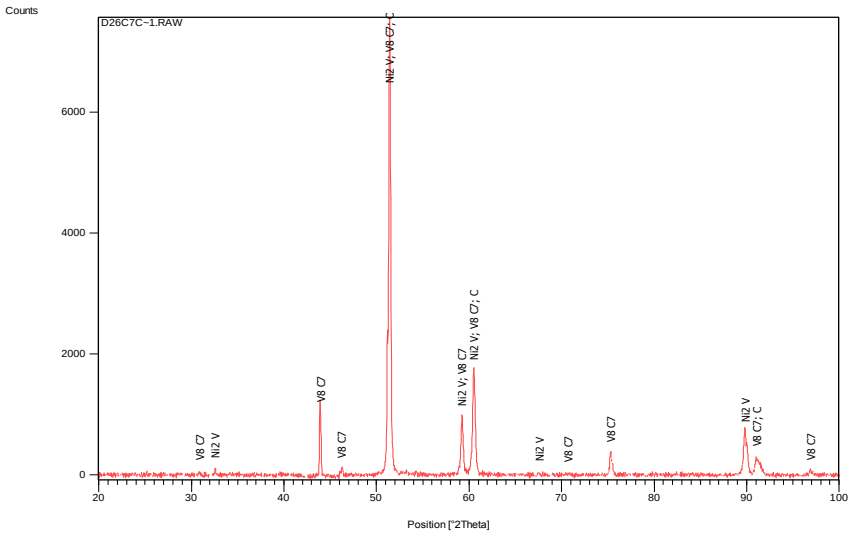


Figure 4.303. XRD pattern of heat treated nominal $Ni_{49}:V_{33.3}:C_{17.7}$ (at.%), Sample 22H, showing all identified peaks.

Table 4.78. XRD peaks for heat treated nominal $Ni_{39}:V_{42.8}:C_{18.2}$ (at.%), Sample 22H.

Position 2θ (º)	Height (counts)	Relative Intensity (%)	Phases
30.8754	37.59	0.57	V_8C_7
32.5521	83.33	1.27	Ni_2V
43.9414	1003.02	15.31	V_8C_7
46.2239	77.62	1.18	V_8C_7
51.4171	6552.92	100.00	V_8C_7, C, Ni_2V
59.2447	932.86	14.24	V_8C_7, Ni_2V
60.5388	1682.98	25.68	V_8C_7, C, Ni_2V
67.6275	20.92	0.32	Ni_2V
70.6771	12.03	0.18	V_8C_7
75.3468	331.71	5.06	V_8C_7
89.8670	661.45	10.09	C
91.0542	270.99	4.14	V_8C_7, C
96.9360	43.01	0.66	Ni_2V

4.2.16 Heat treated nominal $Ni_{22.1}:V_{49.1}:C_{28.8}$ (at.%), Sample 24H

The SEM-BSE images of heat treated nominal $Ni_{22.1}:V_{49.1}:C_{28.8}$ (at.%), Sample 24H, at low and higher magnifications are shown in Figures 4.304 and 4.305. The microstructure in the annealed condition was very different from the as-cast condition (Figures 4.304 and 4.178).

The alloy had two phases, ~V_8C_7 needles which had coarsened and "rounded" considerably losing the finer needles, and the ~Ni_2V matrix. Some of the ~V_8C_7 had transformed back to ~VC.

Table 4.80 gives the phase analyses which are shown in Figure 4.306. Comparing Table 4.80 with Table 4.47, it can be seen that there were slight changes in composition after annealing: ~Ni_2V had gained C and lost V and gained some Ni. The EDX analyses can be found in Appendix B39.

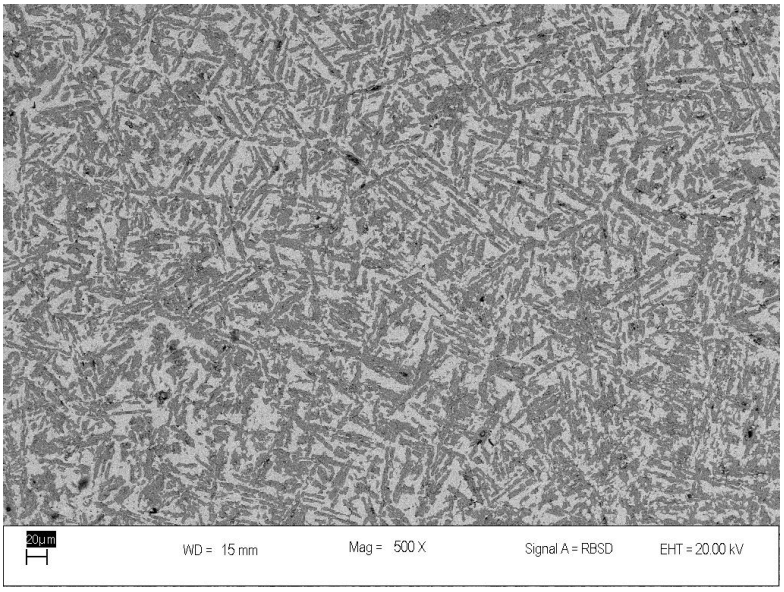


Figure 4.304. BSE-SEM image of heat treated $Ni_{22.1}$:$V_{49.1}$:$C_{28.8}$ (at.%), Sample 24H, showing ~V_8C_7 dendrites (dark) and ~Ni_2V (light).

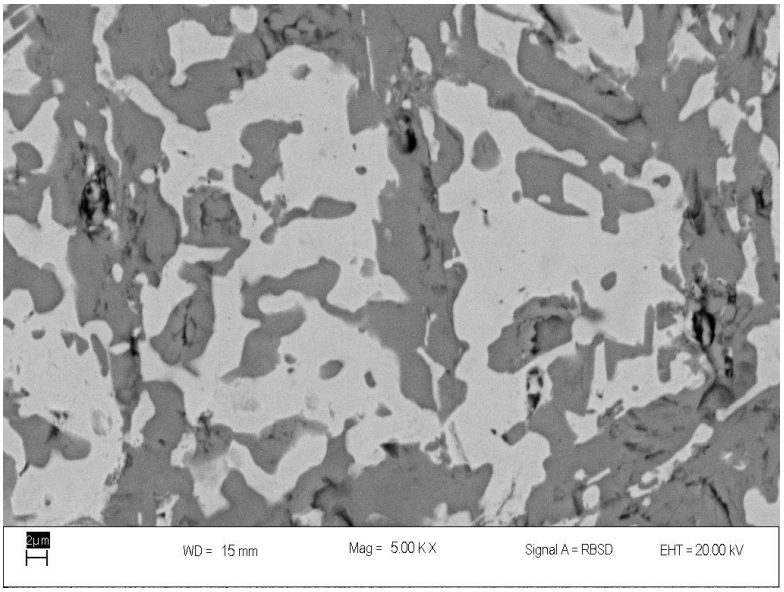


Figure 4.305. BSE-SEM image of heat treated nominal $Ni_{22.1}$:$V_{49.1}$:$C_{28.8}$ (at.%), Sample 24H, showing ~V_8C_7 coarsened needles (dark) and ~Ni_2V matrix (light).

Table 4.79. EDX phase analyses of annealed nominal $Ni_{22.1}$:$V_{49.1}$:$C_{28.8}$ (at.%), Sample 24H.

Phase Description	C	V	Ni	Phase
Overall	35.4 ± 0.5	45.6 ± 1.2	19.0 ± 1.0	-
Dark	45.8 ± 0.5	53.8 ± 0.5	0.4 ± 0.1	~V_8C_7
Light	16.9 ± 0.9	20.5 ± 0.4	62.6 ± 0.7	~Ni_2V

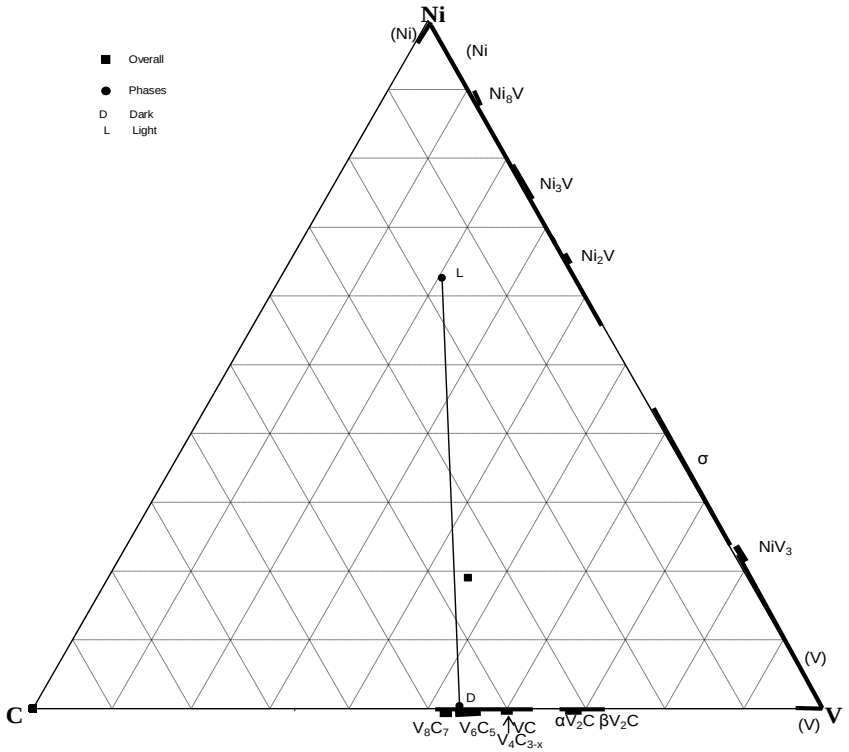


Figure 4.306. EDX analyses of annealed nominal $Ni_{22.1}$:$V_{49.1}$:$C_{28.8}$ (at.%), Sample 24H.

The experimental XRD pattern of the heat treated alloy and the identified peaks for each phase are shown in Figures 4.307 to 4.311 and Table 4.81. The pattern was reasonable with a good signal:background ratio. The highest intensity peak was ~VC at about $2\theta = 48.50^{o}$. The pattern (Figure 4.311) confirmed the presence of ~V_8C_7, ~Ni_2V and ~VC. The pattern was slightly different from that of the as-cast sample, mainly with different peak intensities other than different peaks; all the peaks could be matched.

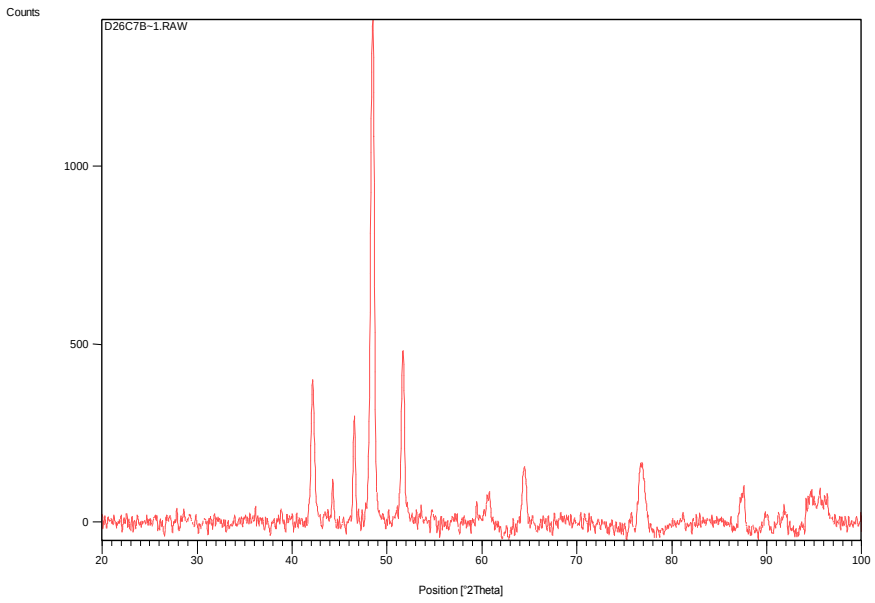


Figure 4.307. Unlabelled XRD pattern of heat treated nominal $Ni_{22.1}$:$V_{49.1}$:$C_{28.8}$ (at.%), Sample 24H.

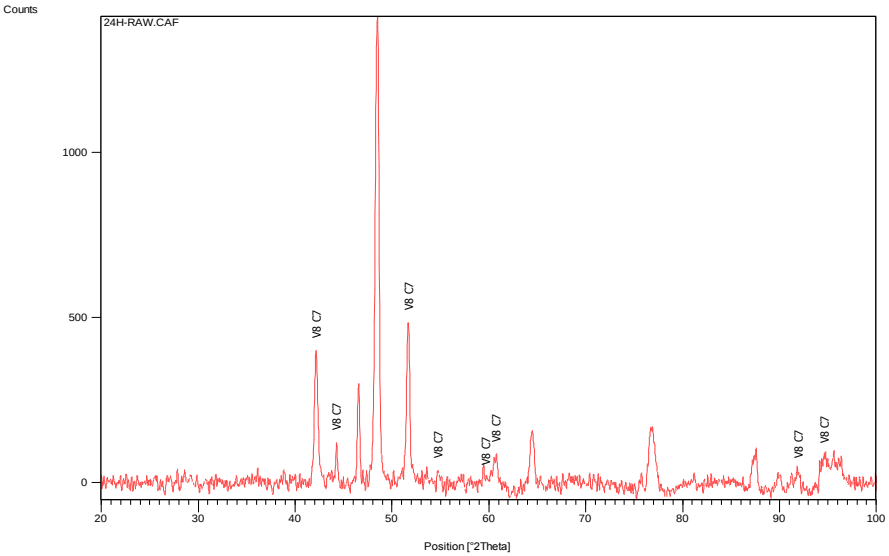


Figure 4.308. XRD pattern of heat treated nominal $Ni_{22.1}$:$V_{49.1}$:$C_{28.8}$ (at.%), Sample 24H, showing identified ~V_8C_7 peaks.

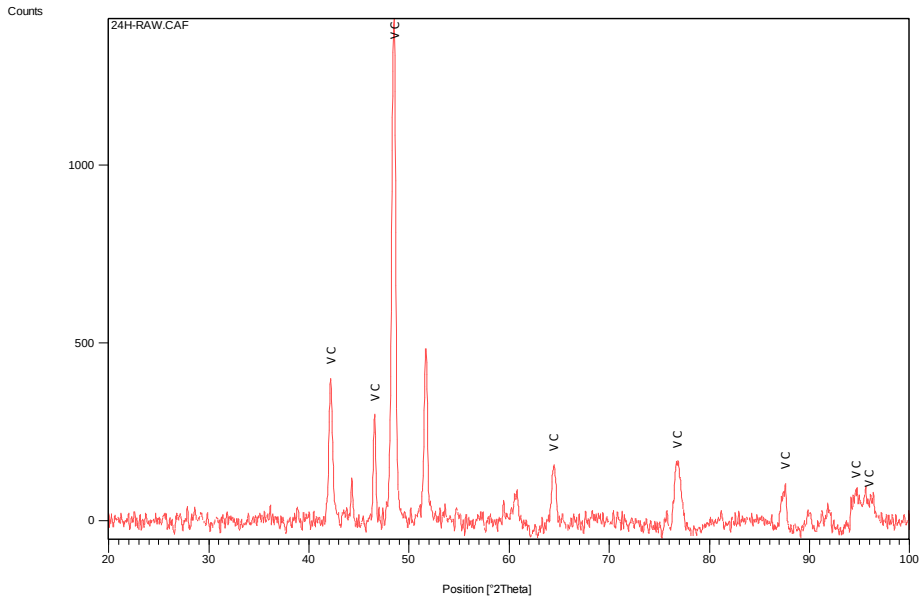


Figure 4.309. XRD pattern of heat treated nominal $Ni_{22.1}$:$V_{49.1}$:$C_{28.8}$ (at.%), Sample 24H, showing identified ~VC peaks.

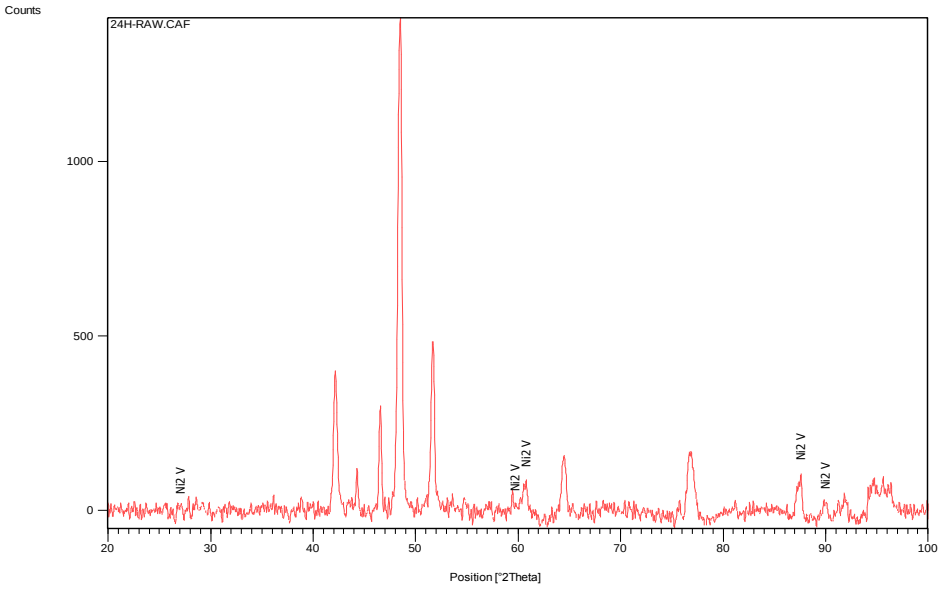


Figure 4.310. XRD pattern of heat treated nominal $Ni_{22.1}$:$V_{49.1}$:$C_{28.8}$ (at.%), Sample 24H, showing identified ~Ni_2V peaks.

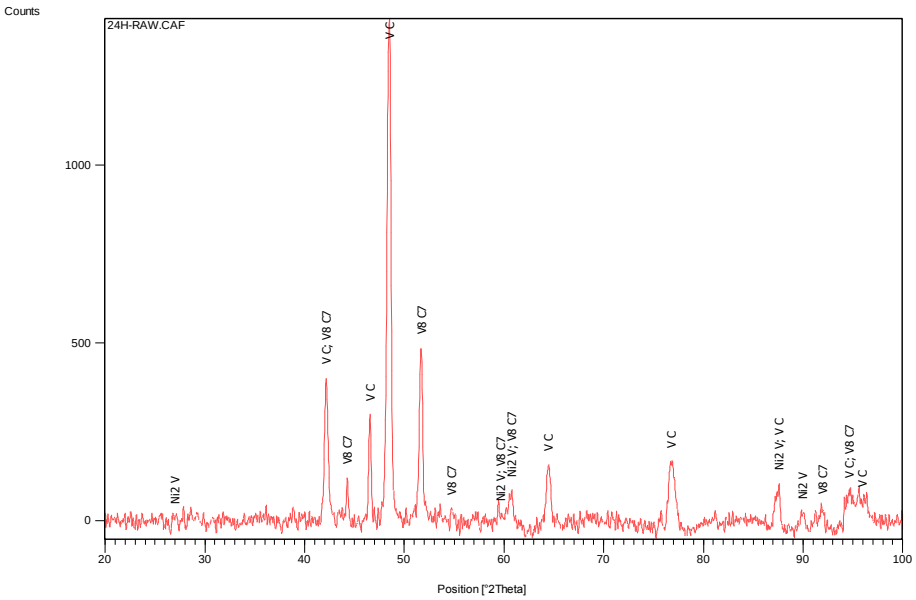


Figure 4.311. XRD pattern of heat treated nominal $Ni_{22.1}$:$V_{49.1}$:$C_{28.8}$ (at.%), Sample 24H, showing all the identified peaks.

Table 4.80. XRD peaks for heat treated nominal $Ni_{22.1}$:$V_{49.1}$:$C_{28.8}$ (at.%), Sample 24H.

Position 2θ (º)	Height (counts)	Relative Intensity (%)	Phases
26.9787	6.69	0.47	Ni_2V
42.1657	398.31	28.17	V_8C_7, VC
44.2848	119.12	8.42	V_8C_7
46.5570	295.00	20.86	VC
48.5032	1414.05	100.00	VC
51.6748	480.09	33.95	V_8C_7
54.7608	31.35	2.22	V_8C_7
59.6316	3.60	0.25	V_8C_7, Ni_2V
60.7761	79.24	5.60	V_8C_7, Ni_2V
64.4507	154.85	10.95	VC
76.7982	162.82	11.51	VC
87.5793	103.87	7.35	VC, Ni_2V
89.9521	21.23	1.50	Ni_2V
91.9420	26.47	1.87	V_8C_7
94.6560	78.69	5.56	V_8C_7, VC
95.8966	51.34	3.63	VC

4.3 Mechanical properties

4.3.1 Hardness test results

Vickers macrohardness tests were carried out on both as-cast and heat treated Ni-C-V alloys. As stated in Section 4.2, hardness tests were not carried out on the following samples: as-cast Sample 16 and heat treated Samples 1H to 5H, which was due to the reaction of the unsealed samples with their boats and Sample 23H which was contaminated by titanium.

4.3.1.1 Hardness results of as-cast specimen

The results of the Vickers macrohardnesses are presented in Table 4.82. All the samples with cracks had their cracks propagated transversely in the microstructure except Samples 1 and 2 which propagated mainly in light phases (Ni_3V, Ni_2V). Samples 19 to 24 with nominal compositions: $Ni_{68}:V_{14}:C_{18}$, $Ni_{59}:V_{27.2}:C_{13.8}$, $Ni_{39}:V_{42.8}:C_{18.2}$, $Ni_{39}:V_{42.8}:C_{18.2}$, $Ni_{24}:V_{58.6}:C_{17.4}$ and $Ni_{22.1}:V_{49.1}:C_{28.8}$ (at.%), had been previously selected for wear tests. Samples 19 to 22 were found to be ductile with no cracks, whereas Samples 23 and 24 were found to be hard and brittle. The hardness indenter that was used was blunt (a new one was unfortunately unavailable), and could have compromised the samples by giving more cracks. Some of the samples were not totally flat (Samples 9, 15) led to out of focus on the sample. Both of these would have made the less valid.

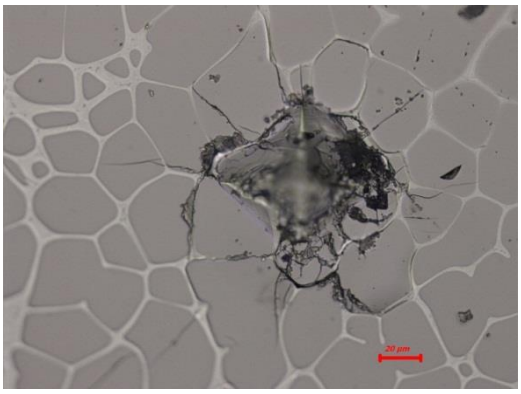
4.3.1.2 Toughness

Figures 4.312 showed the hardness indentations with different slip modes. Cracking around an indentation is an indication of brittleness, while the slip mode around the indentations shows whether the alloy has reasonable toughness (planar slip) or better resistance against cracking (wavy slip) [1988Die]. Cracks were seen in the specimen.

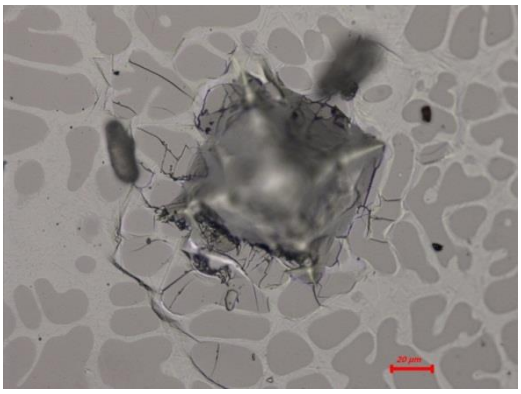
As-cast nominal Samples 5, 8 and 18 with nominal compositions: $Ni_{53}:V_{37}:C_{10}$, $Ni_{60}:V_{30}:C_{10}$ and $Ni_{66.4}:V_{16.1}:C_{17.5}$ (at.%) showed wavy slip, indicating plastic deformation (Figure 4.312). Planar slip was observed in as-cast nominal compositions: $Ni_{24}:V_{50}:C_{26}$, $Ni_{40}:V_{50}:C_{10}$, $Ni_{64}:V_{25}:C_{11}$, $Ni_{70}:V_{10}:C_{20}$, $Ni_{10}:V_{80}:C_{10}$, $Ni_{5}:V_{75}:C_{20}$, $Ni_{68}:V_{14}:C_{18}$, $Ni_{59}:V_{27.2}:C_{13.8}$, $Ni_{39}:V_{42.8}:C_{18.2}$ and $Ni_{49}:V_{33.3}:C_{17.7}$ (at.%) (Samples 3, 4, 6, 7, 11, 12, 19, 20, 21 and 22), indicating reasonable toughness (Figure 4.312).

Table 4.81. Macrohardness measurements of as-cast ternary Ni-C-V alloys using a 5kg load.

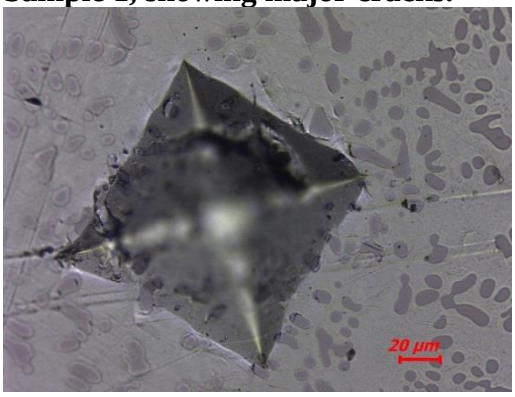
Sample no	Alloy composition (at.%)	Hardness (HV_5)	Phases	Cracks?	Ductile/ Brittle
1	$Ni_{10}:V_{50}:C_{40}$	1575 ± 66	~V_6C_5, ~Ni_3V, C	Cracks	Brittle
2	$Ni_{20}:V_{40}:C_{40}$	646 ± 92	~V_8C_7,(Ni), C	Cracks	Brittle
3	$Ni_{24}:V_{50}:C_{26}$	732 ± 80	~V_6C_5, ~Ni_2V, C, ~$V_4C_{2.66}$	No cracks	Ductile
4	$Ni_{40}:V_{50}:C_{10}$	533 ± 27	~VC, ~Ni_2V, ~$V_4C_{2.66}$	No cracks	Ductile
5	$Ni_{53}:V_{37}:C_{10}$	579 ± 80	~V_6C_5, ~Ni_2V	No cracks	Ductile
6	$Ni_{64}:V_{25}:C_{11}$	686 ± 46	~V_8C_7,~Ni_3V	No cracks	Ductile
7	$Ni_{70}:V_{10}:C_{20}$	211 ± 27	~V_8C_7, (Ni), C	No cracks	Ductile
8	$Ni_{60}:V_{30}:C_{10}$	687 ± 19	~V_8C_7,~Ni_2V	No cracks	Ductile
9	$Ni_{30}:V_{65}:C_5$	378 ± 25	~VC, σ′, ~$V_4C_{2.66}$	Cracks	Brittle
10	$Ni_{20}:V_{35}:C_{45}$	702 ± 81	~V_8C_7, (Ni), C	Cracks	Brittle
11	$Ni_{10}:V_{80}:C_{10}$	536 ± 48	(V), ~VC, ~$V_4C_{2.66}$	No cracks	Ductile
12	$Ni_5:V_{75}:C_{20}$	556 ± 21	(V), ~VC, ~V_2C	No cracks	Ductile
13	$Ni_{14}:V_{64}:C_{22}$	734 ± 27	(Ni), ~VC, ~$V_4C_{2.66}$	Minor cracks	Slightly brittle
14	$Ni_{28}:V_{54}:C_{18}$	1086 ± 86	~VC, σ′, ~$V_4C_{2.66}$	Cracks	Brittle
15	$Ni_{32}:V_{56}:C_{12}$	1093 ± 65	~V_8C_7, σ′, ~$V_4C_{2.66}$	Cracks	Brittle
17	$Ni_{39}:V_{42.8}:C_{18.2}$	624 ± 30	~V_6C_5, ~$V_4C_{2.66}$, ~Ni_2V	Minor cracks	Slightly brittle
18	$Ni_{66.4}:V_{16.1}:C_{17.5}$	275 ± 74	~V_8C_7, ~$V_4C_{2.66}$, (Ni), C	No cracks	Ductile
19	$Ni_{68}:V_{14}:C_{18}$	267 ± 8	~V_8C_7, (Ni)	No cracks	Ductile
20	$Ni_{59}:V_{27.2}:C_{13.8}$	402 ± 20	~V_8C_7, (Ni), C	No cracks	Ductile
21	$Ni_{39}:V_{42.8}:C_{18.2}$	490 ± 34	~V_6C_5, C, ~Ni_2V	No cracks	Ductile
22	$Ni_{49}:V_{33.3}:C_{17.7}$	406 ± 20	~V_8C_7, ~Ni_2V, C	No cracks	Ductile
23	$Ni_{24}:V_{58.6}:C_{17.4}$	1065 ± 56	~V_6C_5, σ′, (V)	Cracks	Brittle
24	$Ni_{22.1}:V_{49.1}:C_{28.8}$	1052 ± 114	~V_8C_7, ~$V_4C_{2.66}$, ~Ni_2V	Cracks	Brittle



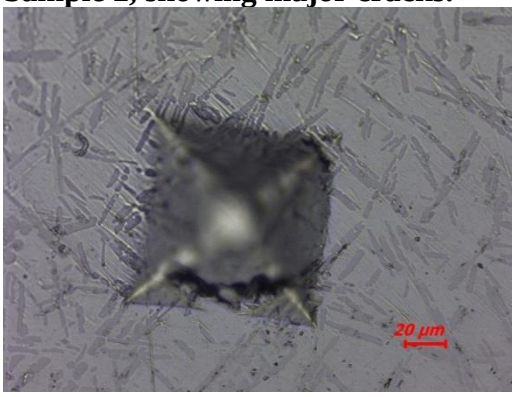
a) As-cast nominal $Ni_{10}:V_{50}:C_{40}$ (at.%), Sample 1, showing major cracks.



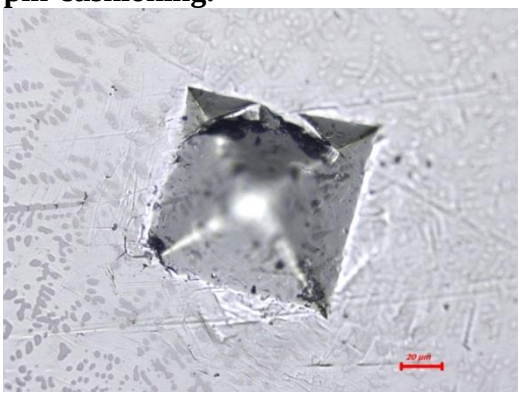
b) As-cast nominal $Ni_{20}:V_{40}:C_{40}$ (at.%), Sample 2, showing major cracks.



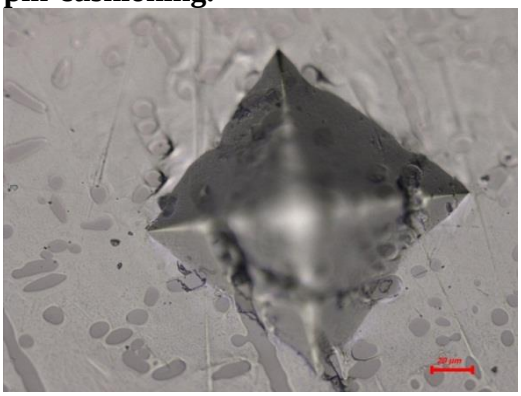
c) As-cast nominal $Ni_{24}:V_{50}:C_{26}$ (at.%) Sample 3, showing planar slip and pin-cushioning.



d) As-cast nominal $Ni_{40}:V_{50}:C_{10}$ (at.%), Sample 4, showing planar slip and slight pin-cushioning.

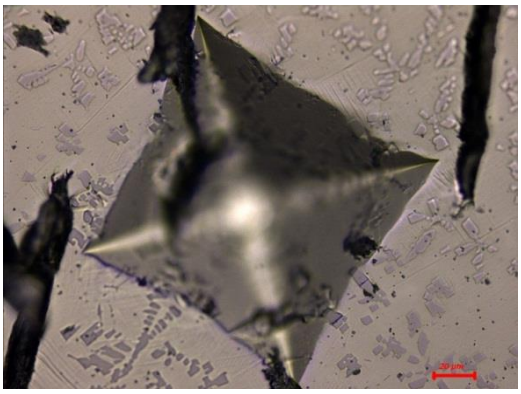


e) As-cast nominal $Ni_{53}:V_{37}:C_{10}$ (at.%), Sample 5, showing planar slip and pin-cushioning.

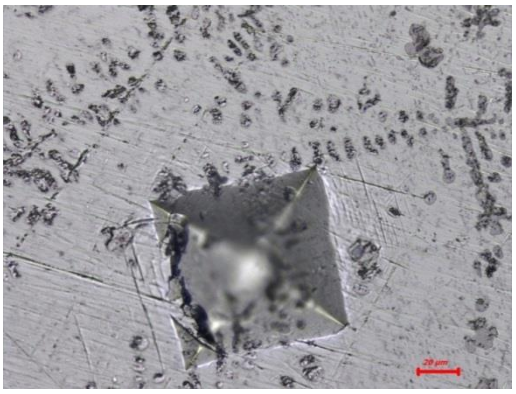


f) As-cast nominal $Ni_{64}:V_{25}:C_{11}$ (at.%), Sample 6, showing planar slip and and pin-cushioning.

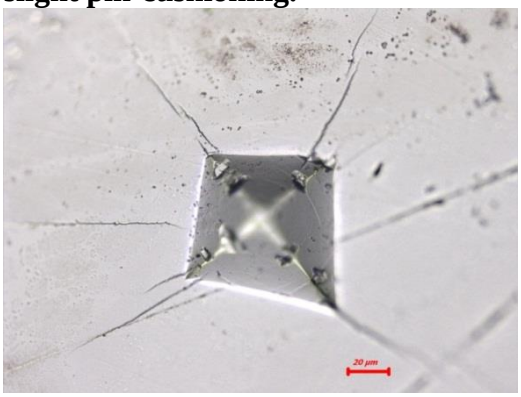
Figure 4.312. Optical micrographs of the macrohardness indentations in the as-cast Ni-V-C samples.



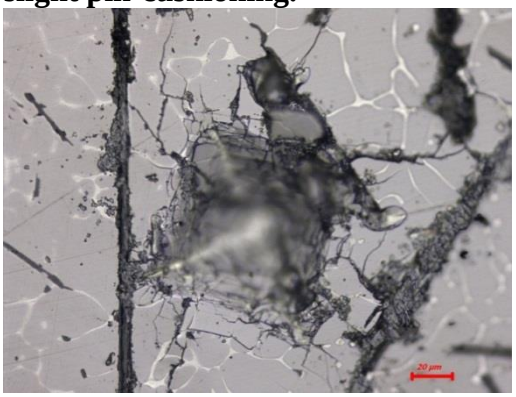
g) As-cast nominal $Ni_{70}:V_{10}:C_{20}$ (at.%), Sample 7, showing planar slip and slight pin-cushioning.



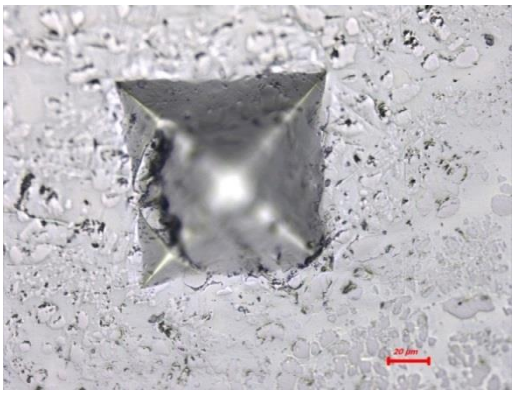
h) As-cast nominal $Ni_{60}:V_{30}:C_{10}$ (at.%), Sample 8, showing wavy slip and slight pin-cushioning.



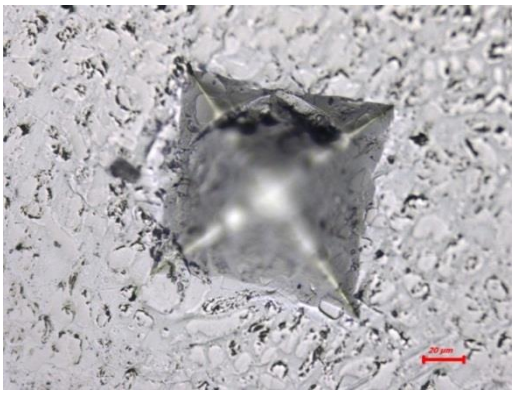
i) As-cast nominal $Ni_{30}:V_{65}:C_{5}$ (at.%), Sample 9, showing major cracks at the corners.



j) As-cast nominal $Ni_{20}:V_{35}:C_{45}$ (at.%), Sample 10, showing major cracking and pin-cushioning.

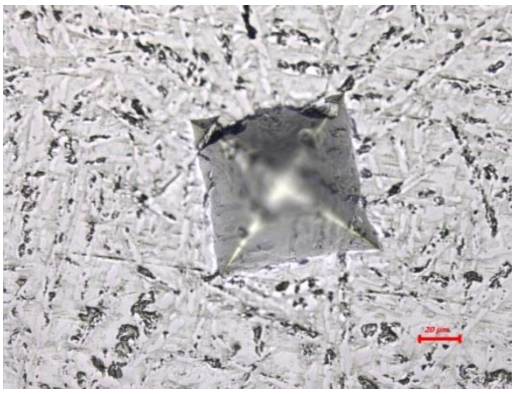


k) As-cast nominal $Ni_{10}:V_{80}:C_{10}$ (at.%), Sample 11, showing planar slip and pin-cushioning.

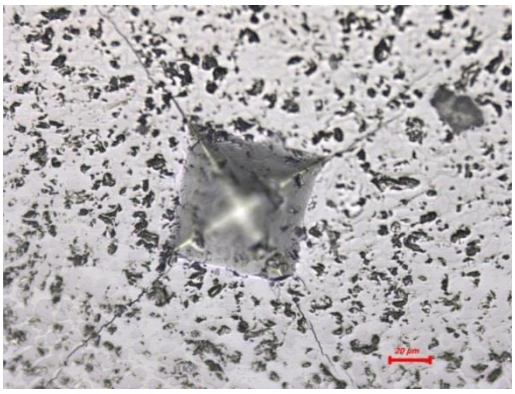


l) As-cast nominal $Ni_{5}:V_{75}:C_{20}$ (at.%), Sample 12, showing planar slip and pin-cushioning.

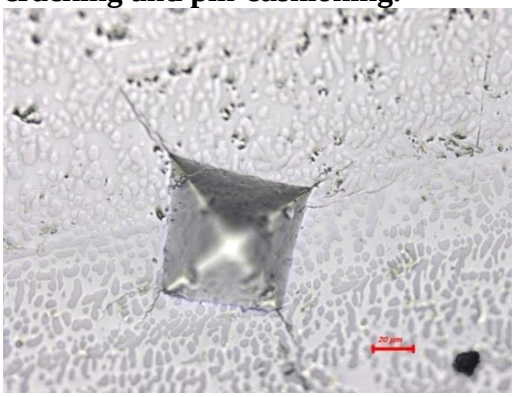
Figure 4.313 (cont.). Optical micrographs of the macrohardness indentations in the as-cast Ni-V-C samples.



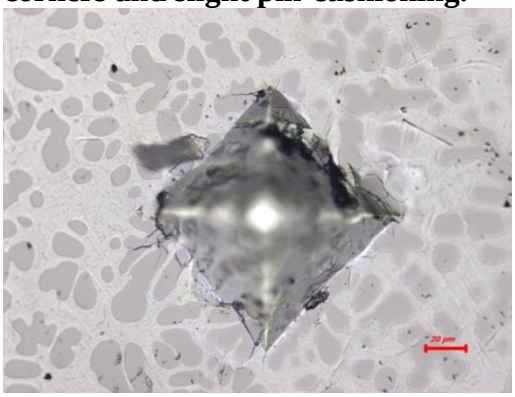
m) As-cast nominal $Ni_{14}:V_{64}:C_{22}$ (at.%), Sample 13, planar slip, minor cracking and pin-cushioning.



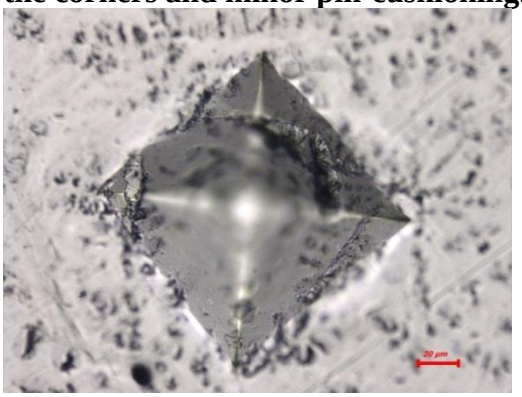
n) As-cast nominal $Ni_{28}:V_{54}:C_{18}$ (at.%), Sample 14, major cracking at the corners and slight pin-cushioning.



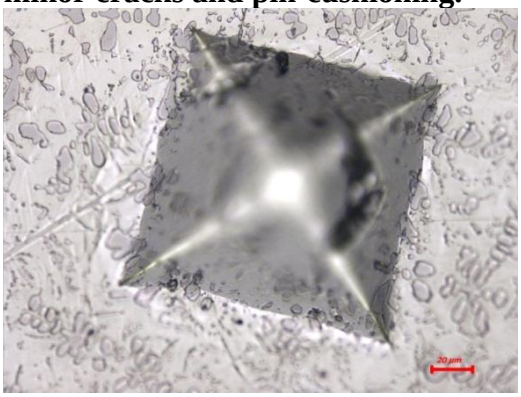
o) As-cast nominal $Ni_{32}:V_{56}:C_{12}$ (at.%), Sample 15, showing cracks at the corners and minor pin-cushioning.



p) As-cast nominal $Ni_{39}:V_{42.8}:C_{18.2}$ (at.%), Sample 17, showing planar slip with minor cracks and pin-cushioning.

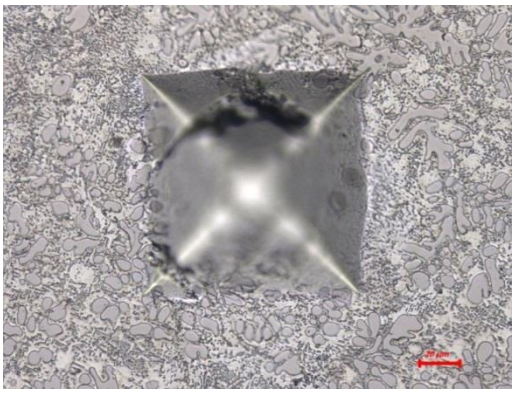


q) As-cast nominal $Ni_{66.4}:V_{16.1}:C_{17.5}$ (at.%), Sample 18, showing wavy slip and pin-cushioning.

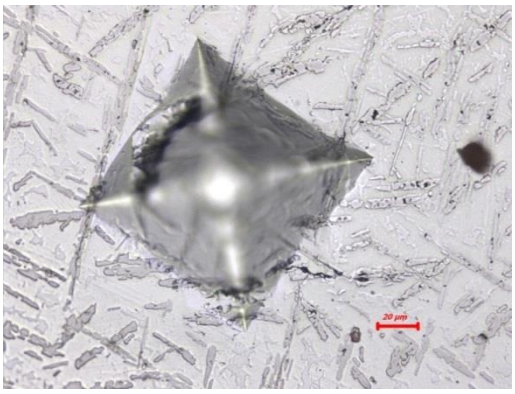


r) As-cast nominal $Ni_{68}:V_{14}:C_{18}$ (at.%), Sample 19, showing planar slip and pin-cushioning.

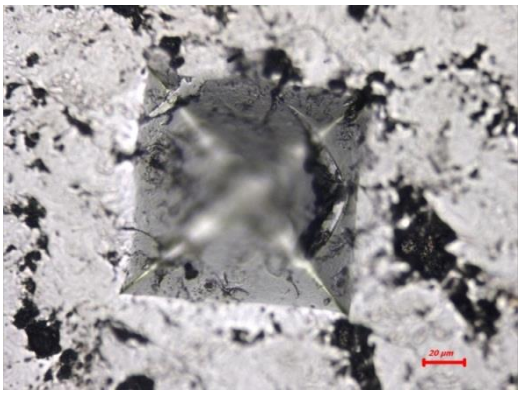
Figure 4.314 (cont.). Optical micrographs of the macrohardness indentations in the as-cast Ni-V-C samples.



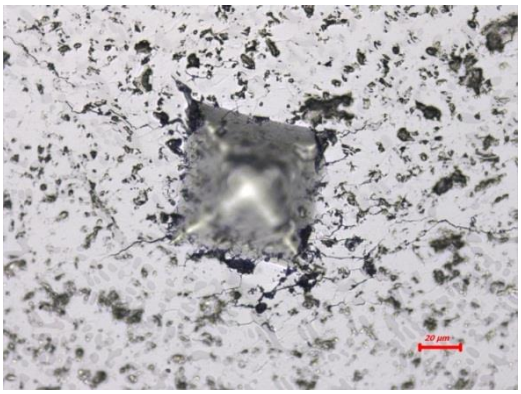
s) As-cast nominal $Ni_{59}:V_{27.2}:C_{13.8}$ (at.%),Sample 20, showing planar slip and barrelling.



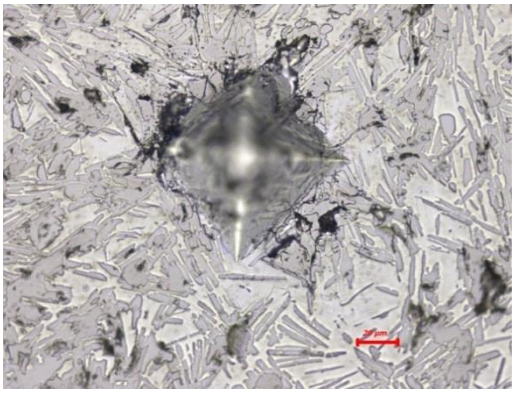
t) As-cast nominal $Ni_{39}:V_{42.8}:C_{18}$ (at.%), Sample 21, showing planar slip and minor pin-cushioning.



u) As-cast nominal $Ni_{49}:V_{33.3}:C_{17.7}$ (at.%), Sample 22, showing planar slip and minor pin-cushioning.



v) As-cast nominal $Ni_{24}:V_{58.6}:C_{17.4}$ (at.%), Sample 23, showing cracking.



w) As-cast nominal $Ni_{22.1}:V_{49.1}:C_{28.8}$ (at.%), Sample 24, showing cracking.

Figure 4.315 (cont.). Optical micrographs of the macrohardness indentations in the as-cast Ni-V-C samples.

Brittleness was observed in nominal compositions: $Ni_{10}:V_{50}:C_{40}$, $Ni_{20}:V_{40}:C_{40}$, $Ni_{30}:V_{65}:C_5$, $Ni_{20}:V_{35}:C_{45}$, $Ni_{28}:V_{54}:C_{18}$, $Ni_{32}:V_{56}:C_{12}$ and $Ni_{24}:V_{58.6}:C_{17.4}$ (at.%), (Samples 1, 2, 9, 10, 14, 15 and 23) by cracks. Propagation of cracks in Samples 1 and 2 was along the light (Ni_3V, Ni_2V) phase.

Nominal compositions: $Ni_{14}:V_{64}:C_{22}$, $Ni_{39}:V_{42.8}:C_{18.2}$ and $Ni_{22.1}:V_{49.1}:C_{28.8}$ (at.%), Samples 13, 17and 24 in as-cast condition showed planar slip behavior with minor cracks.

4.3.1.3 Fracture toughness (K_{IC}), for as-cast samples

Table 4.83 showed the results of the Palmqvist fracture toughness (K_{IC}) of the as-cast Ni-V-C samples. Some alloys had major cracks around the indentations, and this method measures only cracks at corners. If there were more cracks (not just at the corners), then energy was lost, imply minimum reading ($K_{IC} > x$). Highest fracture toughness was with phases (Ni), ~VC, and $\sim V_4C_{2.66}$ and lowest had ~VC, σ′ and $\sim V_4C_{2.66}$

Table 4.82. Palmqvist fracture toughness (MPa√m) values measured from the as-cast Ni-V-C alloys.

Sample no	Alloy composition (at.%)	Fracture toughness (MPa√m)	Phases
1	$Ni_{10}:V_{50}:C_{40}$	4.78 ± 0.1	$\sim V_6C_5$, $\sim Ni_3V$, C
2	$Ni_{20}:V_{40}:C_{40}$	3.00 ± 0.1	$\sim V_8C_7$,(Ni), C
9	$Ni_{30}:V_{65}:C_5$	1.60 ± 0.02	~VC, σ′, $\sim V_4C_{2.66}$
10	$Ni_{20}:V_{35}:C_{45}$	2.68 ± 0.04	$\sim V_8C_7$, (Ni), C
13	$Ni_{14}:V_{64}:C_{22}$	5.22 ± 0.08	(Ni), ~VC, $\sim V_4C_{2.66}$
14	$Ni_{28}:V_{54}:C_{18}$	0.88 ± 0.0	~VC, σ′, $\sim V_4C_{2.66}$
15	$Ni_{32}:V_{56}:C_{12}$	4.05 ± 0.1	$\sim V_8C_7$, σ′, $\sim V_4C_{2.66}$
17	$Ni_{39}:V_{42.8}:C_{18.2}$	5.03 ± 0.2	$\sim V_6C_5$, $\sim V_4C_{52.66}$, $\sim Ni_2V$
23	$Ni_{24}:V_{58.6}:C_{17.4}$	4.03 ± 0.4	$\sim V_6C_5$, σ′, (V)

4.3.1.4 Heat treated hardness test results

The results of the Vickers macrohardness tests carried out on the heat treated Ni-C-V samples are presented in Table 4.84. After the heat treatment, the hardnesses increased, except for Samples 7H and 10H.

Samples 14H and 15H, with sigma phase, still retained the highest hardnesses of 1241 and 1233, respectively, compared to other samples without sigma phase after the heat treatment.

Also, Sample 13 with average hardness value of 734 in the as-cast condition increased to 1266 after annealing and was the highest value. The increment was due to the presence of sigma in the structure after heat treatment.

Samples 6, 7, 8, 12, 18 and 22 still retained their ductility after heat treatment, since there were no cracks before and after heat treatment.

Samples 11 and 17 with minor cracks in the as-cast condition became more cracked in the annealed condition. Figure 4.316 shows the comparison of the hardnesses between the heat treated and as-cast samples.

Micrographs of the hardness indentations of the annealed samples are shown in Figure 4.317. Samples 7H which was not totally flat, 8H, 12H, 18H, and 22H showed planar slip, indicating plastic deformation. Slight brittleness was observed in Samples 11H, 13H, 19H, 20H, and 21H after annealing, as there were minor cracks which were not observed in as-cast condition. The crack in Sample 14H (Figure 4.317 (h)) was not continuous. Also, the cracks in Sample 10H was mainly along the light (Ni) phase.

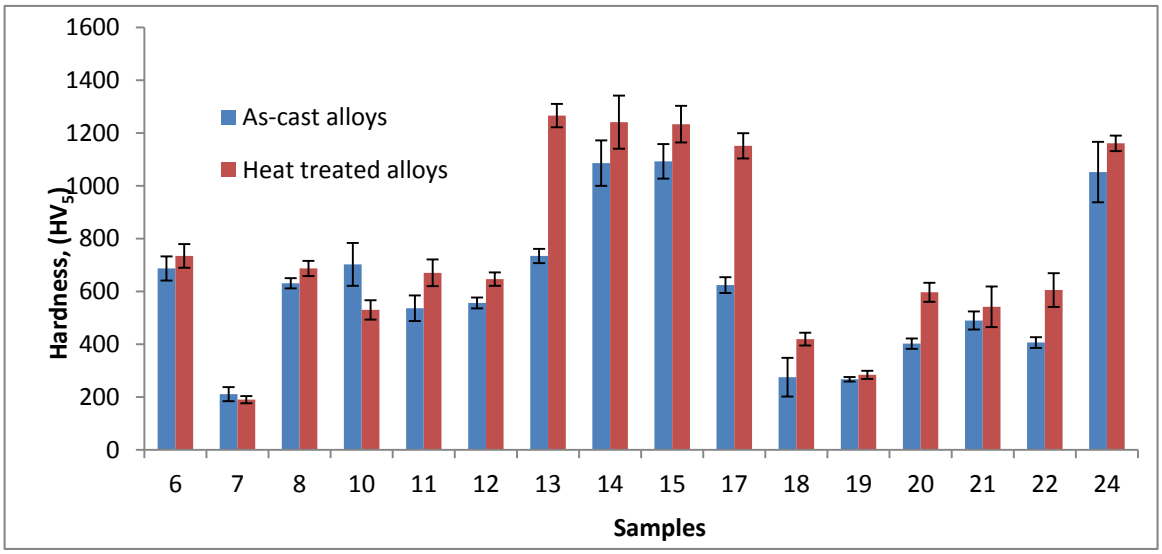
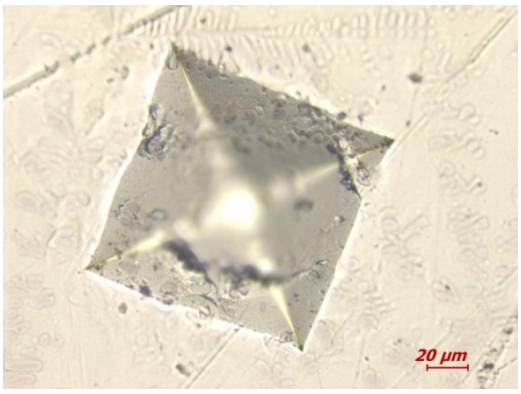


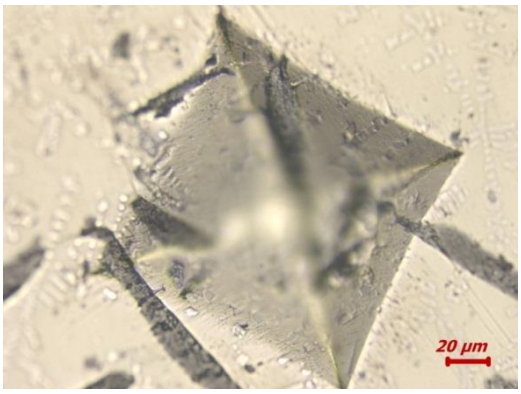
Figure 4.316. Comparison of the hardnesses between the heat treated and as-cast samples.

Table 4.83. Macrohardness measurements of heat treated ternary Ni-C-V alloys using a 5kg load.

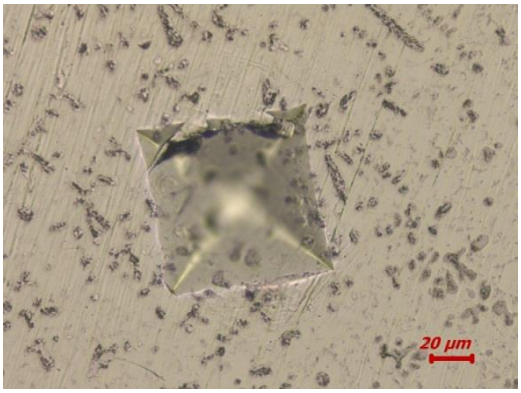
Sample no.	Alloy composition (at.%)	Hardness (HV_5)	Phases	Cracks?	Ductile/Brittle
6	$Ni_{64}:V_{25}:C_{11}$	734 ± 45	~V_8C_7,~Ni_3V	No cracks	Ductile
7	$Ni_{70}:V_{10}:C_{20}$	188 ± 14	~V_8C_7, (Ni), C	No cracks	Ductile
8	$Ni_{60}:V_{30}:C_{10}$	687 ± 29	~V_8C_7,~Ni_2V	No cracks	Ductile
10	$Ni_{20}:V_{35}:C_{45}$	530 ± 37	~V_8C_7, (Ni), C	Cracks	Brittle
11	$Ni_{10}:V_{80}:C_{10}$	670 ± 51	(V), ~VC, ~$V_4C_{2.66}$	Minor cracks	Slightly brittle
12	$Ni_5:V_{75}:C_{20}$	647 ± 26	(V), ~VC, ~V_2C	No cracks	Ductile
13	$Ni_{14}:V_{64}:C_{22}$	1266 ± 44	(Ni), ~VC, σ′, ~$V_4C_{2.66}$	Minor cracks	Slightly brittle
14	$Ni_{28}:V_{54}:C_{18}$	1241 ± 101	~VC, σ′, ~$V_4C_{2.66}$	Cracks	Brittle
15	$Ni_{32}:V_{56}:C_{12}$	1233 ± 70	~V_8C_7, σ′, ~$V_4C_{2.66}$	Cracks	Brittle
17	$Ni_{39}:V_{42.8}:C_{18.2}$	1151 ± 48	~V_6C_5, ~$V_4C_{2.66}$, ~Ni_2V	Cracks	Brittle
18	$Ni_{66.4}:V_{16.1}:C_{17.5}$	419 ±24	~V_8C_7, ~$V_4C_{2.66}$, (Ni), C	No cracks	Ductile
19	$Ni_{68}:V_{14}:C_{18}$	284 ± 15	~V_8C_7, (Ni)	Minor cracks	Slightly brittle
20	$Ni_{59}:V_{27.2}:C_{13.8}$	597 ± 36	~V_8C_7, (Ni), C	Minor cracks	Slightly brittle
21	$Ni_{39}:V_{42.8}:C_{18.2}$	542 ± 77	~V_6C_5, C, ~Ni_2V	Minor cracks	Slightly brittle
22	$Ni_{49}:V_{33.3}:C_{17.7}$	605 ± 54	~V_8C_7, ~Ni_2V, C	No cracks	Ductile
24	$Ni_{22.1}:V_{49.1}:C_{28.8}$	1161 ± 29	~V_8C_7, ~$V_4C_{2.66}$, ~Ni_2V	Minor cracks	Slightly brittle



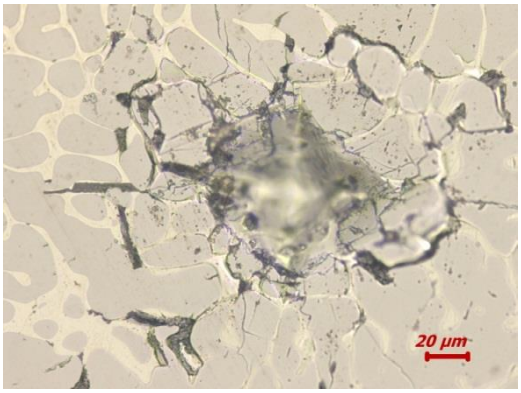
a) Annealed nominal $Ni_{64}:V_{25}:C_{11}$ (at.%), Sample 6H, showing planar slip and slight pin-cushioning.



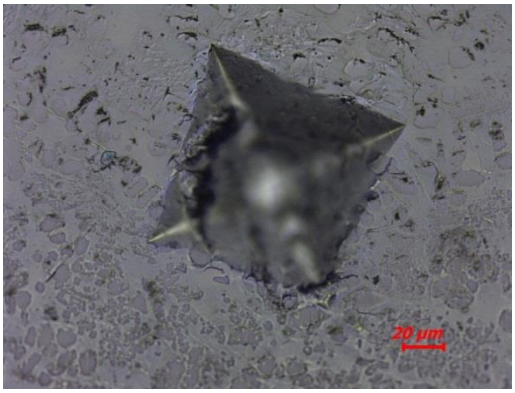
b) Annealed nominal $Ni_{70}:V_{10}:C_{20}$ (at.%), Sample 7H, showing planar slip and pin-cushioning.



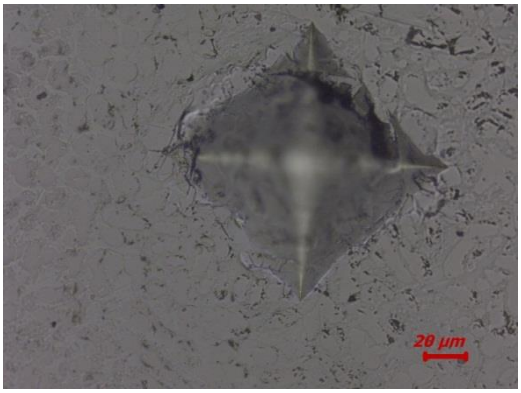
c) Annealed nominal $Ni_{60}:V_{30}:C_{10}$ (at.%),Sample 8H, showing wavy slip and slight pin-cushioning



d) Annealed nominal $Ni_{20}:V_{35}:C_{45}$ (at.%) Sample 10H, showing major cracking along the light phase.

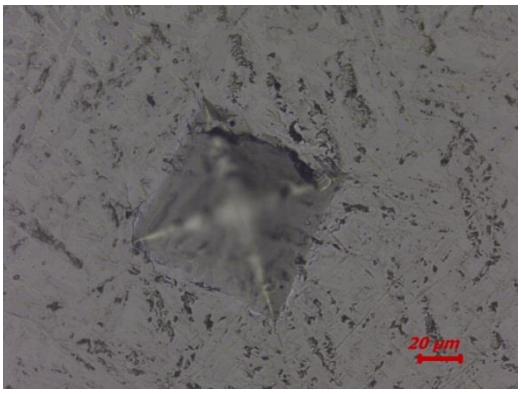


e) Annealed nominal $Ni_{10}:V_{80}:C_{10}$ (at.%), Sample 11H, showing planar slip and pin-cushioning.

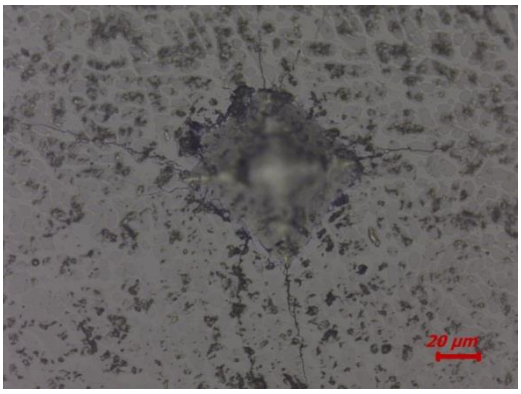


f) Annealed nominal $Ni_{5}:V_{75}:C_{20}$ (at.%), Sample 12H, showing planar slip and slight pin-cushioning.

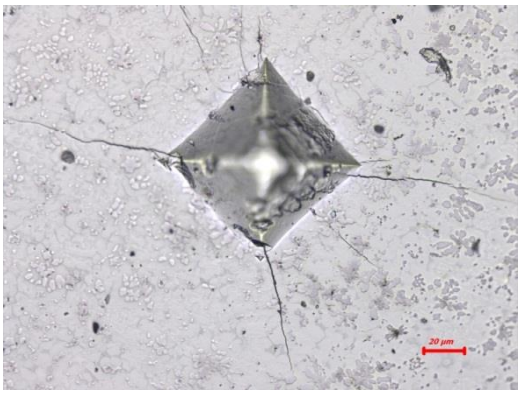
Figure 4.316. Optical micrographs of the macrohardness indentations in the heat treated Ni-V-C samples.



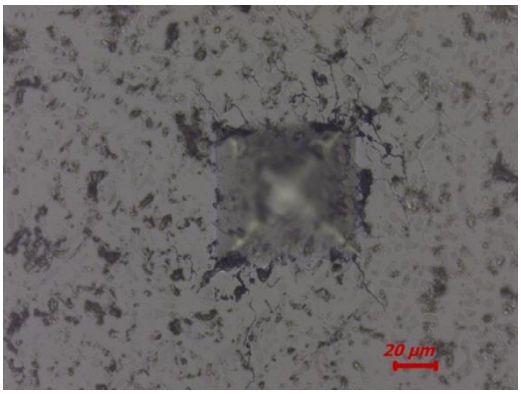
g) Annealed nominal $Ni_{14}:V_{64}:C_{22}$ (at.%), Sample 13H, planar slip, minor cracking and pin-cushioning.



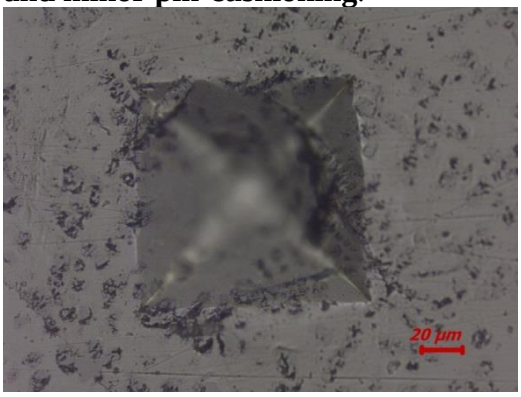
h) Annealed nominal $Ni_{28}:V_{54}:C_{18}$ (at.%), Sample 14H, major cracking and slight pin-cushioning.



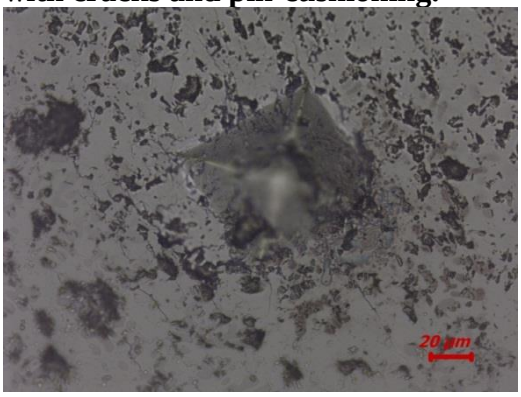
i) Annealed nominal $Ni_{32}:V_{56}:C_{12}$ (at.%), Sample 15H, showing cracking and minor pin-cushioning.



k) Annealed nominal $Ni_{39}:V_{42.8}:C_{18.2}$ (at.%), Sample 17H, showing planar slip with cracks and pin-cushioning.

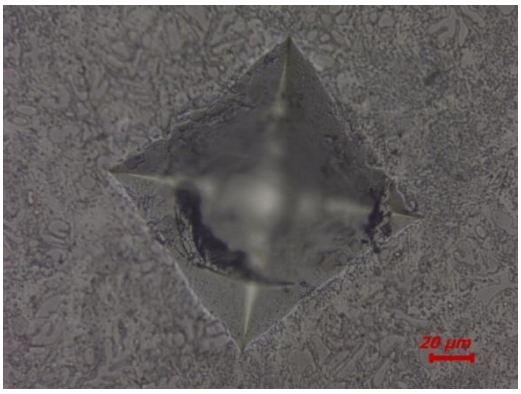


j) Annealed nominal $Ni_{66.4}:V_{16.1}:C_{17.5}$ (at.%), Sample 18H, showing planar slip and pin-cushioning.

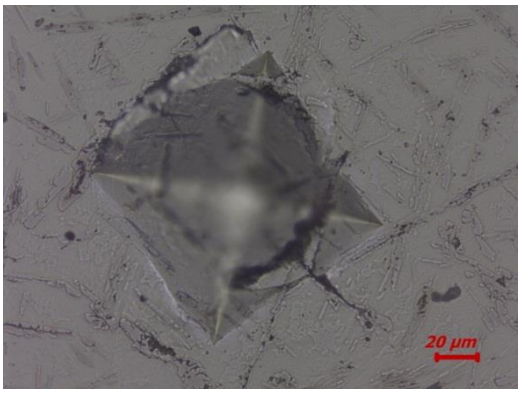


l) Annealed nominal $Ni_{68}:V_{14}:C_{18}$ (at.%), Sample 19H, showing planar slip with cracks and pin-cushioning.

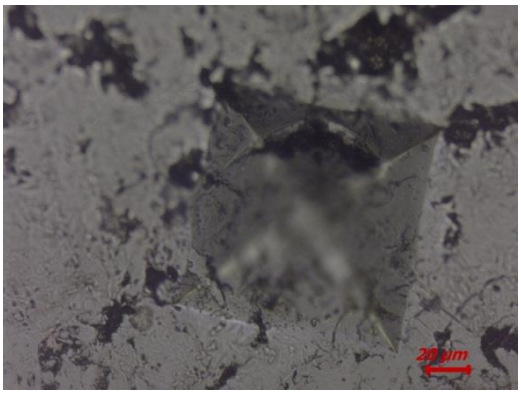
Figure 4.317 (cont.). Optical micrographs of the macrohardness indentations in the heat treated Ni-V-C samples.



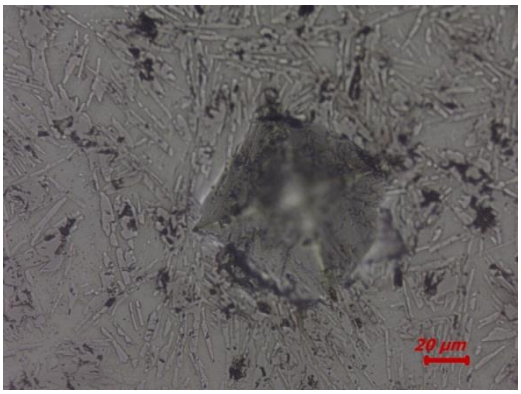
m) Annealed nominal $Ni_{59}:V_{27.2}:C_{13.8}$ (at.%), Sample 20H, showing planar slip and pin-cushioning.



o) Annealed nominal $Ni_{39}:V_{42.8}:C_{18}$ (at.%), Sample 21H, showing planar slip, with minor cracks and pin-cushioning.



n) Annealed nominal $Ni_{49}:V_{33.3}:C_{17.7}$ (at.%), Sample 22H, showing planar slip and minor pin-cushioning.



p) Annealed nominal $Ni_{22.1}:V_{49.1}:C_{28.8}$ at.%), Sample 24H, showing minor cracks.

Figure 4.318 (cont.). Optical micrographs of the macrohardness indentations in the heat treated Ni-V-C samples.

It was interesting to note that "pin-cushioning" of the hardness indentation of the alloy was an anomaly typically observed with annealed material, when metal is sinking in around the faces of the indenter [1988Die]. Also when the crystal structure is complex, without highly close-packed planes and directions, dislocations tend to be immobile. This causes brittleness and high hardness of intermetallic compounds [1988Die].

4.3.1.5 Fracture toughness (K_{IC}) for heat treated samples

Table 4.85 showed the results of the Palmqvist fracture toughness (K_{IC}) of the heat treated Ni-V-C samples. The highest fracture toughness occurred with the (Ni), ~VC, and ~$V_4C_{2.66}$ phases, and lowest had the ~VC, σ′ and ~$V_4C_{2.66}$ phases.

Table 4.84. Palmqvist fracture toughness (MPa√m) values measured from the heat treated Ni-V-C alloys.

Sample no	Alloy composition (at.%)	Fracture toughness (MPa√m)	Phases
10	$Ni_{20}:V_{35}:C_{45}$	2.18 ± 0.1	~V_8C_7, (Ni), C
11	$Ni_{10}:V_{80}:C_{10}$	4.97 ± 1.4	~VC, (V), ~$V_4C_{2.66}$
13	$Ni_{14}:V_{64}:C_{22}$	8.6 ± 0.8	(Ni), ~VC, ~$V_4C_{2.66}$
14	$Ni_{28}:V_{54}:C_{18}$	0.9 ± 0.01	~VC, σ′, ~$V_4C_{2.66}$
15	$Ni_{32}:V_{56}:C_{12}$	3.04 ± 0.1	~V_8C_7, σ′, ~$V_4C_{2.66}$
17	$Ni_{39}:V_{42.8}:C_{18.2}$	5.43 ± 0.04	~V_6C_5, ~$V_4C_{52.66}$, ~Ni_2V
19	$Ni_{68}:V_{14}:C_{18}$	2.79 ± 0.01	~V_8C_7, (Ni)

4.3.2 Sliding wear and friction test results

4.3.2.1 Friction results (as-cast samples) for Samples 19 to 24

Figures 4.320 to 4.325 illustrate the friction curves for Samples 19-24, from sliding tests between pin (Cr steel ball) and as-cast plate specimens.

The friction coefficients of the studied Cr steel ball/VC-Ni tribo-pairs were in the range 0.08 - 0.79. The friction coefficient increased rapidly throughout the first instances of sliding and subsequently decreased. After this initial stage, the variations in the curves became smaller, and the coefficient of friction slightly increased during the remaining testing time. As the wear proceeded further, the wear track became smoother, and the coefficient of friction became steady-state, except for Sample 23 (Figure 4.324), which was more irregular.



Figure 4.319. Friction coefficient evolution with sliding distance for as-cast nominal $Ni_{68}:V_{14}:C_{18}$ (at.%), Sample 19.

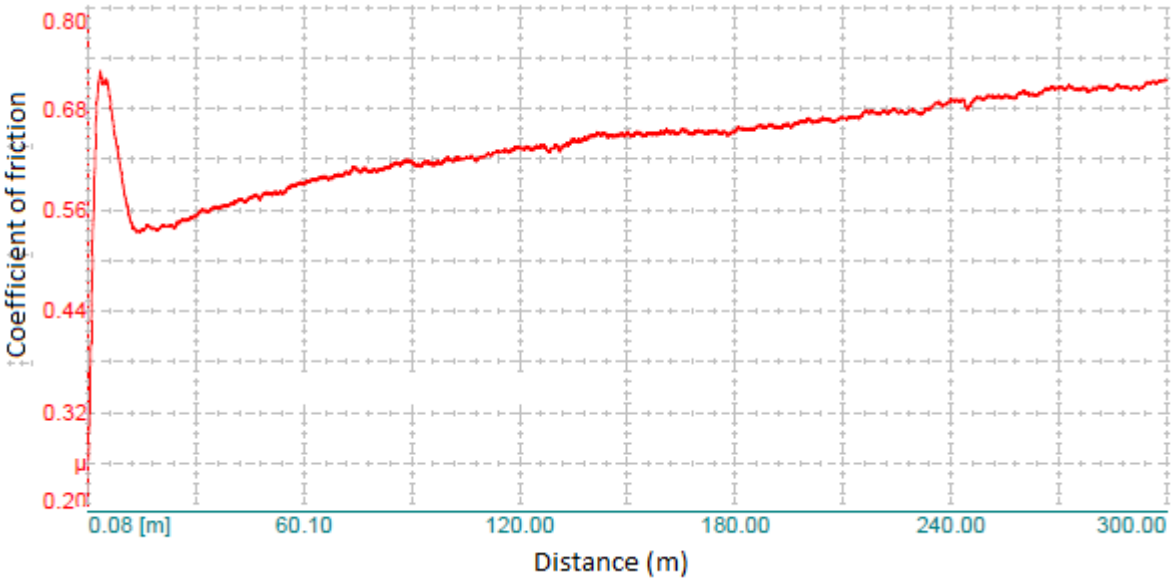


Figure 4.320. Friction coefficient evolution with sliding distance for as-cast nominal $Ni_{59}:V_{27.2}:C_{13.8}$ (at.%), Sample 20.

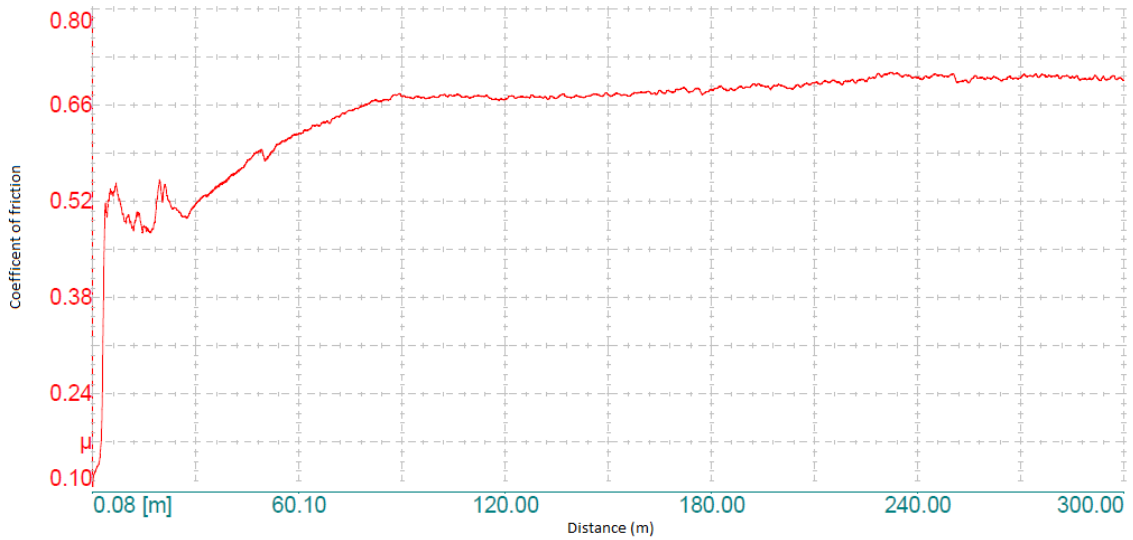


Figure 4.321. Friction coefficient evolution with sliding distance for as-cast nominal $Ni_{39}:V_{42.8}:C_{18.2}$ (at.%), Sample 21.

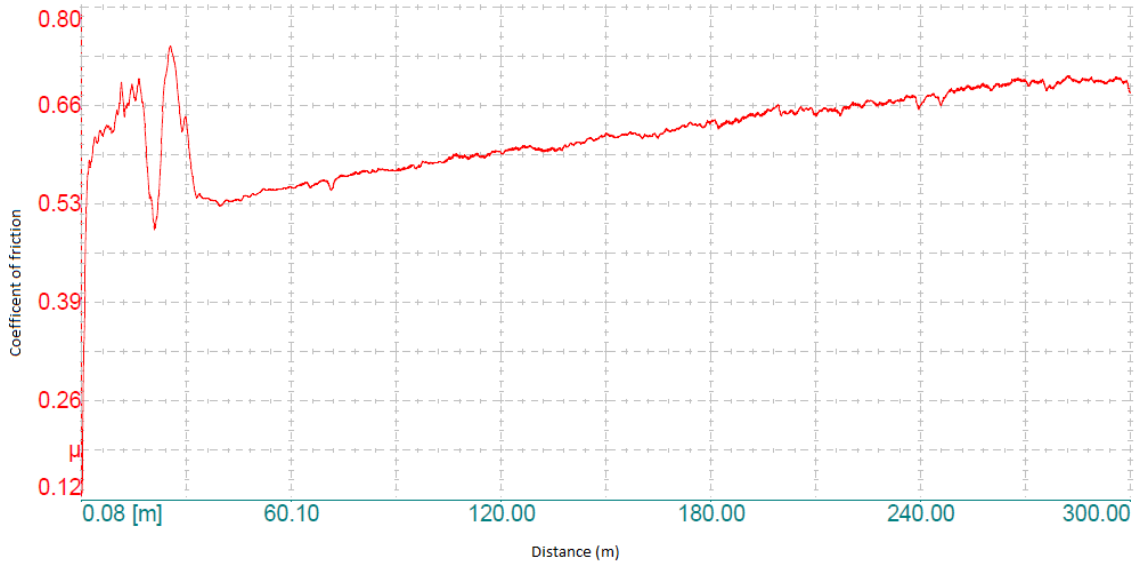


Figure 4.322. Friction coefficient evolution with sliding distance for as-cast nominal $Ni_{49}:V_{33.3}:C_{17.7}$ (at.%), Sample 22.



Figure 4.323. Friction coefficient evolution with sliding distance for as-cast nominal $Ni_{24}:V_{58.6}:C_{17.4}$ (at.%), Sample 23.



Figure 4.324. Friction coefficient evolution with sliding distance for as-cast nominal $Ni_{22.1}:V_{49.1}:C_{28.8}$ (at.%) Sample 24.

The friction responses for Samples 19, 20 and 24 ($Ni_{68}:V_{14}:C_{18}$, $Ni_{59}:V_{27.2}:C_{13.8}$ and $Ni_{22.1}:V_{49.1}:C_{28.8}$ (at.%),) paired with chromium steel ball were similar. During the running-in period, the friction increased to a maximum, after which it decreased and levelled off at a lower level.

Samples 21 and 22 (Ni_{39}:$V_{42.8}$:$C_{18.2}$, Ni_{49}:$V_{33.3}$:$C_{17.7}$ (at.%)) showed similar friction responses. The friction increased during the running-in period, then decreased, increased again, after which it decreased and took longer to level off.

Under the same conditions Sample 23 with nominal composition Ni_{24}:$V_{58.6}$:$C_{17.4}$ (at.%), had the most irregular friction response pattern, and the friction coefficient was higher than other samples.

Table 4.86 showed the summary of the penetration depth of the ball on the as-cast samples. In all cases, the combined ball/sample penetration depth appeared to remain below 2.26µm in 300m wear path. Within the full wear path range, the lowest values of penetration depth were recorded for as-cast Sample 20.

In agreement with the higher friction level for the as-cast Sample 23, the wear depth was the highest.

4.3.2.2 Sliding wear volume of as-cast samples

The volume of material lost during wear was used to calculate the wear coefficients. The dimensional wear coefficient, k, was used to characterise the wear response of the material. Tables 4.86 compares the volumes of material lost and wear coefficients of the samples. Only one sample was measured per composition and condition, due to the shortage of material.

Table 4.85. Sliding wear and friction test results for as-cast samples.

As-cast sample no.	HV_5	Penetration depth (µm)	Friction coefficients	Wear track width (µm)	Wear volume (mm^3)	Wear coefficient, k (mm^3/Nm)
19	267	1.83	0.72	1120.9	2.3E+07	7.6E-06
20	402	1.65	0.73	798.3	1.0E+07	3.4E-06
21	490	2.19	0.71	577.4	7.2E+06	2.4E-06
22	406	1.97	0.75	747.3	1.1E+07	3.6E-06
23	1065	2.26	0.79	1087	2.6E+07	8.8E-06
24	1052	2.16	0.70	611.4	8.0E+06	2.7E-06

4.3.2.3 Wear surface analysis of as-cast samples

Surface view SEM microstructures in SE mode of the worn surfaces of the samples after sliding for 300m at $0.3ms^{-1}$ under a normal contact force 10N against 100Cr steel ball are compared in Figure 4.326 and energy dispersive X-ray (EDX) analysis was done. These images provided a general impression of the variation in wear track widths achieved by the ball which, resulted from several wear mechanism, i.e., abrasion, wear debris formation, adhesion of wear debris layers, surface binder remover, grain fragmentation and grain pull out.

Figure 4.327 illustrates the typical wear scars on the steel ball used to produce the wear tracks on the samples shown in Figure 4.326. Thus Figure 4.327 (a) is the ball used to produce the wear track shown in Figure 4.326, Sample 19 (a).

The wear mechanisms for Samples 19 to 22 (Figure 4.326a-d) were found to be very similar. Severe plastic deformation was evident. Wear debris and roughened surfaces were seen. These wear debris were mainly located in the outer extensions of the wear track, but appeared also occasionally inside, along and adjacent to the wear path.

The ploughing of wear particles was clearly evident and contributed to groove formation and smearing. Figures 4.326 (a-d) illustrate some amounts of wear debris on the roughened surfaces of the samples, grooving and the smearing of the displaced material. The grooving, as well as cutting, was parallel with the sliding direction. The wear surface of Sample 21, Figure 4.326 (c) was covered with more loosely; fine wear debris particles, compared to Samples 19, 20 and 22 Figures 4.326 (a), (b) and (d).

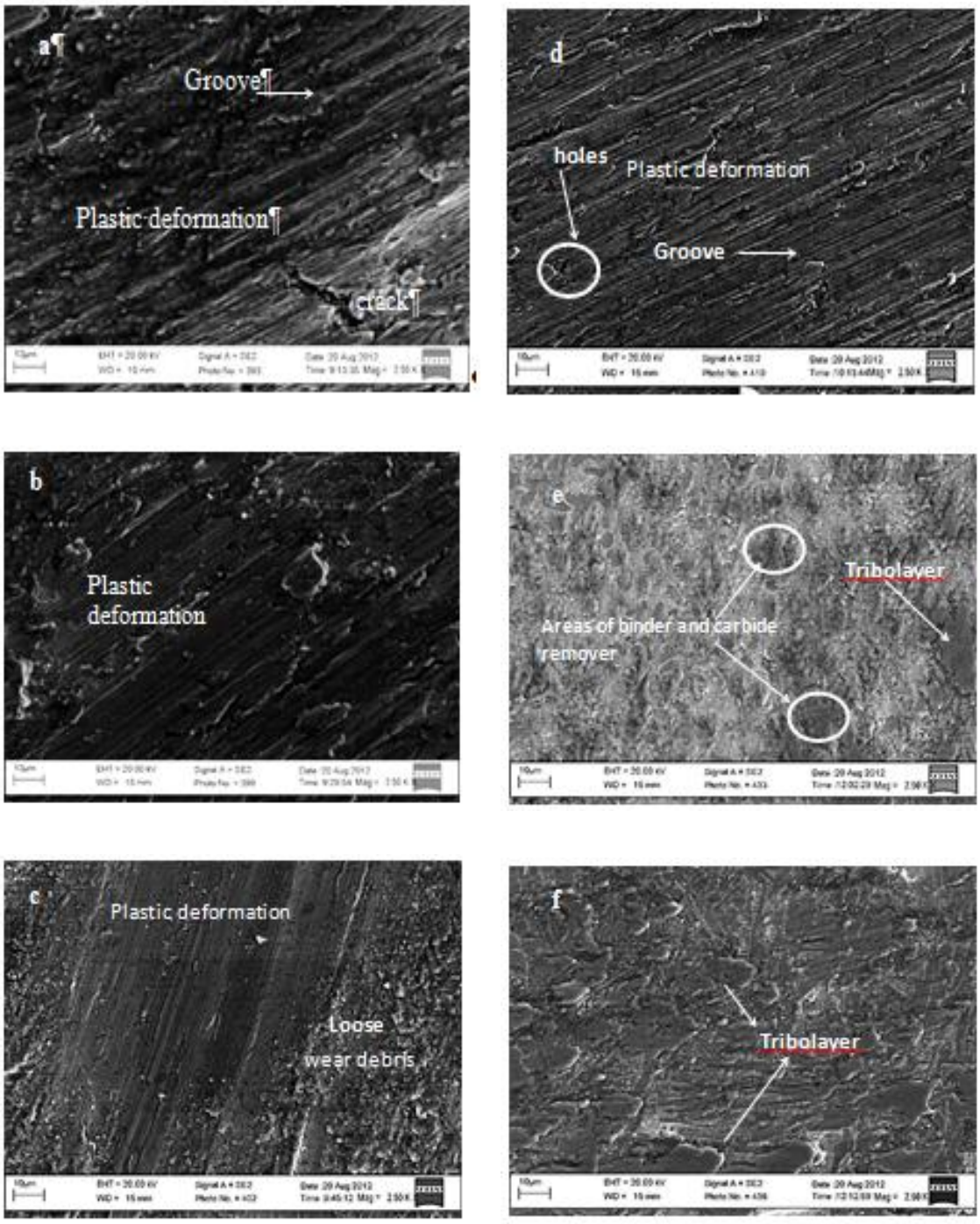


Figure 4.325. SEM images in SE mode of the wear track of: (a) as-cast $Ni_{68}:V_{14}:C_{18}$ (at.%) Sample 19, (b) $Ni_{59}:V_{27.2}:C_{13.8}$ (at.%), Sample 20, (c) $Ni_{39}:V_{42.8}:C_{18.2}$,(at.%) Sample 21, (d) $Ni_{49}:V_{33.3}:C_{17.7}$,(at.%) Sample 22, (e) $Ni_{24}:V_{58.6}:C_{17.4}$ (at.%) Sample 23, and (f) $Ni_{22.1}:V_{49.1}:C_{28.8}$ (at.%), Sample 24, after sliding 300m at $3ms^{-1}$ under a contact load 10N.

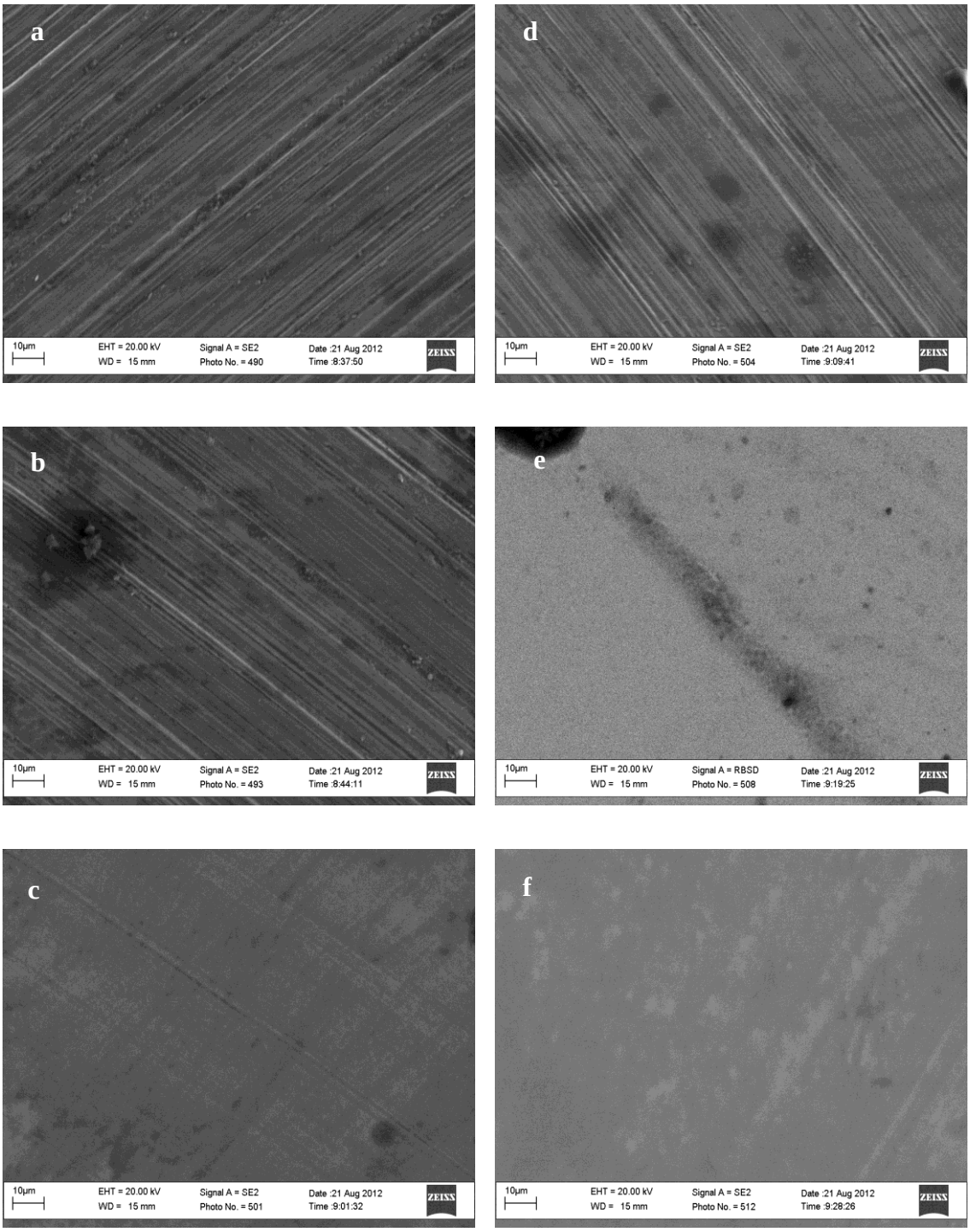


Figure 4.326. SEM images in SE mode of the wear scars on the ball used to produce the as-cast wear tracks shown in Figure 4.317: (a) as-cast $Ni_{68}:V_{14}:C_{18}$ (at.%) Samples 19, (b) $Ni_{59}:V_{27.2}:C_{13.8}$ (at.%), Sample 20, (c) $Ni_{39}:V_{42.8}:C_{18.2}$,(at.%) Sample 21, (d) $Ni_{49}:V_{33.3}:C_{17.7}$,(at.%) Sample 22, (e) $Ni_{24}:V_{58.6}:C_{17.4}$ (at.%) Sample 23, and (f) $Ni_{22.1}:V_{49.1}:C_{28.8}$ (at.%), Sample 24, after sliding 300m at $3ms^{-1}$ under a contact load 10N.

This was evident in the image of the wear scars on the ball (Figure 4.327 (c)), (which was used as the other part of the tribosystem) which was smoother than in Figures 4.326 (a), (b) and (d). Wear debris was seen as bright spots resulting from the fragmentation of carbides that had not been attached yet to the surface. EDX area analyses are given in Table 4.87.

Table 4.86. EDX area analyses of the wear scars on as-cast samples.

Sample no.	Compositions (at.%)				
	C	V	Fe	Ni	O
19A	36.5 ± 0.7	12.4 ± 0.7	3.7 ± 0.0	47.1 ± 0.0	0.3 ± 0.01
20A	38.0 ± 1.3	17.2 ± 0.0	7.2 ± 0.0	36.6 ± 0.7	0.9 ± 0.0
21A	23.2 ± 1.4	34.5 ± 0.7	13.1 ± 0.7	28.3 ± 0.0	0.9 ± 0.02
22A	37.4 ± 0.5	23.5 ± 0.7	3.9 ± 0.7	34.1 ± 0.0	0.8 ± 0.0
23A	37.2 ± 0.7	34.0 ± 0.1	14.5 ± 0.6	13.3 ± 0.0	1.1 ± 0.0
24A	37.7 ± 0.7	41.5 ± 0.7	9.6 ± 0.7	10.4 ± 0.0	1.3 ± 0.0

The binder phase was removed from between the VC grains by abrasion ploughing or/and plastic deformation, which was due to the lower hardness and higher ductility of the binder phase with respect to the carbide phase. Figures 4.326 (Samples 19-22) do not have tribolayers formation compared to Figures 4.326 (Samples 23 and 24). The ploughing was due to abrasion of the binder phase in the direction of movement of sliding, although some holes resulted from the extraction of smaller VC grains and microfractures in larger grains.

With reference to Figures 4.326 (e) and (f) (Samples 23 and 24), wear layer observed was a result of wear debris attachment, i.e. a tribolayer comprising microfragments of both binder phase and VC grains which covered the wear grooves and adhered on the contact surface. The layer contained a high composition of oxygen as shown in Table 4.87.

The damage in Samples 23 and 24 alloys were correlated to their higher hardness. In this case the wear tracks were more heterogeneous, with areas of removal of the binder and carbides fragmentation, and areas where the wear debris was attached to the surface and formed a tribological layer.

4.3.2.4 Friction results of heat treated samples

Figures 4.329 to 4.333 illustrate the friction curves from reciprocating sliding tests between pin (Cr steel ball) and heat treated samples, under the same test conditions. The friction responses for Samples 19H and 20H (Ni_{68}:V_{14}:C_{18} and Ni_{59}:$V_{27.2}$:$C_{13.8}$ (at.%),) paired with chromium steel ball were similar. The friction increased during the running-in period, then decreased and increased again, after which it decreased and took longer to level off.

Samples 21H, 22H and 24 (Ni_{39}:$V_{42.8}$:$C_{18.2}$, Ni_{49}:$V_{33.3}$:$C_{17.7}$ and $Ni_{22.1}$:$V_{49.1}$:$C_{28.8}$ (at.%),) showed similar friction responses. During the running-in period, the friction increased to a maximum then after which it decreased and levelled off at a lower level. The friction curves in Samples 19H and 20H were comparable to hypothetical pattern III. The curves for Cr steel paired heat treated Samples 21H, 22H and 24H (Figures 4.330, 4.331 and 4.331) followed pattern II (Figure.2.15).

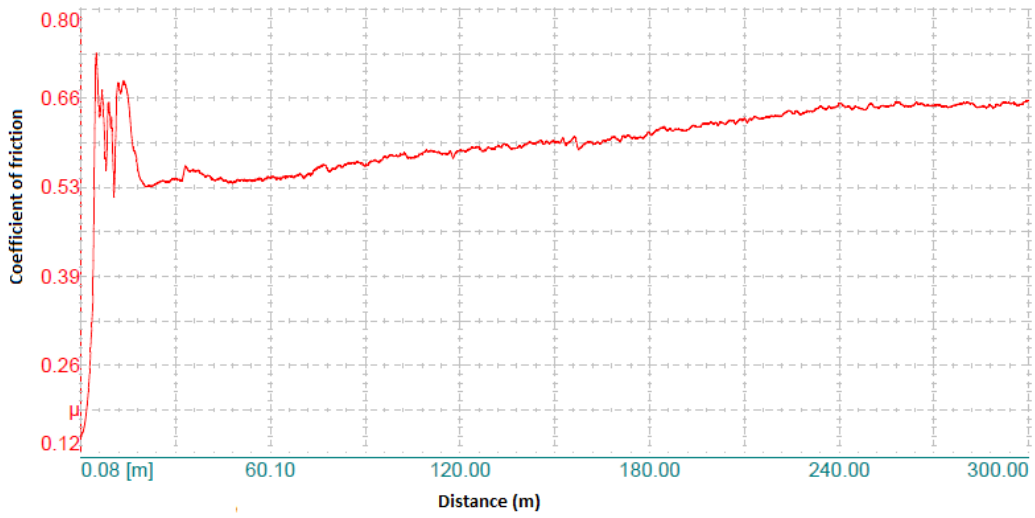


Figure 4.327. Friction coefficient evolution with sliding distance for heat treated Ni_{68}:V_{14}:C_{18} (at.%), Sample 19H.

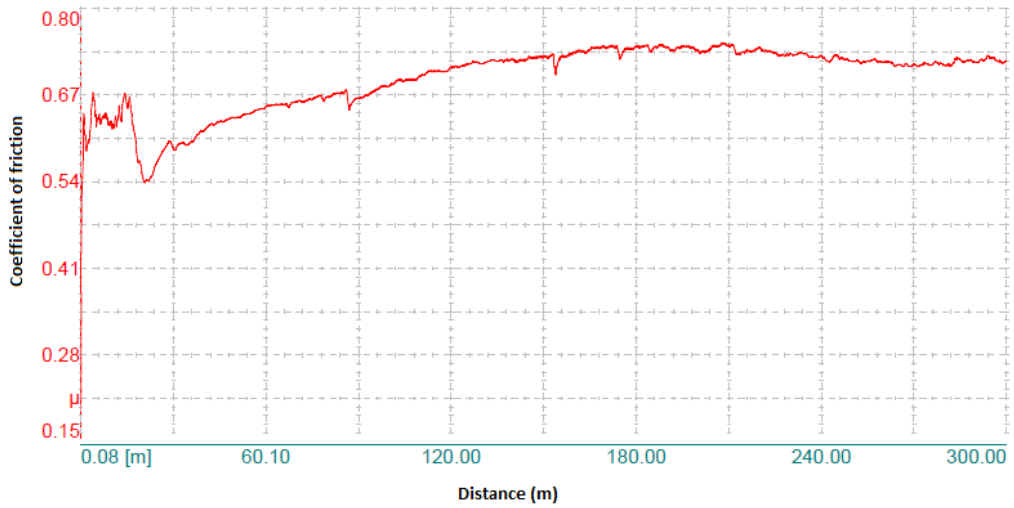


Figure 4.328. Friction coefficient evolution with sliding distance for heat treated $Ni_{59}:V_{27.2}:C_{13.8}$ (at.%), Sample 20H.



Figure 4.329. Friction coefficient evolution with sliding distance for heat treated $Ni_{39}:V_{42.8}:C_{18.2}$ (at.%), Sample 21H.

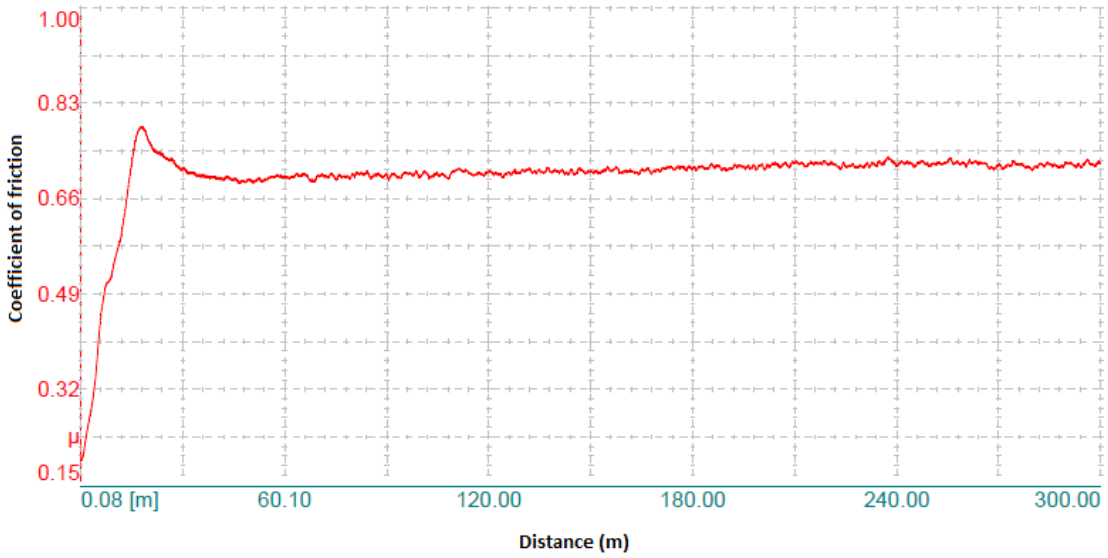


Figure 4.330. Friction coefficient evolution with sliding distance for heat treated $Ni_{49}:V_{33.3}:C_{17.7}$ (at.%), Sample 22H.



Figure 4.331. Friction coefficient evolution with sliding distance for heat treated $Ni_{22.1}:V_{49.1}:C_{28.8}$ (at.%) Sample 24H.

Comparing the friction coefficients of the heat treated samples with the as-cast samples, the measured friction coefficient of the heat treated samples ranged between 0.08 - 0.85, while those of the as-cast samples ranged between 0.08 - 0.79. This showed an increase of ~7.1%

after the heat treatment. Also, the friction coefficients increased rapidly throughout the first stage of sliding, and subsequently decreased as for as-cast samples. Heat treated Samples 19H and 22H had the same running-in period of 30m as the as-cast alloys, but the other samples had different running-in periods. Thus, heat treated Sample 21H had a running-in period of 50m compared to the as-cast Sample 21, which had a running-in period of 30m. Sample 24H had the highest running-in period of 90m after heat treatment, and 50m in the as-cast condition.

Table 4.88 shows the summary of the penetration depth of the ball into the samples after heat treatment. The combined ball/sample penetration depth remained below 2.42µm after a 300m wear path. The lowest value of penetration depth was recorded for Sample 19H.

Figure 4.333 compares the penetration depth of the heat treated samples with as-cast samples. There was increase in penetration depth for Samples 20H, 21H and 24H after heat treatment. This may be due to the presence of carbon and cracks. Sample 19H showed a reduction in penetration depth, which may be attributed to absence of carbon. While there was no change in penetration depth for Sample 22H, there was also no evidence of cracks in the sample after the heat treatment.

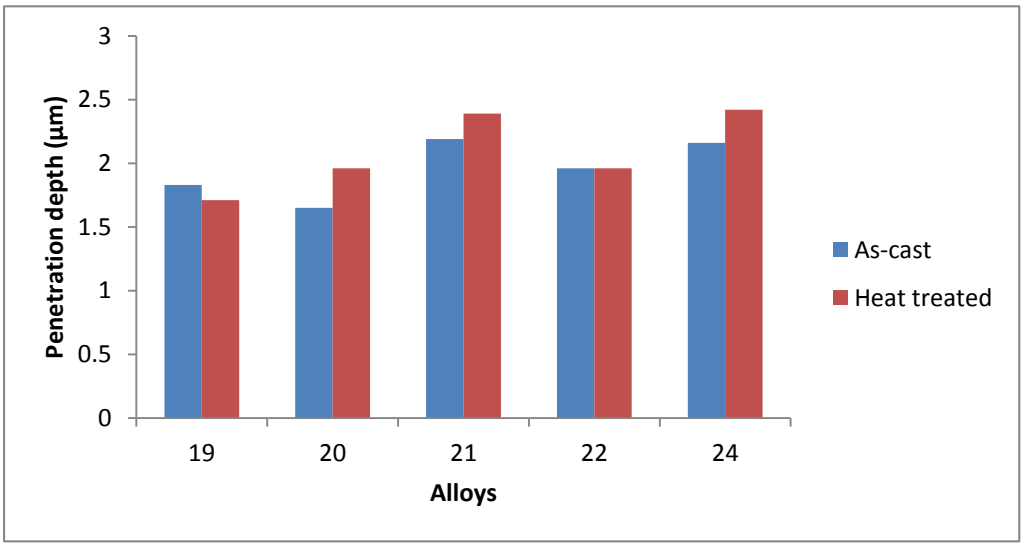


Figure 4.332. Comparison of the penetration depth of the Cr steel ball between heat treated and as-cast samples.

4.3.2.5 Sliding wear volume of heat treated samples

The averaged sliding wear and friction test results for each ball-heat treated sample pair is summarised in Table 4.88. Samples 19H, 20H and 21H, with average hardness values 284, 597 and 542HV, had high wear volume and wear tracks, an indication of high wear rate. Samples 22H and 24H with average hardness values 605 and 1160.8 had the lowest wear loss.

Table 4.87. Sliding wear and friction test results for heat treated samples.

Heat treated Sample no.	HV_5	Penetration Depth (μm)	Friction coefficients	Wear track width (μm)	Wear volume (mm^3)	Wear coefficients, k, (mm^3/Nm)
19H	284	1.71	0.73	1053	1.9E+07	6.3E-06
20H	597	1.96	0.75	1256.8	3.1E+07	1.0E-05
21H	542	2.39	0.86	985	2.3E+07	7.6E-06
22H	605	1.96	0.79	730.3	1.0E+07	3.4E-06
24H	1161	2.42	0.73	747.2	1.3E+07	4.5E-06

4.3.2.6 Wear surface analysis for heat treated samples

SEM microstructures in SE mode of the worn surfaces of the heat treated samples after sliding under the same conditions are shown in Figure 4.334 and their EDX analyses are given in Table 4.89. Figure 4.335 illustrates the typical wear scars on the steel ball used to produce the wear tracks on the heat treated samples.

Tribolayers were observed in Samples 22H and 24H (Figures 4.334 (d), (f)), which was from wear debris attachment. This was also evident in the smoothness of Cr steel balls in Figures 4.335 (e) and (f). The layers contained more oxygen, as shown in the EDX results (Table 4.89), compared to Samples 19H-21H.

Table 4.88. EDX area analyses of heat treated samples.

Sample no.	Compositions (at.%)				
	C	V	Fe	Ni	O
19H	45.6 ± 0.7	7.9 ± 0.7	9.0 ± 0.7	36.5 ± 0.7	1.0 ± 0.0
20H	19.2 ± 0.7	22.0 ± 0.8	9.8 ± 0.7	48.3 ± 0.1	1.1 ± 0.01
21H	17.3 ± 0.4	45.9 ± 1.2	28.2 ± 0.7	6.5 ± 0.7	1.6 ± 0.2
22H	38.7 ± 0.4	21.5 ± 0.7	15.2 ± 0.1	22.5 ± 0.2	2.0 ± 0.1
24H	26.9 ± 1.1	57.6 ± 0.8	12.8 ± 0.3	0.5 ± 0.1	2.3 ± 0.1

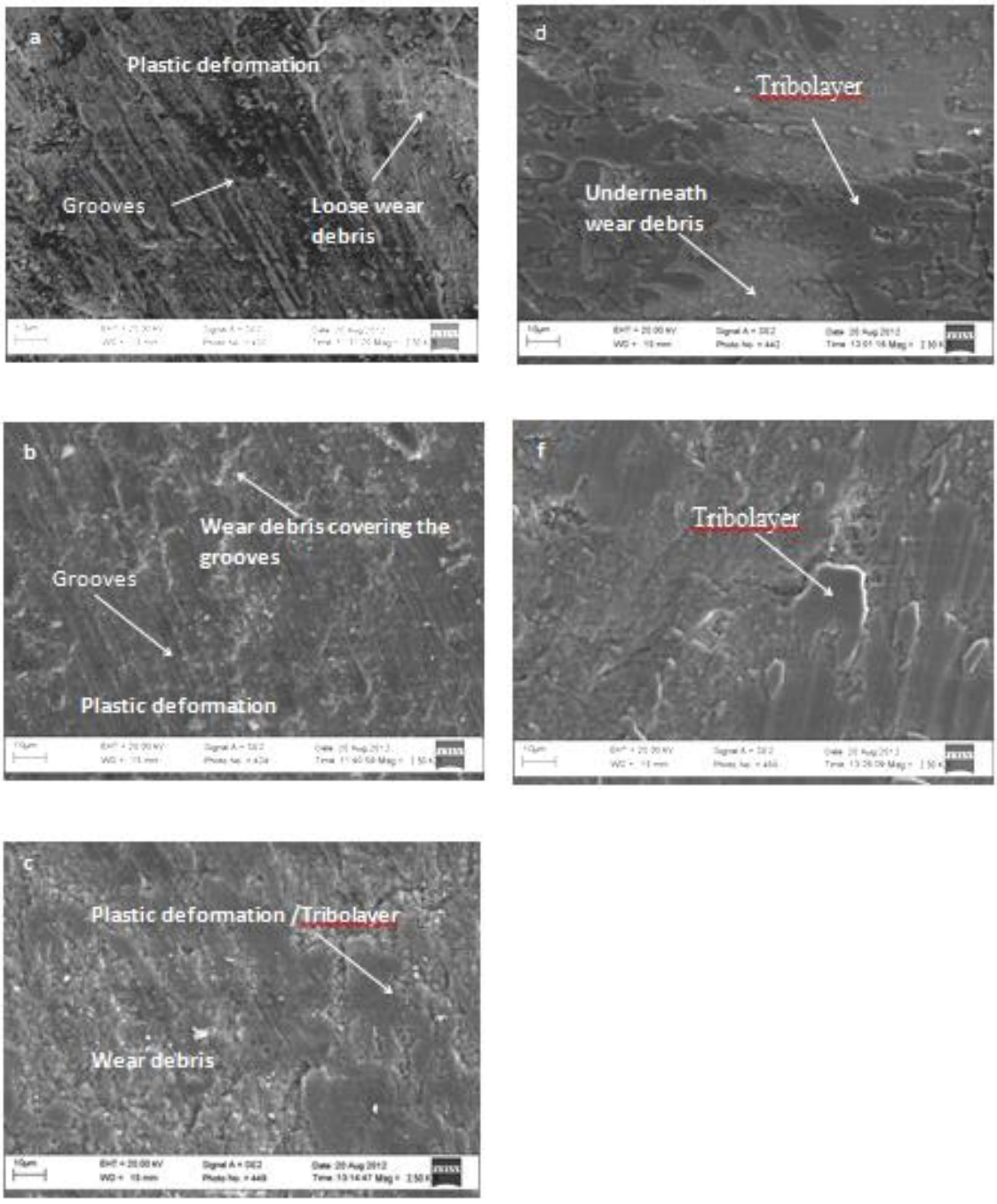


Figure 4.333. SEM images in SE mode of the wear track of: (a) heat treated $Ni_{68}:V_{14}:C_{18}$ (at.%) Samples 19H, (b) $Ni_{59}:V_{27.2}:C_{13.8}$ (at.%) Sample 20H, (c) $Ni_{39}:V_{42.8}:C_{18.2}$,(at.%) Sample 21H, (d) $Ni_{49}:V_{33.3}:C_{17.7}$,(at.%) Sample 22H, (f) and $Ni_{22.1}:V_{49.1}:C_{28.8}$ (at.%), Sample 24H, after sliding 300m at $3ms^{-1}$ under a contact load 10N.

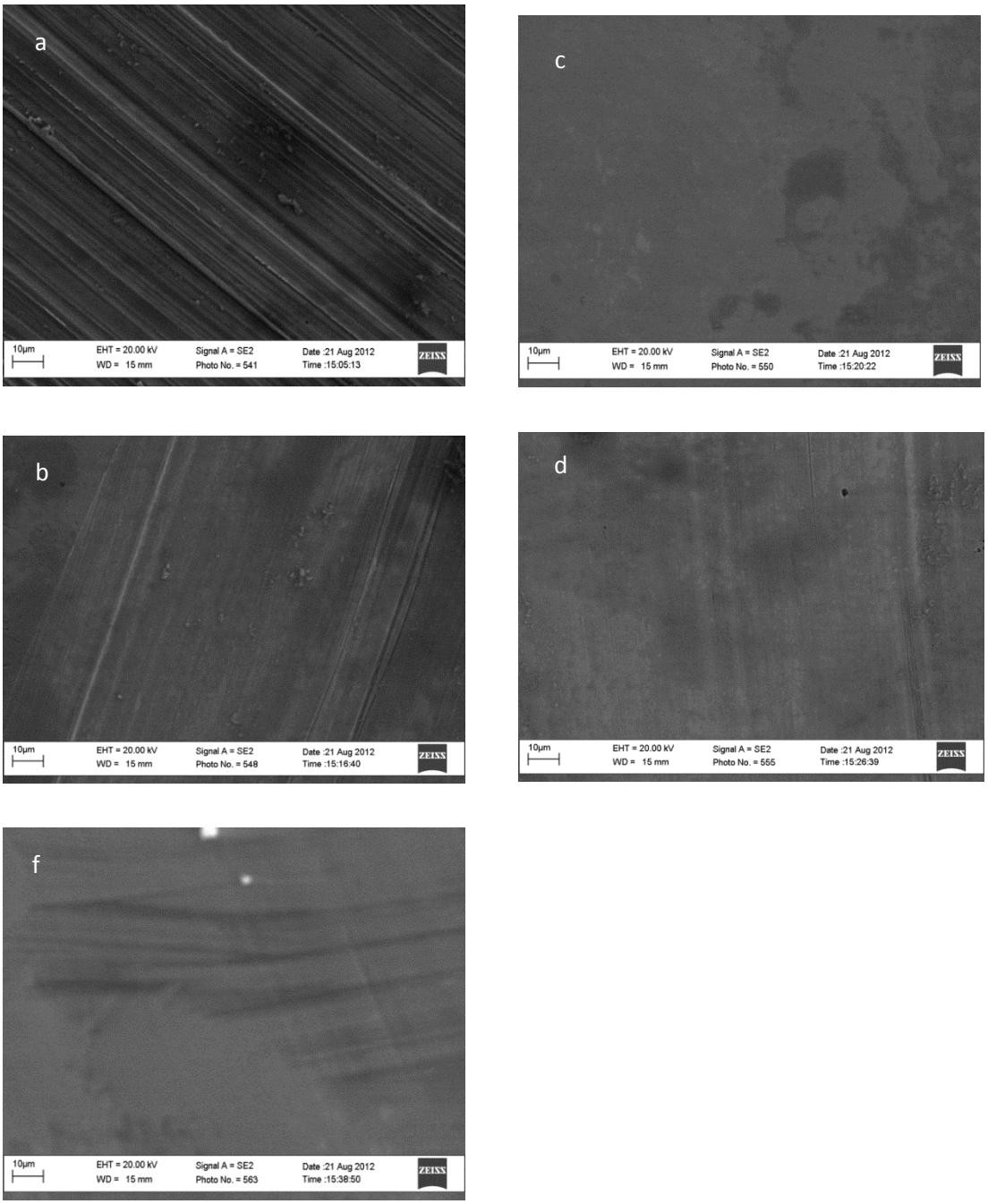


Figure 4.334. SEM images in SE mode of the wear scars on the ball used to produce the heat treated wear tracks shown in Figure 4.334: (a) heat treated $Ni_{68}:V_{14}:C_{18}$ (at.%) Samples 19H, (b) $Ni_{59}:V_{27.2}:C_{13.8}$ (at.%) Sample 20H, (c) $Ni_{39}:V_{42.8}:C_{18.2}$,(at.%) Sample 21H, (d) $Ni_{49}:V_{33.3}:C_{17.7}$,(at.%) Sample 22H, (f) and $Ni_{22.1}:V_{49.1}:C_{28.8}$ (at.%), Sample 24H, after sliding 300m at $3ms^{-1}$ under a contact load 10N.

CHAPTER FIVE

5.0 DISCUSSION

5.1 X-ray results

All of the phases except for σ′ were matched using the International Crystallography Diffraction Database (ICDD) [2001ICD]. Where σ′ was identified by its composition being similar to that in the Ni-V binary [1982Smi], the unidentified peaks were assumed to be from σ′. These are collected in Tables 5.1 and 5.2, and show reasonable agreement, considering the phases had different compositions, and so the peaks would be shifted relative to other.

5.2 Solidification projection

The phases were identified on the basis of composition and comparison to the binary compositions [1982Smi, 1985Car, 1989Sin]. The phase was confirmed by X-ray diffraction. However, there was over-reporting of C in at least ~VC, because the C content was higher than in the binary. In some cases, the XRD was not very beneficial, as so many of the peaks were common between the phases, making distinguishing these phases very difficult. This led to different patterns apparently giving the same phases.

The "~VC" phases had two different morphologies on the V-rich side: dendrites (with or without side arms) and chunky needles. The needles were mainly associated with σ′, and so the morphology difference was thought to be a surface energy effect. There was also a complication in deducing whether the phase was actually ~VC, or one of the lower temperature versions, because of the difficulties with XRD mentioned above. However, some samples (e.g. Sample 13) showed that the phase precipitated in the solid state was ~V_6C_5, and Sample 24 had ~V_8C_7. The ~V_2C phase did not appear in this investigation, partly because the samples were not close to it. This shows that it did not penetrate far into the ternary.

Table 5.2. XRD peaks assumed to be from σ′ in as-cast samples.

Position 2θ (º) Sample 9	Relative Intensity (%)	Position 2θ (º) Sample 12	Relative Intensity (%)	Position 2θ (º) Sample 14	Relative Intensity (%)	Position 2θ (º) Sample 15	Relative Intensity (%)	Position 2θ (º) Sample 23	Relative Intensity (%)
21.3408	0.29	28.3112	2.70	30.7530	15.52	24.8257	5.87	45.9831	10.40
26.3591	2.00	47.4413	0.51	39.7792	1.88	28.8177	0.42	47.7145	22.18
31.0523	0.26	61.7065	10.08	43.2431	2.27	48.0922	67.73	54.0214	55.76
36.9562	2.89			53.0068	42.56	52.6652	22.87	55.4117	78.00
43.5903	7.81			54.1256	12.76	87.1246	2.04	63.9404	1.75
44.7872	30.13			58.8014	44.04	91.0468	19.06	89.6258	5.82
45.7476	76.45			61.4658	1.87	98.5964	0.96	97.4169	1.73
46.9078	17.43			72.5990	2.08				
62.3549	0.49			82.6589	0.88				
68.8426	3.47			88.2293	8.48				

Table 5.2. XRD peaks assumed to be from σ′ in heat treated samples.

Position 2θ (º) Sample 11H	Relative Intensity (%)	Position 2θ (º) Sample 12H	Relative Intensity (%)	Position 2θ (º) Sample 13H	Relative Intensity (%)	Position 2θ (º) Sample 14H	Relative Intensity (%)	Position 2θ (º) Sample 15H	Relative Intensity (%)
33.5594	0.81	20.9275	2.22	25.6893	3.61	26.6783	3.65	48.5043	11.58
35.2787	1.67	26.6896	3.47	34.4576	100.00	31.8853	0.93	53.8534	26.33
44.6700	6.19	29.2194	2.91	40.2886	2.63	47.2194	28.99	56.0604	3.39
52.1066	9.83	36.6567	2.34	42.2133	5.53	50.2607	100.00		
53.1759	17.72	38.9967	0.93	47.9009	70.00	50.9530	21.93		
54.6955	5.02	55.6675	5.26	48.3344	69.50	55.6778	4.74		
69.7797	1.03	56.9477	3.88	51.8923	2.42	56.9227	5.91		
76.1225	2.51			52.6133	13.02	58.7427	12.59		
78.3463	1.88			53.7151	27.28	67.8875	0.63		
				55.2120	14.32	78.3045	5.74		
				57.2105	6.60	87.8292	13.48		
				64.1309	9.57				

The (Ni) phase also transformed to ~Ni_3V or ~Ni_2V. The extent of (Ni) (and its lower temperature phases) was very wide in the ternary, especially on the carbon side. This was surprising since only ~2.5 at.% C dissolves in (Ni) in the binary [1989Sin]. As well as the unexpected C content of (Ni) in the ternary, there were also two binary eutectics which formed with (Ni). These were ~VC + (Ni) which had globular ~VC as the discrete phase, and C + (Ni) which had graphite flakes as the discrete phase. These were often seen in the same samples (Samples 5, 6, 7, 8, 17, 18, 19, 20, 21 and 22), and were distinguished by their different morphologies. Figure 5.1 shows a plot of the phases and overall compositions for all of the as-cast samples.

The solidification temperatures of some of the samples were probably fairly different, because the tie-lines cross. In an isothermal section, the tie-lines are not allowed to cross, but since these are as-cast samples, if the solidification temperature ranges are different, then the tie-lines can cross, as long as they lie at a fairly low angle to each other.

The different samples gave good agreement in most of the phases. Graphite flakes formed first in Samples 1, 2, 7 and 10 of the average overall composition ~$Ni_{4.6}$:$V_{40.7}$:$C_{54.7}$, ~$Ni_{8.4}$:$V_{31.1}$:$C_{60.5}$, ~$Ni_{22.3}$:$V_{4.1}$:$C_{73.6}$ and ~$Ni_{2.4}$:$V_{25.9}$:$C_{71.7}$ (at.%) respectively, before the primary dendrites (~VC). The overall compositions of Samples 1, 2, 7 and 10 were within the tie-triangles of the phases, signifying that the alloys are likely to be in equilibrium and no phase being missed. Also, they had similar microstructures. Carbon was interpreted for the samples because those overalls were on the C sides.

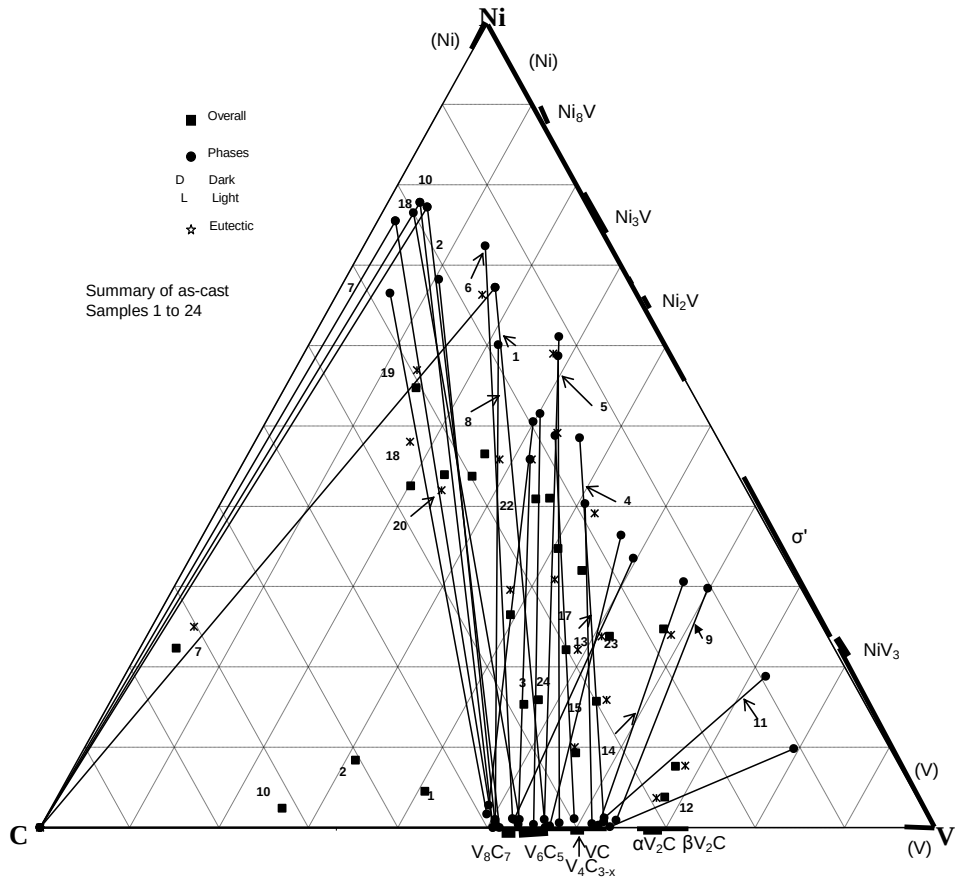


Figure 5.1. Plotted data for as-cast samples of the C-Ni-V system (at.%).

The ~VC carbide formed first in Samples 3, 5, 17, 21 and 23 with average overall compositions ~$Ni_{15.3}$:$V_{46.5}$:$C_{38.2}$, ~$Ni_{41.2}$:$V_{36.4}$:$C_{22.2}$, ~$Ni_{26.5}$:$V_{39.4}$:$C_{34.1}$, ~$Ni_{34.7}$:$V_{40.6}$:$C_{24.7}$ and ~$Ni_{23.8}$:$V_{51.8}$:$C_{24.3}$ respectively, as primary dendrites before the formation of ~V_6C_5 through a solid state transformation.

In Samples 9, 11, 12, 13 and 14 (overall compositions ~$Ni_{24.7}$:$V_{57.4}$:$C_{17.9}$, ~$Ni_{7.6}$:$V_{67.3}$:$C_{25.1}$, ~$Ni_{3.8}$:V_{68}:$C_{28.2}$, ~$Ni_{22.1}$:$V_{47.8}$:$C_{30.1}$ and ~$Ni_{9.3}$:$V_{55.3}$:$C_{35.4}$ (at.%)), the ~VC carbide formed first, without any solid state transformation. The retention of ~VC at lower temperature may be due to the fast cooling of the arc-melting technique.

A eutectics of ~VC + (Ni) had been identified in Samples 2, 7, 8, 10, 13, 18, 19 and 20. The ~VC carbide transformed to ~V_8C_7 by solid state transformation, except in Sample 13. The (Ni) remained as solid solution without transformation.

The eutectic of Samples 1, 3, 4, 5, 17, 21 and 22 were also identified as ~VC + (Ni). The (Ni) of Samples 1 and 6 transformed to ~Ni_3V, whereas those of Sample 4, 5, 8, 17 and 22 transformed to Ni_2V. The ~VC carbide of Samples 1 and 21 transformed to ~V_6C_5 but in Sample 6 it transformed to ~V_8C_7.

A eutectic of C + (Ni) had been identified in Samples 5, 6, 7, 8, 17, 18, 19, 20, 21 and 22. The eutectic of ~VC + σ′ was also identified in Samples 9, 14, 15 and 23. Samples 11 and 12 were the only alloys to form the ~VC + (V) eutectic.

Figure 5.2 shows the solidification projection for C-Ni-V of the as-cast results. The phase boundaries were added taking the above information into account, and by joining the ternary compositions with the binary phases [1982Smi, 1985Car, 1989Sin]. The ~Ni_8V phase was not found in this investigation, partly due to its critical temperature (405°C) that is lower compared to the other intermetallic phases that were observed, and mainly because no samples were manufactured near its composition. The extensions into the ternary were found for most of the phases, and these are given in Table 5.3 and were obtained from the analyses summarised in Figure 5.2. The extensions of (Ni) into the ternary may be larger than shown, and could be due to C pick-up from the eutectic. The phase extensions for the vanadium carbides were very limited, only up to 3 at.%.

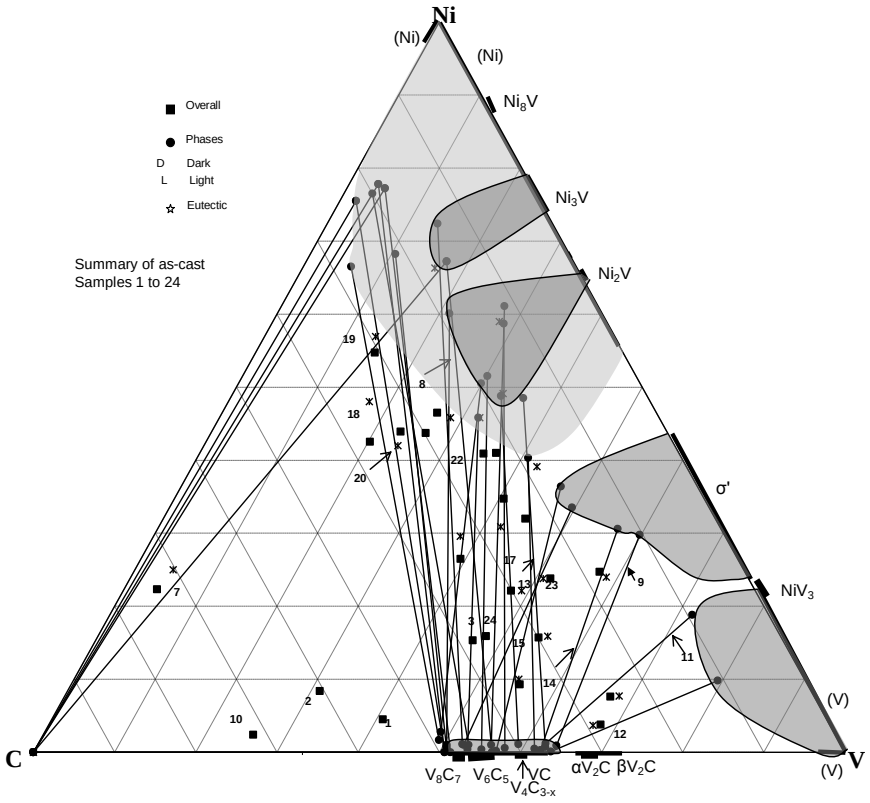


Figure 5.2. Solidification projection for C-Ni-V for the as-cast results (at.%).

Table 5.3. Extents of the binary phases into the C-Ni-V system.

Originated from:	**Phase**	**C extent (at.%)**
Ni-V	~Ni_3V	15
	~Ni_2V	20
	σ′	18
	(V)	12
	(Ni)	27
		Ni extent (at.%)
V-C	~V_8C_7	2
	~V_6C_5	2
	~VC	3

5.3 Liquidus projection surface

Solidification sequences could be clearly identified from the as-cast microstructures by assuming that the dendrites or the graphite flakes were the primary phase. However, there were some samples (Samples 1, 2, 7 and 10) that had both (graphite) flakes as the major phase and small dendrites. It was interpreted that the graphite formed first (it is a high melting point phase), considering the overall compositions, and referring to the binary phase diagrams.

The liquidus projection, which is the projection of solidification reactions delineates the boundaries of different primary solidification phases and was deduced by using the phases derived from the solidification projection as described above, as well as the solidification sequences (Table 5.4).

The eutectic analyses were disappointingly inaccurate, probably because they were too small, and especially too shallow and other non-eutectic phases were also collected. Therefore they were ignored in the solidification projection. There was no ternary eutectic, because the three phases (~VC, (Ni and C)) were not seen together. The liquidus surface as shown in Figure 5.3. Each reaction observed on solidification of the samples had to agree with the liquidus surface.

Most of the reactions were derived from the sample microstructures and EDX results, and are shown as solid lines with dotted lines showing the inferred positions, where there were no data.

Table 5.4. Solidification reactions of the C-Ni-V system.

Sample no.	Nominal sample composition (at.%)	Dendrite morphology	Solidification reactions	Solid state reactions
1	$Ni_{10}:V_{50}:C_{40}$	smooth dendrites	L → graphite L + graphite → ~VC L → ~VC + (Ni)	~VC → $\sim V_6C_5$ (Ni) →$\sim Ni_3V$
2	$Ni_{20}:V_{40}:C_{40}$	smooth dendrites	L → graphite L + graphite → ~VC L → ~VC + (Ni)	~VC → $\sim V_8C_7$
3	$Ni_{24}:V_{50}:C_{26}$	smooth dendrites	L → ~VC L → ~VC + (Ni)	~VC → $\sim V_6C_5$ (Ni) → $\sim Ni_2V$
4	$Ni_{40}:V_{50}:C_{10}$	chunky dendrites	L → ~VC L + ~VC → (Ni) L → ~VC + (Ni)	(Ni) → $\sim Ni_2V$
5	$Ni_{53}:V_{37}:C_{10}$	smooth dendrites	L → ~VC L + ~VC → (Ni) L → ~VC + (Ni L → C + (Ni	~VC → $\sim V_6C_5$ (Ni) → $\sim Ni_2V$
6	$Ni_{64}:V_{25}:C_{11}$	smooth dendrites	L → ~VC L + ~VC → (Ni) L → C + (Ni)	~VC → $\sim V_8C_7$ (Ni) → $\sim Ni_3V$
7	$Ni_{70}:V_{10}:C_{20}$	Facetted dendrites	L → graphite L + graphite → ~VC L → C + (Ni)	~VC → $\sim V_8C_7$
8	$Ni_{60}:V_{30}:C_{10}$	smooth, cracked dendrites	L → ~VC L → ~VC + (Ni) L → C + (Ni)	~VC → $\sim V_8C_7$ (Ni) → $\sim Ni_2V$
9	$Ni_{30}:V_{65}:C_5$	smooth "Lay" dendrites	L → ~VC L → ~VC + σ′	no solid state reaction
10	$Ni_{20}:V_{35}:C_{45}$	smooth dendrites	L → graphite L+ graphite → ~VC L → ~VC + (Ni)	~VC →$\sim V_8C_7$
11	$Ni_{10}:V_{80}:C_{10}$	smooth + facetted dendrites	L → ~VC L → ~VC + (V)	no solid state reaction
12	$Ni_5:V_{75}:C_{20}$	smooth + cracked dendrites	L → ~VC L + ~VC → σ′ L → ~VC + (V)	no solid state reaction
13	$Ni_{14}:V_{64}:C_{22}$	chunky needles	L → ~VC L + ~VC → (Ni) L → ~VC + (Ni)	no solid state reaction

Table 5.4 (cont.). Solidification reactions of the C-Ni-V system.

14	$Ni_{28}:V_{54}:C_{18}$	Smooth long dendrites first, then smooth dendrites, cracked	L → ~VC L → ~VC + σ′	no solid state reaction
15	$Ni_{32}:V_{56}:C_{12}$	smooth globular dendrites cracked	L → ~VC L → ~VC + σ′	~VC → $\sim V_8C_7$
17	$Ni_{39}:V_{42.8}:C_{18.2}$	smooth globular dendrites	L → ~VC L + ~VC → (Ni) L → C + (Ni)	~VC →$\sim V_6C_5$ (Ni) → $\sim Ni_2V$
18	$Ni_{66.4}:V_{16.1}:C_{17.5}$	smooth globular and irregular	L → ~VC L → ~VC + (Ni) L → C + (Ni)	~VC + $\sim V_8C_7$
19	$Ni_{68}:V_{14}:C_{18}$	smooth dendrites	L → ~ VC L → ~VC + (Ni) L → C + (Ni)	~VC → $\sim V_8C_7$
20	$Ni_{59}:V_{27.2}:C_{13.8}$	smooth dendrites	L → ~VC L → ~VC + (Ni) L → C + (Ni)	~VC → $\sim V_8C_7$
21	$Ni_{39}:V_{42.8}:C_{18.2}$	chunky needles	L → ~VC L + ~VC → (Ni) L → ~VC + (Ni) L → C + (Ni)	~VC → $\sim V_6C_5$ (Ni) → $\sim Ni_2V$
22	$Ni_{49}:V_{33.3}:C_{17.7}$	smooth dendrites	L → ~VC L → ~VC + (Ni) L → C + (Ni)	~VC → $\sim V_8C_7$ (Ni) → $\sim Ni_2V$
23	$Ni_{24}:V_{58.6}:C_{17.4}$	smooth dendrites, cracked	L → ~VC L → ~VC + σ′	~VC → $\sim V_6C_5$
24	$Ni_{22.1}:V_{49.1}:C_{28.8}$	chunky needles and clumps	L → ~VC L + ~VC → (Ni) L → ~VC + (Ni)	~VC →$\sim V_8C_7$ (Ni) → $\sim Ni_2V$

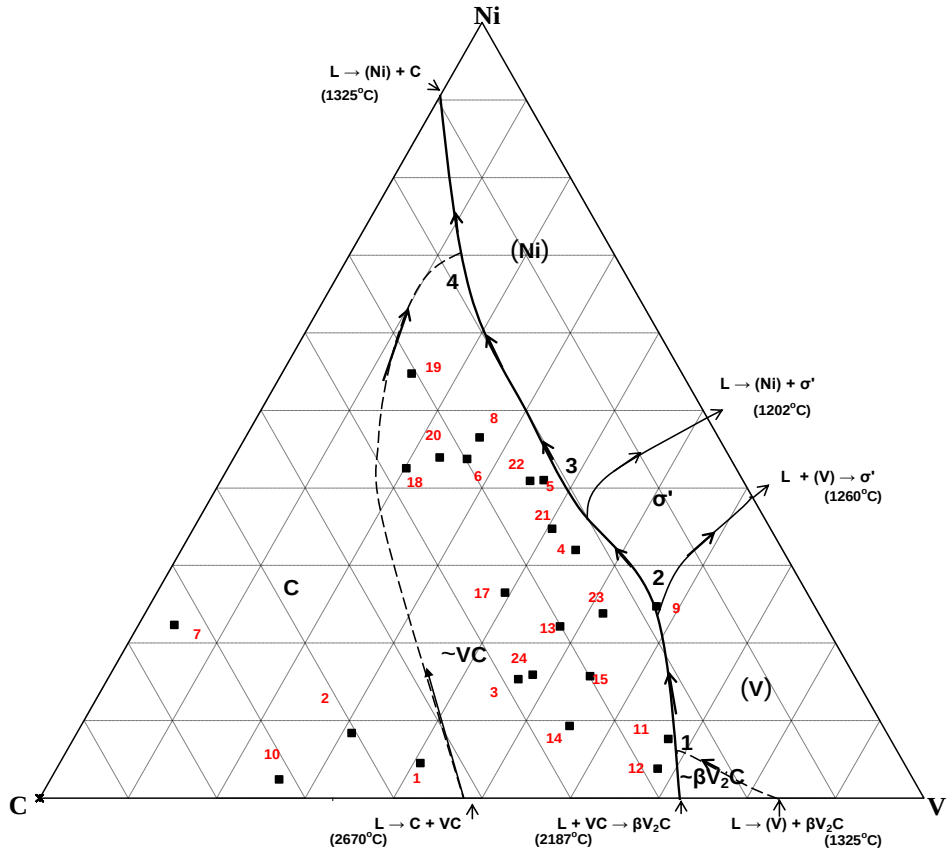


Figure 5.3. Liquidus projection for C-Ni-V for the as-cast results (at.%).

Table 5.6 shows the ternary invariant reactions derived from the liquidus surface.

Table 5.6. Ternary invariant reactions of the C-Ni-V system.

Reaction no.	Invariant reaction	Liquid composition (at.%)
1	$L + \beta V_2C \rightarrow (V) + VC$	$Ni_6:V_{69}:C_{25}$
2	$L + (V) + VC \rightarrow \sigma'$	$Ni_{24}:V_{58}:C_{18}$
3	$L + VC + \sigma' \rightarrow (Ni)$	$Ni_{37}:V_{43}:C_{20}$
4	$L + VC \rightarrow (Ni) + C$	$Ni_{70}:V_{13}:C_{17}$

5.4 Isothermal section at 1000°C

The data from the annealed samples are plotted in Figure 5.4, and using the deduction of the phases by XRD (even realising the difficulties) the boundaries are added in Figure 5.5.

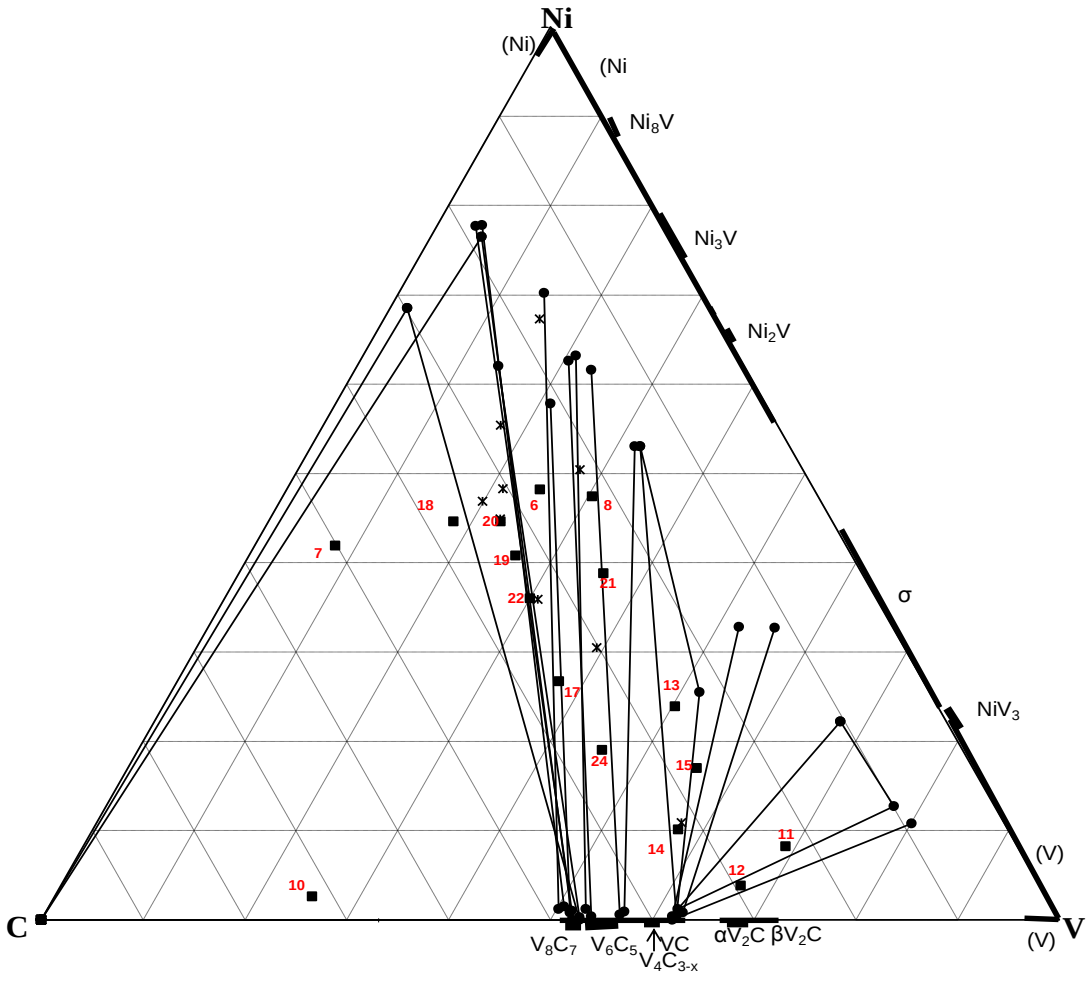


Figure 5.4. Plotted data for isothermal section of the C-Ni-V system (at.%) at 1000°C (Sample numbers in red).

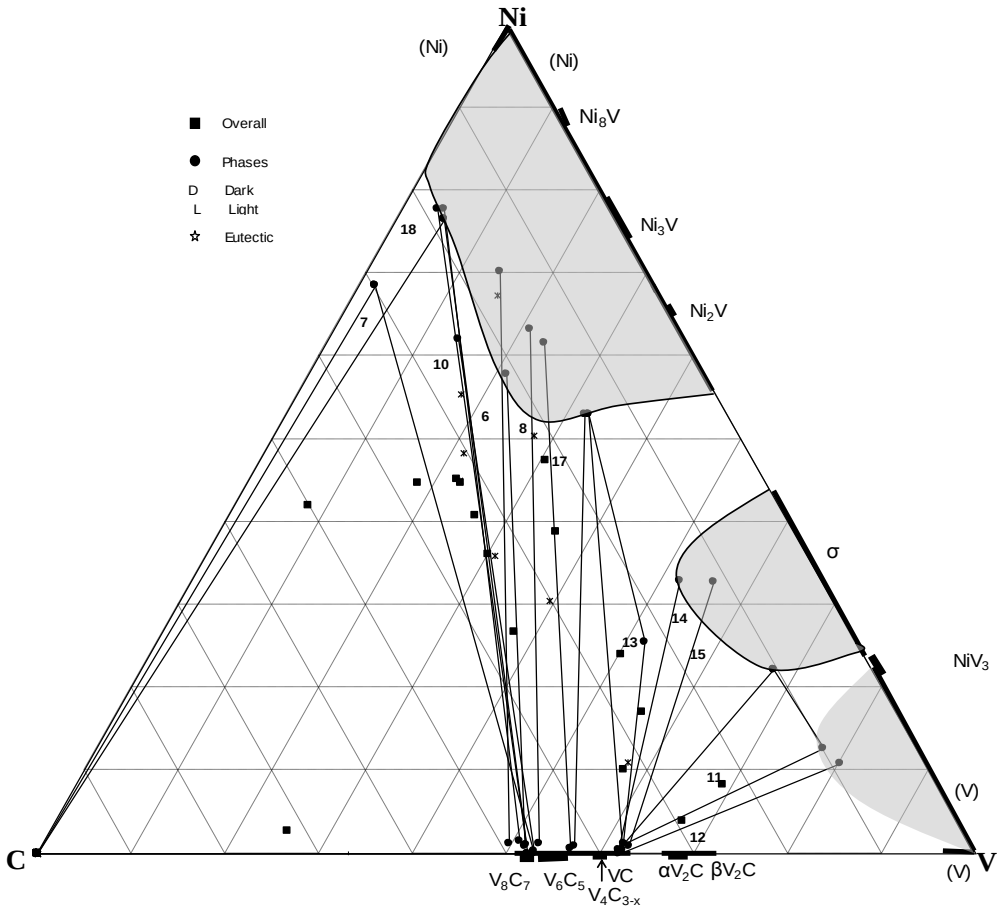


Figure 5.5. Isothermal section of the C-Ni-V system (at.%) at 1000ºC.

After annealing at 1000ºC for 1000h, one of the V_xC_y phases had transformed back to ~VC (Sample 15H), whereas most had not (Samples 6H, 7H, 8H, 10H, 17H, 18H, 19H, 20H, 21H, 22H and 24H). This indicated that there was variation in the transformation temperatures (assuming that XRD interpretations were correct), even for such small differences in Ni content (up to 3 at.%). However, the V-C binary [1985Car] shows that the temperatures of transformation for V_6C_5 and V_8C_7 are very dependent on (V and C) content. The results of this investigation show that the transformation temperatures are around ~1000ºC in the ternary, with some phases transforming (Samples 15H), some not transforming (Samples 11H, 12H, 13H and 14H) and some partially transforming (Sample 24H). The ~$V_4C_{2.66}$ phase was found in several samples (Samples 11H, 14H, 15H, 17H, 18H and 24H), which was unexpected, since in the V-C binary [1985Car], it is

formed peritectoidally from V_2C and VC at 1320°C. If this finding is correct (bearing in mind the problems in interpreting the XRD results), this suggests it must have formed in a different reaction in the ternary, since V_2C was not found.

Annealing produced σ′ in some samples (Samples 11H, 12H, 13H, 14H and 15H), arising from the retreating (V) solvus.

Except for Sample 8H, which transformed back to (Ni), the nickel-rich phase in other samples (Samples 6H,17H, 21H, 22H and 24H) had not transformed after annealing. There were no transformations of the as-cast (Ni) phase after annealing in Samples 7H, 10H, 13H, 18H and 20H. The highest temperature stability of the Ni-V phases must have been around ~1000°C because in the binary they are 1045°C for ~Ni_3V and 922°C for ~Ni_2V [1982Smi].

5.5 Mechanical properties

5.5.1 Hardness

The results of the Vickers hardness measurements (5kg load) on the as-cast (Table 4.82) and heat treated (Table 4.84) samples are superposed on the solidification projection and isothermal sections (Figures 5.6 and 5.7) respectively.

More than half of the as-cast alloys had hardnesses between 400HV_5 and 700 HV_5. The as-cast nominal Ni_{10}:V_{50}:C_{40} (at.%), Sample 1, had the highest hardness value of 1574 HV_5. The sample was very hard and brittle and had major cracks in the indentation. The highest value was due to high proportion of carbide (~V_6C_5) in the microstructure.

Hardnesses in Samples 14, 15 and 23 with nominal compositions: Ni_{28}:V_{54}:C_{18}, Ni_{32}:V_{56}:C_{12} and Ni_{24}:$V_{58.6}$:$C_{17.4}$ (at.%), were high, with average HV_5 values of: 1086, 1093 and 1065 respectively. The high values may be due to σ′ phase which was common to the samples. However, as-cast nominal Ni_{30}:V_{65}:C_5 (at.%), Sample 9, with the same σ′ phase had an average hardness value 378 which was low compared to Samples 14, 15 and 23. The low value may be due to the high proportion of the eutectic in the microstructure, and lower carbide content.

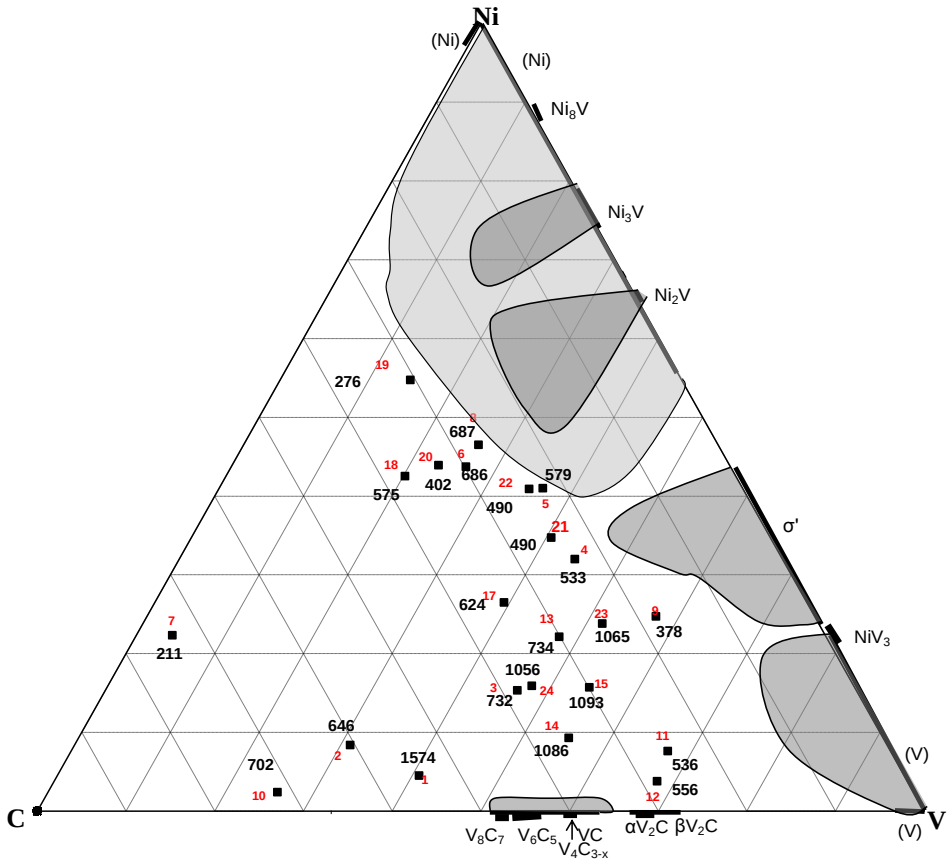


Figure 5.6. Hardness values of as-cast C-Ni-V alloys superposed on the solidification projection (at.%).

Comparing the present work with the hardness values reported by Mohammadpour *et al*. [2012Moh] which ranged from 1375 - 1400HV_{30}, it can be seen that the hardness values of the present work were lower. The high values were reported [2012Moh] to be due to pre-added grain-refining carbides $Ti(C_{0.7}N_{0.3})$ and $(W_{0.24}Ti_{0.76})C$).

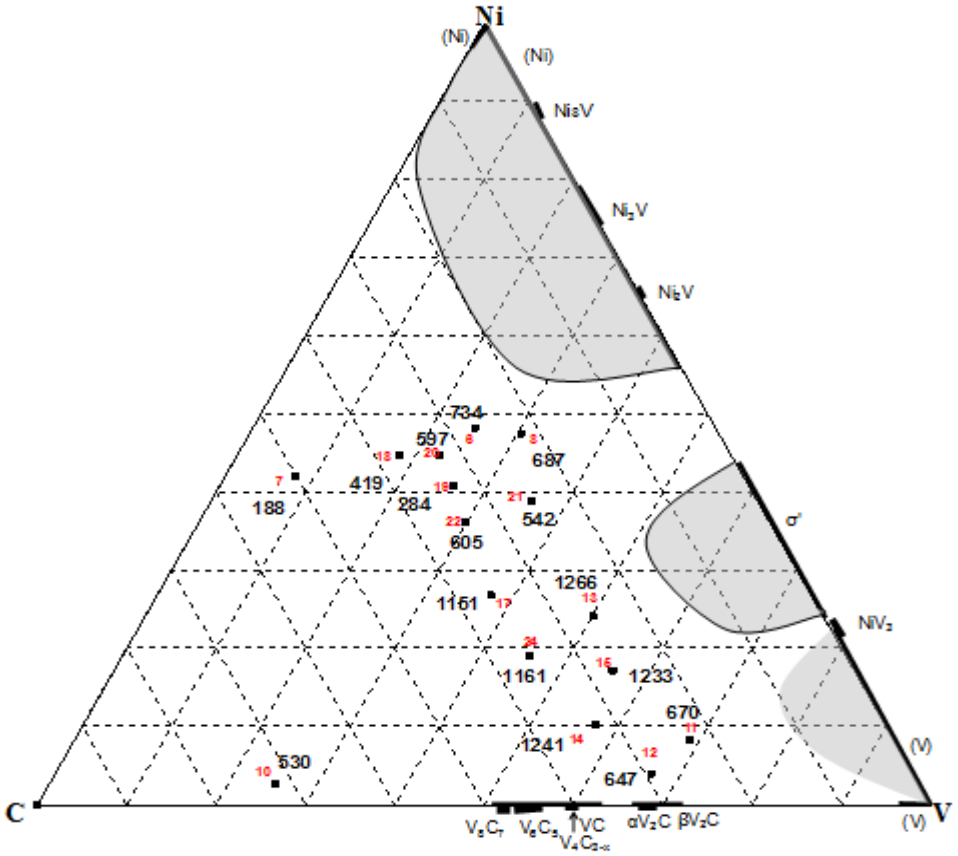


Figure 5.7. Hardness values of C-Ni-V alloys annealed (1000°C, 1000h) and quenched, superposed on the isothermal section (at.%).

After annealing at 1000°C, more than half of the alloys had increased hardnesses. These changes in hardness were due to either a change in phase, or a change in volume fraction of a specific phase.

Three alloys stood out having exceptional high hardness (above 1000 HV_5) compared to the rest, namely Samples 13H, 14H and 15H, all with σ′ phase, which had the highest hardnesses of 1266, 1241 and 1233, respectively compared to other samples without sigma phase. Thus, σ′ phase seemed to be very hard intermetallic compound.

5.5.2 Toughness

The different slip modes of the as-cast are superposed on the solidification projection (Figure 5.8) with deformation responses shown in Figure 5.9. The different slip modes of the heat treated are superposed on isothermal section (Figure 5.10), with their deformation responses are shown in Figure 5.11.

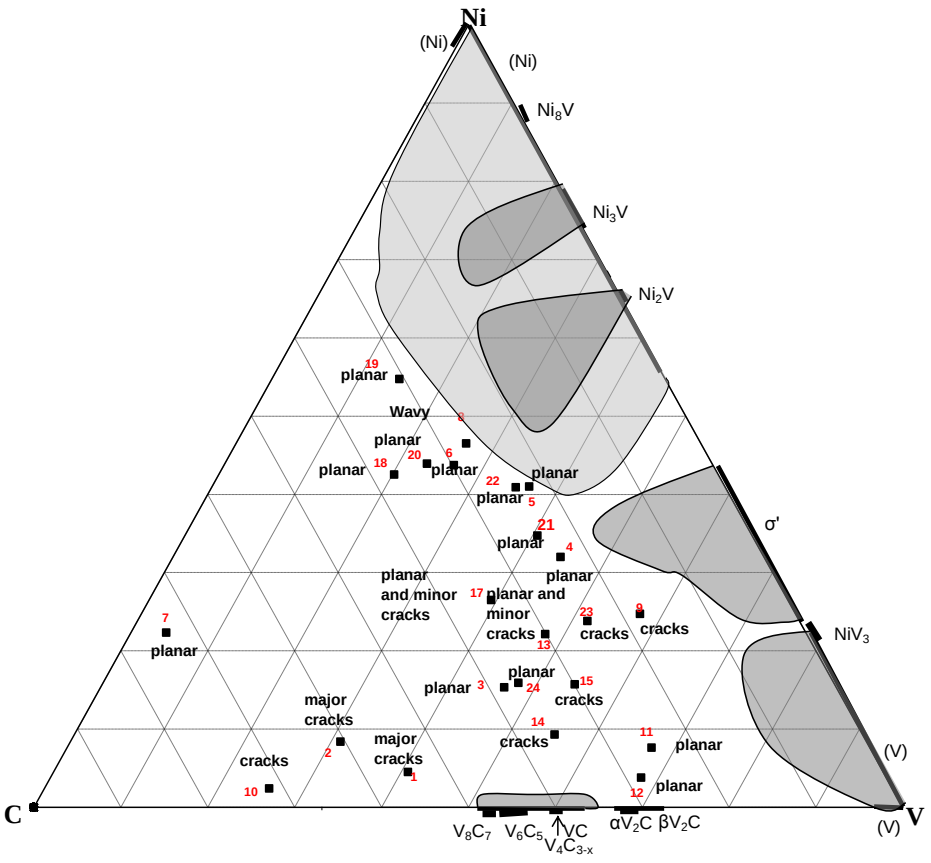


Figure 5.8. Summary of the slip modes of as-cast C-Ni-V alloys, superposed on the solidification projection (at.%).

The as-cast alloys with about ≥30 at.% Ni (actual compositions) exhibited planar or wavy slip, while those with ≤20at.% Ni had cracks, showing their brittleness. Some alloys had major cracks showing their high brittleness.

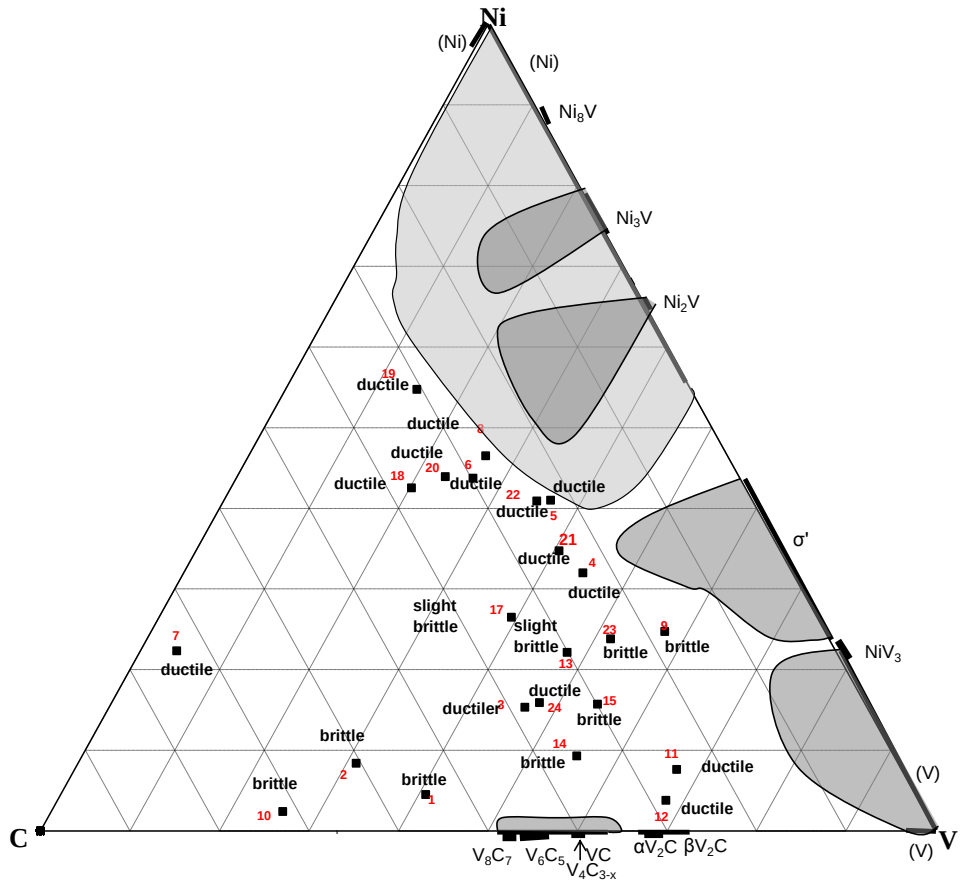


Figure 5.9. Summary of the deformation responses of as-cast C-Ni-V alloys, superposed on the solidification projection (at.%).

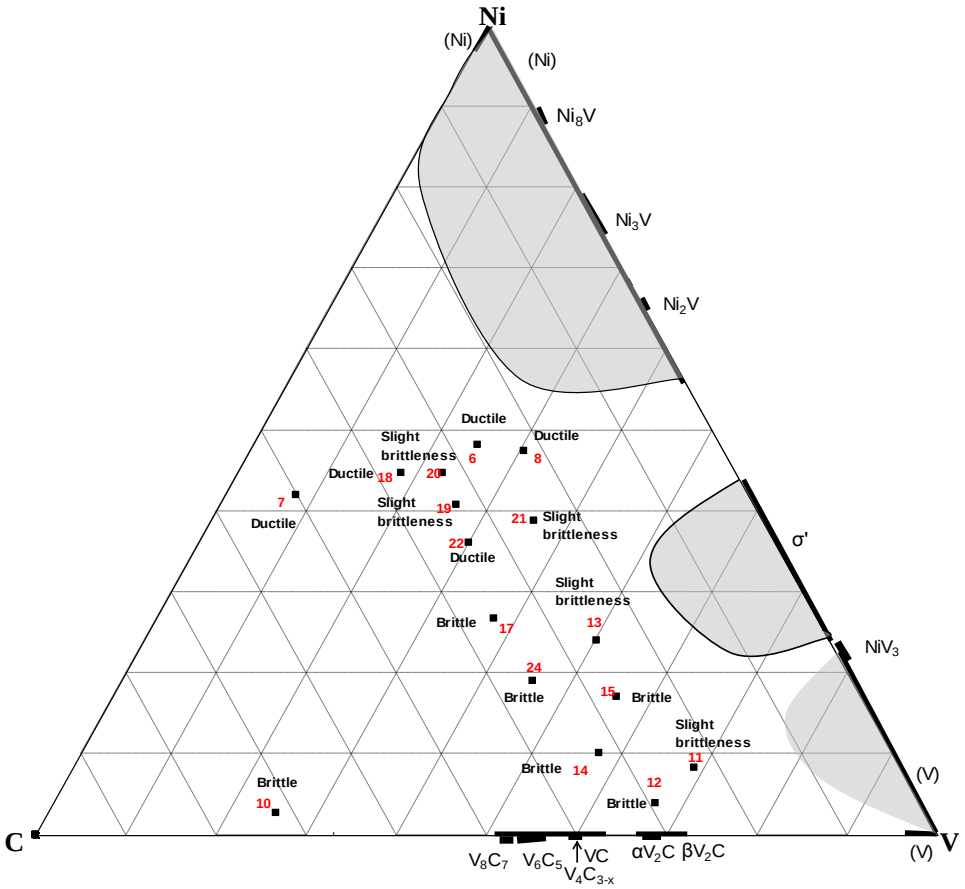


Figure 5.10. Summary of the slip modes of heat treated C-Ni-V alloys, superposed on the isothermal section (at.%).

Comparing Figure 5.10 with Figure 5.8 (as-cast), minor cracks were observed in some of the samples (Samples 11H, 13H, 19H, 20H and 21H) after heat treatment, which were not seen before the annealing. Most of the cracked samples (Samples 11H, 13H, 19H, 20H and 21H) were due to changes in coefficient of expansion and /or change in phase (Sample 13H). Figure 5.10 shows the mechanical behavior superposed on the 1000°C isothermal section. Most of the samples with minor cracks showed slight brittleness, while the planar samples were ductile.

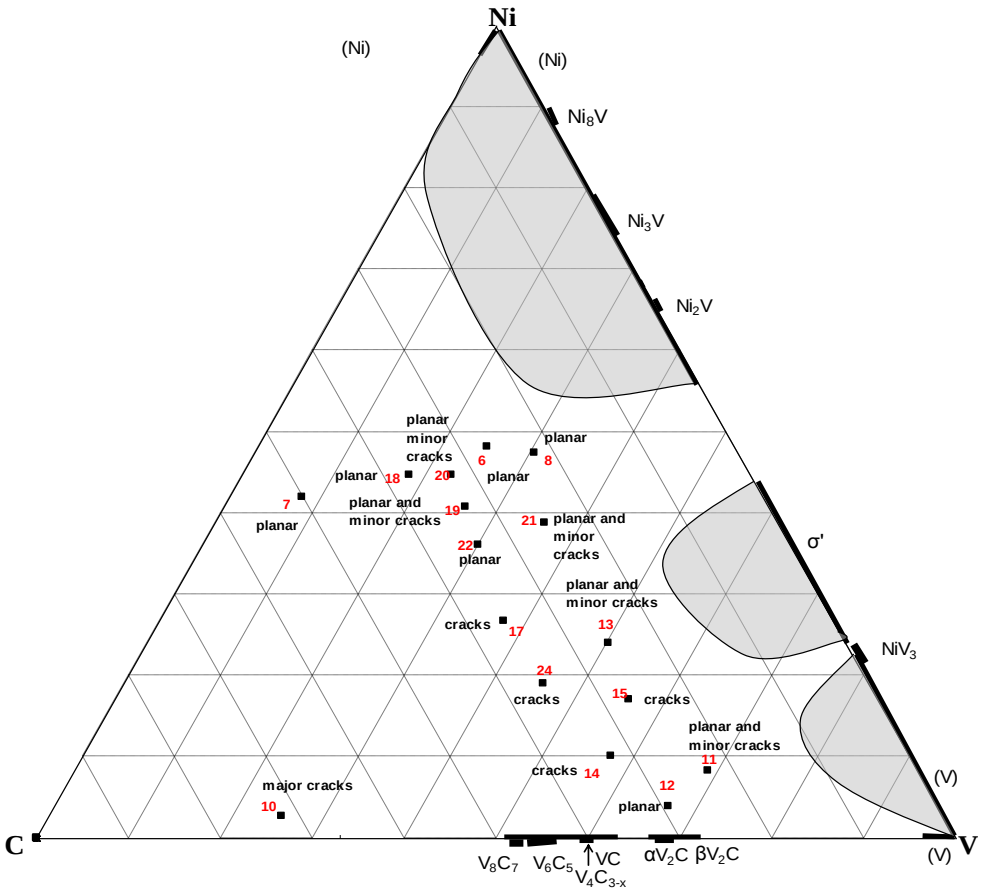


Figure 5.11. Summary of the deformation responses of heat treated C-Ni-V alloys, superposed on the 1000°C isothermal projection (at.%).

5.5.3 Fracture toughness (K_{IC})

In general, fracture toughness (K_{IC}) is low for brittle materials and high for ductile materials. This is shown by the fracture toughness (K_{IC}) values given in Table 5.7 [1993Dow, 1994Cal].

Fracture toughnesses of the as-cast (Table 4.83) and heat treated (Table 4.85) C-Ni-V alloys were found to be very low when compared to other metal alloys, as can be seen in Table 5.7. However, the fracture toughness for this work which ranges between 0.9-5.2 was comparable to the ceramics.

Table 5.7. Examples of room-temperature plane strain fracture toughness values [1993Dow, 1994Cal].

Materials	Fracture toughness ($MPa.m^{-1/2}$)
Metal	
2024-T351 Aluminium alloy	36
4340 Steel (tempered at 260°C)	50
Titanium alloy (Ti-6Al-4V)	44-66
Ceramics	
Aluminium oxide	3.0-5.3
Silicon carbide	3.0-5.0
Soda-lime glass	0.7-0.8
Concrete	0.2-1.4

5.5.4 Friction response of the as-cast samples

The friction response of the cemented carbide/steel sliding pairs can be aligned with one or more of the four hypothetical S shaped patterns defined by Bhushan in Figure 2.14 [2002Bhu]. Table 5.8 indicates the pattern followed by each of the investigated sliding systems.

Table 5.8. Hypothetical friction patterns followed for each sliding system under each test condition [2002Bhu].

Sample no.	Friction pattern
19	II
20	II
21	III
22	III
23	IV
24	I

The obtained curves Cr steel paired as-cast Samples 19 and 20 (Figures 4.320 and 4.321) followed pattern II. Pattern II involves smoothing of the contact surfaces, due to plastic deformation, which resulted in a decrease in the contribution of the ploughing component to friction. Any wear debris present on the surface led to a decrease in the real contact area. The samples had a much lower hardness than the steel ball and thus easily

plastically deformed under the harder material resulting in a high wear rate for the cemented carbide.

Samples 21 and 22 displayed pattern III associated with the constant formation and subsequent expulsion of wear particles during sliding, consequently led to high wear rates (Figures 4.322 and 4.323). During the initial sliding contact, the friction level was high due to very restricted pin-on-plate contact area. The instabilities in the friction coefficient curves can be related to the continuous changes in the sliding contact surface, particularly during the running-in stage. The initial friction was mainly caused by strong asperity interaction (fragmentation and deformation). As sliding proceeded, the asperities were worn down, the initial surface roughness reduced and, hence, the interlocking friction component (i.e. normal contact force (F_n) and tangential force (F_t)) decreases and the fluctuations in the friction curves diminished, indicating that an equilibrium stage had been reached.

Sample 23 (Figure 4.324) resembles pattern IV, with the most irregular friction response pattern, and the friction coefficient was higher than other samples. Pattern four (IV) is similar to pattern (III), although the high and low levels were not repetitive, but rather unpredictable. The fluctuations observed during the evolution of friction coefficient may be due either to low frequency vibrations that occurred in the tribometer [2009Keg] and/or of rupture phenomena and regeneration of a tribological layer of wear debris from the ball and specimen, which changed along the sliding distance [2001Que].

Sample 24 (Figure 4.325) displayed the first pattern (I), the friction stayed at an initial level for a period of time and then slowly increased to another steady state value. This stage is associated with an abrupt removal of fragments of materials, which constituted the tribopair, causing an increased in ploughing and three body wear, and consequently the value of friction coefficient. As the sliding continued, a steady state was reached in which the wear debris was removed and embedded in the wear track to form a tribolayers.

5.5.5 Sliding wear volume of as-cast samples

The wear rates of the materials were defined by the dimensional wear coefficient, k, which is based on the volume of material lost during wear, the applied load and the material hardness. Sliding pairs which displayed high friction values, penetration depth and wear tracks were found to have high wear coefficients which translated into high wear rates.

Figure 5.12 shows that Samples 19 and 23, with average HV hardness values of 267 and 1065, had the highest wear volume, an indication of high wear rate and low wear resistance. Samples 20, 21, 22 and 24 with average hardness values 402, 489.6, 489.6 and 1052 had lower wear volumes, an indication of low wear rate and higher wear resistance. With the exception of Sample 23, the wear rates followed a particular trend, an increase in wear rate with decreased material bulk hardness values. The anomalies in Sample 23 could be attributed to its high coefficient of friction and penetration depth (2.63µm) compared to other samples. Also, they could be attributed to the presence of the sigma phase in the microstructure, because it was the only sample that had the sigma phase.

Figure 5.13 shows the variation of wear tracks and wear coefficients of the as-cast samples with hardness values, with only one result per condition. The wear track and the wear coefficient decreased as the hardness increased, except for Sample 23 with hardness value 1064. The wear track and wear coefficient of Sample 23 increased with the hardness. The increase could be attributed to the presence of the sigma phase in the microstructure, because it was the only sample that had the sigma phase.

5.5.6 Wear surface analysis of as-cast samples

Several mechanisms (abrasive, adhesive, oxidative and plasticity-dominated wear) have been proposed to explain how sliding wear operates. Plastic deformation had been shown to be the main mechanism of wear [1992Hut, 2011Mer]. Combinations of these mechanisms were observed for all the sliding pairs. The extent of damage was found to depend on the interaction between the inherent properties (e.g. hardness) of the materials in contact, the level of mechanical stress exerted under the applied load, the sliding velocity and oxide formation [1992Hut].

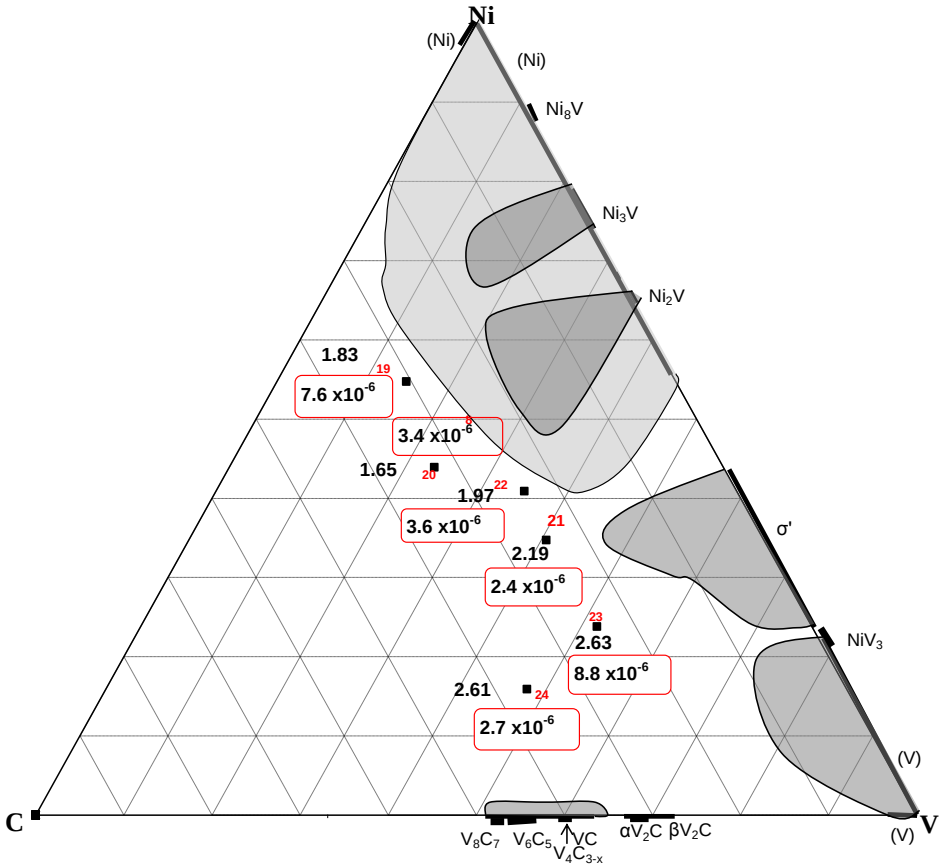


Figure 5.12. Summary of the penetration depth (μm) of the ball on to the as-cast samples and the wear coefficients superposed on the solidification projection (at.%).

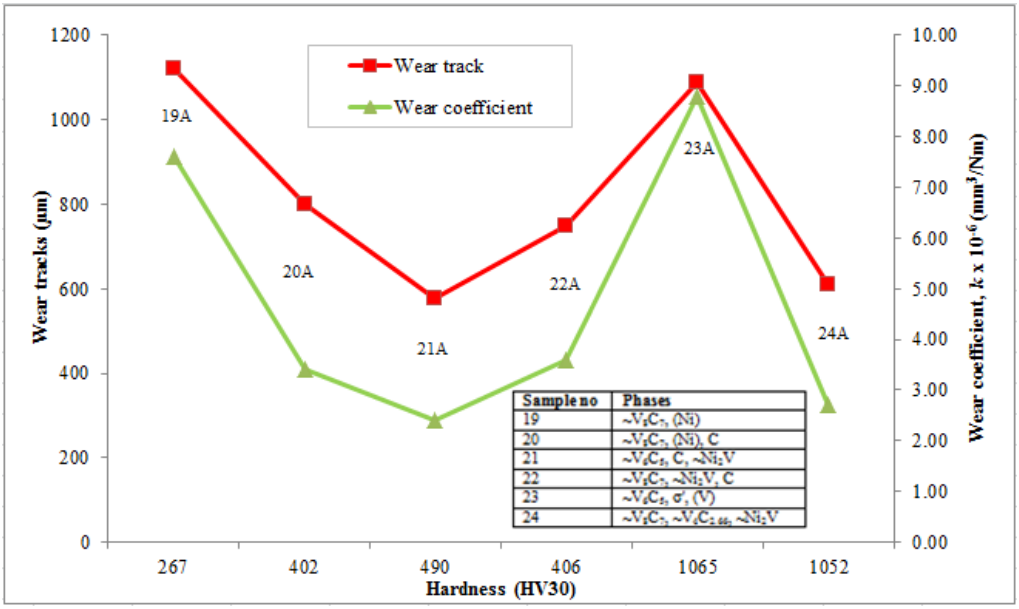


Figure 5.13. The dependence of wear track and wear coefficient on the hardness values in as-cast condition.

Friction and wear are generally believed to be caused by a combination of abrasive ploughing, adhesive interaction and asperity deformation [2011Esp]. The abrasion of the Ni-VC alloys was evidenced by the SEM microstructures presented in Figure 4.326 (Samples 19, 20, 21 and 22). The observed smoothing of the Ni-VC surfaces during sliding wear indicated that asperities were being plastically deformed during the sliding wear contact.

The occurrence of a thin, adhered wear debris film on the wear surface of Samples 23 and 24, as well as the presence of oxygen in the EDX analyses, and the reduced roughness of the wear track demonstrated that tribolayers were formed [2010Bon]. These contained oxides as a result of the compaction of wear debris and the oxidation of binder phase. The expulsion of the binder phase from between the vanadium carbide grains [2009Keg, 2011Esp] was thought to be the initial stage of wear. This was seen for as-cast Samples 23 and 24, and heat treated Samples 22H and 24H in Figures 4.326 and 4.334 and resulted in carbide removal and/or carbide fracture.

5.5.7 Friction response of heat treated samples

The friction response of the heat treated/Cr steel sliding pairs were aligned with one or more of the four hypothetical S shaped patterns in Figure 2.15 [2002Bhu] as shown in Table 5.9.

Table 5.9. Hypothetical friction patterns followed for each heat treated samples sliding system under each test condition [2002Bhu].

Sample no.	Friction pattern
19H	III
20H	III
21H	II
22H	II
24H	I

Samples 19H and 20H (Figures 4.328 and 4.329) followed pattern III after the heat treatment compared to the as-cast which was pattern II. Patterns III was associated with

the constant formation and subsequent expulsion of wear particles during sliding consequently leading to high wear rates.

The curves for Cr steel paired heat treated Samples21H and 22H (Figures 4.330 and 4.331) followed pattern II. The behaviour observed in stage the early stage can be justified by the theory of multi-asperity contacts according to Zhang *et al.* [1991Zha]. This theory explained that when two surfaces are in contact, part of the load is carried by asperity contact over an area, and part of the load is carried by particle debris over a contact area. Thus, the friction coefficient is due to three components, adhesion, asperity ploughing and debris ploughing. According to this theory, the initial drop of the coefficient of friction is due to the reduction of surface roughness and the subsequent increase was associated with increased real area of contact, due to the generation of wear debris from counterpart.

Sample 24H displayed pattern I after heat treatment as its as-cast sample. This stage was associated with an abrupt removal of fragments of materials, which constitute the tribopair, causing an increase in ploughing and three body wear, and consequently the value of friction coefficient.

5.5.8 Sliding wear volume of heat treated samples

The penetration depth and the wear coefficients, k, (in rectangles) were superposed on the isothermal section in (Figure 5.14). Samples 19H, 20H and 21H had high wear volume and high wear tracks, an indication of high wear rate. It could be as a result of high binder content as shown in Table 4.88. It is known that the wear resistance of cemented carbides generally increases with the reduction of grain size and by decreasing binder content, due to increased hardness [2005Gan].

Samples 22H and 24H, with low wear tracks (Table 4.88), had the lowest wear loss. The reason could be attributed to high hardness values, low wear tracks and low binder content. Bonny *et al.* [2010Bon] attributed the decelerating wear rate after running-in to the load-bearing capacity of large carbide grains retained at the sliding surface of the cemented carbide, and their ability to reduce binder-to-binder contact during sliding.

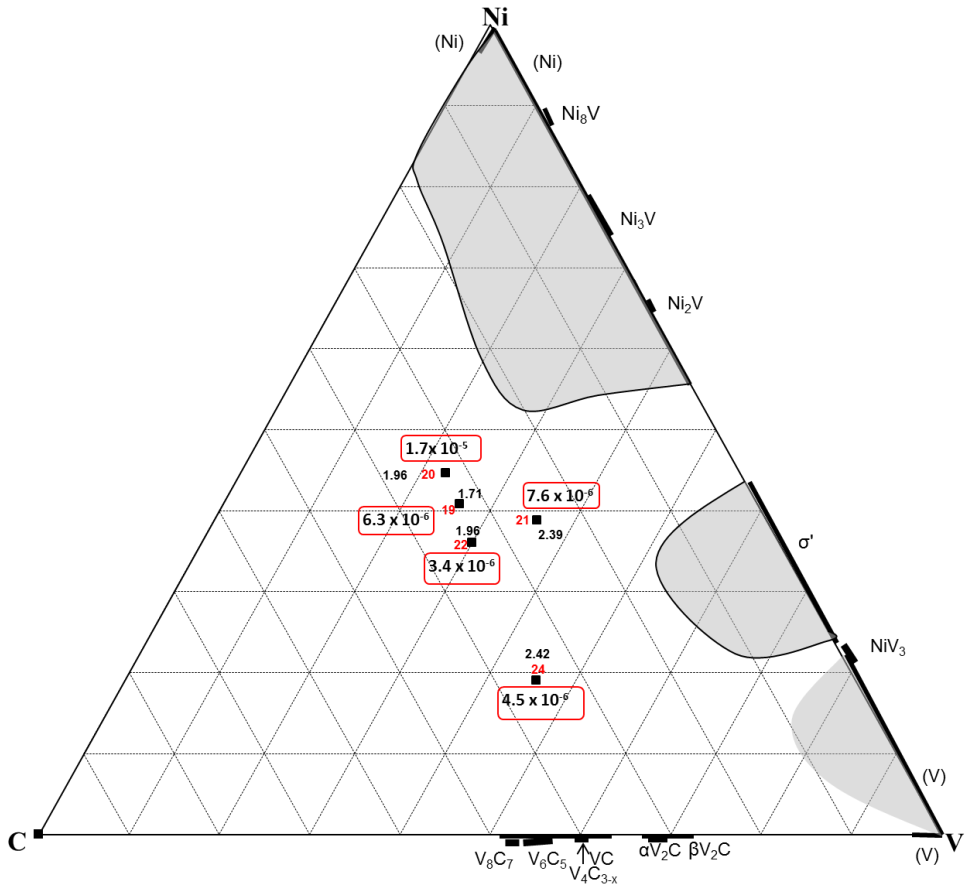


Figure 5.14. Summary of the penetration depth (µm) of the ball on to the heat treated samples and the wear coefficients superimposed on the isothermal section (at.%).

The variation of wear tracks and wear coefficients of the heat treated samples with hardness values are shown in Figure 5.15, with only one result per condition. Samples 19H, 20H and 21H had high wear tracks with an increase in hardness, an indication of high wear rate. It could be as a result of high binder content. Samples 22H and 24H had lowest wear tracks compared to other samples with an increase in hardness values of 605 and 1161 respectively.

Figure 5.16 compared the wear coefficients of the heat treated and as-cast samples. Sample 19H and 22H showed an improvement in wear resistance after heat treatment, with a decrease in wear coefficients. There was an increase in wear coefficients for Samples 20H, 21H and 24H. The large increase in wear coefficients of Sample 20H, 21H

and 24H were as a result of increase in wear tracks: 798.3 to 1256.8µm for Sample 20H, 577.4 to 985µm for Sample 21H and 611.4 to 747.2µm for Sample 24H.

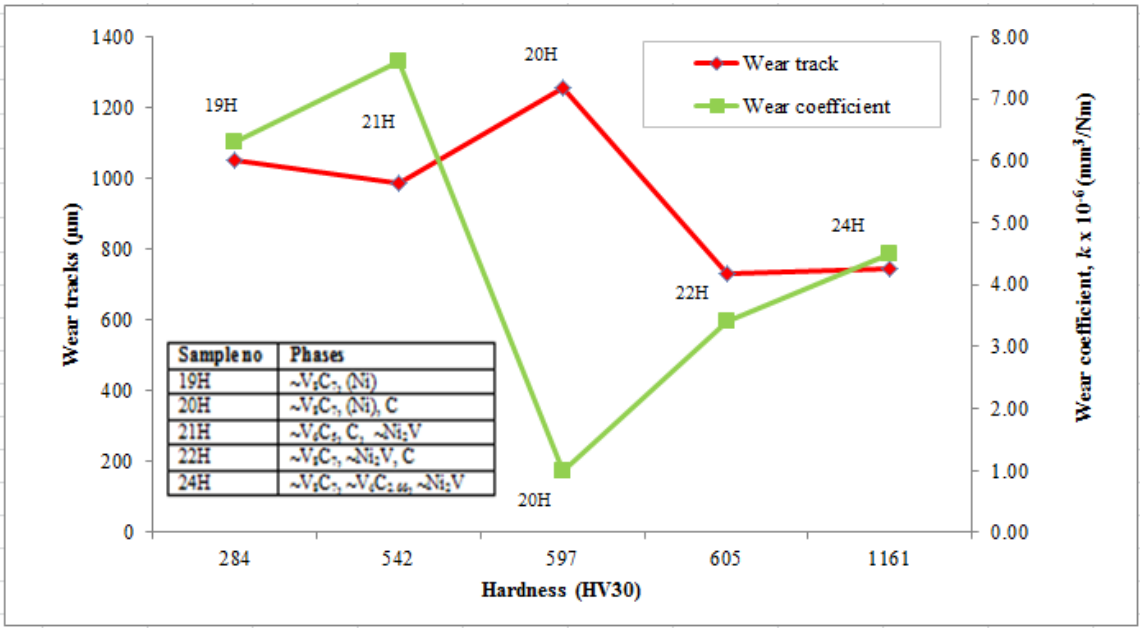


Figure 5.15. Dependence of wear track and wear coefficient on the hardness values in annealed condition.

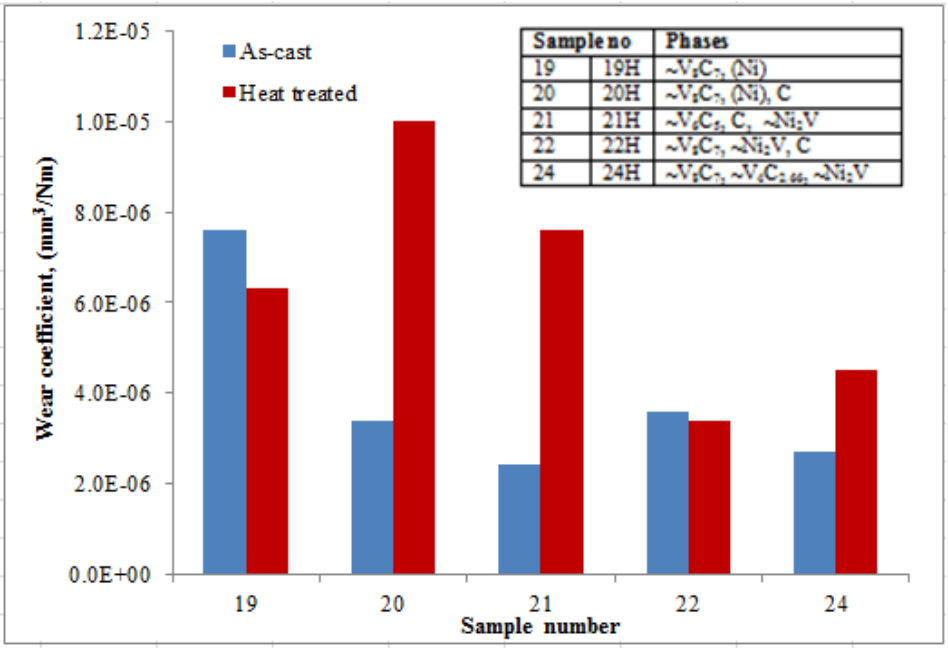


Figure 5.16. Comparison of the wear coefficients of the heat treated and as-cast samples.

5.5.9 Wear surface analysis of heat treated samples

Heat treated Samples 19H, 20H and 21H (Figures 4.334 (a) to (c)) showed similar wear mechanisms to its as-cast samples (Figures 4.326 (a) to (c)), but the plastic deformation were not as severe. Instead, increased wear debris was seen on the samples. The wear resistance of Sample 19H was higher than its as-cast alloy as shown in Figure 5.16. Samples 20H and 21H also had less severe plastic deformation, due to their higher hardness values after heat treatment. Their wear resistances were low, due to the brittleness of the alloys, and had more wear debris which were not adhered to the contact surface and higher wear coefficients, compared to Sample 19H.

High tribolayers observed in Samples 22H and 24H were due to increased amount of debris generated and high temperature (due to surface oxidation) reached in the sliding contact surface. The wear rate was also correlated to their high hardness and low binder content. That is, it is known that the wear resistance of cemented carbides generally increases with the reduction of grain size and by decreasing binder content, due to increased hardness [2005Gan].

After the observation of the different wear mechanisms, a possible sequence of surface damage was envisaged. Wear would start at the binder phase which was removed by a combination of plastic deformation and/or micro-abrasion, which in turn facilitated the removal and/or fracture of the VC grains. The wear debris generated, i.e. ~VC grain fragments and binder debris, would then act as third body, causing further abrasion or could adhere to the contact surface creating a tribolayer.

The metallurgical studies of wear in VC-Ni have been few in relation to other tribological work, the investigations which have been carried out suggested that a link can be established between wear resistance and microstructure.

5.5.10 Comparison with literature data

The reported wear resistances in Tables 5.10 [2010Bon] and 5.11 [1999Yan], indicate that the wear rate of the conventional cemented carbide varied with respect to cemented carbide composition. This was evident in the present work (Table 5.12). It was difficult to compare the wear values measured from this work with those from Table 5.10, as the

experiments from the literature were conducted under different conditions, However, the current results were comparable to the work of Yang [1999Yan] in Table 5.11, despite the fact that the samples compositions were not optimized and were selected after the completion of the phase diagram.

From the present work, the influence of microstructure on wear resistance was noticeable, in particular, composition, nature of the matrix and the effect of the heat treatment, as shown in Tables 5.13 and 5.14 for as-cast and heat treatment respectively. As-cast Samples 19-22 had high binder content which made them to be ductile but low in hardnesses. Sample 23 had reasonable binder but was very brittle due to the presence of σ′ phase. Sample 24 had combined the low binder and high hardness which was the requirement for good wear resistance. Also with the exception of Sample 24 all other samples had eutectics in their microstructures. In annealed condition, all the alloys increased in binder proportion, which made the alloys to be prone to high wear rate.

Table 5.10. Wear scar dimensions and volumetric wear rate for WC–10wt%Co and WC–12wt%Co slid for 10km at 0.3ms−1 against WC–6wt%Co as function of contact load [2010Bon].

Sample compositions (at.%)	Normal force (N)	Width (mm)	Depth (μm)	HV_{10}	Wear coefficient (10^{-6} μm^{3}N^{-1} μm^{-1})
WC-10wt%Co	15	0.75	3.1	1149	22
	35	0.88	5.8	1149	20
	50	1.12	9.2	1149	20
WC-12wt%Co	15	0.69	2.6	1286	18
	35	0.84	4.6	1286	17
	50	0.96	7.0	1286	16

Table 5.11. Wear rate for WC-Co Grade S6 slid for 3800m at 100ms^{-1} [1999Yan].

Sample compositions	Normal force (N)	Tracks width (mm)	Penetration Depth (μm)	HV_{10}	Wear coefficient (mm^3/Nm)
WC-Co GradeS6	500	N/A	1.0	1465	2.4 x10^{-6}

Table 5.12. Wear rate for VC-Ni Slide for 300m at 0.3ms^{-1} (Present work).

Sample compositions	Normal force (N)	Tracks width(mm)	Penetration Depth (µm)	HV_{10}	Wear coefficient (mm^3/Nm)
VC-31wt%Ni	10	0.61	2.2	1052	2.7 x10^{-6}

Sample 24 could be chosen because of the differences in the properties of the as-cast Sample 24 compared to other samples both in as-cast and heat treated condition as shown in Tables 5.10 and 5.11. The high hardness of as-cast alloy 24, together with low binder content is in agreement with Gant *et al.* [2005Gan], for good wear resistance of cemented carbides, which generally increases with decreasing grain size and decreasing binder content. Also, as-cast Sample 24 formed a tribolayer which reduced the friction. This was attributed to the outstanding tribological behaviour of vanadium carbide; high abrasion resistance with a low friction coefficient and high hardness, which is superior to other similar carbide in group IVB and VB except TiC. Also, VC has a fast oxidation kinetics that led to the formation of vanadium oxide (V_5O_2) and oxycarbide surface layers (which suppresses the plasticity-dominated mechanism) which are comparable to the ones of solid lubricants [1997Gri].

With reference to reported wear coefficient work in Table 5.11 for conventional tungsten carbide, slide on medium carbon steel of hardness 1465HV_{10} of WC-Co Grade S6 for 3800m at 100ms^{-1} to be 2.4 x10^{-6} (mm^3/Nm). Comparatively, despite different conditions as shown in Table 5.12, it seems that the wear rate of as-cast alloy 24, obtained from the present study which was 2.7 x10^{-6} (mm^3/Nm) is relatively closer to the one reported by Yang. This result was considered promising, since the sample composition had not been optimised.

Table 5.13. Wear scar dimensions and volumetric wear rate for as-cast samples slid for 300m at 0.3ms^{-1} against Cr steel ball at constant load 10N as a function of compositions.

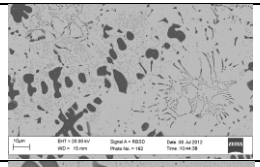
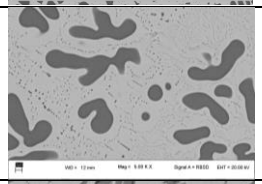
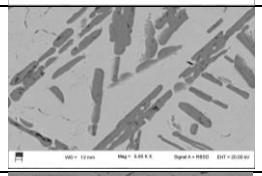
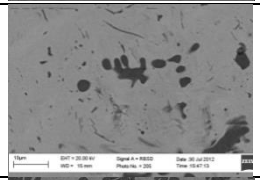
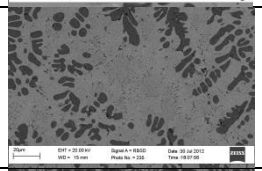
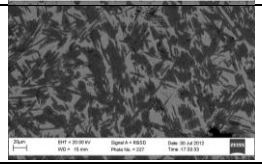
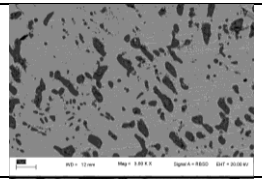
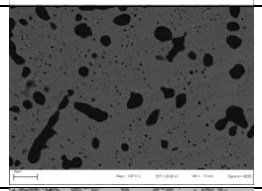
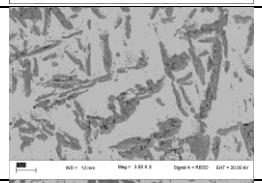
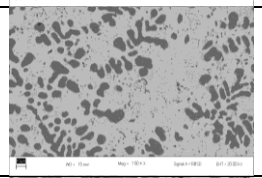
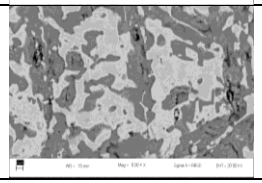
Sample no.	Sample compositions (at.%)	Microstructure	Phases	HV_5	Depth (μm)	Width (mm)	Wear coefficient (mm^3/Nm)
19	$Ni_{68}:V_{14}:C_{18}$		~V_8C_7, (Ni)	267	1.83	1120.9	7.6E-06
20	$Ni_{59}:V_{27.2}:C_{13.8}$		~V_8C_7, (Ni), C	402	1.65	798.3	3.4E-06
21	$Ni_{39}:V_{42.8}:C_{18.2}$		~V_6C_5, C, ~Ni_2V	490	2.19	577.4	2.4E-06
22	$Ni_{49}:V_{33.3}:C_{17.7}$		~V_8C_7, ~Ni_2V, C	406	1.97	747.3	3.6E-06
23	$Ni_{24}:V_{58.6}:C_{17.4}$		~V_6C_5, σ′, (V)	1065	2.26	1087	8.8E-06
24	$Ni_{22.1}:V_{49.1}:C_{28.8}$		~V_8C_7, ~$V_4C_{2.66}$, ~Ni_2V	1052	2.16	611.4	2.7E-06

Table 5.14. Wear scar dimensions and volumetric wear rate for heat treated samples slid for 300m at 0.3ms^{-1} against Cr steel ball at constant load 10N as a function of compositions.

Sample no.	Sample compositions (at.%)	Microstructure	Phases	HV_5	Depth (μm)	Width (mm)	Wear coefficient (mm^3/Nm)
19H	$Ni_{68}:V_{14}:C_{18}$		~V_8C_7, (Ni)	284	1.71	1053	6.3E-06
20H	$Ni_{59}:V_{27.2}:C_{13.8}$		~V_8C_7, (Ni), C	597	1.96	1256.8	1.0E-05
21H	$Ni_{39}:V_{42.8}:C_{18.2}$		~V_6C_5, ~Ni_2V	542	2.39	985	7.6E-06
22H	$Ni_{49}:V_{33.3}:C_{17.7}$		~V_8C_7, ~Ni_2V, C	605	1.96	730.3	3.4E-06
24H	$Ni_{22.1}:V_{49.1}:C_{28.8}$		~V_8C_7, ~$V_4C_{2.66}$, ~Ni_2V	1161	2.42	747.2	4.5E-06

5.5.11. Comparison of phase diagrams with VC-coated Ni

The compositions measured by AES punctual analysis after depositing VC [2009Rui] onto pure Ni by CVD are shown in Table 5.15 and Figure 2.1a and b. They were normalised to eliminate oxygen (which was a minor component).

Table 5.15. Composition of the phases measured by AES punctual analysis on as-coated samples [2009Rui].

	Reported composition (at.%)[2009Rui]				**Normalised to eliminate oxygen (at.%)**			**Phases interpreted from this work**
Regions and phases	C	V	Ni	Sum	C	V	Ni	
A: External layer	15	53	25	93	16.1	57.0	26.9	VC + σ′
B: Discrete carbide in the matrix	26	57	13	96	27.1	59.4	13.5	VC + σ′
C: Continuous carbide	25	50	21	96	26.0	52.1	21.9	VC + σ′
D: Ni_2V	0	35	62	97	0.0	36.1	63.9	~Ni_2V
E: Ni_3V	6	21	69	96	6.3	21.9	71.9	~Ni_3V
F: Ni matrix	0	0	87.5	87.5	0.0	0.0	100.0	Pure Ni

Figure 5.18 shows the solidification projection of the present work with the superposed values from the graded metal-carbide composite [2009Rui], and the phase fields were included in Table 5.15. Ruiz *et al.* [2009Rui] had expected that the phases would progress from VC to Ni, showing any intermediate intermetallic phases. However, this was not seen and instead, they obtained the values in Table 5.15. This can be explained by the current work and their own micrographs Figure 2.1b, where it can be seen that A, B and C layers are actually two phases. The AES technique is not directly comparable to EDX, and the analyses can be done on smaller regions more accurately. The current work found no ternary phases, in disagreement with Holleck [1975Hol]. Given that the thinner layers were actually two-phase, the results agree well, although the second phase in the external layers was σ′.

Ruiz *et al.* [2009]'s D layer was correctly identified as ~Ni_2V, but surprisingly without the carbon observed in the current work. Layer C is a mixture of vanadium carbide and σ′. Layer E was correctly identified as ~Ni_3V, also with rather less carbon content than seen in the current samples. This could mean that all the analyses for this phase (Samples 3, 4, 5, 8, 17, 21, 22 and 24), which pointed towards the E composition, were actually for ~Ni_3V and would have limited carbon content. The result of the current work was due to the fineness of the microstructure, which included carbide. It would not be expected that CVD [2009Rui] allowed time for much diffusion. The bulk substrate F was pure Ni, showing no diffusion.

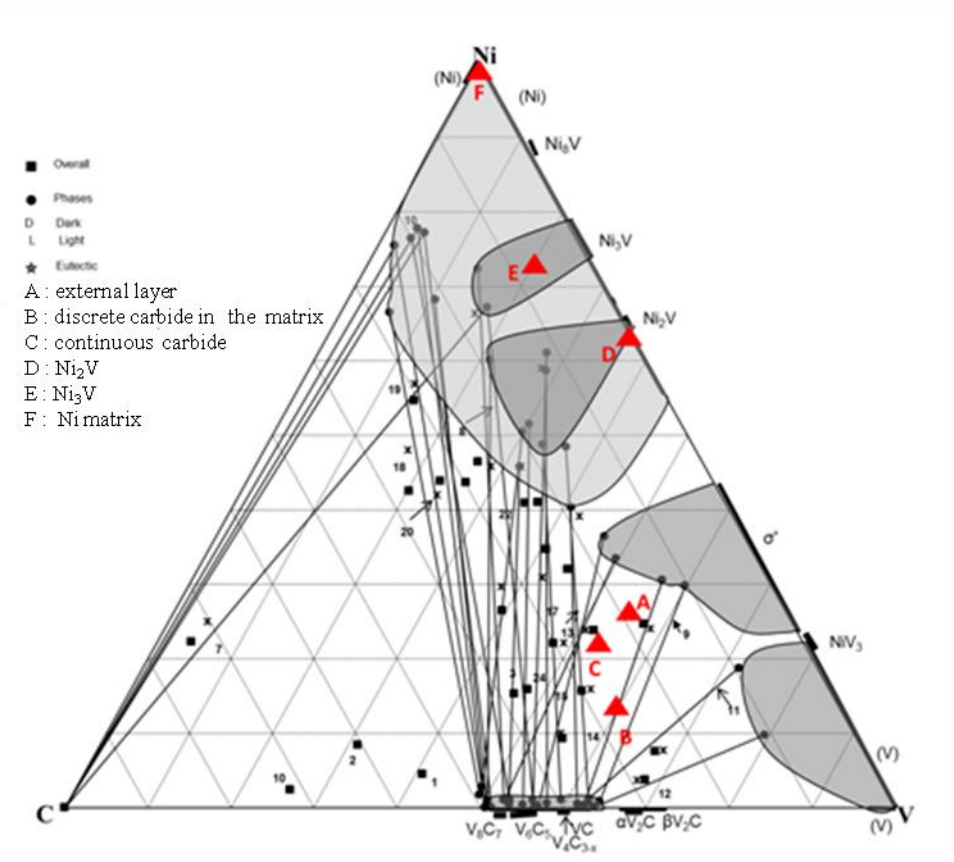


Figure 5.17. Solidification projection showing the superposed VC-coated Ni data (at.%) [2009Rui].

The values from the 1000ºC heat treated VC-coated Ni samples [2009Rui] were superposed onto the 1000ºC isothermal section of the present study, after normalising to remove oxygen (Table 5.16 and Figure 5.18). After the heat treatment of as-coated samples [2009Rui], microstructural changes were reported: V_8C_7 was formed through solid state transformation as a result of C and V diffusion towards the Ni substrate. However, the transformation twins [2009Rui], were not seen in the present work, but might be expected to have annealed twins, being fcc. Comparing their results (Table 5.16 [2009Rui]) with the current study, layer A, the outer layer, was between graphite, vanadium carbide and (Ni). The layer had at least two phases in their microstructure and one was dark, which could have been graphite. The same was true for B, but with more nickel and a lower probability of C (Figure 2.1c and d).

Table 5.16. Composition of the phases in the heat treated samples at 1000ºC, for 45 minutes measured by AES punctual analysis [2009Rui].

Regions and phases	**Reported composition (at.%) [2009Rui]**				**Normalised to eliminate oxygen (at.%)**			**Phases interpreted from this work**
	C	V	Ni	Sum	C	V	Ni	
A: V_8C_7	55	28	16	99	55.6	28.3	16.2	V_8C_7 + C + (Ni)
B: M_2C	36	24	40	100	36.0	24.0	40.0	V_8C_7 + (Ni)
C: M_2C	24	28	47	99	24.2	28.3	47.5	V_6C_5 + (Ni)
D: Ni_3V	0	37	61	98	0.0	37.8	62.2	~Ni_2V
E: About the same with D	0	37	61	98	0.0	37.8	62.2	~Ni_3V
F: Ni matrix	0	0	89	89	0.0	0.0	100.0	Pure Ni

Layer C [2009Rui] was similar to some of the analyses in this work, and contained more ~Ni_2V rather than (Ni). This would mean perhaps ~Ni_2V was missed in the current work, or that there was difficulty in discerning the phases. All of layers A-C were too small to analyse accurately alone. Analysis D was identified as ~Ni_2V [2009Rui], and in the current work, (Ni) was found. The twins [2009Rui] show that the phase was likely to be

(Ni). The F layer was pure Ni, and interestingly, there was another region shown further inside in one of the micrographs, which was not analysed. Other phases: ~V_6C_5, ~$V_4C_{2.66}$, σ′, (V) and ~VC were not reported [2009Rui]. The current work helped explain the phases found in the coating of VC onto Ni [2009Rui], and agreed in that there were no ternary phases, although ~Ni_2V was found [2009Rui], which did not agree with the current work.

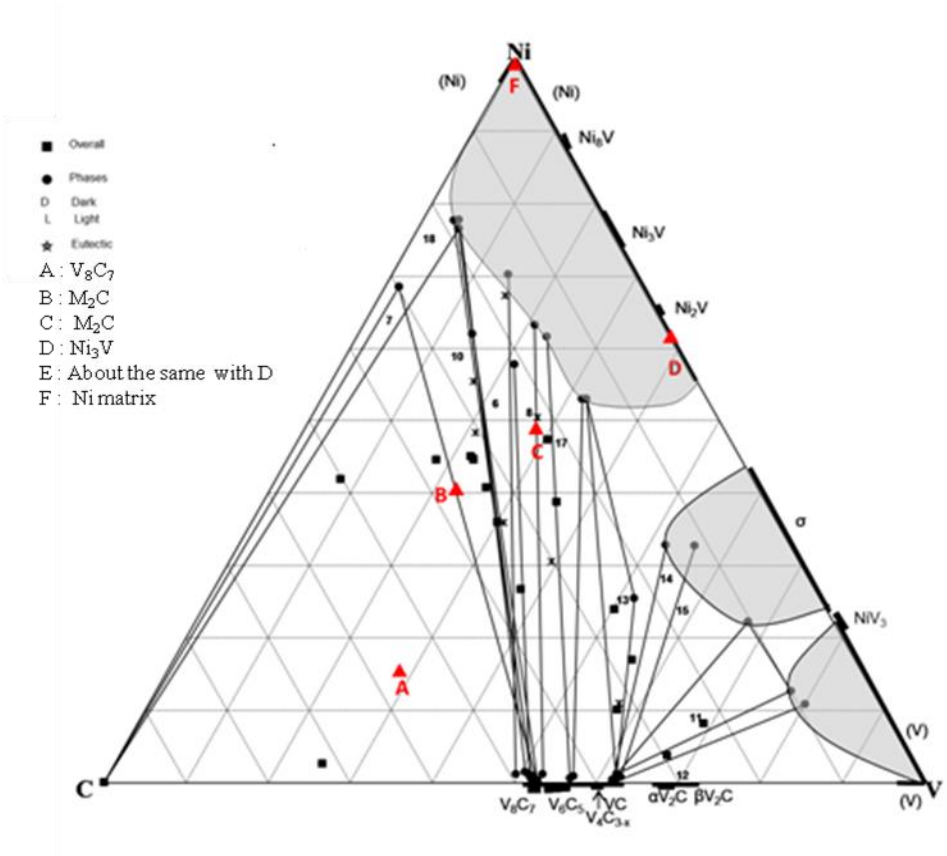


Figure 5.18. Isothermal section showing the superposed VC-coated Ni data (at.%).

5.5.12. Comparison of the investigated C-Ni-V alloyed with rapidly solidified thick deposit of Fe-C-V-Cr-Ni alloy by plasma spraying Hos *et al*. [2009Hos]

The microstructures of the Fe-C-V-Cr-Ni deposit were made up of γ, α, V_8C_7 and Cr_7C_3, while the constituents of Fe-C-V-Cr-Ni in the as-cast condition are made of γ, α, Fe_3C (not seen in plasma sprayed) V_8C_7 and Cr_7C_3 as reported by Hos *et al*. [2009Hos], Figure 5.19. Dendritic vanadium carbides of about 25μm length were reported in the cast sample produced without holding the melt at high temperature (for some time) before casting into the mould (Figure 5.19a), and spheroidised vanadium carbides were reported in the sample which was held at high temperature for 1.9ks before casting (Figure 5.19b). The form of vanadium carbides in the as-sprayed deposit was reported to be more granular compared to that of the cast sample produced by holding the melt before casting (Figure 5.19c). Similar carbide morphologies to Figure 5.19a were seen in the as-cast samples (Figures 4.34, 4.55, 4.147 and 4.172) of the present work. The lamellar structure found to be an iron-chromium carbide in the work of Hos *et al*. [2009Hos] (Figure 5.19a) was not seen in the investigated C-Ni-V alloys, not surprisingly, as there was no iron in the current work. The vanadium carbides in the as-sprayed deposits of Hos *et al*. [2009Hos] were more finer (and granular) than those of the as-cast samples produced in Hos *et al*. [2009Hos] and the present work. The as-sprayed deposits had finer vanadium carbides than in the as-cast samples, because the alloy droplets that accumulate successively on the substrate solidified with a high cooling rate during plasma spraying, Figure 5.19c**.**

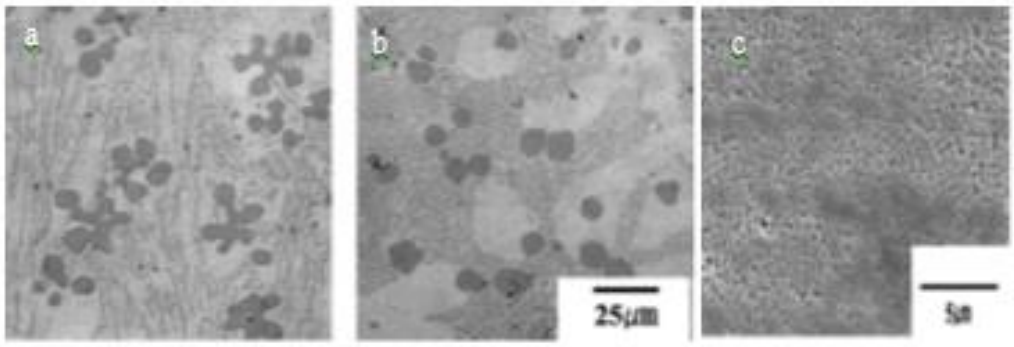


Figure 5.19. SEM images of cross-sections of Fe-C-V-Cr-Ni alloy: (a) as-cast without holding the melt: (b) as-cast after keeping the melt for 1.9ks: (c) as-sprayed deposit [2009Hos].

5.5.13. Comparison of hardnesses of the alloys with σ′ volume fractions

The five as-cast alloys ($Ni_{30}:V_{65}:C_5$, $Ni_5:V_{75}:C_{20}$, $Ni_{28}:V_{54}:C_{18}$, $Ni_{32}:V_{56}:C_{12}$ and $Ni_{24}:V_{58.6}:C_{17.4}$ (at.%)) with σ′ phases had the highest hardness values compared to the samples without σ′ phases. Considering the volume fractions of the σ′ phases, it would be expected that higher volume fractions would give higher hardnesses, but this was not always the case (Tables 5.17, 5.18 and Figure 5.20). Three hardnesses were very similar, around ~1080HV_5, whereas two samples had much lower hardnesses: 378HV_5 and 556HV_5. Relating the lower hardnesses to the microstructure, $Ni_{30}:V_{65}:C_5$ had a much coarser eutectic, and areas with σ′ only, and $Ni_5:V_{75}:C_{20}$ had no eutectic and some occurrences of a lighter phase at the carbide interface. Nominal $Ni_{30}:V_{65}:C_5$ had the highest proportion of σ′ (46 ± 1.3%).

Table 5.17. Nominal compositions (at.%), phases, hardness and approximate σ′ volume fractions (%) of the as-cast samples.

Nominal alloy composition (at.%)	Phases	Hardness (HV_5)	Approximate σ′ volume fraction (%)
$Ni_{30}:V_{65}:C_5$	~VC, σ′, ~$V_4C_{2.66}$	378 ± 25	46 ±1.3
$Ni_5:V_{75}:C_{20}$	(V), ~VC, ~V_2C	556 ± 21	34 ± 3.3
$Ni_{28}:V_{54}:C_{18}$	~VC, σ′, ~$V_4C_{2.66}$	1086 ± 86	26 ± 2.1
$Ni_{32}:V_{56}:C_{12}$	~V_8C_7, σ′, ~$V_4C_{2.66}$	1093 ± 65	38 ± 1.6
$Ni_{24}:V_{58.6}:C_{17.4}$	~V_6C_5, σ′, (V)	1065 ± 56	45 ± 1.9

Table 5.18. Nominal compositions (at.%), phases, hardness and approximate σ′ volume fractions (%) of the heat treated samples.

Nominal alloy composition (at.%)	Phases	Hardness (HV_5)	Approximate σ′ volume fraction (%)
$Ni_{10}:V_{80}:C_{10}$	(V), ~VC, ~$V_4C_{2.66}$	670 ± 51	22 ± 0.8
$Ni_5:V_{75}:C_{20}$	(V), ~VC, ~V_2C	647 ± 26	7 ± 0.7
$Ni_{14}:V_{64}:C_{22}$	(Ni), ~VC, σ′, ~$V_4C_{2.66}$	1266 ± 44	16 ± 0.8
$Ni_{28}:V_{54}:C_{18}$	~VC, σ′, ~$V_4C_{2.66}$	1241 ± 101	32 ± 1.8
$Ni_{32}:V_{56}:C_{12}$	~V_8C_7, σ′, ~$V_4C_{2.66}$	1233 ± 70	41 ± 1.5

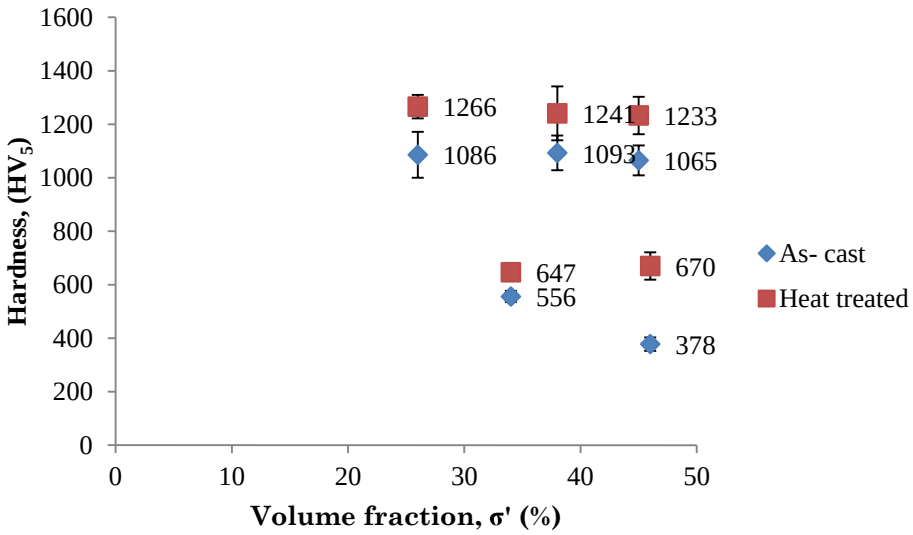


Figure 5.20. Relationship between σ′ volume fractions and hardness of the as-cast and heat treated samples.

Comparison of the hardness values with σ′ volume fractions of the heat treated samples also shows no clear relationship between the hardness and the σ′ volume fractions (Figure 5.20 and Table 5.18). The σ′ phases originated from the alloy with higher V content.

CHAPTER SIX

6.0 CONCLUSIONS AND RECOMMENDATIONS

6.1 CONCLUSIONS

Twenty-four samples of different compositions were studied in as-cast and annealed conditions using SEM with EDX, and the phases were confirmed by X-ray diffraction. Other XRD peaks were identified to belong to the σ′ phases which not currently included in the ICD database. A solidification projection was drawn, showing the phase extents into the ternary (Figure 6.1).

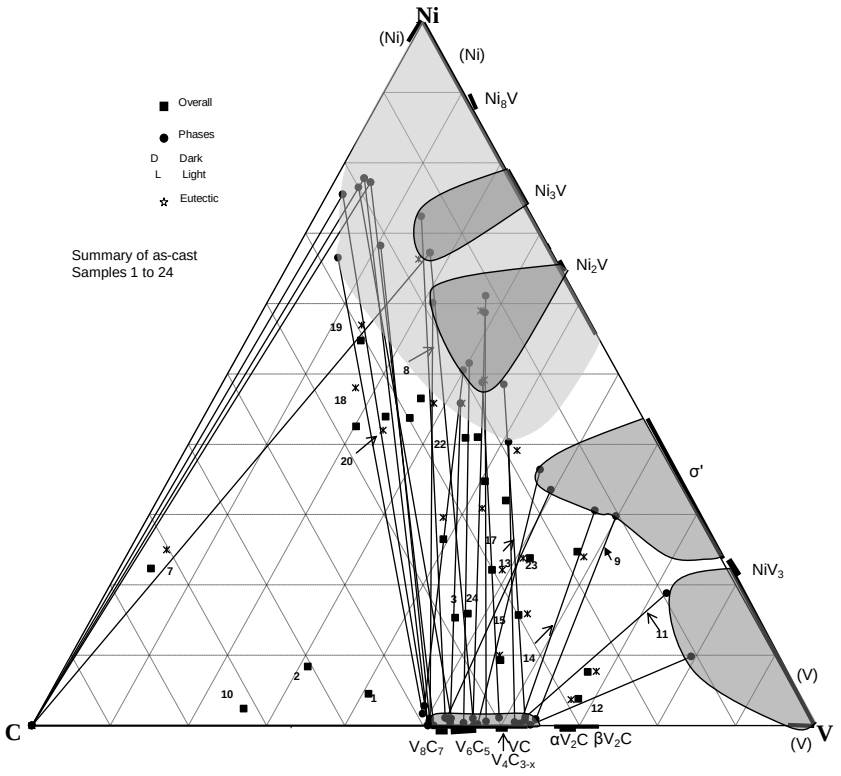


Figure 6.1. Solidification projection for C-Ni-V for the as-cast results (at.%).

The phase extents were:

- ~Ni_3V: ~15 at.% C;

- ~Ni_2V: ~20 at.% C;
- σ′: ~18 at.% C;
- (Ni): ~27 at.% C;
- ~V_8C_7: ~2 at.% Ni;
- ~V_6C_5: ~2 at.% Ni;
- ~VC: ~2 at.% Ni.

The liquidus surface projection was derived from the solidification reactions and the overall compositions, and three ternary invariant reactions were identified. The dotted lines show the inferred positions, where there were no data (Figure 6.2).

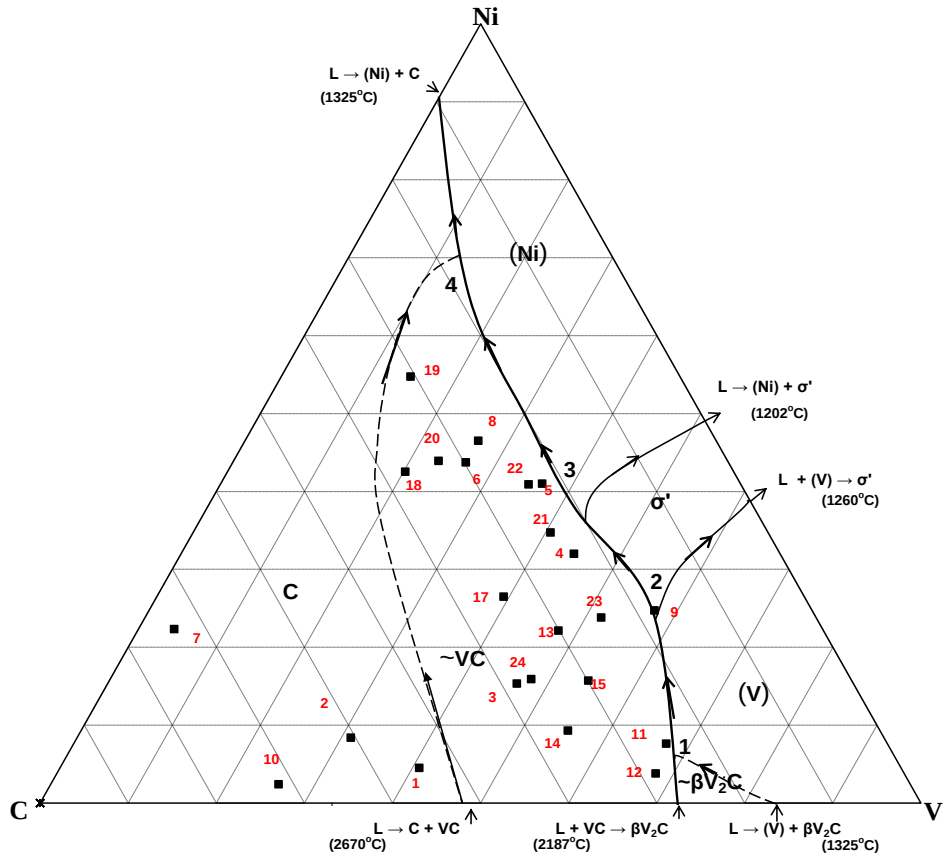


Figure 6.2. Projected liquidus surface for the C-Ni-V system (at.%).

The invariant reactions were:

- L + ~βV_2C → (V) + ~VC
- L + (V) + ~VC → σ′
- L + ~VC → (Ni) + C

The isothermal section at 1000°C was constructed, and was dominated by the (Ni), σ′ and (V) phases. No ternary phase was identified in the investigation (Figure 6.3).

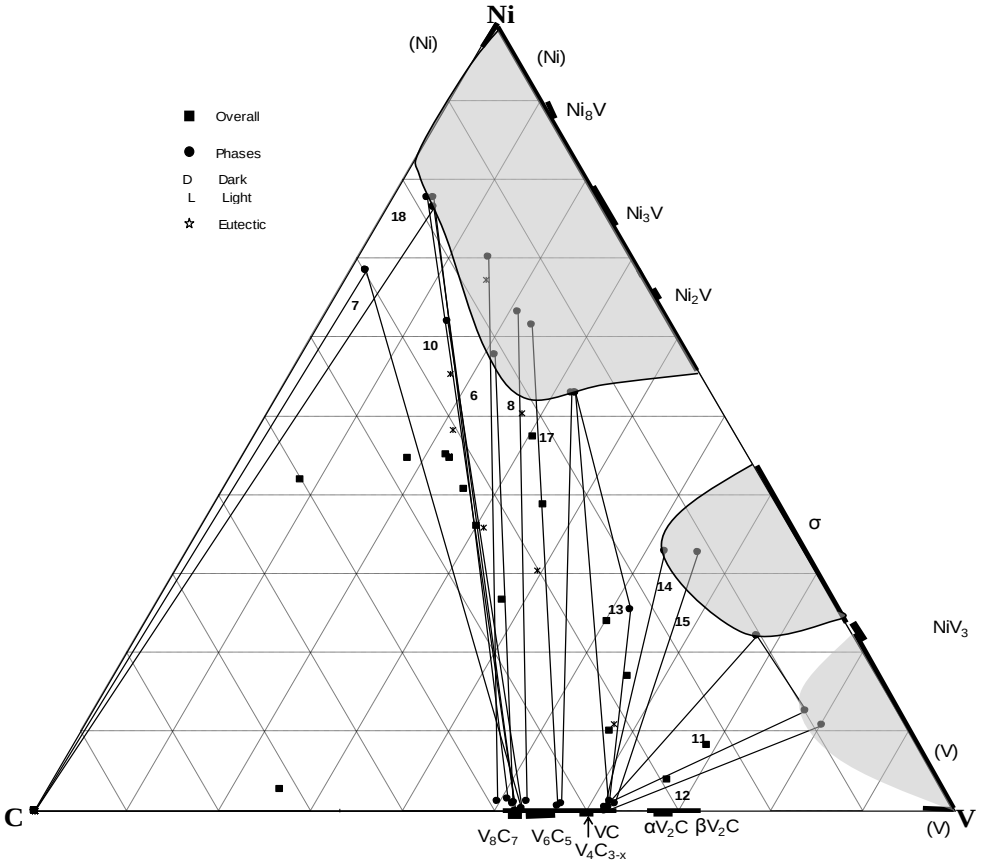


Figure 6.3. Isothermal section of the C-Ni-V system (at.%) at 1000°C.

The form of the vanadium carbides in the as-sprayed deposit from the work of Hos *et al*. [2009Hos] shown more granular and finer vanadium carbide compared with that in the cast produced in the present work. The granular and finer vanadium carbide was because of the alloy droplets that accumulate successively on the substrate solidify at a high cooling rate during plasma spraying.

Vickers hardness measurements were undertaken, and alloys with (Ni) (188 - 402HV_5) were found to be ductile with low hardness. Alloys containing (V), ~Ni_3V and ~Ni_2V were identified as hard phases (533-1052 HV_5). Alloys with σ′ phase were very hard (1065-1266 HV_5) and extremely brittle with many cracks. Comparison of the hardness values with σ′ volume fractions of the as-cast and heat treated samples shows no clear relationship between the hardness and the σ′ volume fractions. The σ′ phases originated from the alloy with higher V content. It can be concluded that more than half of the as-cast alloys had hardnesses between 400HV_5 and 700 HV_5. The as-cast nominal Ni_{10}:V_{50}:C_{40} (at.%), Sample 1, had the highest hardness value of 1574 HV_5. The sample was very hard and brittle and had major cracks in the indentation. The highest value was due to high proportion of carbide (~V_6C_5) in the microstructure. All the as-cast samples with cracks had their cracks propagated transversely in the microstructure except Samples 1 and 2 which propagated mainly in light phases (Ni_3V, Ni_2V). Samples 19 to 22 with nominal compositions: Ni_{68}:V_{14}:C_{18}, Ni_{59}:$V_{27.2}$:$C_{13.8}$, Ni_{39}:$V_{42.8}$:$C_{18.2}$, Ni_{39}:$V_{42.8}$:$C_{18.2}$ (at.%), were found to be ductile with no cracks, whereas Samples 23 and 24 with nominal compositions: Ni_{24}:$V_{58.6}$:$C_{17.4}$ and $Ni_{22.1}$:$V_{49.1}$:$C_{28.8}$ (at.%) were found to be hard and brittle. After annealing at 1000°C, more than half of the alloys had increased hardnesses. These changes in hardness were due to either a change in phase, or a change in volume fraction of a specific phase.

Fracture toughnesses measured by Palmqvist fracture toughness (K_{IC}) of the C-Ni-V alloys 0.9-5.2 (MPa.$m^{-1/2}$) were comparable with some ceramics 0.5-5.3 (MPa.$m^{-1/2}$) [1993Dow, 1994Cal].

Dry sliding experiments on VC-Ni carbides against Cr-steel balls revealed several co-existing wear mechanisms, i.e. abrasion, adhesion and formation of a thin tribolayers. The wear coefficients for a 10N contact load after a sliding wear path of 300m varied between 0.1 x 10^{-6} and 7.6 x 10^{-6} (mm^3/Nm). Comparatively, despite different conditions as shown in Table 5.11, the wear rate of as-cast alloy 24, obtained from the present study which was 2.7 x10^{-6} (mm^3/Nm) is relatively closer to the one reported by Yang [1999Yan] 2.4 x10^{-6} (mm^3/Nm). This result was considered promising, since the sample composition had not been optimised.

The influence of microstructure on wear resistance was noticeable, in particular, composition, nature of the matrix and the effect of the heat treatment. The best wear resistance came from harder alloys with lower binder contents.

The reported wear resistance by Yang [1999Yan] and Bon [2010Bon] indicated that the wear rate of the conventional cemented carbide varied with respect to cemented carbide composition. This was evident in the present work.

The $Ni_{22.1}$:$V_{49.1}$:$C_{28.8}$ (at.%) results from this work were promising, even though they were lower than those of other materials from the literature, because the compositions had not been optimised, and neither had the microstructures been optimised by processing.

6.2 RECOMMENDATIONS

- Differential thermal analysis needs to be conducted on the alloys in order to determine the reaction temperatures and enthalpies of formation for the different phases.
- A newer sample with a high proportion of βV_2C should be made to study that part of the phase diagram.
- A single crystal sample is needed for the proper identification of σ pattern.
- The alloys need to be manufactured by the powder metallurgical route this should allow for the production of homogeneous samples.
- Further investigation using powder metallurgy route will therefore be recommended on composition close to alloy $Ni_{22.1}$:$V_{49.1}$:$C_{28.8}$ (at.%), because it is a promising composition.
- The wear tests should be carried out on more samples, with different compositions where there are more carbides under different conditions (by varying the applied load and velocity), to broaden the current knowledge base.

REFERENCES

[1913Bra] W.L. Bragg. The Diffraction of Short Electromagnetic Waves by a Crystal". *Proceedings of the Cambridge Philosophical Society* 17(1913) 43–57.

[1915Gie] H. Giebelhausen and Z. Anorg. *Chem*., 91 (1915) 251-262.

[1952Pea] W.B. Pearson and W. Hume-Rothery. J. Inst. Met., 80 (1952) 641-648.

[1962Sto] E.K. Storms and R.J. McNeal. The vanadium-vanadium carbide system. *Journal of Physical Chemistry*, 66 (1962) 1401-1408.

[1965Bow] A.L. Bowman, T.C. Wallace, J.L. Yarnell, R.G. Wenzel and E.K. Storms. The crystal structure of UC_2. *Acta Crystallographica*, 21 (1965) 670-671.

[1966Ade] L.M. Adelsberg and L.H. Cadoff. Chemistry of transition metal carbides and nitrides. *Journal of American Ceramics Society*, 49 (1966) 213-220.

[1966Tre] L.A. Tret'yachenko and V.N. Evemenko. Crystal structure; Theory. *Izv. Akad. Nauk SSSR, Neorg. Matter*, 2 (9) (1966) 1568-1573.

[1967Yvo] K. Yvon, W. Rieger and H. Nowotny. Phase transformations in non-stoichiometric vanadium carbide. *Monatsh. Chem.*, 97 (1966) 689- 697.

[1967Rud] E. Rudy and C.E. Brukl. *Journal of American Ceramic Society*, 50 (1967) 265-268.

[1967Rut] C. Ruth and M. Turpin. Determination of the eutectic compositions of binary alloys of nickel-carbon and cobalt-carbon, *C. R. Hebd. Séances Acad. Sci., C*, 9 (1967) 928-929 (in French).

[1968Pre] W. Preeht and G.E. Hollox. Vanadium-Carbide system (experimental). *Journal of Crystal Growth*, 3/4, (1968), 818-823.

[1968Rud] E. Rudy, S. Windisch and C.E. Brukl. Thermodynamic reassessment of the V-C system. *Planseeber, Pulvermetall*, 16 (1968) 3-33

[1968Ven] J.D. Venables, D. Kahn and R.G. Lye. Vacancy short-range order in sub-stoichiometric transition metal carbide. *Philosophical Magazine*. 18 (1968) 177-185.

[1969Luc] L.D. Lucas. Solubility of Carbon in Nickel. *Mém. Sci. Rev. Métall. Levi*, 66 (1969) 747-755 (in French).

[1969Dai] M. Daire and M. Gerspacher. Data on the vanadium- nickel equilibrium diagram between 0 and 40% Ni. *Journal of Less Common Metals*. 17 (1969) 334-335.

[1969Rud] E. Rudy. Compendium of Phase Diagram Data. Air Force Materials Laboratory, Wright-Patterson Air Force Base, OH, Rep. No. AFML-TR-65-2, Part V (1969) 154-156.

[1970Nik] K. Niki and K. Masato. Reaction of carbon with nickel- base solid solution alloy containing carbide- forming element. *Journal of Japanese Institute of Metals* 34, 9 (1970) 879-883

[1970Yvo] K. Yvon and E. Parth'e. The crystal structure of the V, Nb and Ta, *Acta Crystallographica,* 26 (1970) 149-153.

[1970Ste] E.R. Stevens and O.N. Carlson. V-Ni system. *Metallurgical and Materials Transactions B*, 1 (5) 1970) 1267-1271.

[1971Mor] H.A. Moreen, R. Taggart, and D.H. Polonis. Vanadium-Nickel system. *Journal of Materials Science.* 6 (1971) 1425-1432.

[1972Bil] J. Billingham, P.S. Bell and M.H. Lewis. Vacancy Short-Range Order in Substoiehiometrie Transition Metal Carbides and Nitrides with the NaCI Structure. *Acta Crystallographica,* A28 (1972) 602-606.

[1972Tan] L.E. Tanner. The ordering transformation in Ni_2V. *Acta Metalloraphica*, 20 (1972) 1197- 1227.

[1973Sto] E.K. Stoms, A. Lowe, E. Baca and J. Griffin. Vanadium carbides; thermodynamic properties. *High Temp. Science.,* 5 (1973) 276-290.

[1973Hir] K. Hiraga. Vacancy ordering in vanadium carbides based on V_6C_5. *Philosophical Magazine,* 27 (1973) 1301-1321.

[1975Hol] H. Holleck. DTA investigation of high temperature phase equilibra in ternary transition metal-carbon system. *Proceedings of the international conference on thermal analysis,* 3rd, Davos, Switzerland, 1 (1975) 339-348.

[1975San] C. Santafe and C. Borgianni. Study of the oxidation kinetics of vanadium carbide. *Oxidation of Metals,* 9 (1975) 415-425.

[1975Tel] V.S. Telegus. The investigation of transition metals of the fourth with carbon. Visnik L'vivs'kogo Derzhavnogo Universitetu, Seriya Khimichna, 12 (1975) 28-33.

[1976Arb] M.P. Arbuzov, V.G. Fak, and B.V. Khaenko, Izv. Akad. Nauk SSSR, *Neorg. Mater*. 12 (1976) 846-849

[1978Kha] B.V. Khaenko and V.G. Fak. Atomic and vacancy ordering in non-stoichiometric carbides. *Izv. Akad. Nauk SSSR, Neorg. Matter,* 14 (1978) 1294-1301.

[1978Via] P. Viatour, D. Coutsouradis and J.M. Drapier. High temperature alloys for gas turbines. *Journal of Applied Science*, 23 (1978) 875-880.

[1978Kau] L. Kaufman and H. Nesor. Coupled Phase Diagrams and Thermo-chemical Data for Transition Metal Binary Systems – IV. *Calphad*, 2(4) (1978) 295-318.

[1980Ara] T. Arai. Carbide coating process by use of molten borax bath. *Journal of Heat Treatment,* 1 (1979) 15-22.

[1980Vis] R.K. Viswonadham and W. Precht. Preparation and properties of VC+Ni cermets with controlled carbon to metal ratio. *Metallurgical Transactions A*, 11A (1980) 1475-1485.

[1981Ers] T.P. Ershova, D.S. Kamenetskaya and L.P. II'Ina. Calculation of the T-P-X Phase Diagram of the Ni-C System for Pressures up to 100 kbar, *Izv. Akad. Nauk SSSR, Met.,* (4) (1981) 201- 210.

[1981Kun] K.S. Kundig. Tungsten market –from chaos to stability. *Journal of metals*, 33 (1981) 42-47.

[1982Smi] J.F. Smith, O.N. Carlson and P.G. Nash. The Ni-V (Nickel- Vanadium) system. *Bulletin of Alloy Phase Diagrams*. 3, (3) (1982) 342-348.

[1983Fis] H.F. Fischmeister. Development and present status of the science and technology of hard materials. Proceedings of first International Conference on the Science of Hard Materials. New York: Plenum Press (1983) 1- 45.

[1983Emm] G.H. Emmons and W.S. Williams. *Journal of Materials Science.* 18 (1983) 2589–2602.

[1984Gha] A. Ghaneya. "Some Studies on the V-C System," Ph.D. Thesis, Iowa State University, Ames, IA (1984).

[1985Car] O.N. Carlson, A.H. Ghaneya and J.F. Smith. The C-V (Carbon-Vanadium) system. *Bulletin of Alloy Phase Diagrams*, 6 (2) (1985) 115-124.

[1985She] D.K. Shetty, I.G. Wright, P.N. Mincer and A.H. Clauer, *J. Mat. Sci.*, Vol. 20, (1985) 1873.

[1986Yos] M.Yoshinori, S.Kiyoshi and Y.Natsuo. Effect of transition elements on the properties of MC carbides in IN-100 nickel-based super alloy. *Journal of Materials Science*, 21 (1986) 3653-3660.

[1988Ala] E.A. Alamond and B. Roebuck. Identification of optimum binder phase compositions for improved WC hard metals. *Materials Science and Engineering*, A105/106 (1988) 237-248.

[1988Die] G.E. Dieter. Mechanical Metallurgy, McGraw-Hill Book Company, UK (1988).

[1988Shu] A. K. Shurin, G. P. Dmitrieva, N. A. Razumova, and E. L. Khandros. The Phase diagram of the Ni-VC-NbC system. Institute of Metal Physics, Academy of Sciences of the Ukrainian SSR. Translated from Poroshkovaya Metallurgiya. 296 (1988) 67-79.

[1989Sin] M. Singleton and P. Nash. The C-Ni (Carbon-Nickel) system. *Bulletin of Alloy Phase Diagrams*. 10, (2) (1989) 121-126.

[1990Spi] R. Spiegler, S. Schmauder and L. Sigl, *J. Hard Mater.*, 1(3), (1990), p.147.

[1990Van] F.J. Van Loo. Multiphase diffusion in binary and ternary solid-state system. *Prog. Solid st. Chem*, 20 (1990) 47-99

[1991Din] A.T. Dinsdale. SGTE data for pure elements, *Calphad*, 15, (4) (1991) 317-425.

[1991Hua] W.M. Huang. *Z. Metallkd*. 82 (1991) 174.

[1991Zha] J. Zhang, F.A. Moslehy and S.L. Rice, A model for friction in quasi-steady-state sliding Part II. Numerical results and discussion, *Wear*, 149 (1991) pp. 13–25.

[1991Tie] T.Y. Tiegs and R.R. McDonald. Ductile Ni_3Al alloys bonding agents for ceramic materials in cutting tools. *US Patent* 5, 015 (1991) 290.

[1991Lee] B. Lee and D. Lee. A thermodynamic study on the V-C and Fe-V. *Calphad*, 15 (1991) 283-289.

[1992Hut] I.M. Hutchings, Tribology: Friction and Wear of Engineering Materials, Edward Arnold, 1992, London.

[1993Dan] J.L. Dan, H.J. Boving and H.E. Hintermann. Hard coatings. *Journal de Physique* 111**,** 3 (1993) 933-941.

[1993Dow] N.E. Dowling, Mechanical behaivior of Materials: Engineering Methods for Deformation, Fracture, and Fatigue, Prentice Hall (1993) pp. 287-291.

[1994Cal] W. Callister, An Introduction to Material Science and Engineering, 3rd Edition, John Wiley & Sons, Inc. (1994) pp.194-196.

[1994Yak] V.L. Yakyshin, B.A. Kalin, V.I. Polskij, D.V. Strizhnev, V.I. Vasilev and S.S. Tserevitinov. Surface alloying of metals using high-temperature pulse plasma. Izvestiya Akademii Nauk SSSR. Metally. 6 (1994) 74-82.

[1997Lir] J. Lira-Olivares, A.R. Di Giampaolo and M. Velez. Microstructure Development and Mechanical Properties of Ni Matrix/Carbide Composites. *Advanced Performance Materials*, 4 (1997) 95-103.

[1997Luy] S. Luyckx, L. Cornish and C. Osborne. On the preparation of fine V_8C_7-WC and V_4C_3-WC powders. *International Journal of Refractory Metals and Hard Materials*, 15 (1997) 163-168.

[1997Gri] I.C. Grigorescu, J. Ramirez, F. Salcedo and C. Weil. Tribological behaviour of vanadium oxycarbide coatings. *Surface and Coating Technology*, 94 (1997) 437-440.

[1997Wen] E.J. Wentzel and C. Allen. The Erosion-corrosion Resistance of Tungsten carbide Hard Metals. *International Journal of Refractory Metals and Hard Materials*, 15 (1997) 81-87.

[1997Whi] D.J. Whitefield, S. Luyckx, M.J. Witcomb and L.A. Cornish. Microstructure and properties of fine grain WC-VC-Co hard metal with cobalt content ranging from 10-15%. *Proceedings of the 14th International Plansee Semina*r, Tyrol, Austria, 2 (1997) 477-484.

[1998Wie] H. Wiesenberger, W. Lengauer and P. Ettmayer. Reactive diffusion and phase equilibria in the V-C, Nb-C, Ta-C and Ta-N systems. *Acta Materiallia,* 46 (1998) 651-666.

[1999Lip] V.N. Lipatnikov, A.V. Gusev, P. Ettmayer and W. Lengauer. Phase transformations in non-stoichiometric vanadium carbide. *Journal of Physics*: *Condensed. Matter,* 11 (1999) 163-184.

[1999Yan] L.J. Yang. Pin-on-disc wear testing of tungsten carbide with a new moving pin technique. *Wear,* 225-229 (1999) 557-562.

[1999All] A. T. Allen and D. L. Douglass. Internal-Carburizing Behavior of Ni-V, Ni-Cr, and Ni- 3Nb. *Oxidation of Metals,* 51 (1999) 199-219.

[2000Eng] H. Engqvist, U. Beste and N. Axen. The influence of pH on sliding wear of WC-based materials. *International Journal of Refractory Metals & Hard Materials* 18 (2000) 103-109.

[2000Fle] M.C. Flemings. Why materials science and engineering is good for Metallurgy. The 2000 Distinguished Lecture in Materials and Society, *ASM International, Metallurgical and Materials Transactions A,* 32A (2000) 853-860.

[2001Wat1] A. Watson, Q. Chen, Y. Du, A.A. Rampel, J.C. Schuster, P.J. Spencer and H. Yokokawa. The modelling of carbide, nitride and carbon-nitride phases. Materials Research and Advanced Techniques. 92, 6 (2001) 550-559.

[2001Wat2] A. Watson and F.H. Hayes. Some experiences modeling the sigma phase in the Ni–V system. *Journal of Alloys and Compounds* 320 (2001) 199–206.

[2001ICD] International Crystallography Diffraction Database.

[2000Lug] E. Lugscheider, O. Knotek, K. Bobzin and S. Barwulf. Tribological properties, phase stability of tungsten and vanadium oxides deposited by reactive MSIP-PVD process for innovative lubrication applications. *Surface and Coating Technology* (2000) 362-368.

[2001Are] F. Arenas, A. Matos, M. Cabezas, C. DiRauso and C Grigorescu. Densification, mechanical properties and wear behaviour of WC-VC-Co-Al

hard metals. *International Journal of Refractory Metals and Hard Materials*, 29 (2001) 381-387.

[2001And] H.O. Andren. Development of the microstructure during gradient sintering of cemented carbide. *Materials Chemistry and Physics*, 67 (2001) 209-213.

[2001Fle] M.C. Flemings and R.W. Cahn. Organization and trends in materials science and engineering education in the United State and Europe. *Acta Materiallia*, 48 (2000) 371-383.

[2001Mir] J.C. Miranda and A. Ramalho. Abrasion resistance of thermal sprayed composite coatings with a nickel alloy matrix and a WC hard phase. Effect of deposition technique and re-melting. *Tribology Letters*, 11, 1 (2001) 37-48.

[2001Que] G. Quercia, I. Grigorescu, H. Contreras, C. Di Rauso and D. Gutierrez-Campos, Friction and wear behaviour of several hard materials, *International Journal of Refractory Metals and Hard Materials,* 19 (4–6) (2001) pp.359–369.

[2002Bhu] B. Bhushan. Introduction to Tribology, John Wiley & Sons Inc., 2002, New York.

[2002ICS] International Centre for Diffraction standards, Pennsylvania, USA, 2002.

[2002Wit] B. Wittmann, W.D. Schubert. and B. Lux. WC grain growth and grain growth inhibition in nickel and iron binder hard metals. *International Journal of Refractory Metals and Hard Materials,* 20 (2002) 51-60.

[2002Sha] S.V. Shah and N.B. Dadhotre. Laser surface engineered vanadium carbide coating for extended die life. *Journal of Materials Process Technology*, 28 (2002) 105-112.

[2002Lua] J.F. Luan and M. Yan. Effect of Cu-Ni-V-C alloy on properties of laser clad layer. *Journal of Nonferrous Metals.* 12, 5, (2002) 945.

[2003Lee] H.R. Lee, D.J. Kim, N.M. Hwang and D.Y. Kim. Role of VC additive during sintering of WC-Co: mechanism of grain growth inhibition. *Journal of American Ceramics Society*, 86 (2003) 152-154.

[2003Tah] E. Taheri-Nassaj and S.H. Mirhosseini. An in situ WC-Ni composite fabricated by the SHS method. *Journal of Materials Processing Technology*, 142 (2003) 422-426.

[2005Fan] Z. Fang, P. Maheshwari, X. Wang, H.Y. Sohn, A. Griffo and R. Riley. An experimental study of the sintering of nanocrystalline WC-Co powders. *International Journal of Refractory Metals and Hard Materials*, 23 (2005) 249-257.

[2005Gan] A.J. Gant, G.M. Gee and B. Roebuck. Rotating wheel abrasion of WC/Co hardmetals, *Wear*, 258 (2005) pp. 178–188.

[2005Hua] S. Huang, J. Vleugels, L. Li. and O. Biest. Experimental investigation and thermodynamic assessment of the V-W-C system. *Journal of Alloys and Compounds*, 395 (2005) 68-74.

[2006Hu] J. Hu, C. Li, F. Wang and W. Zhang. Thermodynamic re-assessment of the V-C system. *Journal of Alloys and Compounds*, 421 (2006) 120-127.

[2007Wan1] Y. Wang, Y. Ding, J. Wang, F. Cheng and J. Shi. In-situ production of vanadium carbide particulates reinforced iron matrix surface composite by cast- sintering. *Materials and Design*, 28 (2007) 2202-2206.

[2007Wan2] J. Wang, Y. Ding, Y. Wang and W. Gong. Microstructure and Wear-resistance of Fe-(Ti, V) C Composite. *Materials and Design*, 28 (2007) 2207-2209.

[2007Has] N.G. Hashe, J.H. Neethling, P.R. Berndt, H.O. Andren and S. Norgren. A comparison of the microstructures of WC-VC-TiC-Co and WC-VC-Co cemented carbides. *International Journal of Refractory Metals and Hard Materials*, 25 (2007) 207-213.

[2008San] Cemented carbide. www.allaboutcementedcarbide.com. (Accessed September, 2011).

[2008Bon] K. Bonny, P. De Baets, J. Vleugel, S. Huang and B. Lauwers. Dry reciprocating sliding friction and wear response of WC-Ni cemented carbides. *Tribological Letters*, 31 (2008) 199-209.

[2009Che] Chemlink. World production of vanadium pent oxide. www.chemlink.com.au/vanadium. (Accessed March, 2009).

[2009Hos] Y. Hoshiyama, K. Hirano and H. Miyake. Rapidly solidified thick deposit of Fe-C-V-Cr-Ni alloy by plasma spraying, *Plasma Processes and Polymers*, 6 (2009) S944-S947.

[2009Keg] T. Kagnaya, C. Boher, L. Lambert, M. Lazard and T. Cutard, Wear mechanisms of WC–Co cutting tools from high-speed tribological tests, *Wear*, 267 (2009) 890–897.

[2009Rui] A. Ruize, I.C. Grigorescu, L. Matamoras, C. Rojas and D. Morel. Graded metal-carbide composites produced by solid state transformation. *International Journal of Refractory Metals and Hard Material*s, 27 (2009) 261-266.

[2009Xia] W. Xiaoyan, L. Guangze, C. Yanghui and L. Geyang. Microstructure and mechanical properties of vanadium carbide coatings synthesized by reactive magnetron sputtering. *International Journal of Refractory Metals and Hard Material*s, 27 (2009) 611-614.

[2010Bon] K. Bonny, P. De Baets, Y. Perez, J. Vleugels and B. Lauwers, Friction and wear characteristics of WC-Co cemented carbides in dry reciprocating sliding contact, *Wear*, 268 (2010) pp. 1504–1517.

[2011Esp] L. Espinosa, V. Bonache and M.D. Salvador Friction and wear behaviour of WC–Co–Cr_3C_2–VC cemented carbides obtained from nanocrystalline mixtures. *Wear*, 272 (2011) pp. 62-68.

[2011Mer] R. Merwe, Friction and Sliding Wear of WC-Co Inserts Containing Mixed Carbides (TiC, TaC, NbC), MSc Thesis, University of Witwatersrand, Johannesburg, South Africa, (2011).

[2012Bri] M.A. Brieseck, I.B. Hünsche, B.B. Caspers, G.B. Gille, M.C. Bohn and W.A. Lengauer. Diffusion behaviour of the grain-growth inhibitor VC in hardmetals. 8th International Conference on Diffusion in Materials, DIMAT 2011; Dijon, France 323-325 (2012) 509-514.

[2012Moh] M. Mohammadpour, P. Abachi, N. Parvin and K. Pourazrang. Study of cemented carbonitrides with nickel as binder: Experimental investigations and computer calculations. *International Journal of Refractory Metals and Hard Material*s, 31 (2012) 164-170.

APPENDIX A

As-cast sample 1

Elements	At wt	At %	At wt. x at%	Wt %	Wt of the element rqd (g)
Ni	58.7	10	586.90	16.24	0.49
V	50.9	50	2547.00	70.47	2.11
C	12	40	480.40	13.29	0.40
		Σ	3614.30	100	3.00

As-cast sample 2

Elements	At wt	At %	At wt. x at%	Wt %	Wt of the element rqd (g)
Ni	58.7	20	1173.80	31.79	0.95
V	50.9	40	2037.60	55.19	1.66
C	12	40	480.40	13.01	0.39
		Σ	3691.80	100.00	3.00

As-cast sample 3

Elements	At wt	At %	At wt. x at%	Wt %	Wt of the element rqd (g)
Ni	58.7	24	1408.56	33.00	0.99
V	50.9	50	2547.00	59.68	1.79
C	12	26	312.26	7.32	0.22
		Σ	4267.82	100	3.00

As-cast sample 4

Elements	At wt	At %	At wt. x at%	Wt %	Wt of the element rqd (g)
Ni	58.7	40	2347.60	46.81	1.40
V	50.9	50	2547.00	50.79	1.52
C	12	10	120.10	2.39	0.07
		Σ	5014.70	100.00	3.00

As-cast sample 5

Elements	At wt	At %	At wt. x at%	Wt %	Wt of the element rqd (g)
Ni	58.7	53	3110.57	60.81	1.82
V	50.9	37	1884.78	36.84	1.11
C	12	10	120.10	2.35	0.07
		Σ	5115.45	100	3.00

As-cast sample 6

Elements	At wt	At %	At wt. x at%	Wt %	Wt of the element rqd (g)
Ni	58.7	64	3756.16	72.77	2.18
V	50.9	25	1273.50	24.67	0.74
C	12	11	132.11	2.56	0.08
		Σ	5161.77	100.00	3.00

As-cast sample 7

Elements	At wt	At %	At wt. x at%	Wt %	Wt of the element rqd (g)
Ni	58.7	70	4108.30	84.57	2.54
V	50.9	10	509.40	10.49	0.31
C	12	20	240.20	4.94	0.15
		Σ	4857.90	100	3.00

As-cast sample 8

Elements	At wt	At %	At wt. x at%	Wt %	Wt of the element rqd (g)
Ni	58.7	60	3521.40	68.12	2.04
V	50.9	30	1528.20	29.56	0.89
C	12	10	120.10	2.32	0.07
		Σ	5169.70	100.00	3.00

As-cast sample 9

Elements	At wt	At %	At wt. x at%	Wt %	Wt of the element rqd (g)
Ni	58.7	30	1760.70	34.31	1.03
V	50.9	65	3311.10	64.52	1.94
C	12	5.00	60.05	1.17	0.04
		Σ	5131.85	100	3.00

As-cast sample 10

Elements	At wt	At %	At wt. x at%	Wt %	Wt of the element rqd (g)
Ni	58.7	20	1173.80	33.56	1.01
V	50.9	35	1782.90	50.98	1.53
C	12	45	540.45	15.45	0.46
		Σ	3497.15	100.00	3.00

As-cast sample 11

Elements	At wt	At %	At wt. x at%	Wt %	Wt of the element rqd (g)
Ni	58.7	10	586.90	12.27	0.37
V	50.9	80	4075.20	85.22	2.56
C	12	10	120.10	2.51	0.08
		Σ	4782.20	100	3.00

As-cast sample 12

Elements	At wt	At %	At wt. x at%	Wt %	Wt of the element rqd (g)
Ni	58.7	5.00	293.45	6.74	0.20
V	50.9	75	3820.50	87.74	2.63
C	12	20	240.20	5.52	0.17
		Σ	4354.15	100.00	3.00

As-cast sample 13

Elements	At wt	At %	At wt. x at%	Wt %	Wt of the element rqd (g)
Ni	58.7	14	821.66	18.91	0.57
V	50.9	64	3260.16	75.01	2.25
C	12	22	264.22	6.08	0.18
		Σ	4346.04	100	3.00

As-cast sample 14

Elements	At wt	At %	At wt. x at%	Wt %	Wt of the element rqd (g)
Ni	58.7	28	1643.32	35.64	1.07
V	50.9	54	2750.76	59.67	1.79
C	12	18	216.18	4.69	0.14
		Σ	4610.26	100.00	3.00

As-cast sample 15

Elements	At wt	At %	At wt. x at%	Wt %	Wt of the element rqd (g)
Ni	58.7	32	1878.08	38.53	1.16
V	50.9	56	2852.64	58.52	1.76
C	12	12	144.12	2.96	0.09
		Σ	4874.84	100	3.00

As-cast sample 16

Elements	At wt	At %	At wt. x at%	Wt %	Wt of the element rqd (g)
Ni	58.7	38	2230.22	42.94	1.29
V	50.9	57	2903.58	55.90	1.68
C	12	5.00	60.05	1.16	0.03
		Σ	5193.85	100.00	3.00

As-cast sample 17

Elements	At wt	At %	At wt. x at%	Wt %	Wt of the element rqd (g)
Ni	58.7	39	2288.91	48.83	1.46
V	50.9	42.8	2180.23	46.51	1.40
C	12	18.2	218.58	4.66	0.14
		Σ	4687.72	100	3.00

As-cast sample 18

Elements	At wt	At %	At wt. x at%	Wt %	Wt of the element rqd (g)
Ni	58.7	66	3873.54	78.99	2.37
V	50.9	16.1	820.13	16.72	0.50
C	12	17.5	210.18	4.29	0.13
		Σ	4903.85	100.00	3.00

As-cast sample 19

Elements	At wt	At %	At wt. x at%	Wt %	Wt of the element rqd (g)
Ni	58.7	68	3990.92	81.11	2.43
V	50.9	14	713.16	14.49	0.43
C	12	18	216.18	4.39	0.13
		Σ	4920.26	100	3.00

As-cast sample 20

Elements	At wt	At %	At wt. x at%	Wt %	Wt of the element rqd (g)
Ni	58.7	59	3462.71	69.06	2.07
V	50.9	27.2	1385.57	27.63	0.83
C	12	13.8	165.74	3.31	0.10
		Σ	5014.02	100.00	3.00

As-cast sample 21

Elements	At wt	At %	At wt. x at%	Wt %	Wt of the element rqd (g)
Ni	58.7	39	2288.91	48.83	1.46
V	50.9	42.8	2180.23	46.51	1.40
C	12	18.2	218.58	4.66	0.14
		Σ	4687.72	100	3.00

As-cast sample 22

Elements	At wt	At %	At wt. x at%	Wt %	Wt of the element rqd (g)
Ni	58.7	49	2875.81	60.10	1.80
V	50.9	33.3	1696.30	35.45	1.06
C	12	17.7	212.58	4.44	0.13
		Σ	4784.69	100.00	3.00

As-cast sample 23

Elements	At wt	At %	At wt. x at%	Wt %	Wt of the element rqd (g)
Ni	58.7	24	1408.56	30.60	0.92
V	50.9	58.6	2985.08	64.86	1.95
C	12	17.4	208.97	4.54	0.14
		Σ	4602.62	100	3.00

As-cast sample 24

Elements	At wt	At %	At wt. x at%	Wt %	Wt of the element rqd (g)
Ni	58.7	22.1	1297.05	31.30	0.94
V	50.9	49.1	2501.15	60.35	1.81
C	12	28.8	345.89	8.35	0.25
		Σ	4144.09	100.00	3.00

APPENDIX B

APPENDIX B1: As-cast Sample 1

All results in atomic%						
Raw data						
Spectrum	**C**	**V**	**Ni**	**Comment**	**Phase Contrast**	**Remarks**
200x image 1	57.1	37.4	5.49	0verall	Light+Medium+Dark	Not agree
200x image 2	53.61	41.27	5.1	0verall	Light+Medium+Dark	Agree
200x image 3	46.63	50.01	3.34	0verall	Light+Medium+Dark	Not agree
200x image 4	55.96	39.05	4.38	0verall	Light+Medium+Dark	Agree
200x image 5	63.34	32.59	4.05	0verall	Light+Medium+Dark	Not agree
200x image 6	54.46	41.79	3.73	0verall	Light+Medium+Dark	Agree
1000x spot 1	15.44	17.73	66.82	spot	Light	Agree
1000x spot 2	16.64	17.2	66.15	spot	Light	Not agree
1000x spot 3	15.44	17.59	66.96	spot	Light	Agree
1000x spot 4	15.57	16.54	67.87	spot	Light	Agree
1000x spot 5	13.82	40.38	45.79	spot	Light	Not agree
1000x spot 6	43.68	56.31	0	spot	Medium	Agree
1000x spot 7	43.22	56.77	0	spot	Medium	Agree
1000x spot 8	43.64	56.35	0	spot	Medium	Agree
1000x spot 9	48.98	51.01	0	spot	Medium	Not agree
1000x spot 10	47.8	52.19	0	spot	Medium	Not agree
1000x spot 11	100	0	0	spot	dark	Agree
0verall	**C**	**V**	**Ni**	**Comment**	**Phase Contrast**	
200x image 2	53.61	41.27	5.1	0verall	Light+Medium+Dark	
200x image 4	55.96	39.05	4.38	0verall	Light+Medium+Dark	
200x image 6	54.46	41.79	3.73	0verall	Light+Medium+Dark	
MEAN	54.67667	40.70333	4.403333			
STDEV	1.189888	1.455243	0.685298			
Light	**C**	**V**	**Ni**	**Comment**	**Phase Contrast**	
1000x spot 1	15.44	17.73	66.82	spot	Light	
1000x spot 3	15.44	17.59	66.96	spot	Light	
1000x spot 4	15.57	16.54	67.87	spot	Light	
MEAN	15.48333	17.28667	67.21667			
STDEV	0.075056	0.65041	0.570117			
Medium	**C**	**V**	**Ni**	**Comment**	**Phase Contrast**	
1000x spot 6	43.68	56.31	0	spot	Medium	
1000x spot 7	43.22	56.77	0	spot	Medium	
1000x spot 8	43.64	56.35	0	spot	Medium	
MEAN	43.51333	56.47667	0			
STDEV	0.25482	0.25482				
Dark	**C**	**V**	**Ni**	**Comment**	**Phase Contrast**	
1000x spot 11	100	0	0	spot	dark	

APPENDIX B2: As-cast Sample 2

All results in atomic %							
Raw data							
Spectrum	**C**	**V**	**Ni**	**Comment**		**Phase contrasts**	**Remarks**
200x image 1	60.91	30.72	10.76	0verall		Light+Medium+Dark	Agree
200x image 2	61.6	30.49	8.37	0verall		Light+Medium+Dark	Agree
200x image 3	59.41	33.62	7.22	0verall		Light+Medium+Dark	Not agree
200x image 4	61.38	29.6	7.91	0verall		Light+Medium+Dark	Agree
200x image 5	59.58	30.85	6.97	0verall		Light+Medium+Dark	Agree
2000x image 1	50.38	49.62	0	Spot		Medium	Not agree
2000x image 2	49.25	50.75	0	Spot		Medium	Agree
2000x image 3	49.08	50.92	0	Spot		Medium	Agree
2000x image 4	48.63	51.37	0	Spot		Medium	Agree
2000x image 5	46.58	53.42	0	Spot		Medium	Not agree
2000x image 6	45.81	54.19	0	Spot		Medium	Not agree
2000x image 7	47.66	52.34	0	Spot		Medium	Not agree
2000x image 8	48.57	49.9	1.54	Spot		Medium	Not agree
2000x image 9	48.2	51.8	0	Spot		Medium	Agree
2000x image 10	48.14	51.86	0	Spot		Medium	Agree
2000x image 1	18.17	5.53	76.3	Spot		Light	Agree
2000x image 2	13.72	5.44	80.85	Spot		Light	Not agree
2000x image 3	19.98	3.85	76.17	Spot		Light	Agree
2000x image 4	18.87	4.66	76.47	Spot		Light	Agree
2000x image 5	19.52	4.1	76.38	Spot		Light	Agree
2000x image 6	18.14	4.85	77.01	Spot		Light	Agree
2000x image 7	17.73	5.31	76.9	Spot		Light	Not agree
2000x image 8	20.58	5.09	74.33	Spot		Light	Not agree
2000x image 1	98.92	1.08	0	Spot		Dark	Not agree
2000x image 2	100	0	0	Spot		Dark	Agree
2000x image 3	100	0	0	Spot		Dark	Agree
0verall	**C**	**V**	**Ni**	**Comment**		**Phase Contrast**	
200x image 1	60.91	30.72	10.76	0verall		Light+Medium+Dark	
200x image 2	61.6	30.49	8.37	0verall		Light+Medium+Dark	
200x image 3	59.41	33.62	7.22	0verall		Light+Medium+Dark	
200x image 4	61.38	29.6	7.91	0verall		Light+Medium+Dark	
200x image 5	59.58	30.85	6.97	0verall		Light+Medium+Dark	
Mean	60.4925	31.14	7.6175				
STDEV	1.157393	1.734801	0.640072				
Light	**C**	**V**	**Ni**	**Comment**		**Phase Contrast**	
2000x image 1	18.17	5.53	76.3	Spot		Light	
2000x image 3	19.98	3.85	76.17	Spot		Light	
2000x image 4	18.87	4.66	76.47	Spot		Light	
2000x image 5	19.52	4.1	76.38	Spot		Light	
2000x image 6	18.14	4.85	77.01	Spot		Light	

Mean	18.936	4.598	76.466	Spot			
STDEV	0.814819	0.660205	0.323466	Spot			
Medium	**C**	**V**	**Ni**	**Comment**		**Phase Contrast**	
2000x image 2	49.25	50.75	0	Spot		Medium	
2000x image 3	49.08	50.92	0	Spot		Medium	
2000x image 4	48.63	51.37	0	Spot		Medium	
2000x image 9	48.2	51.8	0	Spot		Medium	
2000x image 10	48.14	51.86	0	Spot		Medium	
Mean	48.66	51.34	0				
STDEV	0.501847	0.501847	0				
Dark	**C**	**V**	**Ni**	**Comment**		**Phase Contrast**	
2000x image 2	100	0	0			Dark	
2000x image 3	100	0	0			Dark	
MEAN	100	0	0				
STDEV	0	0	0				

APPENDIX B3: As-cast Sample 3

All results in atomic %						
Raw data						
Spectrum	**C**	**V**	**Ni**	**Comment**	**Phase Contrast**	**Remarks**
300x overall-1	40	46.56	13.45	Overall	Light+Medium+Dark	Not agree
300x overall-2	39.41	45.62	14.97	Overall	Light+Medium+Dark	agree
300x overall-3	36.08	47.29	16.63	Overall	Light+Medium+Dark	agree
300x overall-4	36.32	45.78	17.9	Overall	Light+Medium+Dark	Not agree
300x overall-5	39.01	47.31	13.68	Overall	Light+Medium+Dark	agree
1000x spot 1	45.22	54.11	0.68	spot	Dark	agree
1000x spot 2	44.59	54.91	0.5	spot	Dark	agree
1000x spot 3	44.67	55.33	0	spot	Dark	agree
1000x spot 4	45.34	54.66	0	spot	Dark	agree
1000x spot 5	43.02	56.35	0.62	spot	Dark	not agree
1850x spot 13	17.31	30.7	51.99	spot	Light	agree
1850x spot 14	24.06	29.21	46.73	spot	Llight	not agree
1850x spot 15	18.53	31.7	49.76	spot	Llight	agree
1850x spot 16	11.77	34.22	54.01	spot	Llight	Not agree
1850x spot 17	21.56	28.12	50.32	spot	Llight	Not agree
1850x spot 18	25.32	27.08	47.61	spot	Llight	not agree
1850x spot 19	19.11	28.31	52.58	spot	Llight	agree

0verall	C	V	Ni	Comment	Phase Contrast	
300x overall-2	39.41	45.62	14.97	Overall	Light+Medium+Dark	
300x overall-3	38.08	46.29	15.63	Overall	Light+Medium+Dark	
300x overall-4	36.32	45.78	17.9	Overall	Light+Medium+Dark	
300x overall-5	38.01	46.31	15.68	Overall	Light+Medium+Dark	
Mean	38.15	46.47	15.26		Light+Medium+Dark	
STDEV	0.7889	0.3927	0.3963			
Dark	**C**	**V**	**Ni**	**Comment**	**Phase Contrast**	
1000x spot 1	45.22	54.11	0.68	spot	Dark	
1000x spot 2	44.59	54.91	0.5	spot	Dark	
1000x spot 3	44.67	55.33	0	spot	Dark	
1000x spot 4	45.34	54.66	0	spot	Dark	
Mean	44.56	54.753	0.39			
STDEV	0.3734	0.4415	0.3048			
Llight	**C**	**V**	**Ni**	**Comment**	**Phase Contrast**	
1850x spot 13	16.31	31.7	51.99	spot	Light	
1850x spot 15	16.53	31.7	51.76	spot	Light	
1850x spot 19	16.11	31.31	52.58	spot	Light	
Mean	16.7	31.07	52.11			
STDEV	0.2101	0.2252	0.423			

APPENDIX B4: As-cast Sample 4

All results in atomic%						
Raw data						
Spectrum	**C**	**V**	**Ni**	**Comments**	**Phase contrast**	**Remark**
200x image 1	24.98	44.24	30.77	Overall	Light + Dark	Agree
200x image 2	22.25	44.76	32.98	Overall	Light + Dark	Agree
200x image 3	22.52	45.59	31.87	Overall	Light + Dark	Agree
200x image 4	23.89	43.74	32.35	Overall	Light + Dark	Agree
200x image 5	26.36	42.70	30.92	Overall	Light + Dark	Agree
2000x spot 1	15.18	36.07	48.75	Spot	Medium	Agree
2000x spot 2	14.98	37.01	48.01	Spot	Medium	Agree
2000x spot 3	15.62	37.70	46.68	Spot	Medium	Agree
2000x spot 4	16.44	35.83	47.73	Spot	Medium	Agree
2000x spot 5	16.91	34.51	48.58	Spot	Medium	Agree
2000x spot 1	17.31	34.45	47.24	Spot	Medium	Agree
2000x spot 2	16.22	36.15	47.63	Spot	Light	Agree
2000x spot 3	16.36	36.89	48.75	Spot	Light	Agree

2000x spot 4	16.86	35.68	46.47	Spot	Light	Agree
2000x spot 5	16.50	36.37	47.13	Spot	Light	Agree
2000x spot 6	15.29	36.91	47.81	Spot	Light	Agree
2000x spot 1	36.99	62.50	0.51	Spot	Dark	Agree
2000x spot 2	36.91	62.20	0.81	Spot	Dark	Agree
2000x spot 3	35.99	63.47	0.54	Spot	Dark	Agree
2000x spot 4	36.99	62.69	0.65	Spot	Dark	Agree
2000x spot 5	34.92	64.53	0.56	Spot	Dark	Not agree
2000x Eutectic 1	26.68	45.14	28.18	Area	Light+Dark	Agree
2000x Eutectic 2	26.14	44.33	29.53	Area	Light+Dark	Agree
2000x Eutectic 3	25.78	44.34	29.88	Area	Light+Dark	Agree
2000x Eutectic 4	24.50	43.88	31.62	Area	Light+Dark	Agree
Overall	C	V	Ni	**Comments**	**Phase contrast**	
200x image 1	**24.98**	**44.24**	**30.77**	Overall	**Light + Dark**	
200x image 2	**22.25**	**44.76**	**32.98**	Overall	**Light + Dark**	
200x image 3	**22.52**	**45.59**	**31.87**	Overall	**Light + Dark**	
200x image 4	**23.89**	**43.74**	**32.35**	Overall	**Light + Dark**	
200x image 5	**26.36**	**42.70**	**30.92**	Overall	**Light + Dark**	
Mean	**23.41**	**44.58**	**31.99**			
STDEV	1.27	0.79	0.93			
Light	C	V	Ni	**Comments**	**Phase contrast**	
2000x spot 1	**16.22**	**36.15**	**47.63**	Spot	**Light**	
2000x spot 2	**16.36**	**36.89**	**48.75**	Spot	**Light**	
2000x spot 3	**16.86**	**35.68**	**46.47**	Spot	**Light**	
2000x spot 4	**16.50**	**36.37**	**47.13**	Spot	**Light**	
2000x spot 5	**15.29**	**36.91**	**47.81**	Spot	**Light**	
Mean	**16.09**	**36.58**	**47.83**			
STDEV	**0.55**	**0.38**	**0.68**			
Dark	C	V	Ni	**Comments**	**Phase contrast**	
2000x spot 1	**36.99**	**62.50**	**0.51**	Spot	**Dark**	
2000x spot 2	**36.91**	**62.20**	**0.81**	Spot	**Dark**	
2000x spot 3	**35.99**	**63.47**	**0.54**	Spot	**Dark**	
2000x spot 4	**36.99**	**62.69**	**0.65**	Spot	**Dark**	
Mean	**36.72**	**62.72**	**0.63**			
STDEV	**0.49**	**0.54**	**0.14**			
Medium	C	V	Ni	**Comments**	**Phase contrast**	
2000x spot 1	**15.18**	**36.07**	**48.75**	Spot		

2000x spot 3	**15.62**	**37.70**	**46.68**	Spot		
2000x spot 4	**16.44**	**35.83**	**47.73**	Spot		
2000x spot 5	**16.91**	**34.51**	**48.58**	Spot		
2000x spot 6	**17.31**	**35.45**	**47.24**	Spot		
Mean	16.29	35.91	47.80			
STDEV	0.884347	1.162721	0.878026			
Eutectic	C	V	Ni	**Comments**	**Phase contrast**	
2000x eutectic 1	**26.68**	**45.14**	**28.18**	Area	**Light+Dark**	
2000x eutectic 2	**26.14**	**44.33**	**29.53**	Area	**Light+Dark**	
2000x eutectic 3	**25.78**	**44.34**	**29.88**	Area	**Light+Dark**	
2000x eutectic 4	**24.50**	**43.88**	**31.62**	Area	**Light+Dark**	
Mean	**25.78**	**44.42**	**29.80**			
STDEV	**0.93**	**0.52**	**1.42**			

APPENDIX B5: As-cast Sample 5

All results in atomic%						
Raw data						
Spectrum	**C**	**V**	**Ni**	**Comment**	**Phase Contrast**	**Remarks**
200x image-1	22.16	36.31	41.53	0verall	Light+Medium+Dark	Agree
200x image-2	36.25	29.95	33.8	0verall	Light+Medium+Dark	Not agree
200x image-3	35.24	36.23	28.52	0verall	Light+Medium+Dark	Not agree
200x image-4	22.32	36.39	41.29	0verall	Light+Medium+Dark	Agree
1010ximage-5	22.15	36.78	41.07	0verall	Light+Medium+Dark	Agree
200x image-6	22.91	36.17	41.07	0verall	Light+Medium+Dark	Agree
4000x image 4	16.4	26.99	56.61	spot	Light	Not agree
4000x image 5	11.25	27.63	61.11	spot	Light	Agree
4000x image 6	32.39	36.54	31.07	spot	Light	Not agree
4000x image 7	12.45	27.22	60.33	spot	Light	Agree
4000x image 8	26.46	23.57	49.97	spot	Light	Not agree
4000x image 12	9.87	28.41	61.72	spot	Light	Not agree
4000x image 13	9.69	27.8	62.51	spot	Light	Not agree
4000x image 21	11.11	26.41	62.48	spot	Light	Agree
4000x image 22	11.79	26.8	61.41	spot	Light	Agree
5000x image 2	0	32.45	67.55	spot	Dark	Not agree
4000x image 3	42.32	56.51	1.17	spot	Dark	Not agree
4000x image 9	41.51	57.54	0.95	spot	Dark	Not agree
4000x image 10	43.4	55.7	0.9	spot	Dark	Agree
4000x image 11	43.91	55.2	0.89	spot	Dark	Agree
4000x image 14	43.7	55.46	0.85	spot	Dark	Agree
4000x image 15	13.45	27.17	59.38	Area	Light+Dark	Agree
4000x image 16	19.13	28.06	52.8	Area	Light+Dark	Not agree
4000x image 17	26.43	30.49	43.09	Area	Light+Dark	Not agree
4000x image 18	18.19	27.09	54.72	Area	Light+Dark	Not agree
4000x image 19	14.13	27.07	58.8	Area	Light+Dark	Agree

4000x image 20	13.66	27.42	58.91	Area	Light+Dark	Agree
0verall	**C**	**V**	**Ni**	**Comment**	**Phase Contrast**	
200x image-1	22.16	36.31	41.53	0verall	Light+Medium+Dark	
200x image-2	22.32	36.39	41.29	0verall	Light+Medium+Dark	
200x image-3	22.15	36.78	41.07	0verall	Light+Medium+Dark	
200x image-4	22.91	36.17	41.07	0verall	Light+Medium+Dark	
Mean	22.385	36.4125	41.24			
STDEV	0.358562	0.261327	0.219393			
Dark	**C**	**V**	**Ni**	**Comment**	**Phase Contrast**	
4000x image 10	43.4	55.7	0.9	spot	Dark	
4000x image 11	43.91	55.2	0.89	spot	Dark	
4000x image 14	43.7	55.46	0.85	spot	Dark	
Mean	43.67	55.45333	0.88			
STDEV	0.25632	0.250067	0.026458			
Light	**C**	**V**	**Ni**			
4000x image 5	11.25	27.63	61.11	spot	Light	
4000x image 7	12.45	27.22	60.33	spot	Light	
4000x image 21	11.11	26.41	62.48	spot	Light	
4000x image 22	11.79	26.8	61.41	spot	Light	
Mean	11.65	27.015	61.3325			
STDEV	0.608605	0.526783	0.890183			
Eutectic	**C**	**V**	**Ni**	**Comment**	**Phase Contrast**	
4000x image 15	13.45	27.17	59.38	Area	Light+Dark	
4000x image 19	14.13	27.07	58.8	Area	Light+Dark	
4000x image 20	13.66	27.42	58.91	Area	Light+Dark	
Mean	13.74667	27.22	59.03			
STDEV	0.348186	0.180278	0.308058			

APPENDIX B6: As-cast Sample 6

All results in atomic%						
Raw data						
Spectrum	**C**	**V**	**Ni**	**Comment**	**Phase Contrast**	**Remarks**
200x image1	27.35	25.39	47.26	0verall	Light+Medium+Dark	Agree
200x image2	26.62	26.67	46.72	0verall	Light+Medium+Dark	Agree
200x image3	27.32	25.85	46.83	0verall	Light+Medium+Dark	Agree
200x image4	30.39	22.54	46.55	0verall	Light+Medium+Dark	Not agree
200x image5	27.32	26.14	46.54	0verall	Light+Medium+Dark	Agree
2000x Eutectic 5	17.44	16.89	66.68	Area	Light+Dark	Agree
2000x Eutectic 6	15.84	14.39	69.77	Area	Light+Dark	Not agree
2000x Eutectic 7	16.8	14.52	68.67	Area	Light+Dark	Not agree
2000x Eutectic 8	17.18	16.3	66.52	Area	Light+Dark	Agree
2000x Eutectic 10	18.33	14.67	66.5	Area	Light+Dark	Not agree
2000x Eutectic 13	17.36	16.16	66.47	Area	Light+Dark	Agree

2000x Eutectic 14	18.57	15.03	66.41	Area	Light+Dark	Agree
2000x Eutectic 15	17.2	16.06	66.74	Area	Light+Dark	Agree
2000x Eutectic 16	17.51	16.4	66.09	Area	Light+Dark	Agree
2000x spot 1	47.35	51.96	0.7	Spot	Dark	Agree
2000x spot 9	45.96	53.26	0.78	Spot	Dark	Agree
2000x spot 17	46.39	52.57	0.9	Spot	Dark	Agree
2000x spot 18	46.81	52.56	0.63	Spot	Dark	Agree
2000x spot 19	46.46	51.13	2.42	Spot	Dark	Agree
2000x spot 20	13.63	13.45	72.92	Spot	Light	Agree
2000x spot 2	14.5	12.98	72.52	Spot	Light	Not agree
2000x spot 3	22.98	14.44	62.58	Spot	Light	Agree
2000x spot 4	14.52	13.87	71.61	Spot	Light	Agree
2000x spot 11	14.4	13.12	72.47	Spot	Light	Agree
2000x spot 12	42.54	20.59	36.87	Spot	Light	Not agree

Overall	**C**	**V**	**Ni**	**Comment**	**Phase Contrast**	
200x image1	27.35	25.39	47.26	0verall	Light+Medium+Dark	
200x image2	26.62	26.67	46.72	0verall	Light+Medium+Dark	
200x image3	27.32	25.85	46.83	0verall	Light+Medium+Dark	
200x image5	27.32	26.14	46.54	0verall	Light+Medium+Dark	
Mean	27.1525	26.0125	46.8375			
STDEV	0.355282	0.536182	0.305982			

Eutectic	**C**	**V**	**Ni**	**Comment**	**Phase Contrast**	
2000x Eutectic 1	17.44	16.89	66.68	Area	Light+Dark	
2000x Eutectic 8	17.18	16.3	66.52	Area	Light+Dark	
2000x Eutectic 13	17.36	16.16	66.47	Area	Light+Dark	
2000x Eutectic 14	18.57	15.03	66.41	Area	Light+Dark	
2000x Eutectic 15	17.2	16.06	66.74	Area	Light+Dark	
2000x Eutectic 16	17.51	16.4	66.09	Area	Light+Dark	
Mean	17.54333	16.14	66.485			
STDEV	0.519487	0.615565	0.230716			

Dark	**C**	**V**	**Ni**	**Comment**	**Phase Contrast**	
2000x spot 1	47.35	51.96	0.7	Spot	Dark	
2000x spot 9	45.96	53.26	0.78	Spot	Dark	
2000x spot17	46.39	52.57	0.9	Spot	Dark	
2000x spot18	46.81	52.56	0.63	Spot	Dark	
2000x spot19	46.46	51.13	2.42	Spot	Dark	
Mean	46.6	52.3	1.1			
STDEV	0.5	0.8	0.7			

Light	**C**	**V**	**Ni**	**Comment**	**Phase Contrast**	
2000x spot 2	14.5	12.98	72.52	Spot	Light	
2000x spot 3	22.98	14.44	62.58	Spot	Light	
2000x spot 4	14.52	13.87	71.61	Spot	Light	
2000x spot 11	14.4	13.12	72.47	Spot	Light	
2000x spot 12	42.54	20.59	36.87	Spot	Light	

2000x spot 20	13.63	13.45	72.92	Spot	Light	
Mean	14.2625	13.355	72.38			
STDEV	0.424922	0.395854	0.551422			

APPENDIX B7: As-cast Sample 7

All results in atomic%						
Raw data						
Spectrum	**C**	**V**	**Ni**	**Comment**	**Phase Contrast**	**Remarks**
200x image 1	73.37	4.06	22.57	0verall	Light+Medium+Dark	Agree
200x image 2	73.7	4.01	22.3	0verall	Light+Medium+Dark	Agree
200x image 3	73.19	4.22	22.59	0verall	Light+Medium+Dark	Agree
200x image 4	74.45	3.86	21.69	0verall	Light+Medium+Dark	Not agree
200x image 5	73.56	4.09	22.35	0verall	Light+Medium+Dark	Agree
200x image 6	73.47	4.49	22.03	0verall	Light+Medium+Dark	Agree
1000x spot 1	22.04	1.96	76	spot	Light	Agree
1000x spot 2	21.9	2.11	76	spot	Light	Agree
1000x spot 3	24.06	1.83	74.12	spot	Light	Not agree
1000x spot 4	22.85	1.98	75.17	spot	Light	Agree
1000x spot 5	23.86	2	74.14	spot	Light	Not agree
1000x spot 6	20.43	2.22	77.35	spot	Light	Agree
1000x spot 2	48.52	49.6	1.88	spot	dark	Agree
1000x spot 3	47.54	47.48	5.18	spot	dark	Agree
1000x spot 4	43.5	49.15	7.36	spot	dark	Agree
1000x spot 5	47.89	50.66	1.45	spot	dark	Agree
1000x spot 6	47.5	48.74	3.76	spot	dark	Not agree
1000x spot 1	98.13	0.06	1.81	spot	Very dark	Not agree
1000x spot 2	99.76	0.03	0.21	spot	Very dark	Agree
1000x spot 3	99.8	0	0.2	spot	Very dark	Agree
1000x spot 4	99.59	0.03	0.38	spot	Very dark	Agree
1000x Eutectic1	**75.53**	**3.99**	**20.48**	Area	Medium+Dark	Not agree
1000x Eutectic2	76.3	3.92	19.79	Area	Medium+Dark	Not agree
1000x Eutectic3	69.76	4.71	25.53	Area	Medium+Dark	Agree
1000x Eutectic4	69.55	4.75	25.7	Area	Medium+Dark	Agree
1000x Eutectic5	71.06	4.61	24.33	Area	Medium+Dark	Agree
1000x Eutectic6	71.03	4.63	24.35		Medium+Dark	Agree
0verall	**C**	**V**	**Ni**	**Comment**	**Phase Contrast**	
200x image 1	73.37	4.06	22.57	0verall	Light+Medium+Dark	
200x image 2	73.7	4.01	22.3	0verall	Light+Medium+Dark	
200x image 3	73.19	4.22	22.59	0verall	Light+Medium+Dark	
200x image 5	73.56	4.09	22.35	0verall	Light+Medium+Dark	
200x image 6	73.47	4.49	22.03	0verall	Light+Medium+Dark	
Mean	73.458	4.174	22.368			
STD	0.192795	0.192951	0.228736			
Light	**C**	**V**	**Ni**	**Comment**	**Phase Contrast**	
1000x spot 1	22.04	1.96	76	spot	Light	

1000x spot 2	21.9	2.11	76	spot	Light	
1000x spot 4	22.85	1.98	75.17	spot	Light	
1000x spot 6	20.43	2.22	77.35	spot	Light	
Mean	**21.805**	**2.0675**	**76.13**			
STD	1.007786	0.121484	0.902552			
Dark	**C**	**V**	**Ni**	**Comment**	**Phase Contrast**	
1000x spot 2	48.52	49.6	1.88	spot	dark	
1000x spot 3	47.54	47.48	5.18	spot	dark	
1000x spot 4	47.89	50.66	1.45	spot	dark	
1000x spot 5	47.5	48.74	3.76	spot	dark	
Mean	47.8625	49.12	3.0675			
STD	0.472043	1.346105	1.729034			
Very dark	**C**	**V**	**Ni**	**Comment**	**Phase Contrast**	
1000x spot 2	99.76	0.03	0.21	spot	dark	
1000x spot 3	99.8	0	0.2	spot	dark	
1000x spot 4	**99.59**	**0.03**	**0.38**	spot	dark	
Mean	99.71667	0.02	0.263333			
STD	0.111505	0.017321	0.10116			
Eutectic	**C**	**V**	**Ni**	**Comment**	**Phase Contrast**	
1000x Eutectic3	69.76	4.71	25.53	Area	Medium+Dark	
1000x Eutectic4	69.55	4.75	25.7	Area	Medium+Dark	
1000x Eutectic5	71.06	4.61	24.33	Area	Medium+Dark	
1000x Eutectic6	71.03	4.63	24.35	Area	Medium+Dark	
Mean	70.35	4.675	24.9775			
STD	0.807176	0.066081	0.739431			

APPENDIX B8: As-cast Sample 8

All results in atomic%						
Raw data						
Spectrum	**C**	**V**	**Ni**	**Comments**	**Phase Contrast**	**Remark**
200x image 1	30.31	25.78	43.91	Overall	Light+Medium+Dark	Agree
200x image 2	27.71	26.68	45.61	Overall	Light+Medium+Dark	Not agree
200x image 3	30.35	26.41	43.24	Overall	Light+Medium+Dark	Agree
200x image 4	29.1	26.91	44	Overall	Light+Medium+Dark	Agree
200x image 5	31.11	25.99	42.9	Overall	Light+Medium+Dark	Not agree
200x image 6	29.54	26.93	43.53	Overall	Light+Medium+Dark	Agree
1000x image 7	32.8	26.9	40.3	Overall	Light+Medium+Dark	Not agree
2000x spot 1	16.88	20.73	62.39	Spot	Light	Not agree
2000x spot 2	18.2	21.73	60.07	Spot	Light	Agree
2000x spot 3	18.5	20.87	60.63	Spot	Light	Agree
2000x spot 4	18.88	21.57	59.55	Spot	Light	Agree

2000x spot 5	19.12	20.74	60.14	Spot	Light	Agree
2000x spot 6	14.45	22.5	63.06	Spot	Light	Not agree
2000x spot 1	49.68	41.56	8.76	Spot	Dark	Not agree
2000x spot 2	49.01	50.02	0.97	Spot	Dark	Agree
2000x spot 3	48.79	50.22	0.99	Spot	Dark	Agree
2000x spot 4	48.07	51	0.93	Spot	Dark	Agree
2000x spot 5	48.62	50.34	1.05	Spot	Dark	Agree
2000x eutectic 1	30.4	26.52	43.08	Area	Light+ Dark	Agree
2000x eutectic 2	31.52	25.81	42.68	Area	Light+ Dark	Not agree
2000x eutectic 3	25.03	28.23	46.74	Area	Light+ Dark	Agree
2000x eutectic 4	26.89	28.16	44.995	Area	Light+ Dark	Agree
2000x eutectic 5	25.88	27.68	46.44	Area	Light+ Dark	Agree
2000x eutectic 6	25.56	28.73	45.71	Area	Light+ Dark	Agree
Overall	**C**	**V**	**Ni**	**Comments**	**Phase Contrast**	
200x image 1	30.31	25.78	43.91	Overall	Light+Medium+Dark	
200x image 3	30.35	26.41	43.24	Overall	Light+Medium+Dark	
200x image 4	29.1	26.91	44	Overall	Light+Medium+Dark	
200x image 5	31.11	25.99	42.9	Overall	Light+Medium+Dark	
200x image 6	29.54	26.93	43.53	Overall	Light+Medium+Dark	
Mean	29.825	26.508	43.67			
STDEV	0.831	0.4992	0.5307			
Light	**C**	**V**	**Ni**	**Comments**	**Phase contrast**	
2000x spot 2	18.2	21.73	60.07	Spot	Light	
2000x spot 3	18.5	20.87	60.63	Spot	Light	
2000x spot 4	18.88	21.57	59.55	Spot	Light	
2000x spot 5	19.12	20.74	60.14	Spot	Light	
Mean	18.675	21.228	60.098			
STDEV	0.4067	0.4951	0.4419			
Dark	**C**	**V**	**Ni**	**Comments**	**Phase contrast**	
2000x spot 2	49.01	50.02	0.97	Spot	Dark	
2000x spot 3	48.79	50.22	0.99	Spot	Dark	
2000x spot 4	48.07	51	0.93	Spot	Dark	
2000x spot 5	48.62	50.34	1.05	Spot	Dark	
Mean	48.623	50.395	0.985			
STDEV	0.4014	0.4244	0.05			

Eutectic	**C**	**V**	**Ni**	**Comments**	**Phase contrast**	
2000x eutectic 3	25.03	28.23	46.74	Area	Light+ Dark	
2000x eutectic 4	26.89	28.16	44.995	Area	Light+ Dark	
2000x eutectic 5	25.88	27.68	46.44	Area	Light+ Dark	
2000x eutectic 6	25.56	28.73	45.71	Area	Light+ Dark	
Mean	25.84	28.2	45.971			
STDEV	0.7829	0.4297	0.7815			

APPENDIX B9: As-cast Sample 9

All results in atomic%						
Raw data						
Spectrum	**C**	**V**	**Ni**	**Comments**	**Phase contrast**	**Remark**
200x image 1	17.63	57.75	24.63	Overall	Light + Dark	Agree
200x image 2	16.22	58.55	25.23	Overall	Light + Dark	Not agree
200x image 3	18.34	57.22	24.44	Overall	Light + Dark	Agree
200x image 4	17.42	57.49	25.1	Overall	Light + Dark	Agree
200x image 5	18.13	57.4	24.47	Overall	Light + Dark	Agree
200x image 6	18.22	56.93	24.85	Overall	Light + Dark	Agree
4000x spot 1	10.79	55.79	33.42	Spot	Light	Agree
4000x spot 2	10.28	59.94	29.78	Spot	Light	Agree
4000x spot 3	8.6	55.4	36	Spot	Light	Not agree
4000x spot 4	10.3	57.63	32.07	Spot	Light	Agree
4000x spot 5	9.26	61.68	29.06	Spot	Light	Agree
4000x spot 6	9.92	62.4	27.68	Spot	Light	Not agree
4000x spot 1	31.57	66.25	2.18	Spot	Dark	Not agree
4000x spot 2	35.6	62.43	1.97	Spot	Dark	Agree
4000x spot 3	34.02	64.93	1.05	Spot	Dark	Agree
4000x spot 4	35.4	64.12	0.48	Spot	Dark	Agree
4000x spot 5	35.25	63.59	1.16	Spot	Dark	Agree
4000x spot 6	34.87	62.97	2.16	Spot	Dark	Not agree
2000x eutectic 1	17.75	58.95	23.3	Area	Light+Dark	Agree
2000x eutectic 2	17.99	58.78	23.24	Area	Light+Dark	Agree
2000x eutectic 3	17.82	58.27	23.91	Area	Light+Dark	Agree
2000x eutectic 4	17.26	58.62	24.12	Area	Light+Dark	Agree
2000x eutectic 5	17.44	58.57	23.99	Area	Light+Dark	Agree
2000x eutectic 6	17.26	58.65	24.09	Area	Light+Dark	Agree
2000x eutectic 7	17.45	58.12	24.43	Area	Light+Dark	Agree
2000x eutectic 8	17.99	58.2	23.81	Area	Light+Dark	Agree
2000x eutectic 9	17.91	58.92	23.18	Area	Light+Dark	Agree

2000x eutectic 10	18.75	58.2	23.05	Area	Light+Dark	Not agree
Overall	**C**	**V**	**Ni**	**Comments**	**Phase contrast**	
200x image 1	17.63	57.75	24.63	Overall	Light + Medium + Dark	
200x image 3	18.34	57.22	24.44	Overall	Light + Medium + Dark	
200x image 4	17.42	57.49	25.1	Overall	Light + Medium + Dark	
200x image 5	18.13	57.4	24.47	Overall	Light + Medium + Dark	
200x image 6	18.22	56.93	24.85	Overall	Light + Medium + Dark	
Mean	17.948	57.358	24.698			
STDEV	0.400212	0.306219	0.277435			
Light	**C**	**V**	**Ni**	**Comments**	**Phase contrast**	
4000x spot 1	10.79	59.79	29.42	Spot	Light	
4000x spot 2	10.28	59.94	29.78	Spot	Light	
4000x spot 4	10.3	58.93	30.77	Spot	Light	
4000x spot 5	10.26	60.68	29.06	Spot	Light	
Mean	10.4075	59.835	29.7575			
STDEV	0.255522	0.71789	0.736223			
Dark	**C**	**V**	**Ni**	**Comments**	**Phase contrast**	
4000x spot 2	35.6	63.42	0.98	Spot	Dark	
4000x spot 3	34.02	64.93	1.05	Spot	Dark	
4000x spot 4	35.4	64.12	0.48	Spot	Dark	
4000x spot 5	35.25	63.59	1.16	Spot	Dark	
Mean	35.0675	64.015	0.9175			
STDEV	0.712899	0.678945	0.300929			
Fine eutectic	**C**	**V**	**Ni**	**Comments**	**Phase contrast**	
2000x eutectic 1	17.75	58.95	23.3	Area	Light+Dark	
2000x eutectic 4	17.26	58.62	24.12	Area	Light+Dark	
2000x eutectic 5	17.44	58.57	23.99	Area	Light+Dark	
2000x eutectic 6	17.26	58.65	24.09	Area	Light+Dark	
2000x eutectic 7	17.45	58.12	24.43	Area	Light+Dark	
Mean	17.432	58.582	23.986			
STDEV	0.200425	0.297943	0.417289			
Coarse eutectic	**C**	**V**	**Ni**	**Comments**	**Phase contrast**	
2000x eutectic 2	17.99	58.78	23.24	Area	Light+Dark	
2000x eutectic 3	17.82	58.27	23.91	Area	Light+Dark	
2000x eutectic 8	17.99	58.2	23.81	Area	Light+Dark	
2000x eutectic 9	17.91	58.92	23.18	Area	Light+Dark	
Mean	17.9275	58.5425	23.535			

STDEV	0.080984	0.360775	0.378286			

APPENDIX B10: As-cast Sample 10

All results in atomic%						
Raw data						
Spectrum	**C**	**V**	**Ni**	**Comments**	phase contrast	Remarks
200x image 1	71.61	26.18	2.21	Overall	Light + Medium + Dark	Agree
200x image 2	73.07	24.35	2.57	Overall	Light + Medium + Dark	Not agree
200x image 3	71.48	26.34	2.18	Overall	Light + Medium + Dark	Agree
200x image 4	71.88	25.31	2.81	Overall	Light + Medium + Dark	Agree
200x image 5	73.9	23.36	2.74	Overall	Light + Medium + Dark	Not agree
1000x spot 1	18.34	3.52	78.14	Spot	Light	Agree
1000x spot 2	19.05	3.6	77.35	Spot	Light	Agree
1000x spot 3	18.09	3.51	78.4	Spot	Light	Agree
1000x spot 4	19.11	3.81	77.08	Spot	Light	Agree
1000x spot 5	20.02	6.79	73.2	Spot	Light	Not agree
1000x spot 1	48.81	51.19	0	Spot	Dark	Agree
1000x spot 2	49.39	50.47	0.15	Spot	Dark	Agree
1000x spot 3	49.45	50.33	0.22	Spot	Dark	Agree
1000x spot 4	49.91	50.09	0	Spot	Dark	Agree
1000x spot 5	48.98	50.78	0.24	Spot	Dark	Agree
1000x spot 1	99.87	0.09	0.03	Spot	Very Dark	Agree
1000x spot 2	99.86	0.14	0	Spot	Very Dark	Agree
1000x spot 3	99.88	0.12	0	Spot	Very Dark	Agree
1000x spot 4	94.02	5.57	0.41	Spot	Very Dark	Not agree
Overall	**C**	**V**	**Ni**	**Comments**	**phase contrast**	
200x image 1	71.61	26.18	2.21	Overall	Light + Medium + Dark	
200x image 2	73.07	24.35	2.57	Overall	Light + Medium + Dark	
200x image 3	71.48	26.34	2.18	Overall	Light + Medium + Dark	
200x image 4	71.88	25.31	2.81	Overall	Light + Medium + Dark	
200x image 5	73.9	23.36	2.74	Overall	Light + Medium + Dark	
Mean	71.65667	25.94333	2.4			
STDEV	0.204042	0.554286	0.355387			
Light	**C**	**V**	**Ni**	**Comments**	**phase contrast**	
1000x spot 1	18.34	3.52	78.14	Spot	Light	
1000x spot 2	19.05	3.6	77.35	Spot	Light	
1000x spot 3	18.09	3.51	78.4	Spot	Light	
1000x spot 4	19.11	3.81	77.08	Spot	Light	

1000x spot 5	20.02	6.79	73.2	Spot	Light	
Mean	18.6475	3.61	77.7425			
STDEV	0.510319	0.139284	0.628033			
Dark	**C**	**V**	**Ni**	**Comments**	**Phase contrast**	
1000x spot 1	48.81	51.19	0	Spot	Dark	
1000x spot 2	49.39	50.47	0.15	Spot	Dark	
1000x spot 3	49.45	50.33	0.22	Spot	Dark	
1000x spot 4	49.91	50.09	0	Spot	Dark	
1000x spot 5	48.98	50.78	0.24	Spot	Dark	
Mean	49.308	50.572	0.122			
STDEV	0.431532	0.426169	0.116276			
Very Dark	**C**	**V**	**Ni**	**Comments**	**Phase contrast**	
1000x spot 1	99.87	0.09	0.03	Spot	Very Dark	
1000x spot 2	99.86	0.14	0	Spot	Very Dark	
1000x spot 3	99.88	0.12	0	Spot	Very Dark	
1000x spot 4	94.02	5.57	0.41	Spot	Very Dark	
Mean	99.87	0.116667	0.01			
STDEV	0.01	0.025166	0.017321			

APPENDIX B11: As-cast Sample 11

All results in atomic%						
Raw data						
Spectrum	**C**	**V**	**Ni**	**Comments**	**Phase contrast**	Remark
500x image 1	25.03	67.21	7.76	Overall	**Light + Medium + Dark**	Agree
500x image 2	25.14	67.56	7.3	Overall	**Light + Medium + Dark**	Agree
500x image 3	23.83	68.42	7.76	Overall	**Light + Medium + Dark**	Not agree
500x image 4	23.74	68.26	8	Overall	**Light + Medium + Dark**	Not agree
500x image 5	24.57	67.76	7.67	Overall	**Light + Medium + Dark**	Agree
500x image 6	25.24	67	7.76	Overall	**Light + Medium + Dark**	Agree
500x image 7	25.74	66.78	7.48	Overall	**Light + Medium + Dark**	Agree
2000x spot 1	10.67	70.99	18.34	Spot	**Light**	Agree
2000x spot 2	26.73	57.52	15.75	Spot	**Light**	Not agree
2000x spot 3	9.38	71.83	18.79	Spot	**Light**	Agree
2000x spot 4	9.9	71.99	18.11	Spot	**Light**	Agree
2000x spot 5	12.33	63.96	23.71	Spot	**Light**	Not agree
2000x spot 6	9.75	71.55	18.7	Spot	**Light**	Agree
2000x spot 1	36.3	62.5	1.2	Spot	**Dark**	Agree
2000x spot 2	36.25	62.33	1.42	Spot	**Dark**	Agree
2000x spot 3	36.84	62.76	0.4	Spot	**Dark**	Agree

2000x spot 4	29.58	63.5	6.92	Spot	**Dark**	Not agree
2000x spot 5	36.27	62.48	1.25	Spot	**Dark**	Agree
2000x spot 6	19.34	70.38	10.29	Spot	**Dark**	Not agree
2000x spot 1	9.3	76.25	14.45	Spot	**medium**	Not agree
2000x spot 2	26.64	62.63	10.73	Spot	**medium**	Not agree
2000x spot 3	10.83	71.88	17.29	Spot	**medium**	Agree
2000x spot 4	11.89	69.72	18.39	Spot	**medium**	Agree
2000x spot 5	11.71	70.55	17.74	Spot	**medium**	Agree
1000x eutectic 1	25.06	67.44	7.5	Area	**Light+Dark**	Not agree
1000x eutectic 2	24.06	68.36	7.58	Area	**Light+Dark**	Agree
1000x eutectic 3	24.14	67.94	7.92	Area	**Light+Dark**	Agree
1000x eutectic 4	23.92	68.35	7.73	Area	**Light+Dark**	Agree
1000x eutectic 5	23.82	68.52	7.65	Area	**Light+Dark**	Agree
1000x eutectic 6	30.25	62.84	6.91	Area	**Light+Dark**	Not agree
Overall	**C**	**V**	**Ni**	**Comments**	**Phase contrast**	
500x image 1	25.03	67.21	7.76	Overall	**Light + Medium + Dark**	
500x image 2	25.14	67.56	7.3	Overall	**Light + Medium + Dark**	
500x image 5	24.57	67.76	7.67	Overall	**Light + Medium + Dark**	
500x image 6	25.24	67	7.76	Overall	**Light + Medium + Dark**	
500x image 7	25.74	66.78	7.48	Overall	**Light + Medium + Dark**	
Mean	**25.144**	**67.262**	**7.594**			
STDEV	**0.420393**	**0.40015**	**0.2002**			
Light	**C**	**V**	**Ni**	**Comments**	**Phase contrast**	
2000x spot 1	10.67	70.99	18.34	Spot	**Light**	
2000x spot 3	9.38	71.83	18.79	Spot	**Light**	
2000x spot 4	9.9	71.99	18.11	Spot	**Light**	
2000x spot 6	9.75	71.55	18.7	Spot	**Light**	
Mean	**9.925**	**71.59**	**18.485**			
STDEV	**0.542617**	**0.439394**	**0.316702**			
Dark	**C**	**V**	**Ni**	**Comments**	**Phase contrast**	
2000x spot 1	36.3	62.5	1.2	Spot	**Dark**	
2000x spot 2	36.25	62.33	1.42	Spot	**Dark**	
2000x spot 3	36.84	62.76	0.4	Spot	**Dark**	
2000x spot 5	36.27	62.48	1.25	Spot	**Dark**	
Mean	36.415	62.5175	1.0675			
STDEV	0.28408	0.17858	0.45485			
Medium	**C**	**V**	**Ni**	**Comments**	**Phase contrast**	

2000x spot 3	10.83	71.88	17.29	Spot	**medium**	
2000x spot 4	11.89	69.72	18.39	Spot	**medium**	
2000x spot 5	11.71	70.55	17.74	Spot	**medium**	
Mean	11.47667	70.71667	17.80667			
STDEV	0.567215	1.089602	0.553022			
Area	**C**	**V**	**Ni**	**Comments**	**Phase contrast**	
1000x eutectic 2	24.06	68.36	7.58	Area	**Light+Dark**	
1000x eutectic 3	24.14	67.94	7.92	Area	**Light+Dark**	
1000x eutectic 4	23.92	68.35	7.73	Area	**Light+Dark**	
1000x eutectic 5	23.82	68.52	7.65	Area	**Light+Dark**	
Mean	**23.985**	**68.2925**	**7.72**			
STDEV	**0.14271**	**0.24757**	**0.14674**			

APPENDIX B12: As-cast Sample 12

All results in atomic%						
Raw data						
Spectrum	**C**	**V**	**Ni**	**Comments**	**Phase contrast**	**Remark**
200x image 1	**27.55**	**68.47**	**3.98**	Overall	**Light + Medium + Dark**	Agree
200x image 2	**28.57**	**67.45**	**3.99**	Overall	**Light + Medium + Dark**	Agree
200x image 3	**28.27**	**68.09**	**3.65**	Overall	**Light + Medium + Dark**	Agree
200x image 4	**27.88**	**68.25**	**3.87**	Overall	**Light + Medium + Dark**	Agree
200x image 5	**28.68**	**67.57**	**3.75**	Overall	**Light + Medium + Dark**	Agree
5000x spot 1	**11.56**	**78.78**	**9.65**	Spot	**Light**	Agree
5000x spot 2	**10.79**	**79.23**	**9.98**	Spot	**Light**	Agree
5000x spot 3	**8.6**	**83.7**	**7.71**	Spot	**Light**	Not agree
5000x spot 4	**10.83**	**79.75**	**9.42**	Spot	**Light**	Agree
5000x spot 5	**7.46**	**85.34**	**7.2**	Spot	**Light**	Not agree
5000x spot 6	**10.15**	**79.75**	**10.1**	Spot	**Light**	Agree
5000x spot 1	**36.46**	**63.4**	**0.15**	Spot	**Dark**	Agree
5000x spot 2	**36.45**	**63.37**	**0.18**	Spot	**Dark**	Agree
5000x spot 3	**34.72**	**65.06**	**0.22**	Spot	**Dark**	Not agree
5000x spot 4	**35.41**	**64.59**	**0**	Spot	**Dark**	Agree
5000x spot 5	**32.68**	**64.61**	**2.71**	Spot	**Dark**	Not agree
5000x spot 6	**36.42**	**63.58**	**0**	Spot	**Dark**	Agree
1000x eutectic 1	**28.72**	**67.45**	**3.84**	Area	**Light+Dark**	Agree
1000x eutectic 2	**29.94**	**66.67**	**3.4**	Area	**Light+Dark**	Agree
1000x eutectic 3	28.1	67.77	4.14	Area	**Light+Dark**	Agree
1000x eutectic 4	**28.67**	**67.5**	**3.82**	Area	**Light+Dark**	Agree
1000x eutectic 5	27.5	68.32	4.18	Area	**Light+Dark**	Not agree

1000x eutectic 6	**29.15**	**67.14**	**3.71**	Area	**Light+Dark**	Agree
1000x eutectic 7	29.9	66.43	3.67	Area	**Light+Dark**	Agree
1000x eutectic 8	**29.75**	**66.52**	**3.73**	Area	**Light+Dark**	Agree
Overall	**C**	**V**	**Ni**	**Comments**	**Phase contrast**	
200x image 1	27.55	68.47	3.98	Overall	Light + Medium + Dark	
200x image 2	28.57	67.45	3.99	Overall	Light + Medium + Dark	
200x image 3	28.27	68.09	3.65	Overall	Light + Medium + Dark	
200x image 4	27.88	68.25	3.87	Overall	Light + Medium + Dark	
200x image 5	28.68	67.57	3.75	Overall	Light + Medium + Dark	
Mean	28.19	67.97	3.848			
STDEV	0.4734	0.44	0.147			
Light	**C**	**V**	**Ni**	**Comments**	**Phase contrast**	
5000x spot 1	11.56	78.78	9.65	Spot	Light	
5000x spot 2	10.79	79.23	9.98	Spot	Light	
5000x spot 4	10.83	79.75	9.42	Spot	Light	
5000x spot 6	10.15	79.75	10.1	Spot	Light	
Mean	10.8325	79.38	9.788			
STDEV	0.57645	0.468	0.31			
Dark	**C**	**V**	**Ni**	**Comments**	**Phase contrast**	
5000x spot 1	36.46	63.4	0.15	Spot	Dark	
5000x spot 2	36.45	63.37	0.18	Spot	Dark	
5000x spot 4	35.41	64.59	0	Spot	Dark	
5000x spot 6	36.42	63.58	0	Spot	Dark	
Mean	36.185	63.74	0.083			
STDEV	0.51695	0.577	0.096			
Eutectic	**C**	**V**	**Ni**	**Comments**	**Phase contrast**	
1000x eutectic 1	28.72	67.45	3.84	Area	Light+Dark	
1000x eutectic 2	29.94	66.67	3.4	Area	Light+Dark	
1000x eutectic 3	28.1	67.77	4.14	Area	Light+Dark	
1000x eutectic 4	28.67	67.5	3.82	Area	Light+Dark	
1000x eutectic 6	29.15	67.14	3.71	Area	Light+Dark	
1000x eutectic 7	29.9	66.43	3.67	Area	Light+Dark	
1000x eutectic 8	29.75	66.52	3.73	Area	Light+Dark	
Mean	29.1757	67.07	3.759			
STDEV	0.71412	0.532	0.222			

APPENDIX B13: As-cast Sample 13

All results in atomic%						
Raw data						
Spectrum	**C**	**V**	**Ni**	**Comments**	**Phase contrast**	**Remark**
200x image 1	32.38	46.43	21.19	Overall	Light + Dark	Not agree
200x image 2	30.84	47.72	21.44	Overall	Light + Dark	Agree
200x image 3	30.37	47.61	22.01	Overall	Light + Dark	Agree
200x image 4	30.19	47.68	22.14	Overall	Light + Dark	Agree
200x image 5	29.39	48.14	22.46	Overall	Light + Dark	Agree
200x image 6	29.68	48.13	22.19	Overall	Light + Dark	Agree
2000x spot 1	16.72	42.87	40.41	Spot	Light	Not agree
2000x spot 2	18.02	40.92	41.06	Spot	Light	Agree
2000x spot 3	17.6	42.35	40.05	Spot	Light	Agree
2000x spot 4	18.75	39.33	41.92	Spot	Light	Agree
2000x spot 5	16.01	41.12	42.87	Spot	Light	Not agree
2000x spot 6	17.12	41.48	41.4	Spot	Light	Agree
2000x spot 7	67.34	14.62	18.04	Spot	Light	Not agree
2000x spot 1	37.57	62.13	0.3	Spot	Dark	Agree
2000x spot 2	37.34	62.28	0.38	Spot	Dark	Agree
2000x spot 3	38.1	61.64	0.26	Spot	Dark	Agree
2000x spot 4	37.82	61.73	0.45	Spot	Dark	Agree
2000x spot 5	36.77	62.6	0.63	Spot	Dark	Not agree
2000x spot 6	38.04	61.66	0.3	Spot	Dark	Agree
2000x spot 7	37.46	62.22	0.32	Spot	Dark	Agree
2000x spot 1	35.01	53.56	11.43	Spot	Medium	Agree
2000x spot 2	34.41	52.78	12.81	Spot	Medium	Agree
2000x spot 3	32.56	54.9	12.54	Spot	Medium	Not agree
2000x spot 4	33.04	53.87	13.09	Spot	Medium	Not agree
2000x spot 5	35.54	53.45	11.01	Spot	Medium	Agree
2000x spot 6	35.12	52.13	12.75	Spot	Medium	Agree
2000x spot 7	35.11	52.25	12.64	Spot	Medium	Agree
2000x eutectic 1	45.46	39.28	15.26	Area	Light + Dark	Not agree
2000x eutectic 2	28.27	50.17	21.56	Area	Light + Dark	Agree
2000x eutectic 3	29.93	49.26	20.81	Area	Light + Dark	Agree
2000x eutectic 4	27.17	49.87	22.96	Area	Light + Dark	Agree
2000x eutectic 5	28.4	50.07	21.53	Area	Light + Dark	Agree
2000x eutectic 6	30.9	47.27	21.83	Area	Light + Dark	Not agree
2000x eutectic 7	38.94	40.54	20.52	Area	Light + Dark	Not agree
Overall	C	V	Ni	Comments	Phase contrast	
200x image 2	30.84	47.72	21.44	Overall	Light + Dark	

200x image 3	30.37	47.61	22.01	Overall	Light + Dark	
200x image 4	30.19	47.68	22.14	Overall	Light + Dark	
200x image 5	29.39	48.14	22.46	Overall	Light + Dark	
200x image 6	29.68	48.13	22.19	Overall	Light + Dark	
Mean	30.094	47.856	22.048			
STDEV	0.57204	0.2577	0.3773			
Light	**C**	**V**	**Ni**	**Comments**	**Phase contrast**	
2000x spot 2	18.02	40.92	41.06	Spot	Light	
2000x spot 3	17.6	42.35	40.05	Spot	Light	
2000x spot 4	18.75	39.33	41.92	Spot	Light	
2000x spot 6	17.12	41.48	41.4			
Mean	17.8725	41.02	41.108			
STDEV	0.69096	1.271	0.7887			
Dark	**C**	**V**	**Ni**	**Comments**	**Phase contrast**	
2000x spot 1	37.57	62.13	0.3	Spot	Dark	
2000x spot 2	37.34	62.28	0.38	Spot	Dark	
2000x spot 3	38.1	61.64	0.26	Spot	Dark	
2000x spot 4	37.82	61.73	0.45			
2000x spot 6	38.04	61.66	0.3			
2000x spot 7	37.46	62.22	0.32			
Mean	37.7217	61.943	0.335			
STDEV	0.31346	0.2975	0.0686			
Eutectic	**C**	**V**	**Ni**	**Comments**	**Phase contrast**	
2000x eutectic 2	28.27	50.17	21.56	Area	Light+Dark	
2000x eutectic 3	29.93	49.26	20.81	Area	Light+Dark	
2000x eutectic 4	27.17	49.87	22.96	Area	Light+Dark	
2000x eutectic 5	28.4	50.07	21.53	Area	Light+Dark	
Mean	28.4425	49.843	21.715			
STDEV	1.13482	0.4079	0.8995			
Medium	**C**	**V**	**Ni**	**Comments**	**Phase contrast**	
2000x spot 1	35.01	53.56	11.43	Spot	Medium	
2000x spot 2	34.41	52.78	12.81	Spot	Medium	
2000x spot 5	35.54	53.45	11.01	Spot	Medium	
2000x spot 6	35.12	52.13	12.75	Spot	Medium	
2000x spot 7	35.11	52.25	12.64	Spot	Medium	
Mean	35.038	52.834	12.128			
STDEV	0.40592	0.6607	0.8443			

APPENDIX B14: As-cast Sample 14

All results in atomic%						
Raw data						
Spectrum	**C**	**V**	**Ni**	**Comments**	**Phase contrast**	**Remark**
200x image 1	35.84	55.3	8.86	Overall	Light + Dark	Agree
200x image 2	35.54	55.31	9.15	Overall	Light + Dark	Agree
200x image 3	34.92	55.46	9.63	Overall	Light + Dark	Agree
200x image 4	35.49	55.09	9.42	Overall	Light + Dark	Agree
2000x spot 1	12.63	57.02	30.34	Spot	Light	Agree
2000x spot 2	13.28	56.36	30.36	Spot	Light	Agree
2000x spot 3	27.32	50.38	22.3	Spot	Light	Not agree
2000x spot 4	12.05	56.82	31.15	Spot	Light	Agree
2000x spot 5	21.11	53.82	25.06	Spot	Light	Not agree
2000x spot 1	37.34	62.41	0.25	Spot	Dark needle	Agree
2000x spot 2	37.96	61.81	0.23	Spot	Dark needle	Agree
2000x spot 3	37.01	62.78	0.21	Spot	Dark needle	Agree
2000x spot 4	38.21	61.58	0.21	Spot	Dark needle	Agree
2000x spot 1	37.73	62.06	0.21	Spot	Dark	Agree
2000x spot 2	37.65	61.94	0.41	Spot	Dark	Agree
2000x spot 3	40.33	59.41	0.26	Spot	Dark	Not agree
2000x spot 4	37.39	62.29	0.32	Spot	Dark	Agree
2000x spot 5	31.27	54.12	14.61	Spot	Dark	Not agree
2000x spot 6	36.82	62.97	0.21	Spot	Dark	Agree
2000x eutectic 1	35.23	54.6	10.17	Area	Light+Dark	Agree
2000x eutectic 2	35.15	54.79	10.06	Area	Light+Dark	Agree
2000x eutectic 3	35.75	54.9	9.36	Area	Light+Dark	Agree
2000x eutectic 4	36.25	54.05	9.7	Area	Light+Dark	Not agree
2000x eutectic 5	34.45	55.4	10.15	Area	Light+Dark	Agree
2000x eutectic 6	35.1	54.63	10.27	Area	Light+Dark	Agree
2000x eutectic 7	35.67	54.33	10	Area	Light+Dark	Agree
Overall	**C**	**V**	**Ni**	**Comments**	**Phase contrast**	
200x image 1	35.84	55.3	8.86	Overall	Light + Dark	
200x image 2	35.54	55.31	9.15	Overall	Light + Dark	
200x image 3	34.92	55.46	9.63	Overall	Light + Dark	
200x image 4	35.49	55.09	9.42	Overall	Light + Dark	
Mean	35.448	55.29	9.265			
STDEV	0.3841	0.1521	0.3339			
Light	**C**	**V**	**Ni**	**Comments**	**Phase contrast**	
2000x spot 1	12.63	57.02	30.34	Spot	Light	

2000x spot 2	13.28	56.36	30.36	Spot	Light	
2000x spot 4	12.05	56.82	31.15	Spot	Light	
Mean	12.653	56.733	30.617			
STDEV	0.6153	0.3384	0.462			
Dark needle	**C**	**V**	**Ni**	**Comments**	**Phase contrast**	
2000x spot 1	37.34	62.41	0.25	Spot	Dark	
2000x spot 2	37.96	61.81	0.23	Spot	Dark	
2000x spot 3	37.01	62.78	0.21	Spot	Dark	
2000x spot 4	38.21	61.58	0.21	Spot	Dark	
Mean	37.63	62.145	0.225			
STDEV	0.5519	0.5492	0.0191			
Dark	**C**	**V**	**Ni**	**Comments**	**Phase contrast**	
2000x spot 1	37.73	62.06	0.21	Spot	Dark	
2000x spot 2	37.65	61.94	0.41	Spot	Dark	
2000x spot 4	37.39	62.29	0.32	Spot	Dark	
2000x spot 6	36.82	62.97	0.21	Spot	Dark	
Mean	37.398	62.315	0.2875			
STDEV	0.4115	0.4602	0.0967			
Eutectic	**C**	**V**	**Ni**	**Comments**	**Phase contrast**	
2000x eutectic 1	35.23	54.6	10.17	Area	Light+Dark	
2000x eutectic 2	35.15	54.79	10.06	Area	Light+Dark	
2000x eutectic 3	35.75	54.9	9.36	Area	Light+Dark	
2000x eutectic 5	34.45	55.4	10.15	Area	Light+Dark	
2000x eutectic 6	35.1	54.63	10.27	Area	Light+Dark	
2000x eutectic 7	35.67	54.33	10	Area	Light+Dark	
Mean	35.225	54.775	10.002			
STDEV	0.4681	0.3623	0.3279			

APPENDIX B15: As-cast Sample 15

All results in atomic%						
Raw data						
Spectrum	**C**	**V**	**Ni**	**Comments**	**Phase contrast**	**Remark**
200x image 1	26.54	56.74	16.72	Overall	Light + Dark	Not agree
200x image 2	30.64	53.89	15.47	Overall	Light + Dark	Agree
200x image 3	30.26	53.82	15.92	Overall	Light + Dark	Agree
200x image 4	29.17	55.31	15.53	Overall	Light + Dark	Agree
200x image 5	29.45	54.68	15.87	Overall	Light + Dark	Agree

2000x spot 1	16.11	49.9	33.99	Spot	Light	Agree
2000x spot 2	23.97	53.65	22.38	Spot	Light	Not agree
2000x spot 3	17.21	48.87	33.92	Spot	Light	Agree
2000x spot 4	16.21	49.87	33.92	Spot	Light	Agree
2000x spot 5	17.97	49.65	32.38	Spot	Light	Agree
2000x spot 1	65.09	34.6	0.3	Spot	Dark	Not agree
2000x spot 2	47.09	51.51	1.4	Spot	Dark	Agree
2000x spot 3	46.47	53.28	0.25	Spot	Dark	Agree
2000x spot 4	46.47	52.28	1.25	Spot	Dark	Agree
2000x spot 5	45.89	53.11	1	Spot	Dark	Agree
2000x eutectic 1	28.82	55.3	15.87	Area	Light+Dark	Agree
2000x eutectic 2	29.01	55.25	15.74	Area	Light+Dark	Agree
2000x eutectic 3	28.28	55.87	15.85	Area	Light+Dark	Agree
2000x eutectic 4	28.72	55.27	16.01	Area	Light+Dark	Agree
Overall	**C**	**V**	**Ni**	**Comments**	**Phase contrast**	
200x image 2	30.64	53.89	15.47	Overall	Light + Dark	
200x image 3	30.26	53.82	15.92	Overall	Light + Dark	
200x image 4	29.17	55.31	15.53	Overall	Light + Dark	
200x image 5	29.45	54.68	15.87	Overall	Light + Dark	
Mean	29.88	54.425	15.698			
STDEV	0.6858	0.7072	0.2303			
Light	**C**	**V**	**Ni**	**Comments**	**Phase contrast**	
2000x spot 1	16.11	49.9	33.99	Spot	Light	
2000x spot 3	17.21	48.87	33.92	Spot	Light	
2000x spot 4	16.21	49.87	33.92	Spot	Light	
2000x spot 5	17.97	49.65	32.38	Spot	Light	
Mean	16.875	49.573	33.553			
STDEV	0.8829	0.4814	0.7824			
Dark	**C**	**V**	**Ni**	**Comments**	**Phase contrast**	
2000x spot 2	47.09	51.51	1.4	Spot	Dark	
2000x spot 3	46.47	53.28	0.25	Spot	Dark	
2000x spot 4	46.47	52.28	1.25	Spot	Dark	
2000x spot 5	45.89	53.11	1	Spot	Dark	
Mean	46.48	52.545	0.975			
STDEV	0.49	0.8167	0.5107			
Eutectic	**C**	**V**	**Ni**	**Comments**	**Phase contrast**	
2000x eutectic 1	28.82	55.3	15.87	Area	Light+Dark	

2000x eutectic 2	29.01	55.25	15.74	Area	Light+Dark	
2000x eutectic 3	28.28	55.87	15.85	Area	Light+Dark	
2000x eutectic 4	28.72	55.27	16.01	Area	Light+Dark	
Mean	28.708	55.423	15.868			
STDEV	0.3093	0.299	0.1109			

APPENDIX B16: As-cast Sample 17

All results in atomic%						
Raw data						
Spectrum	**C**	**V**	**Ni**	**Comments**	**Phase contrast**	**Remark**
200x image 1	33.98	39.73	26.29	Overall	Light + Dark	Agree
200x image 2	31.7	40.02	28.27	Overall	Light + Dark	Not agree
200x image 3	34.39	38.92	26.69	Overall	Light + Dark	Agree
200x image 4	32.92	37.72	29.35	Overall	Light + Dark	Not agree
200x image 5	34.03	39.58	26.4	Overall	Light + Dark	Agree
2000x spot 1	12.05	28.72	59.24	Spot	Light	Agree
2000x spot 2	12.46	28.64	58.9	Spot	Light	Agree
2000x spot 3	13.81	30.77	55.42	Spot	Light	Not agree
2000x spot 4	13.22	35.28	51.5	Spot	Light	Not agree
2000x spot 5	12.94	28.92	58.14	Spot	Light	Agree
2000x spot 6	13.38	28.16	58.45	Spot	Light	Agree
2000x spot 1	41.44	58.04	0.52	Spot	Dark	Agree
2000x spot 2	41.86	57.44	0.69	Spot	Dark	Agree
2000x spot 3	41.53	57.96	0.51	Spot	Dark	Agree
2000x spot 4	42.54	56.85	0.61	Spot	Dark	Not agree
2000x spot 5	41.51	57.73	0.75	Spot	Dark	Agree
2000x spot 6	41.66	57.76	0.58	Spot	Dark	Agree
2000x eutectic 1	34.22	36.64	29.14	Area	Light+Dark	Agree
2000x eutectic 2	32.51	40.04	27.45	Area	Light+Dark	Not agree
2000x eutectic 3	31.38	38.87	29.75	Area	Light+Dark	Agree
2000x eutectic 4	33.16	37.51	29.32	Area	Light+Dark	Agree
2000x eutectic 5	31.84	38.11	30.05	Area	Light+Dark	Agree
2000x eutectic 6	33.05	40.09	26.85	Area	Light+Dark	Not agree
Overall	**C**	**V**	**Ni**	**Comments**	**Phase contrast**	
200x image 1	33.98	39.73	26.29	Overall	Light + Dark	
200x image 3	34.39	38.92	26.69	Overall	Light + Dark	
200x image 5	34.03	39.58	26.4	Overall	Light + Dark	
Mean	34.133	39.41	26.46			
STDEV	0.2237	0.431	0.207			

Light	**C**	**V**	**Ni**	**Comments**	**Phase contrast**	
2000x spot 1	12.05	28.72	59.24	Spot	Light	
2000x spot 2	12.46	28.64	58.9	Spot	Light	
2000x spot 5	12.94	28.92	58.14	Spot	Light	
2000x spot 6	13.38	28.16	58.45	Spot	Light	
Mean	12.708	28.61	58.68			
STDEV	0.5773	0.322	0.485			
Dark	**C**	**V**	**Ni**	**Comments**	**Phase contrast**	**Remark**
2000x spot 1	41.44	58.04	0.52	Spot	Dark	Agree
2000x spot 2	41.86	57.44	0.69	Spot	Dark	Agree
2000x spot 3	41.53	57.96	0.51	Spot	Dark	Agree
2000x spot 5	41.51	57.73	0.75	Spot	Dark	Agree
2000x spot 6	41.66	57.76	0.58	Spot	Dark	Agree
Mean	41.6	57.79	0.61			
STDEV	0.1657	0.234	0.106			
Eutectic	**C**	**V**	**Ni**	**Comments**	**Phase contrast**	**Remark**
2000x eutectic 1	34.22	36.64	29.14	Area	Light+Dark	Agree
2000x eutectic 3	31.38	38.87	29.75	Area	Light+Dark	Agree
2000x eutectic 4	33.16	37.51	29.32	Area	Light+Dark	Agree
2000x eutectic 5	31.84	38.11	30.05	Area	Light+Dark	Agree
Mean	32.65	37.78	29.57			
STDEV	1.2902	0.943	0.412			

APPENDIX B17: As-cast Sample 18

All results in atomic%						
Raw data						
Spectrum	**C**	**V**	**Ni**	**Comments**	**Phase contrast**	**Remark**
200x image 1	37.61	19.87	42.52	Overall	Light + Dark	Agree
200x image 2	36.37	21.56	42.08	Overall	Light + Dark	Agree
200x image 3	37.56	19.79	42.65	Overall	Light + Dark	Agree
200x image 4	37.68	19.50	42.82	Overall	Light + Dark	Agree
200x image 5	35.28	18.76	45.96	Overall	Light + Dark	Not agree
2000x spot 1	20.02	3.10	76.88	Spot	Light	Agree
2000x spot 2	20.66	3.62	75.72	Spot	Light	Agree
2000x spot 3	21.17	3.24	75.59	Spot	Light	Not agree
2000x spot 4	19.88	3.38	76.74	Spot	Light	Agree
2000x spot 5	19.50	3.71	76.79	Spot	Light	Agree

2000x spot 1	46.81	52.36	0.83	Spot	Dark	Agree
2000x spot 2	45.99	53.87	0.14	Spot	Dark	Agree
2000x spot 3	42.66	43.98	13.36	Spot	Dark	Not agree
2000x spot 4	45.64	52.70	1.66	Spot	Dark	Agree
2000x spot 5	39.86	54.84	5.30	Spot	Dark	Not agree
2000x spot 6	45.42	53.39	1.19	Spot	Dark	Agree
2000x eutectic 1	34.93	16.74	48.33	Area	Light+Dark	Agree
2000x eutectic 2	34.86	17.49	47.65	Area	Light+Dark	Agree
2000x eutectic 3	34.63	17.88	47.48	Area	Light+Dark	Not agree
2000x eutectic 4	36.66	16.71	46.63	Area	Light+Dark	Agree
2000x eutectic 5	34.00	17.45	48.54	Area	Light+Dark	Not agree
2000x eutectic 6	35.55	19.28	45.17	Area	Light+Dark	Agree
Overall	**C**	**V**	**Ni**	**Comments**	**Phase contrast**	
200x image 1	37.61	19.87	42.52	Overall	Light + Dark	
200x image 2	36.37	21.56	42.08	Overall	Light + Dark	
200x image 3	37.56	19.79	42.65	Overall	Light + Dark	
200x image 4	37.68	19.50	42.82	Overall	Light + Dark	
Mean	37.31	20.18	42.52			
STDEV	0.63	0.93	0.32			
Light	**C**	**V**	**Ni**	**Comments**	**Phase contrast**	
2000x spot 1	20.02	3.10	76.88	Spot	Light	
2000x spot 2	20.66	3.62	75.72	Spot	Light	
2000x spot 4	19.88	3.38	76.74	Spot	Light	
2000x spot 5	19.50	3.71	76.79	Spot	Light	
Mean	20.02	3.45	76.53			
STDEV	0.48	0.27	0.54			
Dark	**C**	**V**	**Ni**	**Comments**	**Phase contrast**	
2000x spot 1	46.81	52.36	0.83	Spot	Dark	
2000x spot 2	45.99	53.87	0.14	Spot	Dark	
2000x spot 4	45.64	52.70	1.66	Spot	Dark	
2000x spot 6	45.42	53.39	1.19	Spot	Dark	
Mean	45.97	53.08	0.96			
STDEV	0.61	0.68	0.64			
Eutectic	**C**	**V**	**Ni**	**Comments**	**Phase contrast**	
2000x eutectic 1	34.93	16.74	48.33	Area	Light+Dark	
2000x eutectic 2	34.86	17.49	47.65	Area	Light+Dark	
2000x eutectic 3	34.63	17.88	47.48	Area	Light+Dark	

2000x eutectic 4	36.66	16.71	46.63	Area	Light+Dark	
2000x eutectic 5	34.00	17.45	48.54	Area	Light+Dark	
2000x eutectic 6	35.55	19.28	45.17	Area	Light+Dark	
Mean	34.61	17.39	48.00			
STDEV	0.42	0.47	0.51			

APPENDIX B18: As-cast Sample 19

All results in atomic%						
RAW DATA						
Spectrum	**C**	**V**	**Ni**	**Comments**	**Phase contrast**	**Remark**
200x image 1	30.1	14.42	55.48	Overall	Light + Dark	Agree
200x image 2	30.38	14.4	55.23	Overall	Light + Dark	Agree
200x image 3	30.05	14.66	55.29	Overall	Light + Dark	Agree
200x image 4	30.78	15.58	53.65	Overall	Light + Dark	Agree
200x image 5	31.72	14.68	53.6	Overall	Light + Dark	Agree
2000x spot 1	26.63	6.03	67.34	Spot	Light	Agree
2000x spot 2	27.21	6.04	66.75	Spot	Light	Agree
2000x spot 3	20.81	5.62	73.57	Spot	Light	Not agree
2000x spot 4	28.81	5.56	65.63	Spot	Light	Agree
2000x spot 5	27.81	5.79	66.4	Spot	Light	Agree
2000x spot 1	49.31	48.82	1.88	Spot	Dark	Agree
2000x spot 2	49.32	49.68	1	Spot	Dark	Agree
2000x spot 3	24.56	6.2	69.24	Spot	Dark	Not agree
2000x spot 4	49.93	48.1	1.97	Spot	Dark	Agree
2000x spot 5	48.14	49.92	1.94	Spot	Dark	Agree
2000x eutectic 1	28.9	13.44	57.66	Area	Light+Dark	Agree
2000x eutectic 2	29.73	13.74	56.52	Area	Light+Dark	Agree
2000x eutectic 3	29.1	13.69	57.21	Area	Light+Dark	Agree
2000x eutectic 4	29.27	14.43	56.29	Area	Light+Dark	Agree
2000x eutectic 5	30.85	13.89	55.27	Area	Light+Dark	Not agree
2000x eutectic 6	29.85	13.42	56.72	Area	Light+Dark	Agree
Overall	**C**	**V**	**Ni**	**Comments**	**Phase contrast**	
200x image 1	30.1	14.42	55.48	Overall	Light + Dark	
200x image 2	30.38	14.4	55.23	Overall	Light + Dark	
200x image 3	30.05	14.66	55.29	Overall	Light + Dark	
200x image 4	30.78	15.58	53.65	Overall	Light + Dark	
200x image 5	31.72	14.68	53.6	Overall	Light + Dark	
Mean	30.606	14.75	54.65			
STDEV	0.6869	0.483	0.9404			

Light	**C**	**V**	**Ni**	**Comments**	**Phase contrast**	
2000x spot 1	26.63	6.03	67.34	Spot	Light	
2000x spot 2	27.21	6.04	66.75	Spot	Light	
2000x spot 4	28.81	5.56	65.63	Spot	Light	
2000x spot 5	27.81	5.79	66.4	Spot	Light	
Mean	27.615	5.855	66.53			
STDEV	0.931	0.228	0.7145			
Dark	**C**	**V**	**Ni**	**Comments**	**Phase contrast**	
2000x spot 1	49.31	48.82	1.88	Spot	Dark	
2000x spot 2	49.32	49.68	1	Spot	Dark	
2000x spot 4	49.93	48.1	1.97	Spot	Dark	
2000x spot 5	48.14	49.92	1.94	Spot	Dark	
Mean	49.175	49.13	1.6975			
STDEV	0.7484	0.833	0.4665			
Eutectic	**C**	**V**	**Ni**	**Comments**	**Phase contrast**	
2000x eutectic 1	28.9	13.44	57.66	Area	Light+Dark	
2000x eutectic 2	29.73	13.74	56.52	Area	Light+Dark	
2000x eutectic 3	29.1	13.69	57.21	Area	Light+Dark	
2000x eutectic 4	29.27	14.43	56.29	Area	Light+Dark	
2000x eutectic 6	29.85	13.42	56.72	Area	Light+Dark	
Mean	29.37	13.74	56.88			
STDEV	0.4074	0.41	0.5524			

APPENDIX B19: As-cast Sample 20

All results in atomic%						
RAW DATA						
Spectrum	**C**	**V**	**Ni**	**Comments**	**Phase contrast**	**Remark**
200x image 1	32.23	23.15	44.62	Overall	Light + Dark	Agree
200x image 2	33.24	23.11	43.65	Overall	Light + Dark	Agree
200x image 3	31.87	23.68	44.45	Overall	Light + Dark	Agree
200x image 4	33.46	22.67	43.87	Overall	Light + Dark	Agree
200x image 5	33.2	23.65	43.15	Overall	Light + Dark	Agree
2000x spot 1	21.86	16.18	61.96	Spot	Light	Not agree
2000x spot 2	21.13	10.13	68.73	Spot	Light	Agree
2000x spot 3	20.83	10.37	68.8	Spot	Light	Agree
2000x spot 4	21.98	10.38	67.69	Spot	Light	Agree
2000x spot 5	21.54	11.03	67.42	Spot	Light	Agree

2000x spot 1	49.14	50.74	0.12	Spot	Dark	Agree
2000x spot 2	48.65	50.56	0.79	Spot	Dark	Agree
2000x spot 3	48.81	50.21	0.98	Spot	Dark	Agree
2000x spot 4	50.15	41.47	8.38	Spot	Dark	Not agree
2000x spot 5	48.42	50.61	0.96	Spot	Dark	Agree
2000x eutectic 1	34.5	24.01	41.5	Area	Light+Dark	Agree
2000x eutectic 2	33.16	24.06	42.78	Area	Light+Dark	Agree
2000x eutectic 3	34.03	23.44	42.53	Area	Light+Dark	Agree
2000x eutectic 4	34.58	24.15	41.27	Area	Light+Dark	Agree
2000x eutectic 5	30.13	21.97	47.9	Area	Light+Dark	Not agree
Overall	**C**	**V**	**Ni**	**Comments**	**Phase contrast**	
200x image 1	32.23	23.15	44.62	Overall	Light + Dark	
200x image 2	33.24	23.11	43.65	Overall	Light + Dark	
200x image 3	31.87	23.68	44.45	Overall	Light + Dark	
200x image 4	33.46	22.67	43.87	Overall	Light + Dark	
200x image 5	33.2	23.65	43.15	Overall	Light + Dark	
Mean	32.8	23.25	43.948			
STDEV	0.703	0.422	0.599			
Light	**C**	**V**	**Ni**	**Comments**	**Phase contrast**	
2000x spot 2	21.13	10.13	68.73	Spot	Light	
2000x spot 3	20.83	10.37	68.8	Spot	Light	
2000x spot 4	21.98	10.38	67.69	Spot	Light	
2000x spot 5	21.54	11.03	67.42	Spot	Light	
Mean	21.37	10.48	68.16			
STDEV	0.5	0.386	0.7078			
Dark	**C**	**V**	**Ni**	**Comments**	**Phase contrast**	
2000x spot 1	49.14	50.74	0.12	Spot	Dark	
2000x spot 2	48.65	50.56	0.79	Spot	Dark	
2000x spot 3	48.81	50.21	0.98	Spot	Dark	
2000x spot 5	48.42	50.61	0.96	Spot	Dark	
Mean	48.76	50.53	0.7125			
STDEV	0.302	0.226	0.4041			
Eutectic	**C**	**V**	**Ni**	**Comments**	**Phase contrast**	
2000x eutectic 1	34.5	24.01	41.5	Area	Light+Dark	
2000x eutectic 2	33.16	24.06	42.78	Area	Light+Dark	
2000x eutectic 3	34.03	23.44	42.53	Area	Light+Dark	
2000x eutectic 4	34.58	24.15	41.27	Area	Light+Dark	

Mean	34.07	23.92	42.02			
STDEV	0.652	0.322	0.7462			

APPENDIX B20: As-cast Sample 21

All results in atomic%						
RAW DATA						
Spectrum	**C**	**V**	**Ni**	**Comments**	**Phase contrast**	**Remark**
200x image 1	25.74	39.58	34.68	Overall	Light + Dark	Agree
200x image 2	24.32	40.89	34.79	Overall	Light + Dark	Agree
200x image 3	22.01	41.88	36.12	Overall	Light + Dark	Not agree
200x image 4	24.87	40.77	34.35	Overall	Light + Dark	Agree
200x image 5	23.96	41.16	34.88	Overall	Light + Dark	Agree
2000x spot 1	18.99	32.96	48.05	Spot	Light	Agree
2000x spot 2	23.72	32.7	43.58	Spot	Light	Not agree
2000x spot 3	16.66	35.27	48.07	Spot	Light	Not agree
2000x spot 4	17.27	34.08	48.65	Spot	Light	Agree
2000x spot 5	16.12	36.92	46.96	Spot	Light	Not agree
2000x spot 6	17.08	33.45	49.47	Spot	Light	Agree
2000x spot 7	18.56	32.25	49.18	Spot	Light	Agree
2000x spot 1	38.83	59.93	1.25	Spot	Dark	Agree
2000x spot 2	40.37	58.98	0.65	Spot	Dark	Agree
2000x spot 3	40.17	58.22	1.61	Spot	Dark	Agree
2000x spot 4	35.8	33.11	31.09	Spot	Dark	Not agree
2000x spot 5	39.45	59.52	1.04	Spot	Dark	Agree
2000x eutectic 1	19.71	35.48	44.81	Area	Light+Dark	Not agree
2000x eutectic 2	26.92	42.29	30.79	Area	Light+Dark	Agree
2000x eutectic 3	26.02	42.37	31.61	Area	Light+Dark	Agree
2000x eutectic 4	27.41	42.36	30.23	Area	Light+Dark	Agree
2000x eutectic 5	27.71	41.48	30.81	Area	Light+Dark	Agree
Overall	**C**	**V**	**Ni**	**Comments**	**Phase contrast**	
200x image 1	25.74	39.58	34.68	Overall	Light + Dark	
200x image 2	24.32	40.89	34.79	Overall	Light + Dark	
200x image 4	24.87	40.77	34.35	Overall	Light + Dark	
200x image 5	23.96	41.16	34.88	Overall	Light + Dark	
Mean	24.723	40.6	34.675			
STDEV	0.7747	0.6993	0.2316			
Light	**C**	**V**	**Ni**	**Comments**	**Phase contrast**	
2000x spot 1	18.99	32.96	48.05	Spot	Light	

2000x spot 4	17.27	34.08	48.65	Spot	Light	
2000x spot 6	17.08	33.45	49.47	Spot	Light	
2000x spot 7	18.56	32.25	49.18	Spot	Light	
Mean	17.975	33.185	48.838			
STDEV	0.9435	0.7738	0.6252			
Dark	**C**	**V**	**Ni**	**Comments**	**Phase contrast**	
2000x spot 1	38.83	59.93	1.25	Spot	Dark	
2000x spot 2	40.37	58.98	0.65	Spot	Dark	
2000x spot 3	40.17	58.22	1.61	Spot	Dark	
2000x spot 5	39.45	59.52	1.04	Spot	Dark	
Mean	39.705	59.163	1.1375			
STDEV	0.7045	0.739	0.4013			
Eutectic	**C**	**V**	**Ni**	**Comments**	**Phase contrast**	
2000x eutectic 2	26.92	42.29	30.79	Area	Light+Dark	
2000x eutectic 3	26.02	42.37	31.61	Area	Light+Dark	
2000x eutectic 4	27.41	42.36	30.23	Area	Light+Dark	
2000x eutectic 5	27.71	41.48	30.81	Area	Light+Dark	
Mean	27.015	42.125	30.86			
STDEV	0.7389	0.4315	0.5677			

APPENDIX B21: As-cast Sample 22

All results in atomic%						
RAW DATA						
Spectrum	**C**	**V**	**Ni**	**Comments**	**Phase contrast**	**Remark**
200x image 1	23.57	35.39	41.05	Overall	Light + Dark	Agree
200x image 2	16.81	36.55	46.65	Overall	Light + Dark	Not agree
200x image 3	24.54	34.93	40.53	Overall	Light + Dark	Agree
200x image 4	23.72	35.41	40.87	Overall	Light + Dark	Agree
200x image 5	24.55	34.16	41.29	Overall	Light + Dark	Agree
2000x spot 1	19.2	29.84	50.97	Spot	Light	Agree
2000x spot 2	19.78	30.22	50.01	Spot	Light	Agree
2000x spot 3	24.35	27.49	48.16	Spot	Light	Not agree
2000x spot 4	20.02	29.84	50.14	Spot	Light	Agree
2000x spot 5	19.38	29.73	50.88	Spot	Light	Agree
2000x spot 1	48.98	48.33	2.69	Spot	Dark	Agree
2000x spot 2	47.7	48.77	3.53	Spot	Dark	Agree
2000x spot 3	48.5	49	2.5	Spot	Dark	Agree
2000x spot 4	48.37	49.21	2.42	Spot	Dark	Agree

2000x spot 5	28.09	26.19	45.72	Spot	Dark	Not agree
2000x eutectic 1	22.51	32.05	45.44	Area	Light+Dark	Agree
2000x eutectic 2	22.64	31.85	45.5	Area	Light+Dark	Agree
2000x eutectic 3	21.84	31.7	46.46	Area	Light+Dark	Agree
2000x eutectic 4	21.3	32.69	46.01	Area	Light+Dark	Agree
2000x eutectic 5	13.41	38.25	48.33	Area	Light+Dark	Not agree
Overall	**C**	**V**	**Ni**	**Comments**	**Phase contrast**	
200x image 1	23.57	35.39	41.05	Overall	Light + Dark	
200x image 3	24.54	34.93	40.53	Overall	Light + Dark	
200x image 4	23.72	35.41	40.87	Overall	Light + Dark	
200x image 5	24.55	34.16	41.29	Overall	Light + Dark	
Mean	24.095	34.973	40.935			
STDEV	0.5232	0.5853	0.3202			
Light	**C**	**V**	**Ni**	**Comments**	**Phase contrast**	
2000x spot 1	19.2	29.84	50.97	Spot	Light	
2000x spot 2	19.78	30.22	50.01	Spot	Light	
2000x spot 4	20.02	29.84	50.14	Spot	Light	
2000x spot 5	19.38	29.73	50.88	Spot	Light	
Mean	19.595	29.908	50.5			
STDEV	0.3729	0.2147	0.495			
Dark	**C**	**V**	**Ni**	**Comments**	**Phase contrast**	
2000x spot 1	48.98	48.33	2.69	Spot	Dark	
2000x spot 2	47.7	48.77	3.53	Spot	Dark	
2000x spot 3	48.5	49	2.5	Spot	Dark	
2000x spot 4	48.37	49.21	2.42	Spot	Dark	
Mean	48.388	48.828	2.785			
STDEV	0.5281	0.3772	0.5094			
Eutectic	**C**	**V**	**Ni**	**Comments**	**Phase contrast**	
2000x eutectic 1	22.51	32.05	45.44	Area	Light+Dark	
2000x eutectic 2	22.64	31.85	45.5	Area	Light+Dark	
2000x eutectic 3	21.84	31.7	46.46	Area	Light+Dark	
2000x eutectic 4	21.3	32.69	46.01	Area	Light+Dark	
Mean	22.073	32.073	45.853			
STDEV	0.623	0.4359	0.479			

APPENDIX B22: As-cast Sample 23

All results in atomic%						
RAW DATA						
Spectrum	**C**	**V**	**Ni**	**Comments**	**Phase contrast**	**Remark**
200x image 1	22.54	52.56	24.9	Overall	Light + Dark	Not agree
200x image 2	24.71	51.93	23.36	Overall	Light + Dark	Agree
200x image 3	23.98	51.78	24.24	Overall	Light + Dark	Agree
200x image 4	24.06	51.96	23.97	Overall	Light + Dark	Agree
200x image 5	24.55	51.69	23.76	Overall	Light + Dark	Agree
2000x spot 1	21.15	42.58	36.27	Spot	Light	Not agree
2000x spot 2	16.74	46.98	36.28	Spot	Light	Agree
2000x spot 3	16.37	46.95	36.68	Spot	Light	Agree
2000x spot 4	17.22	45.74	37.03	Spot	Light	Agree
2000x spot 5	16.69	47.69	35.65	Spot	Light	Agree
2000x spot 1	43.55	56.08	0.37	Spot	Dark	Agree
2000x spot 2	42.25	57.35	0.41	Spot	Dark	Agree
2000x spot 3	42.7	57.3	0	Spot	Dark	Agree
2000x spot 4	38.56	61.44	0	Spot	Dark	Not agree
2000x spot 5	42.98	57.02	0	Spot	Dark	Agree
2000x eutectic 1	25.98	50.54	23.49	Area	Light+Dark	Agree
2000x eutectic 2	24.97	51.78	23.25	Area	Light+Dark	Agree
2000x eutectic 3	25.24	50.69	24.07	Area	Light+Dark	Agree
2000x eutectic 4	25.07	50.49	24.45	Area	Light+Dark	Agree
2000x eutectic 5	23.83	53.77	22.4	Area	Light+Dark	Not agree
Overall	**C**	**V**	**Ni**	**Comments**	**Phase contrast**	
200x image 2	24.71	51.93	23.36	Overall	Light + Dark	
200x image 3	23.98	51.78	24.24	Overall	Light + Dark	
200x image 4	24.06	51.96	23.97	Overall	Light + Dark	
200x image 5	24.55	51.69	23.76	Overall	Light + Dark	
Mean	24.325	51.84	23.833			
STDEV	0.3597	0.1273	0.3712			
Light	**C**	**V**	**Ni**	**Comments**	**Phase contrast**	
2000x spot 2	16.74	46.98	36.28	Spot	Light	
2000x spot 3	16.37	46.95	36.68	Spot	Light	
2000x spot 4	17.22	45.74	37.03	Spot	Light	
2000x spot 5	16.69	47.69	35.65	Spot	Light	
Mean	16.755	46.84	36.41			
STDEV	0.3507	0.8092	0.5921			

Dark	C	V	Ni	Comments	Phase contrast	
2000x spot 1	43.55	56.08	0.37	Spot	Dark	
2000x spot 2	42.25	57.35	0.41	Spot	Dark	
2000x spot 3	42.7	57.3	0	Spot	Dark	
2000x spot 5	42.98	57.02	0	Spot	Dark	
Mean	42.87	56.938	0.195			
STDEV	0.544	0.5898	0.2258			
Eutectic	**C**	**V**	**Ni**	**Comments**	**Phase contrast**	
2000x eutectic 1	25.98	50.54	23.49	Area	Light+Dark	
2000x eutectic 2	24.97	51.78	23.25	Area	Light+Dark	
2000x eutectic 3	25.24	50.69	24.07	Area	Light+Dark	
2000x eutectic 4	25.07	50.49	24.45	Area	Light+Dark	
Mean	25.315	50.875	23.815			
STDEV	0.4571	0.6093	0.5456			

APPENDIX B23: As-cast Sample 24

All results in atomic%						
RAW DATA						
Spectrum	**C**	**V**	**Ni**	**Comments**	**Phase contrast**	**Remark**
200x image 1	35.18	48.92	15.9	Overall	Light + Dark	Agree
200x image 2	37.4	46.89	15.72	Overall	Light + Dark	Agree
200x image 3	35.98	48.12	15.9	Overall	Light + Dark	Agree
200x image 4	36.66	47.16	16.17	Overall	Light + Dark	Agree
200x image 5	34.33	49.28	16.39	Overall	Light + Dark	Not agree
200x image 1	22.9	31.67	45.43	Spot	Light	Agree
2000x spot 2	22.76	31.95	45.29	Spot	Light	Agree
2000x spot 3	21.57	31.55	46.88	Spot	Light	Agree
2000x spot 4	21.8	32.58	45.62	Spot	Light	Agree
2000x spot 5	28.42	27.02	44.56	Spot	Light	Not agree
2000x spot 1	46.64	53.01	0.34	Spot	Dark	Agree
2000x spot 2	45.32	54.11	0.58	Spot	Dark	Agree
2000x spot 3	45.98	53.61	0.41	Spot	Dark	Agree
2000x spot 4	47.15	52.39	0.46	Spot	Dark	Agree
2000x spot 5	38.95	60.59	0.47	Spot	Dark	Not agree
Overall	**C**	**V**	**Ni**	**Comments**	**Phase contrast**	
200x image 1	35.18	48.92	15.9	Overall	Light + Dark	
200x image 2	37.4	46.89	15.72	Overall	Light + Dark	
200x image 3	35.98	48.12	15.9	Overall	Light + Dark	

200x image 4	36.66	47.16	16.17	Overall	Light + Dark	
Mean	36.305	47.773	15.923			
STDEV	0.948	0.9294	0.1855			
Light	**C**	**V**	**Ni**	**Comments**	**Phase contrast**	
200x image 1	22.9	31.67	45.43	Spot	Light	
2000x spot 2	22.76	31.95	45.29	Spot	Light	
2000x spot 3	21.57	31.55	46.88	Spot	Light	
2000x spot 4	21.8	32.58	45.62	Spot	Light	
Mean	22.258	31.938	45.805			
STDEV	0.6701	0.46	0.7293			
Dark	**C**	**V**	**Ni**	**Comments**	**Phase contrast**	
2000x spot 1	46.64	53.01	0.34	Spot	Dark	
2000x spot 2	45.32	54.11	0.58	Spot	Dark	
2000x spot 3	45.98	53.61	0.41	Spot	Dark	
2000x spot 4	47.15	52.39	0.46	Spot	Dark	
Mean	46.273	53.28	0.4475			
STDEV	0.7954	0.7445	0.1011			

APPENDIX B24: Heat treated Sample 6H

All results in atomic%						
RAW DATA						
Spectrum	**C**	**V**	**Ni**	**Comments**	**Phase contrast**	**Remark**
200x image 1	36.05	21.39	42.56	Overall	Light + Dark	Not agree
200x image 2	32.34	22.48	45.19	Overall	Light + Dark	Not agree
200x image 3	26.73	25.02	48.25	Overall	Light + Dark	Agree
200x image 4	26.15	25.27	48.58	Overall	Light + Dark	Agree
200x image 5	27.54	24.81	47.65	Overall	Light + Dark	Agree
200x image 6	26.98	24.46	48.56	Overall	Light + Dark	Agree
2000x spot 2	14.88	14.01	71.11	Spot	Light	Not agree
2000x spot 3	15.66	14.22	70.12	Spot	Light	Agree
2000x spot 4	15.39	14.79	69.83	Spot	Light	Agree
2000x spot 5	19.68	13.9	66.42	Spot	Light	Not agree
2000x spot 6	13.44	14.46	72.09	Spot	Light	Not agree
2000x spot 7	15.31	13.8	70.89	Spot	Light	Agree
2000x spot 8	11.25	14.58	74.17	Spot	Light	Not agree
2000x spot 9	15.56	14.2	70.23	Spot	Light	Agree
2000x spot 2	48.33	50.86	0.82	Spot	Dark	Agree
2000x spot 3	48.37	50.69	0.94	Spot	Dark	Agree

2000x spot 4	48.3	50.05	1.64	Spot	Dark	Agree
2000x spot 5	49.16	49.82	1.02	Spot	Dark	Agree
2000x spot 6	46.15	53.09	0.76	Spot	Dark	Not agree
2000x spot 7	48.96	49.67	1.36	Spot	Dark	Agree
2000x eutectic 1	17.46	15.63	66.91	Area	Light+Dark	Agree
2000x eutectic 2	17.35	15.53	67.12	Area	Light+Dark	Agree
2000x eutectic 3	14.95	14.88	70.18	Area	Light+Dark	Not agree
2000x eutectic 4	20.24	15.42	64.33	Area	Light+Dark	Not agree
2000x eutectic 5	16.48	15.61	67.91	Area	Light+Dark	Agree
2000x eutectic 6	17.72	14.5	67.78	Area	Light+Dark	Agree
2000x eutectic 7	17.74	15.17	67.09	Area	Light+Dark	Agree
Overall	**C**	**V**	**Ni**	**Comments**	**Phase contrast**	
200x image 3	26.73	25.02	48.25	Overall	**Light + Dark**	
200x image 4	26.15	25.27	48.58	Overall	**Light + Dark**	
200x image 5	27.54	24.81	47.65	Overall	**Light + Dark**	
200x image 6	26.98	24.46	48.56	Overall	**Light + Dark**	
Mean	26.85	24.89	48.26			
STDEV	0.5766	0.3428	0.4338			
Light	**C**	**V**	**Ni**	**Comments**	**Phase contrast**	
2000x spot 3	15.66	14.22	70.12	Spot	**Light**	
2000x spot 4	15.39	14.79	69.83	Spot	**Light**	
2000x spot 7	15.31	13.8	70.89	Spot	**Light**	
2000x spot 9	15.56	14.2	70.23	Spot	**Light**	
Mean	15.48	14.253	70.268			
STDEV	0.159	0.4072	0.448			
Dark	**C**	**V**	**Ni**	**Comments**	**Phase contrast**	
2000x spot 2	48.33	50.86	0.82	Spot	Dark	
2000x spot 3	48.37	50.69	0.94	Spot	Dark	
2000x spot 4	48.3	50.05	1.64	Spot	Dark	
2000x spot 5	49.16	49.82	1.02	Spot	Dark	
2000x spot 7	48.96	49.67	1.36	Spot	Dark	
Mean	48.624	50.218	1.156			
STDEV	0.405	0.5296	0.3369			
Eutectic	**C**	**V**	**Ni**	**Comments**	**Phase contrast**	
2000x eutectic 1	17.46	15.63	66.91	Area	Light+Dark	
2000x eutectic 2	17.35	15.53	67.12	Area	Light+Dark	
2000x eutectic 5	16.48	15.61	67.91	Area	Light+Dark	

2000x eutectic 6	17.72	14.5	67.78	Area	Light+Dark	
2000x eutectic 7	17.74	15.17	67.09			
Mean	17.35	15.288	67.362			
STDEV	0.5143	0.478	0.4505			

APPENDIX B25: Heat treated Sample 7H

All results in atomic%							
Raw data							
Spetrum		**C**	**V**	**Ni**	**Comment**	**Phase Contrast**	**Remarks**
200X	1	49.73	10.39	39.88	0verall	Light+Medium+Dark	Not agree
200X	2	51.22	7.78	41	0verall	Light+Medium+Dark	Agree
200X	3	49.99	7.85	42.17	0verall	Light+Medium+Dark	Agree
200X	4	51.44	7.54	41.02	0verall	Light+Medium+Dark	Agree
200X	5	49.32	8.06	42.62	0verall	Light+Medium+Dark	Agree
200X	6	49.13	8.2	42.67	0verall	Light+Medium+Dark	Agree
1500X	1	30.06	1.69	68.25	spot	Light	Agree
1500X	2	30.01	1.73	68.26	spot	Light	Agree
1500X	3	29.21	1.57	69.22	spot	Light	Agree
1500X	4	27.45	1.73	70.81	spot	Light	Not agree
1500X	5	29.96	1.65	68.39	spot	Light	Agree
1500X	1	27.78	4.08	68.14	spot	Dark	Not agree
1500X	2	27.84	2.72	69.44	spot	Dark	Not agree
1500X	3	30.22	1.88	67.9	spot	Dark	Not agree
1500X	4	47.42	1.43	51.15	spot	Dark	Not agree
1500X	5	44.95	50.68	4.38	spot	Dark	Agree
1500X	6	44.21	51.54	4.25	spot	Dark	Agree
1500X	7	45.8	50.48	3.72	spot	Dark	Agree
1500X	8	45.81	51.03	3.16	spot	Dark	Agree
1500X	1	99.22	0.06	0.72	spot	Very dark	Agree
1500X	2	99.26	0.15	0.58	spot	Very dark	Agree
0verall		**C**	**V**	**Ni**	**Comment**	**Phase Contrast**	
200X	2	51.22	7.78	41	0verall	Light+Medium+Dark	
200X	3	49.99	7.85	42.17	0verall	Light+Medium+Dark	
200X	4	51.44	7.54	41.02	0verall	Light+Medium+Dark	
200X	5	49.32	8.06	42.62	0verall	Light+Medium+Dark	
200X	6	49.13	8.2	42.67	0verall	Light+Medium+Dark	
MEAN		50.22	7.886	41.896			
STDEV		1.0653	0.2555	0.8319			
Light		**C**	**V**	**Ni**	**Comment**	**Phase Contrast**	
1500X	1	30.06	1.69	68.25	spot	Light	
1500X	2	30.01	1.73	68.26	spot	Light	
1500X	3	29.21	1.57	69.22	spot	Light	
1500X	5	29.96	1.65	68.39	spot	Light	
MEAN		29.81	1.66	68.53			

STDEV		0.4021	0.0683	0.4644			
Dark		**C**	**V**	**Ni**	**Comment**	**Phase Contrast**	
1500X	5	44.95	50.68	4.38	spot	Dark	
1500X	6	44.21	51.54	4.25	spot	Dark	
1500X	7	45.8	50.48	3.72	spot	Dark	
1500X	8	45.81	51.03	3.16	spot	Dark	
MEAN		45.193	50.933	3.8775			
STDEV		0.7691	0.4644	0.557			
Very dark		**C**	**V**	**Ni**	**Comment**	**Phase Contrast**	
1500X	1	99.22	0.06	0.72	spot	Very dark	
1500X	2	99.26	0.15	0.58	spot	Very dark	
MEAN		99.24	0.105	0.65			
STDEV		0.0283	0.0636	0.099			

APPENDIX B26: Heat treated Sample 8H

All results in atomic%						
Raw data						
Spectrum	**C**	**V**	**Ni**	**Comments**	**Phase contrast**	**Remark**
200x image 1	22.5	30.12	47.38	Overall	Light + Medium + Dark	Agree
200x image 2	21.8	30.55	47.65	Overall	Light + Medium + Dark	Agree
200x image 3	22.2	30.17	47.63	Overall	Light + Medium + Dark	Agree
200x image 4	22.36	30.69	46.95	Overall	Light + Medium + Dark	Agree
200x image 5	16.42	31.67	51.91	Overall	Light + Medium + Dark	Not agree
1500x spot 1	15.8	20.8	63.4	Spot	Light	Agree
1500x spot 2	16.24	21.1	62.66	Spot	Light	Agree
1500x spot 3	18.2	17.02	64.78	Spot	Light	Not agree
1500x spot 4	19.96	16.39	63.65	Spot	Light	Not agree
1500x spot 5	15.79	20.7	63.51	Spot	Light	Agree
1500x spot 6	15.9	20.79	63.31	Spot	Light	Agree
1500x spot 1	14.88	28.87	56.25	Spot	Dark	Not agree
1500x spot 2	16.79	17.46	65.75	Spot	Dark	Not agree
1500x spot 3	30.44	68.08	1.48	Spot	Dark	Agree
1500x spot 4	29.25	68.89	1.86	Spot	Dark	Agree
1500x spot 5	29.72	69.39	0.89	Spot	Dark	Agree
1500x spot 6	29.99	68.7	1.31	Spot	Dark	Agree
1500x area 1	21.19	28.74	50.07	Area	Light+Dark	Agree
1500x area 2	22.51	27.46	50.03	Area	Light+Dark	Agree
1500x eutectic 3	19.79	29.93	50.28	Area	Light+Dark	Not agree
1500x eutectic 4	23.95	28.67	47.39	Area	Light+Dark	Not agree
1500x area 5	22.03	27.56	51.4	Area	Light+Dark	Agree

1500x eutectic 6	20.63	26.96	52.41	Area	Light+Dark	Not agree
1000x area 7	21.94	27.67	50.39	Area	Light+Dark	Agree
Overall	**C**	**V**	**Ni**	**Comments**	**Phase contrast**	
200x image 1	22.5	30.12	47.38	Overall	Light + Medium + Dark	
200x image 2	21.8	30.55	47.65	Overall	Light + Medium + Dark	
200x image 3	22.2	30.17	47.63	Overall	Light + Medium + Dark	
200x image 4	22.36	30.69	46.95	Overall	Light + Medium + Dark	
Mean	22.215	30.383	47.403			
STDEV	0.3026	0.2809	0.3257			
Light	**C**	**V**	**Ni**	**Comments**	**Phase contrast**	
1500x spot 1	15.8	20.8	63.4	Spot	Light	
1500x spot 2	16.24	21.1	62.66	Spot	Light	
1500x spot 5	15.79	20.7	63.51	Spot	Light	
1500x spot 6	15.9	20.79	63.31	Spot	Light	
Mean	15.933	20.848	63.22			
STDEV	0.2109	0.1742	0.3822			
Dark	**C**	**V**	**Ni**	**Comments**	**Phase contrast**	
1500x spot 3	45.9	52.8	1.3	Spot	Dark	
1500x spot 4	46.01	52.59	1.4	Spot	Dark	
1500x spot 5	45.71	53.4	0.89	Spot	Dark	
1500x spot 6	45.8	52.89	1.31	Spot	Dark	
Mean	45.855	52.92	1.225			
STDEV	0.1292	0.3438	0.2278			
Area	**C**	**V**	**Ni**	**Comments**	**Phase contrast**	
1500x area 1	21.19	28.74	50.07	Area	Light+Dark	
1500x area 2	22.51	27.46	50.03	Area	Light+Dark	
1500x area 5	22.03	27.56	51.4	Area	Light+Dark	
1500x area 7	21.94	27.67	50.39	Area	Light+Dark	
Mean	21.918	27.858	50.473			
STDEV	0.5457	0.5946	0.639			
Eutectic	**C**	**V**	**Ni**	**Comments**	**Phase contrast**	
1500x eutectic 3	20.79	28.93	50.28	Area	Light+Dark	
1500x eutectic 4	23.95	28.67	47.39	Area	Light+Dark	
1500x eutectic 6	20.63	26.96	52.41	Area	Light+Dark	
Mean	21.79	28.187	50.027			
STDEV	1.8723	1.0702	2.5196			

APPENDIX B27: Heat treated Sample 10H

All results in atomic%						
Raw data						
Spectrum	**C**	**V**	**Ni**	**Comments**	**Phase contrast**	**Remark**
200x image 1	70.93	26.62	2.45	Overall	Light + Medium + Dark	Agree
200x image 2	72.49	25.16	2.35	Overall	Light + Medium + Dark	Agree
200x image 3	64.44	32.95	2.61	Overall	Light + Medium + Dark	Not agree
200x image 4	71.76	25.31	2.93	Overall	Light + Medium + Dark	Agree
200x image 5	73.16	24.23	2.61	Overall	Light + Medium + Dark	Agree
2000x spot 1	17.06	5.98	76.96	Spot	Light	Agree
2000x spot 2	18.92	4.74	76.34	Spot	Light	Agree
2000x spot 3	47.92	50.63	1.45	Spot	Light	Not agree
2000x spot 4	46.84	52.59	0.57	Spot	Light	Not agree
2000x spot 5	19.49	4.28	76.23	Spot	Light	Agree
2000x spot 1	46.59	53.27	0.14	Spot	Dark	Not agree
2000x spot 2	47.96	51.9	0.15	Spot	Dark	Agree
2000x spot 3	47.08	52.7	0.22	Spot	Dark	Agree
2000x spot 4	48.32	51.47	0.21	Spot	Dark	Agree
2000x spot 5	47.31	52.45	0.23	Spot	Dark	Agree
2000x spot 6	48.02	51.46	0.52	Spot	Dark	Agree
2000x spot 1	99.86	0.14	0	Spot	Very Dark	Agree
2000x spot 2	99.19	0.81	0	Spot	Very Dark	Agree
Overall	C	V	Ni	**Comments**	**Phase contrast**	
200x image 1	70.93	26.62	2.45	Overall	Light + Medium + Dark	
200x image 2	72.49	25.16	2.35	Overall	Light + Medium + Dark	
200x image 4	71.76	25.31	2.93	Overall	Light + Medium + Dark	
200x image 5	73.16	24.23	2.61	Overall		
Mean	**72.085**	**25.33**	**2.585**			
STDEV	**0.959**	**0.9838**	**0.2537**			
Light	**C**	**V**	**Ni**	**Comments**	**Phase contrast**	
2000x spot 1	17.06	5.98	76.96	Spot	Light	
2000x spot 2	18.92	4.74	76.34	Spot	Light	
2000x spot 5	19.49	4.28	76.23	Spot	Light	
Mean	18.49	5	76.51			
STDEV	1.2708	0.8793	0.3936			
Dark	**C**	**V**	**Ni**	**Comments**	**Phase contrast**	

2000x spot 2	47.96	51.9	0.15	Spot	Dark	
2000x spot 3	47.08	52.7	0.22	Spot	Dark	
2000x spot 4	48.32	51.47	0.21	Spot	Dark	
2000x spot 5	47.31	52.45	0.23	Spot	Dark	
2000x spot 6	48.02	51.46	0.52			
Mean	47.738	51.996	0.266			
STDEV	0.5205	0.5646	0.1454			
Very Dark	99.86	0.14	0	**Comments**	**Phase contrast**	
2000x spot 1	99.19	0.81	0	Spot	Very Dark	
2000x spot 2	99.525	0.475	0	Spot	Very Dark	
Mean	0.4738	0.4738	0			
STDEV						

APPENDIX B28: Heat treated Sample 11H

All results in atomic%						
Raw data						
Spectrum	**C**	**V**	**Ni**	**Comments**	**Phase contrast**	**Remark**
500x image 1	23.13	68.58	8.29	Overall	Light + Medium + Dark	Agree
500x image 2	22.51	69.59	7.9	Overall	Light + Medium + Dark	Agree
500x image 3	21.71	69.65	8.64	Overall	Light + Medium + Dark	Not agree
500x image 4	23.26	68.58	8.16	Overall	Light + Medium + Dark	Agree
500x image 5	22.37	69.2	8.43	Overall	Light + Medium + Dark	Agree
2000x spot 1	10.71	67.9	21.39	Spot	Light	Agree
2000x spot 2	10.08	67.61	22.31	Spot	Light	Agree
2000x spot 3	9.93	67.41	22.66	Spot	Light	Agree
2000x spot 4	8.86	68.03	23.11	Spot	Light	Not agree
2000x spot 5	10.74	66.59	22.67	Spot	Light	Agree
2000x spot 6	6.59	70.98	22.43	Spot	Light	Not agree
2000x spot 1	37.27	61.65	1.07	Spot	Dark	Agree
2000x spot 2	37.09	61.72	1.18	Spot	Dark	Agree
2000x spot 3	37.05	61.95	1	Spot	Dark	Agree
2000x spot 4	37.16	62.84	0	Spot	Dark	Not agree
2000x spot 5	36.57	62.43	1	Spot	Dark	Agree
2000x spot 6	36.58	61.83	1.59	Spot	Dark	Agree
2000x spot 1	9.96	77.25	12.79	Spot	medium	Agree
2000x spot 2	8.97	78.83	12.2	Spot	medium	Agree
2000x spot 3	9.23	81.76	9.01	Spot	medium	Not agree
2000x spot 4	9.65	77.08	13.27	Spot	medium	Agree
2000x spot 5	9.99	77.2	12.81	Spot	medium	Agree

2000x spot 6	9.97	77.58	12.45	Spot	medium	Agree
Overall	**C**	**V**	**Ni**	**Comments**	**Phase contrast**	
500x image 1	23.13	68.58	8.29	Overall	Light + Medium + Dark	
500x image 2	22.51	69.59	7.9	Overall	Light + Medium + Dark	
500x image 4	23.26	68.58	8.16	Overall	Light + Medium + Dark	
500x image 5	22.37	69.2	8.43	Overall	Light + Medium + Dark	
Mean	22.818	68.988	8.195			
STDEV	0.4428	0.4967	0.2255			
Light	**C**	**V**	**Ni**	**Comments**	**Phase contrast**	
2000x spot 1	10.71	67.9	21.39	Spot	Light	
2000x spot 2	10.08	67.61	22.31	Spot	Light	
2000x spot 3	9.93	67.41	22.66	Spot	Light	
2000x spot 5	10.74	66.59	22.67	Spot	Light	
Mean	10.365	67.378	22.258			
STDEV	0.4204	0.5622	0.6021			
Dark	**C**	**V**	**Ni**	**Comments**	**Phase contrast**	
2000x spot 1	37.27	61.65	1.07	Spot	Dark	
2000x spot 2	37.09	61.72	1.18	Spot	Dark	
2000x spot 3	37.05	61.95	1	Spot	Dark	
2000x spot 5	36.57	62.43	1	Spot	Dark	
2000x spot 6	36.58	61.83	1.59			
Mean	36.912	61.916	1.168			
STDEV	0.3186	0.309	0.2471			
medium	**C**	**V**	**Ni**	**Comments**	**Phase contrast**	
2000x spot 1	9.96	77.25	12.79	Spot	medium	
2000x spot 2	8.97	78.83	12.2	Spot	medium	
2000x spot 4	9.65	77.08	13.27	Spot	medium	
2000x spot 5	9.99	77.2	12.81	Spot	medium	
2000x spot 6	9.97	77.58	12.45	Spot	medium	
Mean	9.708	77.588	12.704			
STDEV	0.4358	0.7186	0.4054			

APPENDIX B29: Heat treated Sample 12H

All results in atomic%						
Raw data						
Spectrum	**C**	**V**	**Ni**	**Comments**	**Phase contrast**	**Remark**
200x image 1	29	67.03	3.98	Overall	Light + Medium + Dark	Agree
200x image 2	29.82	66.5	3.68	Overall	Light + Medium + Dark	Agree
200x image 3	29.34	66.93	3.73	Overall	Light + Medium + Dark	Agree
200x image 4	29.92	66.23	3.85	Overall	Light + Medium + Dark	Agree
200x image 5	29.02	67.23	3.75	Overall	Light + Medium + Dark	Agree
3000x spot 1	9.55	79.85	10.6	Spot	Light	Agree
3000x spot 2	9.52	79.73	10.75	Spot	Light	Agree
3000x spot 3	32.24	64.68	3.08	Spot	Light	Not agree
3000x spot 4	35.21	61.11	3.68	Spot	Light	Not agree
3000x spot 5	8.71	80.73	10.56	Spot	Light	Agree
3000x spot 6	8.76	80.03	11.21	Spot	Light	Agree
3000x spot 1	38.29	61.71	0	Spot	Dark	Agree
3000x spot 2	38.77	61.07	0.15	Spot	Dark	Not agree
3000x spot 3	37.56	62.44	0	Spot	Dark	Agree
3000x spot 4	38.22	61.78	0	Spot	Dark	Agree
3000x spot 5	38.05	61.95	0	Spot	Dark	Agree
3000x spot 1	8.67	81.27	10.06	Spot	Medium	Agree
3000x spot 2	9.35	80.83	9.82	Spot	Medium	Agree
3000x spot 3	9.16	80.92	9.92	Spot	Medium	Agree
3000x spot 4	8.14	82.01	9.85	Spot	Medium	Agree
3000x spot 5	8.82	81.12	10.05	Spot	Medium	Agree
Overall	**C**	**V**	**Ni**	**Comments**	**Phase contrast**	
200x image 1	29	67.03	3.98	Overall	Light + Medium + Dark	
200x image 2	29.82	66.5	3.68	Overall	Light + Medium + Dark	
200x image 3	29.34	66.93	3.73	Overall	Light + Medium + Dark	
200x image 4	29.92	66.23	3.85	Overall	Light + Medium + Dark	
200x image 5	29.02	67.23	3.75	Overall	Light + Medium + Dark	
Mean	29.42	66.784	3.798			
STDEV	0.4338	0.4088	0.119			
Light	**C**	**V**	**Ni**	**Comments**	**Phase contrast**	
3000x spot 1	9.55	79.85	10.6	Spot	Light	
3000x spot 2	9.52	79.73	10.75	Spot	Light	
3000x spot 5	8.71	80.73	10.56	Spot	Light	
3000x spot 6	8.76	80.03	11.21	Spot	Light	
Mean	9.135	80.085	10.78			

STDEV	0.4625	0.4473	0.2981			
Dark	**C**	**V**	**Ni**	**Comments**	**Phase contrast**	
3000x spot 1	38.29	61.71	0	Spot	Dark	
3000x spot 3	37.56	62.44	0	Spot	Dark	
3000x spot 4	38.22	61.78	0	Spot	Dark	
3000x spot 5	38.05	61.95	0	Spot	Dark	
Mean	38.03	61.97	0			
STDEV	0.3291	0.3291	0			
Medium	**C**	**V**	**Ni**	**Comments**	**Phase contrast**	
3000x spot 1	8.67	81.27	10.06	Spot	Medium	
3000x spot 2	9.35	80.83	9.82	Spot	Medium	
3000x spot 3	9.16	80.92	9.92	Spot	Medium	
3000x spot 4	8.14	82.01	9.85	Spot	Medium	
3000x spot 5	8.82	81.12	10.05	Spot	Medium	
Mean	8.828	81.23	9.94			
STDEV	0.4693	0.4686	0.1111			

APPENDIX B30: Heat treated Sample 13H

All results in atomic%						
RAW DATA						
Spectrum	**C**	**V**	**Ni**	**Comments**	**Phase contrast**	**Remark**
200x image 1	25.63	50.35	24.02	Overall	Light + Medium	Agree
200x image 2	25.42	50.75	23.82	Overall	Light + Medium	Agree
200x image 3	25.31	50.35	24.33	Overall	Light + Medium	Agree
200x image 4	26.95	49.77	23.28	Overall	Light + Medium	Agree
200x image 5	28.23	48.75	23.02	Overall	Light + Medium	Not agree
3000x spot 1	23.95	44.06	31.99	Spot	Light	Not agree
3000x spot 2	14.79	32.73	52.48	Spot	Light	Agree
3000x spot 3	12.63	42.78	44.59	Spot	Light	Not agree
3000x spot 4	13.99	32.45	53.56	Spot	Light	Agree
3000x spot 5	14.95	31.86	53.18	Spot	Light	Agree
3000x spot 6	14.89	32.28	52.83	Spot	Light	Agree
3000x spot 1	38.26	61.18	0.56	Spot	Dark	Agree
3000x spot 2	37.28	62.5	0.22	Spot	Dark	Agree
3000x spot 3	36.93	62.7	0.37	Spot	Dark	Agree
3000x spot 4	34.89	63.79	1.32	Spot	Dark	Not agree
3000x spot 5	37.08	62.49	0.43	Spot	Dark	Agree
3000x spot 1	22.33	51.98	25.69	Spot	Medium	Agree

3000x spot 2	22.53	51.64	25.83	Spot	Medium	Agree
3000x spot 3	22.21	52.94	24.85	Spot	Medium	Agree
3000x spot 4	22.64	51.69	25.68	Spot	Medium	Agree
3000x spot 5	23.56	51.24	25.2	Spot	Medium	Agree
Overall	**C**	**V**	**Ni**	**Comments**	**Phase contrast**	
200x image 1	25.63	50.35	24.02	Overall	Light + Medium	
200x image 2	25.42	50.75	23.82	Overall	Light + Medium	
200x image 3	25.31	50.35	24.33	Overall	Light + Medium	
200x image 4	26.95	49.77	23.28	Overall	Light + Medium	
Mean	25.83	50.31	23.86			
STDEV	0.76	0.403	0.441			
Light	**C**	**V**	**Ni**	**Comments**	**Phase contrast**	
3000x spot 1	14.79	32.73	52.48	Spot	Light	
3000x spot 2	13.99	32.45	53.56	Spot	Light	
3000x spot 3	14.95	31.86	53.18	Spot	Light	
3000x spot 4	14.89	32.28	52.83	Spot	Light	
Mean	14.66	32.33	53.01			
STDEV	0.448	0.364	0.464			
Dark	**C**	**V**	**Ni**	**Comments**	**Phase contrast**	
3000x spot 1	38.26	61.18	0.56	Spot	Dark	
3000x spot 2	37.28	62.5	0.22	Spot	Dark	
3000x spot 3	36.93	62.7	0.37	Spot	Dark	
3000x spot 4	37.08	62.49	0.43	Spot	Dark	
Mean	37.39	62.22	0.395			
STDEV	0.599	0.698	0.141			
Medium	**C**	**V**	**Ni**	**Comments**	**Phase contrast**	
3000x spot 1	22.33	51.98	25.69	Spot	Medium	
3000x spot 2	22.53	51.64	25.83	Spot	Medium	
3000x spot 3	22.21	52.94	24.85	Spot	Medium	
3000x spot 4	22.64	51.69	25.68	Spot	Medium	
3000x spot 5	23.56	51.24	25.2	Spot	Medium	
Mean	22.65	51.9	25.45			
STDEV	0.5335	0.6394	0.4115			

APPENDIX B31: Heat treated Sample 14H

All results in atomic%						
RAW DATA						
Spectrum	**C**	**V**	**Ni**	**Comments**	**Phase contrast**	**Remark**
200x image 1	32.96	57.68	9.36	Overall	Light + Dark	Agree
200x image 2	32.63	57.69	9.68	Overall	Light + Dark	Agree
200x image 3	31.9	57.79	10.31	Overall	Light + Dark	Agree
200x image 4	32.97	56.78	10.25	Overall	Light + Dark	Agree
200x image 5	31.55	57.8	10.64	Overall	Light + Dark	Agree
2000x spot 1	14.8	52.3	32.9	Spot	Light	Agree
2000x spot 2	11.8	57.88	30.32	Spot	Light	Not agree
2000x spot 3	15.33	51.83	32.84	Spot	Light	Agree
2000x spot 4	15.39	51.9	32.71	Spot	Light	Agree
2000x spot 5	15.09	52.32	32.6	Spot	Light	Agree
2000x spot 1	38.43	61.31	0.26	Spot	Dark	Agree
2000x spot 2	23.09	65.54	11.37	Spot	Dark	Not agree
2000x spot 3	37.45	61.9	0.65	Spot	Dark	Agree
2000x spot 4	37.12	62.28	0.6	Spot	Dark	Agree
2000x spot 5	38.22	61.51	0.26	Spot	Dark	Agree
2000x eutectic 1	28.11	58.53	13.36	Area	Light+Dark	Not agree
2000x eutectic 2	31.1	56.94	11.95	Area	Light+Dark	Agree
2000x eutectic 3	31.14	57.58	11.28	Area	Light+Dark	Agree
2000x eutectic 4	32.12	57.64	10.24	Area	Light+Dark	Agree
2000x eutectic 5	32.23	57.53	10.23	Area	Light+Dark	Agree
Overall	**C**	**V**	**Ni**	**Comments**	**Phase contrast**	
200x image 1	32.96	57.68	9.36	Overall	Light + Dark	
200x image 2	32.63	57.69	9.68	Overall	Light + Dark	
200x image 3	31.9	57.79	10.31	Overall	Light + Dark	
200x image 4	32.97	56.78	10.25	Overall	Light + Dark	
200x image 5	31.55	57.8	10.64	Overall	Light + Dark	
Mean	32.402	57.548	10.048			
STDEV	0.645	0.4329	0.5169			
Light	**C**	**V**	**Ni**	**Comments**	**Phase contrast**	
2000x spot 1	14.8	52.3	32.9	Spot	Light	
2000x spot 2	15.33	51.83	32.84	Spot	Light	
2000x spot 3	15.39	51.9	32.71	Spot	Light	
2000x spot 4	15.09	52.32	32.6	Spot	Light	
Mean	15.153	52.088	32.763			
STDEV	0.2684	0.2586	0.1343			

Dark	**C**	**V**	**Ni**	**Comments**	**Phase contrast**	
2000x spot 1	38.43	61.31	0.26	Spot	Dark	
2000x spot 2	37.45	61.9	0.65	Spot	Dark	
2000x spot 3	37.12	62.28	0.6	Spot	Dark	
2000x spot 4	38.22	61.51	0.26	Spot	Dark	
Mean	37.805	61.75	0.4425			
STDEV	0.6213	0.43	0.2117			
Eutectic	**C**	**V**	**Ni**	**Comments**	**Phase contrast**	
2000x eutectic 1	31.1	56.94	11.95	Area	Light+Dark	
2000x eutectic 2	31.14	57.58	11.28	Area	Light+Dark	
2000x eutectic 3	32.12	57.64	10.24	Area	Light+Dark	
2000x eutectic 4	32.23	57.53	10.23	Area	Light+Dark	
Mean	31.648	57.423	10.925			
STDEV	0.611	0.3248	0.8424			

APPENDIX B32: Heat treated Sample 15H

All results in atomic%						
RAW DATA						
Spectrum	**C**	**V**	**Ni**	**Comments**	**Phase contrast**	**Remark**
200x image 1	26.95	55.98	17.06	Overall	Light + Dark	Agree
200x image 2	27.04	55.86	17.1	Overall	Light + Dark	Agree
200x image 3	26.98	55.97	17.05	Overall	Light + Dark	Agree
200x image 4	27.52	55.75	16.74	Overall	Light + Dark	Agree
200x image 5	27.21	55.98	16.8	Overall	Light + Dark	Agree
3000x spot 1	11.96	55.47	32.57	Spot	Light	Agree
3000x spot 2	11.03	56.1	32.87	Spot	Light	Agree
3000x spot 3	11.85	55.45	32.7	Spot	Light	Agree
3000x spot 4	13.35	54.45	32.21	Spot	Light	Not agree
3000x spot 5	11.41	55.77	32.83	Spot	Light	Agree
3000x spot 1	27.19	64.96	7.85	Spot	Dark	Not agree
3000x spot 2	36.83	62.73	0.44	Spot	Dark	Agree
3000x spot 3	36.02	63.64	0.34	Spot	Dark	Agree
3000x spot 4	36.86	61.53	1.6	Spot	Dark	Agree
2000x spot 5	35.11	64.22	0.67	Spot	Dark	Not agree
Overall	**C**	**V**	**Ni**	**Comments**	**Phase contrast**	
200x image 1	26.95	55.98	17.06	Overall	Light + Dark	
200x image 2	27.04	55.86	17.1	Overall	Light + Dark	

200x image 3	26.98	55.97	17.05	Overall	Light + Dark	
200x image 4	27.52	55.75	16.74	Overall	Light + Dark	
200x image 5	27.21	55.98	16.8	Overall	Light + Dark	
Mean	27.14	55.908	16.95			
STDEV	0.2351	0.1018	0.1667			
Light	**C**	**V**	**Ni**	**Comments**	**Phase contrast**	
3000x spot 1	11.96	55.47	32.57	Spot	Light	
3000x spot 2	11.03	56.1	32.87	Spot	Light	
3000x spot 3	11.85	55.45	32.7	Spot	Light	
3000x spot 4	11.41	55.77	32.83	Spot	Light	
Mean	11.563	55.698	32.743			
STDEV	0.4272	0.3057	0.136			
Dark	**C**	**V**	**Ni**	**Comments**	**Phase contrast**	
3000x spot 1	36.83	62.73	0.44	Spot	Dark	
3000x spot 2	36.02	63.64	0.34	Spot	Dark	
3000x spot 3	36.86	61.53	1.6	Spot	Dark	
Mean	36.57	62.633	0.7933			
STDEV	0.4766	1.0583	0.7004			

APPENDIX B33: Heat treated Sample 17H

All results in atomic%						
RAW DATA						
Spectrum	**C**	**V**	**Ni**	**Comments**	**Phase contrast**	**Remark**
200x image 1	35.79	37.45	26.76	Overall	Light + Dark	Agree
200x image 2	34.91	37.7	27.38	Overall	Light + Dark	Agree
200x image 3	35.99	37.49	26.52	Overall	Light + Dark	Agree
200x image 4	36.84	36.78	26.37	Overall	Light + Dark	Agree
200x image 5	35.68	37.9	26.42	Overall	Light + Dark	Agree
3000x spot 1	28.34	52.92	18.74	Spot	Light	Not agree
3000x spot 2	23.72	27.95	48.33	Spot	Light	Not agree
3000x spot 3	23.32	23.26	53.41	Spot	Light	Not agree
3000x spot 4	15.3	22.95	61.75	Spot	Light	Agree
3000x spot 6	15	23.86	61.14	Spot	Light	Agree
3000x spot 7	16.19	22.77	61.04	Spot	Light	Agree
3000x spot 8	14.49	23.13	62.38	Spot	Light	Agree
3000x spot 1	42.59	56.43	0.98	Spot	Dark	Agree
3000x spot 2	37.47	60.96	1.57	Spot	Dark	Not agree
3000x spot 3	42.58	56.85	0.58	Spot	Dark	Agree

3000x spot 4	43.57	56.12	0.31	Spot	Dark	Agree
3000x spot 5	42.82	56.52	0.66	Spot	Dark	Agree
3000x spot 6	38.8	60.27	0.94	Spot	Dark	Not agree
3000x spot 1	40.03	58.76	1.21	Spot	needle	Agree
3000x spot 2	41.52	56.68	1.8	Spot	needle	Agree
3000x spot 3	42.93	55.67	1.4	Spot	needle	Agree
3000x spot 4	39.95	59.05	1	Spot	needle	Agree
3000x eutectic 1	37.89	37.42	24.69	Area	Light + Dark	Agree
3000x eutectic 2	38.74	37.29	23.97	Area	Light + Dark	Agree
3000x eutectic 3	35.86	36.11	28.03	Area	Light + Dark	Not agree
3000x eutectic 4	37.13	36.62	26.25	Area	Light + Dark	Agree
3000x eutectic 5	36.98	38.13	24.89	Area	Light + Dark	Agree
Overall	**C**	**V**	**Ni**	**Comments**	**Phase contrast**	
200x image 1	35.79	37.45	26.76	Overall	Light + Dark	
200x image 2	34.91	37.7	27.38	Overall	Light + Dark	
200x image 3	35.99	37.49	26.52	Overall	Light + Dark	
200x image 4	36.84	36.78	26.37	Overall	Light + Dark	
200x image 5	35.68	37.9	26.42	Overall	Light + Dark	
Mean	35.842	37.464	26.69			
STDEV	0.692	0.4226	0.4139			
Light	**C**	**V**	**Ni**	**Comments**	**Phase contrast**	
3000x spot 4	15.3	22.95	61.75	Spot	Light	
3000x spot 6	15	23.86	61.14	Spot	Light	
3000x spot 7	16.19	22.77	61.04	Spot	Light	
3000x spot 8	14.49	23.13	62.38	Spot	Light	
Mean	15.245	23.178	61.578			
STDEV	0.7132	0.4781	0.6202			
Dark	**C**	**V**	**Ni**	**Comments**	**Phase contrast**	
3000x spot 1	42.59	56.43	0.98	Spot	Dark	
3000x spot 3	42.58	56.85	0.58	Spot	Dark	
3000x spot 4	43.57	56.12	0.31	Spot	Dark	
3000x spot 5	42.82	56.52	0.66	Spot	Dark	
Mean	42.89	56.48	0.6325			
STDEV	0.4667	0.3003	0.2758			
Needles	**C**	**V**	**Ni**	**Comments**	**Phase contrast**	
3000x spot 1	40.03	58.76	1.21	Spot	needle	
3000x spot 2	41.52	56.68	1.8	Spot	needle	

3000x spot 3	42.93	55.67	1.4	Spot	needle	
3000x spot 4	39.95	59.05	1	Spot	needle	
Mean	41.108	57.54	1.3525			
STDEV	1.4133	1.6335	0.3401			
Eutectic	**C**	**V**	**Ni**	**Comments**	**Phase contrast**	
3000x eutectic 1	37.89	37.42	24.69	Area	Light + Dark	
3000x eutectic 2	38.74	37.29	23.97	Area	Light + Dark	
3000x eutectic 4	37.13	36.62	26.25	Area	Light + Dark	
3000x eutectic 5	36.98	38.13	24.89	Area	Light + Dark	
Mean	37.685	37.365	24.95			
STDEV	0.8083	0.6188	0.9525			

APPENDIX B34: Heat treated Sample 18H

All results in atomic%						
Raw data						
Spectrum	**C**	**V**	**Ni**	**Comments**	**Phase contrast**	**Remark**
200x image 1	37.12	18.50	44.38	Overall	Light + Dark	Agree
200x image 2	37.17	18.47	44.36	Overall	Light + Dark	Agree
200x image 3	36.56	18.37	45.07	Overall	Light + Dark	Agree
200x image 4	37.45	18.50	44.05	Overall	Light + Dark	Agree
200x image 5	37.81	17.20	45.00	Overall	Light + Dark	Agree
2000x spot 1	17.82	4.30	77.88	Spot	Light	Agree
2000x spot 2	16.48	4.52	79.00	Spot	Light	Not agree
2000x spot 3	19.19	3.99	76.82	Spot	Light	Agree
2000x spot 4	18.44	3.83	77.73	Spot	Light	Agree
2000x spot 5	18.70	2.99	78.31	Spot	Light	Agree
2000x spot 1	47.79	51.23	0.98	Spot	Dark	Agree
2000x spot 2	47.95	51.06	0.99	Spot	Dark	Agree
2000x spot 3	47.62	51.32	1.06	Spot	Dark	Agree
2000x spot 4	46.70	52.35	0.95	Spot	Dark	Agree
2000x spot 5	46.90	52.07	1.03	Spot	Dark	Agree
2000x eutectic 1	43.14	16.45	40.41	Area	Light+Dark	Not agree
2000x eutectic 2	32.37	22.05	45.58	Area	Light+Dark	Agree
2000x eutectic 3	33.10	23.50	43.40	Area	Light+Dark	Agree
2000x eutectic 4	32.60	22.00	45.40	Area	Light+Dark	Agree
2000x eutectic 5	31.80	23.01	45.19	Area	Light+Dark	Agree
Overall	**C**	**V**	**Ni**	**Comments**	**Phase contrast**	
200x image 1	37.12	18.50	44.38	Overall	Light + Dark	

200x image 2	37.17	18.47	44.36	Overall	Light + Dark	
200x image 3	36.56	18.37	45.07	Overall	Light + Dark	
200x image 4	37.45	18.50	44.05	Overall	Light + Dark	
200x image 5	37.81	17.20	45.00	Overall	Light + Dark	
Mean	37.22	18.21	44.57			
STDEV	0.46	0.57	0.44			
Light	**C**	**V**	**Ni**	**Comments**	**Phase contrast**	
2000x spot 1	17.82	4.30	77.88	Spot	Light	
2000x spot 2	19.19	3.99	76.82	Spot	Light	
2000x spot 3	18.44	3.83	77.73	Spot	Light	
2000x spot 4	18.70	2.99	78.31	Spot	Light	
Mean	18.54	3.78	77.69			
STDEV	0.57	0.56	0.63			
Dark	**C**	**V**	**Ni**	**Comments**	**Phase contrast**	
2000x spot 1	47.79	51.23	0.98	Spot	Dark	
2000x spot 2	47.95	51.06	0.99	Spot	Dark	
2000x spot 3	47.62	51.32	1.06	Spot	Dark	
2000x spot 4	46.70	52.35	0.95	Spot	Dark	
2000x spot 5	46.90	52.07	1.03	Spot	Dark	
Mean	47.39	51.61	1.00			
STDEV	0.56	0.57	0.04			
Eutectic	**C**	**V**	**Ni**	**Comments**	**Phase contrast**	
2000x eutectic 1	32.37	22.05	45.58	Area	Light+Dark	
2000x eutectic 2	33.10	23.50	43.40	Area	Light+Dark	
2000x eutectic 3	32.60	22.00	45.40	Area	Light+Dark	
2000x eutectic 4	31.80	23.01	45.19	Area	Light+Dark	
Mean	32.47	22.64	44.89			
STDEV	0.54	0.74	1.01			

APPENDIX B35: Heat treated Sample 19H

All results in atomic%						
RAW DATA						
Spectrum	**C**	**V**	**Ni**	**Comments**	**Phase contrast**	**Remark**
200x image 1	35.75	15.89	48.35	Overall	Light + Dark	Agree
200x image 2	32.67	16.77	50.57	Overall	Light + Dark	Not agree
200x image 3	36.07	15.31	48.61	Overall	Light + Dark	Agree
200x image 4	35.07	15.64	49.28	Overall	Light + Dark	Agree

200x image 5	35.23	16.62	48.15	Overall	Light + Dark	Agree
200x image 6	33.1	16.47	50.44	Overall	Light + Dark	Not agree
2000x spot 1	18	4.34	77.68	Spot	Light	Agree
2000x spot 2	17.67	4.76	77.56	Spot	Light	Agree
2000x spot 3	17.63	4.57	77.8	Spot	Light	Agree
2000x spot 4	21	5.07	73.93	Spot	Light	Not agree
2000x spot 5	14.54	4.8	80.66	Spot	Light	Not agree
2000x spot 6	17.79	4.1	78.11	Spot	Light	Agree
2000x spot 1	48.43	49.91	1.65	Spot	Dark	Agree
2000x spot 2	49.1	49.64	1.26	Spot	Dark	Agree
2000x spot 3	52.05	47.95	0	Spot	Dark	Not agree
2000x spot 4	47.17	51.53	1.3	Spot	Dark	Agree
2000x spot 5	47.02	51.21	1.77	Spot	Dark	Agree
2000x eutectic 1	36.39	14.92	48.7	Area	Light + Dark	Agree
2000x eutectic 2	38.37	15.41	46.22	Area	Light + Dark	Not agree
2000x eutectic 3	35.07	17.07	47.85	Area	Light + Dark	Agree
2000x eutectic 4	34.91	16.94	48.15	Area	Light + Dark	Agree
2000x eutectic 5	35.51	15.99	48.5	Area	Light + Dark	Agree
Overall	**C**	**V**	**Ni**	**Comments**	**Phase contrast**	
200x image 1	33.5	26.1	40.4	Overall	Light + Dark	
200x image 3	32.07	26.31	41.62	Overall	Light + Dark	
200x image 4	33.07	25.64	41.29	Overall	Light + Dark	
200x image 5	33.28	26.62	40.1	Overall	Light + Dark	
Mean	32.98	26.168	40.853			
STDEV	0.6316	0.4115	0.7191			
Light	**C**	**V**	**Ni**	**Comments**	**Phase contrast**	
2000x spot 1	18	4.34	77.68	Spot	Light	
2000x spot 2	17.67	4.76	77.56	Spot	Light	
2000x spot 3	17.63	4.57	77.8	Spot	Light	
2000x spot 6	17.79	4.1	78.11	Spot	Light	
Mean	17.773	4.4425	77.788			
STDEV	0.1662	0.2857	0.2363			
Dark	**C**	**V**	**Ni**	**Comments**	**Phase contrast**	
2000x spot 1	48.43	49.91	1.65	Spot	Dark	
2000x spot 2	49.1	49.64	1.26	Spot	Dark	
2000x spot 4	47.17	51.53	1.3	Spot	Dark	
2000x spot 5	47.02	51.21	1.77	Spot	Dark	
Mean	47.93	50.573	1.495			

STDEV	1.0041	0.9366	0.2536			
Eutectic	**C**	**V**	**Ni**	**Comments**	**Phase contrast**	
2000x eutectic 1	30.39	20.92	48.7	Area	Light + Dark	
2000x eutectic 2	31.07	21.07	47.85	Area	Light + Dark	
2000x eutectic 3	30.91	20.94	48.15	Area	Light + Dark	
2000x eutectic 4	30.51	20.99	48.5	Area	Light + Dark	
Mean	30.72	20.98	48.3			
STDEV	0.3223	0.0668	0.3764			

APPENDIX B36: Heat treated Sample 20H

All results in atomic%						
RAW DATA						
Spectrum	**C**	**V**	**Ni**	**Comments**	**Phase contrast**	**Remark**
200x image 1	33.85	22.34	43.81	Overall	Light + Dark	Agree
200x image 2	31.9	22.62	45.48	Overall	Light + Dark	Agree
200x image 3	31.96	23.13	44.91	Overall	Light + Dark	Agree
200x image 4	13.15	24.79	62.06	Overall	Light + Dark	Not agree
200x image 5	32.72	23.16	44.12	Overall	Light + Dark	Agree
2000x spot 1	24.38	13.46	62.17	Spot	Light	Agree
2000x spot 2	24.03	14.2	61.77	Spot	Light	Agree
2000x spot 3	23.91	14.35	61.75	Spot	Light	Agree
2000x spot 4	46.57	12.98	40.45	Spot	Light	Not agree
2000x spot 5	24.06	13.55	62.4	Spot	Light	Agree
2000x spot 1	75.35	6.11	18.54	Spot	Dark	Not agree
2000x spot 2	46.86	52.91	0.24	Spot	Dark	Agree
2000x spot 3	36.25	29.32	34.43	Spot	Dark	Not agree
2000x spot 4	47.41	52.4	0.18	Spot	Dark	Agree
2000x spot 5	46.24	53.07	0.69	Spot	Dark	Agree
2000x spot 6	47.35	52.37	0.28	Spot	Dark	Agree
2000x eutectic 1	13.46	22.38	64.17	Area	Light + Dark	Agree
2000x eutectic 2	14.2	22.03	63.77	Area	Light + Dark	Agree
2000x eutectic 3	14.35	22.91	62.75	Area	Light + Dark	Agree
2000x eutectic 4	13.55	22.06	64.4	Area	Light + Dark	Agree
Overall	**C**	**V**	**Ni**	**Comments**	**Phase contrast**	
200x image 1	33.85	22.34	43.81	Overall	Light + Dark	
200x image 2	31.9	22.62	45.48	Overall	Light + Dark	
200x image 3	31.96	23.13	44.91	Overall	Light + Dark	
200x image 5	32.72	23.16	44.12	Overall	Light + Dark	

Mean	32.608	22.813	44.58			
STDEV	0.9085	0.4008	0.7579			
Light	**C**	**V**	**Ni**	**Comments**	**Phase contrast**	
2000x spot 1	24.38	13.46	62.17	Spot	Light	
2000x spot 2	24.03	14.2	61.77	Spot	Light	
2000x spot 3	23.91	14.35	61.75	Spot	Light	
2000x spot 5	24.06	13.55	62.4	Spot	Light	
Mean	24.095	13.89	62.023			
STDEV	0.2007	0.4503	0.3174			
Dark	**C**	**V**	**Ni**	**Comments**	**Phase contrast**	
2000x spot 2	46.86	52.91	0.24	Spot	Dark	
2000x spot 4	47.41	52.4	0.18	Spot	Dark	
2000x spot 5	46.24	53.07	0.69	Spot	Dark	
2000x spot 6	47.35	52.37	0.28	Spot	Dark	
Mean	46.965	52.688	0.3475			
STDEV	0.5425	0.3556	0.232			
Eutectic	**C**	**V**	**Ni**	**Comments**	**Phase contrast**	
2000x eutectic 1	27.17	16.67	56.16	Area	Light + Dark	
2000x eutectic 2	27.83	16.84	55.33	Area	Light + Dark	
2000x eutectic 3	26.83	18.26	54.91	Area	Light + Dark	
2000x eutectic 4	26.72	17.93	55.35	Area	Light + Dark	
Mean	27.138	17.425	55.438			
STDEV	0.4998	0.7884	0.5226			

APPENDIX B37: Heat treated Sample 21H

All results in atomic%						
RAW DATA						
Spectrum	**C**	**V**	**Ni**	**Comments**	**Phase contrast**	**Remark**
200x image 1	15.87	30.9	53.23	Overall	Light + Dark	Agree
200x image 2	13.15	33.37	53.48	Overall	Light + Dark	Agree
200x image 3	15.93	31.59	52.48	Overall	Light + Dark	Agree
200x image 4	15.67	31.5	52.83	Overall	Light + Dark	Agree
200x image 5	12.81	32.96	54.22	Overall	Light + Dark	Not agree
2000x spot 1	31.29	21.76	46.96	Spot	Light	Agree
2000x spot 2	28.82	21.47	50.71	Spot	Light	Agree
2000x spot 3	37.04	20.27	42.69	Spot	Light	Not agree
2000x spot 4	29.18	21.87	48.95	Spot	Light	Agree

2000x spot 5	28.46	22.96	48.58	Spot	Light	Agree
2000x spot 1	42.54	56.77	0.68	Spot	Dark	Agree
2000x spot 2	33.2	32.15	34.65	Spot	Dark	Not agree
2000x spot 3	26.94	29.95	43.11	Spot	Dark	Not agree
2000x spot 4	41.7	57.26	1.04	Spot	Dark	Agree
2000x spot 5	42.7	56.24	1.06	Spot	Dark	Agree
2000x eutectic 1	30.33	38.28	31.38	Area	Light + Dark	Agree
2000x eutectic 2	29.86	39.77	30.38	Area	Light + Dark	Agree
2000x eutectic 3	30.5	39.73	29.77	Area	Light + Dark	Agree
Overall	**C**	**V**	**Ni**	**Comments**	**Phase contrast**	
200x image 1	15.87	30.9	53.23	Overall	Light + Dark	
200x image 2	13.15	33.37	53.48	Overall	Light + Dark	
200x image 3	15.93	31.59	52.48	Overall	Light + Dark	
200x image 4	15.67	31.5	52.83	Overall	Light + Dark	
Mean	15.155	31.84	53.005			
STDEV	1.3413	1.065	0.4406			
Light	**C**	**V**	**Ni**	**Comments**	**Phase contrast**	
2000x spot 1	24.29	36.75	38.96	Spot	Light	
2000x spot 2	25.82	34.47	39.71	Spot	Light	
2000x spot 4	25.18	36.87	37.95	Spot	Light	
2000x spot 5	26.46	34.96	38.58	Spot	Light	
Mean	25.438	35.763	38.8			
STDEV	0.9264	1.227	0.7359			
Dark	**C**	**V**	**Ni**	**Comments**	**Phase contrast**	
2000x spot 1	42.54	56.77	0.68	Spot	Dark	
2000x spot 4	41.7	57.26	1.04	Spot	Dark	
2000x spot 5	42.7	56.24	1.06	Spot	Dark	
Mean	42.313	56.757	0.9267			
STDEV	0.5372	0.5101	0.2139			
Eutectic	**C**	**V**	**Ni**	**Comments**	**Phase contrast**	
2000x eutectic 1	30.33	38.28	31.38	Area	Light + Dark	
2000x eutectic 2	29.86	39.77	30.38	Area	Light + Dark	
2000x eutectic 3	30.5	39.73	29.77	Area	Light + Dark	
Mean	30.23	39.26	30.51			
STDEV	0.3315	0.8489	0.8128			

APPENDIX B38: Heat treated Sample 22H

All results in atomic%						
RAW DATA						
Spectrum	**C**	**V**	**Ni**	**Comments**	**Phase contrast**	**Remark**
200x image 1	34.19	29.39	36.42	Overall	Light + Dark	Agree
200x image 2	34.81	29.75	35.44	Overall	Light + Dark	Agree
200x image 3	34.21	30.08	35.71	Overall	Light + Dark	Agree
200x image 4	33.44	30.44	36.12	Overall	Light + Dark	Agree
200x image 5	33.37	30.15	36.49	Overall	Light + Dark	Agree
2000x spot 1	20.35	21.29	58.36	Spot	Light	Agree
2000x spot 2	21.92	21.12	56.96	Spot	Light	Agree
2000x spot 3	17	21.86	61.14	Spot	Light	Not agree
2000x spot 4	20.39	21.34	58.27	Spot	Light	Agree
2000x spot 5	31.36	18.25	50.4	Spot	Light	Not agree
2000x spot 6	21.66	20.63	57.71	Spot	Light	Agree
2000x spot 1	48.19	51.08	0.73	Spot	Dark	Agree
2000x spot 2	47.19	52.13	0.68	Spot	Dark	Agree
2000x spot 3	51.74	47.64	0.61	Spot	Dark	Not agree
2000x spot 4	48.19	50.99	0.81	Spot	Dark	Agree
2000x spot 5	47	52.07	0.94	Area	Dark	Agree
2000x spot 6	48.14	51.07	0.78	Area	Dark	Agree
2000x eutectic 1	34.71	30.29	35	Area	Light+Dark	Agree
2000x eutectic 2	33.39	30.58	36.03	Area	Light+Dark	Agree
2000x eutectic 3	32.07	31.16	36.77	Area	Light+Dark	Agree
2000x eutectic 4	33.1	30.95	35.95	Area	Light+Dark	Agree
2000x eutectic 5	31.95	30.09	37.96	Area	Light+Dark	Not agree
Overall	**C**	**V**	**Ni**	**Comments**	**Phase contrast**	
200x image 1	34.19	29.39	36.42	Overall	Light + Dark	
200x image 2	34.81	29.75	35.44	Overall	Light + Dark	
200x image 3	34.21	30.08	35.71	Overall	Light + Dark	
200x image 4	33.44	30.44	36.12	Overall	Light + Dark	
200x image 5	33.37	30.15	36.49	Overall	Light + Dark	
Mean	34.004	29.962	36.036	Overall	Light + Dark	
STDEV	0.6014	0.4031	0.4534	Overall	Light + Dark	
Light	**C**	**V**	**Ni**	**Comments**	**Phase contrast**	
2000x spot 1	20.35	21.29	58.36	Spot	Light	
2000x spot 2	21.92	21.12	56.96	Spot	Light	
2000x spot 4	20.39	21.34	58.27	Spot	Light	
2000x spot 6	21.66	20.63	57.71	Spot	Light	
Mean	21.08	21.095	57.825	Spot	Light	

STDEV	0.8268	0.324	0.6444	Spot	Light	
Dark	**C**	**V**	**Ni**	**Comments**	**Phase contrast**	
2000x spot 1	48.19	51.08	0.73	Spot	Dark	
2000x spot 2	47.19	52.13	0.68	Spot	Dark	
2000x spot 4	48.19	50.99	0.81	Spot	Dark	
2000x spot 5	47	52.07	0.94	Spot	Dark	
2000x spot 6	48.14	51.07	0.78	Spot	Dark	
Mean	47.742	51.468	0.788			
STDEV	0.5948	0.5784	0.0983			
Eutectic	**C**	**V**	**Ni**	**Comments**	**Phase contrast**	
2000x eutectic 1	34.71	30.29	35	Area	Light+Dark	
2000x eutectic 2	33.39	30.58	36.03	Area	Light+Dark	
2000x eutectic 3	32.07	31.16	36.77	Area	Light+Dark	
2000x eutectic 4	33.1	30.95	35.95	Area	Light+Dark	
Mean	33.318	30.745	35.938			
STDEV	1.0875	0.3867	0.7259			

APPENDIX B39: Heat treated Sample 24H

All results in atomic%						
RAW DATA						
Spectrum	**C**	**V**	**Ni**	**Comments**	**Phase contrast**	**Remark**
200x image 1	35.21	44.96	19.83	Overall	Light + Dark	Agree
200x image 2	35.91	44.32	19.77	Overall	Light + Dark	Agree
200x image 3	35.54	46.27	18.19	Overall	Light + Dark	Agree
200x image 4	79.16	14.76	6.08	Overall	Light + Dark	Not agree
200x image 5	34.86	47.07	18.06	Overall	Light + Dark	Agree
200x image 1	51.93	13.31	34.76	Spot	Light	Not agree
2000x spot 2	16.8	20.5	62.5	Spot	Light	Agree
2000x spot 3	17	21	63	Spot	Light	Agree
2000x spot 4	16.9	20.2	62.5	Spot	Light	Agree
2000x spot 5	15.18	46.82	38	Spot	Light	Not agree
2000x spot 1	46.42	53.08	0.5	Spot	Dark	Agree
2000x spot 2	45.34	54.34	0.32	Spot	Dark	Agree
2000x spot 3	45.58	53.97	0.35	Spot	Dark	Agree
2000x spot 4	39.18	60.18	0.63	Spot	Dark	Not agree
2000x spot 5	45.83	53.75	0.42	Spot	Dark	Agree
Overall	**C**	**V**	**Ni**	**Comments**	**Phase contrast**	
200x image 1	35.21	44.96	19.83	Overall	Light + Dark	

200x image 2	35.91	44.32	19.77	Overall	Light + Dark	
200x image 3	35.54	46.27	18.19	Overall	Light + Dark	
200x image 5	34.86	47.07	18.06	Overall	Light + Dark	
Mean	35.38	45.655	18.963			
STDEV	0.4494	1.2444	0.9688			
Light	**C**	**V**	**Ni**	**Comments**	**Phase contrast**	
2000x spot 2	16.8	20.5	62.5	Spot	Light	
2000x spot 3	17	21	63	Spot	Light	
2000x spot 4	16.9	20.2	62.5	Spot	Light	
Mean	16.9	20.567	62.667			
STDEV	0.1	0.4041	0.2887			
Dark	**C**	**V**	**Ni**	**Comments**	**Phase contrast**	
2000x spot 1	46.42	53.08	0.5	Spot	Dark	
2000x spot 2	45.34	54.34	0.32	Spot	Dark	
2000x spot 3	45.58	53.97	0.35	Spot	Dark	
2000x spot 5	45.83	53.75	0.42	Spot	Dark	
Mean	45.793	53.785	0.3975			
STDEV	0.4637	0.5293	0.0802			